THE JOURNAL
OF
CHEMICAL PHYSICS

VOLUME 20, NUMBER 3 MARCH, 1952

Comparison of Absorption Spectrum of Uranium Tetrachloride with that of Praseodymium Trichloride and of Uranium Trichloride with that of Neodymium Trichloride*

KENNETH M. SANCIER AND SIMON FREED
Chemistry Department, Brookhaven National Laboratory, Upton, Long Island, New York
(Received October 19, 1951)

The absorption spectra of the following substances were taken at 77°K: crystals of anhydrous uranium tetrachloride, praseodymium trichloride, uranium trichloride, neodymium trichloride, uranium tetrafluoride, and a solution of uranium tetrachloride in a solvent consisting of propyl alcohol, propene, and propane.

The spectra of the "iso-electronic" ions U^{+4} and Pr^{+3} exhibited a match in wave number of the centers of gravity of the separate absorption groups. The correspondence is especially evident between the spectrum of uranium tetrachloride and that of praseodymium chloride. The uranium tetrafluoride furnished a spectrum resembling the chloride but the separations of the absorption regions were not so clear.

These correspondences between U^{+4} and Pr^{+3} lead to term assignments for the basic and activated electronic states of U^{+4} since those of Pr^{+3} are known. Thus, the two least stable electrons of U^{+4} in the basic state and to a good approximation in the excited states lies within the 5*f* shell.

The interaction of the fields of the environment of the ions in the case of U^{+4} is greater than in the case of Pr^{+3} and is especially marked in their $^1I_6$ states. The greater interaction is in agreement with the greater effects of different ionic environments on the spectra of U^{+4}, the greater intensity of the "forbidden" transitions and other physical properties.

The correlation of the spectra of U^{+3} and Nd^{+3} is less distinct even though the same approach may well be valid in view of their similar color. The areas of absorption are not as distinctly separate and may even overlap.

A new method has been developed for obtaining the absorption spectra of very small anisotropic crystals.

INTRODUCTION

IN order to investigate the possible similarity of the quantum character of ions in the transuranic and rare earth series, the spectra of the anhydrous chlorides of the "iso-electronic" combinations $U^{+4}-Pr^{+3}$ and $U^{+3}-Nd^{+3}$ have been taken at 77°K. Salts of both U^{+4} and Pr^{+3} are green in crystals and solutions. While the solutions of the salts of U^{+3} and Nd^{+3} are red, and the color of salts of neodymium are also red, the crystals of uranium trichloride have a greenish cast. Because of presumed differences in effective nuclear charge and in interactions with the ionic environment, there is certainly no *a priori* reason to anticipate a match between the spectra of these iso-electronic combinations. However, simple correspondence has actually been found to occur between the spectra of U^{+4} and Pr^{+3}.

EXPERIMENTAL

The technique depends on the birefringent character of the material. By placing small anisotropic crystals

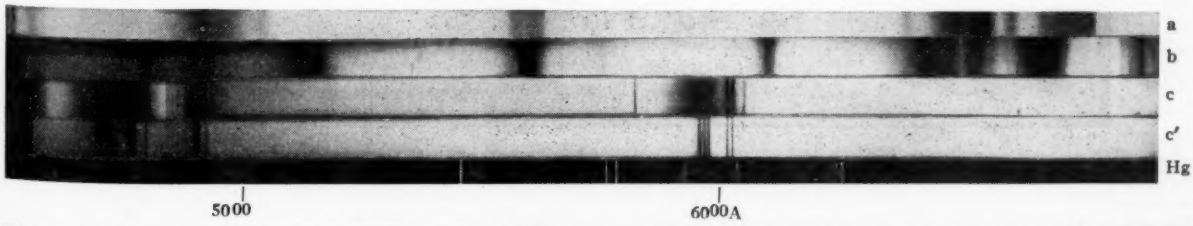

FIG. 1. Absorption spectra at 77°K: (a) UCl_4 solution in 10 percent *n*-propyl alcohol in 1.1 propane-propene, (b) UCl_4 crystals, (c) $PrCl_3$ crystals, and (c') $PrCl_3$ thinner crystals. *Note added in proof.*—The sharp line at 5830A in the spectrum of praseodymium trichloride (c) has been found due to the presence of dissolved neodymium trichloride as an impurity. Its presence does not affect the correspondence drawn between the spectra.

* Research carried out under the auspices of the AEC.

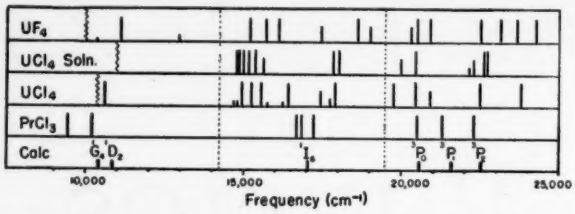

FIG. 2. Comparison of centers of gravity of absorption bands of the "iso-electronic" ions Pr^{+3} and U^{+4}. The lowest row gives the theoretical quantum character of the excited states; the basic state is $^3H_4$.

between crossed nicols, light is transmitted through them because of their birefringence while around them the field is dark. Thus microscopic diaphragming of the separate crystals is obtained. This light is focused on the slit of the grating spectrograph. The intensity of the light scattered and diffracted at the edges of the crystals is much reduced, and consequently a good contrast is achieved between absorption and transmission.

The spectrum obtained is averaged over many orientations but not along an isotropic axis. The method is limited by the transparency of the polarizing prisms.

All the salts were prepared in a vacuum line consisting of glass and fused quartz where necessary. The fused quartz tube used in a series of sublimation constituted the optical cell. For taking spectra at low temperature, the latter was placed in a fused quartz Dewar flask containing liquid nitrogen.

Uranium tetrachloride was dried in an atmosphere of hydrogen chloride while the temperature was slowly raised to 250°C over a period of three hours, and was then sublimed at 450°C in vacuum.

The uranium trichloride was prepared by reducing the tetrachloride with hydrogen at 600–700°C and was sublimed at higher temperatures.

Uranium tetrafluoride was sublimed in vacuum from an incandescent platinum boat onto a quartz plate which was then introduced into the optical cell and dried by heating in the presence of dry hydrogen fluoride.

For purposes of comparison with the spectra of anhydrous uranium tetrachloride, a solution of this salt fluid at 77°K was prepared. Dry *n*-propyl alcohol was condensed on the sublimed uranium tetrachloride which dissolved rapidly. Then a 1:1 mixture of propane-propene was condensed into the alcoholic solution at 190°K making the solution 10 percent alcohol. After thorough mixing at 230°K, the solution was cooled to 77°K where it had about the same fluidity as glycerine at room temperature.

The anhydrous chlorides of neodymium and praseodymium originated in hydrates which were dried in an atmosphere of hydrogen chloride while slowly raising the temperature to 250°C, and the anhydrous salts were sublimed at 850–900°C in vacuum in the optical tube.

DISCUSSION

The wavelengths found for uranium tetrachloride agree with those of Freymann and associates[1] for the most part, but in general, we have found fewer lines.

In Fig. 1 are given parts of the spectra at 77°K of uranium tetrachloride in solution and as crystals, and praseodymium trichloride.

In Fig. 2 comparison is made between the spectra on a wave number scale. Only the centers of gravity of the groups of lines, either discrete or unresolved, are given. It is evident that the spectra of the crystals of uranium tetrachloride, as well as that of its solution at 77°K, fall into separate regions which are roughly the same as those of praseodymium trichloride. The spectrum of uranium tetrafluoride also falls into such clusters, but the regions are not as distinct as those of the tetrachloride. The solution of the tetrachloride is transparent[2] from the last group listed at 4350A to about 3000A where a sharp cutoff occurs and continuous absorption sets in. Except for this continuum of U^{+4}, the spectra of Pr^{+3} and of U^{+4} have their absorptions in the same spectral regions.

The existence of the strong continuum at about 3000A in the spectrum of U^{+4} can be accounted for in terms of the reduction of U^{+4} to U^{+3} where an electron is transferred to the U^{+4} from its environment, a transition analogous to the photographic process in which silver ion Ag^+ is reduced to atomic silver. We have, in fact, observed[3] the photochemical reduction of U^{+4} to U^{+3} in a solution of UCl_4 at 77°K upon irradiating with ultraviolet light below 3000A. The corresponding continuum for Pr^{+3} does not occur because of the instability of Pr^{+2}. A continuum is believed to exist in the spectrum of Pr^{+3} at about 2100A, but this is a result of the ionization of Pr^{+3} to Pr^{+4}; the analogous ionization of U^{+4} to U^{+5} would probably require more energy and its continuum would appear still farther in the ultraviolet.

The centers of gravity of the $PrCl_3$ groups agree very well with those reported by Mukherji[4] for $PrCl_3 \cdot 7H_2O$ as well as with the frequencies calculated by Spedding,[5] and the transitions from the basic state,

FIG. 3. Absorption spectra of crystals at 77°K of UCl_3 and $NdCl_3$.

[1] Freymann, Freymann, and Rohmer, Compt. rend. **230**, No. 17, 1524 (1950).

[2] The transparency of regions of the spectra is relative only since by increasing the light path either through the solution or through the crystals, more and more absorption becomes evident. In addition to weak electronic transitions the origins of these faint absorptions are to be ascribed mostly to various coupling of the ions with their environments.

[3] (To be published).

[4] P. C. Mukherji, Indian J. Phys. **11**, 399–407 (1937).

[5] F. H. Spedding, Phys. Rev. **58**, 255–57 (1940).

$^3H_4$, to the terms given in Fig. 2 are those of Mukherji and Spedding for Pr^{+3} (Pr IV). The over-all centers of gravity of the groups of UCl_4 which have been included within the dotted lines are the same for the crystal and the solution and roughly conform with the centers of gravity of the three groups for $PrCl_3$ identified with the transition to $^1I_6$.† That $PrCl_3$ and UCl_4 have similar color to the eye is consistent with this behavior. The justification for gathering the absorptions in the region of the red into one transition, $^1I_6$, and identifying them as equivalent to one electronic transition is the following: The strong group in the spectra of the crystals UCl_4 at about 16350 cm^{-1} has only an extremely feeble absorption in the solution of these crystals. The omission of such a strong band from the spectrum of a rare-earth ion in different fields is not to be expected. However, by interaction with different external fields it is common to find change in number and spacing of the components within a group corresponding to one electronic transition. The spread in the decomposition of the state of U^{+4} corresponding to the state $^1I_6$ for Pr^{+3} is 3000 cm^{-1}. In Pr^{+3} compounds, this spread is considerably less; in $PrCl_3$ it is 500 cm^{-1}. However, it is 700 cm^{-1} from praseodynium sulfate[6] $Pr(SO_4)_3 \cdot 8H_2O$ and 1200 cm^{-1} from praseodymium molybdate $Pr_2(MoO_4)_3$. The degree of complexity of each subgroup within $^1I_6$ suggests that the coupling of each electronic state with the environment is decidedly more important in U^{+4} than for Pr^{+3}. It must be recalled that when thick crystals of any praseodymium salt are taken, the former background is found to consist of an abundance of absorption having structure (see Fig. 1, spectra c and c′). Further spectroscopic evidence of this large interaction is shown by considerable changes that the spectrum of the ion undergoes in different environments, by the high intensities of transitions in U^{+4} as compared with those in Pr^{+3} in what are accepted as forbidden transitions (nevertheless the intensities of the U^{+4} spectrum are much less than for a permitted transition), and by the magnetic susceptibility data which show strong deviations from the behavior of "free" ions.

The centers of gravity of the groups in the blue region of the spectra of UCl_4 in solid and solution match fairly closely those of $PrCl_3$. We would expect, as has been found, that the transitions to $^3P_0$, $^3P_1$, and $^3P_2$ would not spread out as much as the transition to $^1I_6$ because of their lower values of angular momentum. This behavior holds to an even greater degree for the fluoride. With regard to the groups within the ^3P region (Fig. 2) of UCl_4, the one nearest the red can probably be identified with $^3P_0$ and the group farthest to the blue, with $^3P_2$. We are postponing any detailed assignment of the groups between two extremes. It is likely, in view of the complex structure of the subgroups, especially of those associated with $^1I_6$, that the quantum characters of the states given above for U^{+4} are over-simplified; however, if the intensity of interaction is imagined reduced, they would be expected to approach in character the corresponding state of Pr^{+3}. In the near infrared, the groups of UCl_4 at 10600 cm^{-1} correspond to the transitions to $^1G_4$ and $^1D_2$ of Pr^{+3} in this region. The absorption groups of UF_4 at 11000 cm^{-1} would also correspond adequately if the weak transitions are ignored in this approximation; otherwise the groups are not so distinctly separate. (The broken lines at the left of the spectra in Fig. 2 represent the limits of our examination.)

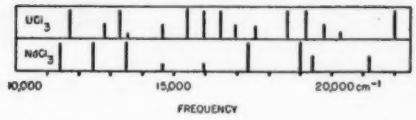

FIG. 4. Comparison of centers of gravity of absorption bands of the "iso-electronic" ions Nd^{+3} and U^{+3}.

The spectra of uranium trichloride and neodymium trichloride reproduced in Fig. 3 are both unusually sharp. It was not possible to obtain spectra of UCl_3 in the ultraviolet because of the transparency limit of the nicol prisms. The centers of gravity and relative intensities of the bands of $NdCl_3$ and UCl_3 are shown in Fig. 4 on a wave-number scale. The correlation of the spectra of the $Nd^{+3}-U^{+3}$ combination is not as clear-cut as in the former case because the groups of absorption do not fall apart into separate areas and may even overlap.

The spectra of the crystals exhibit evidence of strong coupling between the lattice frequencies and the various electronic transitions; these lattice modulations of the electronic frequencies are manifest as feeble repetitions of the main absorption bands displaced slightly toward shorter wavelengths. In UCl_4, where the components of the groups are not well resolved, the lattice modulations appear as a weak unresolved "shadow" on the short wavelength side of the strong parent band. However, there seems to be evidence of "shadows" toward the long wavelengths also. For UCl_3, where the component lines of a band are sharper, the lattice modulations are more discrete and are more obviously a copy of the parent band. The lattice modulations of $PrCl_3$ are even more evident and can be seen in Fig. 1. Ewald[7] first noticed this effect in hydrated magnesium neodymium nitrate.

† *Note added in proof.*—Very recently A. M. Hellwege and K. H. Hellwege [Z. Physik **130**, 549 (1951)] concluded that the state designated as $^1I_6$ should read $^1D_2$ to be consistent with their polarization spectra of two praseodymium salts. E. Trefftz [Z. Physik **130**, 561 (1951)] found theoretically that the state $^1D_2$ is not ruled out as a possibility but the state $^1I_6$ would accompany it rather closely in energy.

The correspondence we have indicated between U^{+4} and Pr^{+3} may be consistent with the $^1D_2$ designation if it be remembered that the actual numbers of groups within the transition in U^{+4} is uncertain because in some instances it is not clear what lines constitute a group.

[6] A. Merz, Ann. Physik **28**, 576 (1937).

[7] H. Ewald, Ann. Physik (5) **34**, 209 (1939).

Lifetimes of Active Molecules. I*

R. A. MARCUS†
University of North Carolina, Chapel Hill, North Carolina
(Received August 3, 1951)

The specific dissociation constants for various vibrationally excited molecules (methane, ethane, and propane) are inferred from an interpretation of experimental data on atomic cracking reactions and on the deuterization of free radicals. As was to be expected, these dissociation constants decrease with increasing number of degrees of freedom of the decomposing molecule.

INTRODUCTION

IN the past, the well-known Rice-Ramsperger, Kassel, and Hinshelwood quasi-unimolecular reaction rate theories have been applied to many unimolecular reactions. However, it is now known that many of these reactions are not simple unimolecular reactions, but rather are complex chain reactions. Thus, for purposes of testing the various unimolecular rate theories and thereby gaining information about intra- and intermolecular energy exchange, it would be well to examine other possible sources of data.

Effectively, the quasi-unimolecular theories were largely concerned with evaluation of the lifetime of the average decomposing molecule. When the pressure in such a reaction system was such that the time between successive collisions was comparable to or greater than this lifetime, the over-all unimolecular rate constant was smaller than the high pressure rate constant.

In the present paper, we shall attempt to deduce the lifetimes of various decomposing molecules from experimental data on the deuterization of methyl radicals and on the atomic-cracking of ethyl and propyl radicals. In a later paper, comparison with theoretical considerations and correlation with data on recombination of free radicals will be given.

To anticipate somewhat, the half-lives deduced below, while probably of the correct order of magnitude, can only be regarded as tentative pending further detailed study of these systems.

A. Deuterization of Methyl Radicals

The mercury photosensitized decomposition of methane results in the production of methyl radicals and hydrogen atoms, and in the presence of deuterium the following reactions can occur:

$$CH_4+Hg(^3P_1)=CH_3+H+Hg(^1S_0) \quad (1)$$

$$D_2+Hg(^3P_1)=2D+Hg(^1S_0) \quad (2)$$

$$CH_3+D=CH_2D+H \quad (3)$$

$$CH_2D+D=CHD_2+H, \text{ etc.} \quad (4)$$

Deuterated methanes then result from the recombination of these radicals with deuterium atoms. At sufficiently high deuterium atom concentrations, the corresponding reactions of hydrogen atoms may be neglected. Furthermore, at sufficiently low temperatures the high activation energy reactions

$$CH_3+D_2=CH_3D+D \quad (5)$$

$$CH_4+D=CH_3+HD \quad (6)$$

may also be disregarded.

It seems reasonable to assume that reactions (3) and (4) together with those of the recombination of radicals and atoms may be written, respectively, in a more fundamental manner as follows:

$$CH_3+D=CH_3D^* \quad (7)$$

$$CH_3D^*+M=CH_3D+M \quad (7')$$

$$CH_3D^* \overset{k_7}{=} CH_2D+H \quad (7'')$$

$$CH_2D+D=CH_2D_2^* \quad (8)$$

$$CH_2D_2^*+M=CH_2D_2+M \quad (8')$$

$$CH_2D_2^* \overset{k_8}{=} CHD_2+H \quad (8'')$$

and a similar sequence for CHD_2 radicals (which shall be designated as reaction sequence (9)). The starred molecules ("active molecules") contain about 100 kcal mole^{-1} of vibrational energy arising from the newly formed C−D bond. M denotes any third body capable of deactivating an active molecule. We wish to evaluate the specific dissociation constants k_7, k_8, and k_9. The corresponding half-life periods are then given by $\tau_i=(\ln_e 2)/k_i$, $i=7, 8, 9$.

In a preliminary investigation of such a system[1] Taylor and co-workers analyzed for the deuteromethanes by infrared methods. Their data are summarized in Table I, where the units may be regarded as arbitrary. The total pressure in the reaction system was 230 mm in each run. The rate constants k_i can be evaluated from this data. Consider the reaction sequence (7). If a CH_3D^* molecule reacts via (7'), CH_3D will be produced, and at small percent conversions this CH_3D will not undergo further reaction. If on the other hand CH_3D^* disappears via (7''), the resulting CH_2D radicals will finally end up as a mixture of CH_2D_2, CHD_3, and CD_4.

* This work was financially assisted by the Office of Naval Research, Contract No. N8onr-77900.
† Present address: Department of Chemistry, Polytechnic Institute of Brooklyn.

[1] Morikawa, Benedict, and Taylor, J. Chem. Phys. 5, 212 (1937).

Thus the relative rate of (7′) and (7″) is given by the ratio, $(CH_3D)/(CH_2D_2+CHD_3+CD_4)$. The rate constant for (7′) is equal to $z_7\lambda_7$, where z_7 is the kinetic theory collision number and λ_7 is some factor equal to or less than unity, representing the efficiency of a deactivating collision.

Thus, if p denotes the total pressure, we have

$$\frac{k_7}{z_7\lambda_7 p}=\frac{k_7(CH_3D^*)}{z_7\lambda_7(CH_3D^*)p}=\frac{(CH_2D_2+CHD_3+CD_4)}{(CH_3D)}, \quad (9)$$

and similarly,

$$k_8=z_8\lambda_8 p \quad (CHD_3+CD_4)/(CH_2D_2)$$
$$k_9=z_9\lambda_9 p \quad (CD_4)/(CHD_3).$$

While the amount of CD_4 produced was not determined, it may be neglected for the present purpose, according to the trends in Table I. For simplicity of notation, set $z_n\lambda_n=z\lambda$ and take $z=5\times10^6$ mm^{-1} sec^{-1} leaving λ arbitrary for the present. Averaging the data of Table I, we find for k_7 and k_8 the values $8\times10^8\lambda$ and $5\times10^8\lambda$ sec^{-1}, respectively. In quasi-unimolecular theories, it is customary to set $\lambda=1$, though there is neither sufficient theoretical nor sufficient experimental justification for this as yet.

B. Atomic Cracking of Ethyl Radicals

The atomic cracking of ethyl radicals, described by Eq. (10), competes with the recombination reaction (11). These reactions

$$H+C_2H_5=2CH_3 \quad (10)$$
$$H+C_2H_5=C_2H_6 \quad (11)$$

may be assumed to occur in the following manner:

$$H+C_2H_5=C_2H_6^* \quad (12)$$
$$C_2H_6^* \overset{k_{12}}{=} 2CH_3 \quad (12')$$
$$M+C_2H_6^*=C_2H_6+M. \quad (12'')$$

With suitable experimental conditions, the methyl radicals will end up largely as methane, which can then be measured. If the rate of (12″) can also be estimated, then from the relative rates of (12′) and (12″), k_{12} can be determined.

In the mercury photosensitized reaction of ethane the occurrence of (12″) (or really, of (11)) has been suggested as a principal cause for the low quantum yields at low ethane pressures and also to account for the

TABLE I. Deuteromethanes produced by mercury photosensitization of CH_4+D_2.

Run	CH_3D	CH_2D_2	CHD_3
47	12	7	2
91	25	12	7
97	16	6	3

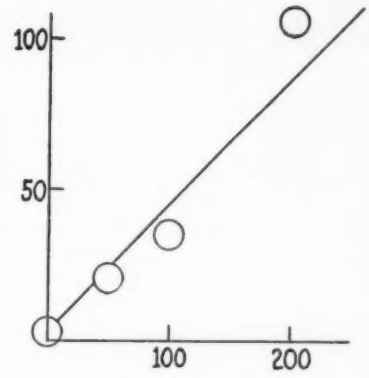

FIG. 1. Experimental data for estimation of k_{12}. Ordinate: $2(1-\phi_{H_2})/\phi_{CH_4}$. Abscissa: pressure in mm.

variation of this yield with pressure. A detailed study of this photosensitized reaction at room temperature has recently been made,[2] and the following mechanism together with Eqs. (10) and (11) (or essentially, (12), (12′), and (12″)), seems to account for most features of the experimental data fairly well.

$$C_2H_6+Hg(^3P_1)=C_2H_5+H+Hg(^1S_0) \quad (13)$$
$$H+C_2H_6=C_2H_5+H_2 \quad (14)$$
$$CH_3+H=CH_4 \quad (15)$$
$$2C_2H_5=C_4H_{10}. \quad (16)$$

These free radicals may also undergo other reactions and several of these are considered in the Appendix. Steady-state equations for CH_3, H, and $C_2H_6^*$ can be shown to lead to the relation,

$$2(1-\phi_{H_2})/\phi_{CH_4}=z\lambda p/k_{12}+3, \quad (17)$$

where ϕ denotes quantum yield. From the data of reference 2 we have plotted in Fig. 1, $2(1-\phi_{H_2})/\phi_{CH_4}$ *vs* the pressure, p. $z\lambda/k_{12}$ is estimated from the slope to be 0.45 mm^{-1}. Setting $z=5\times10^6$ mm^{-1} sec^{-1}, k_{12} is estimated to be $1.1\times10^7\lambda$ sec^{-1}.

C. Atomic Cracking of Propyl Radicals

Hydrogen atoms and propyl radicals may react via (18) and (19).

$$H+C_3H_7=CH_3+C_2H_5 \quad (18)$$
$$H+C_3H_7=C_3H_8. \quad (19)$$

As before, these reactions may also be written as:

$$H+C_3H_7=C_3H_8^* \quad (20)$$
$$C_3H_8^* \overset{k_{20}}{=} CH_3+C_2H_5 \quad (20')$$
$$C_3H_8^*+M=C_3H_8+M. \quad (20'')$$

Data on the mercury photosensitized reaction of propane[3] at room temperature may be interpreted by a

[2] B. de B. Darwent and E. W. R. Steacie, J. Chem. Phys. **16**, 381 (1948).
[3] B. de B. Darwent and E. W. R. Steacie, J. Chem. Phys. **13**, 563 (1945).

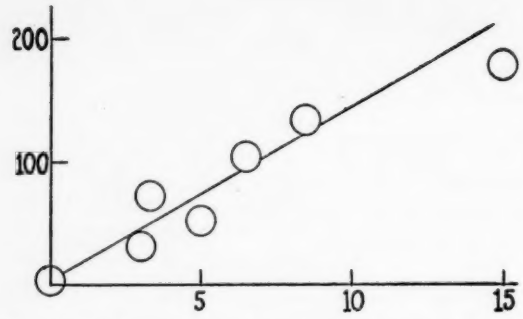

FIG. 2. Experimental data for estimation of k_{20}. Ordinate: $(1-\phi_{H_2})/\phi_{CH_4}$. Abscissa: pressure in mm.

set of reactions analogous to those for ethane:

$$C_3H_8+Hg(^3P_1)=C_3H_7+H+Hg(^1S_0) \quad (21)$$

$$H+C_3H_8=H_2+C_3H_7 \quad (22)$$

$$2C_3H_7=C_6H_{14} \quad (23)$$

together with the sequence (20), (20′), (20″) and some reactions involving the methyl and ethyl radicals produced by (20′).

As before, the methyl radicals are assumed to end up largely as methane. (See Appendix for a discussion of this question.) Experimental data in references 2 and 3 suggest that ethyl radicals react largely via (11) and (16) in the pressure range given in Fig. 2. Steady-state considerations of reactions (15), (20) to (23), and (11) or (16) lead to the relation,

$$(1-\phi_{H_2})/\phi_{CH_4}=z\lambda p/k_{20}+n, \quad (24)$$

where $n=3$ or 2, according as reaction (11) or (16) be included. While only relative quantum yields are given in reference 3, absolute yields were obtained by comparison with the data of another study of this system.[4] We have plotted $(1-\phi_{H_2})/\phi_{CH_4}$ *vs* p in Fig. 2. Evidently from this graph, it makes little difference whether the intercept n equals 2 or 3. Setting $z=5\times10^6$ mm^{-1} sec^{-1}, k_{20} is estimated from the slope to be $3.6\times10^5\lambda$ sec^{-1}.

The half-lives, τ, corresponding to the specific dissociation constants estimated above, are summarized in Table II.

Assuming λ to have roughly the same value in each case, the half-life, τ, is seen to increase with the size of the active molecule, as expected. In each case the active molecule contains about 100 kcal mole^{-1} vibrational energy arising from the newly formed C−H or C−D bond. The larger molecules have more vibrational modes in which this energy can be distributed, so that there is less chance of this energy accumulating in one bond (which could result in decomposition of the molecule). Furthermore, since a C−C bond is about 10–15 kcal mole^{-1} weaker than a C−H bond, the excess of energy over and above that required for reaction is greater for the third and fourth reactions in Table II. If this energy excess were the same for all reactions in this Table, the spread of τ-values would be even greater than that indicated.

TABLE II. Half-lives of various active molecules.

Active molecule	Products	$\tau\times10^9\lambda$sec
CH_3D^*	CH_2D+H	1.4
$CH_2D_2^*$	CHD_2+H	0.9
$C_2H_6^*$	$2CH_3$	60
$C_3H_8^*$	$CH_3+C_2H_5$	2×10^3

APPENDIX

We would like to consider briefly some of the assumptions made in the above treatment.

(a) The low quantum yield in the ethane and propane reactions was attributed to the back reactions (11) and (19), respectively, but not to any possible inefficiency in the primary act. That is, reactions (13) and (21) were assumed to be 100 percent efficient. From the mechanisms given, it can be seen that theoretically, $\phi_{H_2}=1$ at sufficiently high pressures. Extrapolation of the experimental data indicates this to be quite possible, though further study of this question is necessary.

If an efficiency of the primary act, α, $(\alpha\leq1)$ is assumed, it can be shown that Eqs. (17) and (24) need be amended only in that the ϕ's should be replaced by ϕ/α. In the pressure range considered, $1-\phi_{H_2}/\alpha\cong1$ for both photosensitized reactions, so that the k values will be in error by a factor, α. The data[2] suggest that α lies within the range, 0.5 to 1.

(b) In the ethane photosensitized reaction, the following fates for methyl radicals may also be suggested:

$$CH_3+C_2H_6=CH_4+C_2H_5, \quad (25)$$

$$CH_3+C_2H_5=C_3H_8, \quad (26)$$

$$2CH_3=C_2H_6. \quad (27)$$

The experiments discussed above were carried out at room temperature, so that the relatively high activation energy reaction (25) is improbable. Nevertheless, inclusion of (25) in the steady-state equations yields an equation negligibly different from (17).

While the amount of propane produced, if any, was not measured, earlier work[5] on the same system indicated that reaction (26) could be neglected, at least if the ethane pressure exceeded 15 mm. Logically, one would expect the extent of (26) to be intermediate between that of (27) and that of butane production, (16). Since (26) may be neglected, while the butane production exceeds that of propane, (27) may likewise be disregarded.

(c) In these mercury photosensitized reactions, a so-called reaction volume effect enters. Most of the radiation is absorbed close to the incident face, so that the reaction is more or less confined to a small volume, whose dimensions are dependent on the pressure of the hydrocarbon. This effect is generally neglected as a first approximation in quantitative treatments of photosensitized reactions. Nevertheless, repetition of this work at lower mercury concentrations, i.e., under conditions corresponding to a large effective reaction volume, would be helpful in clarifying this question.

Finally, the values of the dissociation constants for ethane and propane may be checked by rather independent methods, e.g., by investigating the reaction of deuterium atoms with these hydrocarbons and analyzing for the amount of methane and deuterated ethanes and propanes produced. While some such data do exist in the literature, the conditions chosen do not appear to be the most desirable ones for evaluation of these constants.

ACKNOWLEDGMENT

I should like to thank Professor O. K. Rice for reading the manuscript and for making several helpful suggestions.

[4] E. W. R. Steacie and D. J. Dewar, J. Chem. Phys. **8**, 571 (1940).

[5] E. W. R. Steacie and N. W. F. Phillips, J. Chem. Phys. **6**, 179 (1938).

Lifetimes of Active Molecules. II*

R. A. MARCUS†
University of North Carolina, Chapel Hill, North Carolina
(Received August 14, 1951)

Experimental data on the atomic cracking of propyl radicals and on the deuterization of methyl radicals are compared with some theoretical calculations. With the aid of some assumptions concerning intramolecular energy transfer in the dissociating molecules involved in these and other reactions and concerning the corresponding activated complexes, data on a number of free radical reactions are correlated.

INTRODUCTION

IN an earlier communication[1] the specific dissociation constants of some vibrationally excited ("active") molecules were estimated from data on the deuterization of free radicals and on atomic cracking reactions. In the present paper, theoretical estimates of these dissociation constants will be made using some equations derived earlier.[2] These calculations will be given in some detail after a comparison of the experimental and theoretical results.

The atomic cracking of ethyl radicals has been considered earlier[3] and assumptions similar to those employed in that treatment will be made here. For brevity some familiarity with these assumptions and notation will be taken for granted.

DISCUSSION OF RESULTS

1. Deuterization of Methyl Radicals

The deuterization of methyl radicals and of deuteromethyl radicals can be interpreted in terms of the following reaction sequence,

$$CH_nD_{3-n}+D \rightleftharpoons CH_nD_{4-n}^*, \tag{1}$$

$$CH_nD_{4-n}^* \overset{k_a}{=} CH_{n-1}D_{4-n}+H, \tag{2}$$

$$M+CH_nD_{4-n}^*=M+CH_nD_{4-n}, \tag{3}$$

where $n=1$, 2, or 3 and M is any third body capable of deactivating the active molecule $CH_nD_{4-n}^*$. From the experimental data k_a was estimated to be[1] *ca* $5\times10^8\lambda$ and $8\times10^8\lambda$ sec^{-1} for $n=2$ and 3, respectively. λ is the efficiency of the deactivating collision (3).

In the following calculations the vibrational degrees of freedom of the active molecule are assumed to be "active" and the rotational degrees of freedom, "adiabatic," using the terminology of reference 2. This is essentially equivalent to assuming that all vibrations can contribute their energy to the breaking bond while the rotations cannot. If one further assumes the activated complex to be "rigid,"[4] then the theoretical value for k_a is found to be 4.4×10^7 and 1.3×10^8 sec^{-1} for $n=2$ and 3, respectively. If, on the other hand, a "loose"[5] activated complex is assumed, k_a is calculated to be 2.6×10^9 and 6.6×10^9 sec^{-1} for $n=2$ and 3, respectively.

A comparison of these theoretical estimates with the data indicates the activated complex to be rigid if one assumes $\lambda\cong0.1$, or loose if $\lambda\sim1$ (λ cannot be greater than unity). We shall return to this question later.

2. Atomic Cracking of Propyl Radicals

Regarding the mechanism of this reaction as given by (4), (5), and (6), k_a was estimated from the data to be *ca* $3.6\times10^5\lambda$ sec^{-1}.

$$H+C_3H_7=C_3H_8^*, \tag{4}$$

$$C_3H_8^* \overset{k_a}{=} CH_3+C_2H_5, \tag{5}$$

$$M+C_3H_8^*=M+C_3H_8. \tag{6}$$

Adopting the previous assumptions of active vibrations and adiabatic rotations k_a is found to be about 2×10^4 and 2×10^8 sec^{-1} for a rigid and loose activated complex, respectively. Clearly, the loose complex gives very poor agreement with the data while if the complex is rigid, $\lambda\cong0.1$.

3. Atomic Cracking of Ethyl Radicals

For comparison with the previous results we recall that using the same assumptions, the loose complex gave[3] very poor agreement with the data while if the complex is rigid, $\lambda\cong0.7$.

4. Effect of Pressure on Recombination of Methyl Radicals

In this case, too, the previous assumptions coupled with a postulated rigid complex were consistent with the data while the loose complex was not.[3]

* This work was financially assisted by the ONR, Contract No. N8onr-77900.
† Present address: Department of Chemistry, Polytechnic Institute of Brooklyn.
[1] R. A. Marcus, J. Chem. Phys. **20**, 352 (1951).
[2] R. A. Marcus, J. Chem. Phys. **20**, 359 (1951).
[3] R. A. Marcus, J. Chem. Phys. **20**, 364 (1952).
[4] The degrees of freedom of this activated complex are similar to those of the active molecule with the exception that a stretching vibration has become a translational motion in the activated complex.
[5] In this complex, the radicals resulting from the decomposition rotate freely.

5. Conclusions

While the experimental data are not very accurate—in some cases an error of a factor of five or ten is possible—it does appear that data on a variety of topics can be correlated in an approximate way by assuming a rigid activated complex, active vibrations, adiabatic rotations and $\lambda \sim 0.1$. If the rotations are treated as adiabatic the data are not consistent with the assumption of a loose complex. Conservation of angular momentum requires that the rotations associated with the two largest moments of inertia of the decomposing molecule will be adiabatic.[2] However, if the remaining rotations acted as energy sinks for the large energy of the active molecule, that is, if they were "active," the calculated lifetime would be increased, k_a decreased, and agreement with the data possibly obtained. Calculations for this assumption were made[3] for data (3) and (4). As pointed out in that discussion, a measurement of the steric factors of the appropriate free-radical-recombination reactions (in the present case, of CH_3+H, $2CH_3$ and $CH_3+C_2H_5$) will throw considerable light on this question. The loose complex is associated with a steric factor of the order of magnitude of unity while the rigid complex, with appreciably smaller steric factors. However, the available data on this question are, at present, conflicting.

CALCULATIONS

1. General

Since no degrees of freedom are assumed to be "inactive," Eq. (17) of reference 2 may be simplified by setting

$$\sum_{E_i \leq E^+} N^*(E_a - E_i + E^+) D(E_i) = N^*(E_a + E^+).$$

This expression for k_a then becomes

$$k_a = \frac{P_1^+ P_R^+ \sum_{E_v \leq E^+} \left(\frac{E^+ - E_v}{kT}\right)^{r/2} P(E_v)}{P_1 \Gamma(1+r/2) h N^*(E_a+E^+)}, \tag{7}$$

where P_1 is the rotational partition function of the active molecule and P_1^+ that of the corresponding rotational degrees of freedom of the activated complex. P_R^+ is the partition function of those r, say, rotational degrees of freedom of the activated complex which originally were vibrations in the active molecule. From the definitions of rigid and loose complexes it follows that $r=0$ for a rigid complex but equals 2 for a nonlinear loose complex consisting of a radical and an atom, and equals 4 for one consisting of two radicals.

$P(E_v)$ is the number of vibrational states of an activated complex whose nonfixed vibrational energy is E_v, while E^+ is the total nonfixed energy of the complex. E_a is the bond strength of the breaking bond and $N^*(E_a+E^+)$ the number of quantum states per unit energy of an active molecule whose energy is (E_a+E^+). In the present calculations the rotational degrees of freedom of the active molecule are assumed to be adiabatic so that N^* is given by the following expression,[2]

$$N^*(E_a+E^+) = \frac{(E_a+E^++E_o)^{s-1}}{\Gamma(s)\prod_i h\nu_i}, \tag{8}$$

where the ν_i are the s vibrational frequencies of the active molecule,

$$E_o = \sum_{i=1}^{s} h\nu_i/2,$$

and Γ is the gamma-function.

The dissociation constants k_a associated with reactions (2) and (5) will now be evaluated with the aid of Eqs. (7) and (8).

2. Deuterization of Methyl Radicals

The rigid and loose activated complexes corresponding to reaction (2) will have[6] a nonfixed energy, E^+, approximately equal to $3kT$ and $5kT$, respectively. Since this energy is smaller than the vibrational quanta[7] of these complexes, $E_v=0$, and the sum in (7) reduces to its first term. Setting $E^+=3kT$ in this equation and noting that $r=0$ and $P_R^+=1$ for the rigid complex, we have

$$k_a = \frac{(P_1^+/P_1)}{hN^*(E_a+3kT)}. \tag{9a}$$

For a loose complex E^+ equals $5kT$ and $r=2$ so that in this case

$$k_a = \frac{5(P_1^+/P_1)P_R^+}{hN^*(E_a+5kT)}. \tag{9b}$$

The moments of inertia of the deuteromethanes needed for the determination of P_1 were, with the exception of CH_2D_2, taken from data given by Herzberg.[8]

---

[6] Defining the dissociation energy of a bond as the energy required to produce an activated complex from the parent molecule, the difference in the C—H and C—D dissociation energies is, for the rigid complex, equal to the difference in the zero-point energies of the corresponding stretching vibrations. Thus, the C—D dissociation energy exceeds that of a C—H bond by an amount approximately equal to 450 cm^{-1} or 1.3 kcal $mole^{-1}$. Clearly the activated complexes of reaction (2) have a nonfixed energy of 1.3 kcal $mole^{-1}$ in addition to the average initial relative kinetic energy (*ca* $kT=0.6$ kcal $mole^{-1}$ at 300°K) of the initial deuteromethyl radical and deuterium atom. The net energy of these complexes is therefore *ca* $3kT$.

In the case of a loose activated complex the difference in the C—H and C—D dissociation energies is equal to the difference in zero-point energies of the one stretching and two bending frequencies of the corresponding bonds. This amounts to *ca* 2.3 kcal $mole^{-1}$, so that the net nonfixed energy, E^+, of the loose activated complexes of reaction (2) is about (2.3+0.6) kcal $mole^{-1}$ $\cong 5kT$ at 300°K.

[7] The corresponding vibration frequencies are inferred from those of the active molecule if the complex is rigid or from the isolated free radicals if the complex is loose.

[8] G. Herzberg, *Molecular Spectra and Molecular Structure* (D. Van Nostrand Company, Inc., New York, 1949), Vol. 2.

The product of the three principal moments of inertia of CH_2D_2 which occurs in the classical expression for P_1, was estimated to be 4.8×10^{-118} (g cm^2 molecule^{-1})^3. Using an equation of Wilson and Hirschfelder[9] the corresponding products for the rigid activated complexes CHD_3^+, $CH_2D_2^+$, CH_3D^+ and CH_4^+ were found to be 4.1, 3.0, 2.1, and 1.4×10^{-117} (g cm^2 molecule^{-1})^3. In these calculations, the hydrogen atom of the activated complex was assumed to be at the apex of a pyramid whose height is 2.8A and whose base is the planar methyl radical. The C—H (and C—D) distance in the radical was taken to be 1.1A.

The rotational partition function of the loose activated complex, $P_1^+P_R^+$, was evaluated as follows: The nonvibrational motion of the radical can be resolved into a rotation about, and a translation of, its center of gravity. The relative motion of the centers of the radical and of the atom may in turn be resolved into radial and transverse motions. The former corresponds to a translation along the reaction coordinate, while the latter may be regarded as the rotation of a diatomic molecule of reduced mass, $\mu=m_am_b/(m_a+m_b)$, where m_a and m_b are the masses of the radical and of the atom, respectively. Thus, the rotational partition function of the loose complex is equal to the rotational partition function of the radical multiplied by that of a diatomic molecule whose moment of inertia is $(2.8)^2\mu$. The products of the three moments of inertia of the radicals which appear in this partition function were estimated from the previously assumed geometry to be 0.55, 1.2, 2.3, and 4.4×10^{-118} (g cm^2 molecule^{-1})^3 for CH_3, CH_2D, CHD_2, and CD_3, respectively.

The vibration frequencies, ν_i, which appear in Eq. (8) were taken from reference 8.[10] Finally, there is a statistical factor equal to the number of alternative C—H bonds of CH_nD_{4-n}* which can be broken (namely n). However, this factor appears automatically via the symmetry numbers in the rotational partition functions of the activated complex and of the active molecule. The C—H bond dissociation energy,[11] E_a is 102 kcal mole^{-1}. With $T=300$°K and the previous data, the k_a values given in Table I were estimated.

Reactions (2) and (3) can occur if $n=4$ though reaction (1) cannot. Nevertheless, the value of k_a for this case is included in Table I for completeness.

TABLE I. k_a for deuteromethanes (sec^{-1}).

n	Loose complex	Rigid complex
1	8.2×10^8	1.2×10^7
2	2.6×10^9	4.4×10^7
3	6.6×10^9	1.3×10^8
4	1.3×10^{10}	3.2×10^8

3. Atomic Cracking of Propyl Radicals

(A) *Rotational Degrees of Freedom*

Because of the geometric complexity of the propane molecule and of the corresponding activated complex, the various rotational partition functions in the expression for k_a will be estimated in a rather approximate manner. However, this estimate should be sufficiently adequate for the present purposes.

The four degrees of freedom of the loose complex which contribute to P_R^+ are two rotations of the methyl group about axes perpendicular to the latter's symmetry axis and two of the ethyl group about axes perpendicular to its own C—C axis. Assuming that the C—H distance in the radical is equal to 1.1A, the appropriate moment of inertia of the methyl group was estimated to be 3.02×10^{-40} g cm^2 molecule^{-1}. The corresponding moment of the ethyl group was inferred from that of ethane to be *ca* 42.3×10^{-40} g cm^2 molecule^{-1}. With this data P_R^+ for the loose complex was found to be 3.6×10^3 at 300°K. As noted earlier P_R^+ equals unity for a rigid complex.

A rough measure of the ratio, P_1^+/P_1, may be inferred in the following way: The three principal moments of inertia of the activated complex will be somewhat larger than those of the active molecule. Furthermore, the rotation of the molecule as a whole has a symmetry number of 2 while the complex is unsymmetrical. These rotations therefore contribute to P_1^+/P_1 a factor somewhat greater than 2. The two internal rotations of the active molecule are hindered while only one is probably hindered in the complex. The partition function of one of these degrees of freedom will be the same in the complex, approximately, as in the active molecule. The remaining internal rotation, which is restricted in the molecule but free in the complex, will contribute to P_1^+/P_1 a factor roughly equal to that obtained for an analogous degree of freedom in ethane[3], namely, 2.0 (at 300°K). Thus the ratio P_1^+/P_1 will be somewhat greater than (2×2). A reasonable value appears to be about 6.

(B) *Vibrational Degrees of Freedom*

The active molecule, C_3H_8*, has an energy[11] of 95 kcal mole^{-1} arising from the formation of the C—H bond in reaction (4). Since only 83 kcal mole^{-1} is required to break the C—C bond in propane[11] the nonfixed energy, E^+, of the activated complex of (5) is[12] approximately 12 kcal mole^{-1}.

Since the number of different vibration frequencies of propane is considerable and E^+ is quite large, the sum in Eq. (7) will have numerous terms corresponding to

[9] E. B. Wilson, Jr., Chem. Revs. **27**, 17 (1940). J. O. Hirschfelder, J. Chem. Phys. **8**, 431 (1940).

[10] See reference 8, p. 306 ff.

[11] See E. W. R. Steacie, *Atomic and Free Radical Reactions* (Reinhold Publishing Corporation, New York, 1946), p. 79.

[12] A more correct value might be 12 plus the difference of the zero-point energies of the activated complexes of (4) and (5). This zero-point energy difference appears to be less than the experimental error in the difference of the C—H and C—C bond strengths and will be disregarded.

all the vibrational energy levels of the activated complex for which $E_v \leq E^+$. In order to make a simpler though less accurate estimate of this sum, the smaller vibration frequencies will be treated in a semiclassical fashion, so that the sum becomes, in part, an integral. The remaining frequencies will, as before, be considered in a quantum manner. While the final results of this calculation still involve a sum, the number of terms involved is significantly less.

With this assumption, E_v becomes a continuous variable and Eq. (7) can be modified by setting

$$\sum_{E_v \leq E^+} (E^+ - E_v)^{r/2} P(E_v) = \int_{E_v=0}^{E^+} (E^+ - E_v)^{r/2} P'(E_v) dE_v, \quad (10)$$

where $P'(E_v)$ is the number of vibrational states per unit energy of an activated complex whose energy is E_v. We next consider a particular set of quantum states for which the energy of the "quantized vibrations" is x_v while that of the "semiclassical vibrations" is $E_v - x_v$. The number of quantum states per unit energy of the semiclassical vibrations is[2]

$$\frac{(E_o' + E_v - x_v)^{q-1}}{\Gamma(q) \prod_i h w_i}, \quad (11)$$

where the w_i are the frequencies of the q semiclassical vibrations and

$$E_o' = \sum_{i=1}^{q} h w_i / 2.$$

When the energy of the quantized vibrations is x_v, let there be $Q(x_v)$ vibrational states of these degrees of freedom and therefore we have

$$P'(E_v) = \sum_{x_v \leq E_v} \frac{(E_o' + E_v - x_v)^{q-1} Q(x_v)}{\Gamma(q) \prod_i h w_i}. \quad (12)$$

after introducing (12) into (10) and interchanging the order of summation and integration so that the new limits are $x_v \leq E^+$ and E_v from x_v to E^+, the right-hand side of Eq. (10) becomes

$$[\Gamma(q) \prod_i h w_i]^{-1} \sum_{x_v \leq E^+} Q(x_v) \times \int_{E_v=x_v}^{E^+} (E_o' + E_v - x_v)^{q-1} (E^+ - E_v)^{r/2} dE_v. \quad (13)$$

In the present calculations r equals 0 and 4 for the rigid and loose complex, respectively, and in the latter case the integral of (13) was evaluated by introducing a new integration variable, $y = (E_o' + E_v - x_v)$.

The discrepancy between (13) and the left-hand side of (10) was estimated for the relatively simple rigid activated complex involved in $C_2H_6 = 2CH_3$. The results of these calculations are given in Table II. The relatively close agreement between the two calculations for large E^+ suggests that (13) will also provide a reasonable approximation to the left-hand side of (10) for the present calculations on propane.

The vibration frequencies of propane used in the calculation of $N^*(E_a + E^+)$ were taken[13] to be 375, 748, 868, 922, 940, 1053, 1155, 1179, 1278, 1355 (3), 1460 (5), and 2950 (8) cm^{-1}. The latter three frequencies were rounded slightly to facilitate some subsequent calculations. By definition these are the vibration frequencies of the rigid complex with the exception that the latter has one C–C stretching frequency while propane has two, namely 868 and 1053 cm^{-1}. The lone C–C frequency of the ethyl group was assumed to be 993 cm^{-1} which is the corresponding frequency in ethane.

The vibration frequencies of the loose activated complex are simply those of the isolated methyl and ethyl radicals. Those of the methyl group were inferred from the frequencies of methyl iodide[14] to be 1252, 1450 (2), and 2960 (3) cm^{-1} while those of the ethyl group were inferred from the characteristic group and bond frequencies[8,13] to be 1000 (5), 1375 (1), 1450 (3), and 2960 (5) cm^{-1}. The remaining vibration of the ethyl radical is a restricted rotation, whose contribution to k_a was considered earlier.

In the calculation for the rigid complex, the frequencies 375, 748, 922, 940, 993, 1155, 1179, and 1278 cm^{-1} were taken to be semiclassical and for the loose complex, 1252 and 1000 (5) cm^{-1} were so adopted.

TABLE II.

E^+ (kcal mole^{-1})	L.H.S. of Eq. No. (10)[a]	Eq. (13)[b]
0	1	7.85
5	11	18.8
8	58	69.8
10	139	188
13	532	670

[a] This sum had been previously estimated in reference 3.
[b] For the vibration frequencies of (see reference 3 for references and discussion) we have chosen: semiclassical vibrations, 827 (2) and 1120 (2) cm^{-1}, i.e., $q = 4$: quantized vibrations, 1380 (2), 1470 (4), 2927 (2), and 2975 (4) cm^{-1}.

TABLE III.

E^+ (kcal mole^{-1})	k_a (Eq. (5)) (sec^{-1})	
	Rigid complex	Loose complex
9.85	1.2×10^4	—
12.85	3.2×10^4	—
14.0	4.6×10^4	3.8×10^8

[13] K. S. Pitzer, J. Chem. Phys. **12**, 310 (1944).
[14] T. Y. Wu, *Vibrational Spectra and Structure of Polyatomic Molecules* (J. W. Edwards, Ann Arbor, Michigan, 1946). The second and third frequencies were rounded to facilitate the calculation of k_a.

k_a is given as a function of the energy of the complex, E^+, in Table III. Clearly the assumption of a loose complex is inconsistent with the data ($E^+=12$ kcal mole^{-1}, $k_a=3.6\times10^5\lambda$ sec^{-1}) so that the corresponding calculations were made for only one value of E^+. Because of a possible error in the present estimates of the C–H and C–C bond strengths E^+ may be slightly different from 12 kcal mole^{-1}. The effect on the calculated value of k_a of assuming a somewhat different value for E^+ may be inferred from Table III.

ACKNOWLEDGMENT

I should like to acknowledge a number of very helpful discussions with Professor O. K. Rice.

THE JOURNAL OF CHEMICAL PHYSICS VOLUME 20, NUMBER 3 MARCH, 1952

Unimolecular Dissociations and Free Radical Recombination Reactions*

R. A. MARCUS†
University of North Carolina, Chapel Hill, North Carolina
(Received August 3, 1951)

The steric and pressure effects associated with the recombination of free radicals both depend on the nature of the activated complex, and are therefore intimately related. From a consideration of the reverse process of unimolecular dissociation, some equations are derived for these properties using an extension of earlier transition state and quasi-unimolecular theories. The present formalism differs from previous formulations of the latter in a number of ways, particularly in the expression used for the density of quantum states of the high energy molecules. Subsequent applications of the theory tentatively suggest that essentially all vibrational degrees of freedom of these molecules can contribute their energy to the vibrationally excited molecules. Consequently, vibrational anharmonicity would appear to be an important factor in intramolecular energy transfer. The present paper is an extension of a previously developed theory for the recombination of methyl radicals and iodine atoms.

INTRODUCTION

RECENTLY,[1] a correlation of the steric effects and pressure dependence of reactions involving the recombination of free radicals was suggested. Such processes are naturally the reverse of those unimolecular dissociations which produce free radicals, and the general theoretical approach was an elaboration of earlier quasi-unimolecular and transition state theories.

The unimolecular reaction rate constant falls off with decreasing pressure when the lifetime of the decomposing (so-called "active") molecules becomes comparable to the time between successive deactivating collisions. The lifetime of these active molecules is a function of the extent of intramolecular energy transfer and also of the nature of the activated complex. Since the steric effects associated with the reverse process of radical recombination are solely dependent on the properties of the same activated complex, there is a close relation between these two effects.

Equations correlating these properties were developed specifically for the decomposition of methyl iodide. The approach was such that several specific assumptions were introduced in the early stages of the derivation, thus necessitating an individual treatment for each different type of molecule and for each specific assumption. A much more general derivation is given in the present paper. Application of the final equations to the available experimental data will be reserved for a later paper.

As before, the unimolecular dissociation is considered initially and then the bimolecular rate constant is estimated with the aid of a calculated equilibrium constant. However, the expressions for the unimolecular rate constant are quite general and could therefore be applied to other unimolecular processes.

UNIMOLECULAR RATE CONSTANT

We consider the following reaction sequence,

$$A+M\underset{k_2}{\overset{k_1}{\rightleftharpoons}}A^*+M, \tag{1}$$

$$A^*\overset{k_a}{=}A^+, \tag{2}$$

$$A^+\overset{k_3}{=}\text{products}. \tag{3}$$

A^* and A^+ denote the active molecule and activated complex respectively, while M is any third body capable of deactivating A^*. Steady-state treatment for A^* and A^+ leads to a relation between the unimolecular rate constant, k_{uni}, and the pressure, p.

$$k_{uni}=k_a(k_1/k_2)/(1+k_a/k_2p). \tag{4}$$

These k's, which are functions of the energy of the

* This work was financially assisted by the ONR Contract No. N8onr-77900.

† Present address: Department of Chemistry, Polytechnic Institute of Brooklyn.

[1] R. A. Marcus and O. K. Rice, J. Phys. and Colloid Chem. 55, 894 (1951).

initial A^* molecule, are first evaluated for a small energy range. k_{uni} is then obtained by integration over all possible energies so that (4) is replaced by

$$k_{uni}=\int \frac{k_a d(k_1/k_2)}{1+k_a/k_2 p}. \tag{5}$$

In Eq. (5) $d(k_1/k_2)$ is the fraction of active molecules having energy in a given energy range. Evaluation of the integrand of (5) will involve a calculation of the number of ways of distributing energy among the various degrees of freedom of the active molecule and of the activated complex. However, the vibrational zero-point energy of A^* and A^+, and also the potential energy of the newly broken bond of the activated complex cannot be so distributed. The remaining energy, which we shall term "nonfixed energy," of the active molecule and of its corresponding activated complex will be denoted by E^* and E^+, respectively. We set $E^*-E^+=E_a$ where the constant E_a is approximately equal to the bond strength of the breaking bond.

The degrees of freedom of the active molecule may be classified with respect to their role in intramolecular energy transfer as "active," "adiabatic," or "inactive." The "active" degrees of freedom are defined as those which can contribute their energy to the breaking bond without restrictions. On the other hand the "adiabatic" ones are assumed to remain in the same quantum state during the course of decomposition of the molecule, and so contribute relatively little energy to the breaking bond. The transfer of energy between the "inactive" degrees of freedom and this bond is assumed to occur with sufficient rapidity only when the molecule has become essentially an activated complex. Since the energy of the latter degrees of freedom is therefore not available to the breaking bond, A^* in Eq. (1) has a nonfixed energy E^* such that $E^*\geq E_a+E_i$, where E_i is the nonfixed energy of the "inactive" degrees of freedom.

Translation of the molecule as a whole makes no contribution to the reaction rate and will not be included in the following. Conservation of angular momentum, which presents some barrier to intramolecular molecular energy transfer, will be treated approximately as follows: The initial molecule may generally be regarded as roughly ellipsoidal in shape and the formation of the corresponding activated complex will frequently correspond to a stretching of the ellipsoid along its major axis (e.g., the rupture of a C—C bond in ethane). On the average, the largest contribution of the angular momentum will come from those two rotational degrees of freedom possessing the larger moments of inertia. This statement applies both to the active molecule and to its activated complex. Conservation of angular momentum thus insures that throughout the course of decomposition the molecule will remain in approximately the same quantum state with respect to these degrees of freedom. Thus these two rotations contribute only the centrifugal energy $J(J+1)h^2/8\pi^2\mu r^2$ to the breaking bond, with J approximately constant. When averaged[2] over all J's the net contribution of these rotations to the reaction rate is a factor P_1^+/P_1, the ratio of the partition functions of these rotations for the activated complex and active molecule, respectively. When, because of additional restrictions, other degrees of freedom (e.g., the remaining rotation) also remain in essentially the same quantum state during the course of reaction, then P_1^+/P_1 becomes the product ratio of the partition functions of all these "adiabatic" degrees of freedom.

In the following, E^*, E^+, and E_i will include neither the energy of translation of the molecule as a whole nor the energy of those degrees of freedom involved in P_1^+/P_1. The results will then be corrected by this factor.

$d(k_1/k_2)$ is equal to the fraction of molecules having energy in the range E^*, E^*+dE^*, where $E^*\geq E_a+E_i$. Let $N^*(E^*-E_i)$ denote the number of energy states per unit energy of the "active" degrees of freedom, and $D(E_i)$, the degeneracy of the inactive ones when they contain the energies (E^*-E_i) and E_i, respectively. We then have

$$d(k_1/k_2)=\frac{\sum_{E_i=0}^{E^*-E_a} N^*(E^*-E_i)D(E_i)\exp(-E^*/kT)dE^*}{\sum_{E_i=0}^{\infty}\int_{E^*=E_i}^{\infty} D(E_i)N^*(E^*-E_i)\exp(-E^*/kT)dE^*}. \tag{6}$$

More exactly $N^*(E^*-E_i)$ should be the number of possible energy states of an active molecule whose energy is (E^*-E_i) and correspondingly the integral in (6) should be a sum. The present treatment anticipates a subsequent semiclassical approximation for $N^*(E^*-E_i)$. Introduction of a new variable $x=(E^*-E_i)$ into the denominator factors the latter into a product which is readily seen to be the product of the partition functions of the active and inactive parts and which will be denoted by the symbol P_2.

k_a may be estimated in the following way: The expressions for $dA^*/dt=0=dA^+/dt$ at complete equilibrium show that the ratio of the equilibrium concentrations of A^+ and A^* is equal to $2k_a/k_3$ if the rate constant for (3) is assumed[3] equal to that for the reverse of (2). The ratio of the equilibrium concentrations of A^+ and A^* molecules of the same energy equals the relative number of quantum states per unit energy of

[2] See O. K. Rice and H. Gershinowitz, J. Chem. Phys. 2, 853 (1934).

[3] This assumption is consistent with the usual assumption of Eyring that motion along the reaction coordinate is a simple translation, so that in our model the velocity is equal in magnitude for the above reactions. We note further that our A^+ refers to those activated complexes which form radicals, rather than the sum of these plus those proceeding in the opposite direction along the reaction coordinate (see reference 1).

A^+ and A^*, respectively. The total number of quantum states per unit energy available to active molecules whose nonfixed energy is E^*, is[4] $N_o^*(E^*)$, where

$$N_o^*(E^*)=\sum_{E_i=0}^{E^*-E_a} N^*(E^*-E_i)D(E_i). \quad (7)$$

One of the degrees of freedom of A^+ is assumed to be a simple translational motion along the reaction coordinate. Let $N_1(x)$ and $N_2(E^+-x)$ denote the number of quantum states per unit energy of this translational motion and of the remaining degrees of freedom of A^+, respectively, when their respective energies are x and (E^+-x). Then the number of quantum states per unit energy of an activated complex which contains a nonfixed energy E^+ is

$$N^+(E^+)=\int_{x=0}^{E^+} N_2(E^+-x)N_1(x)dx. \quad (8)$$

Finally, $2k_a/k_3=N^+(E^+)/N_o^*(E^*)$, where k_3 corresponds to the average value of x. However, the value of k_3 corresponding to a given value of x is equal to $(2x/m)^{\frac{1}{2}}/b$ where m is the reduced mass and b, the extension of the activated complex in coordinate space. Consequently, we may write for k_a,

$$2k_aN_o^*(E^*)=\int_{x=0}^{E^+} N_2(E^+-x)N_1(x)[(2x/m)^{\frac{1}{2}}/b]dx. \quad (9)$$

From the usual expression for the energy levels of a particle in a box, $x=n^2h^2/8b^2m$, we have $N_1(x)(=dn/dx)=2b/h(2x/m)^{\frac{1}{2}}$. On introducing a new variable $y=(E^+-x)$ into (9), the value of k_a, when corrected by the factor P_1^+/P_1, becomes

$$k_a=P_1^+\int_{y=0}^{E^+} N_2(y)dy/P_1h\sum_{E_i=0}^{E^+} N^*(E^*-E_i)D(E_i). \quad (10)$$

From (5), (6), and (10) we find after some cancellation,

$$k_{uni}=\frac{P_1^+\exp(-E_a/kT)}{P_1P_2h}\times\int_{E^+=0}^{\infty}\frac{\int_0^{E^+}N_2(y)dy\exp(-E^+/kT)dE^+}{1+k_a/k_2p}, \quad (11)$$

where k_a is given by (10).[5]

We next derive an expression for $N_2(y)$, the number of quantum states per unit energy of the degrees of freedom of A^+ (not involved in P_1^+ and excluding the translational motion along the reaction co-ordinate) when their energy is y. These degrees of freedom will be vibrational and rotational in nature. We shall assume that the rotations can be treated as independent of each other and of those rotations involved in P_1^+ so that their energy is approximately equal to $\sum_{i=1}^{p} J_i^2h^2/8\pi^2I_i$, where p is the number of rotations while J_i and I_i are the quantum number and moment of inertia of the i'th degree of freedom, respectively. The number of quantum states of the i'th rotation is 2 or $2J_i$ according as it is singly or doubly degenerate. In the former case the factor of two arises since rotation in a plane may occur in 2 (opposite) directions. We shall therefore write this number as $2(J_i)^{d_i-1}$, where d_i is the degeneracy of the i'th rotation ($d_i=1, 2$).[6]

Of the energy y consider first those quantum states of A^+ for which the vibrational energy is E_v and let the degeneracy of the vibrational states be $P(E_v)$. The number of rotational states per unit energy is equal to $(dy)^{-1}\int\cdots\int\prod_i 2(J_i)^{d_i-1}dJ_i$ where the integration is over that region of J_i space where $\sum_i J_i^2h^2/8\pi^2I_i$ lies between $(y-E_v)$ and $(y+dy-E_v)$. The number of rotational-vibrational quantum states per unit energy is simply this multiplied by $P(E_v)$. To obtain $N_2(y)$ we must sum over all vibrational energy levels, E_v, such that $E_v\leq y$. That is,

$$N_2(y)=\sum_{E_v\leq y} P(E_v)(dy)^{-1}\int\cdots\int\prod_i 2(J_i)^{d_i-1}dJ_i. \quad (12)$$

Integration of (12) with respect to all J_i leads to

$$N_2(y)=\sum P(E_v)[\Gamma(r/2)]^{-1}\times(8\pi^2/h^2)^{r/2}(y-E_v)^{r/2-1}\prod_i I_i^{d_i/2}\Gamma(d_i/2), \quad (13)$$

where

$$r=\sum_{i=1}^{p} d_i$$

and Γ is the gamma-function. That is, r is the total number of these rotational degrees of freedom, regarding a d_i-fold degenerate rotation as d_i rotational degrees of freedom.

The product of the partition functions of these de-

[4] The upper limit of the summation arises from the condition that an active molecule has $E^*-E_a\geq E_i$.

[5] We note that at high pressures, the second term in the denominator of (11) is negligible and (11) may be readily integrated by reversing the order of integration so that the limits for E^+ and y become y to ∞ and 0 to ∞, respectively. Integration with respect to E^+ then yields $kT\int_0^\infty N_2(y)\exp(-y/kT)dy=kTP_2^+$ say, which is simply kT multiplied by the partition function of those degrees of freedom of A^+ not involved in P_1^+ and also excluding the internal translation along the reaction co-ordinate. Thus at high pressures, $k_{uni}=(kT/h)\exp(-E_a/kT)P_1^+P_2^+/P_1P_2$, an expression derived by Eyring (J. Chem. Phys. 3, 107 (1935)) and Rice and Gershinowitz. (See reference 2.) However, their approach cannot be used as such for the derivation of the pressure effect.

[6] We observe that it is possible to have several doubly degenerate rotations in an activated complex, although just one in a stable molecule. If, for example, the methyl radicals rotate freely in the activated complex corresponding to the dissociation of ethane, there are three doubly degenerate rotations, one per methyl radical and one for the rotation of the complex as a whole.

grees of freedom is given by[7]

$$P_R^+=\prod_i\int_0^\infty 2(J_i)^{d_i-1}\exp(-J_i^2h^2/8\pi^2I_ikT)dJ_i$$

$$=(8\pi^2kT/h^2)^{r/2}\prod_i\Gamma(d_i/2)I_i^{d_i/2}. \quad (14)$$

Therefore (13) becomes,

$$N_2(y)=\sum_{E_v\leq y}P(E_v)\left(\frac{y-E_v}{kT}\right)^{r/2-1}P_R^+/kT\Gamma(r/2). \quad (15)$$

To calculate $\int_0^{E^+}N_2(y)dy$ from (15), the order of summation and integration is interchanged so that the limits for E_v and for y become $\leq E^+$ and E_v to E^+, respectively. Integration over y then leads to

$$\int_0^{E^+}N_2(y)=\sum_{E_v\leq E^+}P(E_v)\left(\frac{E^+-E_v}{kT}\right)^{r/2}$$

$$\times P_R^+/\Gamma(1+r/2). \quad (16)$$

From (10) and (16) we then obtain:

$$k_a=\frac{P_1^+P_R^+\sum_{E_v\leq E^+}\left(\frac{E^+-E_v}{kT}\right)^{r/2}P(E_v)}{P_1\Gamma(1+r/2)\sum_{E_i\leq E^+}hN^*(E_a+E^+-E_i)D(E_i)}. \quad (17)$$

From (11) and (16) we also find:

$$k_{uni}=\frac{P_1^+P_R^+\exp(-E_a/kT)}{P_1P_2h\Gamma(1+r/2)}$$

$$\times\int_0^\infty\frac{\sum_{E_v\leq E^+}P(E_v)\left(\frac{E^+-E_v}{kT}\right)^{r/2}\exp(-E^+/kT)dE^+}{1+k_a/k_2p}, \quad (18)$$

where k_a is given by (17)

Equation (18) may be further simplified by two approximations. In most of our applications of (18), the vibrational frequencies of A^+ will be assumed to be rather high so that the majority of such activated complexes are produced in their ground vibrational states. Since E_v is the nonfixed vibrational energy, $E_v=0$ and $P(E_v)=1$ for such states. Thus the sum $\sum_{E_v\leq E^+}(E^+-E_v)^{r/2}P(E_v)$ is approximately equal to its first term, $(E^+)^{r/2}$. At very low pressures this approximation results in no error, for unity may be neglected in the denominator of (18) so that this sum cancels out. The error would seem to be largest at $p=\infty$. On integration at $p=\infty$, it is found that k_{uni} is in error by a factor equal to the vibrational partition function of A^+, P_v^+ say. Although P_v^+ generally will be closely equal to unity, the foregoing sum will be replaced by $(E^+)^{r/2}P_v^+$ as a better approximation.

In the summation over E_i in Eq. (17) $N^*(E_a+E^+-E_i)=N^*(E_a)$ to a good approximation; for E_a, which is essentially the bond strength, is of the order of 50 to 100 kcal mole^{-1}, while (E^+-E_i) is less than several kcal mole^{-1} on the average.

Introducing these approximations into (17) and (18), and multiplying (18) by P_T^+/P_T, the ratio of the partition functions for the three external translational degrees of freedom ($P_T^+=P_T$), the following expression for k_{uni} is obtained,

$$k_{uni}=\frac{kT}{h}\frac{P^+}{P}\frac{\exp(-E_a/kT)}{\Gamma(1+r/2)}\int_{w=0}^\infty\frac{w^{r/2}e^{-w}dw}{1+aw^{r/2}}, \quad (19)$$

where we have set $E^+/kT=w$. $P^+(=P_1^+P_R^+P_v^+P_T^+)$ is the partition function for all degrees of freedom of A^+ (excluding the internal translational motion along the reaction coordinate) and $P(=P_1P_2P_T)$, the partition function for A. These are calculated by conventional methods. a is given by (20).

$$a^{-1}=P_1hk_2p\Gamma(1+r/2)N^*(E_a)\sum_{E_i=0}^{wkT}D(E_i)/P_3^+, \quad (20)$$

where $P_3^+=P_1^+P_R^+P_v^+$. The sum in (20) is naturally replaced by integration for those inactive degrees of freedom which can be treated classically. k_2 is simply the kinetic theory collision frequency which, if deactivation does not occur at every collision, should be multiplied by some inefficiency factor.

To complete the derivation, an expression for $N^*(E_a)$ in (20) is needed. $N^*(u)$ is the number of quantum states per unit energy of the "active" part of the active molecule when the energy of that part is u. The majority of these degrees of freedom are vibrational in nature and should therefore, in general, be treated as quantized. A classical treatment of such degrees of freedom is much simpler than the exceedingly laborious quantum treatments but generally gives a gross overestimate of $N^*(u)$. For such quantized vibrations we have found that a good approximation to the average number of vibrational quantum states per unit energy, $N_v^*(u)$ say, is given by the following semiclassical expression[1] when u is large (which it is, for active molecules).

$$N_v^*(u)=(u+E_o)^{s-1}/\Gamma(s)\prod_{i=1}^s h\nu_i, \quad (21)$$

[7] We note here that the present treatment of the rotational degrees of freedom of a molecule leads to the usual classical expression for the partition function of a symmetric top molecule having (or not having) free internal rotation. This provides some justification for our using a very simple expression for the rotational energy levels of a molecule. In the case of an asymmetric top, Eq. (14) leads to the correct classical expression for the partition function if the rotations associated with two moments of inertia, I_1 and I_2, are treated as one doubly degenerate rotation possessing a moment of inertia equal to $(I_1I_2)^{\frac{1}{2}}$.

where

$$E_o=\sum_{i=1}^{s} h\nu_i/2,$$

ν_i is the i'th vibrational frequency of A and s is the number of "active" vibrational modes.

If some rotational degrees of freedom (other than those involved in P_1) are active and if their number of quantum states per unit energy is $N_R^*(x)$ when their energy is x, then $N^*(u)$ is given by (22). Otherwise $N^*(u)$ is equal to $N_v^*(u)$.

$$N^*(u)=\int_{x=0}^{u} N_v^*(u-x)N_R^*(x)dx. \qquad (22)$$

The derivation of an expression for $N_R^*(x)$ is similar to that employed in the treatment of the rotational degrees of freedom involved in (15). Examination of this equation shows that

$$N_R^*(x)=P_a(x/kT)^{(t/2)-1}/kT\Gamma(t/2), \qquad (23)$$

where P_a is the partition function for the t active rotations of the active molecule.

The rotational degrees of freedom associated with $N_2(y)$ and $N_R^*(x)$ have been assumed to be unhindered. If some of these are in fact hindered, then the above treatment will be assumed to provide a reasonable approximation. However, for such degrees of freedom, the correct hindered rotational partition functions will be introduced into P_R^+ and P_a. We have found this procedure to provide a good approximation to some more complicated calculations for the dissociation of ethane to methyl radicals.

BIMOLECULAR RATE CONSTANT

The equilibrium constant for $A \rightleftarrows$ radicals is given by (24).

$$k_{uni}/k_{bi}=\exp(-\Delta H/kT)(P_{\text{rad}}/P)g, \qquad (24)$$

where ΔH is the heat of reaction, P_{rad}, the partition function for radicals, P, that for the molecule, A, and g is the electron spin-orbital degeneracy of the radicals. We have omitted the corresponding factor for A (and A^+) since these are generally in a singlet $\sum$ electronic state. From (19) and (24) we find for k_{bi}

$$k_{bi}=\frac{kT}{h}\frac{P^+\exp[(\Delta H-E_a)/kT]J(a)}{P_{\text{rad}}g}, \qquad (25)$$

where

$$J(a)=\frac{1}{\Gamma(1+r/2)}\int_{w=0}^{\infty}\frac{w^{r/2}e^{-w}dw}{1+aw^{r/2}}.$$

At sufficiently high pressures, $a=0$ and $J(a)=1$. Since there is presumably no potential energy barrier along the reaction co-ordinate, one might argue that the activation energy for the recombination process, $\Delta H-E_a$, should be zero. If there are no orientative restrictions on recombination so that the radicals rotate freely in the activated complex then (assuming no potential energy barrier) $\Delta H=E_a$. If, however, some orientation is necessary so that the activated complex has, in addition to the vibrational frequencies of the isolated radicals, several "bending frequencies," then the activation energy becomes equal to the sum of the zero point energies of these new vibrational modes, when they can be regarded as quantized. When the lifetime, t, of the activated complex is small, the energy levels become appreciably broadened by an amount $\sim h/t$, so that the activation energy is correspondingly less.

The relation between (25) and the simple collision theory expression for k_{bi} may readily be seen from the following approximate considerations. It is assumed that P^+ may be factored into $(8\pi^2Ikt/\sigma h^2)P_{\text{rot}}{}^+P_{\text{vib}}{}^+P_{\text{trans}}{}^+$, where the first factor is the rotational partition function associated with the two larger moments of inertia, I, of the approximately ellipsoidal activated complex and $P_{\text{rot}}{}^+$ is the partition function for the remaining rotations of the complex. The symmetry number, σ, equals 2 or 1 according as the radicals are, or are not, identical. We shall also factor P_{rad} into $P_{\text{rot}}P_{\text{vib}}P_{\text{trans}}$. If the masses of the radicals are m_a and m_b then the translational partition functions per unit volume are:

$$P_{\text{trans}}{}^+=[2\pi(m_a+m_b)kT]^{\frac{3}{2}}/h^3,$$

and

$$P_{\text{trans}}=[2\pi(m_am_b)^{\frac{1}{2}}kT]^3/h^6.$$

In addition, $I=\mu\sigma_{ab}{}^2$, where μ is $m_am_b/(m_a+m_b)$ and σ_{ab} is the distance between the centers of gravity of the radicals in the activated complex. With these expressions Eq. (25) becomes,

$$k_{bi}=(Z/g)(P_{\text{rot}}{}^+/P_{\text{rot}})(P_{\text{vib}}{}^+/P_{\text{vib}})J(a)\times\exp[(\Delta H-E_a)/kT], \qquad (26)$$

where Z is the kinetic theory collision number.

$$Z=\left[\left(\frac{8\pi^2kT}{\mu}\right)^{\frac{1}{2}}\frac{\sigma_{ab}{}^2}{\sigma}\right].$$

If the complex consists of freely rotating radicals then $P_{\text{rot}}{}^+=P_{\text{rot}}$, $P_{\text{vib}}{}^+=P_{\text{vib}}$ and consequently the steric factor is equal to $(1/g)$. If, however, a high degree of mutual orientation of the free radicals is necessary for the formation of an activated complex, then one might assume that the vibrational frequencies of the complex are the same as those of the molecule, A (except that a stretching vibration of A becomes an internal translation of A^+). With this assumption it still follows that $(P_{\text{vib}}{}^+/P_{\text{vib}})\cong 1$ for most reactions. Also, some of the partition functions in $(P_{\text{rot}}{}^+/P_{\text{rot}})$ will approximately cancel and the ratio reduces to a product of the partition functions, f_{rot} say, of those rotational degrees of freedom which are present in the isolated radicals but are "frozen out" when the activated complex is formed. The steric factor then becomes $(gf_{\text{rot}})^{-1}$ (see reference 2).

These extreme types of activated complexes were termed[1] "loose" and "rigid," respectively. The latter is also associated with a high pressure frequency factor of 10^{13} sec^{-1} for the corresponding unimolecular dissociation, since in Eq. (19) we have $P^{+}\cong P$ (and $kT/h\cong 10^{13}$ sec^{-1}) for this case. The corresponding factor for the loose complex is $\cong f_{\text{rot}}\times 10^{13}$ sec^{-1}.

While the true state of the complex would be expected to be intermediate between "loose" and "rigid," it should prove very interesting to see which of the above approximations gives a better explanation of the data. Although one could make some *a priori* calculations, based on potential energy curves, concerning the nature of the activated complex, such calculations should be regarded as highly tentative.

Another important problem is the role of the vibrational degrees of freedom in intramolecular energy transfer. From some applications of the present formalism to the experimental data, it seems quite possible that essentially all the vibrational modes of the molecule, A, are "active" degrees of freedom. Thus the variable, s, in Eq. (21) becomes equal to the number of such modes. It would appear from this that vibrational anharmonicity plays an important role in intramolecular energy transfer, and would have to be taken into account in more fundamental approaches to this problem.

ACKNOWLEDGMENT

I should like to express my appreciation to Professor O. K. Rice for stimulating discussions and suggestions about the many problems associated with these reactions.

THE JOURNAL OF CHEMICAL PHYSICS VOLUME 20, NUMBER 3 MARCH, 1952

Recombination of Methyl Radicals and Atomic Cracking of Ethyl Radicals*

R. A. MARCUS†
University of North Carolina, Chapel Hill, North Carolina
(Received August 14, 1951)

The characteristics of this atomic cracking reaction and of the pressure and steric effects associated with the recombination of methyl radicals are all intimately related. The available data on these reactions are correlated by means of a previously developed theory. Some experimental results on the steric factor and the data on the remaining subjects appear to be consistent with the assumption that the methyl radicals must be highly oriented with respect to each other in order that recombination occur. However, experimental steric factors of unity have also been reported in the literature. The corresponding assumption of no orientation leads to disagreement with the remaining data unless some of the rotational degrees of freedom of the "active" molecule, in addition to the vibrations, are assumed to be "active." Even then, the difficulties are not completely removed. Further experimental work on these reactions is needed.

INTRODUCTION

SEVERAL studies on the pressure and steric effects associated with the recombination of methyl radicals have been reported recently.[1,2] While there seems to be general agreement as to the pressure dependence of the rate constant, different experimental techniques gave widely different values for the steric factor. The reaction appears to be independent of the pressure of inert gases[1b,2b] above 5 mm. No measurements have been reported at lower pressures. Steric factors of unity and 10^{-5} (references 1 and 2, respectively) have been estimated. Still another experimental approach[3] has suggested a steric factor less than 0.1.

The following discussion suggests that the characteristics of the recombination of methyl radicals are closely related, from a theoretical viewpoint, to the relative rates of the "atomic cracking" reaction (1) and the recombination reaction (2). It will be assumed that reactions (1) and (2) may be written in a more illuminating manner as (3), (4), and (5).

$$H+C_2H_5=2CH_3, \tag{1}$$

$$H+C_2H_5=C_2H_6, \tag{2}$$

$$H+C_2H_5=C_2H_6^*, \tag{3}$$

$$C_2H_6^*+M=C_2H_6+M, \tag{4}$$

$$C_2H_6^* \xrightarrow{k_a} 2CH_3. \tag{5}$$

* This work was financially assisted by the ONR, Contract No. N8onr-77900.

† Present address: Department of Chemistry, Polytechnic Institute of Brooklyn.

[1] By use of intermittent light: (a) V. E. Lucas and O. K. Rice, J. Chem. Phys. **18**, 993 (1950). (b) R. Gomer and G. B. Kistiakowsky, J. Chem. Phys. **19**, 85 (1951). (c) R. E. Dodd, Trans. Faraday Soc. **47**, 56 (1951). However, it should be mentioned that there is some slight doubt about the nature of the recombination reaction studied by (a) and (c).

[2] By comparison with reaction of CH_3+NO: (a) R. A. Marcus and E. W. R. Steacie, Z. Naturforsch. **4a**, 332 (1949), and subsequent unpublished work in which the NO was admitted into the reaction system continuously. The latter research, which eliminated some difficulties present in the former, gave a steric factor 10^{-5} to 10^{-6}, while the former gave a steric factor of at least 10^{-3}. (b) D. M. Miller and E. W. R. Steacie, J. Chem. Phys. **19**, 73 (1951).

[3] A. O. Allen and C. E. H. Bawn, Trans. Faraday Soc. **34**, 463 (1937).

$C_2H_6^*$ represents a high energy ("active") molecule containing about 98 kcal mole^{-1} of vibrational energy arising from the newly formed C—H bond. M denotes any molecule capable of deactivating a $C_2H_6^*$ molecule. The value of k_a associated with (5) was estimated to be[4] ca $1.1\times10^7\lambda$ sec^{-1}, where λ is the efficiency of the deactivating collision (4).

The recombination of methyl radicals is closely related to the atomic cracking reactions since it involves the reverse of (5) followed by (4) or alternatively by (5). One important difference is that in this case the average $C_2H_6^*$ molecule has an energy of ca 85 kcal mole^{-1} (the C—C bond strength in ethane) rather than 98 kcal mole^{-1}.

The problem of interpreting the "atomic cracking" and methyl radical recombination reactions reduces to a discussion of the nature of the degrees of freedom of $C_2H_6^*$ and of the activated complex, $C_2H_6^+$, involved in reaction (5). In the following treatment specific assumptions about $C_2H_6^*$ and $C_2H_6^+$ will be introduced into rather general theoretical expressions[5] for pressure and steric effects and for the magnitude of k_a.

THEORETICAL

Before considering these assumptions, a classification[5] of the degrees of freedom of the active molecule will be reviewed briefly. These degrees of freedom were classified into two groups according to whether they do or do not remain in the same "quantum state" during the lifetime of the active molecule. The former group is said to be "adiabatic." Those of the latter group may be further specified with regard to their role in intramolecular energy transfer. They are termed "inactive" if they are not capable of transferring (or receiving) energy to the breaking (or newly formed) chemical bond. Those which are so capable are said to be "active." All vibrational degrees of freedom will be assumed to be active. The rotations corresponding to the two larger moments of inertia of ethane will, for purposes of approximate angular momentum conservation,[5] be assumed to be adiabatic.

Several alternative assumptions will be made about the two remaining degrees of freedom, rotation about the symmetry (C—C) axis and internal hindered rotation. If the active molecule retained its symmetric top configuration during the course of decomposition of the molecule, the angular momenta associated with these rotations would be constants of the motion. The rotations would, in turn, be classified as adiabatic. However, due to the appreciable increase of C—C distance the deviations from a symmetric top configuration may be so large that the rotations become active. Finally if these deviations are only appreciable when the molecule is essentially an activated complex, the rotations would behave as inactive degrees of freedom. As will be seen later, the adiabatic and inactive assumptions lead to rather similar results. In the absence of any suitable guide as to the correct assumptions, calculations will be made for all three cases.

TABLE I. Degrees of freedom of C_2H_6 and of $C_2H_6^+$.

Assumptions		Degrees of freedom of C_2H_6			Degrees of freedom of $C_2H_6^+$	
About $C_2H_6^+$	About two rotations	Adiabatic	Active	Inactive	Adiabatic rotations	Non-adiabatic rotations
loose	adiabatic	4	17	0	4	4
loose	inactive	2	17	2	2	6
loose	active	2	19	0	2	6
rigid	adiabatic	4	17	0	4	0

Two rather extreme assumptions may be made about the activated complex for reaction (5). (1) The complex consists of freely rotating radicals. (2) The degrees of freedom of the complex are very similar to those of ethane with the exception that a C—C stretching vibration in the latter has become, in the former, an internal translational motion along the reaction path.

These complexes are termed "loose" and "rigid," respectively. The rigid complex corresponds to a requirement of a highly oriented collision of methyl radicals, while the assumption of a loose complex is equivalent to a steric factor of the order of magnitude of unity.[5] The absence of an activation energy for these reactions makes a specification of the activated complex rather difficult *a priori*. A more detailed discussion of this problem will be reserved for a later date. For the present, calculations will be made for both complexes.

The various alternative assumptions employed in the following calculations, together with the corresponding specification of the degrees of freedom of ethane and of the activated complex for reaction (5), are summarized in Table I. It will be noted that some alternative assumptions in the case of the rigid complex were not investigated. However, the numerical results for these omitted cases can be roughly extrapolated from the results given in the following.

For purposes of brevity only the detailed calculation of the unimolecular rate constant k_{uni} will be discussed. However, the values of k_a, the dissociation constant of (5), and of k_{bi}, the bimolecular rate constant for the recombination of methyl radicals given in the following, may be estimated in a similar manner using Eqs. (17), (25), and (26) of reference 5 and the data given in Appendix I.

The following expression for k_{uni} as a function of the pressure p was derived earlier.[5]

$$k_{uni}=\frac{kT}{h}\frac{P^+}{P}\cdot\frac{\exp(-E_a/kT)}{\Gamma(1+r/2)}\int_{x=0}^{\infty}\frac{x^{r/2}e^{-x}dx}{1+ax^{r/2}}, \quad (6)$$

where

$$a^{-1}=P_1hk_2p\Gamma(1+r/2)N^*(E_a)\sum_{E_i\leqslant xkT}D(E_i)/P_3^+, \quad (7)$$

[4] R. A. Marcus, J. Chem. Phys. **20**, 352 (1951).
[5] R. A. Marcus, J. Chem. Phys. **20**, 359 (1951); see R. A. Marcus and O. K. Rice, J. Phys. Colloid Chem. **55**, 894 (1951).

TABLE II. Numerical values of integrals in Eqs. (11), (16), and (21).

A^{-1}	$J(A)$	B^{-1}	$K(B)$	C^{-1}	$L(C)$
0	0.00	0	0.00	0	0.00
0.25	0.071	0.25	0.035	8.58	0.26
1	0.19	1	0.11	32.0	0.45
4	0.40	4	0.28	91.1	0.62
16	0.67	16	0.54	250	0.77
36	0.80	36	0.71	1141	0.92
∞	1.00	∞	1.00	∞	1.00

and $N^*(E_a)$ is given by Eqs. (21) or (22) of reference 5 depending on the number of assumed active rotations. E_a is the activation energy for the dissociation of ethane. P and P^+ are the partition functions for all degrees of freedom of C_2H_6 and $C_2H_6^+$, respectively, with the exception that P^+ does not include one degree of freedom of the activated complex, namely, the internal translational motion along the reaction coordinate. P_1 is the partition function for the adiabatic degrees of freedom of ethane, and P_3^+ is the partition function for all rotations and vibrations of the activated complex. These partition functions are estimated by conventional methods from the data given in Appendix I. Γ is the gamma-function and k_2 the collision frequency for the deactivation of active molecules. In the following, the inefficiency of this process is represented by a factor λ. The number of nonadiabatic rotations of the activated complex r is given in the last column of Table I. $D(E_i)$ is the number of quantum states of the inactive degrees of freedom when they have an energy E_i. According to the present assumptions, these are nonvibrational in nature so that the sum in (7) may be replaced by an integral over E_i from 0 to xkT (the rotational energy levels are sufficiently closely spaced). The corresponding integrand is simply the number of rotational quantum states per unit energy for the inactive rotations and is given by an expression similar to Eq. (23) of reference 5. When no degrees of freedom of ethane are assumed to be inactive, the sum over E_i should be replaced by unity. With the previous equations and the data in Appendix I, k_{uni} was evaluated.

The dissociation constant of $C_2H_6^*$, k_a, is given below as a function of the energy of the corresponding activated complex E^+. In the following equations, Z is the frequency of collisions of methyl radicals and $P(E_v)$, the number of vibrational states of an activated complex whose "nonfixed" vibrational energy is E_v. $P(E_v)$ is estimated from the vibrational frequencies of the activated complex by a straight-forward procedure.[6]

The summations in (8), (13), (18), and (23) are over all vibrational energy levels of the complex E_v such that $E_v \leqslant E^+$. The nature of the assumption about the two rotational degrees of freedom discussed earlier is indicated in *italics*. The present calculations correspond to a temperature of 300°K. However, the temperature dependence of the numerical results is rather minor. Pressures are in mm and energies, in kcal mole^{-1}.

1. Loose Activated Complex

(a) *Adiabatic*

$$k_a=\frac{7.4\times10^{40}\sum P(E_v)(E^+-E_v)^2}{(130+E^+)^{16}}\ \text{sec}^{-1}, \tag{8}$$

$$k_{uni}=5.0\times10^{15}J(A)\exp(-E_a/RT)\ \text{sec}^{-1}, \tag{9}$$

$$k_{bi}=0.25ZJ(A), \tag{10}$$

where

$$J(A)=0.5\int_{x=0}^{\infty}\frac{x^2e^{-x}dx}{1+Ax^2} \tag{11}$$

and

$$A=0.69/\lambda p. \tag{12}$$

The integral $J(A)$ may be expressed[7] in terms of exponential sine and cosine integrals. Evaluated from tables[8] of the latter, $J(A)$ is given as a function of A in Table II.

(b) *Inactive*

$$k_a=\frac{4.2\times10^{41}\sum P(E_v)(E^+-E_v)^3}{(130+E^+)^{17}-(130)^{17}}\ \text{sec}^{-1}, \tag{13}$$

$$k_{uni}=5.0\times10^{15}K(B)\exp(-E_a/RT)\ \text{sec}^{-1}, \tag{14}$$

$$k_{bi}=0.25ZK(B), \tag{15}$$

where

$$K(B)=\frac{1}{6}\int_{x=0}^{\infty}\frac{x^3e^{-x}dx}{1+Bx^2} \tag{16}$$

and

$$B=0.23/\lambda p. \tag{17}$$

$K(B)$, estimated in the same manner as $J(A)$, is given in Table II as a function of B.

(c) *Active*

$$k_a=\frac{4.2\times10^{41}\sum P(E_v)(E^+-E_v)^3}{(130+E^+)^{17}}, \tag{18}$$

$$k_{uni}=5.0\times10^{15}L(C)\exp(-E_a/RT)\ \text{sec}^{-1}, \tag{19}$$

$$k_{bi}=0.25ZL(C), \tag{20}$$

[6] For example, let ν_i be the vibrational frequency of the ith oscillator, which is p_i-fold degenerate, say. If the molecule has m different frequencies, then the number of vibrational modes is $(p_1+\cdots+p_m)=\sum_i p_i$. Consider a particular vibrational energy level whose nonfixed energy is $E_v=\sum_i n_i h\nu_i$, the n_i being integers. The number of quantum states associated with the distribution of n_i quanta among p_i vibrational modes is equal to the number of ways, $(n_i+p_i-1)!/n_i!(p_i-1)!$, that n_i identical balls can be distributed among p_i boxes. The total number of vibrational quantum states $P(E_v)$ corresponding to the energy level E_v is

$$\prod_{i=1}^{m}\frac{(n_i+p_i-1)!}{n_i!(p_i-1)!},$$

if the vibrational frequencies are not commensurable.

[7] D. Bierens de Haan, *Nouvelles Tables D'Integrales Definies* (G. E. Stechert and Company, New York, 1939), p. 133.

[8] "Tables of Sine, Cosine and Exponential Integrals" (Federal Works Agency, W. P. A., New York, 1940), Vol. 1.

where

$$L(C)=\frac{1}{6}\int_{x=0}^{\infty}\frac{x^3e^{-x}dx}{1+Cx^3} \tag{21}$$

and

$$C=0.018/\lambda p. \tag{22}$$

In Eqs. (18) and (22) a term, (45)[17], has been neglected in comparison with $(130+E^+)$[17] and (130)[17], respectively. The error thus incurred is negligible.

$L(C)$, calculated in Appendix II as a function of C, is given in Table II.

2. Rigid Activated Complex, *Adiabatic*

$$k_a=\frac{4.4\times10^{38}\sum P(E_v)}{(130+E^+)^{16}}\ \text{sec}^{-1}, \tag{23}$$

$$k_{uni}=\frac{4.3\times10^{13}\exp(-E_a/RT)}{1+0.011/\lambda p}\ \text{sec}^{-1}, \tag{24}$$

$$k_{bi}=\frac{2.2\times10^{-3}Z\exp(-\epsilon/RT)}{1+0.011/\lambda p}. \tag{25}$$

The quantum-mechanical origin of the activation energy ϵ has been discussed elsewhere.[5] According to the present formalism, ϵ is simply equal to the zero-point energy of the four new vibrational modes produced when a rigid activated complex is formed from methyl radicals. The corresponding vibrations in ethane are doubly degenerate (as they are in the complex) rocking vibrations and have a zero-point energy of 5.6 kcal mole^{-1}. ϵ will be somewhat less than 5.6 since the corresponding vibration frequencies of the complex should be smaller than in the molecule, and secondly, the levels may be appreciably broadened as a result of the possibly short lifetime of the activated complex.

Evaluating $P(E_v)$ as indicated in reference 6, k_a is given in Table III.

DISCUSSION

1. k_a

The experimental value associated with reactions (3), (4), and (5) was found to be $1.1\times10^7\lambda$ sec^{-1}. Since the active molecule has, in this case, an energy of 98 kcal mole^{-1} while the C−C bond strength is only 85 kcal mole^{-1}, the activated complex in reaction (5) will have an energy E^+ of $(98-85)=13$ kcal mole^{-1}. From Table III the calculated value of k_a is, if $\lambda\sim1$, seen to be in good agreement with the experimental if the activated complex is assumed to be rigid. It is seen from Table III that an uncertainty in the difference of the C−H and C−C bond strengths of 3 kcal mole^{-1} introduces an uncertainty of a factor of 3 in the calculated value of k_a. On the other hand, k_a calculated on the basis of a loose complex appears to be larger than the observed value by a factor of about $100/\lambda$, and $\lambda\leqslant1$.

TABLE III. Dissociation constant[a] k_a of ethane as a function of E^+.

E^+ (kcal mole^{-1})	Rigid complex (adiabatic)	Loose complex (adiabatic)	Loose complex (inactive)	Loose complex (active)
0	$6.6\ 10^4$	0	0	0
5	$4.0\ 10^5$	$2.0\ 10^8$	$7.2\ 10^7$	$3.4\ 10^7$
8	$1.5\ 10^6$	$7.2\ 10^8$	$2.6\ 10^8$	$1.6\ 10^8$
10	$2.7\ 10^6$	$1.4\ 10^9$	$4.9\ 10^8$	$3.6\ 10^8$
13	$7.5\ 10^6$	$3.5\ 10^9$	$1.2\ 10^9$	$1.0\ 10^9$

[a] Units are sec^{-1}.

2. Recombination of Methyl Radicals

The loose and rigid complexes correspond to markedly different steric factors but, as noted earlier, the present experimental data are in an unsatisfactory state. It will be noted that the steric factor for the recombination of radicals via a loose complex is 0.25 since three-fourths of the collisions lead to a repulsive triplet state and there are no orientative restrictions.

The absence of any pressure dependence of the bimolecular rate constant in the pressure range 5 to 200 mm is quite interesting. This behavior is in complete agreement with that expected from the assumption of a rigid complex (Eq. 25). The predicted behavior of the loose complex is found by plotting the data of Table II *vs* λp using Eqs. (12), (17), and (22). From such graphs one finds that k_{bi} has fallen to one-half its high pressure value when $\lambda p=4.7$, 3.0, and 0.74 mm for the adiabatic, inactive, and active cases, respectively. With the usual assumption of $\lambda\sim1$, it is seen that the assumption of a loose complex corresponds to a large predicted pressure effect in the range 5–200 mm in the first two cases. In the third case the predicted effect would probably be smaller than the probable experimental error (which may be about 20 percent). Thus the observed pressure dependence may be explained on the basis of a loose activated complex only if the two rotational degrees of freedom are assumed to be active. On the other hand, as mentioned earlier, such assumptions do not appear to be consistent with the experimental value of k_a. Nevertheless, further experimental work along these lines, that is, on atomic cracking reactions, is necessary. An inconsistency with the present data can hardly be considered serious.

SUMMARY

The present calculations and discussion appear to favor the assumption of a rigid activated complex. Nevertheless, the dearth of reliable data makes this conclusion highly tentative. A knowledge of the pressure dependence of the rate of recombination of methyl radicals at pressures below 5 mm should prove very illuminating. A reliable estimation of the steric factor would be equally helpful. One might expect the activated complex to be intermediate in nature between the rigid and loose types. If this proves to be true, an interpolation

procedure could be developed for the correlation of the various characteristics discussed in the present paper.

ACKNOWLEDGMENT

I should like to thank Professor O. K. Rice for his constructive criticisms and Professor Wayne A. Bowers for a helpful discussion on approximate integration methods.

APPENDIX I. NUMERICAL DATA

The vibration frequencies of a methyl radical were inferred from those of methyl iodide[9] to be 2855, 1252, 1445 (2), and 3074 (2) cm^{-1}. Those of ethane were taken[10] to be 827 (2), 993, 1120 (2), 1380 (2), 1470 (4), 2927 (2), and 2975 (4) cm^{-1} (slightly rounded to facilitate computation of the $P(E_v)$ associated with a rigid complex). With the exception of the 993 cm^{-1} frequency (C−C stretching), these were assumed to be the vibration frequencies of the rigid activated complex. The loose complex was assumed to have vibration frequencies equal to those of the isolated radicals.

The moments of inertia of ethane were taken to be[11] 42.3, 42.3, and 11.0×10^{-40} g cm^2 $molecule^{-1}$. Assuming a planar configuration of a methyl radical and a C−H distance of 1.1A, its moments of inertia were estimated to be 6.03, 3.02, 3.02×10^{-40} g cm^2 $molecule^{-1}$. The rigid complex was assumed to be an elongated ethane molecule having planar methyl groups and a C−C distance of 3.3A. Its moments of inertia were estimated to be 142, 142, and 12.06 g cm^2 $molecule^{-1}$. The rotational partition function of the loose complex is equal to the product of the individual partition functions for each methyl radical multiplied by the partition function of a diatomic molecule (formed by the centers of gravity of the radicals) whose moment of inertia is $7.5(3.3)^2$.

The collision frequency Z equals $(2\pi kT/\mu)^{\frac{1}{2}}\sigma_1^2$ where μ and σ_1 are the reduced mass ($\mu=7.5$) and collision diameter, respectively σ_1 equals 3.3A.

The partition function for restricted rotation was assumed to equal

$$\sum_{i=1}^{W_{\max}} \exp(-W_i/kT)+\frac{(8\pi^3IkT)^{\frac{1}{2}}}{\sigma h}\exp(-W_{\max}/kT),$$

where I is the effective moment of inertia for internal rotation ($I=(11.0/4)\times10^{-40}$ g cm^2 $molecule^{-1}$) and σ the symmetry number. The energy levels W_i were taken to be[12] 0, 275, 520, 726, and 965 cm^{-1} with the latter equal to $W_{\max}$. Internal rotation in the rigid activated complex was assumed to be free and to have a moment of inertia equal to 3.02×10^{-40} g cm^2 $molecule^{-1}$.

The collision frequency for deactivating collisions was taken to be 5.86×10^8 mm^{-1} sec^{-1}. The values adopted for the C−H and C−C bond strengths of ethane were weighted averages of three independent determinations,[13] (98, 97.5, 96.8) and (85.6, 87.0, 83.4) kcal $mole^{-1}$, respectively.

APPENDIX II. APPROXIMATE EVALUATION OF $\int_{x=0}^{\infty}\frac{ux^3e^{-x}dx}{u+x^3}=R(u)$

We have

$$R(u=\infty)-R(u)=\int_{x=0}^{\infty}\frac{x^6e^{-x}dx}{u+x^3}=\int_{x=0}^{\infty}e^{f(x)}dx, \tag{1A}$$

where

$$f(x)=6\ln x-x-\ln(u+x^3). \tag{2A}$$

This integral approaches $6!/u$ and $3!$ for large and small u, respectively. The Stirling approximation to $n!$ being quite good in this range of n, (1A) will be evaluated by a method which can also be used to derive the Stirling formula. Since $R(u=\infty)=3!$, $R(u)$ is then readily obtained.

Let the maximum value of the Gaussian-like function $\exp(f(x))$ and therefore of $f(x)$ occur at $x=\xi$ and expand $f(x)$ about $x=\xi$ in a Taylor series. Since $f'(\xi)=0$, we have

$$f(x)=f(\xi)+\frac{(x-\xi)^2}{2}f''(\xi) \tag{3A}$$

neglecting the higher order terms. Solving $f'(\xi)=0$ where $f'(x)$ is obtained from (2A), we find

$$6-\xi=3\xi^3/(u+\xi^3) \tag{4A}$$

while from (2A) $-f''(\xi)=N$ is given by

$$N=6/\xi^2+3(2u\xi-\xi^4)/(u+\xi^3)^2. \tag{5A}$$

By introducing (3A) into (1A), changing the lower limit from 0 to $-\infty$ (with but little error) and integrating, we find for $R(u)$

$$R(u)\cong 3!-\left(\frac{2\pi}{N}\right)^{\frac{1}{2}}\frac{(6-\xi)}{3}\xi^3\exp(-\xi), \tag{6A}$$

$$\cong 3!-\frac{2(6-\xi)}{27(3N)^{\frac{1}{2}}}\xi^3\exp(3-\xi). \tag{7A}$$

Equation (7A) is obtained by introducing Stirling's equivalent of $(2\pi)^{\frac{1}{2}}$, namely, $(3!/\sqrt{3})(e/3)^3$ into (6A). This procedure reduces the error in the expression for $R(u)$ to a smaller value, particularly for small values of u.

The error in $3!-R(u)$ as given by (6A) may be roughly estimated by comparing with the known error in Stirling's approximation of $n!$ Evaluation of $R(u)$ directly, instead of via (1A), would have been subject to greater error on the average.

Instead of solving the quartic Eq. (4A) for ξ, various values of ξ were chosen and the equation solved for u. Table II was built up in this manner.

---

[9] T. Y. Wu, *Vibrational Spectra and Structure of Polyatomic Molecules* (Edwards Brothers, Inc., Ann Arbor, Michigan, 1946).

[10] Crawford, Avery, and Linnett, J. Chem. Phys. **6**, 682 (1938).

[11] G. Herzberg, *Molecular Spectra and Molecular Structure* (D. Van Nostrand Company, Inc., New York, 1949), Vol. 2.

[12] Kistiakowsky, Lacher, and Stitt, J. Chem. Phys. **7**, 289 (1939).

[13] E. W. R. Steacie, *Atomic and Free Radical Reactions* (Reinhold Publishing Corporation, New York, 1946).

Cyanogen Flames and the Dissociation Energy of N_2

N. THOMAS AND A. G. GAYDON
Chemical Engineering Department, Imperial College, London, England

AND

L. BREWER*
Department of Chemistry and Chemical Engineering, University of California, Berkeley, California

(Received July 9, 1951)

The behavior of cyanogen flames under a variety of conditions has been observed. Because of the relatively high stability of cyanogen, the behavior is considerably different from that of hydrocarbon flames. Because of the high stability of the combustion products, CO and N_2, the flame temperature can reach temperatures above 4800°K. Thus the cyanogen-oxygen flame is the hottest natural flame known.

Spectroscopic observations have been made of both the reaction zone and the mantle of completely combusted gases. Rotational and vibrational temperature measurements using the CN violet system have indicated that the reaction zone is not in thermal equilibrium but that the mantle is in thermal equilibrium. Comparison of the calculated flame temperatures based on different heats of dissociation of N_2 with the observed mantle temperatures has fixed $D_{N_2}=9.764\pm0.005$ ev and $D_{CN}=8.2\pm0.2$ ev.

INTRODUCTION

THE first extensive studies of the cyanogen flame by Pannetier and Gaydon,[1] Pannetier and Laffitte,[2] and Pannetier[3] have indicated interesting possibilities. To a worker interested mainly in combustion, cyanogen provides an interesting contrast to hydrocarbons as a fuel, while to a thermochemist it provides a means of obtaining very high equilibrium temperatures, owing to the great stability of the flame products.

The work described in this article is a spectroscopic study of various cyanogen flames, and a discussion of the results obtained. It was initiated at Imperial College; the section on vibrational temperature measurement was carried out in collaboration while one of us (L.B.) was temporarily working in England.

EXPERIMENTAL

Cyanogen was prepared by heating mercuric cyanide to a dull red heat in a Pyrex distillation flask. It was stored in a metal gas-holder of 10-liters capacity, over mercury. The gas was fed through the top of the metal float, forcing it up. It was forced out by placing two heavy metal weights on the float (about 20 kg).

The main difficulty in handling cyanogen lay in its high solubility. For this reason mercury had to be used in the gas-holder, and the metering of the gas presented some difficulty. Eventually use was made of the fact that cyanogen was insoluble in a saturated solution of NaCl, acidified with 10 percent HCl. This liquid was accordingly used in a flow-gauge of the normal capillary type, which was calibrated by a simple displacement method, feeding the cyanogen into a vertical calibrated glass cylinder filled with solution and observing the rate of displacement.

No special difficulty was encountered because of the toxic properties of C_2N_2. We consider it less toxic than CO, and its rather pungent odor made it easy to detect.

PRELIMINARY OBSERVATIONS

Exploratory work was first carried out on the cyanogen-air diffusion flame, burning at a small quartz jet. A Hilger Raman spectrograph of $f/4$ was used. The flame was of a purplish-pink color, and unlike hydrocarbon diffusion flames, had a definite rounded contour. It showed no trace of carbon formation. The spectra showed strong CN violet and red systems, also NH, but no trace of C_2.

Pre-mixed flames with air were of a rather similar appearance, but showed a definite reaction zone or "inner cone." The spectra were similar to those of the diffusion flame, but rather more intense, and faint C_2 Swan bands were observed. All preliminary spectroscopic observations were made on the reaction zone or inner cone.

The cyanogen-oxygen pre-mixed flames, however, were of a very different nature. We obtained a small flame with a bright white inner cone, whose brightness was comparable with that of a carbon arc. The spectrum of this inner cone was very different from that of the cyanogen-air flame. The C_2 Swan system was strongly developed, also the 4315 CH, the 3360 NH, and the 3064 and 2811 OH bands. An interesting feature was the very strong and well-developed $\beta-$NO system extending below 2300A. At 3020A a band of unknown origin was found, identical with one previously detected by H. G. Wolfhard in flames supported by N_2O and NO. A number of CN tail-bands, corresponding to those tabulated by Feast,[4] were observed in the 3200–2500A region. The CN system was relatively less intense than in the C_2N_2-air flame.

* John Simon Guggenheim Memorial Fellow, 1950.

[1] G. Pannetier and A. G. Gaydon, Compt. rend. **225**, 1300 (1947).

[2] G. Pannetier and P. Laffitte, Compt. rend. **226**, 72, 341 (1948).

[3] G. Pannetier, Colloque Int. sur Combustion Gazeuse, Paris, p. 142, and thesis, L'Université de Paris, 1949.

[4] M. W. Feast, Proc. Phys. Soc. (London) **62**, 121 (1949).

A diffusion flame of cyanogen-oxygen was then run, using the concentric quartz tubes, C_2N_2 being fed through the inner and oxygen through the outer. This flame was very similar in character to the pre-mixed $C_2N_2-O_2$ flame, being bright white, compact, and giving an identical spectrum, though a rather less intense one. There did not appear to be any carbon formation, in marked contrast to hydrocarbon flames.

It was possible to reduce the intensity of the CH, NH, and OH systems by drying the C_2N_2 and oxygen over P_2O_5-coated glass beads. We also repeated Pannetier's observation of the introduction of water vapor into the $C_2N_2-O_2$ diffusion flame, finding that it produced a marked change in the nature of the flame, which came to resemble a C_2N_2 air diffusion flame, the intensity of the C_2 bands falling off about to zero and the CN violet system becoming more intense.

A similar effect was observed when small amounts of SO_3 were introduced into the flame by bubbling the oxygen supply through oleum. Now Gaydon and Whittingham[5] found that SO_3 in small concentrations induces carbon formation in hydrocarbon flames and greatly reduces the C_2 intensity. It is therefore interesting to note that in the C_2N_2 flame, the C_2 intensity is also reduced.

On the other hand, the cyanogen flame gives little evidence of carbon formation. Only during an attempt to run a large burner of the Meker type on a $C_2N_2-O_2$ mixture did carbon formation occur in rich mixtures. In all other flames it was absent.

Iron carbonyl was introduced into the flame, and the inner cone spectra recorded on a Zeiss Q.24 medium-quartz instrument. Abnormal excitation of iron lines, identical with that reported by Gaydon and Wolfhard[6] for hydrocarbon flames, was found. This did not occur in the C_2N_2 air flames.

A cyanogen fluorine flame was also studied, but its spectrum only showed strong CN violet bands, very little C_2, and some rather faint NO bands. However, on introducing a small amount of hydrogen into the flame, its luminosity was greatly increased, and strong C_2 and CH emission was obtained. Cyanogen did not ignite spontaneously with F_2.

Cyanogen flames supported by N_2O were also examined and their spectra found to be identical with those of C_2N_2 oxygen flames, although the intensity was considerably less.

CHILLED FLAMES

An attempt was made to run a chilled cyanogen-oxygen flame using a burner similar to that described by Gaydon[7] but much smaller. The best operating conditions were as follows.

Cyanogen with a slight admixture of air was fed into the central jet of the burner, and N_2O into the outer jacket, which was water-cooled. A peculiar yellow-pink flame was then stabilized on the outer part, the central jet being maintained well below this level.

Examination of this flame with the Raman spectrograph showed the usual CN systems, some faint C_2, and an apparently new system, degraded to the violet at about 3280A. Examination of this with the Q.24 medium quartz spectrograph gave the following results when the lines were measured up:

	Intensity
3291.4	10
3285.1	7
3279.3	2
3273.8	0
3269.9	0
3264.8	4
3261.2	0
3256.6	0
3254.8	4

These measurements suggest heads at 3291.4, 3264.8, and 3254.8, with rotational structure degraded to the violet. The possibility that this might be an extension of the CN violet system was considered, but these wavelengths do not correspond to any CN heads degraded to the violet that would be expected in this region.

ROTATIONAL TEMPERATURE MEASUREMENTS OF REACTION ZONE OF SMALL FLAME

The pre-mixed C_2N_2 oxygen flame was bright enough to allow a detailed examination of the fine structure of the C_2 and CN systems with a large spectrograph. We used a glass Littrow instrument which gave reasonably short exposure times. The rotational temperature measurements were carried out by the method originated by Ornstein and van Wijk[8] and applied to flames by Gaydon and Wolfhard.[9] The method is a standard one and will not be described in detail here.

The cyanogen-oxygen flame was burnt on a fine quartz jet, and plates were taken both of the reaction zone of the flame and of the white "mantle" which formed immediately above. The intensities of the rotational lines were measured up with a Zeiss microphotometer, the plates being calibrated by use of a rotating step sector. As a source for the calibration marks, we used a tungsten strip lamp in the case of C_2, and an Fe arc in the work on CN. Owing to the variation of plate sensitivity in the C_2 region, it was necessary to calibrate the plate at 50A intervals over the range in which we were working. Ilford Zenith plates were used, and were brushed to avoid the Eberhard effect. The (0, 0) C_2 and (0, 1) CN bands were used. The results

[5] A. G. Gaydon and Whittingham, Proc. Roy. Soc. (London) **A189**, 313 (1947).
[6] A. G. Gaydon and H. G. Wolfhard, Proc. Roy. Soc. (London) **A205**, 118 (1951).
[7] A. G. Gaydon, Proc. Roy. Soc. (London) **A179**, 435 (1942).
[8] L. S. Ornstein and W. R. van Wijk, Z. Physik **49**, 315 (1928).
[9] A. G. Gaydon and H. G. Wolfhard, Proc. Roy. Soc. (London) **A201**, 561 (1950).

obtained are summarized as follows:

C_2 in reaction zone, rich flame	4500°K±400°K
C_2 in reaction zone, stoichiometric (to CO and N_2) flame	4700°K±400°K
C_2 in mantle, rich flame	3500°K±400°K
CN in reaction zone, rich flame	2700°K±400°K
CN in reaction zone, stoichiometric flame	3150°K±400°K
CN in mantle, rich flame	2475°K±400°K

The difference between C_2 and CN rotational temperatures is evident. We shall return to this point in the concluding discussion.

The NO system was well developed enough for temperature measurements to be carried out, though a fairly long exposure was needed (about 20 minutes). The transition probabilities for these bands have been computed numerically by Gaydon and Wolfhard.[10] Using a mercury arc as a source for calibration marks, and a large quartz Littrow instrument, we photographed the system and obtained an apparent rotational temperature of 3800°K. The error in this, however, may have been ±1000°K, or even more, owing to the variation in plate sensitivity over the NO region.

VIBRATIONAL TEMPERATURE MEASUREMENTS AND DETERMINATION OF D_{N_2}

It has been remarked that the cyanogen flame is interesting from the thermochemical viewpoint, since the high dissociation energy of its products, CO and N_2, prevents much heat being used in dissociation reactions, and so a very high equilibrium temperature is attainable. Using high temperature thermochemical data given by Kelley,[11] Latimer,[12] and the National Bureau of Standards Tables[13] and the heat of formation of CN determined by Brewer, Templeton, and Jenkins,[14] we have calculated equilibrium temperatures for certain cyanogen-oxygen mixtures. The main uncertainty in this calculation is the value of D_{N_2}, the dissociation energy of nitrogen, since there is no conclusive evidence in favor of either of the two values usually accepted, 7.38 ev and 9.76 ev.

An account of the past controversy over the correct value of D_{N_2} is given by Gaydon.[15] It is sufficient to say here that the spectroscopic evidence is not conclusive, though of late it has tended to favor the higher value of 9.76 ev. Our calculations indicate that there is a significant difference between the expected maximum temperatures of a stoichiometric $C_2N_2-O_2$ mixture depending upon which value is used for the heat of dissociation of nitrogen. If the flame is not of stoichiometric composition going to CO and N_2 products or if it is diluted by use of some air instead of pure oxygen, the temperature is reduced, which causes a great reduction in the extent of dissociation of N_2 and greatly decreases the difference between the two calculated temperatures.

Assuming the higher heat of dissociation of N_2, we calculate the following compositions in a completely combusted flame formed from an equimolal mixture of C_2N_2 and O_2 which will attain a temperature of 4850°±30°K.

$N_2=0.32$ atmos, CO=0.66 atmos, CN=0.35 to 0.74×10^{-2} atmos,

C=0.355 to 0.255×10^{-2} atmos, N=0.012 atmos,

O=0.69 to 0.96×10^{-2} atmos, NO=3×10^{-4} atmos, and $C_2=10^{-6}$ atmos.

There are also small amounts of CO_2 and C_2N_2 present. The ranges in the compositions given and the uncertainty of 30°K in the maximum temperature are due primarily to the uncertainty of ±6 kcal in the heat of formation of CN as given by Brewer, Templeton, and Jenkins.[13]

Calculations with nonstoichiometric mixtures show that the temperature falls off more rapidly on the rich than on the lean side. A mixture with 11 percent excess O_2 has a calculated temperature of 4500±10°K while 7 percent C_2N_2 brought the temperature down to 4500 ±50°K. If one uses the lower heat of dissociation of 7.38 ev for D_{N_2} in the calculations, the maximum temperature for the stoichiometric mixture is only 4325°K. This difference of 525°K was considered large enough to be detected with certainty.

However, several difficulties had to be overcome before any temperature measurement of the flame at equilibrium was possible. First the temperatures involved were too high for any background source available to us, which ruled out the use of the line-reversal method. We have since learned that xenon arcs under pressure can give background temperatures of 5500°K, but at the time we had only a carbon arc available. Alse we had to deal with the problem of heat loss from the flame and the demonstration of the existence of a region in thermal equilibrium in the flame.

It was finally decided to use a method of measuring the vibrational temperature of the CN molecule, originally developed by Ornstein and Brinkman[16] and applied to the measurement of CN equilibrium temperatures in a King furnace by Brewer, Templeton, and Jenkins.[13] The later workers found very good agreement between the temperatures obtained by this method and those obtained by the optical pyrometer and this led us to try the method. The thermochemical data indicated a fair concentration of CN in the flame, and it seemed

[10] A. G. Gaydon and H. G. Wolfhard (unpublished).
[11] K. K. Kelley, U. S. Bur. Mines Bull. 476 (1949).
[12] W. Latimer, U. S. AEC Report MDDC-1462 (1947).
[13] National Bureau of Standards Selected Values of Chemical Thermodynamic Properties (1950).
[14] Brewer, Templeton, and Jenkins, J. Am. Chem. Soc. **73**, 1462 (1951).
[15] A. G. Gaydon, *Dissociation Energies* (Chapman and Hall, London, 1947).
[16] L. S. Ornstein and H. Brinkman, Proc. Acad. Sci. (Amsterdam) **34**, 33 (1931).

likely that the intensity of the CN violet system would be measurable in the completely combusted gases.

The heat loss problem seemed serious to us because of the low rotational temperature obtained for CN in the small flame used previously. We decided to overcome it by using a burner of the type described later. A $C_2N_2-O_2$ mixture was fed up a central tube, and burned above a small group of holes of 1/50-in. diameter. The small hole size was necessary to prevent flashback. When desired, an oxyhydrogen mixture could be burned at the outer ring of the holes, forming a hot sheath around the central flame. The whole burner was made of copper, on account of the high thermal conductivity of this metal.

We used the Zeiss Q.24 medium-quartz spectrograph for the work, with the rotating-step-sector and a tungsten strip lamp for plate calibration. Ilford Zenith plates were used. We focused a region of the flame several millimeters above the reaction zone on the slit, and tested the effect of variation of the distance above the reaction zone.

Of the two strongest CN sequences, the (0, 1) was well developed in the richer flames, and could be photometered fairly satisfactorily. In leaner mixtures only the (0, 0) was strong enough for adequate measurements.

In practice, it was possible to photometer the first five heads of the (0, 1) sequence, and the first four of the (0, 0). The peak intensity of each band head was measured and from this was subtracted the background intensity just in front of the head. The method of calculating the temperatures from intensity measurements is given in some detail by Ornstein and Brinkman[16] and will not be discussed here. Ornstein and Brinkman's work has been criticized by Lochte-Holtgreven and Maecker[17] who found evidence of error because of reversal and self-absorption effects. However, these effects are only prominent for transitions involving levels of the ground state which have very little excitation. Since the rotational levels which contribute appreciably to the band head peaks in the CN violet system have high K rotational quantum numbers, and since most of the transitions used in this work involved states other than the zero vibrational state of the ground state of CN, it is not believed that the portion of Ornstein and Brinkman's data that was used in our calculations is in error caused by these effects. Other possible sources of error are because of overlapping of the band heads and change of the spacing of rotational lines as one goes from one band head to another. Part of these errors cancel out when one uses Brinkman and Ornstein's data in the same way that they did in their calculations. Possibility of errors because of overlapping was carefully considered by making a careful survey of all the spectroscopic data available for the CN states and calculating the positions of all lines of interest and calculating their contribution to the measured band head peak intensities. These considerations are too extensive to consider in a journal publication, but they will be written up in detail as a private publication by one of us (L.B.). The final result of these considerations was that the method of Ornstein and Brinkman should give satisfactory temperature determinations using the CN violet system.

Our first experiments were intended to give some idea of the probable heat loss due to conduction, convection, and entrainment of air. We obtained temperature measurements from flames with and without a hydrogen-oxygen sheath, and soon found that heat loss was almost inappreciable, since the temperature differences recorded were within the experimental error of $\pm 200°K$. Thus it did not seem that the heat loss was as serious as we had originally suspected.

During this preliminary work we reached temperatures of 4200°K with rich flames. By oxygenating the mixture we obtained consistent values of 4800°K $\pm 200°K$ for approximately stoichiometric flames, and a temperature drop to 4200°K with lean mixtures.

With these leaner mixtures we had some difficulty in bringing up the (0, 1) band strongly enough for satisfactory measurement, and relied mainly on the (0, 0). However, for certain spectra we were able to measure both (0, 0) and (0, 1) bands, and found satisfactory agreement between the temperatures obtained from measurements on both bands.

The main difficulty was caused by a continuum which interfered with photometric measurements, especially of the (0, 1) band. As the use of a hydrogen "sheath" cleared up the background very markedly, we are inclined to attribute it to the CO+O reaction, giving a continuum as in the carbon monoxide flame. This view was supported by the fact that the continuum was strongest in lean mixtures. We checked this idea by surrounding the $C_2N_2-O_2$ flame with a nitrogen sheath, which would presumably cut down the CO+O reaction by reducing accessibility of the hot CO to atmospheric oxygen. As anticipated, the background density was considerably reduced, though not to the same extent as by a hydrogen sheath.

We measured the vibrational temperature at various distances above the reaction zone. It was found that the CN temperature was low immediately above the zone, a value of $3150°K \pm 200°K$ being obtained. It reached equilibrium at 1.5–2 mm above the zone, in our flame. This result confirmed the earlier work on low rotational temperatures for CN in the reaction zone of our small flames, and showed why we had been inclined to overestimate the possible effects of heat loss. About 1/1000 sec is required for the gases to travel 5 mm above the reaction zone which should allow about 10^6 collisions. At high temperatures and for a reactive molecule like CN, considerably less than 1000 collisions should be required for equipartition among vibrational

[17] W. Lochte-Holtgreven and H. Maecker, Z. Physik **105**, 1 (1937).

levels and equilibrium between vibration and translation.

The fact that a constant temperature was obtained in the mantle which was independent of the distance above the reaction zone demonstrates that a steady-state condition is being maintained by the various collision and radiation processes. Because of the low temperatures of most flames, it is not possible to get emission from the mantle of the flame, and emission from the reaction zone, which is definitely not at equilibrium, must be studied. However, in this very hot flame ample emission can be obtained from the mantle where thermal equilibrium might be expected. A possible source of error which we considered carefully is the lack of radiative equilibrium. In a closed container, equilibrium is reached with respect to all processes, radiative and collision. In a flame collision processes may take place to maintain equilibrium, and emission of radiation takes place; but the corresponding absorption of light that one has in a closed system does not take place in a transparent flame. Thus the actual concentrations of excited states of a molecule can be expected to be reduced compared to the equilibrium concentrations if the emission processes are rapid compared to collision processes. For Na in an atmosphere of N_2 at 2000°K, Gaydon and Wolfhard[18] have shown that radiation losses in a flame reduce the population by only 2 percent, equivalent to 3° in temperature. It so happens that in the case of CN, the half-lives of the various vibrational levels of the CN excited state are very closely the same as shown by the data of Ornstein and Brinkman.[15] Thus the relative populations which are important for temperature determinations should not be changed, even if collisions do not re-establish the equilibrium populations. However for a reactive molecule like CN, one might expect the collision processes to retain control of the distribution of various states even with a very short radiative lifetime. Thus we have concluded that no appreciable error in our temperature measurements results from this source of error. This is confirmed by the work of Brewer, Templeton, and Jenkins[13] who used the method of Ornstein and Brinkman in a King Furnace system that was in radiative equilibrium. This point will be discussed in more detail in the private publication previously referred to.

Summarizing, we have measured a temperature of 4800±200°K in stoichiometric $C_2N_2-O_2$ flames. Since the maximum temperature that can be attained if D_{N_2} is 7.38 ev is only 4325°K and a temperature of 4850°K is to be expected if D_{N_2} is 9.76 ev, the other value allowed by spectroscopic data, the heat of dissociation of N_2 has been fixed as 9.76 ev. This together with the heat of formation of CN determined by Brewer, Templeton, and Jenkins[13] fixes D_{CN} as 8.2±0.2 ev. Schmid, Gerö, and Zemplen[19] have previously given D_{CN} as 7.5±0.1 ev, but as Brewer, Templeton, and Jenkins[13] have pointed out, there is enough uncertainty in their extrapolation to allow a value of 8.2 ev from their data. The intermediate value of $D_{N_2}=8.57$ ev which has also been proposed which would be in agreement with Schmid, Gerö, and Zemplen's value of D_{CN} is apparently now excluded by new spectroscopic data.[20] The other related dissociation energies such as $D_{NO}=6.49$ ev, etc., which are now fixed by the determination of D_{N_2} are summarized by Gaydon.[15]

[18] A. G. Gaydon and H. G. Wolfhard, Proc. Phys. Soc. (London) (to be published).

DISCUSSION

In the introduction it was remarked that the cyanogen flame is interesting both to the thermochemist and the combustion physicist. We shall now discuss some of the results obtained.

Our temperature measurements on the $C_2N_2-O_2$ flame provide the first thermochemical estimate of the value of $D(N_2)$. As seen above, they support the value of 9.76 ev since a temperature corresponding to the lower value of $D(N_2)$ lies well outside the possibility of experimental error.

The combusion characteristics of the cyanogen flame present an interesting contrast to those of hydrocarbon flames. The almost complete absence of carbon formation, the similarity between the $C_2N_2-O_2$ pre-mixed flame and the corresponding diffusion flame, and the contrast between $C_2N_2-O_2$ flames and C_2N_2-air flames, are particularly striking.

The key to the difference may lie in the fact that C_2N_2 is an extremely stable compound, as compared with hydrocarbons. In the hydrocarbon diffusion flame Wolfhard and Parker[21] have shown that the hydrocarbon is heated to temperatures approaching 1000°C before it comes into contact with oxygen. As a result extensive pyrolysis occurs, and a great deal of carbon is formed. Owing to the thermal stability of cyanogen, no thermal "cracking" or polymerization occurs till the mixing with the oxygen has been carried out to an appreciable extent, when the reaction proceeds as in a pre-mixed flame.

The absence of carbon formation also illustrates the relative inability of cyanogen to react thermally in the same way as hydrocarbons. Carbon formation only occurs in the top of very large, hot, rich flames, apparently after a high temperature reaction lasting 0.1 sec.

The striking difference between cyanogen-air and cyanogen-oxygen flames may indicate that the nitrogen in air inhibits the reaction leading to the C_2 formation and the bright, high temperature flame. It may be re-

[19] Schmid, Gerö, and Zemplen, Proc. Phys. Soc. (London) **50**, 283 (1938).

[20] Private communication from G. Herzberg, 1950.

[21] H. G. Wolfhard and W. G. Parker, Proc. Phys. Soc. (London) **62**, 722 (1949).

membered that Arthur[22] has found that certain inert gases appeared to inhibit carbon formation, and it is possible that some analogous process is occurring here.

The curious effect of hydrogen on the $C_2N_2-F_2$ flame, mentioned previously, is perhaps analogous to a similar effect noted by R. A. Durie[23] in certain organic halide-fluorine flames. He found that a small addition of hydrogen resulted in heavy carbon formation in these cases.

The process by which C_2 is formed in the hot $C_2N_2-O_2$ flames may not be entirely different from that by which this radical is formed in hydrocarbon flames. The rotational temperature of C_2 in the cyanogen-oxygen flame is approximately the same as that found by Gaydon and Wolfhard[9] in acetylene-oxygen flames.

The strong NO system in the reaction zone and its rather high rotational temperature suggests a possibility that NO may be formed in the reaction zone by a direct "stripping" of nitrogen from C_2N_2, because of a reaction with oxygen, and that some excited C_2 may be among the products of such a reaction. Presumably water, SO_3 and atmospheric nitrogen are all able to inhibit this reaction or group of reactions. But it should be stressed that the foregoing suggestions are tentative.

The presence of abnormal excitation of Fe lines is not surprising in a hot flame with strong C_2 emission. It has been suggested elsewhere that this may be because of direct reaction of C_2 with oxygen.

The unidentified system obtained in the chilled flame could, by analogy with HCO in hydrocarbon chilled flames, be identified by CNO, but this suggestion, also, is very tentative.

The CN radicals do not apparently participate in the reaction sequence which gives rise to C_2 and NO, for, as stated, they have abnormally low temperatures in the reaction zone. It seems quite probable that the rather feeble cyanogen-air flames are due to an oxidation reaction proceeding via CN.

In conclusion, we may say that cyanogen, being a relatively stable molecule, is much less reactive than hydrocarbons but, under suitable conditions, can react vigorously with oxygen. This reaction, when it occurs, may proceed by a path not altogether unlike that in hydrocarbon-oxygen flames.

[22] J. R. Arthur, Nature **165**, 557 (1950).
[23] R. A. Durie (unpublished).

The Combination Band $\nu_1+\nu_2+\nu_3$ of Heavy Water Vapor

F. P. DICKEY, C. A. GUDERJAHN, AND E. D. PALIK
Mendenhall Laboratory of Physics, Ohio State University, Columbus, Ohio

(Received November 16, 1951)

The vibration-rotation band $\nu_1+\nu_2+\nu_3$ in the heavy water vapor (D_2O) spectrum has been remeasured. An analysis of the rotational structure has been carried out. From the interpretation of the data the value of the band center has been determined as well as the values of the reciprocals of inertia effective in this vibration state. The frequency $\nu_1+\nu_2+\nu_3$ is found to be 6533.4 cm^{-1}. The effective reciprocals of inertia are $A(V)=15.70$ cm^{-1}, $B(V)=7.19$ cm^{-1}, and $C(V)=4.69$ cm^{-1}.

I. INTRODUCTION

THE far infrared spectrum of heavy water vapor (D_2O) corresponding to transitions between the rotational energy levels only, has been measured by Fuson, Randall, and Dennison[1] and term values have been assigned. Two of the fundamental vibration-rotation bands, ν_2 and ν_3, have been measured by Dickey and Nielsen[2] and term values have been assigned. The third fundamental vibration band, ν_1, has been observed by Bender[3] as a Raman line. The combination band $\nu_1+\nu_3$ has been measured by Innes, Cross, and Giguère[4] and values for the effective reciprocals of inertia have been given. They have also reworked the data for ν_2 and ν_3 and have given a better set of values for the effective reciprocals of inertia.

The potential constants of H_2O have been evaluated by Bonner[5] from the observed frequencies and from the dimensions for the molecule given by Mecke.[6] By using this information, Bonner has predicted the fundamental vibration frequencies of D_2O. More recently, Darling and Dennison,[7] by using more complete data, have evaluated the normal frequencies of H_2O and D_2O together with values for the vibrational constants of the molecules. Subsequent measurements corroborate essentially the values given by them.

The combination band $\nu_1+\nu_2+\nu_3$ of D_2O has been measured by Norris, Unger, and Holmquist.[8] Their resolution was not good enough to enable them to make any analysis of the rotational structure.

II. EXPERIMENTAL

The band $\nu_1+\nu_2+\nu_3$ of D_2O was examined with a prism grating, automatic recording spectrometer. A

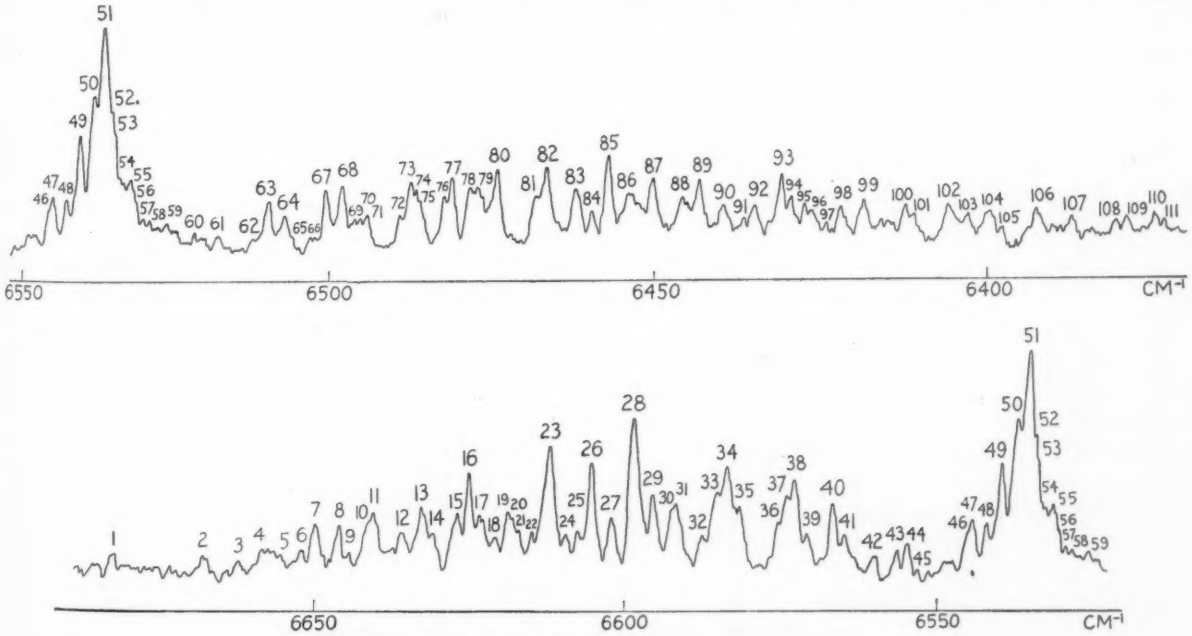

FIG. 1. The heavy water vapor band $\nu_1+\nu_2+\nu_3$ at 6533.4 cm^{-1}.

[1] Fuson, Randall, and Dennison, Phys. Rev. **56**, 982 (1939).
[2] F. P. Dickey and H. H. Nielsen, Phys. Rev. **73**, 1164 (1948).
[3] D. Bender, Phys. Rev. **47**, 252 (1935).
[4] Innes, Cross, and Giguère, J. Chem. Phys. **19**, 1086 (1951).
[5] L. G. Bonner, Phys. Rev. **46**, 458 (1934).
[6] R. Mecke, Z. Physik **81**, 313 (1933).
[7] B. T. Darling and D. M. Dennison, Phys. Rev. **55**, 128 (1940).
[8] Norris, Unger, and Holmquist, Phys. Rev. **49**, 272 (1936).

TABLE I. Frequency positions and identifications of heavy water vapor lines in $\nu_1+\nu_2+\nu_3$.

Line No.	Obs ν(vac) (cm^{-1})	Transition	Line No.	Obs ν(vac) (cm^{-1})	Transition
1	6682.4		56	6531.0	1_0-1_1
2	6668.0		57	6529.5	
3	6662.4		58	6528.6	
4	6658.7		59	6525.9	
5	6655.4		60	6521.3	0_0-1_{-1}
6	6652.4		61	6517.5	$3_{-2}-3_{-1}$
7	6649.8		62	6511.9	1_0-2_{-1}
8	6646.2		63	6509.6	$1_{-1}-2_{-2}$
9	6644.8		64	6507.2	1_1-2_0
10	6641.5				$4_{-3}-4_{-2}$
11	6640.5		65	6503.5	
12	6636.2		66	6501.9	
13	6632.7		67	6500.6	$2_{-1}-3_{-2}$
14	6630.9		68	6498.3	$2_{-2}-3_{-3}$
15	6627.3				2_1-3_0
16	6625.0		69	6496.1	2_2-3_1
17	6623.2		70	6495.2	
18	6621.1		71	6494.0	2_0-3_{-1}
19	6618.6		72	6489.4	$3_{-2}-4_{-3}$
20	6617.9		73	6487.5	$3_{-3}-4_{-4}$
21	6616.8		74	6486.6	3_2-4_1
22	6614.9				3_3-4_2
23	6612.2		75	6486.1	3_0-4_{-1}
24	6609.5		76	6482.1	3_1-4_0
25	6607.2		77	6480.9	$3_{-1}-4_{-2}$
26	6605.3				$5_{-5}-5_{-2}$
27	6601.9		78	6478.0	$4_{-3}-5_{-4}$
28	6598.4	$5_{-1}-4_0$			4_3-5_2
29	6595.3	$5_{-3}-4_{-2}$			4_4-5_3
30	6592.1		79	6476.9	$4_{-4}-5_{-5}$
31	6591.5	$5_{-2}-4_{-1}$			
32	6587.4		80	6474.1	$4_{-1}-5_{-2}$
33	6585.0	$4_{-2}-3_{-1}$			4_1-5_0
		4_0-3_1	81	6468.0	$5_{-4}-6_{-5}$
		4_1-3_2			$4_{-2}-5_{-3}$
		4_2-3_3	82	6466.3	4_0-5_{-1}
34	6583.3	$5_{-5}-4_{-4}$			$5_{-5}-6_{-6}$
		$5_{-4}-4_{-3}$	83	6462.0	$5_{-2}-6_{-3}$
35	6581.4	$4_{-1}-3_0$	84	6459.5	
36	6575.1	$4_{-4}-3_{-3}$	85	6457.0	$5_{-3}-6_{-4}$
37	6573.8	$4_{-3}-3_{-2}$	86	6453.9	$5_{-1}-6_{-2}$
38	6572.6	$3_{-1}-2_0$	87	6450.2	
		3_1-2_2	88	6446.0	
39	6570.4	3_0-2_1	89	6443.3	
40	6566.5	$3_{-3}-2_{-2}$	90	6439.6	
41	6564.2	$3_{-2}-2_{-1}$	91	6436.2	
42	6559.9	2_0-1_1	92	6434.9	
43	6556.3	$2_{-2}-1_{-1}$	93	6431.0	
		$4_{-2}-4_{-3}$	94	6429.5	
44	6554.8	$2_{-1}-1_0$	95	6427.3	
45	6553.1		96	6426.1	
46	6545.2	$1_{-1}-0_0$	97	6424.0	
47	6544.3		98	6421.6	
48	6542.1		99	6418.6	
49	6539.8	4_3-4_4	100	6412.2	
		4_4-4_3	101	6410.5	
50	6537.6		102	6405.5	
51	6535.9	1_1-1_0	103	6402.8	
		3_1-3_0	104	6399.8	
		3_2-3_3	105	6397.6	
		3_3-3_2	106	6392.4	
		4_2-4_1	107	6387.4	
52	6534.8	2_2-2_1	108	6380.6	
		4_1-4_2	109	6379.1	
53	6534.4	2_1-2_2	110	6375.0	
54	6532.9		111	6373.6	
55	6531.6	3_0-3_1			

tungsten filament was used for the energy source. A lead sulfide cell was used for the detector. An ac amplifying system was used, and the radiation was chopped at the rate of 1080 cps. The absorption cell which held the D_2O contained mirrors arranged so that the energy traversed the cell four times giving a path length of 160 cm. A small reservoir of liquid D_2O was connected to the evacuated cell. The reservoir was heated until all the D_2O evaporated into the cell. The cell was heated to about 95°C to keep the D_2O in the vapor state. Thin glass windows were used on the cell.

The sample of D_2O used was obtained from Norsk Hydro-Elektrisk Kvaelstofaktieselkab and contained 99.75 g per 100 g D_2O.

The grating used for the measurement was a replica made by the Perkin-Elmer Corporation. It was ruled with 15,000 lines per inch. The grating constant was obtained by observing lines of the mercury spectrum in high orders. The positions of the lines in wave numbers were reduced to their values in vacuum.

The vibration-rotation band $\nu_1+\nu_2+\nu_3$ was observed in the region from 6370 cm^{-1} to 6670 cm^{-1} with the effective slit width of the spectrometer set to 0.64 cm^{-1}. The results of the measurements may be seen by referring to Fig. 1. The numbers appearing over the various lines are arbitrary numbers assigned to them. These numbers are useful in quickly picking out any one line. Frequencies in wave numbers, corrected to vacuum, for the lines are given in Table I.

III. ANALYSIS OF THE DATA

The identification of lines measured in the band was made by following the method used by Nielsen[9,10] in identifying the lines in the spectrum of water vapor, except that since the effect of the centrifugal stretching coefficients in the D_2O spectrum is 1/16 that of their effect on the H_2O spectrum, the energy formula due Wang[11]

$$F(J_\tau)=\tfrac{1}{2}(B+C)J(J+1)+[A-\tfrac{1}{2}(B+C)]W_\tau$$

and the algebraic equations for W_τ as given by Nielsen[12] were used rather than the more complete equations given by Nielsen[9] which take into account the effect of centrifugal stretching.

The procedure used in carrying out the analysis was as follows. By trial and error some transitions involving low values of J were assigned. Then, term values for the levels $J=0$, $J=1$, and $J=2$ were determined tentatively. By using the sum rules for the asymmetric top as given by Mecke,[6] values for the reciprocals of inertia $A(V)$, $B(V)$, and $C(V)$ were found. These were used to calculate the parameter b from the equation

$$b=C-B/2[A-\tfrac{1}{2}(B+C)].$$

The parameter b, in turn, was used in the algebraic equations for W_τ to find W_τ for higher J values. The

[9] H. H. Nielsen, Phys. Rev. **59**, 565 (1941).
[10] H. H. Nielsen, Phys. Rev. **62**, 422 (1942).
[11] S. C. Wang, Phys. Rev. **34**, 243 (1929).
[12] H. H. Nielsen, Phys. Rev. **38**, 1432 (1931).

W_τ were then used in Wang's equation to determine the rotational term values $F(J_\tau)$ for higher J values.

In making the transition assignments for low J_τ, it was helpful to compare the $\nu_1+\nu_2+\nu_3$ spectrum with the ν_3 spectrum given by Dickey and Nielsen.[2] A definite similarity in the central portion of the two spectra was found.

As a further aid in identifying the lines of the spectrum, the relative intensities of the lines have been calculated by using the line strengths given by Cross, Hanier, and King.[13] That is,

$$\sum_{XYZ}\sum_{M''}\sum_{M'}|(\phi_{Fg}{}^{A})J''\tau''M'';\ J'\tau'M'|^2,$$

where $\phi_{Fg}{}^{A}$ represents the direction cosine element of the asymmetric rotator, and XYZ are the space fixed Cartesian coordinates. Their values of line strengths are tabulated for various values of a parameter of asymmetry. That is,

$$K=(2B-A-C)/(A-C).$$

The values used were those tabulated for $K=-0.5$, since the value of this parameter for the normal state is -0.54 and for the state $\nu_1+\nu_2+\nu_3$ is -0.55.

Term values determined in this manner for the band $\nu_1+\nu_2+\nu_3$ are tabulated through $J=5$ in Table II. The identification of the lines is given in the third column of Table I.

By using the formula

$$W/hc=\sum\dot{\omega}_i(n_i+\tfrac{1}{2})+\sum_{i\geq k}\sum X_{ik}(n_i+\tfrac{1}{2})(n_k+\tfrac{1}{2}),$$

and the constants ω_i and X_{ik} given for D_2O by Darling and Dennison,[7] the band center of the band $\nu_1+\nu_2+\nu_3$ was calculated to be 6529.6 cm^{-1}. Experimentally, it was found to be 6533.4 cm^{-1}.

TABLE II. Vibration-rotation term values for the state $\nu_1+\nu_2+\nu_3$.

J_τ	$\nu_1+\nu_2+\nu_3$	J_τ	$\nu_1+\nu_2+\nu_3$
0_0	6533.4 cm^{-1}	3_{-3}	6602.2
1_1	6556.3	4_4	6808.8
1_0	6553.8	4_3	6808.8
1_{-1}	6545.3	4_2	6741.6
2_2	6608.3	4_1	6741.3
2_1	6608.2	4_0	6696.9
2_0	6582.6	4_{-1}	6691.4
2_{-1}	6575.1	4_{-2}	6673.6
2_{-2}	6568.5	4_{-3}	6648.2
3_3	6692.5	4_{-4}	6645.5
3_2	6692.4	5_{-1}	6762.5
3_1	6646.3	5_{-2}	6749.8
3_0	6643.8	5_{-3}	6736.7
3_{-1}	6622.1	5_{-4}	6700.5
3_{-2}	6606.4	5_{-5}	6698.1

[13] Cross, Hanier, and King, J. Chem. Phys. 12, 210 (1944).

TABLE III. Values of $A(V)$, $B(V)$, $C(V)$, I_A, I_B, I_C, and Δ.

	Calculated	Observed
$A(V)$	15.77 cm^{-1}	15.70 cm^{-1}
$B(V)$	7.20	7.19
$C(V)$	4.68	4.69
I_A	1.774×10^{-40} g cm^2	1.782×10^{-40} g cm^2
I_B	3.886×10^{-40}	3.891×10^{-40}
I_C	5.974×10^{-40}	5.966×10^{-40}
Δ	0.311×10^{-40}	0.293×10^{-40}

In calculating the values of the reciprocals of inertia $A(V)$, $B(V)$, and $C(V)$, extra weight has been given to the term values for lower J, since the effect of the centrifugal stretching coefficients is less for these terms. The values which are then obtained are given in Table III. In the same table are stated the values of the corresponding effective moments of inertia.

Darling and Dennison have shown that the quantity $\Delta=I_C-I_A-I_B$ is one which, for a planar molecule, is independent of the coefficients of the anharmonic part of the potential energy. Its value may therefore be computed from a knowledge of the normal frequencies of the molecule and the shape of the molecule. The value of Δ for the state $\nu_1+\nu_2+\nu_3$ computed with the aid of the relation of Darling and Dennison is given in Table III, together with the experimentally determined value.

The effective reciprocals of inertia may be given by,

$$A(V)=A_e-\sum_{i=1}^{3}\alpha_i{}^{A}(V_i+\tfrac{1}{2})$$

$$B(V)=B_e-\sum_{i=1}^{3}\alpha_i{}^{B}(V_i+\tfrac{1}{2})$$

$$C(V)=C_e-\sum_{i=1}^{3}\alpha_i{}^{C}(V_i+\tfrac{1}{2}).$$

Since there is experimental data for the states (0, 0, 0), (0, 1, 0), (0, 0, 1), and (1, 0, 1), it is possible to calculate values for the $\alpha_i{}^{A}$, $\alpha_i{}^{B}$, and $\alpha_i{}^{C}$. These values have been determined by using the values for the effective reciprocals of inertia given by Innes, Cross, and Giguère and Fuson, Randall, and Dennison. Once the $\alpha_i{}^{A}$, $\alpha_i{}^{B}$, and $\alpha_i{}^{C}$ are known, the values for the effective reciprocals of inertia for the state (1, 1, 1) may be calculated. This has been done, and a comparison of the calculated values with the experimentally determined values may be seen in Table III.

The Infrared Spectrum of Nitrosyl Fluoride.* Part I. Prism Spectrum

P. J. H. Woltz, E. A. Jones,† and A. H. Nielsen‡
K-25 Laboratories, Carbide and Carbon Chemicals Company, Oak Ridge, Tennessee

(Received September 25, 1951)

The prism spectrum of NOF is reported from 2–38μ. Twelve absorption bands were observed and identified in terms of the fundamental frequencies ν_1(N−O) = 1844.03 cm^{-1}, ν_2 (bending) = 521 cm^{-1}, ν_3(N−F) = 765.85 cm^{-1}. Comparison with the companion molecules NOCl and NOBr is made.

NITROSYL fluoride, like nitrosyl chloride and bromide, is assumed to be a nonlinear unsymmetric triatomic molecule with the nitrogen at the apex of a comparatively flat triangle. The infrared spectra of the latter two molecules have been previously investigated by Bailey and Cassie[1] who reported the band positions and gave frequency assignments. Recently, Burns and Bernstein[2] reinvestigated the infrared spectrum of NOBr and listed the fundamental frequencies. For both molecules they computed a set of force constants from their data. Their experimental results were confirmed recently by Wise and Elmer.[3]

In an attempt to complete the infrared vibration spectra on this group of molecules, a study of NOF was undertaken by Jones and Woltz, then of K-25 Laboratories, who published a list[4] of infrared frequencies and their assignments. Recently, Magnuson,[5] working at the University of Tennessee and the K-25 Laboratories, has resolved two of the fundamentals of NOF and observed its microwave spectrum. A full report of the grating measurements, band analysis, and molecular constants is given in Part II.[6]

The present paper is a report on the completed prism work on NOF observed through the spectral interval 2–38μ. A figure showing the spectrum and a table of the NOF frequencies compared with those of NOCl and NOBr are given.

TABLE I. Table of frequencies for NOF, NOCl[2], and NOBr[2].

NOF Observed cm^{-1}	NOF Calculated cm^{-1}	Intensity[a]	Assignment[b]	NOCl Observed cm^{-1}	NOBr Observed cm^{-1}
521	···	vs	ν_2 (bending)	332	265
765.85[6]	···	vs	ν_3(N−X)	592	542
1844.03[6]	···	vs	ν_1(N−O)	1799	1801
1037	1042	m	$2\nu_2$	664	···
1290	1287	m	$\nu_2+\nu_3$	923	807
···	1532	···	$2\nu_3$	1184	···
···	1323	···	$\nu_1-\nu_2$	1207	···
···	1808	···	$2\nu_2+\nu_3$	1248	···
2365	2365	m	$\nu_1+\nu_2$	2131	2066
2612	2610	m	$\nu_1+\nu_3$	2395	2340
3087	3131	w	$\nu_1+\nu_2+\nu_3$	···	···
3652	3688	m	$2\nu_1$	3568	3567
4174	4208	w	$2\nu_1+\nu_3$	4160	4103
4441	4455	w	$2\nu_1+\nu_2$	3898	3831
5417	5532	w	$3\nu_1$	5303	5303

[a] vs = very strong, m = medium, w = weak.
[b] The frequency designations for ν_2 and ν_3 as given by Burns and Bernstein have been reversed in this paper to conform with the usual notation that ν_3 is the bending frequency. Otherwise their assignment and the present one are identical.

EXPERIMENTAL DETAILS

The prism measurements on NOF were made with Perkin-Elmer spectrometers, models 12C and 21, equipped with LiF, NaCl, KBr, and KRS-5 prisms. The rocksalt prism was permanently mounted in the model 21 spectrometer. The NOF gas was prepared by Faloon and Kenna[7] of the K-25 Physics Department. For this experiment, the gas was contained in 10-cm fluorothene[8] absorption cells closed with CaF_2, AgCl, and KRS-5 windows for the respective regions. Pressures of the gas in the cells ranged from less than 0.25 in. Hg for the very intense bands to 1 atmos for the weak bands. Windows of NaCl and KBr were completely unsuitable because they were attacked either by the NOF itself or by some unknown impurities which were present in small amounts in all samples. Windows of CaF_2, AgCl, and KRS-5 were not attacked seriously or rapidly and could generally be used throughout their useful wavelength intervals long enough to make the necessary records.

It was not possible to purify completely the NOF by distillation. Traces of one or more unidentified compounds were present which varied in amount from sample to sample. It was never demonstrated whether it was the NOF or the impurities present which attacked the windows and gave window bands. Sufficient distillations were made from a number of samples so that

* This document is based on work performed for the AEC by Carbide and Carbon Chemicals Company, at Oak Ridge, Tennessee. The subject of this paper was included in a report on Fluorine Compounds given at the Columbus Symposium, June, 1951.

† Physics Department, Vanderbilt University, Nashville, Tennessee. A paper on the force constants and thermodynamic properties is in preparation and will soon appear in this journal.
‡ Physics Department, University of Tennessee, Knoxville, Tennessee.

[1] C. R. Bailey and A. B. D. Cassie, Proc. Roy. Soc. (London) **145**, 336 (1934).
[2] W. G. Burns and H. J. Bernstein, Columbus Symposium on Molecular Structure, June, 1950; W. G. Burns and H. J. Bernstein, J. Chem. Phys. **18**, 1669 (1950).
[3] J. H. Wise and J. T. Elmer, J. Chem. Phys. **18**, 1411 (1950).
[4] E. A. Jones and P. J. H. Woltz, J. Chem. Phys. **18**, 1516 (1950).
[5] D. W. Magnuson, Phys. Rev. **83**, 185 (A) (1951).
[6] D. W. Magnuson, J. Chem. Phys. **20**, 380 (1952).
[7] A. V. Faloon and W. B. Kenna, J. Am. Chem. Soc. **73**, 2937 (1951).
[8] J. S. Kirby-Smith and E. A. Jones, J. Opt. Soc. Am. **39**, 780 (1951).

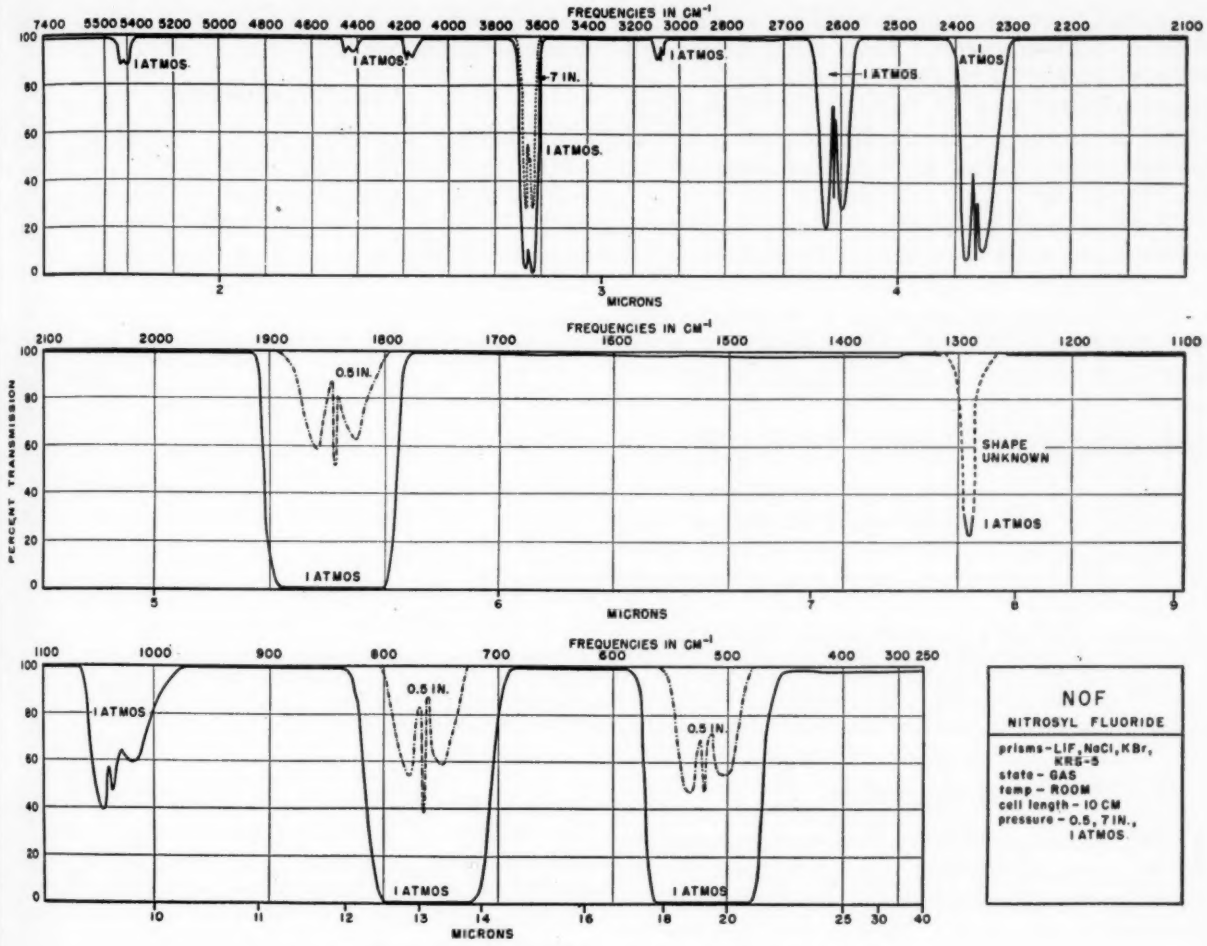

FIG. 1. The infrared prism spectrum of nitrosyl fluoride from 2–38μ.

although the impurities were never entirely eliminated, no spurious bands are included in Table I.

RESULTS AND DISCUSSION

Figure 1 shows the complete infrared prism spectrum from 2–38μ; twelve bands were observed of which three were very intense. These three intense bands were assigned as the fundamentals $\nu_2 = 521$ cm^{-1} (bending), $\nu_3 = 765.85$ (N—F), and $\nu_1 = 1844.03$ (N—O). The frequency values given for ν_3 and ν_1 were taken from the following paper by Magnuson[6] because the grating values were more precise than the prism data. Because the geometry of the nonlinear XYZ molecule possesses no symmetry, except a symmetry plane, all the normal modes are hybrid and have components of the oscillating dipole moment along the least and intermediate axes of inertia. Magnuson[5, 6, 9] has shown from his grating, microwave, and dipole moment experiments that the molecule is very nearly a prolate symmetrical-top rotator with the least axis lying generally in the direction of the O—F bond. All the fundamental bands, therefore, have essentially the same appearance, PQR-type structure, prominent and sharp Q-branch, and a PR spacing of about 32 cm^{-1}. Because of the lack of C_2 symmetry, the normal modes do not have the same general form as in H_2O, H_2S, etc., but the frequency usually denoted as ν_1 is essentially an oscillation of the N—O bond,[10] and the one designated ν_3 is essentially the oscillation of the F—N bond. This is in agreement with observations in NOCl and NOBr[2].

All the other intense vibration-rotation bands observed, with the exception of the one at 1290 cm^{-1}, exhibit the same type of PQR structure, as may be seen in Fig. 1. This characteristic helped to eliminate some impurity bands. The band at 1290 cm^{-1} is heavily flanked on both its high and low frequency sides with intense impurity bands. Its structure was, therefore, never really determined. It is, however, believed that it belongs to the NOF system because of the way its intensity remained constant while the neighboring impurity bands changed with various fractionations. For the much weaker bands at 4174, 4441, and 5417 cm^{-1}, the resolving power was not good enough actually to

[9] D. W. Magnuson, J. Chem. Phys. (to be published).

[10] P. C. Cross and J. H. Van Vleck, J. Chem. Phys. 1, 350 (1933).

resolve the Q branches from the envelope, but they are indicated. All the observed bands could be assigned reasonably in terms of the three fundamentals and these assignments are given in Table I. Also included in Table I for comparison are the fundamental and overtone frequencies observed by Burns and Bernstein[2] for NOCl and NOBr.

A band, reported in the original letter[4] at 1511 cm^{-1}, has been shown to be an impurity and has been omitted from Table I; and the frequency 3635 cm^{-1} has been corrected to 3652 cm^{-1}.

ACKNOWLEDGMENTS

The authors are indebted to A. V. Faloon and W. B. Kenna for the careful preparation of the samples used and for their continued interest. Helpful discussions were held with Dr. D. F. Smith, Mr. D. W. Magnuson, and Mr. T. G. Burke of the K-25 Physics Staff.

THE JOURNAL OF CHEMICAL PHYSICS VOLUME 20, NUMBER 3 MARCH, 1952

The Infrared Spectrum of Nitrosyl Fluoride.*† Part II. Rotational Analysis of ν_1 and ν_3

DALE W. MAGNUSON

K-25 Laboratories, Carbide and Carbon Chemicals Company, Oak Ridge, Tennessee, and the University of Tennessee, Knoxville, Tennessee

(Received September 25, 1951)

Analysis of the rotational structure of ν_1 and ν_3 infrared bands of nitrosyl fluoride at 1844.03 and 765.85 cm^{-1} showed that this molecule is nearly a prolate symmetric top. The following rotational parameters based on symmetric-top theory were found and are expressed in cm^{-1}: for ν_1, $2B''=0.7515$, $2B'=0.7483$, $D_J'+D_J''=0.000027_5$; for ν_3, $2B''=0.7521$, $2B'=0.7503$, $D_J'+D_J''=0.000002_{36}$. The anharmonic term x_{33} was found to be -1.06 cm^{-1} from ν_3. The anharmonic term x_{12} was found to be $+1.03$ cm^{-1} from ν_1.

INTRODUCTION

THE infrared spectrum of NOF was first observed by Jones and Woltz.[1] All of the observed bands were assigned on the basis of the identification of the three most intense bands at 767, 521, and 1844 cm^{-1} as the fundamentals ν_1, ν_2 and ν_3, respectively. A complete report of this work is given in the preceding paper.[2] From some estimates of the shape of the molecule it was suspected that the rotational structure should be observable. It was, therefore, undertaken to complete the study of this molecule by subjecting ν_1 and ν_3 to an examination for their rotational structure, using the high resolution grating spectrometer at the University of Tennessee.[3] The search for the microwave spectrum also was undertaken to complete the structure determination of this molecule. A preliminary report of the microwave spectrum[3,4] has been given, and a complete report on this phase of the work will be submitted for publication at an early date.

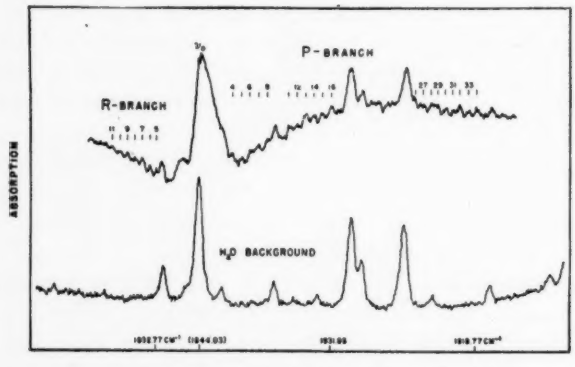

FIG. 1. Grating record of ν_1 for nitrosyl fluoride.

No references were found in the literature concerning the structure of NOF, so it was not possible to estimate accurately the moments of inertia and B values. The structures of NOBr and NOCl were known from electron diffraction data,[5] and the N−Br and N−Cl bond distances were found to be 0.30 and 0.32A larger than the Pauling covalent bond radii.[6] The calculations of the principal moments of inertia $I_a \leqslant I_b \leqslant I_c$ for several variations of the preliminary model suggested by the other nitrosyl halides, indicated that I_a is much smaller than I_b. From the relation $I_a+I_b=I_c$ for planar molecules, it was noted that $I_b \approx I_c$, and hence NOF is nearly a prolate symmetric-top rotator. The spacing of the rotational lines was estimated on the basis of symmetric-top theory to be 0.7 to 0.8 cm^{-1}.

* This document is based on work performed for the AEC by Carbide and Carbon Chemicals Company, at Oak Ridge, Tennessee.

† The work reported herein is included in a doctoral thesis submitted to the University of Tennessee.

[1] E. A. Jones and P. J. H. Woltz, J. Chem. Phys. **18**, 1516 (1950).

[2] Woltz, Jones, and Nielsen, J. Chem. Phys. **20**, 378 (1952).

[3] A preliminary report of this work, and the microwave spectrum, was presented at the Southeastern Section of the American Physical Society, April 5, 1951. D. W. Magnuson, Phys. Rev. **83**, 485(A) (1951).

[4] D. W. Magnuson, J. Chem. Phys. **19**, 1071 (1951).

[5] J. A. A. Ketelaar and K. J. Palmer, J. Am. Chem. Soc. **59**, 2629 (1937).

[6] L. Pauling, *The Nature of the Chemical Bond* (Cornell University Press, Ithaca, New York, 1949), p. 164.

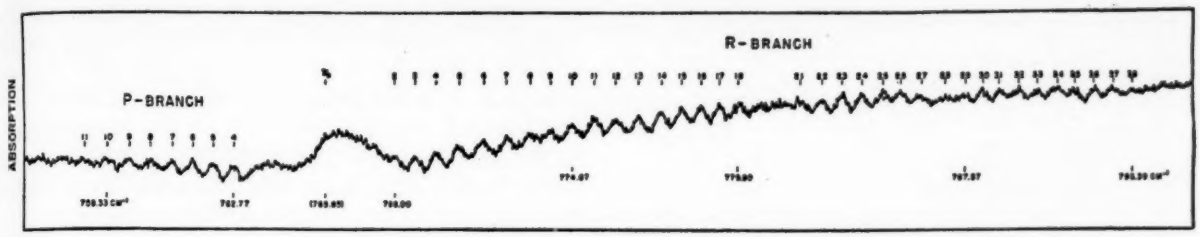

FIG. 2. Grating record of ν_3 for nitrosyl fluoride.

It can be shown from the Slawsky and Dennison[7] equation for the energy levels of a nonrigid symmetric-top rotator,

$$E=BJ(J+1)+(A-B)K^2-D_JJ^2(J+1)^2 -D_{JK}J(J+1)K^2-D_KK^4,$$

that the observed lines for $\Delta J=\pm 1$ and $\Delta K=0$ can be represented by

$$\nu=\nu_0+(B'+B'')m+(B'-B'')m^2-2(D_J'+D_J'')m^3.$$

The D_{JK} terms and the D_J difference terms are neglected. The primes refer to the upper vibrational state and the double primes refer to the ground state. For $\Delta J=+1$, $m=+J'$ and for $\Delta J=-1$, $m=-J''$. The energy difference of the two vibrational states is ν_0, the band center.

EXPERIMENTAL RESULTS

Apparatus

The previously described[8] recording infrared grating spectrometer was used to resolve ν_1 and ν_3 in NOF at 1844 and 767 cm^{-1}, respectively. For ν_1, the gas at 2 cm Hg pressure was contained in a fluorothene cell 10 cm long which had CaF_2 windows sealed with a low-melting polymer of fluorothene. An R. W. Wood replica grating having 7200 lines/in. was used in the spectrometer. It was necessary to dry the air in the spectrometer to reduce the water vapor absorption by flowing dry nitrogen through the enclosure, and by means of trays of P_2O_5 placed in the enclosure. For ν_3, the fluorothene cell had NaCl windows, and a replica grating having 1800 lines/in. was used. A Golay pneumatic infrared detector[9] and amplifier, made by the Eppley Laboratories, was used in conjunction with a Leeds and Northrup, Type G, Speedomax Recorder. Fiducial marks were made on the grating record at 1-minute arc intervals by means of an extra solenoid pen in the recorder. Exact grating angles for an absorption line, measured from the central image, were obtained by linear interpolation.

Data and Calculations

The grating records of ν_1 and ν_3 are reproduced in Figs. 1 and 2. The water-vapor background also is shown with the grating record of ν_1. Because an insufficient number of rotational lines were resolved in the R branch of ν_1 and in the P branch of ν_3, the usual combination relations could not be applied to calculate rotational parameters. Instead, an equation of the form $\nu=\nu_0+am+bm^2+cm^3$ was fitted to the measured line frequencies by grouping the experimental data and solving for the equation constants. Figures 3 and 4 are plots of the line frequencies vs the index number m for ν_1 and ν_3. From the curvature in Fig. 3, it was obvious that a cubic equation was necessary to fit the experimental data. The position of the band center, on which the m identification is based, was determined from the fact that the band center usually lies in the leading or sharp edge of the Q branch. The intervals between successive lines makes it unlikely that the band center could be displaced by one rotational line spacing. The experimental and calculated values for the line frequencies are given in Tables I and II for ν_1 and ν_3, respectively, to show that the derived curve fits the experimental data in all regions. From the coefficients of the fitted curves, the rotational parameters (in cm^{-1}) were determined. For ν_1, $2B''=0.7515$, $2B'=0.7483$, $(D_J'+D_J'')=0.000027_5$. For ν_3, $2B''=0.7521$, $2B'=0.7503$, $(D_J'+D_J'')=0.000002_{36}$. The band centers were: $\nu_1=1844.03$ and $\nu_3=765.85$. The microwave value of $(B+C)=0.7456$ cm^{-1} is to be compared to the $2B''$ values.[3]

On the grating record of ν_3 there is a secondary maximum on the low frequency side of the central Q branch which is suggestive of a Q branch of a higher vibrational transition, $v_3=1\leftarrow 2$. This would be coincident with the Q branch for $v_3=0\leftarrow 1$, except for the anharmonic terms in the potential. The vibrational energy levels including

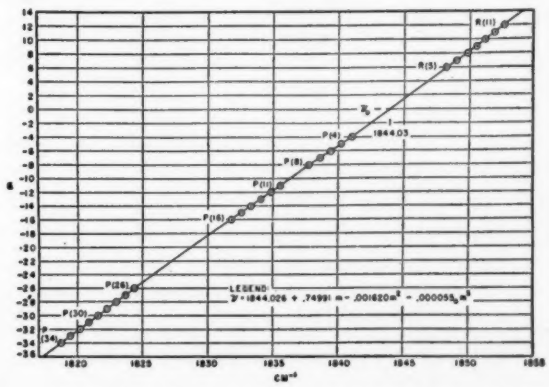

FIG. 3. Plot of the line frequencies vs the line identification for ν_1.

[7] Z. L. Slawsky and D. M. Dennison, J. Chem. Phys. **7**, 509 (1939).
[8] A. H. Nielsen, J. Tenn. Acad. Sci. XXII, No. 4, 241 (1947).
[9] M. J. E. Golay, Rev. Sci. Instr. **20**, 816 (1949).

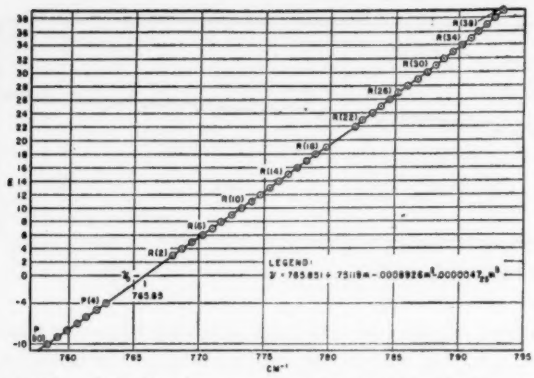

FIG. 4. Plot of the line frequencies *vs* the line identification for ν_3.

anharmonic terms[10] are given by the equation

$$G(v_1v_2v_3)=\sum\nu_i(v_i+\tfrac{1}{2})+\sum x_{ij}(v_i+\tfrac{1}{2})(v_i+\tfrac{1}{2})$$

for a nonlinear XYZ molecule. G, ν_i and x_{ij} are in cm^{-1}. If it is assumed that the maximum is due to $v_3=1\leftarrow2$, then the separation of the Q-branch peaks in ν_3 is

$$\Delta G=2x_{33}=-2.12\ cm^{-1},\quad \text{or}\quad x_{33}=-1.06\ cm^{-1}.$$

In ν_1, there is also an extra maximum on the high frequency side of the Q-branch which cannot be interpreted on a similar basis because the Boltzmann factor for $v_1=1$ is approximately 0.0001. It is also unlikely that these secondary maxima are isotope shifts, because the N^{15} and O^{18} concentrations are 0.0038 and 0.0020, respectively.

TABLE I. Line frequencies of ν_1 for nitrosyl fluoride.

Line	m	Frequency cm^{-1} Calculated	Experimental	Error
$P(34)$	−34	1818.82	1818.77	+0.05
$P(33)$	−33	1819.49	1819.44	+0.05
$P(32)$	−32	1820.17	1820.19	−0.02
$P(31)$	−31	1820.86	1820.89	−0.03
$P(30)$	−30	1921.56	1821.58	−0.02
$P(29)$	−29	1822.26	1822.27	−0.01
$P(28)$	−28	1822.97	1822.98	−0.01
$P(27)$	−27	1823.68	1823.70	−0.02
$P(26)$	−26	1824.40	1824.34	+0.06
$P(16)$	−16	1831.84	1831.86	−0.02
$P(15)$	−15	1832.60	1832.63	−0.03
$P(14)$	−14	1833.36	1833.33	+0.03
$P(13)$	−13	1834.13	1834.11	+0.02
$P(12)$	−12	1834.89	1834.92	−0.03
$P(11)$	−11	1835.65	1835.61	+0.04
$P(8)$	− 9	1837.95	1837.82	+0.13
$P(7)$	− 7	1838.72	1838.68	+0.04
$P(6)$	− 6	1839.48	1839.53	−0.05
$P(5)$	− 5	1840.24	1840.29	−0.05
$P(4)$	− 4	1841.00	1841.12	−0.12
Band Center		1844.03	...	...
$R(5)$	+ 6	1848.46	1848.32	+0.14
$R(6)$	+ 7	1849.18	1849.12	+0.06
$R(7)$	+ 8	1849.89	1849.97	−0.08
$R(8)$	+ 9	1850.60	1850.64	−0.04
$R(9)$	+10	1851.31	1851.30	+0.01
$R(10)$	+11	1852.01	1852.02	−0.01
$R(11)$	+12	1852.70	1852.77	−0.07
	Average deviation			0.046
	Probable error of single measurement			0.040
	Probable error			0.0076

[10] G. Herzberg, *The Infrared and Raman Spectra of Polyatomic Molecules* (D. Van Nostrand Company, Inc., New York, 1944), p. 205.

A possible explanation for the secondary maximum near the Q branch in ν_1 is that the peak is a Q-branch of the $v_1=0\leftarrow1$ for $v_2=1$, i.e., $G(1,1,0)-G(0,1,0)$ or $[(\nu_1+\nu_2)=\nu_1]$. The separation of the maximum from the Q-branch of ν_1 is $+2.03\ cm^{-1}$. On this identification, x_{12} is calculated to be $x_{12}=+1.02\ cm^{-1}$. The Boltzmann factor for the initial state is 0.075, and it does not prevent this type of transition from being observed.

TABLE II. Line frequencies of ν_3 for nitrosyl fluoride.

Line	m	Frequency cm^{-1} Calculated	Experimental	Error
$P(10)$	−10	758.26	758.33	−0.07
$P(9)$	− 9	759.02	759.10	−0.08
$P(8)$	− 8	759.79	759.84	−0.05
$P(7)$	− 7	760.55	760.64	−0.09
$P(6)$	− 6	761.31	761.33	−0.02
$P(5)$	− 5	762.07	762.12	−0.05
$P(4)$	− 4	762.83	762.77	+0.06
Band Center		765.85	...	...
$R(2)$	+ 3	768.10	768.00	+0.10
$R(3)$	+ 4	768.84	768.73	+0.11
$R(4)$	+ 5	769.58	769.49	+0.09
$R(5)$	+ 6	770.33	770.31	+0.02
$R(6)$	+ 7	771.06	771.08	+0.02
$R(7)$	+ 8	771.80	771.72	+0.08
$R(8)$	+ 9	772.54	772.55	−0.01
$R(9)$	+10	773.27	773.30	−0.03
$R(10)$	+11	774.00	774.07	−0.07
$R(11)$	+12	774.73	774.75	−0.02
$R(12)$	+13	775.46	775.48	−0.02
$R(13)$	+14	776.18	776.15	+0.03
$R(14)$	+15	776.90	776.89	+0.01
$R(15)$	+16	777.62	777.58	+0.04
$R(16)$	+17	778.34	778.29	+0.05
$R(17)$	+18	779.06	778.97	+0.09
$R(18)$	+19	779.76	779.80	−0.04
$R(21)$	+22	781.90	782.03	−0.13
$R(22)$	+23	782.60	782.58	+0.02
$R(23)$	+24	783.30	783.35	−0.05
$R(24)$	+25	784.00	784.00	0
$R(25)$	+26	784.70	784.68	+0.02
$R(26)$	+27	785.39	785.30	+0.09
$R(27)$	+28	786.08	786.04	+0.04
$R(28)$	+29	786.77	786.81	−0.04
$R(29)$	+30	787.46	787.57	−0.11
$R(30)$	+31	788.14	788.23	−0.09
$R(31)$	+32	788.82	788.85	−0.03
$R(32)$	+33	789.50	789.52	−0.02
$R(33)$	+34	790.17	790.23	−0.06
$R(34)$	+35	790.85	790.92	−0.07
$R(35)$	+36	791.52	791.45	+0.07
$R(36)$	+37	792.18	792.10	+0.08
$R(37)$	+38	792.85	792.73	+0.12
$R(38)$	+39	793.51	793.39	+0.12
	Average deviation			0.055
	Single measurement probable error			0.047
	Probable error			0.0072

ACKNOWLEDGMENT

The author is indebted to Mr. A. V. Faloon and Mr. W. B. Kenna for the samples used in this work and to Dr. D. F. Smith for many helpful discussions. The valuable suggestions and continued interest of Professor A. H. Nielsen are greatly appreciated. Acknowledgment is made of a Frederick Gardner Cottrell Grant-in-Aid from the Research Corporation of New York which aided in the completion of the infrared grating spectometer at the University of Tennessee.

Proton Relaxation in Paramagnetic Solutions*†

ROBERT L. CONGER AND P. W. SELWOOD
The Department of Chemistry and the Department of Physics, Northwestern University, Evanston, Illinois
(Received October 8, 1951)

Those paramagnetic ions, such as Fe^{+++}, Mn^{++}, and Gd^{+++}, which are in S spectroscopic states; and those ions, such as Cr^{+++} and Cu^{++}, which are effectively in S states through complete quenching of the orbital component, have been shown to produce reciprocal proton relaxation times proportional to the square of the magnetic moment. Those ions such as Co^{++}, Nd^{+++}, and Dy^{+++}, with strong spin-orbital coupling, have been shown to be, in equivalent concentration, about ten times *less* effective.

INTRODUCTION

IT has been shown by Bloch, Hansen, and Packard[1] that paramagnetic solutes in water may act, in effect, like catalysts in diminishing the proton relaxation time. Pure water shows a relaxation time of several seconds, while that in a dilute ferric chloride solution may be only a few milliseconds. Bloembergen, Purcell, and Pound[2] have derived the following formula for the relaxation time for protons in solutions containing paramagnetic ions:

$$1/T_1 = 12\pi^2\gamma^2\eta N\mu^2/5kT^\circ, \quad (1)$$

where T_1 is the longitudinal relaxation time, γ is the gyromagnetic ratio, N is the number of paramagnetic ions per cubic centimeter of solution, μ is the magnetic moment of the paramagnetic ions, k is the Boltzmann constant, and T° is the temperature. In the present paper our principal concern is with the reciprocal proportionality between T_1 and μ^2.

This problem is of interest in connection with the use of nuclear induction to determine accessibility in heterogeneous catalysis. The problem is also of interest as it relates to the paramagnetic process in the ortho-para hydrogen conversion. It is well known that paramagnetic substances catalyze the spin isomerization of hydrogen. Farkas and Sachsse[3] have shown that for this conversion in solutions of rare earth ions the velocity constant (k) is approximately proportional to the square of the magnetic moment of the rare earth, for equivalent concentrations. Actually the Farkas and Sachsse results showed that k/μ^2 varies by about 3-fold in going from one end of the rare earth series to the other, but this drift has been thought to be due to the lanthanide contraction. Because of the parallelism between the ortho-para hydrogen conversion and the proton relaxation experiment it was decided to duplicate, in part, the Farkas and Sachsse experiment but to compare $T_1\mu^2$ rather than k/μ^2 for several rare earth solutions.

EXPERIMENTAL

The Nuclear Induction Apparatus

The apparatus used was similar to that of Bloch and Hansen. It will be described briefly, except for a few new features.

The sample to be studied is placed in a nearly homogeneous field, H_0, of about 3500 gauss in the Z direction, and a 14-mc radiofrequency field of about one gauss in the X direction. At resonance the signal induced in a pick-up coil in the Y direction is amplified and presented as a vertical displacement on a cathode-ray oscilloscope. The field in the Z direction is periodically swept through the resonance value by two coils having a few turns of wire fitted over the magnet poles to produce the required modulation. The ac required for this modulation is obtained from a transformer with its primary winding connected to the 110-volt main.

A variable frequency oscillator using a 6J5 and a 6V6 tube produces the transverse radiofrequency field. Either a vacuum tube power supply or a dynamotor can be used to supply the power for the oscillator. In either case two VR90 tubes in series are used to regulate the voltage.

The pick-up coil of the tuned receiver circuit is wound on a polystyrene form which is placed in a transverse hole in the center of the transmitting coil. The entire coil assembly can be rotated about the axis of the transmitting coil in order to decouple the receiving coil from the modulation of H_0. In addition, the receiving coil form can be adjusted in position with respect to the transmitting coil in order to reduce mutual inductance to a minimum. The coil assembly is quite microphonic in that any sound vibrations vary the mutual inductance between transmitting and receiving coils. The coil assembly and entire magnet are mounted on shear type shock mountings to decrease transmission of the sound, and in addition, the entire apparatus is placed in a sub-basement soundproof room.

The arrangement of the coil assembly between the magnet poles is a feature of the apparatus which is important for its applicability to various problems. The coils are mounted in such a way that a test tube con-

* This is the third paper from these laboratories on applications of nuclear induction to problems in catalysis. The second, by Selwood and Schroyer, appeared in Disc. Faraday Soc. 8, 337 (1950). Inquiries concerning this paper should be addressed to P. W. Selwood.

† This work was done under contract with the ONR.

[1] Bloch, Hansen, and Packard, Phys. Rev. **70**, 474 (1946).
[2] Bloembergen, Purcell, and Pound, Phys. Rev. **73**, 679 (1948).
[3] A. Farkas and H. Sachsse, Z. physik. Chem. **B23**, 1, 19 (1933).

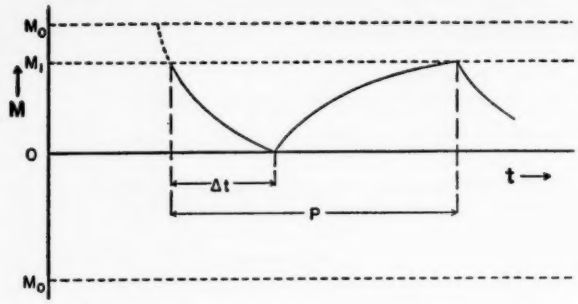

FIG. 1. Plot of M *vs* t.

taining the sample under study may be inserted or removed without difficulty. The varying susceptibility for different samples and test tubes makes some minor readjustments necessary.

The emf induced in the receiver is applied to a vacuum tube circuit consisting of an infinite impedance detector using a 6J5 tube and a preamplifier using a 6SJ7 tube. The signal is then amplified in a General Radio type 814-A audio amplifier and presented as a vertical deflection on a DuMont type 208-B oscilloscope. The linear sweep of the oscilloscope is used so that the time between resonance peaks can be measured. The linearity of the horizontal sweep of the oscilloscope beam was checked by connecting a square wave generator, set at a frequency ten times the modulation frequency, to the vertical displacement of the scope.

In this work all the measurements were made on solutions of paramagnetic ions sufficiently concentrated so that the longitudinal relaxation time T_1 was equal to the transverse relaxation time T_2. Under these conditions T_1 can be measured quite easily with very little apparatus.

Bloch has shown that when T_1 is equal to T_2, the magnitude of the nuclear polarization vector is given by

$$M(t)=\frac{M_0}{T_1}\int_{-\infty}^{t}\frac{\Delta\omega}{(\gamma^2H_1^2+\Delta\omega^2)^{\frac{1}{2}}}e^{-(1/T_1)(t-t')}dt', \qquad (2)$$

where H_1 is the field transverse to the main field H_0, ω is the frequency of the field H_1, γ is the gyromagnetic ratio, t is the time, M_0 is the equilibrium polarization, $\Delta\omega=\gamma H_0-\omega$.

Let

$$\frac{\Delta\omega}{\gamma H_1}=-\Delta \quad \text{for} \quad -\infty<t'<t_1$$
$$=+\Delta \quad \text{for} \quad t_1<t'<t;$$

then $M(t)$ will be given by the equation

$$M(t)=\frac{\Delta M_0}{(1+\Delta^2)^{\frac{1}{2}}}[1-2e^{-(1/T_1)(t-t_1)}]. \qquad (3)$$

Thus the process is exponential with a time constant equal to the relaxation time and $M(t)$ has the limiting value M_0. This equation is the basis of the method used in measuring the relaxation time.

The field H_0 consists of a steady component of about 3500 gauss with a superimposed 60-cycle sine wave component of a few gauss. Although this is not the same as the step function considered in the last paragraph, the results will be the same, if $|\Delta\omega|$ is much larger than $|\gamma H_1|$, because then the quantity

$$\frac{\Delta\omega}{(\gamma^2H_1^2+\Delta\omega^2)^{\frac{1}{2}}}$$

of Eq. (2) will have the value of ±1, regardless of the value of $|\Delta\omega|\gg\gamma H_1|$, and will have the sign of $\Delta\omega$. Thus a sine wave will have the same effect as the square wave if the sine wave goes a considerable distance above and below resonance.

In the nuclear induction apparatus a receiving coil is placed in the Y direction in such a position that a change in the Y component of the polarization vector will induce a voltage in this coil. Thus each time the field H_0 passes through resonance, a voltage will be induced in the receiving coil, and this will be proportional to the magnitude of M as given by Eq. (3). It is possible to adjust the field H_0 so that every second passage through resonance will occur at a time when the magnitude of M is zero, and hence there will be a signal induced in the receiving coil for only every second resonance absorption. From observation of this process the relaxation time T_1 can be determined.

Consider a time t long enough for M of Eq. (3) to equal M_0. Let $\Delta\omega$ change from Δ to $-\Delta$ at t_2. $M(t)$ will be given by the equation

$$M(t)=-M_0[1-2e^{-(1/T_1)(t-t_2)}]. \qquad (4)$$

Thus $M(t)$ will decay exponentially and will become zero when

$$t-t_2=-T\ln\tfrac{1}{2}.$$

By reference to Fig. 1, it may be seen that M will have the value M_1 in a time $-T_1\ln\frac{1}{2}-\Delta t$ and hence M_1 will be given by the equation

$$M_1=-M_0[1-2e^{-(1/T_1)(-T_1\ln\frac{1}{2}-\Delta t)}]$$
$$=M_0(e^{\Delta t/T_1}-1). \qquad (5)$$

When M becomes zero, let $\Delta\omega$ change from $-\Delta$ to Δ. Then M will increase exponentially and will become equal to M_1 again in a time $P-\Delta t$ after reaching zero, or in a time $-T_1\ln\frac{1}{2}+(P-\Delta t)$ after it would have had a value of $-M_0$. For the exponential increase

$$M_1=M_0\{1-2e^{-(1/T_1)(-T\ln\frac{1}{2}+[P-\Delta t])}\}$$
$$=M_0(1-e^{-(P-\Delta t)/T_1}), \qquad (6)$$

and elimination of M_1 and M_0 from these two equations and multiplication by T/P gives the equation used in measuring the relaxation time,

$$\Delta t/P=T_1/P\ln[2/1+e^{-P/T_1}]. \qquad (7)$$

This is the inverse function of that which is desired; however, a plot of it is shown in Fig. 2 from which the value T_1/P may be found as a function of $\Delta t/P$. The graph shows that measurements will be unreliable for relaxation times much longer than the maximum practical modulation period.

Experimentally, the quantity $\Delta t/P$ is obtained from measurements made on a cathode-ray oscilloscope connected to the receiving coil. At resonance a series of "pips," which are alternately up and down, will appear on the scope. The "pips" which are up represent a passage through resonance by the increasing field H_0 while those that are down represent a passage through resonance by the decreasing field. By adjusting the field H_0, the "pips" which are down can be made to disappear, corresponding to a value of zero for M at resonance. The ratio of the distance between a "pip" which is up and one which has just disappeared to the distance between two "pips" which are up, is the value of $\Delta t/P$. T_1/P as a function of $\Delta t/P$ is read off the graph of Fig. 2, and since the modulation period P is known (1/60 second), this gives the value of the relaxation time T_1.

Preparation of Materials

Measurements of relaxation times were made on aqueous solutions containing the ions Cr^{+3}, Mn^{+2}, Fe^{+3}, Fe^{+2}, Co^{+2}, Ni^{+2}, and Cu^{+2}. These were all dissolved in water as cp nitrates, chlorides or sulfates, except for the Fe^{+2} which was used as ferrous ammonium sulfate.

Measurements were also made with solutions containing the ions La^{+3}, Ce^{+3}, Pr^{+3}, Nd^{+3}, Sm^{+3}, Eu^{+3}, Eu^{+2}, Gd^{+3}, Tb^{+3}, Dy^{+3}, Er^{+3}, and Yb^{+3}. All these were made up by dissolving the oxides in dilute nitric acid, except for the Ce^{+3} and Eu^{+2} which were obtained by reduction from solutions containing Ce^{+4} and Eu^{+3}, respectively. The purity of the various rare earth samples turned out to be a matter of major importance in this work. Source and purity (as estimated by magnetic susceptibility and spectroscopic measurements) were as follows: La^{+3}, Ce^{+3}, Nd^{+3}, Sm^{+3}, and Gd^{+3} were from the senior author's collection, had all been the object of repeated magnetic studies, and are considered to be of "atomic weight" purity. Pr^{+3} and Er^{+3} were obtained from the University of Illinois through the courtesy of Professor Therald Moeller, and contained about 2 percent lanthanum for the Pr^{+3}, and 35 percent yttrium for the Er^{+3}. Magnetic susceptibilities were measured and found to be $\chi_{Pr}=28.3$ $(\times 10^{-6})$, and $\chi_{Er}=133$ per gram of crude sesquioxide. Sm^{+3} and Eu^{+3} were from samples given to the senior author by the late Professor Herbert N. McCoy. The Sm^{+3} contained about 10 percent Gd^{+3}, and the Eu^{+3} was spectroscopically pure. Pr^{+3}, Tb^{+3}, and Dy^{+3} were obtained from the National Bureau of Standards through the courtesy of Dr. Raleigh Gilchrist. Except for the Pr^{+3} which was substantially pure, all samples contained about 10 percent of impurities for which correction was possible. Yb^{+3} was obtained from the Argonne National Laboratory. It appeared to be spectroscopically pure.

In all the work the relaxation time produced by a 0.10 M solution of cupric nitrate was taken for calibration purposes. The magnetic moment of the Cu^{+2} ion was taken to be 2.0 Bohr magnetons. This procedure is that adopted by Bloembergen, Purcell, and Pound. Direct evaluation of the term $12\pi^2\gamma^2\eta/5kT^\circ$ by substituting values for the gyromagnetic ratio, etc., gave apparent magnetic moments about 10 percent higher than those reported below.

Measurements of densities and viscosities of the solutions used showed that the various dilute solutions had the same density and viscosity as water, within required limits of accuracy. Relaxation time measurements on concentrated solutions were corrected for density and viscosity in accordance with Eq. (1).

The concentration of paramagnetic ions in solution was usually adjusted so that the relaxation times would be in a region where greatest sensitivity was obtained. Measurements made on different concentrations of the same paramagnetic ion showed that the apparent (effective) moment derived from the observed relaxation time was not a function of concentration unless the concentration was so great that a substantial change in viscosity occurred. Some data on the effect of concentration, viscosity, and of change of solvent are given below.

It must be emphasized that the results presented here show that great stress must be placed on chemical purity. As little as 1 percent of gadolinium in rare earths such as samarium or in terbium may halve the observed relaxation time.

RESULTS

Table I shows the observed proton relaxation times for the various solutions studied. The series of values for Nd^{+3} shows the change of relaxation time with changing concentration. It will be recalled that some

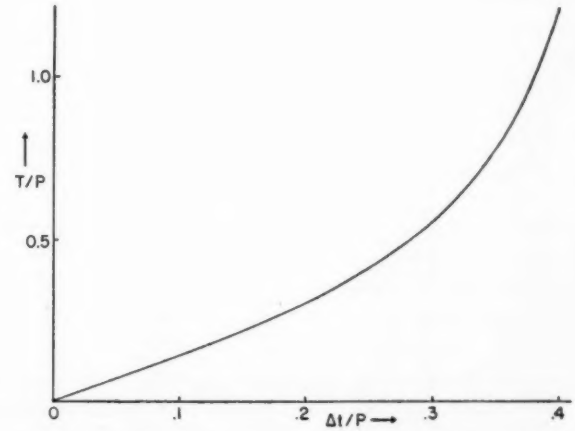

FIG. 2. Plot of T/P *vs* $\Delta t/P$ for the inverse function of $\Delta t/P = T/P \ln(2/1+\epsilon^{-P/T})$.

TABLE I. Proton relaxation times in solutions of paramagnetic salts.

Ion	Molar concentration	Relaxation times
Cr^{+3}	0.0131	0.0107 sec
Mn^{+2}	0.015	0.0085
Fe^{+3}	0.013	0.0077
Fe^{+2}	0.161	0.0102
Co^{+2}	0.46	0.0115
Ni^{+2}	0.27	0.0062
Cu^{+2}	0.10	0.0092
Ce^{+3}	0.60	0.060
Pr^{+3}	0.782	0.0313
Nd^{+3}	0.575	0.060
Nd^{+3}	0.970	0.042
Nd^{+3}	1.31	0.025
Nd^{+3}	1.53	0.020
Nd^{+3}	1.74	0.020
Nd^{+3}	2.08	0.0113
Nd^{+3}	2.40	0.0077
Sm^{+3}	0.804	0.060
Eu^{+3}	1.26	0.0666
Eu^{+2}	0.0408	0.0145
Gd^{+3}	0.0030	0.0105
Tb^{+3}	0.0232	0.0417
Dy^{+3}	0.0617	0.277
Er^{+3}	0.080	0.0233
Yb^{+3}	0.522	0.031

of the rare earth samples were not very pure. Where the impurity was known to be diamagnetic, such as yttrium, a correction has been made for the actual paramagnetic ion content. The value for terbium can be considered as approximate only.

Further tests made to determine the influence, if any, of varying conditions on the relaxation times all gave not unexpected results. Thus, gadolinium dissolved in 1:1 nitric acid-water gave the same result as in pure water. The relaxation time for neodymium at 80°C was essentially the same as at 25°. Neodymium dissolved in 90 percent ethyl alcohol gave the same result as in pure water. A mixture of neodymium and lanthanum in water gave a result which was strictly linear with composition, as did a mixture of samarium and gadolinium. A mixture of neodymium and iron (+3) gave results which were certainly not very significantly different from linear with composition.

TABLE II. Comparison of μ_S and μ_N for paramagnetic ions.

Ion	Term	μ_S	μ_N	μ_S/μ_N
Cr^{+3}	$3d^3\ {}^5D_0$	3.8	4.8	1.2
Mn^{+2}	$3d^5\ {}^6S$	5.9	6.1	1.0
Fe^{+3}	$3d^5\ {}^6S$	5.9	5.6	0.95
Fe^{+2}	$3d^6\ {}^5D_4$	5.3	1.5	0.28
Co^{+2}	$3d^7\ {}^4F_{9/2}$	5.0	0.89	0.18
Ni^{+2}	$3d^8\ {}^3F_4$	3.1	1.4	0.45
Cu^{+2}	$3d^9\ {}^2D_{52}$	2.0	2.0[a]	1.0
Ce^{+3}	$4f\ {}^2F_{5/2}$	2.1	0.35	0.17
Pr^{+3}	$4f^2\ {}^3H_4$	3.4	0.38	0.11
Nd^{+3}	$4f^3\ {}^4I_{92}$	3.5	0.35	0.10
Sm^{+3}	$4f^5\ {}^6H_{5/2}$	1.6	0.30	0.18
Eu^{+3}	$4f^6\ {}^7H_0$	3.9	0.20	0.05
Eu^{+2}	$4f^7\ {}^8S$	7.9	0.30	0.38
Gd^{+3}	$4f^7\ {}^8S$	7.9	10.8	1.4
Tb^{+3}	$4f^8\ {}^7F_6$	9.8	1.95	0.20
Dy^{+3}	$4f^9\ {}^6H_{15/2}$	10.9	1.47	0.14
Er^{+3}	$4f^{11}\ {}^4I_{15/2}$	9.5	1.75	0.18
Yb^{+3}	$4f^{13}\ {}^2F_{7/2}$	4.5	0.50	0.11

[a] Assumed.

DISCUSSION OF RESULTS

In Table II there are shown spectroscopic ground terms, magnetic moment (μ_S) obtained from susceptibility measurements, and apparent moment (μ_N) obtained from the nuclear induction experiment and Eq. (1). It is well known that μ_S varies somewhat with changing ionic environment and that for some ions the coordination may have a large effect. The μ_S values chosen are those for magnetically dilute systems in which covalent coordination is thought to be negligible. This problem is of small importance for the rare earths, but may be of great significance for ions such as Ni^{+2}.

Where they overlap, these results are in reasonably satisfactory agreement with the results of Bloembergen, Purcell, and Pound except for erbium, for which they found $\mu_N = 8.5$. Careful reinvestigation of this case suggests that their sample of erbium may have contained a substantial percentage of gadolinium, a not unlikely impurity.

TABLE III. Effect of viscosity and density of Nd^{+3} solutions on μ_N.

Molar concentration of Nd^{+3}	Viscosity	Density	μ_N
0.575	1.1	1.19	0.28
0.970	1.5	1.37	0.21
1.31	2.3	1.45	0.19
1.54	3.3	1.54	0.15
1.74	4.8	1.62	0.12
2.08	10.2	1.78	0.093
2.40	20.0	1.93	0.072

The results show clearly that those ions in S states, such as Fe^{+3} and Gd^{+3} give μ_N approximately equal to μ_S. Furthermore, those ions such as Cr^{+3} which, through quenching of the orbital component, are "effectively" in S states, likewise give $\mu_N = \mu_S$. The nuclear induction experiment appears thus to yield a measure of spin-orbital coupling. For instance, Cr^{+3} normally has a μ_S which may be calculated from the spin-only formula, but the ions Ni^{+2} and especially Co^{+2} have μ_S values higher than the spin-only formula would predict, and we find that for these two ions μ_N is, respectively, somewhat smaller and much smaller than μ_S. The case of Eu^{+2} is especially interesting. It is known[4] that this ion, which is isoelectronic with Gd^{+3} offers an example of the Sommerfeld-Kossel rule and is in an S state. The observed μ_N is much nearer μ_S than is the case for Eu^{+3}. For Eu^{+2} the fraction μ_N/μ_S does not reach unity, but this is attributed partly to the difficulty of keeping europium reduced during the measurements, and partly possibly to the different radius of the Eu^{+2} ion as compared with the trivalent rare earths. It will be clear

[4] P. W. Selwood, J. Am. Chem. Soc. **55**, 4869 (1933).

also from the unique magnetic properties of Sm^{+3} and Eu^{+2} that the subnormal μ_N values for these ions could probably be explained quite easily. But the low μ_N values for Nd^{+3}, Er^{+3}, and other rare earths make it clear that a more general explanation must be found, and that the large high frequency term in the susceptibilities of Sm^{+3} and Eu^{+3} cannot be blamed for the effect.

Table III shows the effects of viscosity and density on the values of μ_N for Nd^{+3} solutions. The units are such that water has a density and viscosity of 1.0. It will be noticed that the values of μ_N decrease with increasing concentration and for this series μ_N is approximately inversely proportional to the viscosity. The values of μ_N given in Table II are for solutions sufficiently dilute so that their densities and viscosities are approximately that of water.

It would be interesting to determine experimentally what effect the Stark field of the solvent molecules has on the effective magnetic moment μ_N of the rare earth ions. Unfortunately, the rare earth ions are in general not soluble in nonpolar liquids. The effective moment μ_N of the Nd^{+3} ion in alcohol solution is the same as the moment in water solution.

The authors are indebted to Dr. N. Bloembergen in connection with correspondence concerning this effect.

THE JOURNAL OF CHEMICAL PHYSICS VOLUME 20, NUMBER 3 MARCH, 1952

Kinetics of a Fixed Bed System for Solid Diffusion into Spherical Particles*†

J. B. ROSEN‡
Committee on Applied Mathematics, Columbia University, New York
(Received July 27, 1951)

A solution is presented to the general problem of the transient behavior of a linear fixed bed system where the rate of adsorption is determined by the combined effect of a liquid film and solid diffusion into spherical particles. The result obtained is an expression for the effluent following a sudden change in the influent concentration. It is given in two forms: (a) An exact solution to the problem in the form of an infinite integral suitable for numerical integration. (b) An approximation to the exact solution together with an expression for the leading error term in this approximation. The approximate solution and the error term are given as closed trigonometric expressions which can be easily evaluated.

I. INTRODUCTION

A CHEMICAL system consisting of a single solute liquid solution flowing through a fixed bed passes through a period of transient behavior following a sudden change of the influent concentration in the liquid solution. The kinetic behavior of the system is determined by the mechanism controlling the rate at which material in solution is taken up by the particles of the packed bed. It is likely for many systems, and in particular for resinous ion exchangers, that the rate determining factor is a process of solid diffusion into the particle itself.[1] An additional delay may be introduced by the diffusion of material through a liquid film surrounding the particle. If all other processes taking place are very rapid compared to the diffusion of material the behavior of the system during the transient period will be determined by this diffusion process. The kinetics of such a system are the subject of investigation in this paper. The system considered consists of a bed of homogeneous spherical particles of uniform radius, through which the liquid solution flows with a constant linear velocity.

The result obtained is an expression for the effluent concentration $c(x, \theta)$ as a function of time and bed length following a step increase in the influent concentration from zero to c_0 at $t=0$. Certain simplifying assumptions are made in obtaining this result, which may, however, be approximately satisfied in many cases of practical application. The two primary assumptions are: (a) The liquid film coefficient and the solid diffusion coefficient are independent of position, and of concentration over the range of its variation. (b) The system has a linear isotherm so that under equilibrium conditions the concentration q_s, of adsorbed material at the surface of the solid is given by $q_s=Kc$, where K is an effective equilibrium constant which can be considered to be defined by this relation.

With these two assumptions the system is a linear one which can be solved to give the general result for the case of combined surface film and internal solid diffusion. The exact solution to this problem is given here as an infinite integral in a form suitable for numerical integration. A relatively simple approximation to this infinite integral is also given. This approximation is obtained by a saddle point integration of the Laplace transform inversion integral.

* A part of a dissertation written under the Faculty of Pure Science, Columbia University, as part of the requirements for the degree of Doctor of Philosophy.

† This research was supported by an AEC Predoctoral Fellowship.

‡ Present address, Forrestal Research Center, Princeton University, Princeton, New Jersey.

[1] F. Nachod (editor), *Ion Exchange* (Academic Press, New York, 1949), contribution by H. C. Thomas, pp. 29–43.

The author is aware of two previous solutions to a similar problem.[2,3,§] A method of obtaining numerical results is given by Lowan, while the solution is left in the form of a Laplace transform by Wicke. Numerical results can be obtained more easily by means of the infinite integral given here than by the method of Lowan. For those cases where the saddle point approximation is accurate enough, the work required is reduced by at least a factor of ten.

Experimental verification, under conditions of high ionic concentration, of the results given here has been obtained by Raseman[4] using an ion exchange column consisting of spherical particles of Dowex 50. A 0.5 normal solution of NaCl with Na^{24} as a tracer was used in this work. Experimental results obtained with this system when the influent concentration was varied sinusoidally also follow closely the theoretical curves given for the sinusoidal case when solid diffusion is the rate controlling mechanism.[5]

II. DERIVATION OF EQUATIONS

The problem can be formulated exactly in terms of the equations and boundary conditions to be satisfied. It is assumed that any variations in concentration or velocity over a given cross section of the bed can be neglected. The concentration then depends only on the single space variable the bed length z and time t. The equation of conservation is then given by

$$v(\partial c/\partial z)+\partial c/\partial t=-(\partial q/\partial t)/m \tag{1}$$

where v is the constant linear flow velocity and q is the average over a particle of the concentration of adsorbed material, per unit volume of solid. We have also neglected the effect of a possible longitudinal diffusion term $-D_L(\partial^2 c/\partial z^2)$ on the left-hand side of (1) which we assume to be much smaller than $v(\partial c/\partial z)$. By the change of variables $x=z/mv$ and $\theta=t-z/v$, (1) can be written as

$$\partial c/\partial x=-\partial q/\partial\theta. \tag{2}$$

The rate $\partial q/\partial t=\partial q/\partial\theta$ at which material is taken up from solution by the solid particles is determined by the combined effect of a liquid surface film and solid diffusion into the particles.

All material diffusing into the interior of a solid particle must first reach the surface of the particle by diffusing through a static layer of fluid surrounding the particle. In order to be able to take account of the effect of this layer we idealize the situation in the following way. We assume that a uniform liquid surface film surrounds each solid spherical particle and that the concentration at the outer surface of the liquid film is that in the body of the fluid at that value of x and θ, i.e., $c(x,\theta)$. The rate at which the film diffusion takes place is then taken as proportional to the concentration change across the film, $c-q_s/K$. It is possible that because of the flow pattern around the particle, the static layer of fluid may not surround the particle uniformly. However, it may be possible to choose the value of the liquid film coefficient h, so that $h(c-q_s/K)$ gives the average rate of flow of material across the surface film surrounding a particle, per unit of surface area. In this case the idealized model above is valid and we can define an effective surface film resistance $R_f=b/3h$. It is clear that this model will apply only where the particles are small enough so that the change in concentration over a length equal to the particle diameter can be neglected. That is, we require $2b(\partial c/\partial z)\ll c$, where b is the particle radius.

With these conditions, the rate $\partial q/\partial\theta$ is given in terms of the surface concentration q_s by solving the two equations,

$$\partial q/\partial\theta=3h/b[c-q_s/K]=1/R_f[c-q_s/K], \tag{3}$$

$$\partial q_i/\partial\theta=D\nabla^2 q_i=(D/r^2)\partial/\partial r[r^2(\partial q_i/\partial r)], \tag{4}$$

where $q_i=q_i(r,x,\theta)$ is the concentration distribution of adsorbed material in the interior of spheres and $q_s(x,\theta)=q_i(b,x,\theta)$. A table defining all quantities is given at the end of the article. The average concentration in the particles is given by

$$q(x,\theta)=3/b^3\int_0^b q_i(r,x,\theta)r^2dr. \tag{5}$$

The initial and boundary conditions may be taken as the bed being initially free of adsorbed material and a step function in the influent concentration.

$$q_i(r,x,0)=0,\quad 0\leqq r<b,\quad x\geqq 0,$$

$$u(0,\theta)=c(0,\theta)/c_0=\begin{cases}0, & \theta=t\leqq 0\\ 1, & \theta=t>0\end{cases}. \tag{6}$$

Because of the linearity of the system the expression for $u(x,\theta)=c(x,\theta)/c_0$ obtained with these initial and boundary conditions can be used to give the effluent concentration for the much more general conditions of the bed initially at equilibrium with the constant value $q(x,0)=q_i(r,x,0)=q_0$ throughout the bed and an influent concentration of c_0 for $\theta>0$. Then the effluent is given by

$$c(x,\theta)=q_0/K+[c_0-q_0/K]u(x,\theta). \tag{7}$$

For $c_0=0$ this gives the effluent for the elution of a saturated column, $c(x,\theta)=(q_0/K)[1-u(x,\theta)]$.

[2] A. N. Lowan, Phil. Mag. **7**, 914 (1934).
[3] E. Wicke, Kolloid-Z. **86**, 295 (1939).
§ *Note added in proof.*—A solution to the above stated problem, considering internal diffusion only, has recently appeared in this Journal [H. C. Thomas, J. Chem. Phys. **19**, 1213 (1951)]. The inversion integral given there is equivalent to the integral (22) in this paper after replacing $Y_r(s)$ by its value $Y_D(s)$ for no surface film. The inversion integral is evaluated by Thomas by means of a triple infinite series.
[4] C. J. Raseman, Ph.D. thesis (Dept. of Chem. Eng. Cornell University, Ithaca, New York, 1951).
[5] J. B. Rosen and W. E. Winsche, J. Chem. Phys. **18**, 1587 (1950).

The mathematical formulation of the originally stated physical problem is now complete. It consists of finding the three functions $c(x, \theta)$, $q(x, \theta)$, and $q_i(r, x, \theta)$ which satisfy the system of equations (2), (3), (4), and (5), with the initial and boundary conditions (6). Since it is difficult to solve the system of equations directly in this form, it is desirable to simplify the system before attempting to obtain a solution. This is accomplished in what follows by eliminating two of the unknown functions and obtaining a single equation in the single unknown function $c(x, \theta)$.

By means of Duhamel's theorem[6] we can obtain an expression for q_i in terms of q_s. For $q_i(r, x, 0)=0$ we have

$$q_i(r, x, \theta)=\int_0^\theta q_s(x, \lambda)\frac{\partial}{\partial\theta}H(r, \theta-\lambda)d\lambda \qquad (8)$$

where $H(r, \theta)$ is the solution of the problem of solid diffusion into an initially empty spherical particle for a constant imposed surface concentration of unity for $\theta\geqq 0$, i.e., $H(r, \theta)$ is the solution of (4) for $q_i(r, \theta)=0$, $0\leq r<b$, at $\theta=0$, and $q_s(\theta)=1$, $\theta>0$. The value of $H(r, \theta)$ is given by[7]

$$H(r, \theta)=1-2\sum_{n=1}^{\infty}\frac{(-1)^{n+1}}{\sigma_n r}\sin(\sigma_n r)\exp[-D\sigma_n^2\theta], \qquad (9)$$

where $\sigma_n=n\pi/b$. In the various differentiations and integrations which are carried out it can be shown that the required condition of uniform convergence of the original or derived series is satisfied. The details of the proof of this are straightforward but rather lengthy and will be omitted. We will therefore proceed to carry out all operations formally without further consideration of convergence questions. Then (9) gives

$$\frac{\partial H(r, \theta)}{\partial\theta}=2D\sum_{n=1}^{\infty}(-1)^{n+1}\sigma_n\frac{\sin(\sigma_n r)}{r}\exp[-D\sigma_n^2\theta].$$

The substitution of this in Eq. (8) and the interchange of the order of integration and summation leads to

$$q_i(r, x, \theta)=2D\sum_{n=1}^{\infty}(-1)^{n+1}\sigma_n\frac{\sin(\sigma_n r)}{r}\times\int_0^\theta q_s(x, \lambda)\exp[-D\sigma_n^2(\theta-\lambda)]d\lambda.$$

If this expression is used in (5) and the integration and summation interchanged again we get

$$q(x, \theta)=\frac{6D}{b^2}\sum_{n=1}^{\infty}\int_0^\theta q_s(x, \lambda)\exp[-D\sigma_n^2(\theta-\lambda)]d\lambda, \qquad (10)$$

after performing the integration with respect to r. To get an expression for the rate $\partial q/\partial\theta$, consider

$$\frac{\partial}{\partial\theta}\int_0^\theta q_s(x, \lambda)\exp[-D\sigma_n^2(\theta-\lambda)]d\lambda=\int_0^\theta\frac{\partial q_s(x, \lambda)}{\partial\lambda}\exp[-D\sigma_n^2(\theta-\lambda)]d\lambda,$$

after integration by parts and making use of the fact that $q_s(x, 0)=0$. Using this relation we can give the time rate of change of the average concentration q in terms of the time rate of change of the surface concentration q_s. Equation (2) can be written in the form

$$\frac{\partial c}{\partial x}=-\frac{\partial q}{\partial\theta}=-\frac{6D}{b^2}\sum_{n=1}^{\infty}\int_0^\theta\frac{\partial q_s(x, \lambda)}{\partial\lambda}\exp[-D\sigma_n^2(\theta-\lambda)]d\lambda. \qquad (11)$$

We wish to obtain an equation involving only the single unknown function $c(x, \theta)$ and its derivatives. From (2) and (3) we get q_s in terms of c

$$q_s=K\left[c+R\frac{\partial c}{\partial x}\right]. \qquad (12)$$

This gives the desired equation as a linear partial integro—differential equation which must be satisfied by $c(x, \theta)$

$$\frac{\partial c}{\partial x}=-2\gamma\sum_{n=1}^{\infty}\int_0^\theta\left[\frac{\partial c}{\partial\lambda}+R\frac{\partial^2 c}{\partial x\partial\lambda}\right]\times\exp[-D\sigma_n^2(\theta-\lambda)]d\lambda, \qquad (13)$$

where $\gamma=3DK/b^2$. We have now reduced the problem to that of solving a single equation in the unknown concentration $c(x, \theta)$ which it is the purpose of this paper to determine. We proceed by obtaining an exact solution to Eq. (13).

III. EXACT SOLUTION

To solve this equation subject to the boundary conditions previously given we use the Laplace transform,[8] and transform (13) with respect to the variable θ. We denote by $L\{f(x, \theta)\}=F(x, s)$ the transform with respect to θ of $f(x, \theta)$. We let $C(x, s)=L\{c(x, \theta)\}$. We will also use the relations

$$L\{(\partial/\partial\theta)f(x, \theta)\}=sF(x, s)-f(x, 0), \qquad (14)$$

$$L\{(\partial/\partial x)f(x, \theta)\}=\partial F(x, s)/\partial x, \qquad (15)$$

$$L\left\{\int_0^\theta f_1(x, \lambda)f_2(x, \theta-\lambda)d\lambda\right\}=F_1(x, s)F_2(x, s), \qquad (16)$$

$$L\{\exp[-D\sigma_n^2\theta]\}=1/(s+D\sigma_n^2). \qquad (17)$$

[6] H. S. Carslaw and J. C. Jaeger, *Conduction of Heat in Solids* (Oxford University Press, London, 1947), p. 20.

[7] See reference 6, p. 200.

[8] R. V. Churchill, *Modern Operational Mathematics in Engineering* (McGraw-Hill Book Company, Inc., New York, 1944), Chapters I, II, and VI.

TABLE I. Summary of functions and limiting values used in computing $u(x, \theta)$.

Function	Complete expression	Limiting values $\lvert s\rvert \to 0$ or $\lambda \to 0$	Limiting values $\lvert s\rvert \to \infty$ or $\lambda \to \infty$
$Y_D(s)$	$\gamma[w(s)\coth w(s)-1]$	$-\gamma[w^2/3+w^4/45+\cdots]$	$(2\lvert s\rvert/\sigma)^{\frac{1}{2}}-1$
$Y_D(i\beta)$	$\gamma[H_{D1}(\lambda)+iH_{D2}(\lambda)]$	See H_{D1} and H_{D2}	
$H_{D1}(\lambda)$	$\lambda[\sinh 2\lambda+\sin 2\lambda]/[\cosh 2\lambda-\cos 2\lambda]-1$	$(4/45)\lambda^4$	$\lambda-1$
$H_{D2}(\lambda)$	$\lambda[\sinh 2\lambda-\sin 2\lambda]/[\cosh 2\lambda-\cos 2\lambda]$	$(2/3)\lambda^2$	λ
$Y_T(s)$	$Y_D(s)/[1+R_fY_D(s)]$	$Y_D(s)$	$1/R_f$
$Y_T(i\beta)$	$\gamma[H_1(\lambda, \nu)+iH_2(\lambda, \nu)]$	See H_1 and H_2	
$H_1(\lambda, \nu)$	$[H_{D1}+\nu(H_{D1}^2+H_{D2}^2)]/[(1+\nu H_{D1})^2+(\nu H_{D2})^2]$	H_{D1}	$1/\nu$
$H_2(\lambda, \nu)$	$H_{D2}/[(1+\nu H_{D1})^2+(\nu H_{D2})^2]$	H_{D2}	$1/2\nu^2\lambda$

$s=\alpha+i\beta$, $w(s)=i(2s/\sigma)^{\frac{1}{2}}$, $w(i\beta)=(i-1)\lambda$, $\lambda=(\beta/\sigma)^{\frac{1}{2}}$, $\nu=\gamma R_f$

Relation (16) is the Faltung integral theorem. Now taking the transform of (12) and using (15), $Q_s(x, s)=K\{C(x, s)+R_f[\partial C(x, s)/\partial x]\}$, while from (14)

$$L\{(\partial q_s(x, \theta)/\partial\theta)\}=sQ_s(x, s)-q_s(x, 0)=sQ_s(x, s).$$

If we take the transform of Eq. (11) and use the relation above together with (16) and (17) we get

$$\frac{\partial C(x, s)}{\partial x}=-2\gamma\sum_{n=1}^{\infty}\frac{s}{s+D\sigma_n^2}\left[C(x, s)+R_f\frac{\partial C(x, s)}{\partial x}\right]$$

$$=-\left[C(x, s)+R_f\frac{\partial C}{\partial x}\right]Y_D(s),$$

where

$$Y_D(s)=2\gamma\sum_{n=1}^{\infty}\frac{s}{s+D(n\pi/b)^2}. \tag{18}$$

After solving for $\partial C/\partial x$

$$\partial C(x, s)/\partial x=-Y_T(s)C(x, s), \tag{19}$$

$$Y_T(s)=Y_D(s)/[1+R_fY_D(s)], \tag{20}$$

are obtained. From Eqs. (19) and (2) it follows that the quantity $Y_T(s)$ can be thought of as the factor which relates the rate at which material is diffusing into the particles at a given point to the concentration at that point. By analogy with the corresponding term in electric circuit theory we call $Y_T(s)$ the total system admittance. For the special case where the effect of the surface film can be neglected, ($R_f=0$) the quantity $Y_D(s)$ plays the same role, and may therefore be called the system admittance for solid diffusion only.

Equation (19) is the transform of Eq. (13). It can be treated as an ordinary differential equation with s as a parameter. Its solution, satisfying the initial condition $C(0, s)/c_0=1/s$ obtained from (6) is given by

$$U(x, s)=C(x, s)/c_0=(1/s)e^{-xY_T(s)}. \tag{21}$$

The desired result $u(x, \theta)$ is given by the contour integral representing the inverse transform of $U(x, s)$

$$u(x, \theta)=\frac{1}{2\pi i}\int_{-i\infty}^{\alpha+i\infty}\frac{1}{s}e^{s\theta-xY_T(s)}ds, \tag{22}$$

where the path of integration is the straight line parallel to the imaginary axis given by $\Re(s)=\alpha>0$. The expression for $u(x, \theta)$ in this form can be shown to satisfy the Eq. (13) and the boundary conditions by making use of the limiting values of $Y_T(s)$ as given in Table I. We wish to obtain (22) in the form of a real infinite integral from which numerical results can be more readily obtained.

Let us first obtain a trigonometric expression for $Y_D(s)$. The relation[9]

$$2\sum_{n=1}^{\infty}\frac{-z^2}{n^2-z^2}=\pi z\cot(\pi z)-1, \tag{23}$$

holds for all complex $z\neq 0, \pm 1, \pm 2, \cdots$. Let $z^2=-b^2s/\pi^2D$, then after multiplying top and bottom of each term of (18) by b^2/π^2D,

$$Y_D(s)=\gamma[w\cot w-1], \tag{24}$$

where $w=w(s)=ib(s/D)^{\frac{1}{2}}=i(2s/\sigma)^{\frac{1}{2}}$ and $\sigma=2D/b^2$. The principle properties of the functions $Y_D(s)$ and $Y_T(s)$ are summarized in Table I. Their values for $s=i\beta$, β real, are the ones required for the evaluation of the infinite integral expression for $u(x, \theta)$. The functions $H_{D1}(\lambda)$ and $H_{D2}(\lambda)$ are tabulated in Table II. Curves of these functions have also been given.[5]

It is of interest to determine the initial value of the effluent as given by (22) for $\theta=0$. To do this, we evaluate the integral (22) by closing the path of integration by an infinite arc to the right and making use of the limiting values given in Table I. We let $\nu=\gamma R_f$ and consider two cases separately, $\nu>0$ and $\nu=0$.

(a) $\nu>0$.—This is the general case where the effect of the surface-film resistance is taken into account. The above method of evaluation then gives $u(x, 0)=e^{-\gamma x/\nu}$. This result also follows directly from Eqs. (2) and (3) for $q_s(x, 0)=0$. Physically, this means that the effect of a surface film resistance will be clearly indicated by the initial value of the effluent provided the effective bed length γx can be made small enough relative to ν.

[9] K. Knopp, *Theory and Application of Infinite Series* (Blackie and Son, Ltd., London, 1928), p. 419.

(b) $\nu=0$.—We assume here, that the effect of the surface film can be neglected. We see from Table I that $H_1(\lambda, 0)=H_{D1}(\lambda)$ and $H_2(\lambda, 0)=H_{D2}(\lambda)$ so that in general for $\nu=0$ we have $Y_T(i\beta)=Y_D(i\beta)$, a considerable simplification. Using this fact we get that for any $\gamma x>0$, $u(x, 0)=0$, i.e., the initial value of the effluent is zero, regardless of bed length. This result is caused by infinite initial rate of adsorption required by the condition $q_s=Kc$ which must now be satisfied. Physically, of course, this situation will never be realized completely. However, for $\gamma x/\nu>5$ the error in the initial value caused by neglecting the effect of a film resistance will be less than possible experimental errors. In those cases where it can be shown that the error for $\theta>0$ is of the same order as that at $\theta=0$, the solution $u(x, \theta)$ for the mathematically simpler case $\nu=0$ will be a satisfactory approximation to the general case $\nu>0$, provided $\gamma x/\nu>5$.

We now return to the job of simplifying the integral (22). It can readily be seen from its series form that $Y_D(s)$ has an infinite number of first-order poles along the negative real axis at the points $s=-D\sigma_n^2$, $n=1, 2, \cdots$. Except for these poles $Y_D(s)$ is analytic throughout the s-plane. In particular, $Y_D(s)$ is analytic in the half-plane $\Re(s)>-\pi^2D/b^2$. In view of these properties the function $(1/s)e^{-xY_D(s)}$ has an essential singularity at each pole of $Y_D(s)$, a simple pole at $s=0$, and is analytic everywhere else. The situation with respect to $U(x, s)=(1/s)e^{-xY_T(s)}$ is similar except that in this case the essential singularities are given by $s=-\alpha_i$, where the α_i are the roots of $(2\alpha/\sigma)^{\frac{1}{2}}\cot(2\alpha/\sigma)^{\frac{1}{2}}+(1/\nu)-1=0$. Since the roots are real and positive the corresponding singularities are again along the negative real axis.

Because there exist an infinite number of essential singularities the usual method of evaluation of the inverse transform by residues is not practical. However, since $U(x, s)$ is analytic for $\Re(s)\geqq 0$, except at $s=0$, we can take the path of integration to be along the imaginary axis with a small semicircle Γ of radius $\epsilon\to 0$ excluding the origin. Then

$$u(x, \theta)=\frac{1}{2\pi i}\lim_{\epsilon\to 0}\left[\int_{-i\infty}^{-i\epsilon}+\int_{i\epsilon}^{i\infty}+\int_{\Gamma}\right]_{s}^{1}e^{s\theta-xY_T(s)}ds.$$

To evaluate the integral around Γ transform to polar coordinates and use $Y_T(s)\to 0$ as $|s|\to 0$. Then it readily follows that for $\epsilon\to 0$ the last integral contributes an amount $\frac{1}{2}$ to $u(x, \theta)$. The first and second integrals can be combined by making the substitution $s=-i\beta$ and $s=i\beta$, respectively, and taking the limit. This gives

$$u(x, \theta)=\tfrac{1}{2}+\frac{1}{2\pi}\int_0^\infty\left[e^{i\beta\theta}U(x, i\beta)+e^{-i\beta\theta}U(x, -i\beta)\right]d\beta.$$

Since $U(x, s)$ is a Laplace transform $U(x, \bar{s})=\bar{U}(x, s)$, where the bar indicates the complex conjugate.[10]

[10] See reference 8, p. 149.

Further, for any complex quantity F we have $F+\bar{F}=2\Re(F)$. Then

$$u(x, \theta)=\tfrac{1}{2}+\frac{1}{\pi}\int_0^\infty\Re\left[e^{i\beta\theta}U(x, i\beta)\right]d\beta.$$

By using (21) and the expression for $Y_T(i\beta)$ with the change of variable $\beta=\sigma\lambda^2$, we get finally

$$u(x, \theta)=\tfrac{1}{2}+\frac{2}{\pi}\int_0^\infty e^{-\gamma xH_1(\lambda, \nu)}\times\sin\left[\sigma\theta\lambda^2-\gamma xH_2(\lambda, \nu)\right]\frac{d\lambda}{\lambda}. \quad (25)$$

This is the solution to the problem in the form of an infinite integral which is a function only of the three dimensionless parameters γx, $\sigma\theta$, and ν. The convergence of this infinite integral follows from the asymptotic expressions for $H_1(\lambda, \nu)$ and $H_2(\lambda, \nu)$. The integrand is bounded for all λ including $\lambda=0$, and for $\nu>0$ and large λ the integrand approaches $(1/\lambda)e^{-\gamma x/\nu}\sin(\sigma\theta\lambda^2)$ which has a convergent infinite integral. For $\nu=0$, convergence

TABLE II. Values of $H_{D1}(\lambda)$ and $H_{D2}(\lambda)$.

λ	$H_{D1}(\lambda)$	$H_{D2}(\lambda)$
0 to 0.5	$(4/45)\lambda^4$	$(2/3)\lambda^2$
0.6	0.0115	0.2392
0.7	0.0212	0.3247
0.8	0.0359	0.4223
0.9	0.0569	0.5313
1.0	0.0856	0.6504
1.1	0.1233	0.7784
1.2	0.1709	0.9133
1.3	0.2291	1.054
1.4	0.2982	1.196
1.5	0.3781	1.340
1.6	0.4678	1.482
1.7	0.5663	1.621
1.8	0.6719	1.755
1.9	0.7830	1.884
2.0	0.8978	2.006
2.1	1.015	2.123
2.2	1.132	2.234
2.3	1.249	2.340
2.4	1.364	2.443
2.5	1.477	2.542
2.6	1.588	2.639
2.7	1.697	2.734
2.8	1.803	2.829
2.9	1.907	2.924
3.0	2.010	3.019
3.1	2.112	3.114
3.2	2.212	3.209
3.3	2.311	3.306
3.4	2.410	3.403
3.5	2.509	3.501
3.6	2.608	3.599
3.7	2.706	3.698
3.8	2.805	3.797
3.9	2.903	3.897
4.0	3.002	3.997
4.1	3.101	4.097
4.2	3.201	4.197
4.3	3.300	4.298
4.4	3.400	4.398
4.5	3.500	4.499
4.5 to ∞	$\lambda-1$	λ

TABLE III. Functions and derivatives used to compute u_0 and δ_0.

n	$D_n(\lambda)=(1/\gamma)\alpha^n Y_D^{(n)}(\alpha)$	$T_n(\lambda)=(1/\gamma)\alpha^n Y_T^{(n)}(\alpha)$[a]	$E_n(\lambda)=\alpha^n F^{(n)}(\alpha)$
0	$A-1$	$D_0/[1+\nu D_0]$	$\sigma\theta\lambda^2/2-\gamma x T_0(\lambda)-\log\alpha$
1	$\frac{1}{2}[A-B]$	$D_1/[1+\nu D_0]^2$	$\sigma\theta\lambda^2/2-\gamma x T_1(\lambda)-1$
2	$-\frac{1}{4}[A+B-2AB]$	$[D_2+\nu(D_0D_2-2D_1^2)]/[1+\nu D_0]^3$	$1-\gamma x T_2(\lambda)$
3	$\frac{1}{8}[3(A+B)-2B^2-4A^2B]$	$T_2'(\lambda)$	$-2-\gamma x T_3(\lambda)$
4	$-\frac{1}{16}[15(A+B)+6AB-4B^2-8A^2B-8AB(2B+A^2)]$	$T_3'(\lambda)$	$6-\gamma x T_4(\lambda)$

$A=\lambda\coth\lambda$, $B=[\lambda\operatorname{csch}\lambda]^2$, $\lambda=(2\alpha/\sigma)^{\frac{1}{2}}$

[a] Obtained by formally taking derivative using $T_{n+1}=T_n'(\lambda)$, $D_n'(\lambda)=D_{n+1}(\lambda)$. For $\nu=0$, $T_n=D_n$.

is assured by the factor $e^{-\gamma x(\lambda-1)}$. In general the convergence of this integral may be rather slow, necessitating a large amount of numerical work. However, for $\nu<\gamma x/5$ the exponential factor in the integrand will be the controlling factor and bring about more rapid convergence. In particular, for the limiting case of no surface film resistance we have

$$u(x,\theta)=\tfrac{1}{2}+\frac{2}{\pi}\int_0^\infty e^{-\gamma x H_{D1}(\lambda)}\times\sin[\sigma\theta\lambda^2-\gamma x H_{D2}(\lambda)]\frac{d\lambda}{\lambda}. \quad (26)$$

This has been evaluated numerically as a function of $\sigma\theta$ for the case of $\gamma x=1$. The results of this exact integration are given in Table IV together with the values obtained by the approximate method given below.

IV. APPROXIMATE SOLUTION

We now investigate an approximate method of evaluating the integral (22), using the method of saddle point integration or the method of steepest descents.[11] Let

$$F(s)=s\theta-xY_T(s)-\log s. \quad (27)$$

Then (22) can be written in the form

$$u(x,\theta)=\frac{1}{2\pi i}\int_{\alpha-i\infty}^{\alpha+i\infty}e^{F(s)}ds.$$

We are free to choose for α any positive real number. We take $\alpha=\alpha_0$, where α_0 is the positive real root of $F'(\alpha)=0$, where the prime denotes differentiation with respect to the argument. Then if we expand $F(s)$ about $s=\alpha_0$ in a finite Taylor series with a remainder and use the fact that along the path of integration $s-\alpha_0=i\beta$, we get

$$F(s)=F(\alpha_0)+F''(\alpha_0)(i\beta)^2/2!+F'''(\alpha_0)(i\beta)^3/3!+F^{IV}(\alpha_0)(i\beta)^4/4!+I_5(\beta),$$

where $I_5(\beta)$ is a remainder term involving β^5. Then

$$u(x,\theta)=u_0(x,\theta)+\frac{1}{2\pi}e^{F(\alpha_0)}\times\int_{-\infty}^{\infty}\eta_3(\beta)\exp\left[-\frac{F''(\alpha_0)}{2}\beta^2\right]d\beta, \quad (28)$$

where $\eta_3(\beta)$ is a power series in β, starting with β^3, with derivatives $F^{(n)}(\alpha_0)$ as coefficients. The value of $u_0(x,\theta)$ is given by

$$u_0(x,\theta)=\frac{1}{2\pi}e^{F(\alpha_0)}\int_{-\infty}^{\infty}\exp\left[-\frac{F''(\alpha_0)}{2}\beta^2\right]d\beta=\frac{e^{F(\alpha_0)}}{(2\pi F''(\alpha_0))^{\frac{1}{2}}}. \quad (29)$$

The function $u_0(x,\theta)$ exists provided $F''(\alpha_0)>0$, and in this case the second integral in (28) gives the error involved in the approximation $u(x,\theta)\cong u_0(x,\theta)$. The net contribution of the odd order terms in $\eta(\beta)$ is zero since the contributions to the integral from the positive and negative portions of the path cancel. As a result of this there is no contribution from the β^3, β^5, and β^7 terms. Taking account of the β^4 and β^6 terms we get

$$u(x,\theta)=u_0(x,\theta)[1+\delta_0+\delta_1], \quad (30)$$

$$\delta_0=1/8[E_4(\lambda_0)/E_2^2(\lambda_0)-(5/3)E_3^2(\lambda_0)/E_2^3(\lambda_0)], \quad (31)$$

$\delta_1=$ remainder term.

The functions $E_n(\lambda)$ are defined by $E_n(\lambda)=\alpha^n F^{(n)}(\alpha)$, where $\lambda=(2\alpha/\sigma)^{\frac{1}{2}}$. Formulas for their evaluation are given in Table III for $n=0,\cdots,4$. The value λ_0 corresponds to the root α_0, but actually is determined directly by Eq. (32).

The term δ_0 gives the magnitude of the error involved in the approximation $u\cong u_0$, and in some cases may actually be used as a correction term (see Table IV). However, it does not appear possible to show in general that $\delta_1\ll\delta_0$. In view of this the best procedure is probably to compute $u(x,\theta)$ from (25) for several widely separated values of $\sigma\theta$, with γx and ν fixed. If the value of δ_0 given by (31) is close to $u-u_0$ for the values computed it is reasonable to assume it will remain so for all $\sigma\theta$.

We now obtain an expression for $u_0(x,\theta)$ which involves only the functions $E_n(\lambda)$. As a result of the logs term, $F'(\alpha)$ has a first-order pole at $\alpha=0$. Then the roots of $F'(\alpha)=0$ are given by $\alpha F'(\alpha)=E_1(\lambda)=0$, i.e., by the roots of

$$E_1(\lambda)=(\sigma\theta\lambda^2/2)-(\gamma x/2)[(A-B)/[1+\nu(A-1)]^2]-1=0. \quad (32)$$

[11] R. H. Fowler, *Statistical Mechanics* (Cambridge University Press, London, England, 1936), p. 36.

It can readily be shown that this equation has a unique positive root λ_0. Also from (29) we get

$$u_0(x,\theta)=\frac{\exp[(\sigma\theta\lambda_0^2/2)-\gamma x T_0(\lambda_0)]}{(2\pi E_2(\lambda_0))^{\frac{1}{2}}}, \qquad (33)$$

where we have used the fact that $e^{-\log\alpha}=1/\alpha$. It is clear from this that once λ_0 has been determined by (32) both $u_0(x,\theta)$ and the leading error term δ_0 can readily be obtained by the formulas given in Table III. It can also be shown from the expression for $E_2(\lambda)$ that $F''(\alpha)>0$ for all $\alpha>0$.

For $\nu=0$ the approximate solution reduces to the very simple expression

$$u_0(x,\theta)=\frac{\exp[(\sigma\theta\lambda_0^2/2)-\gamma x(A-1)]}{(2\pi[1+\frac{1}{4}\gamma x(A+B-2AB)])^{\frac{1}{2}}}, \qquad (34)$$

with λ_0 the root of

$$\sigma\theta\lambda^2-\gamma x[A(\lambda)-B(\lambda)]-2=0. \qquad (35)$$

Values obtained from this expression for $\gamma x=1$ are compared in Table IV with the exact solution. Consideration of asymptotic expressions for $A(\lambda)$ and $B(\lambda)$ in (35) gives the following explicit formulas for λ_0, accurate to 0.5 percent,

$$\begin{aligned}\lambda_0^2&=(15/4\gamma x)\{-(3\sigma\theta/2-\gamma x)\\&\quad+[(3\sigma\theta/2-\gamma x)^2+8\gamma x/5]^{\frac{1}{2}}\}, \quad \text{for} \quad \lambda_0\leqq 1,\\ \lambda_0&=\gamma x/2\sigma\theta+[(\gamma x/2\sigma\theta)^2+2/\sigma\theta]^{\frac{1}{2}}, \quad \text{for} \quad \lambda_0\geqq 4.\end{aligned} \qquad (36)$$

V. DISCUSSION

A further result which gives a physical insight into the nature of the solution obtained will be discussed briefly. For $\gamma x\geqq 50$ and $\nu\leqq 0.01$, the following expression, accurate to 1 percent, can be obtained directly from the integral (25)[12]

$$u(x,\theta)=\tfrac{1}{2}\left[1+\operatorname{erf}\left(\frac{3\sigma\theta/2-\gamma x}{2(\gamma x/5)^{\frac{1}{2}}}\right)\right]. \qquad (37)$$

This is the expected $\int$ shaped curve for the effluent concentration, and in addition is symmetrical about the value $\frac{1}{2}$. This value of the concentration travels down the bed with a velocity given by $dz/dt=mv/m+K$, which corresponds to the result required by consideration of conservation of material. Thus for a large effective bed length the half-value of concentration travels down the bed with the velocity $mv/m+K$, while because of the term $(\gamma x)^{\frac{1}{2}}$ in the denominator, the slope of the $\int$ curve becomes less and less steep as it moves down the bed.

[12] Compare this result with that obtained by Wicke, reference 3, for the problem of equilibrium with a linear isotherm with longitudinal diffusion taken into account.

TABLE IV. Comparison of exact and approximate solutions for $\gamma R_f=0$ and $\gamma x=1$.

$\sigma\theta$	λ_0	u_0	u	δ_0	$u_0[1+\delta_0]$
0.0	∞	0	0	0	0
0.1	11.71	0.0042	0.004	−0.002	0.0042
0.3	4.75	0.186	0.185	−0.015	0.183
0.5	3.21	0.435	0.427	−0.017	0.428
0.7	2.50	0.634	0.622	−0.014	0.625
1.0	1.91	0.820	0.808	−0.019	0.805
1.5	1.43	0.953	[a]	−0.031	0.923
∞	0	1.083	1.000	−0.083	0.994

[a] Not computed.

VI. SUMMARY

The exact solution $u(x,\theta)$, to the complete problem with both a liquid film and internal solid diffusion as rate determining factors, is given by the integral (25) as a function of the three dimensionless parameters γx, $\sigma\theta$, and ν. If the effect of the film resistance can be neglected the exact solution reduces to the simpler integral (26). The functions $H_1(\lambda,\nu)$ and $H_2(\lambda,\nu)$, needed to evaluate the integral (25), are defined in terms of $H_{D1}(\lambda)$ and $H_{D2}(\lambda)$ in Table I, while the integrand of (26) is given directly in terms of these latter functions. The values of $H_{D1}(\lambda)$ and $H_{D2}(\lambda)$ are tabulated against λ in Table II.

The approximate solution $u_0(x,\theta)$, to the complete problem, is given by (33) in terms of $T_0(\lambda_0)$ and $E_2(\lambda_0)$. The functions $E_n(\lambda)$ and $T_n(\lambda)$ are defined in terms of ν and hyperbolic functions of λ in Table III. The required value λ_0 is the unique positive root of (32). The leading error term δ_0 is given by (31) in terms of the functions $E_n(\lambda_0)$. For $\nu=0$, the approximate solution reduces to Eq. (34), with λ_0 given implicitly by (35) or explicitly by (36).

VII. ACKNOWLEDGMENT

Many helpful suggestions and comments by Professor F. J. Murray, Department of Mathematics, Columbia University, are gratefully acknowledged. The author also wishes to thank Professor H. S. Snyder, Department of Physics, Princeton University for suggesting the use of the saddle point integration method, and Professor R. H. Wilhelm, Department of Chemical Engineering, Princeton University, and Professor R. H. Bretton, Department of Chemical Engineering, Yale University, for their suggestions concerning the chemical aspects of this paper. The computing work in Tables II and IV was done by Mrs. Theresa Ames and Miss Anna Potter of the Brookhaven National Laboratory, through the cooperation of the Laboratory. The research described in this paper was made possible by a NRC–AEC Predoctoral Fellowship grant.

NOMENCLATURE AND SYMBOLS

A consistent system of units is given in brackets.

$A=A(\lambda)=\lambda\coth\lambda$.

b = radius of spherical particles; assumed uniform throughout bed (cm).
$B = B(\lambda) = (\lambda \operatorname{csch}\lambda)^2$.
$c = c(x, \theta)$ = concentration of material in fluid (mm/cc).
$c_0 = c(0, \theta)$ = concentration (constant) at input face of bed (mm/cc).
$C(x, s)$, $Q(x, s)$, $U(x, s)$ = Laplace transforms of $c(x, \theta)$, $q(x, \theta)$, $u(x, \theta)$, respectively.
D = effective coefficient of solid diffusion in spherical particles; assumed constant (cm²/sec).
D_L = longitudinal diffusion coefficient (cm²/sec).
h = liquid film coefficient (cm/sec).
K = effective equilibrium constant.‖
m = void volume per unit volume of adsorbent.‖
$q = q(x, \theta)$ = average (over particle) of concentration of adsorbed material (mm/cc adsorbent).
$q_0 = q(x, 0)$ = initial (constant) concentration of adsorbed material (mm/cc).
$q_i = q_i(r, x, \theta)$ = internal concentration distribution of adsorbed material (mm/cc).
$q_s = q_i(b, x, \theta)$.
r = radial distance from center of spherical particle (cm).
$R_f = b/3h$ = effective surface film resistance (sec).
$s = \alpha + i\beta$, complex variable.
t = time measured from instant of step input (sec).
$u = u(x, \theta) = c(x, \theta)/c_0$.
$u_0(x, \theta)$ = approximation to $u(x, \theta)$ obtained by saddle point integration.
v = linear flow velocity; assumed constant (cm/sec).
$w(s) = i(2s/\sigma)^{\frac{1}{2}}$.
$x = z/mv$ = time required for fluid to flow distance z/m (sec).
$Y_D(s)$ = system admittance for solid diffusion only (sec^{-1}).
$Y_T(s) = Y_D(s)/[1 + R_f Y_D(s)]$ = total system admittance for combined surface film and solid diffusion (sec^{-1}).
z = distance measured from input face of bed (cm).
$\gamma = 3DK/b^2$ (sec^{-1}).
δ_0 = leading term of error in $u_0(x, \theta)$.
$\theta = t - z/v$ = time measured from instant point is reached by fluid (sec).
λ = variable of integration.
$\nu = \gamma R_f = DK/bh$.‖
$\sigma = 2D/b^2$ (sec^{-1}).
$\sigma_n = n\pi/b$ (cm^{-1}).
$\gamma x = 3DKz/mvb^2$ = effective bed length.‖
$\sigma\theta = 2D(t - z/v)/b^2$.‖
$\gamma x/\nu = 3hz/mvb$.‖

‖ Indicates dimensionless quantity.

THE JOURNAL OF CHEMICAL PHYSICS VOLUME 20, NUMBER 3 MARCH, 1952

On the Frequency Dependence of the Viscosity of High Polymer Solutions

ROGER CERF*
Department of Chemistry, Cornell University, Ithaca, New York
(Received November 13, 1951)

The ultrasonic shear waves technique introduced by Mason offers the possibility of measuring the viscosity of a liquid in laminar flow at ultrasonic frequencies. A dilute high polymer solution exhibits, besides the usual shear viscosity, a shear elasticity as well for rather low frequencies (of the order of 10^5). A theory is given for infinitely dilute solutions using as a model for the chain molecule an elastic sphere. This model, which the author has used previously for the theory of flow birefringence, represents the limiting case of complete impermeability. The theory is compared with experimental results of Baker, Mason, and Heiss and of Rouse on polystyrene. The theory gives a good picture of the phenomena as a whole and is particularly successful in describing the apparently anomalous temperature dependence of the elasticity coefficient of polystyrene solutions at high frequencies. The interest of combining results on flow birefringence and on high frequency viscosity measurements is emphasized, as well as the possibilities of the latter technique for determining the molecular elasticity and internal viscosity as a function of frequency. On the basis of preliminary results for a sample of polystyrene of molecular weight 130,000, the tentative conclusion is given that the elastic sphere model will not have a quantitative significance for chains of such a low molecular weight and that it might be necessary to take into account the effect of permeation.

I. INTRODUCTION

1. Relaxation Process in Pure Liquids

MAXWELL[1] in 1867 predicted that an instantaneous shear distorsion in a liquid would have a relaxation time τ given by the formula

$$\tau=\eta/\mu, \tag{1}$$

where η is the shear viscosity and μ the shear elasticity. Therefore if liquids were sheared rapidly enough they would exhibit a shear elastic effect as well as a viscous effect.

A liquid subjected to an instantaneous strain may show elasticity just like a solid body. There is, however, a difference between the solid body and the liquid, namely that for the latter any stress will gradually disappear, the rate of disappearance depending on the viscosity of the medium. Maxwell supposes this rate proportional to the stress F and therefore arrives at the following equation:

$$dF/dt=\mu(dS/dt)-F/\tau, \tag{2}$$

where S is a strain of some kind which is here supposed to be a simple shear. The corresponding coefficient of elasticity then is the shear elasticity coefficient μ. If S is constant,

$$F=\mu Se^{-(t/\tau)}, \tag{3}$$

showing that F gradually disappears, the coefficient τ being the relaxation time of the process.

If dS/dt is constant, that is, if there is a steady motion of the body which continually increases the displacement

$$F=\mu\tau(dS/dt)+\text{const}\times e^{-(t/\tau)}, \tag{4}$$

showing that F tends to a constant value depending on the rate of displacement. The quantity $\mu\tau$, by which the rate of displacement must be multiplied in order to obtain the force is the ordinary coefficient of viscosity, and Eq. (1) is established.

Special attention will be given herein to periodic motions; their study will be made easier by the use of a *complex viscosity coefficient*. For a periodic motion with circular frequency ω, Eq. (2) may be written

$$F=[\eta/(1+i\omega\tau)](dS/dt);\quad i=\sqrt{-1}. \tag{5}$$

It replaces the conventional equation

$$F=\eta(dS/dt), \tag{6}$$

relating stress and rate of shear for a liquid at zero frequency.

In a more precise form, we may say that at the frequency ω the viscosity coefficient η has to be replaced in the hydrodynamic equations by the complex viscosity coefficient

$$\eta^*=\eta/(1+i\omega\tau). \tag{7}$$

This is because of the fact that the equations of hydrodynamics express the equilibrium between the frictional forces acting on an element of volume and the other forces such as pressure, inertial forces, body forces.

2. Behavior of Liquids and Polymer Solutions Undergoing Ultrasonic Shear Waves

The torsion crystal technique introduced by W. P. Mason[2] has made possible the measurement of the viscous and elastic properties of liquids in oscillatory shear gradient at ultrasonic frequencies. A cylindrical crystal cut from piezoelectric material, undergoing a twisting deformation about the cylinder axis is oscillated in the liquid. Highly attenuated waves are set up, extending under ordinary experimental conditions to a distance of a few hundredths of a millimeter. The radius of the cylinder can therefore be taken as infinite and the

* Rockefeller Fellow, 1951. Home address: Centre d'Etudes de Physique Macromoléculaire. Faculté des Sciences de Strasbourg, France.

[1] J. C. Maxwell, Phil. Trans. Roy. Soc. (London) **157**, 49 (1867).

[2] W. P. Mason, Trans. Amer. Soc. Mech. Eng. **69**, 359 (1947); J. Coll. Sci. **3**, 147 (1948).

hydrodynamic problem replaced by that of an infinitely extended plane yz oscillating parallel to itself.

This problem of laminar motion has been considered by Stokes. In the case of a simple harmonic motion, assuming a time factor $e^{i\omega t}$ and for a liquid extending to infinity in the direction of the x-positive perpendicular to the yz plane, the velocity u of a sheet at the distance x from the moving plane is given by the following formulas:

$$\left.\begin{aligned} u&=u_0e^{-(1+i)\beta x}\times e^{i\omega t}\\ \beta&=(\rho\omega/2\eta)^{\frac{1}{2}},\end{aligned}\right\}, \tag{8}$$

where u_0 is the maximum velocity of the plane yz and ρ the density of the liquid.

The length $l=\beta^{-1}$ is of great importance as indicating the extent to which the motion penetrates into the liquid; l is the length over which the velocity is attenuated by a factor of $e^{-1}=0.37$. For a liquid having a viscosity $\eta=0.015$ centipoise, a density $\rho=1$ g/cm^3 and for a frequency 2×10^4 cps, $l\sim5\times10^4$A.

The mechanical impedance Z_M of the liquid is readily shown to be

$$Z_M=R_M+iX_M=(1+i)[(\omega\rho\eta/2)^{\frac{1}{2}}], \tag{9}$$

where R_M and X_M are respectively the mechanical resistance per cm^2 and the mechanical reactance per cm^2. As a result of the liquid reaction the electrical resistance of the crystal is increased by an amount ΔR_E while the resonant frequency is reduced by an amount Δf. As shown by Mason[2] the experimentally determined quantities ΔR_E and Δf enable us to determine the mechanical resistance R_M and the mechanical reactance X_M.

If the viscosity of the liquid is a real quantity, the resistive and reactive part of the impedance are equal. However, if the liquid shows shear elasticity, that is if the viscosity is complex, R_M and X_M will no longer be equal. For ordinary light liquids the relaxation frequency $f_r=1/2\pi\tau$ as calculated by Frenkel[3] is of the order of magnitude of 10^{11} cps which is considerably above the capacity of any present day ultrasonic equipment. Indeed, for such liquids no departure from the ordinary viscous behavior was apparent within the accuracy of the method.[2] However, for very viscous liquids such as polymerized castor oil, Mason found that the resistive and reactive components are not equal, the resistance becoming progressively larger than the reactance at high frequencies. These liquids show the behavior expected when the viscosity is complex. Giving the viscosity in Eq. (9) the complex value (7), one obtains for the real coefficients η and τ the following formulas previously derived by Mason using the electrical analogy:[2]

$$\left.\begin{aligned} \eta&=(R_M^2+X_M^2)^2/(2R_MX_M\omega\rho)\\ \tau&=(R_M^2-X_M^2)/(2\omega R_MX_M).\end{aligned}\right\}. \tag{10}$$

If the liquid under study is a solution of long chain molecules, certain new significant effects appear. Long chain molecules are flexible and can take up many different configurations, some of which are more probable than others; and if a molecule is distorted, it tends to return to a more probable shape when the stress is removed, with a speed which determines the relaxation time of the process.

Long chain molecules liquids had previously been studied by means of other devices by various authors, in particular by Ferry.[4] As shown by Mason,[2] the shear viscosity η as well as the shear elasticity μ of polymer liquids can be determined by the torsion crystal technique. The improved precision recently obtained has made it possible to carry out similar measurements in dilute solutions of long chain molecules and to obtain results extrapolated to infinite dilution.[5,6] We therefore may expect to obtain in this way information about the mechanical properties of a single chain molecule.

For a solution of chain molecules, formula (9) cannot be applied without further attention because, due to the disturbances caused by the dissolved molecule, the motion is no more a purely laminar one, as in the case of a pure liquid. However, for the approximations we shall make in this paper, in the frequency range and for the molecular dimensions we shall consider, the solution will behave like an equivalent pure liquid having the same density ρ as the solvent but a complex viscosity η^*. For an infinitely dilute solution at a given frequency, we shall use a complex viscosity having the same form as that of a pure liquid: $\eta^*=\eta/(1+i\omega\tau)$. This particular form of the complex viscosity of the solution, which is chosen arbitrarily, is of secondary significance. The real coefficients η and τ, however, will depend on the concentration and the frequency in addition to the individual properties of the molecule. It will principally be our aim to find these relations, which will permit relating the experimentally determined quantities R_M and X_M to the molecular parameters.

The existence of a complex viscosity for a solution of chain molecules had first been found by Kirkwood[7] using the Kirkwood-Riseman model of a necklace with partial draining.[8] But there seems to be some difficulty in obtaining practically useful conclusions from the theory because of mathematical complexity, and therefore it seems reasonable to use simplified models, which may be suitable for understanding the essential features.

II. VISCO-ELASTIC PROPERTIES OF AN INFINITELY DILUTE SOLUTION OF ELASTIC SPHERES

3. The Molecular Model

For studying the streaming double refraction of high polymer solutions the author has recently used as a

[3] J. Frenkel, *Kinetic Theory of Liquids* (Oxford University Press, London, 1946).

[4] J. D. Ferry, Rev. Sci. Instr. **12**, 79 (1941); Ann. New York Acad. Sci. 44, 313 (1943).

[5] Baker, Mason, and Heiss (to be published in the J. Polymer Sci.)

[6] P. E. Rouse (private communication to the office of Rubber Reserve).

[7] J. G. Kirkwood, Proc. Int. Coll. Macromol. (Amsterdam, 1949), p. 133.

[8] J. G. Kirkwood and J. Riseman, J. Chem. Phys. **16**, 565 (1948).

model for the chain molecule a visco-elastic sphere characterized by the shear elasticity coefficient μ of Lamé and the internal viscosity η_i.[9] This model represents the limiting case of complete impermeability just as Einstein's rigid sphere[10] does in the Brinkman-Debye theory[11,12] of viscosity of high polymers. The predictions of the theory of flow birefringence of solutions of elastic spheres have been shown to be in qualitative agreement with experimental results on polystyrene solutions.[13]

The elastic sphere has also been shown to have in a steady flow velocity field with constant gradient a behavior somewhat similar to that of a liquid drop.[9]

The same model will be used here, with the assumption that the elastic sphere be made of incompressible material. This assumption was not made for the theory of flow birefringence, but even then the elastic sphere behaves as incompressible, since the velocity field to which it is subjected is free from cubic dilatation. The λ coefficient of Lamé therefore does not appear in either of these theories.

The solution will be supposed herein to be infinitely dilute. The pure liquid will be assumed to show no shear elasticity in the frequency range under investigation.

4. Approximations

(a) One of the fundamental assumptions in the previously mentioned work of Einstein, concerning the viscosity of a solution of rigid spheres, is that one can find a volume large compared with the dimensions of the molecule, over which the components of the velocity vary slowly enough so that only linear terms with respect to the space coordinates may be retained. In other words, the velocity gradient should be sufficiently constant over a distance d great compared with the diameter $2a$ of the molecule. For the particular motion[8] we are dealing with here, the velocity gradient G is given by the following formula:

$$G=\partial u/\partial x=-u_0(1+i)\beta[1-(1+i)\beta x+[(1+i)^2/2]\beta^2x^2+\cdots]e^{i\omega t}. \quad (12)$$

It may be considered as constant over a distance d such as

$$\beta d\ll 1. \quad (13)$$

With the numerical values chosen previously for ω, ρ, η_0 the length $l=\beta^{-1}$ is of the order of 5×10^4A. The preceding conditions thus require that $d\sim5\times10^3$A, $2a\sim5\times10^2$A. The diameter $2a$ of the molecule is about one-tenth of d, which itself is about one-tenth of l. This gives an idea of the approximation involved. Since the value 2×10^4 chosen for the frequency N is not the highest frequency used in the torsion crystal method (this highest value is about 10^5), a finer approximation may be necessary subsequently. However, the ideal conditions assumed to be fulfilled here could always be approached by increasing the viscosity of the solvent; this procedure would both increase l and lower the relaxation frequency f_r. The increase of viscosity can be easily obtained by decreasing the temperature.

The numerical value of the velocity gradient is of great significance since it enables us to calculate the amplitude of the periodic rotation of the molecule. The value of the velocity gradient depends on that of the amplitude u_0. A numerical example has been given by Mason[2] for the case of dimethyl-phtalate ($\eta_0=0.178$ poise, $\rho=1.186$). For a frequency $N=13{,}948$ the maximum linear velocity at the end of the torsion crystal was $u_0=1.13\times10^{-4}$ cm/sec, so that the maximum value G_0 of the velocity gradient was of the order of 10^{-1} sec^{-1}. Let us now suppose a rigid sphere to be suspended in such a liquid. The instantaneous angular velocity Ω of the sphere being $G/2$, the angular distance θ between the extreme positions attained by the sphere is G_0/Ω, and therefore θ is of the order of 5×10^{-6}. In other words the molecule undergoes an angular displacement which is only a very small fraction of a complete rotation.

Once having accepted the approximation of homogeneity of the velocity gradient over a distance great compared with the molecular dimensions, it is readily shown that all inertia terms may be neglected in calculating the viscosity of the solution. For example, a rigid sphere, with the previously considered diameter of 5×10^2A could be considered as following both the translation and the rotation of the fluid with an approximation far better than that we have just accepted (phase shift of the order of 7×10^{-5} for the translation, of the order of 2×10^{-5} for the rotation); also the disturbances resulting from the inertia term $\rho(\partial\mathbf{u}/\partial t)$ in the hydrodynamic equations are not significant here, and these terms will be omitted below in Eqs. (15) and (16).

As a consequence of the assumption that we may find an element of volume $\mathfrak{V}$ great compared with the dimensions of the molecule over which the gradient is constant, we shall also be able to replace the solution by an equivalent pure liquid. At the surface of $\mathfrak{V}$ the disturbance of the velocity caused by the presence of the molecule can be neglected. For a macromolecule in which the concentration of segments is ordinarily of the order of 1–2 percent it is reasonable to assume a specific weight equal to that of the surrounding liquid. Thus the center of gravity of the volume $\mathfrak{V}$ moves as if this volume consisted of pure liquid. Since the velocity gradient can be considered as constant over $\mathfrak{V}$, elements like $\mathfrak{V}$ may be taken as infinitely small elements of a pure liquid subjected to the velocity field (8). It follows immediately that for an infinitely dilute solution formula (9) is still valid. It only remains to calculate the complex viscosity of the solution.

[9] R. Cerf, J. chim. phys. **48**, 59 (1951).
[10] A. Einstein, Ann. Physik **19**, 289 (1906); **34**, 591 (1911).
[11] H. C. Brinkman, Proc. Acad. Sci. Amsterdam **50**, No. 6 (1947); App. Sci. Res. **A1**, 27 (1947).
[12] P. Debye and A. M. Bueche, J. Chem. Phys. **16**, 573 (1948).
[13] R. Cerf, J. chim. phys. **48**, 85 (1951); J. Coll. Sci. **6**, 293 (1951).

(b) For molecules of the dimensions here considered the usual question of the influence of configurations deviating from the mean form arises. In order to study the effect of these configurations one may represent the chain molecule as has been done for the theory of streaming double refraction[9] by a sphere and a series of spheroids instead of a single sphere. Let us denote by $a=a_0(1+d)$ any one of the principal axes of one of the preceding spheroids, a_0 being the radius of the undeformed sphere. It has been shown[9] that the mean square value of the coefficient d is related to the elasticity coefficient μ by the formula

$$\bar{d}^2=kT/3v\mu, \tag{14}$$

where v is the volume of the molecule, k Boltzmann's constant, and T the absolute temperature. For the samples of polystyrene for which μ has been measured (molecular weight of the order of 150,000 and 200,000), $\bar{d}^2$ is of the order of 0.06. Since the specific viscosity of a suspension of ellipsoids of revolution is a parabolic function of the axial ratio p and varies only slightly when p is about equal to one (variation of a few percent of the specific viscosity as long as $p<2$), it seems reasonable as a first approximation to neglect the effect of elongated configurations. It should also be noted that since the molecules undergo only an extremely small rotation in the ultrasonic field, no preferential orientation of elongated configurations occurs.

5. Visco-Elastic Properties of the Solution[14]

The problem of finding the velocity inside the molecule as well as outside is now reduced to integrating with the proper boundary conditions at the surface of the particle the following system of equations.

(a) Outside the molecule:

$$\left.\begin{aligned}\eta_0\Delta\mathbf{u}&=\mathbf{gradp}\\ \mathrm{div}\mathbf{u}&=0\end{aligned}\right\}; \tag{15}$$

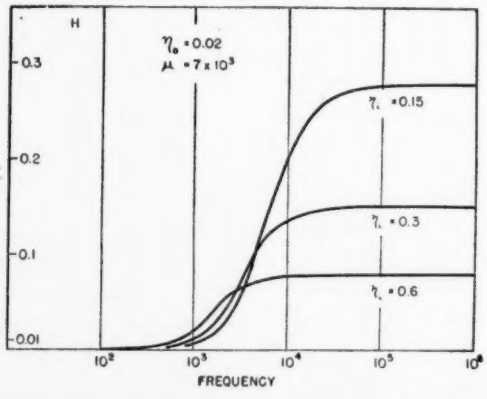

FIG. 1. Behavior of the specific viscosity as a function of the frequency. H for given values of μ and η_0 and different values of η_i.

[14] R. Cerf, Compt. rend. **233**, 1099 (1951).

(b) Inside the incompressible molecule:

$$\left.\begin{aligned}\eta_i\Delta\mathbf{u}+\mu\Delta\boldsymbol{\sigma}&=0\\ \mathrm{div}\boldsymbol{\sigma}&=0\end{aligned}\right\}, \tag{16}$$

where $\boldsymbol{\sigma}$ is the displacement inside the molecule. Since $\Delta\mathbf{u}=(d/dt)\Delta\boldsymbol{\sigma}$ for a periodic motion, the system (16) can also be written:

$$\left.\begin{aligned}\eta_i^*\Delta\mathbf{u}&=0\\ \mathrm{div}\mathbf{u}&=0\end{aligned}\right\}, \tag{17}$$

with

$$\eta_i^*=\eta_i+(\mu/i\omega). \tag{18}$$

At the surface of the particle we shall write the usual boundary conditions, namely the continuity of the velocity as well as that of the stress. As soon as the velocity is known the viscosity of the solution is easily calculated along familiar lines.

For solving a problem concerning the behavior of liquid drop subjected to a laminar flow, G. I. Taylor[15] has determined a velocity distribution which precisely obeys the conditions here required. The system of equations was both inside and outside the molecule identical to the system (15), the viscosity being replaced inside the particle by the viscosity η' of the drop. G. I. Taylor showed that, as long as small deformations are concerned, the term **gradp** vanishes inside the drop. Consequently the solution obtained by G. I. Taylor is also the solution of our problem, provided the viscosity η' of the drop be replaced by the complex viscosity (18).

The condition that the deformation of the molecule be small is automatically fulfilled at small frequencies. At high frequencies it is satisfied by making the additional assumption the real part η_i of the internal complex viscosity be great compared with η_0. At very high frequencies the external form of the molecule is time independent and the principal axes of the deformed molecule are respectively parallel and perpendicular to the direction of propagation of the shear waves.

The viscosity of the solution is readily deduced from G. I. Taylor's calculations for the case where the internal viscosity is a real quantity. The viscosity η_s of an infinitely dilute solution is given by the following formula:

$$\eta_s=\eta_0\left[1+2.5c\frac{\eta'-\eta_0}{\eta'+1.5\eta_0}\right], \tag{19}$$

where c is the volume concentration of the solution.

Giving η' the complex value (18), the viscosity η_s becomes a complex quantity η^* to which we may give the form (7) and deduce the corresponding values of the real coefficients η and τ; η, of course, differs only slightly from η_0, so that we may define a real specific viscosity

$$(\eta_{sp})_{real}=\frac{\eta-\eta_0}{\eta_0}=2.5c\left[1-2.5\frac{\eta_0(\eta_i+1.5\eta_0)\omega^2}{\mu^2+(\eta_i+1.5\eta_0)^2\omega^2}\right]. \tag{20}$$

[15] G. I. Taylor, Proc. Roy. Soc. (London) **A146**, 501 (1934).

The relaxation time τ is given by the following formula:

$$\tau = 6.25c\frac{\mu\eta_0}{\mu^2+(\eta_i+1.5\eta_0)^2\omega^2}. \quad (21)$$

Since τ is proportional to the concentration c of the solution, the coefficient η in the formula (7) is also here in first approximation the real part of η^* as well as the absolute value of η^*.

One will notice that the radius of the particle does not appear in formulas (20) and (21).

Formula (20) shows that for $\omega=0$ the intrinsic viscosity is equal to $[\eta]_E=2.5$, which is Einstein's value for a solution of rigid spheres. This zero-frequency or steady-flow viscosity can be measured by means of a capillary tube. For increasing ω the real part of the intrinsic viscosity $[\eta]_{\text{real}}$ decreases. We may write

$$\frac{[\eta]_{\text{real}}}{[\eta]_E}=1-H, \quad (22)$$

where the term H has the following value:

$$H=2.5\frac{\eta_0(\eta_i+1.5\eta_0)\omega^2}{\mu^2+(\eta_i+1.5\eta_0)^2\omega^2}. \quad (23)$$

For large values of ω, H tends towards the limiting value

$$H_{\omega=\infty}=2.5\frac{\eta_0}{\eta_i+1.5\eta_0}, \quad (24)$$

which is smaller than one, since we have assumed η_i to be great compared with η_0.

On the other hand, the relaxation time τ, which for small concentrations c is proportional to c, tends toward zero for very high frequencies; in other words, for very high frequencies the behavior of the solution approaches that of a pure liquid. For very small values of ω the ratio τ/c tends toward the limit

$$(\tau/c)_{\omega=0}=6.25(\eta_0/\mu). \quad (25)$$

Although the coefficients μ and η_i will usually depend on the frequency, we shall give for purposes of illustration the curves for the case where μ and η_i are frequency independent, that is to say, for the case of a single retardation process. Figure 1 shows the behavior of the term H with respect to the frequency for given values of μ and η_0 and different values of the internal viscosity η_i. Figure 2 shows the corresponding τ curves. The frequency range on both figures has been limited to an upper value such as $\omega=10^6$.

The frequency of the inflexion point both for the H curve and the τ curve is given by

$$\omega_f=\frac{1}{\sqrt{3}}\frac{\mu}{\eta_i+1.5\eta_0}. \quad (26)$$

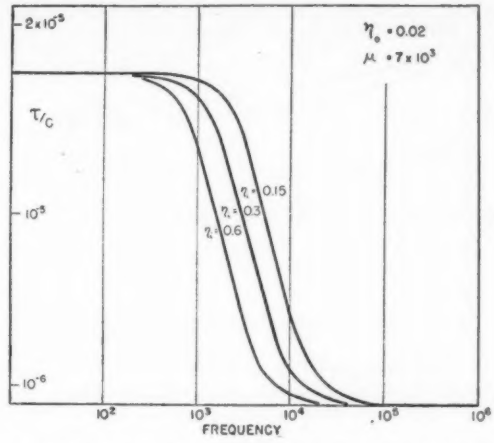

FIG. 2. Behavior of the relaxation time as a function of the frequency. τ/c for given values of μ and η_0 and different values of η_i.

Some important conclusions may be drawn from Eqs. (20) and (21).

(a) These formulas allow us to determine for each value of the frequency the molecular parameters μ and η_i. One will remember that streaming double refraction measurements also allowed one to determine these coefficients[9,13] but only for the case when $\omega=0$. There is obviously a great advantage of combining the information obtained by both techniques, ultrasonic shear waves and streaming double refraction; this point will be discussed in more detail in the following section.

(b) The formula (21) shows that the temperature dependence of the elasticity coefficient μ_s of the solution is reversed at high frequencies. Indeed, writing $\nu=\eta_i+1.5\eta_0$ we can deduce from (21) that

$$d\mu_s/dt=1/6.25c\mu^2[(\mu^2-\nu^2\omega^2)(d\mu/dT)+2\mu\nu\omega^2(d\nu/dT)]. \quad (27)$$

Assuming μ to be proportional to T and ν to be of the form

$$\nu=\text{const}\times e^{-\alpha T}, \quad (28)$$

where α is a constant, it is seen that at the temperature T, $d\mu_s/dt=0$ for

$$\omega=\mu/\nu(1+2\alpha T). \quad (29)$$

For low frequencies, when $\omega<\mu/\nu(1+2\alpha T)$, $(d\mu_s/dT)>0$. For high frequencies, when $\omega>\mu/\nu(1+2\alpha T)$, $(d\mu_s/dT)<0$. In other words one would expect the elasticity coefficient μ_s of the solution to show at high frequencies an apparently abnormal temperature dependence, that is to say to decrease when the temperature increases.

III. COMPARISON WITH EXPERIMENTS

6. Qualitative Comparison

The comparison between theory and experiments will be carried out on the basis of the previously mentioned

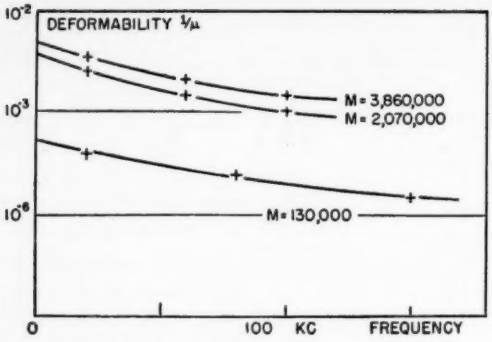

FIG. 3. Deformability $1/\mu$ of polystyrene as a function of frequency and molecular weight. Molecular coefficient calculated by formula (32) from data of Rouse and of Baker, Mason, and Heiss.

results of Baker, Mason, and Heiss[5] and of Rouse.[6] The whole of the experimental results is in qualitative agreement with the preceding theory.

(a) The curves in Figs. 1 and 2 give qualitatively the right frequency dependence of $[\eta]_{real}$ and τ/c, that is to say, a decrease of $[\eta]_{real}$ as well as of τ/c when the frequency increases. The dispersion occurs in a frequency range which is not out of reason considering the numerical values of μ and η_i obtained for polystyrene by means of streaming double refraction measurements.[13] This point, however, will be discussed in more detail in Sec. 8.

(b) The experiments show that the elasticity coefficient of the solution calculated according to formulas (10) and (1) indeed increases very rapidly when the concentration decreases, at least in the field of small concentrations, according to formula (21).

(c) One would expect the molecular coefficient μ to be the factor mainly affected by changes in molecular weight and in solvent power in the expression of the term H (formula (23)); also μ should decrease both when the molecular weight increases and the solvent power increases. Therefore one would expect H to increase, that is to say, the solution to depart more and more from the ordinary viscous behavior as the molecular weight increases or the solvent power increases, which the experiments indeed show.

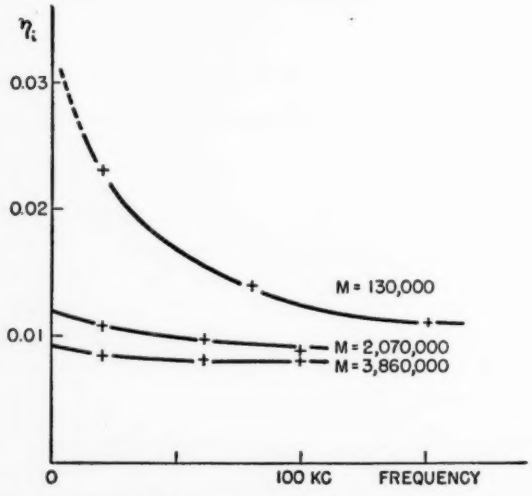

FIG. 4. Internal viscosity η_i of polystyrene as a function of frequency and molecular weight (molecular coefficient calculated by formula (33) from data of Rouse and of Baker, Mason, and Heiss).

The temperature dependence of the elasticity coefficient μ_s of the solution will be examined in full detail in Sec. 8.

7. Determination of the Molecular Coefficients μ and n_i

The assumption previously made of a complete impermeability of the coil means that the steady flow viscosity is given by the formula of Einstein for a solution of rigid spheres.[10] The volume concentration c of the solution can thus be obtained from the steady flow viscosity, and the formulas (20) and (21) then allow us to calculate from the experimentally determined quantities the molecular coefficients μ and η_i for each value of the frequency. Putting

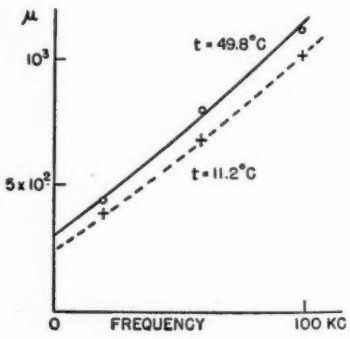

FIG. 5. Elasticity coefficient μ for polystyrene $(B+C)$ as a function of frequency and temperature (molecular coefficient calculated by formula (32) from data of Rouse).

$$r=\frac{1}{6.25\eta_0}(\tau/c)_{c=0}, \tag{30}$$

$$s=\frac{(H)_{c=0}}{2.5\eta_0\omega^2}, \tag{31}$$

μ and $\nu=\eta_i+1.5\eta_0$ are given by the following formulas:

$$\mu=\frac{r}{r^2+\omega^2 s^2}, \tag{32}$$

$$\nu=\frac{s}{r^2+\omega^2 s^2}. \tag{33}$$

These formulas will be used for interpreting the results of P. E. Rouse,[6] who has investigated among other polymers four samples of polystyrene dissolved in toluene designated as $(B+C)$, (A_2), (A), (A_1). The molecular weight determined from viscosity measurements is, respectively, 2,070,000, 2,570,000, 3,800,000,

and 6,860,000. Polymers (A_1) and (A_2) are fractions. The measurements were carried out at two temperatures: 11.2°C and 49.8°C. The results are expressed by means of a modified Maxwell element, that is to say, the complex viscosity of the solution is expressed in the form

$$\eta^*=\eta_\infty+[\eta_m/(1+i\omega\tau)]. \tag{34}$$

Before using formulas (30)–(33) we have therefore made a transformation so as to express the data by means of an ordinary Maxwell element according to Eq. (7).

Rouse has carefully investigated the concentration dependence of the effect. The quantity τ/c involved in Eq. (30) appears to be particularly difficult to extrapolate to zero concentration. The extrapolated value is, however, quite reliable for sample $(B+C)$ at both temperature 11.2°C and 49.8°C and for sample (A_2) and (A) at 11.2°C.

Figures 3 and 4 show respectively the behavior of $1/\mu$ and η_i with the frequency for samples $(B+C)$ and (A) at 11.2°C. On the same figure are reported results of Baker, Mason, and Heiss[16] on polystyrene of molecular weight 130.000. This sample, designated as P_{III}, is the one the author of this paper has previously studied by means of streaming double refraction measurements.[13] The results, which have been obtained at 30°C using benzene as a solvent, will be discussed in detail in Sec. 9.

The coefficient μ appears to increase with the frequency while η_i is rather frequency independent for polymers $(B+C)$ and (A) and decreases when the frequency increases for polymer P_{III}. The fact that the coefficient μ is frequency dependent is evidence for a distribution of retardation processes. It is believed that giving the frequency dependence of the molecular coefficients will be a convenient way of expressing the existence of such a distribution.

The deformability $1/\mu$ increases when the molecular weight increases, while the internal viscosity decreases as the molecular weight increases.

Figures 5 and 6 show the μ and η_i values for polymer $(B+C)$ at both temperatures 11.2°C and 49.8°C. The coefficient μ increases, while the coefficient η_i decreases for increasing temperature. It can be seen that the zero frequency value of η_i does not seem to depend very much on the frequency. Since the zero frequency value of η_i is that which is obtained by streaming double refraction measurements (see Sec. 9), this last conclusion gives some support to the assumption we had made for interpreting flow birefringence data, i.e., η_i is as a first approximation temperature independent.[13]

8. Temperature Dependence of the Elasticity Coefficient μ_s of the Solution

The prediction of the theory concerning the apparently anomalous temperature dependence of μ_s at high frequencies is illustrated in Fig. 7 which gives the $(c\mu_s)_{c=0}$ values for polymer $(B+C)$ deduced from the data of Rouse. Indeed at high frequencies the coefficient μ_s is a decreasing function of the temperature.

[16] Baker, Mason, and Heiss (personal communication).

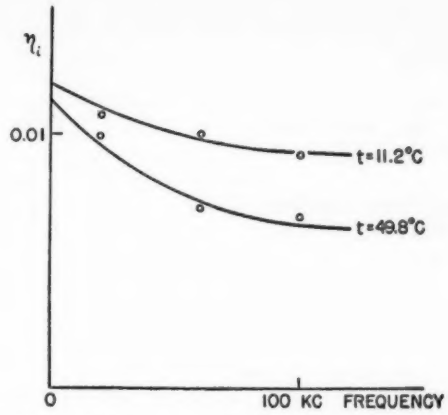

FIG. 6. Internal viscosity η_i for polystyrene $(B+C)$ as a function of frequency and temperature (molecular coefficient calculated by formula (33) from data of Rouse).

Figure 5 on the other hand, shows that over the whole range of frequencies the molecular coefficient μ has apparently a normal behavior. From Fig. 5 a reasonable zero frequency value of this coefficient at 11.2°C and 49.8°C can be obtained. Formula (25) then gives the value of the coefficient μ_s for the solution at zero frequency, where it has a normal behavior, that is to say increases when the temperature increases. The zero frequency values of $(c\mu)_{c=0}$ are also given in Fig. 7.

Although it is difficult to draw curves since few experimental points are available, one can obtain a tentative value for the frequency at which both curves corresponding to the temperature 11.2°C and 49.8°C should cut each other. This frequency, which is about $N=900$ cps seems to correspond well to the theoretical one evaluated on the basis of formula (27). The coefficient α appearing in that formula is easily evaluated from the experimental data. The question as to whether

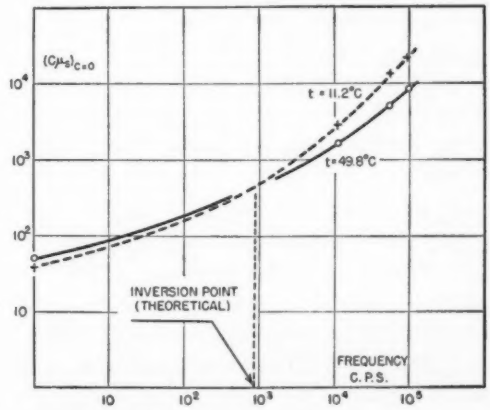

FIG. 7. Behavior of the elasticity coefficient μ_s of the solution as a function of frequency and temperature for polystyrene $(B+C)$ (from data of Rouse).

TABLE I. The μ and η_i values for polystyrene P_{III}.

Method	Solvent	Temperature	μ	η_i
Flow birefringence	cyclohexanone	20°C	7×10^3	0.3
Ultrasonic shear waves	benzene	30°C	2×10^3	0.035

this coincidence between theory and experiments is significant will have to be reinvestigated as soon as data are available for lower frequencies.

9. Comparison with Flow Birefringence Measurements

Flow birefringence measurements provide a method for determining the coefficients μ and η_i in a steady flow at zero frequency from the zero gradient behavior of the extinction angle of the solution.[13]

If the elastic sphere model has a quantitative significance for chain molecules, the values of μ and η_i thus obtained must coincide with those one can deduce from shear waves measurements by extrapolating to zero frequency. The previously mentioned results of Baker, Mason, and Heiss[16] on the polystyrene sample P_{III} allow a comparison which, however, has a very tentative character because of the following reasons: (a) The sample P_{III} is not fractionated. (b) It has not been possible so far to use in the ultrasonic measurements the solvent which had been used in the streaming double refraction measurements (cyclohexanone). (c) The ultrasonic measurements were carried out only at one concentration, namely 1 percent. However, according to Baker, Mason, and Heiss one can extrapolate linearly to zero concentration the experimentally determined quantities R_M and X_M for a polymer of such low molecular weight.

While the extrapolation to zero frequency of μ seems to be rather reliable, the extrapolation for η_i is more difficult. The resultant zero frequency values of μ and η_i are tabulated herein together with the values obtained by means of flow birefringence measurements.

Since benzene is a better solvent than cyclohexanone, it is not surprising to obtain lower values both for μ and η_i, when using benzene. However, the gap for the η_i values seems hard to explain on that basis. Considering the previously mentioned tentative character of the present comparison we shall draw from these experiments only very preliminary conclusions, namely that theories based on the elastic sphere model lead to the right order of magnitude of the molecular coefficients, but do not have a quantitative value, at least for low molecular weights, of the order of a few hundred thousand.

At high frequencies there are some limitations to the presented theory which concern the inertia terms and the relative magnitude of the internal viscosity η_i and the solvent viscosity η_0 (see Secs. 4 and 5). These limitations, however, cannot be responsible for the lack of agreement, since we are dealing with the zero frequency values of the molecular coefficients. It seems, therefore, that the model itself is insufficient, at least for low molecular weights. This is not an unexpected conclusion, and it would seem desirable to take into account the permeation effect using, for example, the Brinkman-Debye model.[11,12]

IV. CONCLUSIONS

(1) The present theory for the frequency dependence of the viscosity of dilute solutions of elastic spheres, which represents for solutions of chain molecules the limiting case of complete impermeability, gives a good qualitative representation of all the experimental results on ultrasonic shear waves. This theory seems in particular to provide an explanation for the apparently anomalous temperature dependence of the elasticity coefficient of dilute solutions at high frequencies.

(2) It is of great interest to combine results of high frequency viscosity and flow birefringence measurements, since they should, in the ideal case of elastic spheres, lead to the determination of both the μ elasticity coefficient and the internal viscosity of the particle. While flow birefringence measurements only lead to the zero frequency values of these coefficients, measurements by ultrasonic shear waves give them as a function of frequency, thus providing method of great value for investigating the mechanical properties of high polymers.

(3) For polystyrene the μ elasticity coefficient increases rapidly with the frequency, showing the existence of a distribution of retardation processes.

(4) On the basis of preliminary measurements of high frequency viscosity and of flow birefringence on a sample of polystyrene of molecular weight 130.000, it is seen that the elastic sphere model leads to an order of magnitude for the molecular coefficients which is not out of reason. However, it seems likely that this model will not have a quantitative significance for a chain molecule of such low molecular weight. This quite expected conclusion, if confirmed, will make it desirable to take into account the effect of permeation.

ACKNOWLEDGMENT

The author wishes to express his deepest gratitude to Professor Peter Debye for invaluable advice, inspiring talks, and for the charming hospitality at his laboratory.

The Rockefeller grant which made possible the trip to America and sojourn at Cornell University is gratefully acknowledged.

Thanks are also expressed to Doctors Baker, Mason, and Heiss who have kindly carried out ultrasonic shear waves measurements on polystyrene P_{III} with the equipment of the Bell Telephone Laboratories, and given permission to quote the results.

The Pyrolysis of *n*-Propyl-Benzene and the Heat of Formation of Ethyl Radical

C. H. LEIGH AND M. SZWARC
Chemistry Department, University of Manchester, Manchester 13, England
(Received August 14, 1951)

The investigation of the pyrolysis of *n*-propyl-benzene by the "toluene carrier" technique revealed that this compound decomposes initially into benzyl and ethyl radicals:

$$C_6H_5\cdot CH_2\cdot C_2H_5 \rightarrow C_6H_5\cdot CH_2\cdot + C_2H_5.$$

Ethyl radicals decompose rapidly into ethylene and hydrogen atoms. The hydrogen atoms reacting with toluene produce H_2 or CH_4. The rate of the initial dissociation process can be measured by the rate of formation of C_2 hydrocarbons.

It was shown that the decomposition is a homogeneous, first-order gas reaction. The activation energy was estimated at 57.5 kcal/mole, the frequency factor at 3.10^{12} sec^{-1}. It appears that the activation energy is equal to $D(C_6H_5\cdot CH_2-C_2H_5)$. Since the heat of formation of benzyl radicals is known, the estimation of $D(C_6H_5\cdot CH_2-C_2H_5)$ leads to the value for the heat of formation of ethyl radicals, i.e.,

$$\Delta H_f(C_2H_5)\approx 22 \text{ kcal/mole}.$$

The latter value makes it possible to evaluate various relevant bond dissociation energies, i.e., $D(C_2H_5-H)$ $\approx 94\pm 4$ kcal/mole.

THE purpose of this paper and of the following one is to report our experimental results, which enable us to estimate the C—H bond dissociation energies in some simple aliphatic hydrocarbons. The method used in these studies has been reported elsewhere,[1] and consequently we are giving here only a brief account of the principles involved.

One way in which the R—H bond dissociation energy might be determined involves the investigation of the pyrolysis of a derivative of R, namely $C_6H_5\cdot CH_2\cdot R$. Since the resonance energy of benzyl radicals is large, one might expect that the $C_6H_5\cdot CH_2-R$ bond would be the weakest one in the molecule $C_6H_5\cdot CH_2\cdot R$. Consequently, the pyrolysis of such a compound would result in the rupture of the $C_6H_5\cdot CH_2-R$ bond, i.e.,

$$C_6H_5\cdot CH_2\cdot R \rightarrow C_6H_5\cdot CH_2\cdot + R\cdot. \qquad (1)$$

In the presence of an excess of toluene, reaction (1) might be followed by a fast reaction (2)

$$C_6H_5\cdot CH_3 + R\cdot \rightarrow C_6H_5\cdot CH_2\cdot + RH, \qquad (2)$$

which would remove radicals R as rapidly as they were formed. Under these conditions, the rate of formation of RH would measure the rate of the initial dissociation process (1).

The mechanism of decomposition suggested above has indeed been verified on several occasions; e.g., the pyrolysis of ethylbenzene[2] appears to proceed according to the equation

$$C_6H_5\cdot CH_2\cdot CH_3 \rightarrow C_6H_5\cdot CH_2\cdot + CH_3\cdot,$$

the latter dissociation process being followed by the reaction

$$C_6H_5\cdot CH_3 + CH_3\cdot \rightarrow C_6H_5\cdot CH_2\cdot + CH_4.$$

Similarly, the pyrolysis of benzyl-amine[3] appears to be correctly described by the equations

$$C_6H_5\cdot CH_2\cdot NH_2 \rightarrow C_6H_5\cdot CH_2\cdot + NH_2\cdot,$$

and

$$C_6H_5\cdot CH_3 + NH_2\cdot \rightarrow C_6H_5\cdot CH_2\cdot + NH_3.$$

These results imply, therefore, that one might determine the $C_6H_5\cdot CH_2-R$ bond dissociation energy by measuring the activation energy of the pyrolysis of $C_6H_5\cdot CH_2\cdot R$ in an excess of toluene. Having obtained the value for $D(C_6H_5\cdot CH_2-R)$ one proceeds to calculate the heat of formation of radical R, $\Delta H_f(R)$, by making use of the relationship,

$$D(C_6H_5\cdot CH_2-R)=\Delta H_f(C_6H_5\cdot CH_2) + \Delta H_f(R)-\Delta H_f(C_6H_5\cdot CH_2\cdot R).*$$

The evaluation of $\Delta H_f(R)$ makes it possible to calculate the required R—H bond dissociation energy by applying the equation

$$D(R-H)=\Delta H_f(R)+\Delta H_f(H)-\Delta H_f(R\cdot H).$$

In the present investigation the method described above has been used for determining the C—H bond dissociation energy in ethane. We studied the pyrolysis of *n*-propyl-benzene, using toluene as carrier gas. It seems that *n*-propyl-benzene decomposes into benzyl and ethyl radicals.†

$$C_6H_5\cdot CH_2\cdot C_2H_5 \rightarrow C_6H_5\cdot CH_2\cdot + C_2H_5\cdot. \qquad (3)$$

However, at the high temperatures (above 600°C) in

[1] M. Szwarc, Chem. Revs. **47**, 75 (1950); Proc. Roy. Soc. (London) **A207**, 5 (1951).
[2] M. Szwarc, J. Phys. Chem. **17**, 431 (1949).
[3] M. Szwarc, Proc. Roy. Soc. (London) **A198**, 285 (1949).

* $\Delta H_f(C_6H_5\cdot CH_2)$—i.e., the heat of formation of benzyl radicals, has been estimated at 37.5 kcal/mole by investigating the pyrolysis of toluene (see e.g., reference 1). The heat of formation of $C_6H_5\cdot CH_2\cdot R$ can be obtained by the standard thermochemical methods.

† A similar conclusion might be drawn from the results of pyrolysis of *n*-propyl-benzene investigated by A. Dobryanskii, Chem. Abstracts **31**, 5334 (1937).

TABLE I. Analysis of the C_2 fraction.

Run	P_{C_2} mm Hg	P_{H_2} used in hydrogenation mm Hg	C_2H_4 / C_2 hydrocarbons
8	37	33	0.90
9	48	38	0.80
10	39	33	0.85
11	136	137	1.00
13	110	112	1.00
44 P	85	76	0.90
45 P	31	30	0.97
47 P	33	29	0.88

which our experiments have been carried out, ethyl radicals do not appear to react with toluene according to Eq. (2) but rather to decompose according to Eq. (4),

$$C_2H_5\cdot \rightarrow C_2H_4+H. \quad (4)$$

This behavior of ethyl radicals is not at all surprising in view of the very low dissociation energy of the C−H bond in the ethyl radical[1] $D(\cdot CH_2\cdot CH_2-H)\sim 40$ kcal/mole, and indeed similar observations have been reported recently by Bywater and Steacie.[4]

Hydrogen atoms, produced in reaction (4), seem to react rapidly with toluene, and the previous studies by one of us[5] suggest that the following reactions take place:

$$C_6H_5\cdot CH_3+H\rightarrow C_6H_5\cdot CH_2\cdot +H_2 \quad (5)$$

and

$$C_6H_5\cdot CH_3+H\rightarrow C_6H_6+CH_3\cdot, \quad (6)$$

followed by

$$C_6H_5\cdot CH_3+CH_3\cdot \rightarrow C_6H_5\cdot CH_2\cdot +CH_4. \quad (7)$$

This mechanism of pyrolysis of *n*-propyl-benzene requires therefore that one mole of $C_6H_5\cdot C_3H_7$ decomposed should produce one mole of ethylene, one mole of H_2 or CH_4, and one mole of dibenzyl. The experimental evidence seems to support these conclusions. The pyrolysis of *n*-propyl-benzene produced C_2 hydrocarbons, and hydrogenation of the latter proved it to be composed mainly of ethylene (see Table I). In addition to the C_2 hydrocarbons, permanent gases composed of H_2 and methane were formed in the pyrolysis, their amounts corresponding roughly to the required molar proportion of one C_2H_4 for one H_2+CH_4 (see Table II).

Previous studies of the pyrolysis of toluene[5] indicated that the molar ratio of hydrogen to methane produced by reactions (5) and (6) should be approximately 6:4 (i.e., about 60 percent of hydrogen should be present in the mixture of H_2+CH_4 formed in the pyrolysis). Also this conclusion seems to be confirmed by our results (see Table III). Finally, the formation of dibenzyl proves beyond any doubt that the pyrolysis of *n*-propyl benzene occurs via a radical split.

The significance of the formation of dibenzyl in this reaction becomes evident when one compares the results of the pyrolysis of *n*-propyl-benzene with those obtained by us for the pyrolysis of ethyl-bromide. These experiments have been carried out under the same experimental conditions as those performed with *n*-propyl-benzene. The products were ethylene and HBr accompanied by minute quantities of dibenzyl and permanent gases (see Table IV). It seems therefore that the pyrolysis of ethyl bromide takes place mainly by the molecular decomposition

$$C_2H_5\cdot Br\rightarrow C_2H_4+HBr,$$

the latter being accompanied to a very small extent by the radical decomposition

$$C_2H_5\cdot Br\rightarrow C_2H_5\cdot +Br.$$

We have to consider now the two possible deviations from the scheme suggested above. The analysis of the C_2 hydrocarbons fraction does indicate the presence of small amounts of ethane (see Table I), and the molar ratio of $(H_2+CH_4)/(C_2$ hydrocarbons) is slightly smaller than the predicted value of 1. Both these ob-

TABLE II.

Exp.	T°K	$(H_2+CH_4)/C_2H_4$	Exp.	T°K	$(H_2+CH_4)/C_2H_4$
30	887	0.82	27	940	0.94
26	888	1.13	16	943	0.89
25	889	0.82	12	944	0.87
31	891	0.99	13	945	0.83
29	893	0.91	28	947	0.91
47 P	900	0.95	8	948	0.99
23	904	0.72	40	949	0.91
21	906	0.90	32	956	0.91
43	912	1.50 (?)	6	969	0.88
41	917	0.97	9	969	0.91
24	918	0.96	17	984	0.83
42	920	0.97	18	987	0.84
22	921	1.00	33	987	0.89
39	927	0.92	34	1000	0.83
44 P	927	0.86	7	1004	0.54 (?)
14	930	0.96	37	1005	0.77
10	932	1.05	38	1017	0.80
11	935	0.91	36	1019	0.81
45 P	937	0.86	35	1036	0.80
15	938	0.90			

TABLE III.

Run	T°K	$H_2/(H_2+CH_4)$
30	887	0.60
41	917	0.60
42	920	0.61
39	927	0.60
44 P	927	0.58
14	930	0.52 (?)
10	932	0.59
45 P	937	0.59
13	945	0.61
8	948	0.27 (?)
40	949	0.55
6	969	0.64
9	969	0.70
7	1004	0.60

[4] S. Bywater and E. W. R. Steacie, J. Chem. Phys. **19**, 326 (1951).
[5] M. Szwarc, J. Chem. Phys. **16**, 128 (1948).

servations suggest that a small fraction of ethyl radicals, produced in the initial dissociation process, react with toluene according to Eq. (8)

$$C_6H_5\cdot CH_3+C_2H_5\cdot\rightarrow C_6H_5\cdot CH_2\cdot+C_2H_6. \quad (8)$$

The extent of reaction (8) can be estimated by the following calculations. The activation energy of reaction (8) might be taken at 8–10 kcal/mole by analogy with the value of E for the reaction $C_6H_5\cdot CH_3+CH_3\cdot\rightarrow C_6H_5\cdot CH_2\cdot+CH_4$,[6] its temperature independent factor being most probably of the order of 10^{11} cc/moles sec.[7] The concentration of toluene is of the order of 3.10^{-7} mole/cc, the temperature about 900°–1000°K, and, therefore, the rate of reaction (8) appears to be of the order of $10^2\cdot[C_2H_5]$ moles/cc sec. On the other hand, the rate of the unimolecular decomposition of ethyl radicals, i.e., the rate of reaction (7), is most likely given by the expression $\sim 10^{13}\exp(40{,}000/RT)\cdot[C_2H_5]$ moles/cc sec,‡ i.e., it appears to be of the order of $10^3[C_2H_5]$ moles/cc sec. It seems, therefore, that a few percent of ethyl radicals would react according to Eq. (8), and this proportion might be sufficient to account for the amount of ethane observed and for the values of the ratio $(H_2+CH_4)/(C_2$ hydrocarbons) listed in Table II.

TABLE IV. Pyrolysis of ethyl-bromide.

T°K	P_{total} mm Hg	$P_{C_2H_5Br}$ mm Hg	HBr / C_2H_5Br	C_2H_4 / C_2H_5Br	Dibenzyl / C_2H_5Br	(H_2+CH_4) / C_2H_5Br
906	13.1	2.44	···	0.71	0.0012	0.0087
941	12.9	2.39	0.83	···	···	0.012
978	13.0	2.41	···	0.80	0.0054	0.018

One has to consider also the possibility of disproportionation of ethyl radicals. Their rate of formation is given by the rate of reaction (3), and the rate of their disappearance is probably 10^3–$10^4[C_2H_5\cdot]$ moles/cc sec (computed from the preceding calculations). The concentration of n-propyl-benzene is about 10^{-8} mole/cc, and thus the stationary concentration of ethyl radicals appears to be of the order 10^{-11}–10^{-12} mole/cc. If the activation energy for disproportionation is zero and the temperature independent factor even as high as 10^{12}–10^{13} cc/moles sec then only a few percent of ethyl radicals might undergo disproportionation.

KINETICS

The above discussion convinces us that the rate of initial dissociation (3) can be conveniently measured by the rate of formation of C_2 hydrocarbons, and all the kinetic results reported in this section are calculated on the assumption that one mole of C_2 hydrocarbons formed corresponds to one mole of n-propyl-benzene decomposed.

TABLE V.

Exp.[a]	T°K	$k\cdot10^2$ sec^{-1}	$k_{900°K}\cdot10^2$ sec^{-1}
29	893	3.0	3.5
47 P	900	3.5	3.5
23	904	5.0	3.7
			$k_{927°K}\cdot10^2$ sec^{-1}
39	927	11.6	11.6
44 P	927	11.0	11.0
14	930	11.0	10.0
			$k_{937°K}\cdot10^2$ sec^{-1}
11	935	12.0	12.9
45 P	937	17.7	17.7
15	938	14.0	13.6
			$k_{975°K}\cdot10^2$ sec^{-1}
6	969	34	41
9	969	35	42
49 P	971	61	69
50 P	982	88	66
17	984	54	30

[a] Experiments carried out in the packed reaction vessel are denoted by P. The surface was increased by a factor of 15.

The apparatus and experimental technique have been described elsewhere (see e.g., reference 2), and these subjects are omitted therefore, in the present communication. Two samples of n-propyl-benzene were investigated: one acquired commercially from B.D.H. and the second kindly supplied to us by Professor F. D. Rossini.§ The results of pyrolyses of both samples were identical, proving that our observations were not affected by any impurities which might be present in either sample.

The pyrolysis of n-propyl-benzene was studied in the temperature range of 610°–760°C. The packing of the reaction vessel with silica wool, which increased the surface by a factor of 15, affects only slightly the rate of decomposition (see Table V and Fig. 1), thus proving

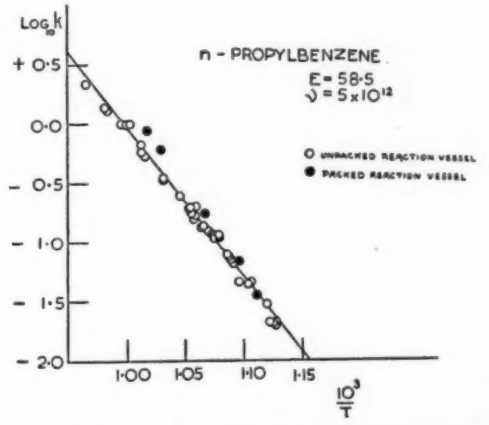

FIG. 1. (In the nomenclature change $E=58.5$ to $E=57.5$ kcal/mole; change $\nu=5\times10^{12}$ to 3×10^{12} sec^{-1}.)

[6] A. F. Trotman-Dickenson and E. W. R. Steacie, J. Chem. Phys. **19**, 329 (1951).

[7] M. G. Evans and M. Szwarc, Trans. Faraday Soc. **45**, 940 (1949); M. Szwarc, Faraday Soc. Disc. **10**, 143 (1951).

‡ The value of ~40 kcal/mole for the activation energy of this reaction is derived in the last part of this paper.

§ We take this opportunity of thanking Professor Rossini for his kind assistance.

TABLE VI.

Exp.[a]	T°K	P_{total} mm Hg	$P_{Ph\cdot C_3H_7}$ mm Hg	Time of contact sec	% decomp.	$k\cdot10^2$ [b] sec^{-1}
30	887	16.1	1.27	2.1	4.4	2.1
26	888	16.0	1.63	2.1	4.0	2.0
25	889	16.0	1.30	2.1	4.2	2.0
31	891	16.1	1.24	2.1	4.3	2.1
29	893	16.1	1.35	2.2	6.2	3.0
47 P	900	12.7	0.67	0.44	1.6	3.5
23	904	13.8	0.58	0.74	3.3	5.0
21	906	13.6	0.44	0.75	3.2	4.4
43	912	12.1	0.35	0.46	2.1	4.6
41	917	11.8	0.30	0.47	3.1	6.6
24	918	13.8	0.76	0.72	4.8	6.9
42	920	11.4	0.33	0.45	3.4	7.6
22	921	13.9	1.27	0.71	5.3	8.0
39	927	12.0	0.28	0.46	5.2	11.6
44 P	927	12.7	0.64	0.43	4.6	11.0
14	930	14.3	0.94	0.41	4.4	11.0
10	932	12.3	0.85	0.44	5.1	12.0
11	935	11.7	0.73	0.44	5.3	12.0
45 P	937	12.7	0.89	0.42	7.1	17.7
15	938	11.9	0.54	0.45	5.9	14.0
27	940	16.2	1.30	2.1	24.0	13.0
16	943	11.6	0.63	0.43	8.2	20.0
12	944	11.9	0.84	0.43	7.1	17.0
13	945	5.5	0.88	0.51	7.6	15.0
28	947	16.2	1.48	2.0	30.0	17
8	948	12.3	1.28	0.40	7.6	20
40	949	11.8	0.28	0.44	8.15	19
32	956	12.0	0.30	0.44	10.3	25
6	969	11.8	0.74	0.41	13.0	34
9	969	12.3	0.93	0.41	13.0	35
49 P	971	12.8	0.64	0.41	22.2	61
50 P	982	12.9	0.71	0.41	30.1	88
17	984	12.1	0.33	0.41	20.0	54
18	987	12.0	0.43	0.40	24.0	67
33	987	12.2	0.31	0.43	21.9	57
34	1000	12.1	0.29	0.42	29.6	83
7	1004	12.3	0.87	0.40	33.0	98
37	1005	12.0	0.29	0.42	34.0	99
38	1017	12.2	0.33	0.42	42.0	129
36	1019	12.1	0.30	0.42	43.0	136
35	1036	12.1	0.39	0.41	59.0	215

[a] Experiments carried out in the packed reaction vessel are denoted by P.
[b] The quoted values of k are rounded up to two decimals.

that the process investigated was a homogeneous gas reaction. The first-order character of the decomposition was demonstrated by varying the partial pressure of *n*-propyl-benzene by a factor of 5 (from 0.3 mm Hg to 1.5 mm Hg), and the time of contact by a factor of 5 (from 0.4 sec to 2 sec). Finally, it was shown that the variation of the partial pressure of toluene from about 5 mm Hg to 16 mm Hg also did not affect the rate of the pyrolysis of *n*-propyl benzene. Table VI summarizes all the results obtained over the whole temperature range of about 150°C. The plot of $\log \cdot k$ *versus* 1/T is given in Fig. 1, the straight line corresponding to the activation energy of 57.5 kcal/mole and the frequency factor of 3.10^{12} sec^{-1}.‖

BOND DISSOCIATION ENERGIES

The experimental results discussed in previous sections support the conclusion that the activation energy of the initial dissociation process

$$C_6H_5\cdot CH_2\cdot C_2H_5 \rightarrow C_6H_5\cdot CH_2\cdot + C_2H_5\cdot$$

is 57.5 kcal/mole. Making the plausible assumption that the reverse process, i.e., the recombination of benzyl and ethyl radicals, takes place without any activation energy, we deduce that

$$D(C_6H_5\cdot CH_2-C_2H_5)=57.5 \text{ kcal/mole.}$$

Using the equation

$$D(C_6H_5\cdot CH_2-C_2H_5)=\Delta H_f(C_6H_5\cdot CH_2)+\Delta H_f(C_2H_5)-\Delta H_f(C_6H_5\cdot C_3H_7)$$

in conjunction with the values for $\Delta H_f(C_6H_5\cdot CH_2)=37.5$ kcal/mole[1] and $\Delta H_f(C_6H_5\cdot C_3H_7)=1.9$ kcal/mole, we calculate the heat of formation of ethyl radicals at

$$\Delta H_f(C_2H_5)\approx 22 \text{ kcal/mole,}$$

and in view of various uncertainties we regard this value as not better than ±4 kcal/mole.

Having the heat of formation of ethyl radicals we are now able to calculate various relevant bond dissociation energies, namely:

$$D(C_2H_5-H)\approx 94\pm4 \text{ kcal/mole}$$
$$D(C_2H_5-CH_3)\approx 80\pm4 \text{ kcal/mole}$$
$$D(C_2H_5-C_2H_5)\approx 76\pm8 \text{ kcal/mole}$$
$$D(\cdot CH_2\cdot CH_2-H)\approx 41.5\pm4 \text{ kcal/mole.}$$

The following interpretation can be given to the last result. If the activation energy for the reaction

$$C_2H_4+H\rightarrow C_2H_5$$

is negligible, then the dissociation of ethyl radicals corresponds to an activation energy of about 40 kcal/mole (see in this connection reference 4).

‖ Calculated by the least square method without taking into account the results obtained in the packed reaction vessel.

THE JOURNAL OF CHEMICAL PHYSICS VOLUME 20, NUMBER 3 MARCH, 1952

The Pyrolysis of *n*-Butyl-Benzene and the Heat of Formation of *n*-Propyl Radical

C. H. LEIGH AND M. SZWARC
Department of Chemistry, University of Manchester, Manchester 13, England
(Received August 14, 1951)

It has been shown that the pyrolysis of *n*-butyl-benzene results in its dissociating into benzyl and *n*-propyl radicals,

$C_6H_5\cdot CH_2\cdot CH_2\cdot CH_2\cdot CH_3 \rightarrow C_6H_5\cdot CH_2\cdot + \cdot CH_2\cdot CH_2\cdot CH_3$, (1)

and the propyl radicals subsequently decompose to give ethylene and methyl radicals, $CH_3\cdot CH_2\cdot CH_2\cdot \rightarrow CH_3\cdot + C_2H_4$. By the use of the toluene-carrier technique, it has been possible to measure the rate of reaction (1) by measuring the rate of formation of ethylene. The activation energy of reaction (1) has been thus determined at 65 kcal/mole. The latter value has been identified with the $C_6H_5\cdot CH_2-C_3H_7$ bond dissociation energy, i.e., $D(C_6H_5\cdot CH_2-CH_2\cdot CH_2\cdot CH_3)=65$ kcal/mole. Since $D(C_6H_5\cdot CH_2-C_3H_7)=\Delta H_f(C_6H_5\cdot CH_2)+\Delta H_f(n-C_3H_7)-\Delta H_f(n\cdot C_6H_5\cdot C_4H_9)$ and $\Delta H_f(C_6H_5\cdot CH_2)=37.5$ kcal/mole, one may compute the unknown value for $\Delta H_f(n-C_3H_7)$, namely, $\Delta H_f(CH_3\cdot CH_2\cdot CH_2\cdot)\approx 24$ kcal/mole. Having $\Delta H_f(n-C_3H_7)$, we calculated the dissociation energy of the primary C—H bond in propane at $D(C_3H_7-H)=\Delta H_f(n-C_3H_7)+\Delta H_f(H)-\Delta H_f(C_3H_8)\approx 100$ kcal/mole. This value for $D(CH_3\cdot CH_2\cdot CH_2-H)$ is compared with the findings of other workers. It agrees well with the recent findings of Stevenson, although the existing indirect chemical evidence seems to require a lower value.

THE investigation of the pyrolysis of *n*-butyl-benzene provides some data of use for the calculation of the dissociation energy of the primary C—H bond in propane. It appears that the pyrolysis of *n*-butyl-benzene takes place by its dissociation into benzyl and *n*-propyl radicals,

$$C_6H_5\cdot CH_2\cdot CH_2\cdot CH_2\cdot CH_3 \rightarrow C_6H_5\cdot CH_2\cdot + \cdot CH_2\cdot CH_2\cdot CH_3. \quad (1)$$

At the high temperatures of our experiments (i.e., above 600°C), the propyl radicals, produced by reaction (1), decompose rapidly into ethylene and methyl radicals

$$CH_3\cdot CH_2\cdot CH_2\cdot \rightarrow CH_3\cdot + C_2H_4. \quad (2)$$

This reaction is facilitated by the low dissociation energy of the $CH_3-CH_2\cdot CH_2\cdot$ bond which is probably less than 25 kcal/mole. The presence of an excess of toluene in these experiments facilitates a rapid removal of methyl radicals by reaction (3)

$$C_6H_5\cdot CH_3 + CH_3\cdot \rightarrow C_6H_5\cdot CH_2\cdot + CH_4. \quad (3)$$

The mechanism of decomposition described by reactions (1), (2), and (3) demands, therefore, the formation of one mole of ethylene, of methane, and of dibenzyl for every mole of *n*-butyl-benzene decomposed; and indeed, it appears that this simple scheme applies to the main mode of decomposition of *n*-butyl-benzene. Ethylene,[1] methane, and dibenzyl were found to be the main products of the pyrolysis, and the formation of the latter compound leaves no doubt as to the radical character of the decomposition. It seems, however, that the main decomposition, described by Eqs. (1)–(3), is accompanied by some side processes. This is indicated by the presence of small quantities of hydrogen in the products of the pyrolysis, and by the molar ratio of CH_4/C_2H_4, which was smaller than unity (Tables I and IA).

The formation of hydrogen might be a result of reaction (4)

$$C_6H_5\cdot CH_2\cdot CH_2\cdot C_2H_5 \rightarrow C_6H_5\cdot CH{:}CH\cdot C_2H_5 + H_2. \quad (4)$$

The occurrence of this reaction does not affect our further conclusions, and it is, therefore, of no great importance in our present studies. On the other hand, the

TABLE I.

Run	T°K	$(CH_4+H_2)/C_2H_4$	$H_2/(CH_4+H_2)$
37	879	0.71	...
32	883	0.69	...
38	888	0.65	...
30	900	0.75	0.18
7	907	0.79	0.20
15	910	0.95	0.22
11	911	0.81	0.15
9	912	0.71	0.27
14	916	0.69	...
31	917	0.66	...
10	918	0.69	...
16	928	0.72	0.23
13	931	0.79	...
12	936	0.78	0.39
8	948	0.71	...
4	952	0.71	...
3	958	0.73	0.18
17	963	0.79	0.24
6	965	0.63	0.34
5	967	0.67	...
34	971	0.67	0.20
33	972	0.74	...
35	973	0.85	...
36	974	0.65	...

TABLE IA. Packed reaction vessel.

Run	T°K	$(CH_4+H_2)/C_2H_4$	$H_2/(CH_4+H_2)$
46 P	891	1.07	0.16
44 P	916	1.08	0.16
45 P	918	0.81	0.13
48 P	943	0.89	0.14
41 P	943	1.37 (?)	0.17
50 P	944	0.77	...
42 P	949	0.64	0.25
51 P	950	0.72	...
43 P	955	0.75	0.15
49 P	960	0.74	0.27

[1] Hydrogenation of the C_2 hydrocarbon fractions showed that they were composed of ethylene only.

TABLE II.

Run	T°K	Dibenzyl/C_2H_4
50	944	0.42
51	950	0.44
49	960	0.45

low value of the molar ratio CH_4/C_2H_4 might indicate the occurrence of some processes, the participation of which in the over-all decomposition might affect our final calculations.

The low value of the molar ratio CH_4/C_2H_4 can be explained by postulating either the occurrence of some process, different from reactions (1) and (2), which produces ethylene, e.g.,

$$\begin{matrix} C_6H_5\cdot CH_2\cdot CH_2 \\ | \\ CH_3CH_2 \end{matrix} \rightarrow \begin{matrix} C_6H_5\cdot CH_2 \\ | \\ CH_3 \end{matrix} + \begin{matrix} CH_2 \\ \| \\ CH_2 \end{matrix}, \qquad (5)$$

or it might be caused by some reactions, other than (3), which consume methyl radicals, e.g.,

$$C_6H_5\cdot CH_2\cdot + \cdot CH_3 \rightarrow C_6H_5\cdot CH_2\cdot CH_3 \qquad (6)$$

or

$$C_6H_5\cdot CH_2\cdot + CH_3\cdot CH_2\cdot CH_2\cdot \rightarrow C_6H_5\cdot CH_2\cdot CH_3 + C_2H_4. \qquad (7)$$

Neither of these possible schemes seems to be fully satisfactory; yet, we are unable to offer any better explanation. The quantitative determination of the amount of dibenzyl formed in the pyrolysis might be helpful in disentangling this problem. Unfortunately, technical difficulties made such a determination unfeasible. Although we could isolate a considerable portion of pure dibenzyl produced in the reaction (Table II), it was impracticable to recover quantitatively that portion which was condensed together with the undecomposed toluene and *n*-butyl-benzene.

In spite of all these difficulties, we are confident that the rate of formation of ethylene provides a reasonable measure of the rate of the initial dissociation (1). While

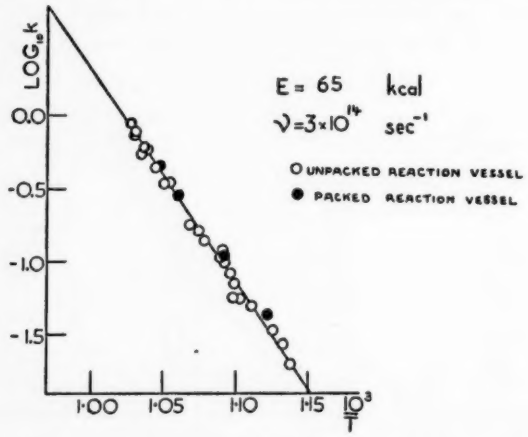

FIG. 1. *n*-butyl-benzene. In nomenclature $\nu = 3\times10^{14}$ sec^{-1} "based on $d[C_2H_4]/dt$."

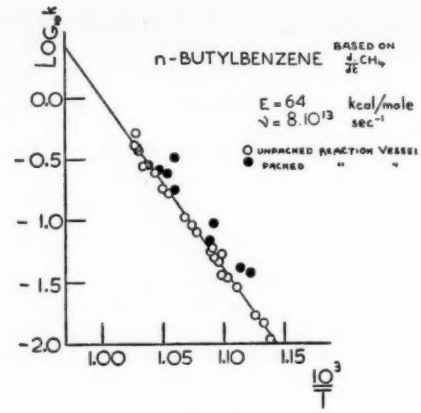

FIG. 2.

the ratio of CH_4/C_2H_4 varies considerably, and apparently depends on the magnitude of the surface of the reaction vessel (Table I and Fig. 2), the rate of formation of ethylene obeys well first-order kinetics, and it is not affected by the packing of the reaction vessel (Tables III, IV, and IVA and Fig. 1). We conclude, therefore, that the low ratio of CH_4/C_2H_4 is caused by the participation of some reactions consuming methyl radicals, and not to the occurrence of reactions producing additional quantities of ethylene. Consequently, all the rate constants listed in the following tables are computed on the assumption that one mole of ethylene formed corresponds to one mole of *n*-butyl-benzene decomposed.

EXPERIMENTAL

The pyrolysis of *n*-butyl-benzene was studied by a flow technique which used toluene as a carrier gas. The apparatus and the details of experimentation have been described elsewhere,[2] and are therefore omitted in the present communication. Three samples of *n*-butyl-

TABLE III. Effect of packing the reaction vessel.

Run	T°K	$k\cdot10^2$ sec^{-1}	Interpolated to const. temp.
			$k_{931}\cdot10^2$ sec^{-1}
38	888	4.9	5.3
46 P	891	4.3	4.3
30	900	5.6	4.1
			$k_{917}\cdot10^2$ sec^{-1}
14	916	9.8	10.1
44 P	916	11.1	11.4
31	917	12.1	12.1
45 P	918	10.6	10.3
10	918	10.7	10.4
			$k_{950}\cdot10^2$ sec^{-1}
18	948	35	37
42 P	949	50	51
51 P	950	41	41
4	952	34	32
			$k_{960}\cdot10^2$ sec^{-1}
3	958	44	47
59 P	960	53	53
17	963	59	54

[2] M. Szwarc, J. Chem. Phys. **17**, 431 (1949); Proc. Roy. Soc. (London) **A198**, 285 (1949).

TABLE IV. Variation of the partial pressure of *n*-butyl-benzene.

Run	T°K	$P_{C_6H_5\cdot C_4H_9}$ mm Hg	$k\cdot10^2$ sec^{-1}	Interpolated to const. temp.
				$k_{914}\cdot10^2$ sec^{-1}
11	911	0.49	5.6	5.8
44	916	0.49	11.2	10.5
45	918	0.70	10.6	9.3
15	910	1.49	7.0	7.8
9	912	1.49	8.3	8.8
				$k_{950}\cdot10^2$ sec^{-1}
48	943	0.21	25.5	32.0
41	943	0.26	29.0	36.0
4	952	0.29	34.0	31.0
43	955	0.36	45.0	37.0
50	944	0.37	31.0	38.0
51	950	0.43	41.5	41.5
49	960	0.48	52.5	37.0
18	948	1.24	34.5	37.0
17	963	1.54	59.0	36.0

benzene were investigated,[3] identical results being obtained in every case. We are thus satisfied that our observations were not affected by any impurities which might have been present in the pyrolyzed samples.

The investigation was carried out over a temperature range of about 100°C (from 600°C to 700°C). The packing of the reaction vessel with silica wool which increased the surface by a factor of 15 did not affect the rate of decomposition as measured by the rate of formation of ethylene (Table III). Changing the partial pressure of *n*-butyl-benzene by a factor of 7 (from 0.21 mm Hg to 1.54 mm Hg), and the time of contact by a factor of 5 did not affect the unimolecular rate constants (Table IV and IVA). The unimolecular rate constants were shown also to be independent of the partial pressure of toluene (Table V). Table VI summarizes all the experimental results, and the plot of log$k$ *versus* 1/T is shown in Fig. 1. The experimental activation energy has been estimated at 65 kcal/mole, and the frequency factor at 3.10^{14} sec^{-1}.

BOND DISSOCIATION ENERGIES

All these observations are in accord with the suggestion that the initial dissociation process is represented by reaction (1)

$$C_6H_5\cdot CH_2\cdot CH_2\cdot CH_2\cdot CH_3 \rightarrow C_6H_5\cdot CH_2\cdot + \cdot CH_2\cdot CH_2\cdot CH_3, \quad (1)$$

TABLE IVA. Variation of the time of contact.

Run	T°K	Time of contact sec	$k\cdot10^2$ sec^{-1}	Interpolated to const. temp.
				$k_{950}\cdot10^2$ sec^{-1}
18	948	2.10	35	37
4	952	0.44	34	32
				$k_{963}\cdot10^2$ sec^{-1}
17	963	2.04	59	59
3	958	0.45	44	51
6	965	0.42	60	56.5

[3] We are indebted to Professor F. D. Rossini and to Shell Company, Amsterdam, for generously supplying samples of pure *n*-butyl-benzene.

TABLE V. Variation of the total pressure.

Run	T°K	P_{total} mm Hg	$k\cdot10^2$ sec^{-1}	Interpolated to const. temp.
				$k_{931}\cdot10^2$ sec^{-1}
13	931	6.6	16.2	16.2
16	926	16.3	14.0	16.3
12	936	19.8	18.0	15.3
				$k_{914}\cdot10^2$ sec^{-1}
14	916	6.6	9.8	9.2
9	912	16.3	8.3	8.8
31	917	16.4	12.1	10.9
11	911	19.6	5.6	6.2

which is rate-determining in the formation of ethylene. Hence, the observed activation energy of 65 kcal/mole appears to be the activation energy of reaction (1). By making the plausible assumption that the recombination of radicals does not require any activation energy, we conclude that

$$D(C_6H_5\cdot CH_2-CH_2\cdot CH_2\cdot CH_3)=65 \text{ kcal/mole}.$$

We consider the uncertainty in this value to be not less than ~3 kcal/mole (by taking into account the experimental errors and the possible ambiguity in the interpretation of the results).

Heats of formation of radicals are connected with bond dissociation energies by the equation

$$D(R-R_1)=\Delta H_f(R)+\Delta H_f(R_1)-\Delta H_f(R\cdot R_1).$$

TABLE VI. *n*-butyl-benzene.

Run	T°K	P_{total} mm Hg	$P_{C_6H_5\cdot C_4H_9}$ mm Hg	Time of contact sec	% dec.	$k\cdot10^2$ sec^{-1}
37	879	16.4	1.40	2.35	4.6	1.99
32	883	16.3	2.0	2.12	5.6	2.71
38	888	16.5	1.2	2.37	7.6	3.36
46-P	891	12.8	0.8	0.37	1.6	4.35
30	900	16.2	1.2	2.17	10.1	4.90
7	907	16.0	0.9	2.25	11.8	5.56
15	910	16.3	1.5	2.16	14.1	7.04
11	911	19.6	0.5	1.99	10.6	5.62
9	912	16.3	1.5	2.07	15.8	8.3
14	916	6.6	2.0	3.72	30.6	9.8
44-P	916	12.7	0.5	0.44	4.7	11.2
31	917	16.4	1.6	2.09	22.3	12.05
45-P	918	12.7	0.7	0.43	4.4	10.56
10	918	16.3	1.0	2.14	20.5	10.7
16	928	16.3	1.3	2.15	27.0	14.0
13	931	6.6	1.8	3.76	45.8	16.25
12	936	19.8	0.7	1.94	29.5	18.0
48-P	943	12.6	0.2	0.43	10.4	25.5
41-P	943	12.5	0.3	0.42	11.4	28.8
50-P	944	12.8	0.4	0.43	12.6	31.3
18	948	16.8	1.2	2.10	51.8	34.7
42-P	949	12.7	0.9	0.40	18.2	50.0
51-P	950	12.8	0.4	0.43	16.2	41.5
4	952	11.8	0.3	0.44	14.0	34.2
43-P	955	12.7	0.4	0.42	17.2	45.1
3	958	12.2	0.3	0.45	18.0	43.8
49-P	960	12.8	0.5	0.41	19.6	52.6
17	963	16.9	1.5	2.04	69.9	58.8
6	965	12.1	0.8	0.42	22.5	60.0
5	967	12.3	0.5	0.44	21.3	54.6
34	971	12.5	0.4	0.44	28.8	77.4
33	972	12.4	0.3	0.44	27.1	71.6
35	973	12.3	0.3	0.44	30.0	81.4
36	974	12.5	0.4	0.44	32.1	88.4

In this case the relevant equation is

$$D(C_6H_5\cdot CH_2-CH_2\cdot CH_2\cdot CH_3)=\Delta H_f(C_6H_5\cdot CH_2\cdot)+\Delta H_f(CH_3\cdot CH_2\cdot CH_2\cdot)-\Delta H_f(n-C_6H_5\cdot C_4H_9).$$

By taking $D(C_6H_5\cdot CH_2-C_3H_7)$ at 65 kcal/mole and $\Delta H_f(C_6H_5\cdot CH_2)=37.5$ kcal/mole,[4] we derive

$$\Delta H_f(CH_3\cdot CH_2\cdot CH_2\cdot)\approx 24 \text{ kcal/mole.}$$

The latter value makes it possible to calculate the dissociation energy of the primary C−H bond in propane, namely,

$$D(CH_3\cdot CH_2\cdot CH_2-H)=\Delta H_f(CH_3\cdot CH_2\cdot CH_2\cdot)+\Delta H_f(H)-\Delta H_f(C_3H_8)$$

and thus

$$D(CH_3\cdot CH_2\cdot CH_2-H)\approx 100\pm 5 \text{ kcal/mole.}$$

The value for $D(C_3H_7-H)$ derived above appears to be rather high. We examined, therefore, the possible side processes which might render our determination of $D(C_6H_5\cdot CH_2-C_3H_7)$ too high. One may suggest that some propyl radicals, produced in the initial dissociation process, react with toluene according to equation

$$C_6H_5\cdot CH_3+C_3H_7\cdot\rightarrow C_6H_5\cdot CH_2\cdot+C_3H_8,$$

and that the participation of this reaction in the over-all decomposition influences the determination of the activation energy. To check this suggestion special experiments were designed for isolating and estimating any C_3 hydrocarbons possibly formed in the pyrolysis. The results were, however, negative.[5]

Another possibility which should be considered is the participation of reaction (5) at higher temperatures of the pyrolysis

$$\begin{matrix} C_6H_5\cdot CH_2\cdot CH_2 \\ | \\ CH_3\cdot CH_2 \end{matrix} \rightarrow \begin{matrix} C_6H_5\cdot CH_2 \\ | \\ CH_3 \end{matrix} + \begin{matrix} CH_2 \\ \| \\ CH_2 \end{matrix}. \qquad (5)$$

Although it is not possible to refute decisively this suggestion, we are inclined to consider reaction (5) as not a probable one (see the discussion in the preceding section of this paper). The specific requirement that this reaction is more important at higher temperature range is particularly improbable. This would mean that the activation energy of reaction (5) is higher than that of reaction (1). On the other hand it is expected that the entropy of activation is also higher for reaction (5) than for reaction (1), which would then make the frequency factor of the former reaction lower than that of the latter. Consequently, the rate of reaction (5) would be negligible as compared with that of reaction (1).

Our conclusion about the high value of the C−H bond dissociation energy in propane cannot be changed substantially by abandoning the assumption that the rate of the initial dissociation process is measured by the rate of formation of ethylene, and assuming instead that it is measured by the rate of formation of methane. The plot of $\log k_{CH_4}$ *versus* 1/T is given in Fig. 2. (k_{CH_4} is the unimolecular rate constant computed on the assumption that one mole of methane produced corresponds to one mole of *n*-butyl-benzene decomposed.) The activation energy has been estimated at 64 kcal/mole, the latter value making $D(CH_3\cdot CH_2\cdot CH_2-H)=99$ kcal/mole.

Finally, one might consider the estimation of the activation energy as unreliable (assuming the occurrence of some unspecified side processes) and base the calculation on the assumption that the frequency factors for the dissociations

$$C_6H_5\cdot CH_2\cdot C_2H_5\rightarrow C_6H_5\cdot CH_2\cdot+C_2H_5\cdot$$

and

$$C_6H_5\cdot CH_2\cdot C_3H_7\rightarrow C_6H_5\cdot CH_2\cdot+n-C_3H_7\cdot$$

are identical. If this assumption is approximately correct, then $D(CH_3\cdot CH_2-H)\approx D(CH_3\cdot CH_2\cdot CH_2-H)$, the calculation being based on the values of the rate constants observed at the lower temperature range of the pyrolysis.

DISCUSSION OF OTHER METHODS OF DETERMINING $D(CH_3\cdot CH_2\cdot CH_2-H)$

The work of Butler and Polanyi[6] provided the first data on the C−H bond dissociation energy in propane. These workers determined the C−I bond dissociation energy in *n*-propyl-iodide, by investigating pyrolyses of this compound and assuming the frequency factor for the unimolecular dissociation process,

$$C_3H_7I\rightarrow C_3H_7+I$$

to be 10^{13} sec^{-1}. By applying the usual thermochemical calculations the value of $D(CH_3\cdot CH_2\cdot CH_2-H)=95$ kcal/mole was then derived from the value of $D(CH_3\cdot CH_2\cdot CH_2-I)$ estimated at 50 kcal/mole.

However, the kinetics of the pyrolysis of organic iodides is not at all simple (see, e.g., reference 4 where this problem is discussed fully), and, therefore, the bond dissociation energies derived by Butler and Polanyi might be incorrect by 3–4 kcal/mole.

Recently, an electron impact study of some hydrocarbons enabled Stevenson[7] to estimate $D(CH_3\cdot CH_2\cdot CH_2-H)$ at 99.4±0.9 kcal/mole. This determination agrees very well with the value reported here.

Indirect chemical evidence, on the other hand, seems to favor a lower value for $D(CH_3\cdot CH_2\cdot CH_2-H)$. Our results, as well as those of Stevenson, lead to the inequality

$$D(CH_3\cdot CH_2\cdot CH_2-H)>D(CH_3\cdot CH_2-H),$$

while the sodium flame investigations require a reverse order for the magnitude of these bond dissociation

[4] M. Szwarc, Chem. Revs. **47**, 75 (1950).

[5] The minimum amount of the C_3 hydrocarbons which could be detected in our experiments was about 5 percent of ethylene formed.

[6] E. T. Butler and M. Polanyi, Trans. Faraday Soc. **39**, 19 (1943).

[7] D. P. Stevenson, private communication.

energies,[8] i.e.,

$$D(CH_3\cdot CH_2\cdot CH_2-H)<D(CH_3\cdot CH_2-H).$$

The latter inequality agrees better with other evidence based on the relative reactivity of relevant compounds.

Furthermore, the extensive studies of reactions

$$R\cdot H+CH_3\cdot\rightarrow R\cdot+CH_4$$

by Trotman-Dickenson and Steacie[9] indicate that all the primary C—H bond dissociations are roughly equal.

In conclusion we have to state that the direct evidence seems to indicate a high value for $D(CH_3\cdot CH_2\cdot CH_2-H)$. However, in view of the existing indirect evidence this value should be treated with some reservation. Further direct evidence seems to be highly desirable.

[8] E. Warhurst, Quart. Rev. **5**, 44 (1951).

[9] A. F. Trotman-Dickenson and E. W. R. Steacie, J. Chem. Phys. **19**, 329 (1951).

THE JOURNAL OF CHEMICAL PHYSICS VOLUME 20, NUMBER 3 MARCH, 1952

Kinetics of Solidification of Supercooled Liquid Mercury Droplets

DAVID TURNBULL
General Electric Research Laboratory, Schenectady, New York

(Received September 21, 1951)

The solidification rate of supercooled liquid mercury droplets is strongly dependent upon the nature of foreign substances on their surface or suspended in them. Droplets (2–8 microns diameter) coated with mercury laurate solidify at rates that are proportional to droplet volume and satisfactorily described by the theory of homogeneous nucleation of crystals. Droplets coated with mercury acetate solidify with frequencies that are proportional to droplet area and in good agreement with the theory of heterogeneous nucleation.

The results on Hg_2I_2-coated droplets are interpreted on the hypothesis that nucleation is effected by suspended crystallites of one kind. For some droplet dispersions the kinetic results are apparently best described by a multiplicity of solidification frequencies/area or volume. Various hypotheses for this multiplicity are considered.

BECKER and Döring[1] have developed the theory for the rate of homogeneous nucleation[2] of liquid droplets in supersaturated one-component vapors. This theory predicts values of the supersaturation ratios required to nucleate liquid droplets rapidly in several one-component systems in excellent agreement with the measured values of Volmer and Flood,[3] with the exception of that for methyl alcohol.

By following the basic assumptions of the Becker-Döring theory, Turnbull and Fisher[4] have developed a theory for the rate of homogeneous nucleation in condensed systems according to which the frequency of formation, I, of crystal nuclei/volume of supercooled liquid is:

$$I=K_v\exp[-a\sigma^3/(\Delta F_v)^2kT], \quad (1)$$

where

$$K_v=n^*(A/9\pi)^{\frac{1}{2}}n(kT/h)\exp[-\Delta F_A/kT], \quad (2)$$

σ = interfacial energy/area between crystal nuclei and the liquid,

ΔF_v = the free energy change/volume for the transition liquid→crystal,

n^* = number of atoms in the surface of a nucleus of critical size,

n = number of atoms/volume of liquid,[5]

ΔF_A = free energy of activation/atom for transport across the liquid-crystal interface, and

a = constant determined by the nucleus shape.

A is defined by the equation

$$\Delta F/kT=Ai^{\frac{1}{2}}+Bi, \quad (3)$$

where ΔF is the free energy of forming crystal embryos containing i atoms. For nuclei that are spherically shaped $a=16\pi/3$ and

$$(A/9\pi)^{\frac{1}{2}}=(\sigma/kT)^{\frac{1}{2}}(2v/9\pi)^{\frac{1}{2}}, \quad (4)$$

where v = volume/atom of the crystal.

The free energy of forming crystal embryos and nuclei on the surface of nucleation catalysts can be described[2] in terms of i, σ, ΔF_v, and θ, the equilibrium contact angle between the crystal nucleus and catalyst when surrounded by supercooled liquid. By combining earlier concepts[2,4] an approximate expression for the frequency of nucleation/area of catalyst, I_s, may be written as follows,

$$I_s=K_s\exp[-a\sigma^3f(\theta)/(\Delta F_v)^2kT], \quad (5)$$

where

$$K_s=n^*(A/9\pi)^{\frac{1}{2}}n_s(kT/h)\exp[-\Delta F_A/kT]. \quad (6)$$

[1] R. Becker and W. Döring, Ann. Physik [5] **24**, 719 (1935).

[2] Nucleation that occurs without the catalytic acid of foreign bodies is designated "homogeneous." "Heterogeneous" nucleation is catalyzed by such bodies. D. Turnbull, J. Chem. Phys. **18**, 198 (1950).

[3] M. Volmer and H. Flood, Z. physik. Chem. **170A**, 273 (1934).

[4] D. Turnbull and J. C. Fisher, J. Chem. Phys. **17**, 71 (1949).

[5] In earlier publications, n was erroneously defined as the number of atoms/sample though the calculations were based upon a correct definition of n. The author is indebted to R. S. Bradley for calling his attention to the error made in the definition. A. D. Turnbull, J. Appl. Phys. **21**, 1022 (1950). D. Turnbull, J. Chem. Phys. **18**, 768 (1950).

n_s = number of liquid atoms in contact with catalyst/area. For nuclei having the form of spherical sectors,

$$f(\theta)=(2+\cos\theta)(1-\cos\theta)^2/4$$
$$(A/9\pi)^{\frac{1}{3}}=(\sigma/kT)^{\frac{1}{3}}(2v/9\pi)^{\frac{1}{3}}[(2-\cos\theta+\cos^2\theta)/4]^{1/6}.$$

The factors that, according to Eqs. (1) and (5), determine I and I_s are at least approximately known excepting σ[6] and θ. Therefore, the validity of the nucleation theory can be tested by measuring the variation of I or I_s with temperature and comparing the values of $(K_v)_{exp}$ or $(K_s)_{exp}$ computed from these experimental results with the theoretical values predicted by Eqs. (1) or (5).

Crystal nucleation frequencies of large continuous masses of supercooled liquid are generally unsuitable for testing the predictions of nucleation theory because these masses almost inevitably contain nucleation catalysts of unknown composition and variable potency.[2,7,8] Let the number of these accidental catalytic centers in a given mass of liquid be m_0. It has been postulated[2,8,9] that if the mass is broken into a number of isolated droplets $m \gg m_0$ crystal nuclei must form in the major portion of the droplets homogeneously or with the aid of a known crystalline film sometimes used to isolate the droplets. The evidence supporting this postulate has been fully summarized elsewhere.[5,10] If a mass of liquid is dispersed to a number of droplets $m \gtrsim m_0$, it may be found that the rate of nucleation in the majority of the droplets, though greater than the rate of homogeneous nucleation, is very much less than the rate of nucleation of the original mass. This result is explained if, following Levine,[11] the additional hypothesis is made that the concentration of accidental catalytic centers with a given catalytic potency, $p=1/f(\theta)$, increases as p decreases. Levine has given a formal treatment of the problem that is analogous to the statistical theory of brittle fracture by stress raisers of variable potency developed by Weibull[12] and Fisher and Hollomon.[13] Levine's theory successfully describes the experimental results of Dorsch and Hacker[14] on the freezing of water droplets.

It appears that the most promising method of testing the predictions of the theory of crystal nucleation in supercooled liquids is the measurement of the nucleation frequency in a collection of small droplets sufficiently dispersed to make $m \gg m_0$.[2,9] Then crystal nucleation in droplets isolated by films that are not nucleation catalysts should be homogeneous and describable by Eq. (1). In droplets coated with crystalline films that catalyze nucleation, the nucleation frequency should be proportional to the surface area of the films and describable by Eq. (5).

It has been demonstrated[2,15] that the rate determining step in the solidification of very small metal droplets is nucleation. Thus the nucleation frequency in small droplet dispersions can be computed from direct measurement of the solidification rate on the basis that the period of crystal growth is negligible in comparison with the nucleation period.

Consider the kinetics of isothermal solidification of a dispersion of droplets having a wide distribution of diameters. We make the following definitions: D = diameter of the droplet, v_D = volume of droplets of diameter D, a_D = surface area of droplets of diameter D, and V_D = total volume of all droplets of diameter D that remain liquid at time, t. A function $y(t)$ is defined by the equation

$$y(t)=\sum_{D=0}^{D=D} V_D/\sum_{D=0}^{D=\infty} V_D=(1/V)\int_0^D V_D dD. \quad (7)$$

At $t=0$

$$y(t)=y^0=(1/V^0)\int_0^D V_D{}^0 dD. \quad (8)$$

Also from (7) and (8) $dy(t)/dD=V_D/V$ and $dy^0/dD=V_D{}^0/V^0$. Let the nucleation frequency per droplet $=k_D$; it follows from the assumptions that the volume rate of solidification of droplets of diameter D conforms to the radioactive decay law and is given by,[2]

$$-dV_D/dt=k_D V_D. \quad (9)$$

The total volume rate of solidification is,

$$-dV/dt=\sum_{D=0}^{D=\infty} k_D V_D=\int_0^\infty k_D V_D dD. \quad (10)$$

Integration of (9) and (10) gives

$$V_D=V_D{}^0\exp[-k_D t], \quad (11)$$

$$V=\sum_{D=0}^{D=\infty} V_D{}^0\exp[-k_D t]$$
$$=\int_0^\infty V_D{}^0[\exp(-k_D t)]dD. \quad (12)$$

For homogeneous nucleation

$$k_D=Iv_D, \quad (13)$$

[6] There is a good possibility (particularly in view of the quantitative success of the Becker-Döring theory applied to the nucleation of droplets) that σ may be approximately equal to the appropriate liquid-crystal interfacial tension σ' measured in macroscopic systems. As yet σ' has not been measured with sufficient accuracy to test this possibility.

[7] M. Avrami (Now Melvin) J. Chem. Phys. **7**, 1103 (1939).

[8] D. Turnbull, J. Appl. Phys. **20**, 817 (1949).

[9] D. Turnbull, Trans. Am. Inst. Mining Met. Engrs. **188**, 1144 (1950).

[10] D. Turnbull, *Thermodynamics in Physical Metallurgy* (Am. Soc. Metals, Cleveland, Ohio, 1950), pp. 282–306.

[11] J. Levine, Nat. Advisory Comm. Aeronaut. Repts., Tech. Mem. Notes 2234 (1950).

[12] W. Weibull, Roy. Swed. Inst. Eng. Research No. 151, (1939).

[13] J. C. Fisher and J. H. Hollomon, Metals Technol. **14**, No. 5 (1947).

[14] R. G. Dorsch and P. T. Hacker, Nat. Advisory Comm. Aeronaut. Repts. Tech. Mem. Notes 2142 (1950).

[15] D. Turnbull and R. E. Cech, J. Appl. Phys. **21**, 804 (1950).

TABLE I. Summary of methods used to prepare dispersions of mercury droplets.

Coating on droplets	Designation[a]	Method of dispersion	Composition of dispersing mixture: Fluid	Oxidizing agent	Acid	Droplet diameter range (microns)	Dilatometer fluid
Mercury sulfide (black)	Hg(S)	Manual shaking	CS_2 (30 cc)	Sulfur 0.05 g	···	50–200	Ethyl alcohol (EtOH)
Sodium oleate (adsorbed)	Na Oleate	Manual shaking	EtOH saturated with Na Oleate	···	···	100–400	EtOH
Mercury iodide (yellow)	Hg_2I_2[b]	Manual shaking	EtOH (30 cc)	0.3 g iodine	···	15–70	EtOH
Mercury acetate	Hg(Ac)	Waring blendor	Silicone oil (150 cc)	0.2 g acetyl peroxide	···	4–12	Methyl cyclopentane
Mercury stearate	Hg(St)	Waring blendor	Mineral white oil (150 cc)	Air	0.5 g stearic acid	2–7	Methyl cyclopentane
Mercury laurate	Hg(Lau)	Waring blendor	Silicone oil (150 cc)	0.5 g lauroyl peroxide	0.1 g lauric acid	2–8	Methyl cyclopentane
Mercury benzoate	Hg(Bz)	Waring blendor	Silicone oil (150 cc)	0.7 g benzoyl peroxide	0.3 g stearic acid	2–8	Methyl cyclopentane

[a] These designations are not intended to indicate the precise chemical formula of the film but only the method of its formation. The author did not find the data necessary for calculating whether the Hg_2^{++} or Hg^{++} salts are thermodynamically more stable under the experimental conditions. Also, it is possible that some of the carboxylates are oxy salts.

[b] According to thermodynamic calculations, Hg_2I_2 is the more stable phase (relative to HgI_2) in equilibrium with mercury under the experimental conditions.

and Eq. (12) may be rewritten

$$V=\sum_{D=0}^{D=\infty} V_D{}^0 \exp(-Iv_Dt)$$

$$=\int_0^\infty V_D{}^0 [\exp(-Iv_Dt)]dD. \quad (14)$$

In case nucleation is catalyzed by the film on the droplet surface,

$$k_D=I_sa_D \quad (15)$$

and Eq. (12) becomes

$$V=\sum_{D=0}^{D=\infty} V_D{}^0 \exp(-I_sa_Dt)$$

$$=\int_0^\infty V_D{}^0 [\exp(-I_sa_Dt)]dD. \quad (16)$$

Experimentally, we obtain $y^0=f(D)$ and $V=f(t)$ at various constant temperatures. By using the relation $y^0=f(D)$, Eqs. (14) and (16) may be compared with the experimental relation $V=f(t)$ by a numerical or analytical procedure. From this comparison it may be decided whether the data are fit best by assuming the nucleation frequency proportional to the volume of the droplet [Eq. (14)] or to its surface area [Eq. (16)].

It follows that $\partial^2X/\partial t\partial T|_{x=x_1}$, where $X=(V_0-V)/V_0$, is proportional to dI/dT or dI_s/dT for a given dispersion. Therefore $d\ln I/dT$ or $d\ln I_s/dT$ can be evaluated from $V=f(t)$ for a given dispersion at various constant temperatures even though $y^0=f(D)$ is not known.[5b]

Vonnegut[16] has measured the isothermal rate of solidification of tin droplets (1–10 micron diameter) isolated from each other by an oxide film as a function of temperature. Analysis of his data[5b] indicated that the magnitude of $\partial^2X/\partial t\partial T|_{x=x_1}$ is in approximate agreement with the prediction of Eq. (14). However, $y^0=f(D)$ was not determined. Later measurements of Pound and LaMer[17] of $V=f(t)$, in conjunction with measurements of $y^0=f(D)$, on oxide-coated tin droplets showed that $(\partial X/\partial t)_T$ decreased much too rapidly with time to be compatible with a single value of I or I_s.

We have measured $V=f(t)$ at various temperatures for dispersions of mercury droplets coated with various surface films. Preliminary reports of some of the results have been published elsewhere.[5b,18,19] The purpose of this paper is to describe and analyze these and additional results more completely.

EXPERIMENTAL

A. Materials and Preparation of Dispersions

Purified triple-distilled mercury was used in all the preparations to be described. In forming one group of dispersions 2 cc of mercury and the forming solution were shaken up in a test tube. To form the second group, 5 cc of mercury and the forming solution were agitated in a Waring Blendor for net times of three to eight minutes. The agitation was interrupted at intervals in order to prevent excessive heating of the blendor contents.

The method of forming the dispersions, the composition of the forming solutions, and the range of droplet diameters contributing significantly to the volume of the dispersed mercury are indicated in Table I. All of

[16] B. Vonnegut, J. Colloid Sci. 3, 563 (1948).

[17] G. M. Pound and V. K. LaMer, J. Am. Chem. Soc. (to be published).

[18] D. Turnbull, Science 112, 448 (1950).

[19] D. Turnbull, Phys. Rev. 83, 880 (1951).

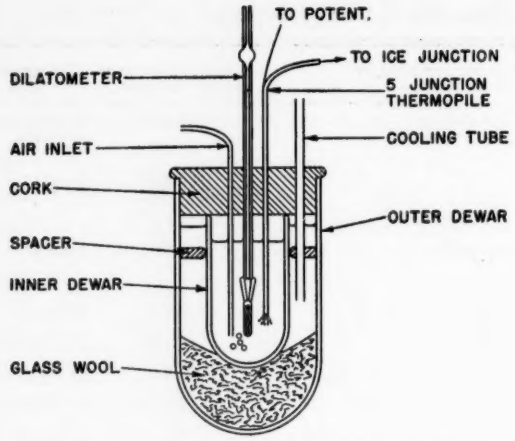

FIG. 1. Schematic drawing of bath for maintaining constant temperature.

the organic compounds used in the preparations were Eastman cp chemicals, excepting that purified lauroyl peroxide[20] was furnished by W. E. Cass and acetyl peroxide was obtained in the form of 25 percent dimethyl phthallate solution from Buffalo Electrochemical Company. The iodine and sulfur used were reagent grade materials.

It is believed that the film on the droplet surface consisted of a mercury compound in all cases excepting for the dispersion formed in the alcoholic sodium oleate solution. When the air pressure in the blendor containing the stearic acid solution was reduced to about 0.001 atmosphere, the mercury did not break up into droplets. Therefore, it is believed that the Hg(St) film formed as a result of reaction of the stearic acid with an oxide film formed by the interaction of air and mercury. The chemical film formed in peroxide solution is believed to result from the acid catalyzed direct addition of mercury to peroxide

In all cases the amount of the film forming agent used was less than that required to form by complete reaction an Hg_2^{++} salt constituting a volume fraction of 0.02 of the dispersed mercury.

Measurements of the droplet size distribution $[(y^0=f(D)]$ in the dispersions where time, temperature, and medium of dispersion were varied to the extent used in the experiments established that $y^0=f(D)$ was not measurably affected by these variations, with the possible exception of Hg(S) dispersions (on which such observations were not made) and the Na Oleate dispersions. However, Hg_2I_2 dispersions did coarsen with time when one-half the indicated amount of iodine was used in forming them.

B. Temperature Measurement and Control

The extent of solidification of mercury was measured dilatometrically. In these measurements two schemes were used on occasion to maintain the temperature constant. The first of these schemes was used in the experiments on Hg(St) and Hg_2I_2 coated aggregates. The constant temperature chamber consisted of a well-insulated can containing freon 11 entirely surrounded, excepting for outlets, by a bath of the same fluid. Further details on the construction of this bath have been published.[9] To maintain the temperature of the outer bath constant to within ± 0.2°C the potential developed by a five junction thermopile, having one set of junctions in the outer bath and the other set in a Dewar flask containing a constant temperature mixture, was used to activate a General Electric Recording potentiometer. The recorder was part of a relay circuit so that as the bath reached the control temperature, the recorder needle closed a relay circuit thus causing the bath heater circuit to open. Liquid nitrogen was circulated in cooling coils in the outer bath. This method of temperature control requires a compound in the Dewar flask at a phase transition temperature within 5 to 10° of the bath temperature to be maintained. With the indicated degree of control of the outer bath, the inner bath temperature remained constant to within ± 0.01°C. The inner bath was agitated by bubbling air through it and its temperature was checked every three to five minutes.

In the other isothermal experiments, a much simpler and equally effective method was used to control temperature. In this method the outer bath was a 4-liter Dewar filled to a level well above the fluid level in the inner bath with a partly melted compound at a temperature 20 to 30° lower than the temperature to be maintained in the inner bath. The container for the inner bath was a 1-liter unsilvered Dewar flask maintained in position by glass wool support and Teflon spacers so that its top was 2 in. to 3 in. below the top of the outer Dewar. The space between the top of the outer and inner Dewars was filled with a cork insulator. Figure 1 shows the arrangement schematically. Heat leaked slowly from the inner to the outer bath. To compensate for this loss, air originally at the ambient temperature was passed through the inner bath. This rate of air flow was regulated by a flowmeter and valve arrangement sufficiently sensitive so that a given pressure differential could be maintained to within a millimeter of water. After the system reached thermal equilibrium with a given rate of air flow, the temperature in the inner bath was held constant to within 0.01°C by small manual adjustments of the rate at intervals ranging from three to fifteen minutes. To determine when these adjustments would be necessary, the temperature of the inner bath was measured every two to five minutes. In the isothermal measurements on Hg(Lau) coated droplets (-117 to -120°) freon 12 was used in the inner bath and an equilibrium mixture of liquid and solid freon 12 in the outer bath.

The temperature was calculated from the potential developed by a five junction copper-constantan thermopile. This potential was measured on a Type K poten-

[20] The source and purity is described elsewhere. W. E. Cass, J. Am. Chem. Soc. 72, 4915 (1950).

tiometer. One set of thermocouple junctions was placed in the bath a small distance from the middle of the dilatometer bulb. The other set was immersed in a Dewar containing an equilibrium mixture of distilled water and ice made from distilled water. After each set of measurements, the thermocouple calibration was checked against the melting temperature of pure mercury. In all cases, this calibration agreed with the standard calibration charts for copper-constantan thermocouples to within 0.05°C.

C. Dilatometry

A general description of the dilatometer has been published.[9] The dilatometer bulbs were about 6- to 7-cm long and ~0.5-cm internal diameter. Five to seven g of mercury (*ca* ½cc) droplets from a given dispersion were introduced into the dilatometer bulb and the dispersing medium changed to the fluid indicated in Table I by several decantations and additions. The capillary bores of the various dilatometers were from 0.055- to 0.065-cm diameter. The drop in fluid level in the dilatometer capillaries caused by the complete isothermal solidification of mercury ranged from 4.5 to 6.5 cm. The fluid level in the capillary was measured, relative to a fixed point on the outer surface of the capillary, to within 0.02 cm by means of a cathetometer.

Preliminary experiments were made on each of the dispersions to determine the temperature range in which solidification occurs at a reasonable rate. The experimental procedure used in these "continuous" cooling experiments has been described.[9] Figure 2 shows the dilatometer readings obtained from a cooling-heating cycle on Hg(St)-coated droplets. A linear section of the cooling curve AB was established corresponding to the thermal contraction curve for the dilatometer fluid and the liquid mercury. It was confirmed that the curve $B \rightarrow A$ was identical to $A \rightarrow B$ and it was therefore concluded that no appreciable solidification had taken place at $T > T_B$. The curve CD is the thermal expansion curve of dilatometer fluid and solid mercury.

xy, the vertical displacement of the lines AB and CD at T_{xy} is the dilatometer contraction, Δh_0, proportional to the change in volume of the dispersion if all the mercury contained in it solidified isothermally at T_{xy}. The variation of Δh_0 with temperature in the range of rapid solidification is negligible. Δh_0 was measured to within one percent uncertainty.

Temperatures of beginning solidification T_i and of final solidification T_f measured in the cooling-heating experiments are defined as the temperatures between which the points on the cooling curves do not fall, within experimental error, on the extrapolation of either of the lines AB or CD. Actually, T_f and T_i are weak functions of the rate of cooling and in this investigation are specified for a cooling rate of 1°/minute.

No values of T_f and T_i were accepted as characteristic of a given dispersion unless two additional conditions were established as follows: (1) The volume contraction presumed to be associated with solidification was registered as an expansion during the heating cycle at the accepted melting temperature of mercury. (2) The sample evolved a substantial quantity of heat (heat of solidification) when cooled through the temperature range T_i to T_f.

The temperature range in which the heat of solidification was evolved was determined by measuring as a function of temperature the deflection, δ, of a sensitive galvanometer activated by a differential thermocouple having one junction in a well embedded in the sample and the other junction embedded in a well in the temperature bath. When the bath was cooled at a constant rate of 1°/min, δ exhibited a pronounced maximum at a temperature between T_i and T_f. Values of T_i and T_f measured by this method were in excellent agreement with values measured dilatometrically in all cases, excepting for some experiments where a dispersing fluid was used that gelled at $T < T_i$.

In the isothermal dilatometric experiments the sample bulb was always thoroughly dispersed by shaking immediately before the experiment in order to insure that the rate of volume contraction would not be limited by the flow of fluid into the mercury. The dilatometer bulb and part of the capillary, which had been precooled to a temperature about 10° above that of the inner bath, were immersed in the inner bath after a constant temperature T_C had been established in it, and dilatometer readings $h(t)$ were taken as a function of time. After measuring $h(t)$ over a three- or four-hour period, the sample was either (a) quickly quenched into an auxiliary bath maintained at a temperature about 10° below T_f, held in this bath for about 15 minutes then returned to the original bath at T_C, or (b) the bath at T_C was slowly cooled to about 10° below T_f, held for 15 minutes at the lower temperature, and then warmed back up to T_C. In either event after about 15 minutes more of thermal equilibration at T_C a final dilatometer reading h_f was taken. The dilatometer reading h_i corresponding to the fraction of sample

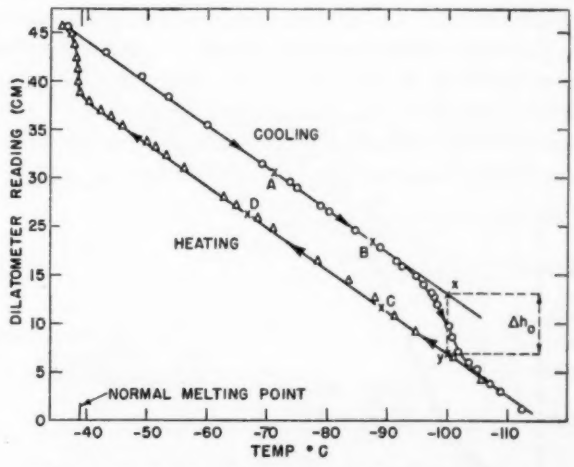

FIG. 2. Cooling-heating cycle for dispersion of Hg(St)-coated Hg droplets.

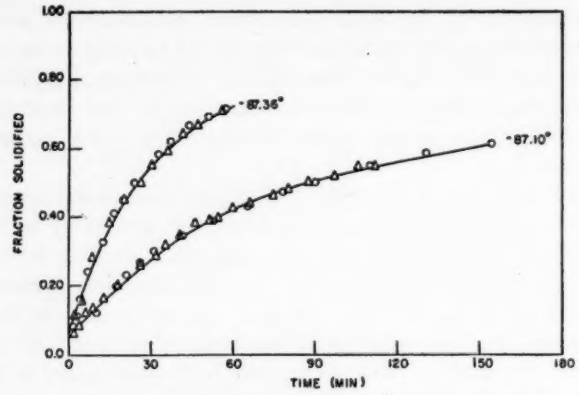

FIG. 3. Comparison of duplicate isotherms on a dispersion of Hg_2I_2-coated Hg droplets.

solidified $X=0$ at T_C is calculated from the equation $h_i=h_f+\Delta h_0$. $X=f(t)$ is given by $X=[h_i-h(t)]/\Delta h_0$. The time origin was taken as the ordinary time when $h(t)=h_i$.

Additional experiments were carried out on the Hg(Lau)-coated droplets to find out how closely the temperature of the sample approached the temperature of the bath. For this purpose, a dilatometer was used containing an embedded thermocouple well. The potential difference developed in a thermocouple with one junction in the well and the other in the bath was measured as a function of time at constant bath temperatures. In the same experiments $X=f(t)$ was measured. It was found that for transformation rates $R\leqslant$ than 0.05 g of mercury/min the temperature difference registered by the differential couple was <0.02°C. After quenching the precooled dilatometer into the bath at T_C, the temperature inside the dilatometer generally approached T_C within a period of about five minutes. In most of the isothermal data to be reported R was well below 0.05 g/min.

The reproducibility of the isotherms was checked by repeating measurements on several for each dispersion. For all, $X=f(t)$ was reproduced to within the accuracy of the $h(t)$ measurements. Figure 3 illustrates the reproducibility of two isotherms on the Hg_2I_2 coated mercury droplets. The second experiment at -87.10°C was made immediately after the first one, but one week's time elapsed between the two experiments at -87.36°.

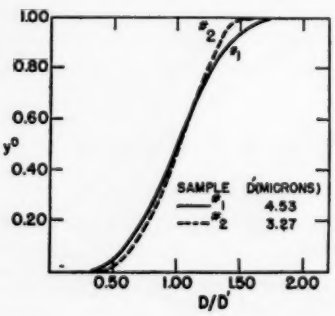

FIG. 4. Hg droplet size distribution in Hg(Lau) dispersions.

D. Droplet Diameter Measurement

To measure droplet diameter, a Spencer microscope with an apochromat lens and Aplanat eyepiece was used. The lens had a 4-mm objective and was fitted with a correction collar. Illumination was provided by transmitted light from a zircon arc source. A prism was used to project the field on the wall and the diameter of the image measured, after bringing it into focus, to within $\frac{1}{2}$ mm. For droplets having diameters in the range 2–12 microns, the magnification factor was 1160. Samples were taken directly from the dilatometer after the isothermal measurements and dispersed in mineral white oil. Due precautions were taken to obtain representative samples and to insure that the droplets would not be flattened by the microscope cover glass.

Droplet size determinations were made on two or more withdrawals from each dilatometer sample. The droplet size distributions for these withdrawals checked satisfactorily. The diameter of a total of about 2000 droplets in each dilatometer sample was measured. The volume of sample having droplet diameters between

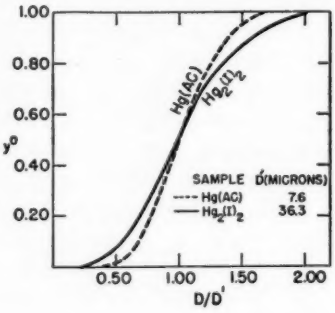

FIG. 5. Hg droplet size distributions in Hg_2I_2 and Hg(Ac) dispersions.

D and $D+\P D$ (where $\P D=500/1160$ microns for the magnification factor of 1160) was plotted against D. From smoothed curves $[(V^0dy^0/dD)=f(D)]$ through these points curves were constructed of the function $y^0=f(D)$ (see Figs. 4 and 5). D' is defined by

$$0.5=(1/V^0)\int_0^{D'} V_D{}^0dD=(1/V^0)\int_{D'}^{\infty} V_D{}^0dD. \quad (17)$$

RESULTS

A. Continuous Cooling Experiments

Figure 6 is a diagram that compares the results of the continuous cooling (rate ~1°/minute) experiments for the various dispersions. The ordinate is the supercooling, ΔT ($\Delta T=T_m-T$ where T_m is the melting temperature), and the abscissa is the logarithm of the droplet volume. T_m-T_i and T_m-T_f calculated from the continuous cooling experiments are the ΔT coordinates of the corners of each rectangle. The log$v$ coordinates of the corners define the range of volume of droplets that contribute significantly to the total volume of the mercury. A change of a factor of 10 in the cooling

rate shifts the ΔT coordinate of the rectangles 1° or less. These experiments prove conclusively that a very small droplet size in itself is not a sufficient condition for marked supercooling of liquids, for in most instances the size distribution in the various dispersions overlap considerably or even completely yet their nucleation frequencies differ by many orders of magnitude.

It must be concluded that the most important factor determining the position of a dispersion in the solidification diagram (Fig. 6) is the potency of the most effective nucleation catalyst on the surface or in the volume of the constituent droplets. Compared to this factor, the effects of droplet volume and cooling rate are second order. Nucleus formation must be initiated by catalysts in all of the dispersions with the possible exception of Hg(Lau) and Hg(Bz).

The chemical composition and structure of the effective catalytic substance may not correspond to that of the compound covering the major part of the droplet surface. Minute amounts of impurity in the forming compound could have formed a catalyst more potent than that formed by the compound itself, (though different samples of the forming substance gave the same result). However, the fact that the supercooling of the dispersions varies so widely even though their droplet size distributions overlap proves that, with the exception of Hg(Lau), Hg(Bz), and Na Oleate dispersions, the effective catalysts could not have been bodies suspended in the mercury prior to the formation of the dispersion. Further, the fact that the solidification range of a given dispersion is very narrow indicates that the effective catalytic substances in the dispersion must be chemically identical or closely related.

It has been established[9] that the solidification of Na Oleate dispersions is coincident with a breakdown in the protective action of the absorbed film. Therefore, the position on the solidification diagram may not indicate the actual $\Delta T-\log v$ relationship for Na Oleate dispersions. The main interest attaching to the Na Oleate results is that droplets so large (0.4-mm diameter) can be supercooled so much (35°).

After long holding periods at room temperature, the solidification behavior of Hg(Lau) and Hg(St) dispersions changed discontinuously from that defined by the Hg(St) and Hg(Lau) rectangles in Fig. 6 to that defined by the HgX rectangle with no accompanying change in droplet size distribution. Before this transition is complete, two discrete ranges of solidification [HgX and Hg(St) or Hg(Lau)] are found in the same dispersion. No measurable part of dispersions coated with Hg(Bz) reverted to the Hg(X) class over a two-week period. Holding Hg(Lau) dispersions at −40°C or lower completely suppressed the transition for at least several weeks.

Addition of small amounts of glacial acetic acid to HgX dispersions in methyl cyclopentane caused a marked increase (by a factor of 10 to 20) in the mean droplet diameter and a discontinuous transition in solidification behavior to that characteristic of Hg(Ac) dispersions.

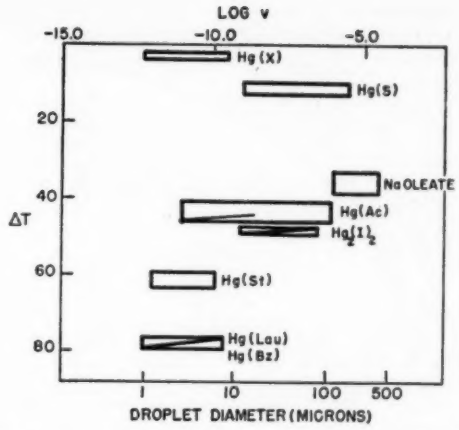

FIG. 6. Solidification diagram for mercury—curves in certain rectangles are isokinetic relations.

These facts seem consistent with the following hypotheses: (a) Hg(Lau) and Hg(St) films hydrolyze to form patches of mercury oxide on the surfaces of the droplets. (b) Mercury oxide is an effective catalyst for the nucleation of mercury crystals. (c) Acetic acid converts the oxide to mercury acetate. In further support of these ideas, it was observed that the transition to Hg(X) was made markedly slower by increasing the viscosity of the dispersing medium and in some instances by greatly increasing the shortest available diffusion path between the droplets and atmospheric components.

B. Homogeneous Nucleation

Isothermal Solidification of Hg(Lau) Coated Droplets

From our interpretation of the continuous cooling experiments, it follows that the temperature range of rapid homogeneous nucleation should either correspond to or fall below $T_i > T > T_f$ for Hg(Lau) or [Hg(Bz)] coated droplets. Therefore, it is important to find whether or not the isothermal solidification behavior of these dispersions follows the predictions of the homogeneous nucleation theory.

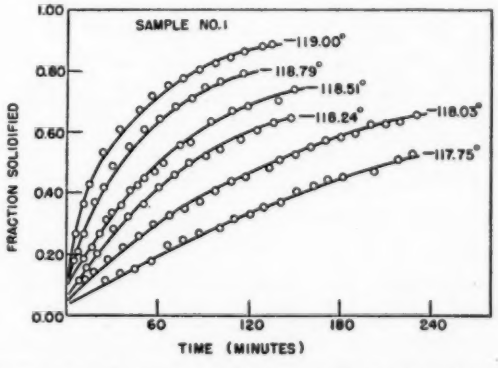

FIG. 7. Solidification isotherms of Hg(Lau)-coated droplets—Sample No. 1.

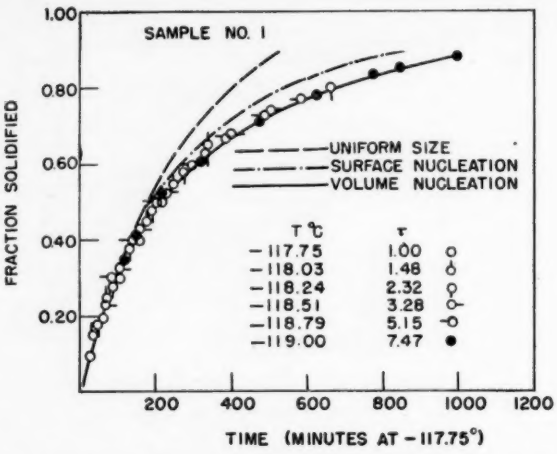

FIG. 8. Comparison of isotherms calculated on the basis of volume or surface nucleation hypotheses with master isotherm for solidification of Hg(Lau)-coated Hg droplets—Sample No. 1. The "uniform size" curve was calculated on the assumption of a uniform droplet diameter.

For the isothermal experiments, two Hg(Lau) dispersions having different droplet size distributions were prepared. $y^0=f(D)$ for these dispersions is given in Fig. 4. To prepare the dispersion (Sample No. 2) having the smaller D' value, the blendor was run for a longer period of time than for Sample No. 1.

$X=f(t)$ curves for Sample No. 1, calculated from dilatometric data at six temperatures in the range -117.75 to $-119.00°$, are plotted in Fig. 7. In order to test the volume and surface nucleation hypotheses, it is convenient to shrink all the data to a "master isotherm" by letting the magnitude of the time unit vary with temperature. Figure 8 shows the master isotherm and the best multiplying factors τ to apply to the ordinary time units to obtain the best superposition of the isotherms.

In constructing this isotherm, the data obtained at the shortest times at the lowest temperatures were disregarded because the transformation rate under these conditions substantially exceeded 0.05-g Hg/min. In order to test Eq. (14) derived from the homogeneous (or volume) nucleation, hypothesis $X=f(t')$, where $t'=\alpha t$ and t is expressed in time units at $-117.75°$ ($\tau=1.0$), was calculated from (14) with the use of the relation $y^0=f(D)$. Then α is evaluated by making $X=f(t')$ coincide with the experimental $X=f(t)$ relation at two values of X, in this instance 0.10 and 0.30. Making the substitution $t'=\alpha t$ in $X=f(t')$ gives the relation $X=f_v(t)$ predicted by Eq. (14) (volume nucleation). An analogous procedure where the calculated and experimental isotherms are made coincident at the same values of X as in testing the volume nucleation hypothesis, was used to calculate a relation $X=f_a(t)$ predicted by Eq. (16) (surface nucleation).

The comparison of $X=f_v(t)$ and $X=f_a(t)$ with the master isotherm $X=f(t)$ determined experimentally is shown in Fig. 8. The data are described by $X=f_v(t)$ to well within the experimental uncertainty but $X=f_a(t)$ falls somewhat outside the range of uncertainty in the experimental points for $X>0.5$.

The same order of agreement of $X=f_v(t)$ and $X=f_a(t)$ with the data was obtained when the unsmoothed droplet diameter distribution was used in place of the smoothed $y^0=f(D)$. From this result, it is concluded that the errors that may have been made in determining the droplet size distribution are not of sufficient magnitude to affect the validity of the conclusion that the data are best fitted on the basis of the volume nucleation hypothesis.

From the described analysis, values of k_D and [from Eq. (13)] I are calculated for $-117.75°$. I for the other temperatures is found by multiplying I at $-117.75°$ by the appropriate τ-factor listed in Fig. 8.

The sources and probable magnitude of the principal errors that affect the intercomparison of I values measured on the same sample are as follows:

1. $\pm0.02°$ uncertainty in the control and measurement of temperature may cause ±3 percent error in I.
2. ±0.03 cm uncertainty in final cathetometer reading may lead to ±1 percent error in I.

Thus the probable deviation of I values measured on the same dispersion at the same temperature is of the order of 4 percent.

The greatest part of the probable deviation of I values measured on different samples, prepared in the same way, is contributed by the uncertainty in the measured droplet size distribution, for any error in the measurement of D is magnified three times when I is calculated. It is estimated that (considering errors in sampling, microscope magnification, measurement, and curve smoothing) D' was measured with an accuracy of ±5 percent, therefore, the corresponding probable error in I is ±15 percent. An additional term, affecting the intercomparison of different samples is the ±2 percent probable error in I caused by ±0.05 cm, uncertainty in Δh_0. By taking all these terms into account, the maximum probable error in the absolute magnitude

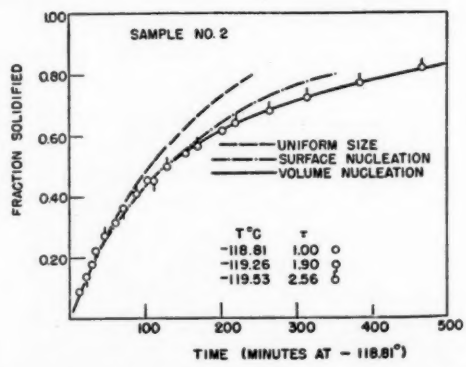

FIG. 9. Comparison of isotherms calculated on the basis of volume or surface nucleation hypotheses with master isotherm for solidification of Hg(Lau)-coated Hg droplets—Sample No. 2. The "uniform size" curve was calculated on the assumption of a uniform droplet diameter.

of I and the maximum probable deviation when samples prepared in the same way are intercompared is ±21 percent.

Three isotherms were measured on Sample No. 2. The master isotherm and τ-values calculated from these data are given in Fig. 9. Analysis of the results by the same method used on Sample No. 1 established that they are best described (and satisfactorily so) on the basis of the volume rather than the surface nucleation hypothesis. I values were calculated as before.

Equation (1) gives $I=f(T)$ based on the homogeneous nucleation theory. From thermodynamic principles,

$$d(\Delta F_v)/dT=-\Delta S_v, \tag{18a}$$

where ΔS_v is the entropy of solidification/volume. According to the existing thermodynamic data,[21] ΔS_v is virtually independent of temperature;[22] therefore, to a good approximation,

$$\Delta F_v=-(\Delta S_v)\Delta T \tag{18b}$$

and Eq. (1) may be rewritten

$$I=K_v \exp[-a\sigma^3/(\Delta S_v)^2(\Delta T)^2kT]. \tag{19}$$

If σ is assumed to be independent of temperature, it follows that $\ln I$ is a linear function of $1/T(\Delta T)^2$ having the slope,

$$d\ln I/d[1/T(\Delta T)^2]=-a\sigma^3/(\Delta S_v)^2k; \tag{20}$$

$\log I$ is plotted against $1/T(\Delta T)^2$ for both samples in Fig. 10, and an excellent straight line relation obtains for each sample as required by Eq. (1). The average deviation from the mean value of I between Samples 1 and 2 in the overlapping temperature range of the two sets of measurements is 14.5 percent and within the calculated maximum deviation of 21 percent.

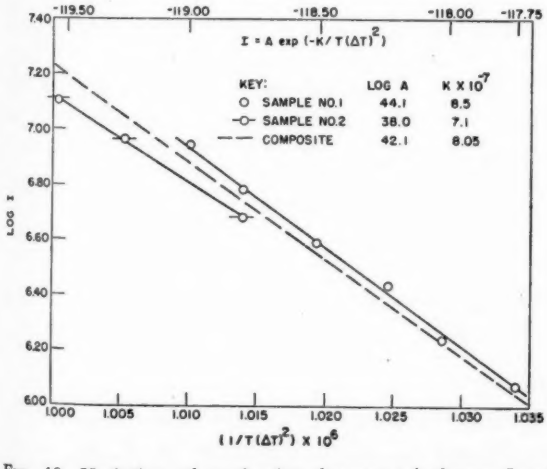

FIG. 10. Variation of nucleation frequency/volume, I, with supercooling, ΔT, in the solidification of Hg(Lau)-coated Hg droplets.

[21] K. K. Kelley, Bureau of Mines Bulletins No. 371 (1934) and No. 393 (1936).

[22] The author is indebted to R. A. Oriani for establishing this fact.

TABLE II. Summary of results on kinetics of homogeneous and heterogeneous nucleation in mercury.

Surface coating	Type of nucleation	σ erg/cm²	θ	$\log K_v$ Exptl.	$\log K_v$ Calc	$\log K_s$ Exptl.	$\log K_s$ Calc
Hg(Lau)	Volume (Homogeneous)	31.2	···	42.1	35.1	···	···
Hg(Ac)	Surface (Heterogeneous)	31.2	72°	···	···	26.8	27.3
Hg_2I_2	Volume (Heterogeneous)	[a]	···	69.6	35.5	···	···
Hg(St)	Heterogeneous	31.2	87°	31.	35.	27.4	27.3

[a] The nucleation frequency in iodide coated droplets can be satisfactorily described by an *apparent* value of $\sigma=29.2$ erg/cm².

A further check on the validity of the volume nucleation hypothesis is obtained from these data by comparing the measured value of k_D' for Sample No. 2 with the values calculated from the results on Sample No. 1 on the basis of the surface $(k_D')_a$ and volume $(k_D')_v$ hypothesis. At the temperature −118.81° in Sample No. 2, the experimental value of $k_D'=0.0052$ min^{-1} in fair agreement with $(k_D')_v=0.0065$ min^{-1} and in marked disagreement with $(k_D')_a=0.0095$ min^{-1}. Though it is recognized that the deviation between $X=f(t)$ and $X=f_a(t)$ for any one set of data is hardly large enough to be convincing, it is believed that the result just cited and the fact that $X=f(t)$ is in best agreement with $X=f_v(t)$ for two dispersions fully substantiates the conclusion that k_D' in these experiments is proportional to droplet volume.

From the $\ln I$ *vs* $1/T(\Delta T)^2$ lines for the two samples a composite straight line was constructed as shown in Fig. 10. Assuming that mercury crystal nuclei are spherically shaped ($a=16\pi/3$), σ was calculated from the slope of the composite line [Eq. (20)] to be 31.2 ergs/cm². (Also see summary of results—Table II.) The radius of the nucleus[23] $r^*=-2\sigma/(\Delta F_v)$ was calculated to be 11.8A° at −118°; whence it follows that it contains 830 atoms and $n^*=220$.

To calculate K_v from the theory of homogeneous nucleation [Eq. (2)] it was assumed that $\Delta F_A=(\Delta F_A)_{vis}$, where $(\Delta F_A)_{vis}$ the free energy of activation for viscous flow is calculated from the viscosity of mercury using the equation for viscosity calculated from absolute rate theory.[24] In the temperature range of the measurements $\exp(-\Delta F_A/kT)\approx 10^{-2}$. With this assumption $\log K_v$ calculated from Eq. (2) is 35.1 and is to be compared with the experimental value of 42.1±2 determined from the intercept of the composite line in Fig. 10 on the $\log I$ axis.

To explain this disagreement of a factor of at least 10^5 between the K_v and $(K_v)_{exp}$, some of the assumptions made in deriving and applying the theory have to

[23] M. Volmer, *Kinetik der Phasenbildung* (Steinkopff, Leipzig, Germany (1939).

[24] Glasstone, Laidler, and Eyring, *The Theory of Rate Processes* (McGraw-Hill Book Company, Inc., New York, 1941), pp. 477–516.

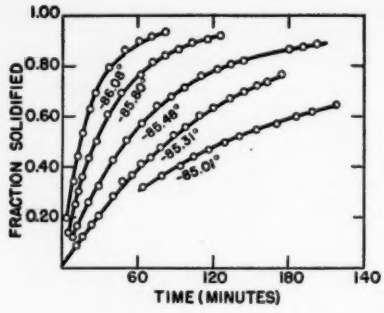

FIG. 11. Solidification isotherms of dispersion of Hg(Ac)-coated Hg droplets.

be examined more critically. In the derivation of the theory the frequency factor for the addition of an atom to the nucleus from the liquid was assumed to be (kT/h) from the absolute rate theory. There is no assurance that this assignment is valid for an atomic process as complex as the nucleation reaction. In addition, it is assumed that crystal embryos mix ideally with the supercooled liquid. It is believed that together these factors might lead to an uncertainty as large as $10^{\pm 2}$ in the calculated K_v. However, the assumptions that ΔS_v and σ are temperature independent are probably of more importance. The term $\exp[-a\sigma^3/(\Delta F_v)^2 kT]$ is very temperature sensitive (such that I changes by a factor of 5/°C) so that even a very small dependence of σ or ΔS_v upon temperature has a potent effect upon the measured slope $[d \ln I/d(1/T(\Delta T)^2]$ and hence on $\log(K_v)_{\text{exp}}$. For example, suppose that σ depends upon temperature according to the equation: $\sigma=\sigma_0+bT$ and that ΔF_v is given by $\Delta F_v=-\Delta S_v{}^0(\Delta T)(1+c\Delta T)^{\frac{1}{2}}$. It follows,

$$d \ln I/d[1/T(\Delta T)^2] \approx [-a\sigma^3/(\Delta S_v)^2 k] \times\{1+[T(T_m-T)/(3T-T_m)][3b/\sigma+c]\}. \quad (21)$$

In Eq. (21) the factor $-a\sigma^3/(\Delta S_v)^2 k$ is the slope that would be measured if σ and ΔS_v were temperature independent.

If $c=0$ a value of $b\approx 0.0008/°$ is sufficient to change the slope 18 percent and the apparent value of K_v by a factor of 10^6. In order to cause a change of the same order of magnitude when $b=0$, c must be 0.0016/°.

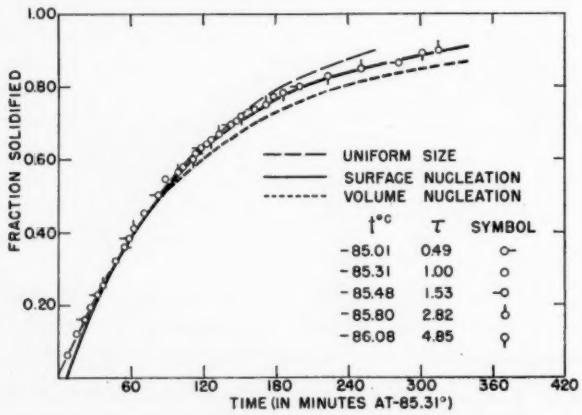

FIG. 12. Comparison of isotherms calculated from volume and surface nucleation hypotheses with master isotherm for Hg(Ac)-coated Hg droplets.

It seems reasonable to suppose that the combined effect of b, $c\neq 0$, and the relatively large ΔT values obtaining in the experiments accounts for the major part of the disagreement between K_v and $(K_v)_{\text{exp}}$.[25] On the basis of this analysis, it may be concluded that the experimental results are compatible with the predictions of the homogeneous nucleation theory.

The only other possible interpretation of the data that seem to merit serious consideration is that nucleation is catalyzed by inclusions colloidally suspended in the mercury. In order to account for the results, the minimal concentration of the inclusions would have to be 10^{13} to 10^{14}/cm³ (corresponding to a volume fraction 10^{-5} to 10^{-8}) all having equal catalytic effectiveness/cm². Since the same results are obtained in continuous cooling experiments with Hg(Bz), and two-Hg(Lau) dispersions gave the same I within experimental error, it is concluded that these inclusions could not have had their origin in the preparation of the dispersion but, if present, must have been suspended in the original mercury sample.

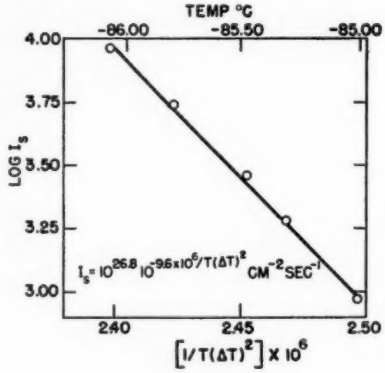

FIG. 13. Variation of I with ΔT for solidification of Hg(Ac)-coated Hg droplets.

The arguments that make the colloidal catalyst interpretation less plausible are:

(1) The homogeneous nucleation theory describes the results semiquantitatively.

(2) Hg(Lau) dispersions from different lots of mercury exhibited the same solidification behavior within experimental error in continuous cooling experiments.

Since $I=f(T)$ and k_D is given by Eq. (13), it follows that

$$k_D=f(T)v_D. \quad (22)$$

From (22) we may derive "isokinetic" relations between v_D and T at constant k_D as follows,

$$[v_D=f'(T)]_{k_D=\text{constant}}. \quad (23)$$

One such isokinetic curve for Hg(Lau)-coated droplets is drawn in Fig. 6. The k_D value of this curve is

[25] We do not assert that the signs of b and c are actually as indicated. Intuitively it might be believed that b should be negative rather than positive. However, our knowledge of liquid-crystal nuclei interfaces is not sufficiently advanced to justify such a belief. Our purpose is to show that the neglect of the factors b and c might, so far as our present knowledge goes, account for the disagreement between K_v and $(K_v)_{\text{exp}}$.

fixed by the co-ordinates of a corner of the Hg(Lau) rectangle.

C. Heterogeneous Nucleation

1. k_D *Proportional to Droplet Area: Isothermal Experiments on Hg(Ac)-Coated Droplets*

The primary purpose of this investigation was to measure the kinetics of homogeneous nucleation of mercury crystals. Consequently, the isothermal solidification behavior of dispersions in which nucleation is believed to be heterogeneous was studied in less detail than that of the Hg(Lau) dispersions.

Figure 11 shows the $X=f(t)$ isotherms obtained at five different temperatures on a dispersion of Hg(Ac) coated droplets. The isotherm at $-85.01°$ does not extrapolate to $X=0$ at $t=0$ because the dispersion was inadvertently precooled to a temperature just below $-85.01°$ for a short time prior to the running of the isotherm.

The data were analyzed by the same methods used to analyze the data on the Hg(Lau) dispersion. Figure 12

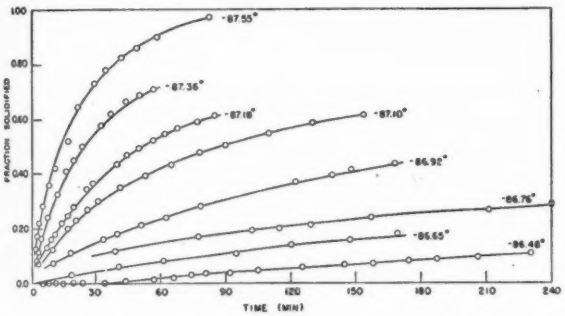

FIG. 14. Solidification isotherms of dispersion of Hg_2I_2-coated Hg droplets.

shows the master isotherm and Fig. 5 the smoothed curve for $y^0=f(D)$. In evaluating α the calculated and experimental curves were made coincident at $X=0.3$ and 0.5. Comparison of the calculated curves with the master isotherm is made in Fig. 12. Clearly the data are most satisfactorily described on the basis of the surface nucleation hypothesis [Eqs. (15) and (16)]. For $0 \lesssim X \lesssim 0.2$ the experimental rate is greater than calculated on the basis of either the surface or volume nucleation hypotheses, but this departure is not considered significant in view of the small values of X and t.

I_s was calculated at various temperatures from the τ values shown in Fig. 12. $\text{Log}I_s$ is a linear function of $1/T(\Delta T)^2$ as shown in Fig. 13. From the measured slope and the value of σ obtained from the experiments on homogeneous nucleation, the contact angle θ was calculated to be [see Eq. (5)] 72°. $\text{Log}(K_s)_{exp}$ was found to be 26.8 which compares well with the value 27.4 calculated from Eq. (6) on the assumption that all elements of area in the droplet surface are equally effective for nucleation catalysis.

This excellent agreement between theory and experiment fully supports the concept developed earlier that the kinetics of heterogeneous nucleation can be described with the use of a single parameter, θ, in addition to those required to describe homogeneous nucleation. Deviations between theory and experiment due to any temperature dependence of ΔS_v and σ will be smaller in these experiments[26] than in the case of homogeneous nucleation because ΔT is much smaller.

An isokinetic relation between $\log v$ and ΔT for this dispersion is indicated on the solidification diagram in Fig. 6.

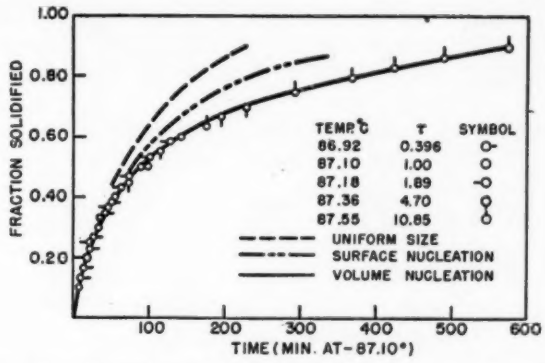

FIG. 15. Comparison of isotherms calculated from volume and surface nucleation hypotheses with master isotherm for Hg_2I_2-coated Hg droplets.

2. k_D *Proportional to Droplet Volume: Isothermal Experiments on Hg_2I_2-Coated Mercury Droplets*

$X=f(t)$ curves measured at eight temperatures on a Hg_2I_2-coated dispersion are plotted in Fig. 14. Because of the extraordinary magnitude of the temperature coefficient of the rate, every isotherm was rechecked, with the exception of the one at $-87.55°C$. In all cases, the agreement is excellent.

$y^0=f(D)$ for this dispersion is given in Fig. 5. The master isotherm and the test of its agreement with the volume and surface nucleation hypotheses is shown in Fig. 15. A much better fit (also an entirely satisfactory one) is obtained on the basis of the volume than on the

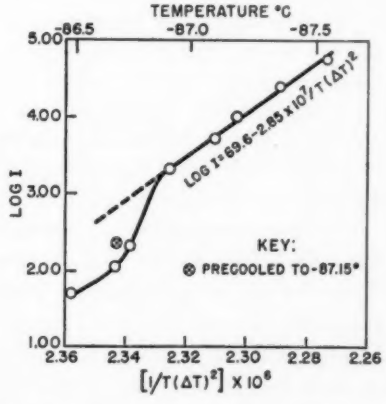

FIG. 16. Variation of I with ΔT for the solidification of of Hg_2I_2-coated Hg droplets.

[26] Of the order of 10^2 if it is accepted that the deviation in the homogeneous nucleation results is caused by the temperature dependence of σ and ΔS_v.

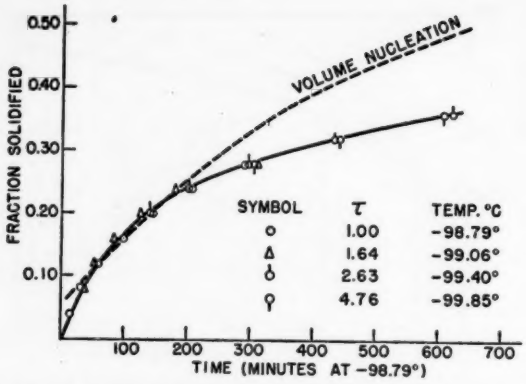

FIG. 17. Comparison of isotherm calculated from volume nucleation hypothesis with master isotherm for dispersion of Hg(St)-coated Hg droplets.

surface nucleation hypothesis. Log$I$ is plotted against $1/T(\Delta T)^2$ in Fig. 16. A good straight line relation is obtained at the five lowest temperatures; $(K_v)_{exp}$ and the apparent σ value derived from the constants of this line are listed in Table II. At temperatures higher than $-86.9°$ I is much lower (by a factor of 4) than predicted by the low temperature linear relation. When the dispersion was precooled below $-86.9°$ then warmed to a temperature above $-86.9°$, the transformation rate at the higher temperature was significantly larger than if the sample had not been precooled.

These results can be explained on the hypothesis that the nucleation is catalyzed by colloidal particles suspended throughout the volume of the mercury droplet. For reasons already given it seems likely that these catalysts must have had their origin in the preparation of the dispersion rather than in some earlier stage of the mercury processing.

The greater total catalytic effect of the suspended particles in comparison with the Hg_2I_2 film on the droplet surface might be accounted for in one of the following ways:

(1) The suspended particles are not chemically identifiable as Hg_2I_2 and their catalytic potency, p, is greater than p for Hg_2I_2.

(2) The suspended particles are Hg_2I_2 having the same p as the surface film. However, the total area of these particles/droplet considerably exceeds the film area/droplet. For example, if the suspended particles were 0.01 micron in diameter and their volume fraction ~ 0.001, their total area/droplet would exceed the droplet area by a factor of 4.

(3) The thermodynamic properties and undoubtedly also the lattice parameters of crystals 0.01 micron in diameter differ significantly from those of crystals exceeding one micron size. Therefore, p for 0.01 micron Hg_2I_2 particles might exceed p for the larger Hg_2I_2 crystals constituting the surface film.

As a consequence of the exceptionally marked dependence of I on T (a factor of about $200/°$) $(K_v)_{exp}$ $\sim 10^{70}$ is many orders of magnitude larger than maximum $K_v \sim 10^{35}$ calculable from nucleation theory. On the basis of the known facts, it is not possible to reconcile this disagreement with nucleation theory without an additional hypothesis. It can be verified from the theory that the temperature coefficient of nucleation in heterogeneous processes is larger, the nearer the process is in temperature to the equilibrium temperature. Therefore, the results on the Hg_2I_2 dispersion suggest that the rate controlling process is the formation of the nucleus of a phase in equilibrium with liquid mercury (or with Hg_2I_2) at a temperature well below the normal melting point of mercury. Two possible rate-controlling mechanisms to account for the results are suggested:

1. Formation of a nucleus of a new Hg_2I_2 phase having a greater catalytic potency for formation of mercury crystals than the parent Hg_2I_2 phase.

2. Nucleation of a crystalline mercury phase, β, having a melting temperature well below $-38.87°C$. It is supposed that the nucleation of β is more strongly promoted by Hg_2I_2 than is the nucleation of the most stable crystalline phase α. Also it is assumed that the nucleation of α in β is rapid by comparison with the nucleation of β in liquid.

The experimental results can be reconciled with theory on the basis of mechanism (2) if β melts around $-70°C$.

An isokinetic relation $\Delta T = f(\log v)$, for the Hg_2I_2 dispersion is indicated in Fig. 6.

3. *Heterogeneous Nucleation Showing Multiplicity of I_s at Constant T*

(*a*) *Results on Hg(St) Dispersion.*—$y^0 = f(D)$ for this dispersion was practically identical in shape with $y^0 = f(D)$ for Sample No. 1 shown in Fig. 4 but with $D' = 3.8$ microns. $X = f(t)$ was measured at four temperatures and the master isotherm constructed from these data is plotted in Fig. 17. After an earlier analysis[5b] of these results, it was concluded that the conditions for homogeneous nucleation were approached in these experiments. However, it proved impossible to describe the data on the basis of the volume nucleation hypothesis with a single value of I and the discovery was made that Hg(Lau) and Hg(Bz) dispersions supercool to temperatures 18–20° lower than Hg(St) dispersions. Therefore, it is believed that the earlier conclusion was mistaken and that mercury crystals are nucleated heterogeneously in the Hg(St) dispersion. The comparison of the master isotherm with the curve calculated on the basis of volume nucleation is given in Fig. 17. The experimental rate of solidification decreases with increasing X much more sharply than does the calculated rate. These facts can be interpreted on the hypothesis that two or more fractions of the dispersed droplets have different I_s values at constant temperature.

k_D' may be roughly estimated at a specified value of X by assuming the validity of the relation

$$k_D' = dX/dt(1-X). \quad (24)$$

Apparent values of I and I_s were evaluated from k_D' at $X=0.3$ using Eqs. (13) and (15). The constants θ and $(K_s)_{exp}$ of Eq. (5) calculated from these data and the τ-values in Fig. 17 are listed in Table II. In calculating the log $K_s=27.3$ given in the table, it was assumed that every mercury atom in the droplet surface was in the catalyst surface. Actually, it seems probable that the fraction of surface mercury atoms also in the catalyst surface was substantially less than unity.

Since Hg(Lau) films apparently do not catalyze the nucleation, it is not considered likely that any one of the effective catalysts in the Hg(St) dispersion is a mercury stearate. It seems more likely that the catalysts are mercury oxystearates and/or substances formed by the reaction of minor components in the stearic and forming solution with mercury.

(*b*) *Hg(X) Dispersion.*—Rates of solidification of Hg(X) dispersions increased slowly as a result of room temperature aging. Four isotherms measured over a two-day period, during which time aging is hardly perceptible, are plotted in Fig. 18. These isotherms can only be described by several values of I_s that differ widely (by factors of at least 1000) at constant temperature. Apparently, the curves approach in time an X asymptote, $X\simeq 0.2$ at $-41.72°$ to $X\sim 0.9$ at $-42.77°$. This general behavior is similar to that observed by Vonnegut[16] and by Pound and LaMer[17] in the solidification of tin.

(*c*) *Interpretation.*—The $X=f(t)$ relations for both the Hg(X) and Hg(St) dispersions can be described by the general analytical relation,

$$X=X_1^0[1-\exp(-k_1t)] + X_2^0[1-\exp(-k_2t)]\cdots X_i^0[1-\exp(-k_it)], \quad (25)$$

where X_1^0, $X_2^0\cdots X_i^0$ are fractions of the total dispersion, each characterized by a single nucleation frequency (k_1, k_2, $\cdots k_i$ per droplet). It is assumed for simplicity, and for the present purpose without a significant loss in rigor, that the droplet size in a given dispersion is uniform. So we have then to interpret directly a multiplicity in k that corresponds to a multiplicity in I_s.

Two terms of Eq. (25) with $X_1^0=0.3$ and $k_1\sim 100\ k_2$ are sufficient to describe the Hg(St) isotherms. At least five terms are required for the description of the HgX isotherms.

Two basic interpretations of the multiplicity of k seem worthy of serious consideration. First, it may be supposed that each k value characterizes the catalytic potency of a different chemical substance. In our experiments these were introduced during the dispersion forming process or formed in a subsequent chemical reaction (as was definitely the case for the HgX dispersion). An essential requirement of this interpretation is that the average number, m, of crystallites or surface patches per droplet of the most potent catalytic substance should not greatly exceed unity.

A second basic interpretation is that catalysis is effected by one chemical substance having different catalytic potencies in different parts of its surface or when formed on droplets of different size. For example, it may be supposed that nucleation takes place preferentially at nonthermally equilibrated defects in the surface of the catalytic crystallite. A specific example of such a defect is the step present in a crystal surface caused by the termination of a screw dislocation in it.[27] The specific structure and catalytic potency of these defects may vary considerably and considering the small mass of their containing crystallites, the average number m/droplet of the defects most effective in nucleation catalysis can be of the order unity. It follows that the formal treatment of the problem of the kinetics of nucleation catalyzed by such defects is entirely analogous to the treatment of k multiplicity as a result of catalysis by a variety of chemical substances.

A second possible explanation for a differing catalytic potency in the same chemical substance follows from the fact that the thickness of the droplet surface coating is only of the order of 0.05 micron. Therefore, its thermodynamic properties, lattice parameter, and catalytic potency will be comparatively sensitive functions of its thickness and surface charge density. It is conceivable that the film thickness and its surface charge density may be related to the droplet size in such a way that $X=f(t)$ is described by equations of type (25).

The kinetic treatment of the k multiplicity caused by suspended crystallites, surface patches, and structural defects must take into account the statistical distribution of units of a particular catalyst among the droplets. Kimball and Halford[28] have treated this problem formally considering only one kind of catalyst. Their method was to write an equation of type (25) where each term corresponds to a droplet class containing a specified number of catalytic units. Then the X_i^0's and k_i's are

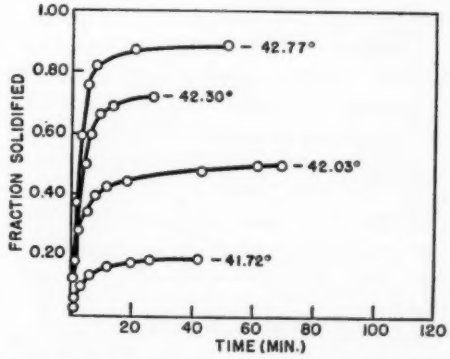

FIG. 18. Solidification isotherms of dispersion of Hg(X)-coated Hg droplets.

[27] Burton, Cabrera, and Frank, Nature **163**, 398 (1949).
[28] Kimball and Halford (private communication to Pound and LaMer, reference 17).

related to m and k, the nucleation frequency of a droplet containing one unit, through the Poisson distribution law. The resulting $X=f(t)$ relation is,

$$X=1-\exp\{-m[1-\exp(-kT)]\} \qquad (26)$$

and X approaches an asymptote $[1-\exp(-m)]$ at $t\to\infty$, for small values of m (26) reduces to $X=m[1-\exp(-kt)]$ which corresponds to a single term in Eq. (25) with $m=X_i^0$.

None of the existing data showing multiplicity of k values can be described by the Kimball-Halford theory on the assumption of a single catalyst; to fit the data to this theory requires several more terms of Eq. (26), approximately the same number as would be required with Eq. (25), corresponding to the additional active catalysts. For example, the Hg(St) data require two Kimball-Halford terms.

Pound and LaMer[17] have fitted two of their isotherms on tin with the Kimball-Halford formula. Their analysis shows that at least two specific catalysts were active and inspection of their other isotherms indicates that several other catalysts were probably active. The simple Kimball-Halford theory predicts that m is proportional to droplet volume if catalysis is effected by suspended crystallites or to droplet area if effected by chemical or structural heterogeneities in the droplet surface. Pound and LaMer's results are better described on the assumption that m is proportional to droplet area.

Applying the procedure used on the Hg(St) data Pound and LaMer's data gives $(K_s)_{\text{exp}}\sim 10^{31}$, compared with $K_s=10^{27.5}$ calculated on the assumption that every atom in the droplet surface is in an active catalytic surface.

It seems probable that the different catalysts responsible for the k multiplicity in the Hg(St) and Hg(X) dispersions are very closely related chemically, and in the case of Hg(X) they may be chemically the same and differ only structurally. The basis of this conclusion is that the solidification diagram (Fig. 4) shows that different crystalline compounds differ widely in their catalytic potency, and it seems very unlikely that two or more wholly unrelated compounds formed in the same dispersion process would exhibit nearly the same catalytic activity. It seems even more unlikely that several unrelated compounds exhibiting catalytic activity characterized by the narrow Hg(X) band in the solidification diagram could all be formed from the Hg(St) dispersion by approximately the same kinetics and all catalytically deactivated by small amounts of acetic acid.

CONCLUSIONS

In this investigation it has been demonstrated unequivocally for the first time, to the best of the author's knowledge, that the rate of crystal nucleation in several dispersions of supercooled mercury droplets follows first-order reaction kinetics described at constant temperature for a given dispersion by a single value of nucleation frequency/volume or area.

Convincing evidence has been obtained that 2–8 micron diameter mercury droplets coated by a mercury laurate film solidify from nuclei formed homogeneously. It is demonstrated that the data are in satisfactory agreement with the Turnbull-Fisher theory of homogeneous nucleation in condensed systems. This agreement lends credence to the use made of the theory[5a] to calculate liquid-crystal nucleus interfacial energies of metals where the homogeneous nucleation frequency is known at only a single temperature. (In calculating σ from I and a theoretical value of K_v, it should be remembered that an uncertainty of only one percent is introduced into σ for every factor of ten uncertainty in K_v.)

In an earlier publication,[5a] it was pointed out that "gram-atomic interfacial energies" σ_g of the strictly metallic elements calculated from presumed homogeneous nucleation frequencies are related to the corresponding gram atomic heats of fusion, ΔH_f, by the equation,

$$\sigma_g/\Delta H_f=0.46\pm 0.04. \qquad (27)$$

When treated according to the earlier procedure, for purposes of comparison, the new data on mercury give $\sigma_g/\Delta H_f=0.61$. This deviation from the average for the other metallic elements, though significant, is not sufficient to invalidate the generalization that $\sigma_g/\Delta H_f \approx$ constant for the metallic elements.

The first instance has been established, in the Hg(Ac) dispersion data, in which the nucleation frequency is proportional to the surface area of the supercooled droplet. These results are in good agreement with the theory of heterogeneous nucleation kinetics derived from concepts advanced in earlier papers.[2,4,5a] In this case the nucleation catalytic potency of the surface film can be conveniently characterized by a contact angle θ.

For two mercury dispersions and for all tin dispersions thus far studied a multiplicity of I_s values measured at constant temperature is found. It is believed that the catalysts responsible for this multiplicity in mercury are either structural defects of different severity in a common crystalline substance or very closely related chemical substances.

ACKNOWLEDGMENT

The author was ably assisted by W. A. Rocco throughout this investigation. Mr. Rocco is mainly responsible for the design of the simple and effective method used to maintain the temperature constant. E. F. Fullam advised and assisted in the droplet size distribution measurements.

The author has been stimulated by discussions of various aspects of this investigation with J. C. Fisher, J. H. Hollomon, and G. W. Sears. He is also indebted to V. K. LaMer for making the Pound-LaMer manuscript available to him in advance of publication.

The Structure and Internal Motion of 1,2-Dichloroethane

J. AINSWORTH AND J. KARLE
U. S. Naval Research Laboratory, Washington 25, D. C.
(Received October 29, 1951)

The structure and internal motion of 1,2-dichloroethane were investigated by means of electron diffraction. Values were obtained for several distances involving hydrogen atoms. In addition, the average amplitude of vibration was found for many of the distances. The predominant isomer was in the *trans*-form and the less abundant one was in the *gauche*-positions at 109±5° from the *trans*-equilibrium position. The amount of *gauche*-isomer was found to be 27±5 percent at 22°C.

THE molecule 1,2-dichloroethane has been the subject of a considerable number of investigations because of the interest in its restricted internal rotation and the nature of the potential barrier associated with this motion. Recent investigations have shown that the *trans*-equilibrium position predominates, that two secondary equilibria occur in the *gauche*-positions which occur roughly 120° from the *trans*- and that there is no indication of the *cis*-(eclipsed) position. In addition, some of the equilibrium distances involving the carbon and chlorine atoms have been reported.

Debye[1] and later Ehrhardt[2] found that the data from x-ray diffraction of gaseous 1,2-dichloroethane could be explained by the occurrence of molecules in the *trans*-configuration.

By using electron diffraction data obtained by the visual method, Weirl[3] concluded that 1,2-dichloroethane consisted of the *cis*- and *trans*-forms. It was pointed out by Glockler[4] that Weirl had mistakenly attributed the distance corresponding to *gauche*- to the *cis*-form, and therefore, he had actually discovered a mixture of *gauche*- and *trans*-isomers.

Beach and Palmer[5] by using visual electron diffraction data established that the *trans*-configuration was the main position of equilibrium. Yamaguchi, Morino, Watanabe, and Mizushima,[6] using visual electron diffraction data, confirmed that the *trans*-position was predominant and estimated that about twenty percent of the molecules occupied the *gauche*-position. There was no evidence for an equilibrium occurring in the *cis*-position. Hassel and Viervoll,[7] using a sector method for electron diffraction, studied the *trans*-form and determined the carbon-chlorine and chlorine-chlorine distances. They found 1.79A and 2.70A for the C−Cl distances and 4.29A for the Cl−Cl distance.

By using the change of mean dipole moment with temperature, Mizushima, Morino, Watanabe, Simanouti, and Yamaguchi[8] report a value of 1.21 kcal/mole, for the difference, ΔE, between the equilibrium energies of the *trans*- and *gauche*-forms. From the change of infrared absorption with temperature, they report a value of 1.03 kcal/mole for ΔE. Bernstein[9] finds a value of 1.10 kcal/mole from the temperature variation of infrared bands.* From the change of mean moment with temperature, Mizushima *et al.*[8] obtain 25 percent *gauche*-form at about 83°C, the boiling point of 1,2-dichloroethane. Bernstein[10] reports 22 percent *gauche* at 25°C and 27 percent at 83°C.

Bernstein[11] has also demonstrated from a product rule for *cis*- and *trans*-isomers that the less stable rotational isomer is the *gauche*-form. On the basis of a force model for 1,2-dichloroethane[12] he finds a barrier of 2.81 kcal/mole between the *trans*- and *gauche*-equilibria and a barrier of 4.50 kcal/mole at the *cis*-position.

Mizushima *et al.*[8] report that Raman spectra indicated that in the solid state dihalogenoethanes were solely in the *trans*-form. The x-ray measurements of Lipscomb[13] substantiate this.

In the light of these extensive investigations of the structures and energies of the rotational isomers of 1,2-dichloroethane, it was of interest to apply the method of electron diffraction by gases, based on quantitative intensity measurements.[14,15] This method permits the evaluation not only of the equilibrium distances occurring in the molecule but also the mean deviation of the interatomic distances from equilibrium caused by the internal motion of the molecule. It was of special interest to study the nature of the rotational isomers.

METHOD

The sample of 1,2-dichloroethane was obtained from the Eastman Kodak Company and was carefully re-

[1] P. Debye, Physik. Z. **31**, 142 (1930).
[2] F. Ehrhardt, Physik. Z. **33**, 605 (1932).
[3] R. Weirl, Ann. d. Physik **13**, 453 (1932).
[4] G. Glockler, Revs. Modern Phys. **15**, 155 (1943).
[5] J. Y. Beach and K. J. Palmer, J. Chem. Phys. **6**, 639 (1938).
[6] Yamaguchi, Morino, Watanabe, and Mizushima, Sci. Papers Inst. Phys. Chem. Research (Tokyo) **40**, 417 (1943).
[7] O. Hassel and H. Viervoll, Arch. Math. Naturvidenskab **47B**, No. 13 (1944).
[8] Mizushima, Morino, Watanabe, Simanouti, and Yamaguchi, J. Chem. Phys. **17**, 591 (1949).
[9] H. J. Bernstein, J. Chem. Phys. **17**, 258 (1949).
* *Note added in proof.*—Earlier work had been performed by Mizushima *et al.* See Mizushima, Morino, Watanabe, and Simanouti, J. Chem. Phys. **17**, 663 (1949), and Mizushima, Morino, and Simanouti, J. Chem. Phys. **17**, 663 (1949).
[10] From reference 9 corrected for the structural model reported in this paper.
[11] H. J. Bernstein, J. Chem. Phys. **17**, 256 (1949).
[12] H. J. Bernstein, J. Chem. Phys. **17**, 262 (1949).
[13] Private communication from W. Lipscomb.
[14] J. Karle and I. L. Karle, J. Chem. Phys. **18**, 957 (1950).
[15] I. L. Karle and J. Karle, J. Chem. Phys. **18**, 963 (1950).

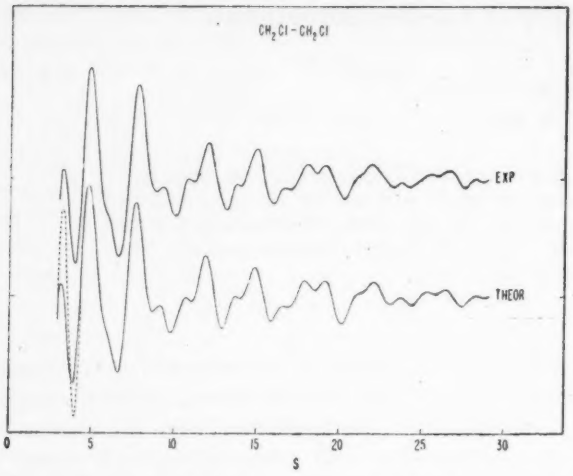

FIG. 1. Experimental intensity curve and theoretical curve from best model. The dotted curve corresponds to the intensity of a purely *trans*-model in the region $3<s<5$.

distilled, having a bp 82.8°C at 767 mm. The methods used in obtaining the structure of dichloroethane have been described in previous publications.[14–16] An experimental molecular scattering curve essentially characteristic of the scattering from bare nuclei was obtained. From the scattering curve, a radial distribution curve, $f(r)$, was computed using Eq. (1) of reference 15, and decomposed into individual peaks for each interatomic distance. The positions of the maxima of the decomposed peaks indicate the equilibrium interatomic distances except in the case of the *trans*-Cl−Cl in which the equilibrium position is shifted slightly beyond the maximum in the direction of increasing r. In all cases, the shapes of the peaks indicate the nature of the vibrational motion between pairs of atoms.

The analysis of the *trans*-Cl−Cl required special treatment since it is asymmetric as a consequence of the combined torsional motion and the over-all vibration of the molecular frame. For the analysis of the Cl−Cl radial distribution peak, Eq. (26) of reference 16 was used and for the computation of corresponding theoretical intensity curves, Eq. (45) of reference 16 was employed. This yields an estimate of the value of β which determines the potential function, V, for small angles in the vicinity of the *trans*-position in the following manner,[16]

$$V=\beta c_2 kT\phi^2/2, \qquad (1)$$

where k is Boltzmann's constant, T is the absolute temperature, and $c_2=(l_2^2-l_1^2)/2$ where l_2 is the largest possible value of the Cl−Cl distance in the course of a complete rotation (*trans*-position) and l_1 is the smallest possible value (*cis*-position), and ϕ is the angle of rotation measured from the *trans*-position as the origin.

RESULTS

The experimental molecular scattering curve and the resulting radial distribution curve are shown in Figs. 1 and 2. Analysis of the radial distribution curve gives the values listed in the second and third columns of Table I. It is customary procedure to establish the limits of error for the parameters taken from the radial distribution curve by means of theoretical intensity curves computed with reasonably exhaustive variations in these parameters. In the case of a system as complicated as a mixture of *gauche*- and *trans*-1,2-dichloroethane, it is not feasible to exhaust the possible variations of the parameters. The procedure which was followed with 1,2-dichloroethane involved plotting the separate scattering curves for each of the distances given by the radial distribution curve. When a component distance or damping constant was varied, the remaining components could be studied to ascertain whether any difficulties introduced into the theoretical intensity curves could be corrected by variations in these remaining components. This procedure was essentially equivalent to the computation of theoretical intensity curves in which several parameters are varied simultaneously in order to produce the best possible comparison with experiment. The final values from studying the radial distribution and theoretical intensity curves are given in the fourth and fifth columns of Table I. The values for the vibrational amplitudes which represent the root mean deviations projected on the lines connecting the pairs of atoms at equilibrium were corrected for finite sample size.[15] Using the final values, a theoretical intensity curve was computed for comparison with the experimental curve and is shown in Fig. 1. Corrections for the difference in the shapes of the atomic scattering factors of hydrogen, carbon, and chlorine and for the effect of secondary scattering[15] have been included in the calculation of the theoretical curve. The comparison of maxima and minima between the theoretical and experimental curves gives an s/s_0 ratio of 0.998 ± 0.004.

If a Gaussian curve is fitted as well as possible to the asymmetric *trans*-Cl−Cl peak, a value of 0.066A is obtained for the average amplitude of vibration. This approximate measure of the amplitude is of interest since this amplitude is relatively small for so large an equilibrium distance compared to the values for the other distances.

Gutowsky, Kistiakowsky, Pake, and Purcell[17] have

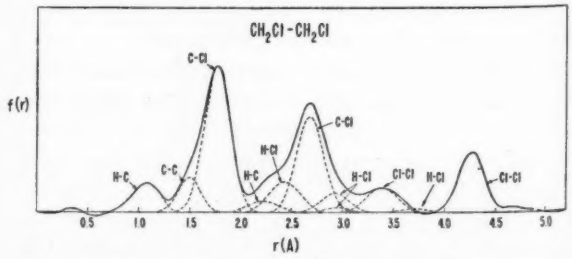

FIG. 2. Radial distribution curve showing component distances.

[16] J. Karle and H. Hauptman, J. Chem. Phys. 18, 875 (1950).

[17] Gutowsky, Kistiakowsky, Pake, and Purcell, J. Chem. Phys. 17, 972 (1949).

reported from measurement of absorption line shapes at nuclear magnetic resonance an H—H distance of 1.71±0.02A. By using our value of 1.12A for the C—H distance, this leads to an H—C—H angle between 98° and 101° which is, as pointed out by the above authors, a considerable decrease from the tetrahedral value. In our best model given in Table I, the H—C—H angle is 93°. In the many models which we have tried, a satisfactory one was never found with an H—C—H angle larger than 102°. This is in very good agreement with the results of Gutowsky *et al.*[17] However, in view of the complexity of the system, it is not possible to state with certainty that we have demonstrated that 102° is an upper limit.

The limits of uncertainty for the interatomic distances appearing in Table I should be functionally related to one another. It is not feasible to discover these functional relationships and therefore the limits are somewhat larger than that which is demanded by the uncertainty in the data. Thus, in addition to many satisfactory models, the limits also contain combinations of parameters which would compare quite unfavorably with the experimental intensity curve.

ROTATIONAL ISOMERS

The electron diffraction results confirm the findings of Mizushima *et al.*[8] and Bernstein[9] that the less stable rotational isomer is of the *gauche*-form. The *gauche*- and *trans*-forms appear in the radial distribution curve, Fig. 2, and their ratio, N_g/N_t is measured by the areas under their respective curves by means of the formula,

$$N_g/N_t = A_g r_g / A_t r_t, \qquad (2)$$

where A_g and A_t are the areas and r_g and r_t are the equilibrium distances for the *gauche*- and *trans*-forms, respectively. The application of this formula leads to a value of 25 percent for the amount of *gauche*.

Another way to evaluate the amount of *gauche* is from a study of the intensity curves. It was found that the height between the maximum and minimum at $s=3.2$ and $s=4.0$ is very sensitive to the relative amounts of *trans*- and *gauche*-forms. Taking into account the variable atomic scattering factors in this region of small s values, in addition to the effect of multiple scattering, it is found that a composition of 27 percent *gauche* agrees very well with experiment, whereas the omission of the *gauche*-form would produce an error of about 135 percent in the intensity curve (see dotted curve, Fig. 1). Although the accuracy of the intensity curve for the region about $s=3-4$ is less than that for larger values of s,[18] the result from this inner region serves as very good confirmation of the percentage of *gauche*- found from the radial distribution curve and other portions of the theoretical intensity curves. The percentage of *gauche* reported in Table I, 27±5 percent at 22°, is slightly larger than that reported by Bernstein[10] who found 22 percent at 25°C and by Mizushima *et al.* who found 25 percent at 83°C.

TABLE I. Results from analysis of radial distribution curve and final results from additional study of theoretical intensity curves. The average amplitudes of vibration are indicated by $\langle l_{ij}^2 \rangle^{\frac{1}{2}}$.

	From radial distribution curve			Final results	
	Distance	A	$\langle l_{ij}^2 \rangle^{\frac{1}{2}}$	A	$\langle l_{ij}^2 \rangle^{\frac{1}{2}}$
trans	C—H	1.10	0.066	1.12±0.04	0.066±0.025
	C—C	1.51	···	1.49±0.03	0.030 assumed
	C—Cl	1.78	0.064	1.78±0.01	0.064±0.010
	H—C	2.21	0.086	2.21±0.04	0.086±0.030
	H—Cl	2.40	0.104	2.42±0.04	0.104±0.02
	C—Cl	2.69	0.064	2.69±0.02	0.070±0.010
	H—Cl	2.91	0.085	2.91±0.04	0.085±0.030
	Cl—Cl	4.29	(peak value)	4.31±0.02	$1.0<\beta<\infty$
gauche	H—Cl	2.94	···	2.94±0.12	0.090 assumed
	Cl—Cl	3.38	0.084	3.35±0.06	0.068±0.020
	H—Cl	3.70	···	3.70±0.12	0.100 assumed
	gauche=25% at 22°C			*gauche*=27±5% at 22°C ∠ of *gauche*[a] 109±5° ∠CCCl 110°23′±3°	

[a] Assuming frame same as for *trans*-form.

The equilibrium angle for the *gauche*-isomer was computed on the assumption that the structural frame of the molecule did not change with rotation. The uncertainty in this angle was consequently based upon the limits of variation of the *gauche*-Cl—Cl distance. The equilibrium angle from Bernstein's[12] potential function was 117°. The value of 109±5° found in this investigation indicates that this potential function should be modified somewhat to reduce the equilibrium values.

The torsional motion of 1,2-dichloroethane about the C—C bond causes the *trans*-Cl—Cl peak to be asymmetric and shifts the position of the maximum. The position of the maximum of the *trans*-Cl—Cl peak at 4.28–4.29A in the radial distribution curve, which borders the lower limit of the value 4.31A obtained from a study of the intensity curves, is an indication of this effect. Although the peak is asymmetric, the uncertainty in the shape is sufficient to prevent an accurate evaluation of β. If $\beta>4$, the effect of the torsional motion is not noticeable and the shape of the peak is practically Gaussian. The value of β consistent with the potential function of Bernstein[12] for small angles, which may be obtained from formula (1), is $\beta=3.5$. Since the torsional oscillation appears in combination with the over-all vibration of the frame, an independent evaluation of the contribution of the over-all vibration of the frame by spectroscopic means would be very helpful in the study of the torsional oscillation and the evaluation of β.

We wish to thank the Computing Laboratory of the National Bureau of Standards for their excellent cooperation in performing the calculations required for this investigation.

[18] The uncertainty is estimated to be about 15 percent between maxima and minima in the vicinity of $s=3$, whereas it is between 5–10 percent for larger values of s up to $s=20$, where it again begins to increase.

Theory of Resonance Topology of Fully Aromatic Hydrocarbons. I

M. GORDON
Royal Technical College, Glasgow, Scotland

AND

W. H. T. DAVISON
Dunlop Research Centre, Birmingham, England

(Received September 24, 1951)

The computation of resonance forms of any specified number of unpaired electrons ("radicality") of aromatic hydrocarbons is reduced to combinatorial problems, many of which can be solved on the basis of five simple lemmas. In this first of two papers, only unexcited (Kekulé) forms are computed. Algorithms are deduced for deriving the number N of such forms for classes covering practically all nonreticulate aromatic hydrocarbons and a number of singly, doubly, or triply infinite series of reticulate ones. One lemma leads to a simplification of the combinatorial problems from the hexagonal to the square lattice ("dot diagrams"). Points of purely mathematical interest arise and may merit further study.

1. INTRODUCTION

THE computation of the number of resonance forms of aromatic hydrocarbons has been developed by Wheland,[1] Pullman,[2] and Daudel and Pullman.[3] The results may be used in quantum-mechanical calculations of molecular energies, etc., in which case a set of *linearly independent* resonance forms is required. Rumer, Teller, and Weyl[4] have given the classical method for constructing such sets, but Klement[5] first realized that the method is not applicable to reticulate structures, i.e., in which one or more carbons participate in three rings. Moreover, the classical method does not automatically give a "reasonable" set of independent forms, i.e., one comprising the forms of low excitation. In practice it appears useful to be able to construct and compute all the resonance forms of a specified degree of excitation, particularly the unexcited (Kekulé) ones, and on this basis qualitative inferences on relative stabilities of structures are commonly and usefully drawn without elaborate quantum-mechanical calculations or considerations of linear dependence. We are not aware of any previous general methods for deriving *complete sets of resonance forms of a specified degree of excitation*, other than by trial and error.

From five simple mathematical lemmas we derive in this paper an approach to this problem which yields (a) algorithms for the number N of possible Kekulé forms of any nonreticulate hydrocarbon, (b) general formulas for N in the case of numerous classes of reticulate structures, and (c) easy methods of *constructing* resonance forms. The same method of attack will be shown in the second paper to be applicable to the enumeration and construction of excited forms, but this rapidly becomes a cumbersome procedure with increase in molecular complexity and degree of excitation. Indications will be given of how the number of possible forms with a given single or double bond can be found. As no account is taken of linear dependence, our results for excited forms may occasionally be higher than the highest obtainable by the classical method because of the inclusion of forms linearly dependent upon others included.

We shall mainly base ourselves on the more commonly occurring "graphitic" hydrocarbons, i.e., such as can be fitted to the unlimited plane graphitic lattice of hexagons shown in Fig. 1, in which every carbon has the coordination number three. As examples, triphenyl and styrene are shown in heavy type and in the form of "coordination schemes," i.e., without reference to the multiplicity of individual bonds. In all figures after the first, the coordination schemes are further simplified by omitting all hydrogens and showing the carbons only by implication (one at each junction of bonds). Our general method of computing nonhexagonal hydrocarbons will be seen to be reduction to equivalent hexagonal structures. By this means unity and simplicity of approach can be maintained.

2. CLASSIFICATION OF RESONANCE FORMS, COMPOUNDS, AND RADICALS

A hydrocarbon, in which each carbon is three-coordinate, is here termed *fully aromatic*. In these a Kekulé form is a resonance form in which each carbon has a share in exactly one double bond and two single bonds. If such a form can be written, the hydrocarbon will exist as a *compound*, as distinct from a *radical*, (provided the singlet state corresponds energetically to the ground state, as is usually the case). In radical forms there are one or more trivalent carbons carrying three single bonds and an unshared electron; the number of such carbons in a given form will be called its *radicality* R. The elementary mathematical basis of the computational side of both papers follows in the form of five lemmas. The first of these applies to any alternant

[1] G. W. Wheland, J. Chem. Phys. **3**, 356 (1935).
[2] A. Pullman, Compt. rend. **222**, 736 (1946).
[3] R. Daudel and A. Pullman, J. phys. radium (sér. VIII), **7**, 74 (1946).
[4] Rumer, Teller and Weyl, Gött. Nachr. (Math. phys. Klasse), 499 (1932).
[5] O. Klement, Helv. Chim. Acta **32**, 1777 (1949).

hydrocarbon,[6] i.e., any which has no odd-numbered rings. It embodies a classification of the carbon atoms in such structures, and its simple inductive proof will here be omitted.

First Lemma

Every alternant hydrocarbon has two sets of carbon atoms, such that atoms of the first set are linked only to atoms of the second, and vice versa. On the graphitic lattice we shall, for a given orientation on the page, call one set male

(of the form),

and one female

.

The designation of the sets is interchanged by rotating the hydrocarbon in its plane through an odd multiple of 60°, but the membership of the sets is preserved. The number of bonds along any path joining atoms of equal sex in an alternant hydrocarbon is even, between atoms of opposite sex it is odd. A *double* bond may conveniently be compared to a "marriage" The excess number of atoms of either sex over those of the other in a given structure will be called the *disparity D*. It will be shown that structures with any value of D can be constructed. The disparity of a graphitic hydrocarbon can, moreover, be read off at sight as the excess or deficiency of the number of "corners" pointing north (thus $\wedge$) over those pointing south (thus $\vee$). The corners pointing north are, of course, those carbons on the upper part of the circumference of a structure which are linked by a vertical bond to a hydrogen (omitted in our figures). The simple rule given follows from the fact that all vertical bonds linking two carbons account for one male and one female atom and thus make no contribution to the disparity. We note the corollary that $D=0$ for any graphitic hydrocarbon which has a plane of symmetry at right angles to some bond. It will be shown in the second paper that $R \geqslant D$ in any alternant aromatic hydrocarbon.

Second Lemma

The number of Kekulé forms of a fully aromatic hydrocarbon in which two fixed parts are linked together only by single bonds, is equal to the product of the number of forms of the two parts. The parts are cut from the whole by "hydrogenation" across the single C−C bonds linking them. By induction, the lemma is extended to any number of parts linked exclusively by single bonds: the number of forms of the total hydrocarbon is the product of the number of forms of the parts.

As an example, consider the triphenyl of Fig. 1. It can be cut by hydrogenation across bonds a and b to form three benzenes with two Kekulé forms each. According to the lemma there are $2\times2\times2=8$ forms in triphenyl in which bonds a and b are both single. The next lemma shows that the triphenyl has no other Kekulé forms. The proof of the second lemma follows directly from the definition given above for Kekulé and radical forms and the fact that C−H bonds are single.

[6] C. A. Coulson and H. C. Longuet-Higgins, Proc. Roy. Soc. (London) **A192**, 16 (1947).

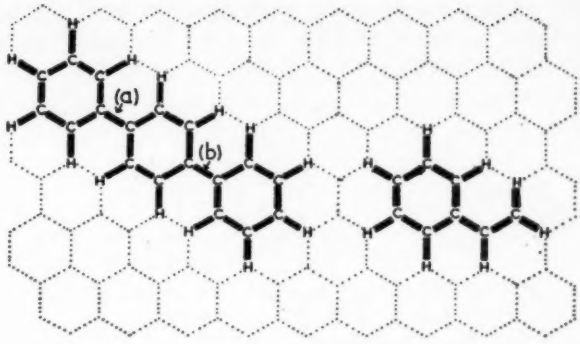

FIG. 1. Graphitic lattice with triphenyl and styrene molecules.

Third Lemma

If two fully aromatic alternant hydrocarbon *compounds* are joined together by bonds through dehydrogenation, the resulting structure is formally a compound. If the joining bonds all commence at one of the constituent hydrocarbons from atoms of the same sex, then all joining bonds are single in all forms.

The proof of this lemma and its inductive generalization to more than two hydrocarbons will become obvious from the discussion of various individual examples given later.

Fourth Lemma

If in a finite fully aromatic graphitic hydrocarbon the multiplicity (i.e., single or double nature) of all bonds parallel to any one bond has been assigned, then there is at most one Kekulé form which satisfies the assignment.

There are three sets of parallel bonds in a graphitic hydrocarbon, each set being arranged in rows. A row of bonds is defined as a set having a common perpendicular bisector. For instance the set of vertical bonds of the lattice in Fig. 1 is arranged in horizontal rows. By considering two adjacent rows of these in a compound on this lattice and assigning their nature, one readily proves that the nature of all the bonds lying between the two rows (and belonging to the other two sets of parallel bonds) is fully determined. Hence the lemma follows.

Fifth Lemma

In any Kekulé form of a graphitic hydrocarbon compound the number of parallel *double* bonds lying in a given row, is equal to the disparity of either of the two collections of atoms lying wholly on one or other side of the line bisecting the bonds of the given row.

The proof of this lemma will become obvious later.

3. UNIFILAR ARRANGEMENTS OF HEXAGONS

We consider first the general case of unbranched strings of hexagons termed "unifilar," which may be straight or have any number of "kinks." The example with four kinks shown in Fig. 2 has 79 unexalted forms, and it may serve for describing the computation of such forms for unifilar arrangements in general. One carries out a summation, starting at one end of the molecule

and adding one figure for each hexagon, until the last hexagon on the right gives the total number of forms. At the left-hand end the numbers start with 2, 3..., one unit being added for each hexagon. Once a kink has been passed, the figure added for each hexagon is no

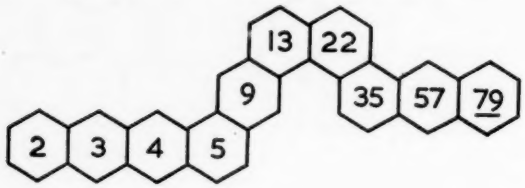

FIG. 2.

longer unity but the figure which immediately preceded the last kink passed, (e.g., after 5 is reached, 4 is added to give 9). One proves this mode of computation by considering the effect of adding one hexagon at the right-hand end of an arbitrary unifilar chain (Fig. 3). We lose no generality by adding it in a straight (unkinked) position, as shown. As each carbon in the added ring must, in a given form, carry one double bond, the bonds marked *a* and *b* are invariably either both single or both double. In the former case we find by the second lemma (i.e., cutting *a* and *b*) the number X of such forms equal to the number of forms of the original, unaugmented structure since the butadiene fragment has

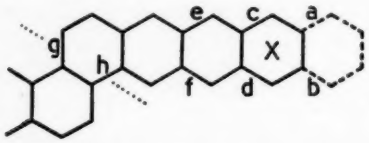

FIG. 3.

exactly one form. On the other hand, in the forms where both *a* and *b* are double bonds, so are *c* and *d*, and *e* and *f*, etc. Thus there is a rigidly fixed bond structure until we reach the first kink to the left, where bonds *g* and *h* are obviously both single. Using the second lemma for these two bonds, we get two fragments as in Fig. 4. As we have noted, the right-hand fragment is rigidly restricted to one form, while the left fragment has Y forms, say. Then the whole augmented unifilar structure of Fig. 3 has $(X\times1)+(1\times Y)=X+Y$ Kekulé forms, as was to be shown. In the special case where there are no kinks at all, Y reduces to unity, so that the *straight* unifilar chain of n hexagons has $(n+1)$ forms,

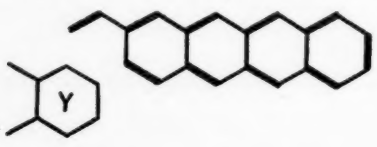

FIG. 4.

benzene having two, naphthalene three, anthracene four, and so on for the other acenes. (Later we shall meet other cases of Y being set equal to unity in the absence of relevant kinks.) At the other extreme one can consider the completely and regularly kinked series of unifilar graphitic hydrocarbons beginning with benzene, naphthalene, phenanthrene, and whose sixth member is shown in Fig. 5. The number of forms of the members of this series is 2, 3, 5, 8, 13, 21, etc., in which evidently each number is the sum of the two preceding.

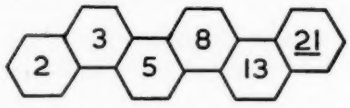

FIG. 5.

They are variously known as the Fibonacci numbers or Lamé series, are encountered in the theory of continued fractions, matrices, etc., and are associated with the "golden section" in classical geometry. Other points of mathematical interest arise, in particular the fact that the computation process for filar structures is invariant if the end at which the computation starts is changed.

Clearly the presence of kinks generally increases the number of forms. While this factor will tend to stabilize the structures concerned, special reactivity may be concentrated at the bend. As a biochemical application of this work, consider the structure of Fig. 6. By the rule given it has seven forms. It is readily seen that as many

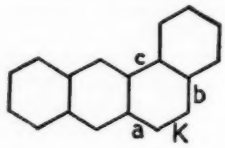

FIG. 6.

as six of these have a double bond in position K; for *when K is double*, bonds *a*, *b*, and (by the first and third lemmas) *c* are necessarily single and we can cut them according to the second lemma. The result is one benzene, one naphthalene, and one ethylene molecule, whence the number of such forms is $2\times3\times1=6$. Pullman[7] and later Anderson[8] have connected such regions of high electron density in the K region with the carcinogenic activity of the structure.

4. POLYFILAR ARRANGEMENTS OF HEXAGONS

The essential part of the process of computing unifilar forms is the progressive inscription in the hexagons of

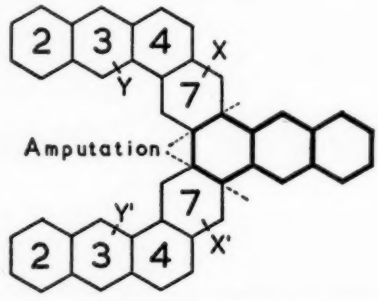

FIG. 7.

numbers, each of which is the sum of its predecessor plus the number immediately preceding the last kink which has been passed in this process of inscription. This

[7] A. Pullman, Compt. rend. **221**, 140 (1945).
[8] W. Anderson, Nature **160**, 892 (1947).

process is capable of generalization. In trifilar structures (Fig. 7) three unifilar arms converge at a juncture. Their number of forms is computed through the construction of an auxiliary unifilar structure by amputating two of the arms at the juncture and replacing them by one

FIG. 8.

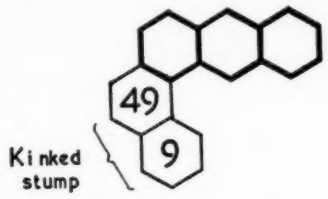

kinked stump of two rings. Into these two rings numbers XX' and YY' (see next paragraph) are respectively inscribed (Fig. 8). This permits the generalized process of computation to be commenced for the auxiliary unifilar structure, whose final result agrees with the desired number of resonance forms of the trifilar structure. Thus Fig. 9 shows that the structure in Fig. 7 has 156 resonance forms, a result which applies to the analogous known compound listed in the Ring Index as No. 3965, since the replacement of $-CH=$ by $-N=$ leaves the result unaffected.

It will be noted that X and X' are the number of

FIG. 9.

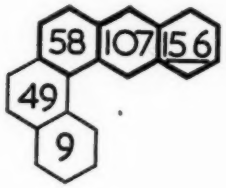

forms of the two amputated arms, found as in 3. Y and Y' are the respective numbers of the two arms up to the last kink before and including the juncture, i.e., when finding "the last kink before the juncture" the arm must not be considered cut off but the juncture ring taken into account. Y must be put equal to unity (again as in 3) when an amputated arm has no kinks. The reader may verify this by amputating in Fig. 7 the straight arm on the right in place of the kinked arm at the top, when the computation proceeds as shown in Fig. 10. The method described, consisting of the amputation of two arms, their replacement by *two* rings

FIG. 10.

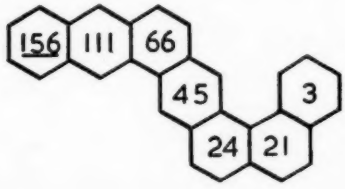

forming a kinked stump and carrying the numbers XX' and YY', and the computation of the auxiliary structure thus obtained, universally applies to trifilar forms of hexagons however large and kinked.

More highly branched (polyfilar) structures can be computed by an analogous successive reduction of branches. Any two arms converging at a juncture are replaced by their equivalent kinked stump, thus forming a single auxiliary arm. This is computed up to the next juncture and, together with one of the arms with

FIG. 11.

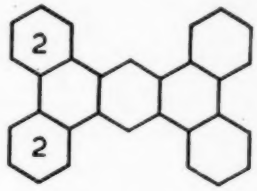

which it converges there, is replaced by the equivalent kinked stump. The process is continued until a unifilar structure remains, whose final number gives the desired result. A simple example is shown in stages in Figs. 11–13. Thus a method has been described whereby for any compound consisting of hexagons (other than for reticulate structures in which certain carbons partake of three rings, or for those containing closed loops of hexagons) the number of resonance forms can be found. Even in cases larger than those exemplified in the figures, only rapid mental arithmetic is involved after very little practice. The procedure for trifilar structures

FIG. 12.

described above can be simplified, the number of forms being obtained as $XX'X''+YY'Y''$, where the obvious notation applies to the three arms. However, this procedure cannot be generalized to more highly branched structures.

5. FILAR STRUCTURES CONTAINING NONHEXAGONAL RINGS

We show how alternant hydrocarbons, i.e., those having only even-membered rings, are reduced to equivalent hexagonal structures having the same number of forms, first in the unifilar case and then in the polyfilar case with one juncture ring only. The same

FIG. 13.

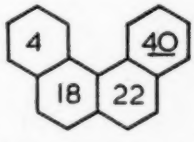

range of compounds modified by the presence of odd-membered rings are also reducible to purely hexagonal structures.

Unifilar alternant hydrocarbons are simply reduced to hexagon ones by inserting or cutting out $-CH-CH-$

groups wherever necessary, which leaves the number of Kekulé forms invariant. Thus Fig. 14 is transformed into the hexagonal form of Fig. 15, merely a distorted version of Fig. 16, which is normally computed. In large rings two or more contiguous $-CH-CH-$ may

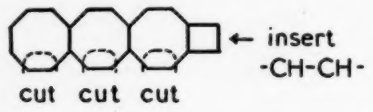

FIG. 14.

have to be removed. (Note that the "straight" structure of Fig. 14 happens to be equivalent to a kinked structure (16) in terms of hexagons.)

Star-shaped polyfilar forms with a single juncture ring are computed as a sum of two products, thus:

$$N=(X_1X_3X_5\ldots Y_2Y_4Y_6\ldots)+(X_2X_4X_6\ldots Y_1Y_3Y_5\ldots). \quad (1)$$

The arms are labeled and the X and Y terms subscripted accordingly, for which purpose the *sides of the juncture ring* are enumerated circularly, starting from a point which is arbitrary because of the symmetry of the formula. Figure 17 illustrates the enumeration, Fig. 18 the rest of the computation. Each arm is again computed from its free end by use of the unifilar process of 3 to give X_n. The Y_n term for a given arm refers as usual to

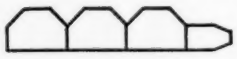

FIG. 15.

the number of forms up to the last kink before (and including) the juncture.

Thus note particularly that $Y_6=2$ because the arm in question is affixed to the central decagon in a kinked position, and this *kink* must be *included* in the counting. On the other hand $Y_1=1$ for the opposite arm on the left because of the total absence of kinks. Even-membered rings other than hexagons forming part of the arms are, of course, rectified to hexagons by insertion or excision of $-CH-CH-$ groups, as is always possible and shown in Fig. 18. The result of this figure shows that the compound Fig. 17 has $X_1X_9Y_4Y_6+X_4X_6Y_1Y_9=3\times2\times3\times2+5\times3\times1\times1=51$ forms.

In unifilar *compounds* the number of odd-membered rings must be even, and one considers them in pairs *from one end of the chain*. Thus in Fig. 19 we have two pairs of odd-membered rings: the pair $A-B$ and the

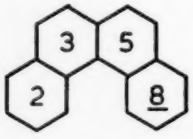

FIG. 16.

pair $a-b$. Next we consider the system of rings formed by any such pair plus all the even-membered rings (if any) intervening between the two members of the pair. The computation consists simply in dissolving all the cross-bonds in each system as in Fig. 20, thereby converting each system into one large even-membered ring. The system $A-B$ becomes C, and the system $a-b$ becomes c. In other words, and quite generally:

An equivalent even-membered ring is constructed for each system consisting of a pair of odd-membered rings

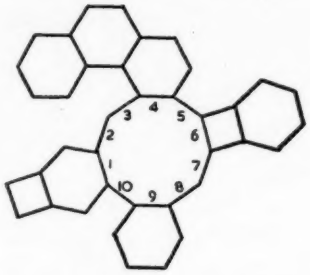

FIG. 17.

plus any even membered rings lying between them, *viz.*, by dissolving all the cross-bonds which are common to any two rings of the system. Figure 21 completes the process in the usual way by cutting out enough $-CH-CH-$ groups to leave a purely hexagonal structure. In the same way an odd-membered *juncture* ring will form part of a system with one other odd-membered ring. The system is reduced to an even-membered juncture ring by dissolution of cross-bonds. This process is illustrated in Figs. 22 and 23, where $A-B$ becomes

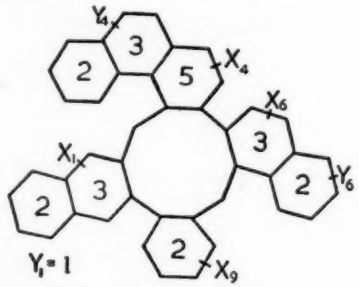

FIG. 18.

C and two four-membered rings are incidentally converted to hexagons by the standard process of inserting $-CH-CH-$ groups. By formula (1), Fig. 23 (and hence 22) has $2\times1\times1+3\times3\times1=11$ forms. The whole procedure can be derived with the aid of the second lemma; in particular, the dissolution of cross-bonds lying between certain pairs of odd-membered rings in a unifilar chain (or an arm of a polyfilar one) is justified because such cross-bonds are readily shown to be single in all possible Kekulé forms.

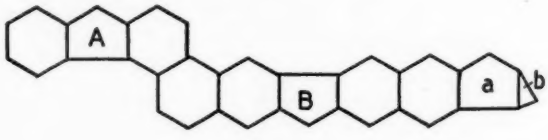

FIG. 19.

Care must, however, be taken to pair off the odd-membered rings correctly (i.e., from the end of any arm). For example, in a unifilar string containing 4 odd-membered rings, cross-bonds must not be dissolved between the second and third, but only between the

first and second and between the third and fourth odd ring, respectively (Fig. 20).

Although occasional simple examples can be computed more quickly by other methods, the procedures described are both of completely general application and

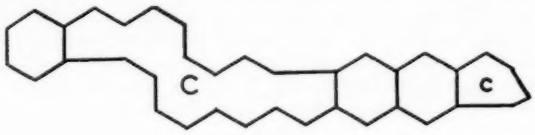

FIG. 20.

the simplest known in the case of more complex structures. They seem to be sufficient to ensure that the classes covered by rigid algorithms include all known filar fully aromatic compounds, whose number of forms are thus found by simple (usually mental) arithmetic. In fact, all nonreticular structures, except some having a multiplicity of nonhexagonal juncture rings and whose calculation is more complex, have been treated above, and we proceed to reticulate structures in which at least one atom partakes of 3 rings.

FIG. 21.

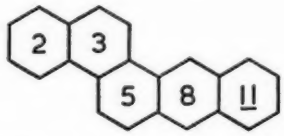

6. RETICULATE GRAPHITIC STRUCTURES

The number of Kekulé forms of several specific classes of fused ring graphitic hydrocarbons are given by formulas listed in Table I. The rationale of deducing these formulas consists in constructing, on the basis of lemmas 4 and 5, all permissible assignments of the set of vertical bonds in the coordination schemes shown in the table. The problem will thus be simplified by passing from the hexagonal to the square lattice, and setting up a one-to-one correspondence between the Kekulé forms and so-called dot diagrams on the square lattice. These constructions lead to a notable class of purely combinatorial problems, only a limited number of which have so far yielded solutions. The simplest example, the parallelogram-shaped series $P_{m,n}$ at the head of Table I, deserves detailed discussion.

FIG. 22.

In this doubly infinite series, each member requires two parameters for its specification; thus $P_{m,n}$ denotes a general member with m hexagons along one, and n hexagons along the other side of the parallelogram. $P_{3,4}$ is actually illustrated in Fig. 14. We show that the number of forms of $P_{m,n}$ generally equals ${}^{m+n}C_m = {}^{n-1}H_m$ (in the usual notation for binomial coefficients and homogeneous products), by actually constructing that number of forms and proving that there are no others. For an example, the reader may consult a paper by

FIG. 23.

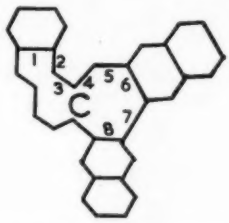

Robertson and White[9] who have drawn the ${}^4C_2 = 6$ forms of pyrene ($= P_{2,2}$). In the construction of a typical form (Fig. 24) all vertical bonds are assigned to be double, with the exception of precisely one single vertical bond on each of the horizontal rows in which the vertical bonds are arranged. The position of this single bond in a given row may vary from one form to another, but in each constructed form one restriction applies: neighboring rows must have their single bonds in adjacent positions. According to the fourth lemma there can be only one form for a given assignment of vertical bonds. This form actually exists: we complete the construction (e.g., Fig. 24) by making all oblique bonds single, with the exception of those which lie between two of the vertical single bonds, i.e., every oblique bond joining two carbons bearing single vertical bonds is made double. This complete construction satisfies the definition of a Kekulé form, since every carbon has been assigned precisely one double bond (vertical or oblique).

FIG. 24.

FIG. 25.

[9] J. M. Robertson and J. G. White, J. Chem. Soc. 358 (1947).

The total number of such forms, which can be constructed by varying the position of the vertical single bonds—subject always to the restriction which limits their position in neighboring rows to adjacent places—is readily shown to be ${}^{m+n}C_m$. Two instructive proofs follow.

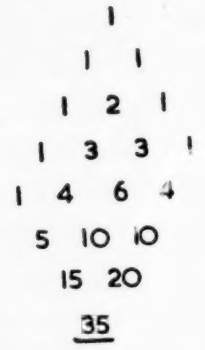

FIG. 26.

For the first proof we construct a "dot diagram" in which every vertical bond is represented by a dot. The dots form an array as in Fig. 25. The number of constructed forms is equal to the number of ways in which the top dot can be linked to the bottom dot by "direct paths" such as that shown in Fig. 25, which symbolizes precisely and unambiguously the form of Fig. 24. Every dot on the path of arrows in 25 stands for a vertical single bond in 24, and every dot *not* on

FIG. 27.

the path for a vertical double bond. Each direct path takes in one dot from each row, dots taken in on neighboring rows being in adjacent positions. The top and bottom dot are on every such path, since they symbolize C—H bonds which are single in every form. Each path consists of m like unit vectors parallel to one side of the parallelogram and n like vectors parallel to the other. Each permutation of these vectors yields a different permissible path, hence the number of paths is ${}^{m+n}C_m$.

FIG. 28.

In the second proof one symbolizes each vertical bond, not by a dot, but by a binomial coefficient arranged exactly as in Pascal's triangle (Fig. 26). Thus each number is the sum of the two numbers immediately above it. But the number of paths linking a given dot (Fig. 25) to the top dot is precisely equal to the sum of the number of such paths for the two dots lying immediately above it. Hence the rest of the proof is obvious and Fig. 26 shows that $P_{3,4}$ has ${}^7C_3 = 35$ forms, of which Fig. 24 provides one.

We have noted earlier that it is useful to be able to read off the number of forms in which a given bond is single, say. The reader will readily convince himself with the aid of the diagrams, that the number out of the constructed ${}^{m+n}C_m$ forms in which the vertical bond symbolized in Fig. 26 by ${}^sC_r$ is single, is given by ${}^sC_r \times {}^{m+n-s}C_{m-r}$. This product of two coefficients disposed symmetrically in a figure such as 26, gives, in fact, the number of different paths passing through the corresponding dot and can be

FIG. 29.

read off at sight. Such calculations underline the essentially combinatorial nature of resonance topology.

To complete the proofs, one shows that there are no other forms than these ${}^{m+n}C_m$ already constructed. The fifth lemma proves that every form must in fact have one single bond exactly in every row of vertical bonds. The restriction of these to adjacent positions in neighboring rows is proved by reference to Fig. 27. This shows that if a single bond s were flanked by two double bonds d in the adjacent positions, no Kekulé form could be constructed, since some one of the carbons would be forced to have either no or two double bonds.

The method of dot-diagrams is generalizable to apply to all graphitic hydrocarbons. While the parallelograms $P_{m,n}$ have only one path for each dot diagram, in general the number of paths is equal to the number n of C—H bonds pointing north (see under first lemma). There are still as many forms of a graphitic compound as it has dot diagrams. But each dot diagram must have each dot corresponding to a C—H bond pointing north linked by a direct path to a dot representing a C—H bond pointing south, and all paths must be *free*, i.e., not touch or cross other paths in the same dot diagram. A dot diagram typical for coronene (Fig. 29) is shown in

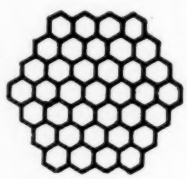

FIG. 30.

Fig. 28. Each vertical bond is represented by a dot; two free paths link the two top dots to the two bottom dots. Vertical bonds corresponding to the dots on the paths are single, the others double, in the resonance form corresponding to the dot diagram.

Thus the problem of finding N is reduced to a simpler combinatorial one, which aids in the deduction of the general formulas of Table I and in all cases facilitates the systematic construction of the forms (as distinct from computation of the number). Table I is restricted to simple series where all the n corners pointing north (or

TABLE I. Number of Kekulé forms of various classes of reticulate hydrocarbons.

SERIES	EXAMPLE	GENERAL FORMULA FOR N
$P_{m,n}$ PARALLELOGRAMS	$P_{4,5}$ N=126	$N = {}^{m+n}C_m$
$A_{3,n}$ 3 TIER STRIPS BOTH ENDS INDENTED	$A_{3,5}$ N=36	$N = (n+1)^2$
$B_{3,n}$ 3 TIER STRIPS ONE END INDENTED	$B_{3,4}$ N=55	$N = 1+\sum_{n=1}^{n=n} A_{3,n} = (n+1)(n+2)(2n+3)/6$
$C_{3,n}$ 3 TIER STRIPS	$C_{3,4}$ N=105	$N = 1+\sum_{n=1}^{n=n} B_{3,n} = (n+1)(n+2)^2(n+3)/12$
$A_{5,n}$ 5 TIER STRIPS BOTH ENDS INDENTED	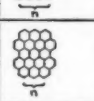 $A_{5,3}$ N=650	$N = (n+1)(n+2)^3(n+3)(n^2+4n+5)/120$
$B_{5,n}$ 5 TIER STRIPS ONE END INDENTED	$B_{5,3}$ N=805	$N = 1+\sum_{n=1}^{n=n} A_{5,n}$
$C_{5,n}$ 5 TIER STRIPS	$C_{5,4}$ N=4116	$N = 1+\sum_{n=1}^{n=n} B_{5,n}$
$CH_{1,m,n}$ CHEVRONS DEPENDING ON THREE PARAMETERS	$CH_{3,4,4}$ N=798	$N = 1+\sum_{s=1}^{s=m} {}^{s+1}C_s \, {}^{m+n-s}C_n$

south) line in one row and in adjacent positions. Nevertheless, some of the formulas for the number of forms listed are quite complicated and contain interesting information on the influence of molecular shape on the number of Kekulé forms. Particular instances of three of the series listed are pyrene $P_{2,2}$, benzperylene $B_{3,2}$, coronene $C_{3,2}$, and ovalene $C_{3,3}$ whose 6, 14, 20, and 50 unexalted forms, respectively, have been drawn and discussed from the valency bond viewpoint by Robertson.[10]

The series $C_{2n-1,n}$ representing hexagonal assemblages of hexagons, is illustrated by its second and fourth members in Figs. 29 and 30. Although the synthesis of the compound of Fig. 30 may be a matter of the remote future, our methods permit the somewhat laborious computation of N as shown in Table II.

We are grateful to Mr. R. M. Everett for suggesting a general formula for N in the series $C_{m,n}$, which contains the hexagonal series of Table II as the special case where $m=2n-1$. The formula which has since been shown to be a special case of a more general equation established

[10] J. M. Robertson, Acta Cryst. **1**, 101 (1948); Proc. Roy. Soc. (London) **A207**, 107 (1951).

TABLE II.

Member of hexagonal series	N
$C_{1,1}$ (Benzene)	2
$C_{3,2}$ (Coronene)	20
$C_{5,3}$	980
$C_{7,4}$ (Fig. 30)	232,848

by Mr. M. Woodger,[11] when expressed in terms of binomial coefficients, reads:

$$N \text{ (for } C_{m,n}) = \frac{\prod_{1}^{m} {}^{n+a}C_n}{\prod_{1}^{\frac{1}{2}(m-1)} {}^{n+a}C_n}, \qquad (2)$$

the products extending over the values of a shown. Apart from the inherent mathematical interest, the problems adumbrated in this paper justify consideration because of their bearing on *chemical reactivities*. The theory of *chemical structure*, on the other hand, has benefitted from studies of isomerism topology based upon the theory of "graphs,"[12,13] differing from resonance topology in specifying only one kind of line (bond) between any pair of atoms. Topological problems similar to those treated here have arisen in the theory of binary solutions,[14] and a typical dot-diagram problem was recently solved by Kuhn[15] in connection with the number of possible configurations of a polymer chain. Both isomerism and resonance topology have a bearing on chemical systematics, nomenclature and cipher notations.[16]

ACKNOWLEDGMENTS

The authors are indebted to Professor C. A. Coulson for helpful criticism and suggestions, and for drawing their attention to much of the previous work; to Mr. M. Woodger for his proof of the validity of Eq. (2), and for permission to publish the result prior to his publication; and to the Dunlop Rubber Company for facilities in the preparation of this paper.

[11] M. Woodger (to be published).
[12] G. Pólya, Z. Krist. **93**, 415 (1936); Ann. math. **68**, 145 (1937).
[13] T. L. Hill, J. Phys. Chem. **47**, 253 (1943).
[14] R. H. Fowler and G. S. Rushbrooke, Trans. Faraday Soc. **33**, 1272 (1937).
[15] H. Kuhn, Helv. Chim. Acta **31**, 1677 (1948).
[16] Gordon, Kendall, and Davison, Proc. XIth Intern. Congr. Pure and Appl. Chem. (in press); *Chemical Ciphering* (Royal Inst. Chem. London, 1948).

Diffusion Coefficients of the Systems CO_2-CO_2 and CO_2-N_2O*

I. Amdur, J. W. Irvine, Jr., E. A. Mason† and J. Ross‡
Department of Chemistry, Massachusetts Institute of Technology, Cambridge, Massachusetts
(Received October 8, 1951)

The radioactive tracer, $C^{14}O_2$, has been used to measure diffusion coefficients for the systems CO_2-CO_2 and CO_2-N_2O in the temperature range $-78°$ to 90°C. The apparatus, which is the Loschmidt type, uses saturation ionization currents as a measure of the extent of diffusion. The characteristics of this type of apparatus have been analyzed in detail to obtain working equations which permit use of experimental measurements at both small and large values of the time.

The present results, whose accuracy is estimated at 1.5 percent, agree with those obtained by other investigators using different experimental methods. Although the difference is small, 2.6±0.3 percent, the diffusion coefficient for the system CO_2-N_2O is consistently larger than that for CO_2-CO_2 over the entire temperature range.

THE influence of intermolecular forces on gaseous transport properties has long been recognized[1] and a great deal of information concerning molecular interactions has been obtained from determinations of the coefficient of viscosity as a function of temperature.[2] Relatively little diffusion coefficient data exists, however, which can be used satisfactorily for this purpose. Harteck and Schmidt,[3] Hutchinson,[4] and Winn[5] have measured gaseous self-diffusion coefficients over a sufficient temperature range and with adequate accuracy to permit evaluation of the potential energy between like molecules, but comparable measurements of mutual diffusion coefficients for calculating interaction potentials between unlike molecules do not seem to exist. Additional determinations of self- and mutual diffusion coefficients as a function of temperature are therefore of interest.

The availability of radioactive tracers facilitates the study of gaseous diffusion. First, the determination of self-diffusion coefficients becomes particularly straightforward because intermolecular forces between like molecules are unchanged when stable atoms are replaced by radioactive isotopes. Second, mutual diffusion coefficients can be measured with tracer concentrations of one of the components of the diffusing mixture to avoid uncertainties of interpretation which arise from the variation of the mutual diffusion coefficient with composition.[6] It is the object of the present article to describe an apparatus which is suitable for measuring gaseous diffusion coefficients in the range $-78°$ to 90°C by means of radioactive tracers, and to analyze in detail the effects which must be considered in order to obtain accurate diffusion coefficients. Values of the diffusion coefficients for two systems, CO_2-CO_2 and CO_2-N_2O, will be presented to illustrate the results which have been obtained with the apparatus.

APPARATUS AND PROCEDURE

The diffusion cell, shown in Fig. 1, is mounted horizontally in a thermostat whose temperature is constant to ±0.01° in the range $-78°$ to 90°C. The cell is similar to one first used by Loschmidt[7] and consists of a brass tube, separated by a slide, 1, into two sections, one of which, 2, is fixed, and the other, 3, capable of limited motion through the bellows. By turning the shaft, 4, the slide may be rotated to bring a hole of the same diameter as the tube, or a lead insert, 5, into axial alignment with the sections of the cell. To segregate the sections prior to a diffusion run, the steel nut, 6, is turned to imbed the movable section in the lead insert. The resulting seal is vacuum tight.

Each section of the cell contains a collecting electrode, 7, insulated from the tube with the plastic, 2,5-dichloropolystyrene, and functions as an ionization chamber. A potential of -450 volts on the electrode was found necessary to insure saturation currents. These currents, of the order of 10^{-11} amp, are measured with a single stage dc amplifier. The essential elements of the amplifier are a 10^{11}-ohm grid resistor, a Raytheon subminiature electrometer tube, type CK 571AX, and a Leeds and Northrup galvanometer, type E 2430-d, in the plate circuit. Extreme precautions are taken to minimize leakage currents and pick-up. The housing, 8, at the end of each section of the cell is evacuated to prevent condensation of moisture. Each grid lead, which consists of coaxial cable whose shield is at -450 volts, passes from the housing, through heavy wall iron pipe, to a brass vacuum chamber which contains the grid resistor and electrometer tube. The chamber is kept at a potential of -450 volts and serves as a guard ring and electric shield. All components of the amplifier are housed in a thermostated, heavy wall, iron cabinet.

* Supported in part by a du Pont grant-in-aid of fundamental research.
† Charles A. Coffin Fellow, 1949–1950.
‡ Eastman Kodak Company Fellow, 1949–50.
[1] S. Chapman and T. G. Cowling, *The Mathematical Theory of Non-Uniform Gases* (Cambridge University Press, Teddington, England, 1939), p. 380 ff.
[2] See reference 1, Chapter 12; Hirschfelder, Bird, and Spotz, J. Chem. Phys. **16**, 968 (1948); Chem. Rev. **44**, 205 (1949).
[3] P. Harteck and H. W. Schmidt, Z. physik. Chem. **B21**, 447 (1933).
[4] F. Hutchinson, J. Chem. Phys. **17**, 1081 (1949).
[5] E. B. Winn, Phys. Rev. **80**, 1024 (1950).
[6] See reference 1, Chapter 14.
[7] J. Loschmidt, Sitz. Akad. Wiss. Wien **61**, 367 (1870).

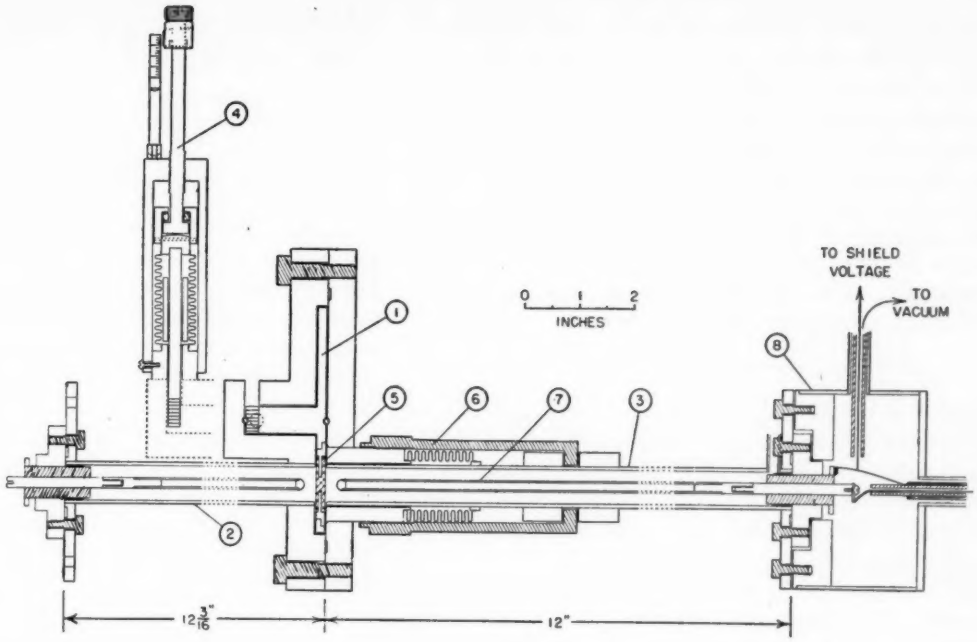

FIG. 1. Details of diffusion cell.

The amplifier is used as a null instrument by including in the circuit a variable reference voltage which is measured potentiometrically. The voltage developed when the ionization chamber current flows through the grid resistor is opposed by this reference voltage until the amplifier indicates no net voltage input. The circuit is capable of measuring ionization currents with a precision of 0.1 percent.

The experimental procedure for determining diffusion coefficients using radioactive tracers may be illustrated by summarizing the steps which were followed for the system CO_2-CO_2.

$BaCO_3$ containing $BaC^{14}O_3$ was fused with $PbCl_2$ to generate a mixture of CO_2 and $C^{14}O_2$.[8] This gas mixture was diluted with normal CO_2 to produce the desired tracer concentration. The diffusion cell was evacuated and the sections segregated to permit introduction of radioactive mixture into one section and normal gas into the other. Before transfer to the diffusion cell, the gases were thoroughly dried and then purified by distillation from bulbs at dry ice temperature and condensation in bulbs cooled with liquid nitrogen. The pressure of the normal CO_2 was adjusted to that of the labeled CO_2 within 0.1 mm of Hg as read on a differential manometer filled with silicone fluid, type DC 200. A cathetometer was used to read the absolute pressure on a mercury manometer. After the pressures in the sections of the cell were equalized, the ionization current in the section containing radioactive gas was measured. The separating slide was then opened, and the rate of diffusion was followed by measuring the decrease in the ionization current as a function of time. Before and after each diffusion run both sections of the cell were filled with normal gas, and background currents were measured.

[8] Zwiebel, Turkevich, and Miller, J. Am. Chem. Soc. **71**, 376 (1949).

ANALYSIS

For the case of one-dimensional diffusion in a system of two components at constant molecular density, the mutual diffusion coefficient D_{12} may be defined by Fick's second law in the form

$$\partial c_1/\partial t = (1/\omega)(\partial/\partial x)[D_{12}\omega(\partial c_1/\partial x)], \qquad (1)$$

where $\partial c_1/\partial t$ is the time rate of change in the concentration of component 1 at a point x on the axis along which diffusion is occurring. The concentration gradient of this component at the given point is $\partial c_1/\partial x$, and the area across which diffusion takes place is ω. If the components are indistinguishable, the diffusion coefficient is referred to as the self-diffusion coefficient D_{11}. Since in the present case the component whose concentration changes are being followed is always the radioactive tracer, component subscripts will be omitted henceforth. The case of self-diffusion will be distinguished from that of mutual diffusion by indicating that the tracer-free gas is CO_2 rather than N_2O.

The solution of Eq. (1) for certain boundary conditions is well known for the case where ω and D are independent of x.[9] In the present apparatus, the cross-sectional area of the cell is not constant since the collecting electrodes cannot extend the full length of the sections. The procedure for solving Eq. (1) in this case is suggested by the solution of the problem of one-dimensional heat flow through contiguous rods having different thermal conductivities.[10] It is assumed that the

[9] P. Frank and R. v. Mises, *Die Differential- und Integralgleichungen der Mechanik und Physik*, (Friedr. Vieweg und Sohn, Braunschweig, Germany), 8th edition, Vol. 2, pp. 576–579.

[10] See reference 9, p. 539 ff.

diffusion cell may be represented by three regions of constant cross section, two of which have the same uniform cross section and extend from the closed end of each section of the cell to the tip of each collecting electrode. The third region, of different cross section, is in the center of the cell between the electrode tips. Appropriate particular solutions of Eq. (1) for the three regions are matched at the planes where the changes in cross section occur by applying conditions of continuity of concentration and of diffusion current Γ, which is defined by Fick's first law as

$$\Gamma = -D\omega(\partial c/\partial x). \tag{2}$$

Inclusion of the initial and boundary conditions results in a general solution for the concentration of the tracer as a function of time at any point along the axis of the diffusion cell. Since the central electrodes in the cell sections measure the total current resulting from the disintegration of the tracer, the total quantity of tracer at any time in an entire section is of interest rather than the concentration at any point. The general solution for the concentration as a function of time and position is therefore integrated over the volume of the section to give an equation of the form

$$n(t)/n(0) = a + be^{-k^2Dt} + \cdots, \tag{3}$$

where $n(t)/n(0)$ is the ratio of the total quantity of tracer at time t to that at time 0 in the section of the cell originally filled with labeled mixture, and a, b, and k are known constants for a given apparatus and set of initial conditions.

The use of Eq. (3) for calculating D would be very convenient since a single experimental value of $n(t)/n(0)$ would be sufficient to obtain a value of D. Unfortunately, this is not possible in the present case because the ratio of measured ionization currents (corrected for background), $i(t)/i(0)$,[11] is not equal to $n(t)/n(0)$. There are two effects which are responsible for this inequality. The first, known as cross-over ionization, results in the production of current in one section of the diffusion cell by particles, capable of producing ionization, which originate in the other section. The second is the dependence of the current in a given section of the cell upon the manner in which the tracer is distributed in the section, as well as upon the total quantity of tracer present. This distribution effect results from the difference in average effective path lengths of ionizing particles produced by disintegrations. For example, the average effective path traversed by an ionizing particle which originates near the center of a section of the cell is longer than that of a particle which originates near the ends. Consequently, the current resulting from a given number of radioactive particles near the center of the section is greater than that arising from the same number of particles near the ends.

In principle, it is possible to correct measured currents for cross-over ionization and to eliminate the distribution effect by further correcting all currents to the values they would have if referred to a common distribution. The most convenient distribution for this purpose is a uniform one, such as exists at $t=0$. In practice, these corrections cannot be made numerically because of insufficient knowledge of the dynamics of the ionization processes which occur in the diffusion cell. It is possible, however, to make the corrections in formal fashion, and this is sufficient for the purpose of evaluating diffusion coefficients from the experimental measurements.

At time t, the relation between the current, corrected for the effects of cross-over ionization and distribution $i^*(t)$ and the measured current $i(t)$ may be written as

$$i^*(t) = i(t)\left[\frac{i(t,d)}{i(t,d)+i(t,c)}\right]\frac{i(t,u)}{i(t,d)}$$

$$= i(t)\left[\frac{i(t,u)}{i(t,d)+i(t,c)}\right]. \tag{4}$$

The functions, $i(t,d)$, $i(t,c)$, and $i(t,u)$, are formal expressions for the currents, at time t, in a given section of the cell, and may be identified, respectively, as follows:

$i(t,d)$, the current produced by the total quantity of tracer present in its actual distribution;

$i(t,c)$, the additional current resulting from cross-over ionization; and

$i(t,u)$, the current produced by the total quantity of tracer present in uniform distribution.

To obtain the expression for $i(t,d)$ it is necessary to consider the current produced in volume dV' of a given section of the diffusion cell by ionizing particles which originate from disintegrations in volume dV of the same section. If $c(x,t)$ is the tracer concentration in dV, the total current in the section will be given by

$$i(t,d) = \int\int fc(x,t)dVdV', \tag{5}$$

where f takes into account all aspects of the dynamics of the ionization process and the effect of solid angle on the number of ionizing particles which reach dV' from dV. The double integration extends over the entire volume of the given section of the cell. Since $c(x,t)$ is the known general solution of Eq. (1) for any portion of the cell section where the cross section may be taken as constant,[9,10] the expression for $i(t,d)$ may be reduced to

$$i(t,d) = \alpha + \beta e^{-k^2Dt} + \cdots. \tag{6}$$

[11] In referring to $i(t)$ as the measured ionization current at time t, it is assumed that the separating slide between the section of the diffusion cell has been opened instantly at $t=0$, and that the electrical measuring circuit has zero response time. The nature of the corrections which are required when these conditions are not fulfilled will be discussed in detail below.

The constants α and β are independent of time or position and contain integrals remaining from Eq. (5) after terms in $c(x, t)$ which involve the time have been taken outside the integral signs. The relation for $i(t, c)$ is obtained in similar manner, except that the volume elements dV' and dV are in different sections of the cell and the function f is replaced by f' to allow for the difference in the details of the ionization processes. Thus

$$i(t, c) = \int\int f'c(x, t)dVdV', \tag{7}$$

where the integration with respect to V' is taken over the volume of the section in which the current is being measured, while that with respect to V is taken over the volume of the other section. Again, by proper substitutions for $c(x, t)$, Eq. (7) may be put in the form

$$i(t, c) = \gamma + \delta e^{-k^2Dt} + \cdots, \tag{8}$$

where γ and δ are constants similar to α and β in Eq. (6). Finally, since $i(t, u)$ is the current produced in a given section of the cell by ionizing particles which originate in that same section when the tracer concentration is assumed to be uniformly distributed, it may be written as

$$i(t, u) = \int\int f\bar{c}(t)dVdV', \tag{9}$$

where $\bar{c}(t)$ is the average tracer concentration. It is equal to $n(t)/V$ where V is the volume of the section over which the integrations in Eq. (9) are performed. Since, according to Eq. (3),

$$\bar{c}(t) = c(0)(a + be^{-k^2Dt} + \cdots), \tag{10}$$

Eq. (9) may be reduced to

$$i(t, u) = (a + be^{-k^2Dt} + \cdots)\epsilon, \tag{11}$$

where ϵ is another constant of the type of α, β, γ, and δ of Eqs. (6) and (8).

The corrections which must be applied to the initial measured current, $i(0)$, are simpler than those required for $i(t)$. There is no correction for cross-over ionization since the separating slide between the sections of the cell is closed, and there is no distribution correction since the existing distribution is the uniform one to which corrected $i(t)$ values are referred. However, the fact that the slide is closed during the measurement of $i(0)$ necessitates two other corrections. The first is required because of the change in the quantity or in the concentration of tracer which occurs when the separating slide between the sections of the cell is rotated to permit diffusion to proceed. The rotation introduces into the cell the small volume of gas, either radioactive or normal, which filled the hole in the slide when the sections were segregated during filling. The second correction is required because of the change of pressure in the cell when the bellows are extended to permit rotation of the slide. The relation between the corrected initial current $i^*(0)$ and the corresponding measured current $i(0)$ may be written

$$i^*(0) = i(0)\zeta, \tag{12}$$

where ζ is an unknown constant containing a ratio of double integrals similar to those in α or β in Eq. (6), and a multiplicative term which, at a given temperature and pressure, depends only upon the fixed ratio of the pressures in the cell corresponding to the open and closed positions of the slide.

Substitution of Eqs. (6), (8), and (11) into Eq. (4) and division of the result by Eq. (12) leads to

$$\frac{i^*(t)}{i^*(0)} = \frac{i(t)\epsilon(a + be^{-k^2Dt} + \cdots)}{i(0)\zeta[(\alpha+\gamma) + (\beta+\delta)e^{-k^2Dt} + \cdots]}. \tag{13}$$

This expression for $i^*(t)/i^*(0)$ may be set equal to $n(t)/n(0)$ in Eq. (3) to give the desired relation involving the measured quantities $i(t)$, $i(0)$, and t, namely,

$$i(t)/i(0) = \eta + \theta e^{-k^2Dt} + \cdots, \tag{14}$$

where $\eta = (\zeta/\epsilon)(\alpha+\gamma)$ and $\theta = (\zeta/\epsilon)(\beta+\delta)$. It is interesting to observe that the form of Eq. (14) is identical with that of Eq. (3). However, since η and θ are parameters which can be determined only from the actual experimental measurements, whereas a and b are known constants, it is more difficult to obtain accurate values of D from Eq. (14) than from Eq. (3). Since it is not possible to measure $n(t)/n(0)$ directly, there is no choice but to use Eq. (14) and to attempt to increase the accuracy of the experimental measurements in an effort to compensate for the necessity of determining the constants η, θ, and D, simultaneously.

There is a slight convenience introduced by the use of Eq. (14) which partly offsets the disadvantage of solving for the three disposable constants. Since the slide between the sections of the cell cannot be opened instantaneously, the question arises as to the proper origin for the time which appears in the equation. The fact that η and θ are not known *a priori* makes it possible to select as the origin an unspecified time when the slide has been fully opened and lateral inequalities of composition caused by the opening have disappeared. The effect of such a shift in the time origin is equivalent to assuming a different set of initial conditions than those which led to Eq. (3). In Eq. (14) this change in initial conditions merely changes the observed values of η and θ.

The presence of but two terms in Eq. (14) limits the use of the equation, for reasons of convergence, to large values of Dt. In the present case, these values lie in the range 185 cm² to 750 cm², corresponding to values of t between 800 seconds and 3200 seconds, at the experimental temperatures and pressures. Since measurements start at about 85 seconds, it would appear desirable either to add higher terms to Eq. (14), or to develop an additional relation, with suitable convergence characteristics, for smaller values of Dt. The

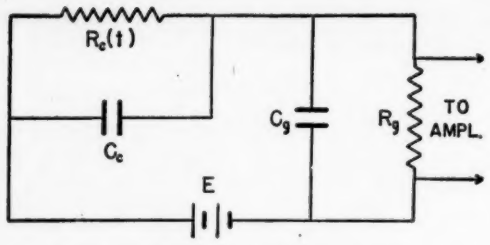

FIG. 2. Equivalent electrical circuit.

addition of higher terms to Eq. (14) does not produce the desired result, since the introduction of such terms requires inclusion of additional adjustable parameters similar to η and θ, because of the effects of cross-over ionization and distribution. The additional experimental results which can be used because of the presence of the higher terms merely serve to determine the new parameters, and essentially no new information is obtained with respect to the value of D. The second alternative for using experimental results at early times, namely, development of a new relation with proper convergence properties, can be realized by applying the method of Laplace transforms,[12] with the following results.

For the ideal case of one-dimensional diffusion in a cell initially divided into two identical sections, each of the same uniform cross section and length, $l/2$ the ratio of the total quantity of tracer at time t to that at time 0 in the section originally filled with labeled mixture, is given by

$$n(t)/n(0)=1-(1/w)\{1+2\sum_{j=1}^{j=\infty}(-1)^j[\exp(-j^2w^2/\pi) -jw\,\mathrm{erfc}(jw/\pi^{\frac{1}{2}})]\}, \quad (15)$$

where $w=(l/2)(\pi/Dt)^{\frac{1}{2}}$. The error function, $\mathrm{erfc}(jw/\pi^{\frac{1}{2}})$, is defined by the integral

$$\mathrm{erfc}(jw/\pi^{\frac{1}{2}})=2/\pi^{\frac{1}{2}}\int_{jw/\pi^{\frac{1}{2}}}^{\infty}\exp(-z^2)dz. \quad (16)$$

For the non-ideal geometry of the present diffusion cell, it was not feasible to use the method of Laplace transforms for solving the fundamental differential diffusion equation, Eq. (1), or to derive the form of the corrections which are required to convert Eq. (15) into the corresponding relation for the ratio $i(t)/i(0)$. Accordingly, by analogy with the relation between Eq. (14) and Eq. (3), it was assumed that the desired relation, valid for small values of Dt, could be written as

$$i(t)/i(0)=1-s(Dt)^{\frac{1}{2}}, \quad (17)$$

where s is an unknown parameter. Higher order terms, originating from the summation in Eq. (15), have not been included, since their contribution is negligible for the range of Dt of interest, namely, about 25 cm^2 to 250 cm^2, corresponding to times between about 85 seconds and 900 seconds. Since s must be evaluated from experimental results, it is not possible to use Eq. (17) to obtain absolute values of D. However, it can yield relative values as a function of temperature and thus makes use of experimental results at early times to improve the accuracy of the absolute values of D as calculated from Eq. (14).

The time t in Eq. (17) must be referred to the proper origin, since this equation, unlike Eq. (14), cannot include in the unknown parameter s a constant displacement of the time origin. In an actual experiment, the slide which separates the sections of the diffusion cell was rotated with constant angular velocity from $t=0$, when it started to open, until it was fully open at $t=\tau$. Therefore, a time origin t_0 was chosen between 0 and τ such that, if the slide could be opened instantly at t_0, the quantity of radioactive gas mixture which would diffuse between t_0 and τ would be the same as that which actually diffused during a run between 0 and τ. This quantity is calculated by applying the treatment given by Ney and Armistead[13] and by Hutchinson[4] for diffusion between two chambers connected by a tube of small diameter. For the present apparatus and operating procedure (rotation of the separating slide with constant angular velocity) the final result may be written

$$t_0=0.7894\tau. \quad (18)$$

For all runs the values of τ were between 10.5 seconds and 23.0 seconds.

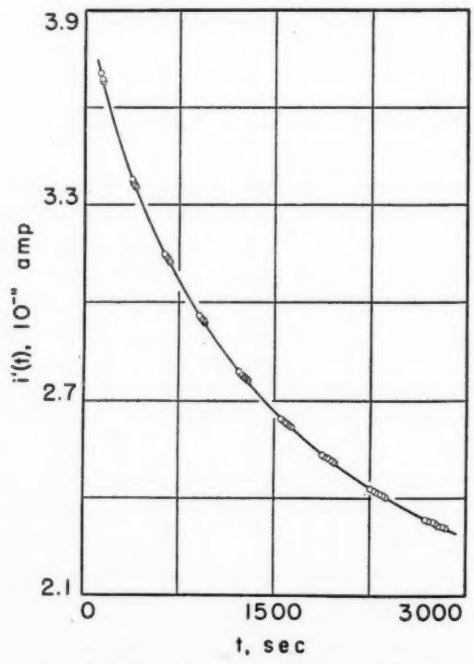

FIG. 3. Typical experimental measurements.

[12] H. S. Carslaw and J. C. Jaeger, *Conduction of Heat in Solids* (Oxford University Press, London, England, 1947), pp. 240–246, 250–253; *Operational Methods in Applied Mathematics*, second edition (Oxford University Press, London, England, 1948), pp. 88–94, 271–276.

[13] E. P. Ney and F. C. Armistead, Phys. Rev. **71**, 14 (1947).

In addition to the correction for the finite time required to open the slide, it is necessary to take into account the effect of the response time of the electrical circuit. This arises from the fact that the current $i(t)$, which appears in Eqs. (14) and (17), refers to the saturation current in the ionization chamber, whereas the current which is actually measured is that which flows through the 10^{11} ohm grid resistor in series with the chamber. Since there is capacity as well as resistance in the electrical circuit, these currents will not be the same, particularly at early times when $i(t)$ is changing rapidly.

The correction for the effect of the response time may be obtained by considering the equivalent circuit, shown in Fig. 2, which consists of a source of emf E, the grid resistor R_g, the effective dc resistance of the ionization chamber $R_c(t)$, which varies with time, and the capacities C_g and C_c. C_g is the interelectrode capacity of the electrometer tube and the distributed capacity of its leads, while C_c is the capacity of the ionization chamber and the distributed capacity of its leads. Application of Kirchoff's laws to the circuit in Fig. 2 leads to the relation

$$di'(t)/dt+i'(t)/(R_gC)=i(t)/(R_gC), \qquad (19)$$

where $i'(t)$ is the measured current through R_g, $i(t)$ is the saturation current through $R_c(t)$, and C is equal to C_g+C_c. (Because of the difference in the length of the leads, C, in the present apparatus, has different values for the two sections of the diffusion cell, 83 $\mu\mu$f and 123 $\mu\mu$f.) There are two solutions to Eq. (19): one which is obtained by eliminating $i(t)$ through Eq. (14), and the other by eliminating $i(t)$ through Eq. (17). The boundary conditions are the same in both cases, namely, $i'(0)=i(0)$ and $i'(\infty)=i(\infty)$. Substitution of $i(t)$ from Eq. (14) yields an expression for $i'(t)$ which, within the accuracy justified by the presence of but two terms in Eq. (14), differs from $i(t)$ only in that the values of η and θ are changed. Since these are determined from experiment, it follows that measured values of $i'(t)$ may be substituted directly into Eq. (14) without correction for the time of opening the slide or for the effect of the response time of the measuring circuit. Substitution of $i(t)$ from Eq. (17), however, and inclusion of the correction for the time of opening the slide produces the following final equation for use at early values of the time:

$$i'(t)/i'(0)$$
$$=1-s(Dt^*)^{\frac{1}{2}}\left[1-(1/y)\exp(-y^2)\int_0^{y/2}\exp(z^2)dz\right], \qquad (20)$$

where $t^*=t-0.7894\tau$ and $y=[t^*/(R_gC)]^{\frac{1}{2}}$. For large values of y^2 the integral in Eq. (20) approaches $[\exp(y^2)]/(2w)$. When this approximation is not adequate, values of the integral may be obtained from tables.[14]

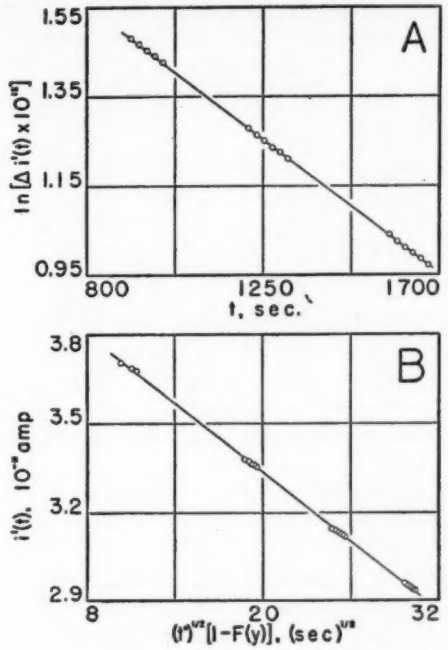

FIG. 4. Applicability of equations for evaluating D: A. Eq. (14); B. Eq. (20).

RESULTS

Experimental results for a typical diffusion run are shown in Fig. 3 where the ionization current $i'(t)$, as measured on the dc amplifier and corrected only for background, is plotted against the elapsed time t, since the separating slide began to open. The full range of results shown in the plot were used to calculate a value of the diffusion coefficient by applying both Eqs. (14) and (20) as follows.

An absolute value of D, at the temperature and pressure existing during the run, was obtained by using Eq. (14) for measurements between 900 seconds and 2660 seconds. A special calculating procedure was used[15] which requires values of $i'(t)$ at equally spaced time intervals from the smooth curve. A plot was made of $\ln\Delta i'(t)$ *vs* t, where $\Delta i'(t)$ is the change in ionization current in a given constant time interval and t is the initial time (the final time is also suitable) in the interval to which $\Delta i'(t)$ refers. If Eq. (14) is valid, a straight line of slope $-k^2D$ should result, as shown in Fig. 4A. As previously indicated, k is a known constant whose value for the present apparatus depends slightly upon the absolute temperature T, because of thermal expansion of the brass tube in the diffusion cell. Its value may be represented by

$$k=0.05363/(1+1.25\times10^{-5}T+9.8\times10^{-9}T^2). \qquad (21)$$

[14] W. L. Miller and A. R. Gordon, J. Phys. Chem. **35**, 2785 (1931); H. M. Terrill and L. Sweeney, J. Franklin Inst. **237**, 495 (1944); **238**, 220 (1944).

[15] J. Lipka, *Graphical and Mechanical Computation* (John Wiley and Sons, Inc., New York, 1918), pp. 142–145.

TABLE I. Experimental values of the diffusion coefficient, D.

T, °K	P, mm	D, cm²/sec [Eq. (14)]	D, cm²/sec [Eq. (20)]	D, cm²/sec (smoothed)	Percent deviation
A. The system, CO_2-CO_2.					
194.8	157.0	0.0509	0.0518	0.0516	−0.4
273.2	307.2	0.0956	0.0966	0.0970	+0.4
312.8	490.4	0.1201	0.1220	0.1248	+2.3
362.6	468.4	0.1707	0.1682	0.1644	−2.3
				Av=	1.4
B. The system, CO_2-N_2O.					
194.8	203.7	0.0550	0.0526	0.0531	+1.0
273.2	319.7	0.0989	0.1006	0.0996	−1.0
312.8	510.0	0.1297	0.1244	0.1280	+2.9
312.8	323.3	0.1245	0.1292	0.1280	−0.9
362.6	507.4	0.1709	0.1715	0.1683	−1.9
				Av=	1.5

The measurements shown in Fig. 3 between 115 seconds and 940 seconds were then used in Eq. (20) to adjust slightly the value of D derived from Eq. (14) to obtain a new value which is valid, within the estimated experimental error, over the entire time range. Values of $i'(t)$ were plotted against $(t^*)^{\frac{1}{2}}[1-F(y)]$, where

$$F(y)=(1/y)\exp(-y^2)\int_0^{iy^2}\exp(z^2)dz, \qquad (22)$$

to give a straight line with a slope of $-i'(0)s(D)^{\frac{1}{2}}$ and an intercept of $i'(0)$ as shown in Fig. 4B. (In all cases the intercept agreed with the measured value of $i'(0)$ within 0.1 percent, the experimental uncertainty.) The intercept was combined with the value of D previously obtained from Eq. (14) to calculate a value of s for the run in question. If Eq. (20) is valid, not only should the type of plot shown in Fig. 4B be a straight line for every run, but the value of s, except for a small temperature coefficient which is the same as that given for k in Eq. (21), should be the same for all runs in a given system. In fact, the similarity of the present systems, CO_2-CO_2 and CO_2-N_2O, suggests that s should be the same for all runs since only *differences* in the effects of cross-over ionization and distribution would result in different average values for s for the two systems. Accordingly, all runs were treated in the manner just described for the typical run in Fig. 3 to obtain preliminary values of D and corresponding individual values of s. These s values showed a maximum deviation of 4.0 percent and the average deviation from the mean was 1.1 percent. They showed no trends and their average value for both systems was the same within ±0.6 percent. Final experimental values of D for each run were obtained by combining a single average value of s and the appropriate value of $i'(0)$ with the slope, $-i'(0)sD^{\frac{1}{2}}$. These slopes, as well as those from Eq. (14), were obtained analytically by the method of averages.

The results of the present investigation are summarized in Table I. The diffusion coefficients have been referred to 1 atmosphere. Their values at the tabulated pressures existing during the runs may be obtained from the inverse relation between the diffusion coefficient and the pressure. Since the mass of the radioactive tracer was different from that of the normal gas, the tabulated values of D were corrected to refer to diffusion systems in which all molecules had the molecular weight of the normal gas. The correction factor, which is the square root of the ratio of the reduced mass of the experimental system to that of the system of like molecules, amounts to 1.011 in the present case. The basis for the correction is to be found in the Chapman-Enskog expression for the first approximation to the diffusion coefficient.[16] The smoothed values of D shown in Table I have been taken from the curves in Figs. 5A and 5B, which were drawn to provide the best fit for the values calculated from Eq. (20) without introducing inflections or curvatures which could only arise from unrealistic forms of molecular interaction. The last column shows the percent deviations between these final smoothed values of D and those calculated from Eq. (20).

DISCUSSION

In addition to the results of the present investigation, Figs. 5A and 5B show the values of D obtained by other investigators. For the system CO_2-CO_2, the only other measurements over a large range of temperature are those made by Winn,[5] who used a mass spectrometer to follow the diffusion of $C^{13}O_2$ in a system similar to that of Ney and Armistead.[13] For the complete temperature range the average absolute deviation of his values from those on the smooth curve of Fig. 5A is 1.7 percent. The average probable error cited by Winn for his results is 1.2 percent, and the internal consistency of the present results is 1.4 percent, as measured by the average of the percent deviations in Table I. Winter[17] also used a mass spectrometer to follow the diffusion of $C^{12}O^{16}O^{18}$ in an apparatus similar to that of Winn. After correction for the increased mass of the oxygen isotope, his mean values, which are reproducible to ±1.8 percent, lie within 0.8 percent of the present smoothed values.

For the system CO_2-N_2O there are no investigations over a large range of temperature. Loschmidt[18] determined the extent of diffusion by chemical analysis and obtained two values of D near room temperature. His results, which are reproducible to ±1 percent, show an average deviation of 0.8 percent from the curve of Fig. 5B. Using similar types of Loschmidt apparatus, Boardman and Wild[19] and Wall and Kidder[20] also obtained room temperature values of the diffusion coefficient for this system. Boardman and Wild analyzed

[16] See reference 1, p. 165.
[17] E. R. S. Winter, Trans. Faraday Soc. **47**, 342 (1951).
[18] J. Loschmidt, Sitz. Akad. Wiss. Wien **62**, 468 (1870).
[19] L. E. Boardman and N. E. Wild, Proc. Roy. Soc. (London) **A162**, 511 (1937).
[20] F. T. Wall and G. A. Kidder, J. Phys. Chem. **50**, 235 (1946).

their gas mixtures chemically and obtained six separate values of D within a temperature range of 1.9 degrees. After correction to a common temperature, these values show an average absolute deviation of 1.7 percent from their mean, which, in turn, is 2.6 percent lower than the corresponding present value. Similarly, Wall and Kidder obtained four independent values of D at a single temperature in a series of experiments in which gas mixtures were analyzed interferometrically. The average absolute deviation of the four values from the reported mean is 0.4 percent. The deviation between this mean value and the curve of Fig. 5B is fortuitously small, 0.1 percent. The remaining points shown in the figure are those obtained by Obermayer[21] who used a Loschmidt apparatus and analyzed his gas mixtures chemically. Although the reproducibility of his results is good, ±0.4 percent, the accuracy seems to be poor as shown by the abnormally large average deviation, 5.1 percent, from the present results, and the lack of agreement with the results of the other investigators.

The accuracy of the present D values for both systems is estimated to be at least 1.5 percent. The estimate takes into account the reproducibility of the experimental measurements, the accuracy with which Eqs. (14) and (20) can represent these measurements, the percentage deviations in the last column in Table I, and the agreement of the present smoothed values with the results of other investigators. It is interesting to observe that the final D values for the system CO_2-N_2O are consistently higher than those for CO_2-CO_2 by 2.6 ±0.3 percent. Since this consistent difference is greater than the estimated error, the authors feel that the result can be attributed to the lack of complete physical identity of the isosteres CO_2 and N_2O. Small differences must certainly exist between the intermolecular forces of CO_2 and N_2O as compared with those of CO_2 and CO_2, and such differences could give rise to the observed trend.

[21] A. v. Obermayer, Sitz. Akad. Wiss. Wien **81**, 1102 (1880).

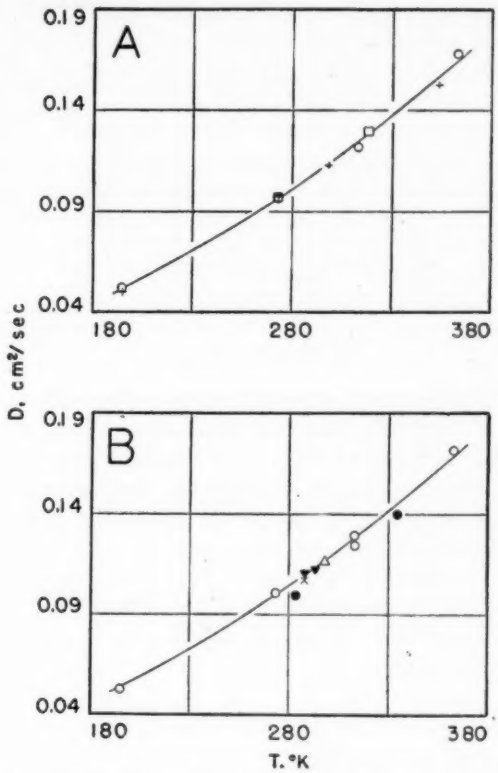

FIG. 5. Experimental values of D. A. CO_2-CO_2: + Winn; □ Winter; ○ present investigation. B. CO_2-N_2O: ▼ Loschmidt; × Boardman and Wild; Δ Wall and Kidder; ● Obermayer; ○ present investigation.

ACKNOWLEDGMENTS

The authors wish to express their appreciation to Mr. K. Wilhelmson for aid in constructing the apparatus, and to Mr. T. F. Schatzki for assisting with the measurements and calculations.

Polarized Infrared Spectrum of Sodium Nitrite*

ROGER NEWMAN
Gates and Crellin Laboratories,† California Institute of Technology, Pasadena, California
(Received September 6, 1951)

The infrared spectra of single crystals of $NaNO_2$ were obtained in polarized light. The polarization behavior of the strong absorptions leads to the following assignment of the nitrite fundamentals $\nu_1=1325$ cm^{-1}, $\nu_2=831$ cm^{-1}, and $\nu_3=1360$ cm^{-1}. Other bands of lower intensity are observed. A combination band $(\nu_1+\nu_3)$ at 2670 cm^{-1} shows a polarization behavior in accord with site group selection rules. An effect is discussed which results from the use of an infrared microscope in the investigation of polarization spectra.

INTRODUCTION

THE present investigation of the polarized spectra of crystalline $NaNO_2$ was undertaken with two purposes in mind. First it was anticipated that this study might definitely establish the fundamental frequencies of the nitrite ion. Previous investigations of this subject were not entirely conclusive.[1–3] Second, the simplicity of both the nitrite spectrum and the crystal structure[4] of $NaNO_2$ allows us an opportunity to test with some confidence certain aspects of a theory of the spectra of crystals.[5]

EXPERIMENTAL

Crystals of $NaNO_2$ were grown by evaporation of aqueous solutions at room temperature. The crystal habit is such that (001) plates are usually formed.‡ The thickness of the plates depends upon the rate of evaporation. By a very rapid evaporation (under vacuum) of a film of solution spread on a glass surface, very thin crystal plates several mm on an edge were formed. By slow evaporation, plates about a mm thick and several mm on an edge could be formed. For the studies of the (001) plates, the sections were suitably mounted for use with our microilluminator[6] and appropriate spectra taken. It was also possible to obtain thin (001) plates of sufficient size to use directly in the parallel light beam between source and spectrometer. (010) sections were prepared from the thicker crystal plates by the hand polishing technique previously described.[7] These were likewise suitably mounted for use in the microilluminator.

The spectra were taken using a Beckman IR-2 spectrometer (NaCl optics). The microilluminator was equipped with a low temperature cell so that samples could be cooled to liquid nitrogen temperature. A silver chloride polarizer was used.

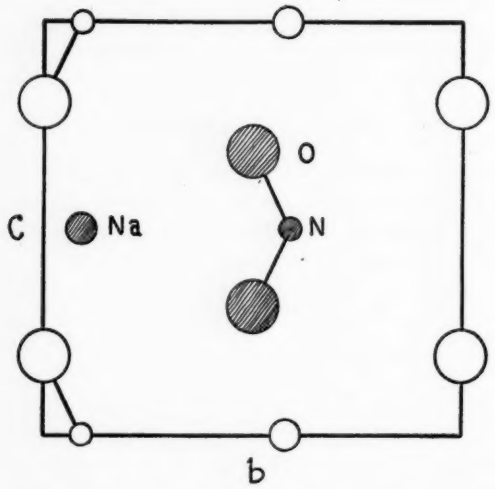

FIG. 1. Diagram of unit cell of $NaNO_2$. Clear circles at $a=0$, shaded circles at $a=\frac{1}{2}$ (after Ziegler).

SELECTION RULES

Sodium nitrite forms orthorhombic crystals having space group symmetry $C_{2v}{}^{20}$ with two molecules per unit cell.[4] The NO_2^- groups are found to be isoceles triangles with the N–O bond distance equal to 1.13A and the O–N–O bond angle equal to 132°. The nitrite groups occupy sites of full C_{2v} symmetry. The two occupied sites of the unit cell have parallel symmetry elements. A diagram of the unit cell is shown in Fig. 1.

Under the site symmetry just described the selection rules of the nitrite ion in the crystal are those of the isolated ion. Namely, ν_1, the symmetric stretch and ν_2, the symmetric bend should be active parallel to the C_2 axis, while ν_3, the asymmetric stretch should be active only perpendicular to the C_2 axis. All activity, of course, takes place in the molecular plane. In terms of the crystal axes, therefore, it is to be expected that ν_1 and ν_2 should be polarized along b and ν_3 should be polarized

* The work herein described was supported by the ONR under Contract N6-ori-102, VI.
† Contribution No. 1631 from the Gates and Crellin Laboratories.
[1] C. R. Bailey and J. W. Thompson, Nature **135**, 913 (1935).
[2] D. Williams, J. Am. Chem. Soc. **61**, 2987 (1939).
[3] A. Langseth and E. Walles, Z. physik. Chem. **B27**, 209 (1934).
[4] G. E. Ziegler, Phys. Rev. **38**, 1040 (1931).
[5] H. Winston and R. S. Halford, J. Chem. Phys. **17**, 607 (1949).
‡ Identification of crystal orientations was achieved both through simple goniometric measurement and by observation of the refractive indices. The latter were compared with Ziegler's (reference 4) values. In this connection we have found that the principal refractive indices were $\alpha=1.35$, $\beta=1.41$, and $\gamma=1.62$, as compared to $\alpha=1.35$, $\beta=1.46$, and $\gamma=1.65$ reported by Ziegler. Our standard liquids were uncalibrated but they are probably good to 0.01 of a unit.
[6] R. M. Badger and R. Newman, Rev. Sci. Instr. **22**, 935 (1951).
[7] R. Newman and R. S. Halford, J. Chem. Phys. **18**, 1276 (1950).

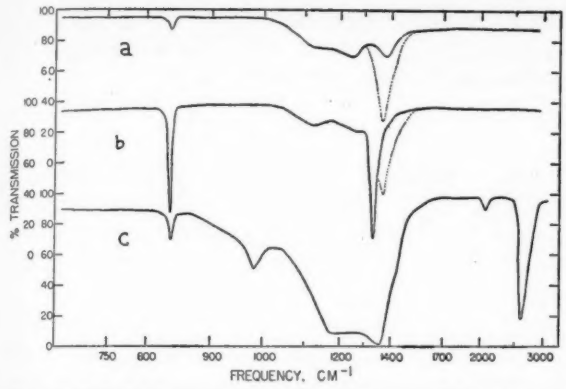

FIG. 2. Polarized spectra of $NaNO_2$. The *a* and *b* spectra were taken in parallel light from a (001) crystal about 15μ thick. The dotted curves show the additional absorption resulting from the use of the microilluminator. The *c* spectrum was taken in the microilluminator from a (010) crystal about 30μ thick.

along *c*. The *a* spectrum should be devoid of any activity involving nitrite fundamentals alone.

Results and Discussion

In Fig. 2, we have shown the polarized spectra of $NaNO_2$. The frequencies observed are listed in Table I. The spectra shown were obtained either with the microilluminator or by using parallel light, as indicated in the caption.

Fundamentals

An examination of the *b* spectrum for the very thin samples shows that there are two strong sharp bands present, one of 831 cm^{-1} and the other at 1325 cm^{-1}. A search down to 400 cm^{-1} with a KBr spectrometer failed to show the presence of any bands below that at 831 cm^{-1}. It would therefore seem reasonable from polarization and intensity considerations that the two strong bands are the ν_1 and ν_2 fundamentals. Their frequencies almost necessitate their assignment as $\nu_1=1325$ cm^{-1} and $\nu_2=831$ cm^{-1}. When (001) crystals are studied in the convergent light beam of the microilluminator the *a* and *b* spectra show the presence of a band at 1360 cm^{-1}. This phenomenon will be discussed below.

The *c* spectrum shows the presence of a wide region of intense absorption extending from about 1170 to 1370 cm^{-1}. There are also several much weaker absorption bands in the spectrum. No section was obtained which was thin enough to completely resolve the region of intense absorption into its component bands. However, for reasons which will be discussed later there is a mixing of the orthogonal spectra, *a*, *b*, and *c* when the microilluminator is used. It is our view that the band at 1360 cm^{-1}, which only appears in the *a* and *b* spectra when these are obtained with convergent light (the dotted curves of Fig. 2) is derived from *c*. Its intensity in the thinnest samples suggests most strongly that we assign it as the *c* active fundamental, $\nu_3=1360$ cm^{-1}.

The absorption bands which we have ascribed to fundamentals are quite intense. The intensity ratios $I(\nu_3)/I(\nu_1)$ for other molecular groups of a structure similar to the nitrite ion (e.g., NO_2, O_3, H_2O, etc.) are always large. This would also be expected to be the case for the nitrite spectrum. Considering the strength of the ν_1 band it is, therefore, not surprising that, even for the thinnest (010) sections at our disposal, the ν_3 band showed complete absorption. The bands are notably sharp. The 831 band is particularly so. At room temperature it has a width at half-height of 8 cm^{-1}. At liquid nitrogen temperatures this is reduced to 6.5 cm^{-1}. For ν_1 the width changes from 15 cm^{-1} at room temperature to 10 cm^{-1} at liquid nitrogen temperature, for ν_3 the corresponding change is from 20 cm^{-1} to 15 cm^{-1}.

One can obtain some check on the validity of the proposed assignment of fundamentals by seeing how well it satisfies a valence force field. Employing the reported apex angle of 132° one finds that our frequencies satisfy such a field to about 5 percent in the sense of the consistency of the three determining equations.[8] This is about the order of agreement that one often finds for other bent symmetrical triatomic groups. The force constants calculated on this basis are $k_1=6.0\times10^5$ and $k_\delta/l^2=2.8\times10^5$ dynes/cm for the stretching and bending constants, respectively.

Using the more general force field of the form

$$2V=k_1(Q_1^2+Q_2^2)+2k_{12}Q_1Q_2+k_\delta\delta^2$$

one finds the following sets of force constants

$$k_1=7.5 \text{ or } 7.0\times10^5 \text{ dynes/cm},$$
$$k_{12}=1.5 \text{ or } 1.0\times10^5 \text{ dynes/cm},$$
$$k_\delta/l^2=1.8 \text{ or } 2.0\times10^5 \text{ dynes/cm}.$$

As a companion study we have also observed the spectrum of powdered crystalline KNO_2.§ We find that there are apparently three strong bands at 1290, 1250, and 805 cm^{-1}. On comparing these frequencies with those found for the sodium salt it would seem reasonable to make the following assignment: $\nu_1=1250$ cm^{-1}, $\nu_2=805$ cm^{-1}, $\nu_3=1290$ cm^{-1}. The decrease in the fre-

TABLE I. Frequencies (cm^{-1}) observed for $NaNO_2$.

a		*b*	*c*		Assignment
		831		s	ν_2
			970	w	
1130	=	1130		w	
			1170		$(NO_2^-)+$(Lattice)
1230	=	1230	to	ms	
			1300		
		1325		s	ν_1
			1360	vs	ν_3
			2120	w	$(\nu_2+\nu_3)$?
			2670	s	$\nu_1+\nu_3$

[8] G. Herzberg, *Infra-Red and Raman Spectra of Polyatomic Molecules* (D. Van Nostrand Company, Inc., New York, 1945), p. 169.

§ To avoid the complications resulting from the deliquescence of this substance, samples were cooled to dry ice temperature in vacuum.

quencies in going from $NaNO_2$ to KNO_2 varies from 3 to 6 percent. Qualitatively this shift is perhaps predictable, since the potassium salt possesses a more open lattice than does the sodium salt.[9] However, an elementary attempt to calculate the magnitude of the shift, using nearest neighbor interactions, met with no conspicuous success.

Combinations

Of the bands observed in the $NaNO_2$ spectra, other than those which we have assigned as fundamentals, there are only two, a weak band at 2120 cm^{-1} and a very intense band at 2670 cm^{-1} that can be assigned with reasonable assurance as combination bands arising from molecular modes. We have assigned these as $\nu_2+\nu_3$ and $\nu_1+\nu_3$, respectively. It is of interest that a strong $\nu_1+\nu_3$ band is often observed in the spectra of other bent XY_2 molecules.

A number of other bands are found throughout the spectrum. We have indicated that these are probably combinations of molecular modes and lattice modes. There is, however, no apparent regularity in their frequency pattern. The strongest of these bands are found in the 1300 cm^{-1} regions. The Raman spectrum of crystalline $NaNO_2$ was reported to have shown broad diffuse bands in this vicinity.[10]

It is notable that the bands which we have been discussing show good polarization effects. Particularly impressive is the fact that the $\nu_1+\nu_3$ band is active in the sense predicted by site group (factor group) selection rules. The general group theoretical approach to crystalline spectra allows for a complete relaxation of selection rules for combinations.[5] Our result may then perhaps be taken as evidence that the simpler site group (factor group) critique provides a more useful description of experimental facts in cases of this sort.

Use of Convergent Light

Before concluding we should like to mention an interesting effect that has been observed using the convergent light beam of the microilluminator. This effect is typified by the behavior of the 1360 cm^{-1}, ν_3 band.

It will be recalled that the *a* and *b* spectra were taken from a naturally grown (001) crystal plate. When used with the microilluminator, this was placed at the focus of the convergent light beam with its normal parallel to the axis of the beam. In this situation it is obvious that what we nominally term the *a* and *b* spectra will contain contributions from the *c* spectrum. Estimates based upon the geometry of the microilluminator suggest that the contribution of the *c* spectrum to the observed spectra would be of the order of 25 percent. Empirical evidence, based on the residual transmission in the 831 and 1325 bands in thick crystals suggest that this contribution is about 20 percent. Thus, we would expect that the 1360 cm^{-1} band should appear in the *a* and *b* spectra absorbing at most about 20–25 percent of the available light. In contrast to this stands the observed fact that this band absorbs 60 to 70 percent of the available light. That this arises solely through the use of convergent light is shown by the virtual absence of such absorption for spectra taken with the sample in parallel light. We do not, at present, fully understand this apparent enhancement in absorption. However, our observation at least points out a serious problem in the use of infrared microscopes for quantitative polarization work.

[9] G. E. Ziegler, Z. Krist. 94, 491 (1936).
[10] W. R. Angus and A. H. Lechie quoted in reference 1.

The Molecular Structure of MoF_6, WF_6, and UF_6 from Infrared and Raman Spectra*†

T. G. Burke, D. F. Smith, and A. H. Nielsen‡
K-25 Laboratories, Carbide and Carbon Chemicals Company, Oak Ridge, Tennessee
(Received November 16, 1951)

This paper is a report of the complete investigation and interpretation of the Raman and infrared spectra of MoF_6, WF_6, and UF_6. The Raman photographs of MoF_6 and WF_6 exhibit three intense lines in accord with earlier measurements on UF_6 in solution. The exploration of the infrared spectra of MoF_6 and WF_6 from 2–40μ yielded a great many bands for each molecule. Two of these were quite intense in each case and were identified as fundamentals while the remaining weaker ones were identified as overtones and combinations. The infrared spectrum of UF_6 was repeated from 2–17μ with substantially the same results as in the earlier work. Extension of this spectrum from 17–40μ was made and three new bands were discovered.

Because of the great similarity of the spectra of these three molecules, an interpretation of the bands was made along lines suggested by Bigeleisen, Mayer, Stevenson, and Turkevich for UF_6, that the molecule belongs to the point group O_h and has totally symmetric octahedral structure. It was possible to fit all but five very weak bands into an identification scheme based on this model. The success of this effort is taken to be conclusive evidence in favor of the O_h type symmetry.

INTRODUCTION

THE question as to whether the molecule UF_6 belongs to the totally symmetric point group O_h or has some lower symmetry has not, up to the present, been settled, although a number of different types of investigations have been made. It was, therefore, the purpose of this investigation to perform such additional infrared experiments on UF_6 as seemed necessary and to observe the infrared and Raman spectra of the analogous molecules MoF_6 and WF_6 in order to settle this point or at least to throw some new light on the problem.

The structure of the hexafluorides of molybdenum, tungsten, and uranium have been studied with electron diffraction techniques by Braune and Pinnow.[1] The model most consistent with their measurements was an octahedron in which the X–F distances lay along the rectangular axes and were in the ratio 1.00 to 1.12 to 1.22 for all three compounds. They did not, however, entirely exclude the regular octahedron in which the X–F distances were all equal.

More recently, Bauer[2] has studied the electron diffraction by UF_6. He found that, while his experimental results were to some extent in harmony with those of Braune and Pinnow, a more careful interpretation appeared to rule out the structure proposed by them, as well as the totally symmetric one. He proposed, instead, a model without a center of symmetry as the one which best fit his data.

Bauer, himself, pointed out two major difficulties with this model: the first was the inferred zero dipole moment from dielectric constant measurements of Smyth and Hannay.[3] They found the dipole moment to be less than 0.5 and probably less than 0.3 Debye unit. Bauer suggested that differences in bond characteristics could yield zero or at least small dipole moments. More precise measurements have recently been made by Magnuson[4] using a microwave refractometer. His measurements indicate that the dipole moment is less than his minimum detectable dipole moment of 0.15 Debye unit.

The second difficulty was in connection with the success of Bigeleisen, Mayer, Stevenson, and Turkevich[5] who interpreted the observed vibration spectrum of UF_6 on the basis of the totally symmetric model. The infrared data were obtained on the gas from 2–17μ and the Raman frequencies were obtained from solutions of UF_6 in C_7F_{16}, as well as from limited exposures on pure UF_6.

After the present Raman spectra of MoF_6 and WF_6 had been obtained, a recently published paper by Tanner and Duncan[6] was discovered in the literature in which they give substantially the same results for the Raman effect of these two molecules as are herein reported. As there were differences in technique which might be of sufficient interest to merit inclusion, comment will be made on the present Raman work later in the paper.

EXPERIMENTAL DETAILS

Sample Preparation and Handling

The samples of MoF_6, for which the infrared and Raman spectra were obtained, were prepared by W. L. Colvin by direct fluorination of molybdenum metal. The WF_6 was prepared by A. V. Faloon and W. B. Kenna by direct fluorination of tungsten. Mr. G. Oliver furnished

* This document is based on work performed for the AEC by Carbide and Carbon Chemicals Company at Oak Ridge, Tennessee.

† The data on MoF_6 were presented at the S. E. S. A. P. S. in Chattanooga (Phys. Rev. 83, 485(A) (1951)), and the material of this paper was presented at the Columbus Symposium, June, 1951.

‡ Department of Physics, University of Tennessee, Knoxville, Tennessee.

[1] H. Braune, and P. Pinnow, Z. physik. Chem. **B35**, 239 (1937).

[2] S. H. Bauer, J. Chem. Phys. **18**, 27 (1950); **18**, 994 (1950).

[3] C. P. Smyth and N. B. Hannay, Princeton University, October 1, 1944 (MDDC-441).

[4] D. W. Magnuson, J. Chem. Phys. (to be published).

[5] Bigeleisen, Mayer, Stevenson, and Turkevich, J. Chem. Phys. **16**, 442 (1948).

[6] K. N. Tanner and A. B. F. Duncan, J. Am. Chem. Soc. **73**, 1164 (1951).

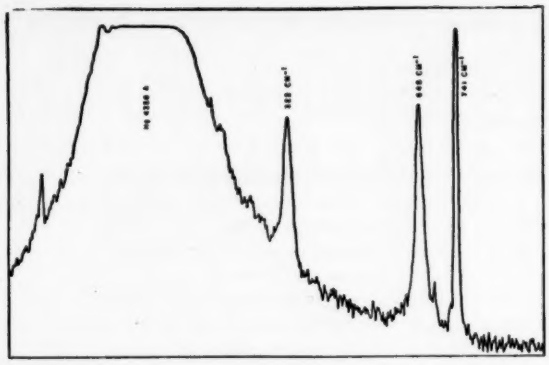

FIG. 1. Microphotometer trace of the Raman spectrum of MoF_6.

a number of samples of UF_6 of high purity for the infrared measurements on that gas. Further purification by a series of fractional distillations was carried out during the course of measurement of the spectra. The MoF_6 and WF_6 samples were nearly water-clear liquids with fairly large vapor pressures. Sample purification, preparation, and handling was carried out exclusively in copper, nickel, or fluorothene systems. The metal systems were carefully conditioned for fluorine compounds before the samples were admitted. Several flushings of the systems with the samples were then carried out in order to maintain sample purity throughout the investigation. In the case of the infrared spectra, repeated runs were made on successive fractions until the records showed no apparent changes in the observed bands from record to record. The crude distillations performed between records made possible the detection and elimination of several impurity bands. Several impurities were detected in this way though the impurity itself was never actually eliminated from the sample. Bands ascribed to impurities have been omitted from the records shown herein. The gases were never exposed to glass or silica, and no traces of SiF_4 were observed. Small amounts of HF were, however, never entirely eliminated.

Raman Spectra

The Raman spectra of MoF_6 and WF_6 were photographed on a Lane-Wells Raman spectrograph and source unit. The exciting lines were the mercury 4047A with no filter, and the mercury 4358A filtered by Rhodamine 5 GDN extra and paranitrotoluene. Satisfactory exposures were made with minimum line breadth in about 20 minutes. Raman tubes of fluorothene[7] were used for all three molecules. Such Raman tubes have the advantage that they prevent reaction between the sample and the vessel, but they have the disadvantage that they prevent the making of polarization measurements because of the innate inhomogeneity of the material. Purity of sample is preserved at the expense of polarization data.

[7] J. S. Kirby-Smith and E. A. Jones, J. Opt. Soc. Am. 39, 780 (1949).

Attempts were made to obtain Raman photographs of liquid UF_6 in the fluorothene Raman tubes. Because of the sublimation of UF_6 it was necessary to operate at elevated temperatures and pressures to keep it liquid. The fluorothene, which is thermoplastic, ruptured under these conditions and this phase of the investigation was abandoned.

Infrared Spectra

The infrared spectra of all three compounds were observed from 2 to about 40μ with Perkin-Elmer spectrographs models 12C and 21 equipped with NaCl, KBr, and KRS-5 prisms. The gases were contained in 10-cm fluorothene[7] cells closed with AgCl, KBr, or KRS-5 windows depending upon the region investigated. The windows were sealed to the cells with a low melting polymer of trifluoro-monochloroethylene. The cells were maintained at room temperature and the maximum pressure of the gas in the cells was the vapor pressure of the liquid for that temperature. Several records were made with gas in a modified Perkin-Elmer one-meter cell. No appreciable increase in information was obtained over the 10-cm cell.

Although the cell windows were attacked to some extent by these corrosive gases, and their transmission was impaired in certain spectral regions, it was generally possible to make observations over long enough periods to obtain the data without having to repolish the windows.

EXPERIMENTAL RESULTS

Raman Spectra

Microphotometer traces of the Raman photographs of MoF_6 and WF_6 are shown in Figs. 1 and 2, respectively. For each molecule three quite intense lines were observed. This is in agreement with the observations of Tanner and Duncan.[6] The Raman data for MoF_6, WF_6, and UF_6 obtained by the various investigators have been collected in Table I for comparison. It may be seen that the agreement between the present values and Tanner and Duncan's for MoF_6 and WF_6 is very good.

The polarization data of Tanner and Duncan[6] make it

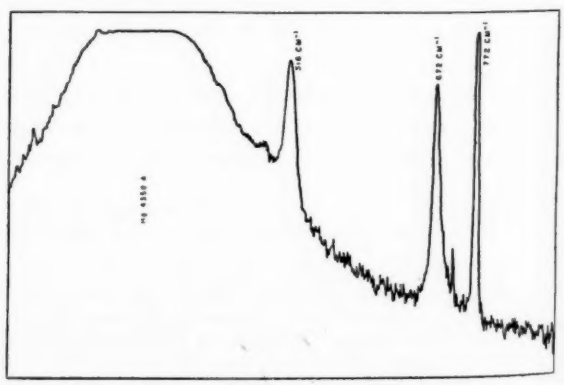

FIG. 2. Microphotometer trace of the Raman spectrum of WF_6.

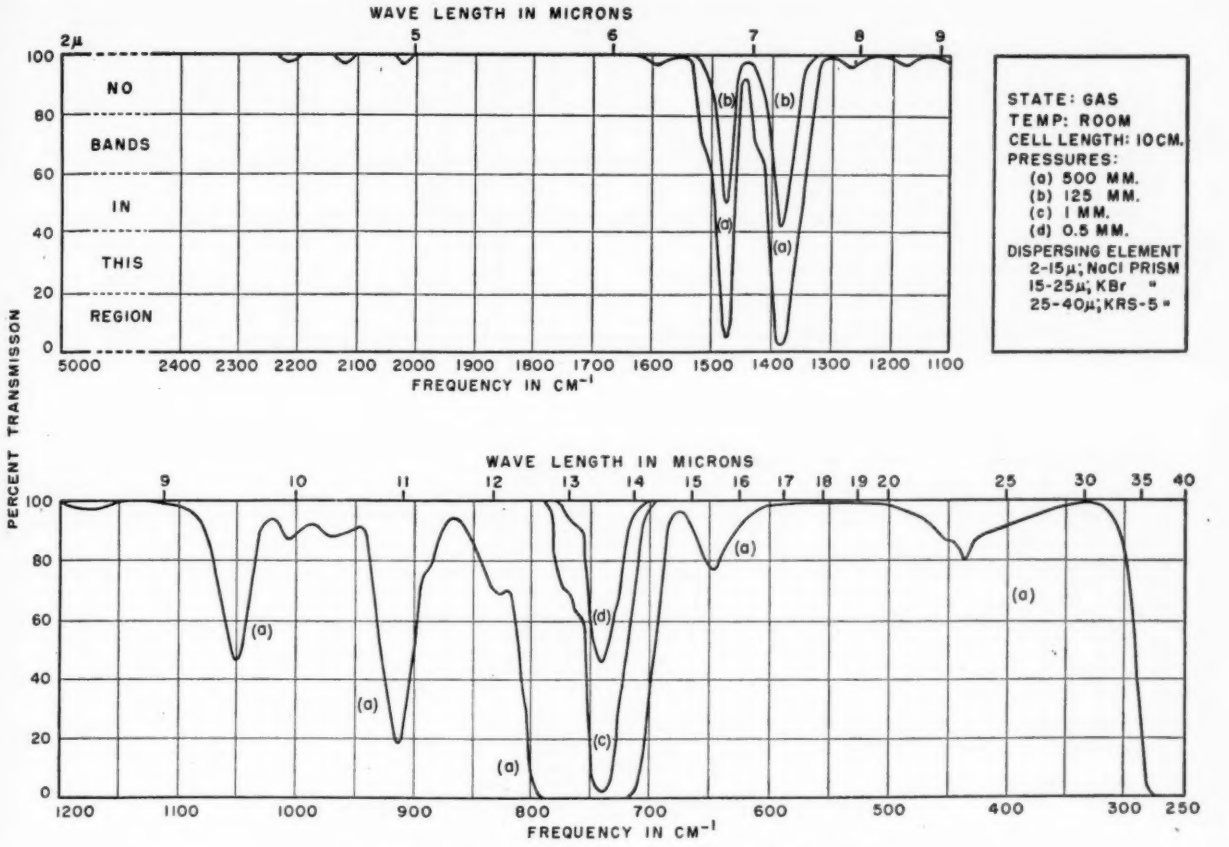

FIG. 3. The infrared prism spectrum of MoF_6 from 2–40μ.

reasonable to assign the intense lines 741 cm^{-1} and 772 cm^{-1} in MoF_6 and WF_6, respectively, to the totally symmetric mode ν_1. The mode ν_2 is probably of higher frequency than the deformation frequency ν_5, and thus ν_2 is probably best identified as 672 cm^{-1} and 645 cm^{-1}, while ν_5 is 316 cm^{-1} and 322 cm^{-1} for the two molecules, respectively.

Infrared Spectra

The infrared spectra of MoF_6, WF_6, and UF_6 are shown in Figs. 3, 4, and 5, respectively. No infrared information on the first two of these was to be found in the literature, and the data given here is thus completely new. The region from 17–38μ in UF_6 had not previously been explored and is new information. The repetition of the 2–17μ region in UF_6 confirms the work of Bigeleisen, Mayer, Stevenson, and Turkevich.[5]

TABLE I. Observed Raman lines (cm^{-1}) for MoF_6, WF_6, and UF_6.

		MoF_6	WF_6	UF_6
ν_1	Burke, Smith, Nielsen	741	772	...
	Tanner, Duncan[a]	736	769	...
	Bigeleisen, Mayer[b] Stevenson, Turkevich	...	...	656
ν_2	Burke, Smith, Nielsen	645	672	...
	Tanner, Duncan	641	670	...
	Bigeleisen, Mayer Stevenson, Turkevich	...	...	511
ν_5	Burke, Smith, Nielsen	322	316	...
	Tanner, Duncan	319	322	...
	Bigeleisen, Mayer Stevenson, Turkevich	...	...	200

[a] See reference 6.
[b] See reference 5.

MoF_6

In Fig. 3 is shown the complete infrared spectrum of MoF_6 plotted in percent transmission *versus* frequency in cm^{-1} for several different pressures of gas and recorded with NaCl, KBr, and KRS-5 prisms in the appropriate regions.

Twenty-two absorption bands were detected of which the two at 260 cm^{-1} and 741 cm^{-1} were very intense and were assumed to be fundamentals. The remainder were taken to be overtones and combination bands and, with the exception of four, have been identified in terms of permitted transitions in the totally symmetric octahedral model. The frequency assignment is discussed in a later section. No structure was discernible in any of the bands although an effort was made to discover structure with the best resolution afforded by the prisms. The complete list of frequencies and assignments for MoF_6 are given in Table VI.

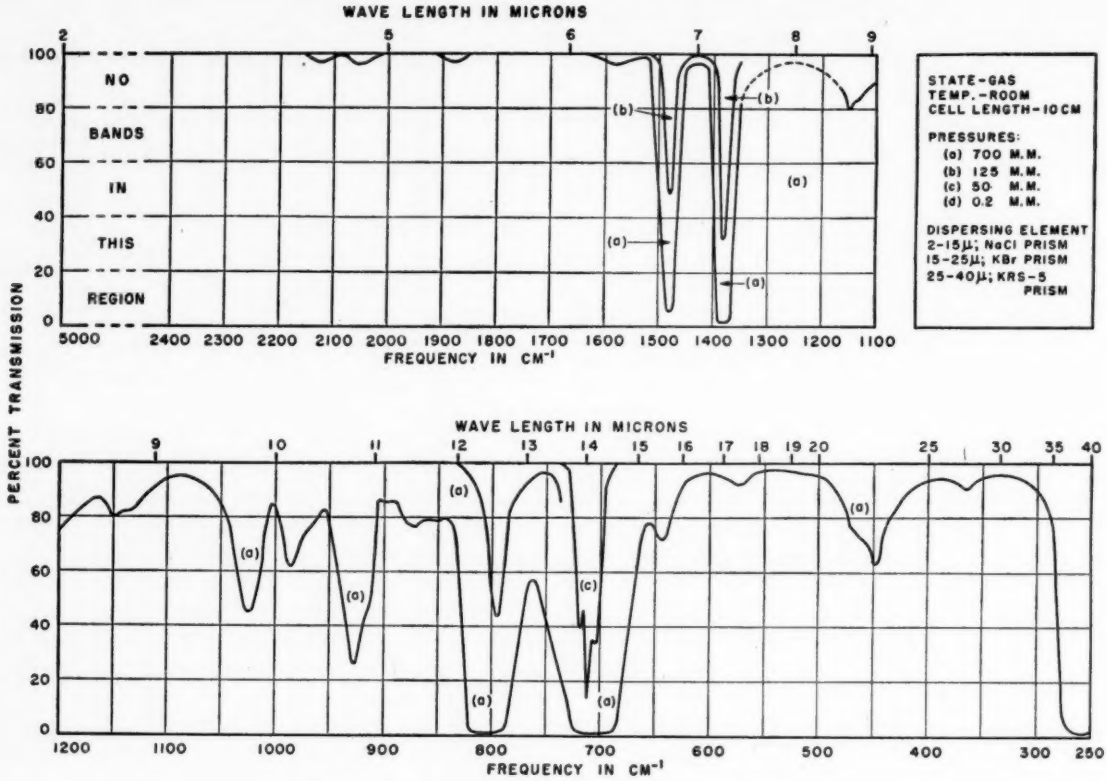

FIG. 4. The infrared prism spectrum of WF_6 from 2–40μ.

WF_6

The complete infrared spectrum of WF_6 is shown in Fig. 4 plotted in percent transmission *versus* frequency in cm^{-1} for various pressures, and recorded with the prisms available.

Nineteen absorption bands were detected of which the two at 258 cm^{-1} and 712 cm^{-1} were very intense and were assumed to be fundamentals. The remaining bands, with the exception of one, have been fitted into an identification scheme which is consistent with permitted transitions for the assumed model. In this case the band at 712 cm^{-1} appears to resolve into three maxima, the central line being sharp and intense. No other band, however, exhibited any structure. A complete list of the observed bands is given in Table VII.

UF_6

The infrared spectrum of UF_6 displayed in Fig. 5 is plotted in the same manner as is shown in Figs. 3 and 4. The very intense band at 623 cm^{-1} is very likely a fundamental corresponding to the two intense bands at 741 cm^{-1} and 712 cm^{-1} in MoF_6 and WF_6, respectively. This band, like the one in WF_6, shows indications of having three maxima. The low frequency fundamental in UF_6 which corresponds to the 260 cm^{-1} band in MoF_6 and to the 258 cm^{-1} band in WF_6 lay beyond the range of the spectrographs, but was predicted at 200 cm^{-1} by Bigeleisen *et al.* A band, reported by these authors at 675 cm^{-1}, showed doublet structure under the present higher resolution. The maxima occur at 671 cm^{-1} and 677 cm^{-1}, respectively. Though these maxima are only 6 cm^{-1} apart and it is believed that this is a single band, it is conceivable that two bands overlap here to make this region as intense as it is. The remainder of the bands were ascribed to overtones and combinations and are listed in Table VIII.

The region 2–17μ reported by Bigeleisen and coworkers was repeated for confirmation and was found to be virtually identical with their measurements. Three new bands at 279 cm^{-1}, 350 cm^{-1}, and 392 cm^{-1} were discovered between 17–40μ in the extended region.

Discussion and Band Assignment

The great similarity of these spectra is immediately apparent from a comparison of Figs. 1–5 inclusive. Each

TABLE II. Observed frequency, symmetry, activity, and assignments of fundamentals in MoF_6, WF_6, and UF_6.

Assignment	Symmetry	Activity	MoF_6	WF_6	UF_6
ν_1	A_{1g}	R	741 cm^{-1}	772 cm^{-1}	656 cm^{-1}
ν_2	E_g	R	645	672	511
ν_3	F_{1u}	IR	741	712	640[a]
ν_4	F_{1u}	IR	260	258	200 (calc)
ν_5	F_{2g}	R	322	316	200
ν_6	F_{2u}	Inactive	234 (calc)	215 (calc)	130 (calc)

[a] Unperturbed value of ν_3 which is in resonance with $\nu_1+\nu_6$.

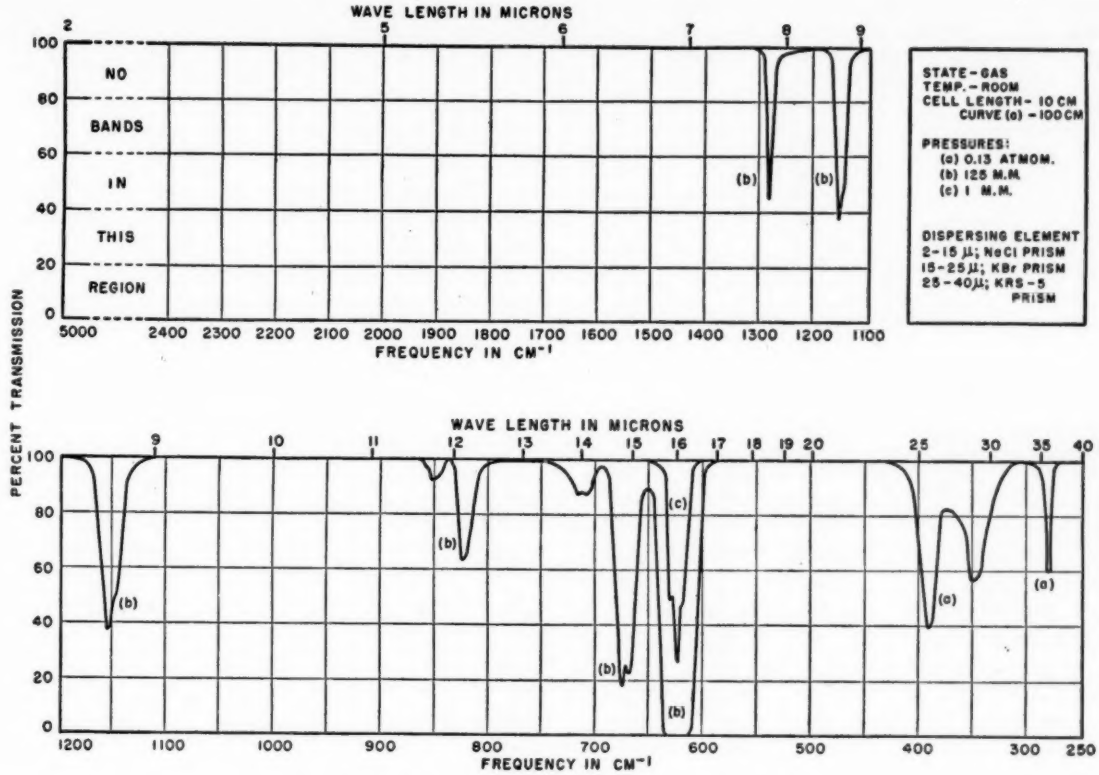

FIG. 5. The infrared prism spectrum of UF_6 from 2–40μ.

spectrum is characterized by three intense Raman lines and two§ intense infrared absorption bands.

A seven-atom totally symmetric molecule with octahedral structure belongs to the point group O_h and has six normal frequencies, ν_1 (singly degenerate), ν_2 (doubly degenerate), and ν_3, ν_4, ν_5, and ν_6 (triply degenerate). Of these, ν_1, ν_2, and ν_5 are Raman-active, ν_3 and ν_4 are infrared-active, and ν_6 is inactive in both Raman and infrared. The observed spectra of the fundamentals of MoF_6, WF_6, and UF_6, therefore, satisfy the predicted spectrum of a molecule with this type of symmetry. The normal modes of vibration and their symmetry classes have been discussed in some detail by Herzberg.[8] The further test which the model must stand is whether or not the remaining observed bands in the infrared can be accounted for in terms of combinations permitted by the symmetry rules applicable to this model. Such an investigation follows for all the observed bands of the three molecules.

TABLE III. Binary summation bands permitted by symmetry rules.

Binary combination	Symmetry
$\nu_1+\nu_3$	F_{1u}
$\nu_1+\nu_4$	F_{1u}
$\nu_2+\nu_3$	$F_{1u}+F_{2u}$
$\nu_2+\nu_4$	$F_{1u}+F_{2u}$
$\nu_2+\nu_6$	$F_{1u}+F_{2u}$
$\nu_3+\nu_5$	$A_{2u}+E_u+F_{1u}+F_{2u}$
$\nu_4+\nu_5$	$A_{2u}+E_u+F_{1u}+F_{2u}$
$\nu_5+\nu_6$	$A_{1u}+E_u+F_{1u}+F_{2u}$

The fundamental frequencies in MoF_6 and WF_6 have been assigned in accord with the frequency assignment made by Bigeleisen *et al.*[5],‖ for UF_6. These frequencies are collected in Table II together with the symmetry species and activity of the vibration mode.

Only vibrations of symmetry species F_{1u} are active in the infrared spectrum of a regular octahedral XY_6 molecule. To make assignments of the remaining observed bands it was necessary to investigate the activity of overtones, binary, and ternary combination bands. Tables 29, 31, 32, and 33 given by Herzberg[9] were consulted for the rules which apply in forming combinations. It may easily be seen that all of the first overtones are forbidden. Of the fifteen possible combinations of the fundamentals into binary summation bands only the eight given in Table III are permitted, i.e., contain an F_{1u} component. Binary difference bands are permitted in all cases where the summation bands are permitted. Difference bands would, however, be likely involving only the low frequencies ν_4, ν_5, and ν_6 as for example

§ The low frequency infrared band ν_4 of UF_6 lies beyond instrument range.

[8] G. Herzberg, *Infrared and Raman Spectra* (D. Van Nostrand Company, Inc., New York, 1945), p. 122.

‖ The present numbering of the frequencies follows Herzberg (see reference 8). Thus, in the present notation ν_1 and ν_2 are the same as given by Bigeleisen *et al.*, but ν_3, ν_4, ν_5, and ν_6 are the same as their ν_6, ν_5, ν_3, ν_4, respectively.

[9] See reference 8, pp. 123, 126, 127, and 129.

TABLE IV. Binary combination bands.

Assignment	MoF_6 Obs freq.	MoF_6 Calc freq.	Summation WF_6 Obs freq.	WF_6 Calc freq.	UF_6 Obs freq.	UF_6 Calc freq.
$\nu_1+\nu_3$	1480 cm^{-1}	1482 cm^{-1}	1481 cm^{-1}	1484 cm^{-1}	1288 cm^{-1}	1296 cm^{-1}
$\nu_1+\nu_4$	1002	1001	1025[a]	1030	850	856
$\nu_2+\nu_3$	1385	1386	1383	1384	1159[a]	1151
$\nu_2+\nu_4$	913	905	928	930	715[a]	711
$\nu_2+\nu_6$	882	879	871	887	674[b]	641
$\nu_3+\nu_5$	1052	1062	1025[a]	1028	825	840
$\nu_4+\nu_5$	...	582	573	574	392[a]	400
$\nu_5+\nu_6$	...	556	...	531	350	330
			Difference			
$\nu_2-\nu_4$	...	385	...	414	...	311
$\nu_2-\nu_6$	435[a]	411	448	457	392[a]	381
$\nu_3-\nu_5$	435[a]	419	...	396	...	440

[a] Indicates possible alternative assignments for this frequency (see Table V).
[b] Perturbed value caused by resonance with ν_3.

TABLE V. Ternary combination bands.

Assignment	Symmetry	MoF_6 Obs freq. cm^{-1}	MoF_6 Calc freq. cm^{-1}	WF_6 Obs freq. cm^{-1}	WF_6 Calc freq. cm^{-1}	UF_6 Obs freq. cm^{-1}	UF_6 Calc freq. cm^{-1}
$3\nu_3$	$A_{2u}+2F_{1u}+F_{2u}$	2215	2223	2130	2136	[b]	1920
$2\nu_1+\nu_2$	F_{1u}	2125	2127	...	2216	[b]	1512
$2\nu_2+\nu_3$	$2F_{1u}+F_{2u}$	2030	2031	2050	2056	[b]	1662
$2\nu_3+\nu_4$	$A_{1u}+E_u+3F_{1u}+2F_{2u}$	1740	1742	...	1682	[b]	1480
$\nu_3+2\nu_4$	$2F_{1u}+F_{2u}$	1265[a]	1261	...	1228	[b]	1040
$3\nu_4$	$2F_{1u}+F_{2u}$	770	780	796	774	[b]	600
$\nu_1+\nu_5-\nu_6$	$A_{1u}+E_u+F_{1u}+F_{2u}$	833	829	855	873	715[a]	726
$2\nu_4-\nu_6$	$A_{1u}+E_u+2F_{1u}+3F_{2u}$	...	286	...	301	279	270
$2\nu_5-\nu_4$	$A_{1u}+E_u+3F_{1u}+2F_{2u}$	...	384	367	374	...	200
$2\nu_1-\nu_6$	$F_{1u}+2F_{2u}$	1265[a]	1248	...	1329	1159[a]	1182
$\nu_1+\nu_5+\nu_6$	$A_{1u}+E_u+F_{1u}+F_{2u}$	...	1297	1316	1303	[b]	986
$2\nu_2+\nu_6$	$F_{1u}+2F_{2u}$	1585	1524	1580	1559	1159[a]	1152
$2\nu_2-\nu_6$	$F_{1u}+2F_{2u}$	...	1056	1148	1129	...	892
$2\nu_4+\nu_6$	$A_{1u}+E_u+2F_{1u}+3F_{2u}$	764	754	...	731	...	530

[a] Indicates possible alternative assignments (see Table IV).
[b] Unobserved with 0.14 meter equivalent path length at S. T. P.

$\nu_2-\nu_4$, $\nu_3-\nu_5$, etc. A great many of the difference bands would lie beyond the limits of observation of most infrared spectrometers. After the assignment of the binary bands the remaining bands were ascribed to ternary combinations of which there are a great many having an F_{1u} component. The interpretations of the infrared spectra of the three molecules have been listed in Tables II, IV, and V. Table II gives the fundamentals, Table IV the binary combinations and Table V, the ternary bands and any others of higher order.

In connection with their work on sulfur hexafluoride, Yost, Steffens, and Gross[10] developed the expression, $\nu_1^2=\nu_2^2+\frac{3}{2}\nu_5^2$, which relates the three Raman-active frequencies. They also quote an expression $\nu_5^2/\nu_6^2=2$, which they attribute to Dr. E. B. Wilson, from which the inactive frequency may be computed. When the first of these two expressions is applied to the fundamentals of MoF_6 and WF_6 good agreement is achieved, but for UF_6 the calculated value of $\nu_1=565$ cm^{-1} agrees poorly with the observed $\nu_1=656$ cm^{-1}. The second relation applied to the three molecules gives about the same agreement for all three. The relation was used only to give the order of magnitude of ν_6, and values were chosen in this vicinity which gave the best agreement among the binary combinations. In any case the difference between the computed value and the value used is no more than 8 percent. This is probably within the accuracy of the relation. Bigeleisen *et al.* chose the value 130 cm^{-1} for ν_6 in UF_6 because when combined with ν_2 to form $\nu_2+\nu_6$ this frequency was accidentally degenerate with ν_3. It was with this device that they explained the positions of the bands at 623 cm^{-1} and at 674 cm^{-1}. It was not possible to pick more satisfactory frequency values for the fundamentals in UF_6 than those suggested by Bigeleisen *et al.* They are, therefore, the values used in Tables II, IV, V, and VIII.

Four very weak infrared bands in the spectrum of MoF_6 remain unassigned. Their frequencies are 455 cm^{-1}, 648 cm^{-1}, 970 cm^{-1}, and 1175 cm^{-1}. They are assumed to belong to the MoF_6 system because it was not possible to show experimentally that they were impurities. It is perhaps likely that they are combina-

[10] Yost, Steffens, and Gross, J. Chem. Phys. **2**, 311 (1934).

tion bands of higher order than ternary. Several coincidences are worth pointing out: the bands at 455 cm^{-1} and 648 cm^{-1} agree closely with the calculated positions of the forbidden $2\nu_6$ and $2\nu_5$ respectively, and the band at 970 cm^{-1} falls within 5 cm^{-1} of the calculated position of the forbidden binary $\nu_1+\nu_6$. Another interesting coincidence is the degeneracy of ν_1 observed in Raman effect and ν_3 observed in the infrared. Both have the frequency 741 cm^{-1}. These are the strongest lines in the spectra. Eighteen of the twenty-two observed bands can easily be accounted for by assuming the totally symmetric model.

In WF_6 only the weak band at 985 cm^{-1} cannot be satisfactorily explained. This band agrees closely with either of the forbidden binaries $\nu_1+\nu_6$ at 987 cm^{-1} or $\nu_2+\nu_5$ at 988 cm^{-1}. A more likely assignment would probably be that it is a higher order combination band. Six of the eight permitted binaries were observed while none of the forbidden overtones were observed.

No bands were left unexplained in UF_6. It was pointed out by Bigeleisen *et al.*[5] that there appeared to be a resonance interaction between ν_3 and $\nu_2+\nu_6$ in UF_6. This was a likely explanation of the facts that $\nu_2+\nu_6$ calculated at 641 cm^{-1} actually occurred at 674 cm^{-1} and was much too intense compared with other binaries (Fig. 5) and that from other combination bands the value of ν_3 appeared to be nearer 640 cm^{-1} than 623 cm^{-1} where it was observed. Such an explanation is further substantiated by the fact that no such resonance occurs in MoF_6 and WF_6, and the binary bands are considerably weaker than $\nu_2+\nu_6$ in UF_6.

Because of the weakness of the few unexplained bands the inconsistencies noted above are considered negligible objections to the totally symmetric octahedral model for MoF_6, WF_6, and UF_6. It is concluded that the generally successful assignment of these observed bands provides overwhelming evidence in favor of the O_h point group symmetry.

The frequencies for each molecule have been collected into separate Tables VI, VII, and VIII for convenience of reference.

TABLE VI. Frequencies and assignments of observed bands in MoF_6.

Obs freq. (cm^{-1})	Calc freq. (cm^{-1})	Assignment	Intensity
Inactive	234	ν_6	
260 *IR*	···	ν_4	m
322 *R*	···	ν_5	
435 *IR*	419 or 411	$\nu_3-\nu_5$ or $\nu_2-\nu_6$	vw
455 *IR*	(468?)	$(2\nu_6?)$[a]	vw
645 *R*	···	ν_2	
648 *IR*	(644?)	$(2\nu_5?)$[a]	w
741 *R*	···	ν_1	
741 *IR*	···	ν_3	vs
764 *IR*	754	$2\nu_4+\nu_6$	m
777 *IR*	780	$3\nu_4$	m
833 *IR*	829	$\nu_1+\nu_5-\nu_6$	vw
882 *IR*	879	$\nu_2+\nu_6$	vw
913 *IR*	905	$\nu_2+\nu_4$	w
970 *IR*	(975?)	$(\nu_1+\nu_6?)$[a]	vw
1002 *IR*	1001	$\nu_1+\nu_4$	vw
1052 *IR*	1062	$\nu_3+\nu_5$	w
1175 *IR*	···	?	vw
1265 *IR*	1261 or 1248	$2\nu_4+\nu_3$ or $2\nu_1-\nu_6$	vw
1385 *IR*	1368	$\nu_2+\nu_3$	m
1480 *IR*	1482	$\nu_1+\nu_3$	m
1585 *IR*	1524	$(2\nu_2+\nu_6?)$	vw
1740 *IR*	1742	$2\nu_3+\nu_4$	vw
2030 *IR*	2031	$2\nu_2+\nu_3$	vw
2125 *IR*	2127	$2\nu_1+\nu_2$	vw
2215 *IR*	2223	$3\nu_3$	vw

[a] Forbidden transitions.

TABLE VII. Frequencies and assignments of observed bands in WF_6.

Observed frequency (cm^{-1})	Calculated frequency (cm^{-1})	Assignment	Intensity
Inactive	215	ν_6	
258 *IR*	···	ν_4	s
316 *R*	···	ν_5	
367 *IR*	374	$2\nu_5-\nu_4$	w
448 *IR*	457	$\nu_3-\nu_6$	w
573 *IR*	574	$\nu_4+\nu_5$	vw
672 *R*	···	ν_2	
712 *IR*	···	ν_3	vs
772 *R*	···	ν_1	
796 *IR*	774	$3\nu_4$	w
855 *IR*	873	$\nu_1+\nu_5-\nu_6$	vw
871 *IR*	887	$\nu_3+\nu_6$	vw
928 *IR*	930	$\nu_2+\nu_4$	m
985 *IR*	988? 987?	$\nu_2+\nu_5?$ $\nu_1+\nu_6?$ [a]	w
1025 *IR*	1030	$\nu_1+\nu_4$	w
1148 *IR*	1129	$2\nu_2-\nu_6$	vw
1316 *IR*	1303	$\nu_1+\nu_5+\nu_6$	vw
1383 *IR*	1384	$\nu_2+\nu_3$	m
1481 *IR*	1484	$\nu_1+\nu_3$	m
1580 *IR*	1559	$2\nu_2+\nu_6$	vw
1880 *IR*	1875	$2\nu_2+\nu_5+\nu_6$	vw
2050 *IR*	2056	$2\nu_2+\nu_3$	vw
2130 *IR*	2136	$3\nu_3$	vw

[a] Forbidden transitions.

TABLE VIII. Frequencies and assignments of observed bands in UF_6.

Observed frequency (cm^{-1})	Calculated frequency (cm^{-1})	Assignment	Intensity
Inactive	130	ν_6	
IR act. (unobs.)	200	ν_4	
200 *R*	···	ν_5	
279 *IR*	270	$2\nu_4-\nu_6$	w
350 *IR*	330	$\nu_4+\nu_6$	w
392 *IR*	400	$\nu_4+\nu_5$	w
511 *R*	···	ν_2	
623[a] *IR*	···	ν_3	vs
656 *R*	···	ν_1	
674[a] *IR*	641	$\nu_2+\nu_6$	s
715 *IR*	711	$\nu_2+\nu_4$	w
825 *IR*	840	$\nu_3+\nu_5$	m
850 *IR*	856	$\nu_1+\nu_4$	w
1159 *IR*	1151	$\nu_2+\nu_3$	m
1288 *IR*	1296	$\nu_1+\nu_3$	m

[a] Perturbed value of ν_3 (after B. M. S. T., see reference 5) = 640 cm^{-1}. Perturbed value of $\nu_2+\nu_6$ (after B. M. S. T., see reference 5) = 641 cm^{-1}.

While the investigation reported herein on the infrared and Raman spectra of MoF_6, WF_6, and UF_6 was being prepared for publication it was learned that Dr. R. C. Lord and co-workers of M. I. T. were carrying on concurrent and independent infrared measurements on MoF_6 and WF_6. The two efforts have been compared and both groups of authors come to essentially the same conclusions. The results of the other work will be submitted for publication elsewhere.

ACKNOWLEDGMENT

The authors are indebted to A. V. Faloon, W. B. Kenna, W. L. Colvin, and G. D. Oliver for the samples of MoF_6, WF_6, and UF_6 used in this investigation.

THE JOURNAL OF CHEMICAL PHYSICS VOLUME 20, NUMBER 3 MARCH, 1952

Substituted Methanes. VIII.* Vibrational Spectra, Potential Constants, and Calculated Thermodynamic Properties for Dibromodichloromethane†

ABRAM DAVIS,‡ FORREST F. CLEVELAND, AND ARNOLD G. MEISTER
Spectroscopy Laboratory, Department of Physics, Illinois Institute of Technology, Chicago 16, Illinois

(Received December 12, 1951)

Raman displacements, semiquantitative relative intensities, and quantitative depolarization factors for the liquid, and infrared absorption wave numbers and percent transmission curves for both the liquid and the gas, have been obtained for CBr_2Cl_2. The present and previous data were critically examined and probable values of the wave numbers corresponding to the fundamental vibrational frequencies were determined. Assignments were made for all observed Raman and infrared bands. As a check on the assignments, a normal coordinate treatment was undertaken, using a potential function containing all possible quadratic interaction constants. A reasonable set of potential constants was obtained. The observed fundamentals then were used to calculate to a rigid rotator, harmonic oscillator approximation the heat content, free energy, entropy, and heat capacity for 12 temperatures from 100° to 1000°K, for the ideal gaseous state at 1-atmos pressure.

RAMAN displacements for liquid CBr_2Cl_2 have been obtained in 2 investigations,[1,2] but in only one of these[2] were depolarization factors and estimated relative intensities determined. Infrared bands have been reported only for the liquid: Lecomte, Volkringer, and Tchakirian[1,3] give results for the region 500 to 1500 cm^{-1}, while Plyler[4] reports 4 bands between 350 and 450 cm^{-1}. The disagreement between the results of the different investigations is in many cases far larger than would be expected from experimental errors.

A normal coordinate treatment, using a Urey-Bradley potential function, was carried out by Simanouti.[5] His calculated fundamentals agree better with the observed values of Delwaulle and Francois[2] than with those of Lecomte, Volkringer, and Tchakirian.[1,3]

Glockler and Edgell[6] have calculated the heat capacity at constant pressure for 12 temperatures between 250° and 600°K, but their calculations were based upon frequencies which now seem questionable. No other observed or calculated values were found in the literature.

The present investigation was undertaken in an attempt to remove the uncertainties that exist in the previous Raman and infrared spectral data for the liquid; to obtain infrared data for the gas; to carry out a normal coordinate treatment with a more complete potential function; to establish probable values for the fundamental vibrational frequencies; and to calculate more reliable values for the heat capacity as well as values for the heat content, free energy, and entropy.

EXPERIMENTAL DETAILS

Purification of the Sample

The sample of CBr_2Cl_2 was obtained from the Eastman Kodak Company, Rochester, New York, and was further purified as follows: a distilling flask with a side arm leading to a collecting tube was filled, pumped briefly without cooling to remove dissolved air, surrounded by dry ice while the pumping continued, and finally, when thoroughly cold, was sealed off. The bulb containing the impure liquid was now placed in a beaker

* For previous papers of this series, see J. Chem. Phys. **18**, 346, 1073, 1076, 1081 (1950); **19**, 119, 784, 1561 (1951).

† Supported in part by Office of Ordnance Research Contract DA-11-022-ORD-464.

‡ Based upon an investigation carried out in partial fulfillment of the requirements for the degree of Master of Science. Present address: Hooker Electrochemical Company, Niagara Falls, New York.

[1] J. Lecomte, H. Volkringer, and A. Tchakirian, Compt. rend. **204**, 1927 (1937).

[2] M. L. Delwaulle and F. Francois, Compt. rend. **214**, 226 (1942).

[3] Volkringer, Lecomte, and Tchakirian, J. phys. et radium **9**, 105 (1938).

[4] E. K. Plyler, J. Chem. Phys. **17**, 218 (1949). *Note added in proof.*—A recent paper by E. K. Plyler and W. S. Benedict, J. Research Natl. Bur. Standards **47**, 202 (1951) gives infrared spectral data and some potential constant calculations, with an approximate potential function, for CBr_2Cl_2 as well as 17 other halogen-substituted methanes.

[5] T. Simanouti, J. Chem. Phys. **17**, 245 (1949).

[6] G. Glockler and W. F. Edgell, Ind. Eng. Chem. **34**, 532 (1942).

TABLE I. Raman and infrared spectral data for dibromodichloromethane (CBr_2Cl_2).[a]

Raman										Infrared						Theoretical Assignment		
		$\Delta\nu_l$				I	ρ		PS		ν_t	I_l		ν_g	I_g			
PR	LVT	DF	N	PV	AD	PR	DF	PR		LVT	Pl	PR	PR	PR	PR	ν_c		Type
154	141	154	2	**154**	0.0	36	0.65	0.51	P							**154**	ν_4	A_1
175	164	174	2	**175**	0.5	18	0.65	0.82	D							**175**	ν_5	A_2
229		230	2	**230**	0.5	21	7/8	0.73[b]	D							**230**	ν_7	B_1
	230																	
242		241	2	**242**	0.5	64	0.24	0.45	P							**241**	ν_3	A_1
262	252	262	2	**262**	0.0	12	7/8	0.84	D							**262**	ν_9	B_2
313	318		1	313		1										*308*	$2\nu_4$	A_1
											351					*350*	$2\nu_5$	A_1
380	370	380	2	**380**	0.0	100	0.05	0.00	P		375					**381**	ν_2	A_1
											397					*396*	$\nu_3+\nu_4$	A_1
											442					*442*	$\nu_6-\nu_8$	B_1
610			1	610		1						607	*m*	607	*vw*	*610*	$\nu_2+\nu_7$	B_1
684	672	683	2	**684**	0.5	24	D	0.84	D	680		681	*s*	698	*m*	**684**	ν_6	B_1
734	720	733	2	**734**	0.5	13	P	0.64	P	727		731	*s*	746	*s*	**735**	ν_1	A_1
771	759	769	2	**770**	1.0	3	D	0.86	D	764		770	*s*	781	*m*	**770**	ν_8	B_2
												857	*w*			*859*	$\nu_5+\nu_6$	B_2
												883	*w*			*888*	$\nu_1+\nu_4$	A_1
												925	*w*			*926*	$\nu_3+\nu_6$	B_1
												1072	*w*			*1064*	$\nu_2+\nu_6$	B_1
												1118	*vw*			*1114*	$\nu_1+\nu_3$	A_1
												1146	*w*			*1150*	$\nu_2+\nu_8$	B_2
1364			1	1364		*w*										*1368*	$2\nu_8$	A_1
1380			1	1380		*w*						1382	*vw*			*1376*	$\nu_1+\nu_2+\nu_9$	B_2
1464			1	1464		*vw*										*1468*	$2\nu_1$	A_1
												1485	*m*			*1504*	$\nu_1+\nu_8$	B_2

[a] $\Delta\nu_l$ = Raman displacement for the liquid in cm^{-1}; I = relative intensity; ρ = depolarization factor; PS = the deduced polarization state (P = polarized, D = depolarized); ν_l and ν_g = wave numbers in cm^{-1} for the liquid and gas, respectively; I_l and I_g = the corresponding intensities (*s* = strong, *m* = medium, *w* = weak, *v* = very); ν_c = calculated wave number in cm^{-1}; PR = present results; LVT = Lecomte, Volkringer, and Tchakirian, references 1 and 3; DF = Delwaulle and Francois, reference 2; Pl = Plyler, reference 4; N = number of apparently reliable, independent determinations; PV = probable values (mean of the N values); and AD = average deviation from the mean value.

[b] This value is less reliable than the others because of the overlapping by the strong, polarized 242 line.

of water and slowly warmed and the collecting tube was cooled with dry ice. When $\frac{1}{3}$ of the liquid had distilled into the collecting tube, the bulb containing the remaining $\frac{2}{3}$ also was surrounded with dry ice, and warm water was poured over the connecting glass tube to remove all of the sample from it so there would be no decomposition when the sample tube was sealed off. The sample tube was then sealed off at the greatest possible distance from the sample. This first $\frac{1}{3}$ was discarded since it might have contained low boiling impurities.

The remaining $\frac{2}{3}$ was transferred with a capillary tube "medicine dropper" and a capillary tube funnel to a 2nd distilling flask with 2 attached sample tubes, one for the infrared sample, the other for the Raman sample. The Raman tube is sealed beforehand to the Raman sample container. The system was evacuated and sealed, and the liquid was distilled into the sample tubes (as before) until only $\frac{1}{3}$ of the original material remained in the bulb of the distilling flask. The connecting tubes were heated with warm water and sealed off, as before. Any high boiling impurity in the original material may be expected to have remained behind in the final $\frac{1}{3}$. Finally, the Raman tube was filled by cooling the back end (away from the window) and warming the sample container so that the sample distilled slowly over into the Raman tube.

By this procedure, the sample is kept at the lowest possible temperature and is kept out of contact with air, which minimizes decomposition and formation of new compounds. The samples prepared in this way gave exceedingly low continuous background in the Raman spectrum and showed no evidence of impurities.

Spectroscopic Technique

The Raman displacement spectrograms were obtained by the use of a 2-prism spectrograph, constructed in this laboratory, having a dispersion of 162 cm^{-1}/mm (33A/mm) at 4500A. The depolarization spectrograms were obtained by the use of a Hilger E-518 spectrograph having a dispersion of 307 cm^{-1}/mm (63A/mm) at 4500A. Eastman 103-J plates were used and the exciting line was Hg4358A. The relative intensities[7] and depolarization factors[8] were determined by previously described methods. In order to check the depolarization factors for closely spaced lines, use was made of a Leeds and Northrup microphotometer. The results agreed very well with the depolarization factors determined by the use of the Gaertner microdensitometer.

The infrared records were obtained at room temperature with a Beckman IR-2 (KBr optics) spectrophotometer. Records of the atmospheric absorption were taken immediately preceding the record of the sample in order to eliminate spurious bands.

[7] F. F. Cleveland, J. Chem. Phys. **11**, 1 (1943).
[8] F. F. Cleveland, J. Chem. Phys. **13**, 101 (1945).

RESULTS

The Raman spectral data are summarized in Table I. In determining the probable values for the displacements, only the values of Delwaulle and Francois[2] were taken since the values of Lecomte, Volkringer, and Tchakirian differ from their values and the present results in many instances by more than 10 cm^{-1}, far beyond the normal experimental error. The present depolarization factors are in qualitative agreement with those of Delwaulle and Francois. The present results, however, remove the uncertainty as to which of the 2 lines at 154 and 175 cm^{-1} is polarized; establish quantitative values for the lines at 230, 262, 684, 734, and 770 cm^{-1}; and seem to remove all doubt as to the polarization state of the lines. Depolarization factors were obtained for all the fundamentals, but, because decomposition of the sample prevented long exposures, values could not be obtained for the observed overtones and combinations.

The infrared spectral data also are summarized in Table I, and the percent transmission curves are shown in Fig. 1. Bands observed at 5900, 5680, and 5400 cm^{-1} for the liquid were not included because of the low dispersion and resolution of the prism in this region. As for the Raman data, the observed values do not agree very well with those of Lecomte, Volkringer, and Tchakirian.[1,3] This suggests the possibility that their sample may have been impure, or that some other source of error existed in their work. In view of these discrepancies for the fundamentals, the values observed by them for the combinations and overtones are not included in Table I.

SYMMETRY, SELECTION RULES, AND ASSIGNMENTS

The CBr_2Cl_2 molecule has the symmetry of the C_{2v} point group and has 9 normal vibrations: 4 type A_1; 1 type A_2; 2 type B_1; and 2 type B_2. According to the selection rules, all fundamentals, overtones, and combinations are allowed in the Raman spectrum, while all fundamentals (except A_2), all overtones (except A_2^n, n odd), and all combinations (except $A_1 \times A_2$ and $B_1 \times B_2$) are allowed in the infrared. In the Raman spectrum, the A_1 vibrations correspond to polarized lines, the others to depolarized lines; in the infrared, the A_1 vibrations correspond to parallel bands, and the B_1 and B_2 vibrations to perpendicular bands.

The assignments shown in Table I were made after consideration of the selection rules and the observed depolarization factors. Only binary combinations and 1st overtones were used, except for the 1380 cm^{-1} band, which had to be assigned as a ternary combination.

In Table II are given the probable values for the fundamentals of CBr_2Cl_2. These were determined by critical examination of both the present and previous spectral data, given in Table I.

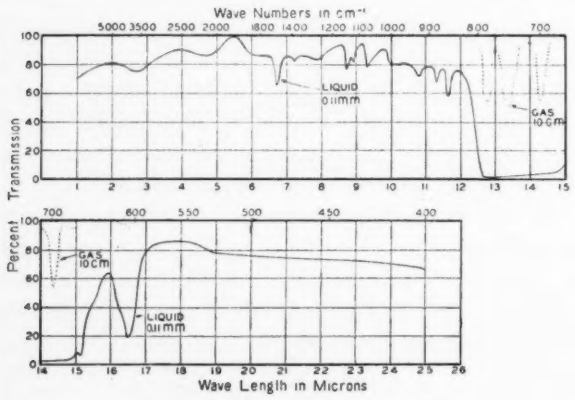

FIG. 1. Infrared bands for CBr_2Cl_2.

NORMAL COORDINATE TREATMENT

As a check on the assignments, as well as to obtain reliable values of the potential (force) constants, a normal coordinate treatment (Wilson **FG** matrix method[9]) was carried out, using the most general quadratic potential function.

For simplicity in comparing the potential energy constants for different molecules, and in order to be able to recognize instantly upon sight the nature of the potential constant, the following descriptive notation will be adopted in this and subsequent papers on the substituted methanes and ethanes: for the bond distances

h=C−H, f=C−F, b=C−Br, m=C−C,
d=C−D, c=C−Cl, i=C−I; and xy=X−C−Y

for the interbond angles (x or y=h, d, f, c, b, i, or m). The C−C bond in the ethanes is the *middle* bond, hence the choice of m for this bond distance. The possible types of potential constants are illustrated by the following examples:

f_b C−Br stretching;
f_{bc} Br−C−Cl bending;
$f_b{}^c$ C−Br, C−Cl interaction;
$f_b{}^{ch}$ C−Br, Cl−C−H interaction;
$f_{bb}{}^{cc}$ Br−C−Br, Cl−C−Cl interaction;
$f_b{}^{bc}$ C−Br, Br−C−Cl interaction, with the C−Br bond forming one side of the angle;
$f_b{}^b$ C−Br, C−Br interaction between different C−Br bonds;
$f_b{}^{b'c}$ C−Br, Br−C−Cl interaction, with the C−Br bond different from the C−Br bond which forms one side of the Br−C−Cl angle;
$f_{bc}{}^{b'c'}$ Br−C−Cl, Br−C−Cl interaction for which neither side of one angle is a side of the other angle;
$f_{bc}{}^{b'c}$ Br−C−Cl, Br−C−Cl interaction, with only the C−Cl bond common to the 2 angles; and
$f_{bc}{}^{bc}$ Br−C−Cl, Br−C−Cl interaction for which the angles are at opposite ends of a substituted ethane.

[9] E. B. Wilson, Jr., J. Chem. Phys. **7**, 1047 (1939); **9**, 76 (1941).

The symbols used for the equilibrium values of the bond distances and interbond angles for CBr_2Cl_2 are:

$c_1=C-Cl_1$, $b_1=C-Br_1$,
$c_1c_2=Cl_1-C-Cl_2$, $c_1b_2=Cl_1-C-Br_2$,
$c_2=C-Cl_2$, $b_2=C-Br_2$,
$b_1b_2=Br_1-C-Br_2$, $c_2b_1=Cl_2-C-Br_1$,

and,

$$c_1b_1=Cl_1-C-Br_1, \quad c_2b_2=Cl_2-C-Br_2.$$

Wherever it is unnecessary to distinguish between identical atoms, the subscripts will be dropped.

The symmetry coordinates were: for the A_1 vibrations,

$$R_1=\tfrac{1}{2}(\Delta c_1+\Delta c_2+\Delta b_1+\Delta b_2),$$
$$R_2=\tfrac{1}{2}(\Delta c_1+\Delta c_2-\Delta b_1-\Delta b_2),$$
$$R_3=2^{-\frac{1}{2}}(\Delta cc-\Delta bb),$$
$$R_4=12^{-\frac{1}{2}}(2\Delta cc+2\Delta bb-\Delta c_1b_1-\Delta c_2b_1-\Delta c_1b_2-\Delta c_2b_2),$$

and

$$R'=6^{-\frac{1}{2}}(\Delta cc+\Delta bb+\Delta c_1b_1+\Delta c_1b_2+\Delta c_2b_1+\Delta c_2b_2)\equiv 0 \text{ (redundant coordinate)};$$

for the A_2 vibration,

$$R_5=\tfrac{1}{2}(\Delta c_2b_1-\Delta c_1b_1+\Delta c_1b_2-\Delta c_2b_2);$$

for the B_1 vibrations,

$$R_6=2^{-\frac{1}{2}}(\Delta b_1-\Delta b_2),$$

and

$$R_7=\tfrac{1}{2}(\Delta c_1b_2-\Delta c_1b_1+\Delta c_2b_2-\Delta c_2b_1);$$

and for the B_2 vibrations,

$$R_8=2^{-\frac{1}{2}}(\Delta c_1-\Delta c_2),$$

and

$$R_9=\tfrac{1}{2}(\Delta c_2b_1-\Delta c_1b_1-\Delta c_1b_2+\Delta c_2b_2).$$

The numbering of these coordinates corresponds to the numbering of the fundamentals in Table I.

From the **f** matrix (Table III) and the **U** matrices formed from the coefficients of the symmetry coordinates, one gets the following **F** matrix elements:

for the A_1 vibrations,

$$F_{11}=\tfrac{1}{2}(f_c+f_b+f_c{}^c+f_b{}^b+4f_b{}^c),$$
$$F_{12}=\tfrac{1}{2}(f_c-f_b+f_c{}^c-f_b{}^b),$$
$$F_{13}=2^{-\frac{1}{2}}(f_c{}^{cc}+f_b{}^{cc}-f_c{}^{bb}-f_b{}^{bb}),$$
$$F_{14}=3^{-\frac{1}{2}}(f_c{}^{cc}+f_b{}^{cc}+f_c{}^{bb}+f_b{}^{bb}-f_c{}^{bc}-f_c{}^{bc'}-f_b{}^{bc}-f_b{}^{b'c}),$$
$$F_{22}=\tfrac{1}{2}(f_c+f_b+f_c{}^c+f_b{}^b-4f_b{}^c),$$
$$F_{23}=2^{-\frac{1}{2}}(f_c{}^{cc}-f_b{}^{cc}-f_c{}^{bb}+f_b{}^{bb}),$$
$$F_{24}=3^{-\frac{1}{2}}(f_c{}^{cc}-f_b{}^{cc}+f_c{}^{bb}-f_b{}^{bb}-f_c{}^{bc}-f_c{}^{bc'}+f_b{}^{bc}+f_b{}^{b'c}),$$
$$F_{33}=\tfrac{1}{2}(f_{cc}+f_{bb}-2f_{bb}{}^{cc}),$$
$$F_{34}=6^{-\frac{1}{2}}(f_{cc}-f_{bb}-2f_{bc}{}^{cc}+2f_{bb}{}^{bc}),$$

and

$$F_{44}=(f_{cc}+f_{bb}+2f_{bb}{}^{cc}-4f_{bc}{}^{cc}-4f_{bb}{}^{bc}+f_{bc}+f_{bc}{}^{bc'}+f_{bc}{}^{b'c}+f_{bc}{}^{b'c'})/3;$$

for the A_2 vibration,

$$F_{11}=(f_{bc}-f_{bc}{}^{bc'}-f_{bc}{}^{b'c}+f_{bc}{}^{b'c'});$$

for the B_1 vibrations,

$$F_{11}=(f_b-f_b{}^b),$$
$$F_{12}=2^{\frac{1}{2}}(f_b{}^{b'c}-f_b{}^{bc}),$$

and

$$F_{22}=(f_{bc}+f_{bc}{}^{bc'}-f_{bc}{}^{b'c}-f_{bc}{}^{b'c'});$$

and for the B_2 vibrations,

$$F_{11}=(f_c-f_c{}^c),$$
$$F_{12}=2^{\frac{1}{2}}(f_c{}^{bc'}-f_c{}^{bc}),$$

and

$$F_{22}=(f_{bc}+f_{bc}{}^{b'c}-f_{bc}{}^{bc'}-f_{bc}{}^{b'c'}).$$

The **G** matrix elements, obtained by use of the Decius[10] tables, are as follows:

for the A_1 vibrations,

$$G_{11}=\tfrac{1}{2}(\mu_{Cl}+\mu_{Br}),$$
$$G_{12}=\tfrac{1}{2}(\mu_{Cl}-\mu_{Br}),$$
$$G_{13}=0,$$
$$G_{14}=0,$$
$$G_{22}=\tfrac{1}{2}(\mu_{Cl}+\mu_{Br}+8\mu_C/3),$$
$$G_{23}=-4(b^{-1}+c^{-1})\mu_C/3,$$
$$G_{24}=8^{\frac{1}{2}}(b^{-1}-c^{-1})3^{-\frac{1}{2}}\mu_C,$$
$$G_{33}=c^{-2}\mu_{Cl}+b^{-2}\mu_{Br}+4(c^{-1}+b^{-1})^2\mu_C/3,$$
$$G_{34}=6^{-\frac{1}{2}}[3c^{-2}\mu_{Cl}-3b^{-2}\mu_{Br}+4(c^{-2}-b^{-2})\mu_C],$$

and

$$G_{44}=3\mu_{Cl}/2c^2+3\mu_{Br}/2b^2+2(c^{-1}-b^{-1})^2\mu_C;$$

for the A_2 vibration,

$$G_{11}=3(\mu_{Cl}/c^2+\mu_{Br}/b^2)/2;$$

TABLE II. Wave numbers and degeneracies for the fundamentals of CBr_2Cl_2.

Designation	Degeneracy	Type	Wave number in cm^{-1}
ν_1	1	A_1	746[a]
ν_2	1	A_1	380
ν_3	1	A_1	242
ν_4	1	A_1	154
ν_5	1	A_2	175
ν_6	1	B_1	698[a]
ν_7	1	B_1	230
ν_8	1	B_2	781[a]
ν_9	1	B_2	262

[a] Gaseous state.

[10] J. C. Decius, J. Chem. Phys. **16**, 1025 (1948).

TABLE III. The f matrix.

	Δc_1	Δc_2	Δb_1	Δb_2	Δc_1c_2	Δb_1b_2	Δb_1c_1	Δb_2c_1	Δb_1c_2	Δb_2c_2
Δc_1	f_c	f_c^c	f_b^c	f_b^c	f_c^{cc}	f_c^{bb}	f_c^{bc}	f_c^{bc}	$f_c^{bc'}$	$f_c^{bc'}$
Δc_2		f_c	f_b^c	f_b^c	f_c^{cc}	f_c^{bb}	$f_c^{bc'}$	$f_c^{bc'}$	f_c^{bc}	f_c^{bc}
Δb_1			f_b	f_b^b	f_b^{cc}	f_b^{bb}	f_b^{bc}	$f_b^{b'c}$	f_b^{bc}	$f_b^{b'c}$
Δb_2				f_b	f_b^{cc}	f_b^{bb}	$f_b^{b'c}$	f_b^{bc}	$f_b^{b'c}$	f_b^{bc}
Δc_1c_2					f_{cc}	f_{bb}^{cc}	f_{bc}^{cc}	f_{bc}^{cc}	f_{bc}^{cc}	f_{bc}^{cc}
Δb_1b_2						f_{bb}	f_{bb}^{bc}	f_{bb}^{bc}	f_{bb}^{bc}	f_{bb}^{bcc}
Δb_1c_1							f_{bc}	$f_{bc}^{b'c}$	$f_{bc}^{bc'}$	$f_{bc}^{bb'}$
Δb_2c_1								f_{bc}	$f_{bc}^{b'c'}$	$f_{bc}^{bc'}$
Δb_1c_2									f_{bc}	$f_{bc}^{b'c}$
Δb_2c_2										f_{bc}

Since the matrix is symmetric, with $f_{ij}=f_{ji}$, the elements below the diagonal may easily be determined. The primed and unprimed symbols refer to different bonds of the same type; for example, b and b' are different C−Br bonds.

for the B_1 vibrations,

$$G_{11}=\mu_{Br}+4\mu_C/3,$$
$$G_{12}=2(b^{-1}+3c^{-1})\mu_C/3,$$

and

$$G_{22}=3\mu_{Cl}/2c^2+\mu_{Br}/2b^2+(3c^{-1}+b^{-1})^2\mu_C/3;$$

and for the B_2 vibrations,

$$G_{11}=(\mu_{Cl}+4\mu_C/3),$$
$$G_{12}=2(c^{-1}+3b^{-1})\mu_C/3,$$

and

$$G_{22}=3\mu_{Br}/2b^2+\mu_{Cl}/2c^2+(3b^{-1}+c^{-1})^2\mu_C/3.$$

Here μ_C, μ_{Br}, and μ_{Cl} are, respectively, the reciprocals of the masses of the C, Br, and Cl atoms while $b(=1.93A)$ and $c(=1.75A)$ are the equilibrium values[11] for the C−Br and C−Cl bonds.

In order to get approximate potential constants, values were transferred from CCl_3X,[12] CBr_3X,[13] $CHBrCl_2$,[14] and $CDBrCl_2$.[14] After several modifications, the resulting potential constants yielded calculated fundamentals that were all within 0.5 percent of the observed values for the liquid. These potential constants are given in Table IV along with those obtained from relations given by Simanouti, who based his calculations on a Urey-Bradley potential energy function and adjusted his constants to fit the frequencies observed for a group of D, Cl, and Br substituted methanes. For CBr_2Cl_2, his calculated fundamentals agreed better with the observed values of Delwaulle and Francois[2] than with those of Lecomte, Volkringer, and Tchakirian,[1] which seems to cast additional doubt on the validity of the results of the latter workers. In the present investigation, the potential constants were modified so as to obtain agreement with the liquid values of the fundamentals since only a few gas values for the fundamentals were available.

[11] P. Capron and S. Perlinghi, Bull. soc. chim. Belges **45**, 730 (1936).
[12] Zietlow, Cleveland, and Meister, J. Chem. Phys. **18**, 1076 (1950).
[13] Meister, Rosser, and Cleveland, J. Chem. Phys. **18**, 346 (1950).
[14] Polo, Meister, Cleveland, Bernstein, and Sherman (to be published).

THERMODYNAMIC PROPERTIES

The heat content, free energy, entropy, and heat capacity at constant pressure were calculated for 12 temperatures from 100° to 1000°K, using the wave numbers and degeneracies given in Table II. A rigid rotator, harmonic oscillator model was assumed, and the values were calculated for the ideal gaseous state at 1-atmos pressure. The principal moments of inertia were determined by the Hirschfelder[15] formulas, using the electron diffraction data.[11] The values obtained were:

$$I_{xx}=369 \text{ awu } A^2 \ (613\cdot10^{-40} \text{ g cm}^2),$$
$$I_{yy}=621 \text{ awu } A^2 \ (1031\cdot10^{-40} \text{ g cm}^2),$$

and

$$I_{zz}=542 \text{ awu } A^2 \ (900\cdot10^{-40} \text{ g cm}^2).$$

TABLE IV. Potential constants for CBr_2Cl_2.[a]

Type	Present results	Simanouti
f_c	3.3713[b]	2.50
f_b	2.7530	2.48
f_c^c	0.35134	0.467
f_b^b	0.21296	0.355
f_b^c	0.32465	0.412
f_c^{cc}	0.36022	0.466
f_b^{bb}	0.34088	0.376
f_c^{bb}	−0.20547	—
f_b^{cc}	−0.16258	—
f_c^{bc}	0.36022	0.405
f_b^{bc}	0.35007	0.441
$f_c^{bc'}$	−0.20547	—
$f_b^{b'c}$	−0.17178	—
f_{cc}	1.1360	1.44
f_{bb}	1.2391	1.25
f_{bb}^{cc}	−0.028036	—
f_{bc}^{cc}	0.077883	0.198
f_{bb}^{bc}	0.12944	0.198
f_{bc}	1.1383	1.25
$f_{bc}^{b'c}$	0.087897	0.198
$f_{bc}^{bc'}$	0.074897	0.198
$f_{bc}^{b'c'}$	−0.018668	—

[a] Bond stretching and bond interaction constants are in units of md/A; angle-bond interaction constants are in md/rad; angle, and angle interaction, constants are in md A/rad.
[b] This number of significant figures is not really justified but is necessary to give the best reproduction of the observed wave numbers and to secure internal consistency in the calculations.

[15] J. O. Hirschfelder, J. Chem. Phys. **8**, 431 (1940).

The symmetry number is 2 and $I_{xy}=I_{xz}=I_{yz}=0$. Birge's[16] values of the physical constants were used throughout.

The values obtained for the thermodynamic properties are given in Table V. The values of the heat capacity calculated by Glockler and Edgell,[6] for the temperatures given here, do not differ too greatly from the present values (average difference 0.11 cal deg^{-1} M^{-1}), but the wave numbers used by them seem less reliable than the ones used in the present work. Hence, the heat capacity values given in Table V are to be preferred.

TABLE V. Heat content, free energy, entropy, and heat capacity of CBr_2Cl_2 for the ideal gaseous state at 1-atmos pressure.[a]

T	$(H^0-E_0^0)/T$	$-(F^0-E_0^0)/T$	S^0	C_p^0
100	9.62	55.04	64.65	13.09
200	12.74	62.71	75.45	18.08
273.16	14.47	66.95	81.43	20.23
298.16	14.98	68.24	83.23	20.80
300	15.02	68.33	83.35	20.84
400	16.70	72.89	89.59	22.50
500	17.97	76.76	94.73	23.50
600	18.95	80.13	99.07	24.12
700	19.72	83.11	102.82	24.53
800	20.34	85.79	106.13	24.82
900	20.85	88.21	109.06	25.02
1000	21.27	90.44	111.72	25.16

[a] T is in °K and the other quantities are in cal deg^{-1} M^{-1}.

ACKNOWLEDGMENTS

The Hilger E-518 spectrograph used for the depolarization spectrograms was obtained in part with a grant from the American Academy of Arts and Sciences, and the work was further aided by a later grant from this society. The optical parts of the 2-prism spectrograph used for the Raman displacement spectrograms were secured with a grant from the Society of the Sigma Xi. The diagram used as Fig. 1 was prepared by Mr. Alfons Weber. The authors are grateful for this assistance.

[16] R. T. Birge, Revs. Modern Phys. **13**, 233 (1941).

THE JOURNAL OF CHEMICAL PHYSICS VOLUME 20, NUMBER 3 MARCH, 1952

The Reaction of Nitrous Acid with Hydroxylamine*

A. BOTHNER-BY AND L. FRIEDMAN
Department of Chemistry, Brookhaven National Laboratory, Upton, Long Island, New York

(Received July 23, 1951)

Approximately equal quantities of $N^{14}N^{15}O^{16}$ and $N^{15}N^{14}O^{16}$ are produced by reaction of hydroxylamine hydrochloride and N^{15}-enriched sodium nitrite in solution in O^{18}-enriched water. The same reaction when carried out in a solution brought to a pH of 1 with gaseous HCl produces an excess of $N^{14}N^{15}O^{16}$. In both experiments the concentration of $N^{15}N^{15}O^{16}$ was accounted for on the basis of the reaction of nitrous acid with hydroxylamine to yield nitrous oxide molecules containing one nitrogen atom from each source. O^{18} exchange occurred to a greater extent in acid medium and the double tagged N_2O so produced was mainly $N^{14}N^{15}O^{18}$ rather than a mixture of the isomers $N^{14}N^{15}O^{18}+N^{15}N^{14}O^{18}$.

These observations lead to the following conclusions concerning the reaction mechanisms. In neutral solution most of the nitrous oxide produced is formed by dehydration of a symmetrical intermediate, probably hyponitrous acid. In acid medium a competitive dehydration of an unsymmetrical intermediate plays an important role. Mechanisms involving nitroxyl as an intermediate are untenable. Oxygen exchange is acid catalyzed and occurs exclusively with nitrous acid or with an unsymmetrical intermediate formed in the course of this reaction. Oxygen atoms from either nitrous acid or hydroxylamine appear in the product nitrous oxide.

INTRODUCTION

THE end products of the reaction between hydroxylamine and nitrous acid are water and nitrous oxide.[1] The reaction has been assumed to proceed via the compound nitroxyl,[2] NOH. The implied reaction mechanism may be written as follows

$$H_2NOH+HO-N=O\rightarrow 2NOH+H_2O, \quad (1)$$

$$2NOH\rightarrow HO-N=N-OH, \quad (2)$$

$$HON=NOH\rightarrow N\rightleftarrows N=O+H_2O. \quad (3)$$

Audrieth[3] has demonstrated the presence of hyponitrous acid in a slowly decomposing solution of hydroxylammonium nitrite, and has proposed as another species possibly present in the reaction mixture N-nitroso-hydroxylamine, pointing out that some N-substituted hydroxylamines give relatively stable nitroso derivatives.

Nitroxyl has been assumed as a hypothetical intermediate in the decomposition of nitrohydroxylamic acid, $H_2N_2O_3$,[4] and has also been postulated as an intermediate in the oxidation of ammonia.[5] Both hyponitrous acid and nitroxyl have been eliminated as

* Research carried out under the auspices of the AEC.

[1] V. Meyer, Ann. **175**, 141 (1875). W. Wislicenus, Ber. **26**, 772 (1893).

[2] W. M. Latimer and J. H. Hildebrand, *Reference Book of Inorganic Chemistry* (MacMillan Company, New York, 1941), pp. 196–197.

[3] L. F. Audrieth, J. Phys. Chem. **34**, 538 (1930).

[4] A. Angeli, Gazz. Chim. **33**, II, 245 (1903).

[5] L. Andrussow, Ber. **59**, 458 (1926); Z. angew. Chem. **48**, 593 (1935).

TABLE I.

Mass	Relative ion intensity a	Relative ion intensity b	% Total a	% Total b	Ions contributing to peak
47	0.57	2.1	0.083	0.313	$N^{15}N^{14}O^{18}$, $N^{14}N^{15}O^{18}$, $N^{15}N^{15}O^{17}$
46	2.24	5.1	0.325	0.75	$N^{14}N^{14}O^{18}$, $N^{15}N^{15}O^{16}$, $N^{14}N^{15}O^{17}$, $N^{15}N^{14}O^{17}$
45	223.0	221.0	32.2	32.3	$N^{14}N^{15}O^{16}$, $N^{15}N^{14}O^{16}$, $N^{14}N^{14}O^{17}$
44	463.0	450.0	67.4	66.6	$N^{14}N^{14}O^{16}$
33	0.086	0.51	···	···	$N^{15}O^{18}$
32	0.60	1.7	···	···	$N^{14}O^{18}$, $O^{16}O^{16}$ (background)
31	28.2	35.8	···	···	$N^{15}O^{16}$
30	136.8	131.0	···	···	$N^{14}O^{16}$, $N^{15}N^{15}$

possible intermediates in the controlled thermal decomposition of ammonium nitrate.[6] However, in view of Audrieth's[3] findings, the reaction of nitrous acid with hydroxylamine seemed attractive to study in search of the often proposed, but rarely detected nitroxyl.[7]

EXPERIMENTAL

Sodium Nitrite-N^{15}.—Sodium nitrate, prepared from nitric acid containing 31.9 atom percent N^{15}, was converted to sodium nitrite by reduction with lead.[8]

Hydroxylamine Hydrochloride.—Eastman Kodak Company white label grade was used without purification.

Water-O^{18}.—Water enriched to 1.5 percent O^{18} was obtained from the Stuart Oxygen Co., California.

Preparation of Nitrous Oxide.—(*a*) Solutions of 0.080 g of N^{15}-enriched sodium nitrite in 1.00 ml of O^{18}-enriched water and 0.080 g of hydroxylamine hydrochloride in 1.00 ml of O^{18}-enriched water were placed in the legs of a two-legged flask. The flask was connected to a vacuum manifold, the solutions were frozen and noncondensed gases pumped off. The flask was then closed off by means of a stopcock, and the solutions were thawed and mixed at room temperature. A rapid evolution of gas was observed. The speed of the reaction may be ascribable to a slight acidity of the solution.[3] The aqueous phase was refrozen and the evolved gas was passed through a trap held at −80°C and condensed in a storage bulb cooled with liquid nitrogen. No residual pressure was observed.

(*b*) A solution of 0.250 g of N^{15}-enriched sodium nitrite in 2.00 ml of O^{18}-enriched water was cooled to −5°C in one leg of a two-legged flask, 0.240 g of hydroxylamine hydrochloride was placed in the other leg. Dry hydrogen chloride was bubbled through the nitrite solution bringing it to *p*H 1, determined by Hydrion test paper. The flask was then connected to the vacuum manifold and the sequence of operations described in experiment (*a*) was carried out.

Analysis of the gas samples in the Consolidated Nier mass spectrometer seemed to indicate the presence of some carbon dioxide. The gas was therefore transferred to other storage bulbs partly filled with dry sodium hydroxide pellets and stored for 24 hours. The gases thus purified were analyzed in the mass spectrometer; CO_2 was absent.

DISCUSSION OF RESULTS

The mass spectra of the N_2O produced in the reactions forementioned are presented in Table I. The sub-columns *a* and *b* refer to the products of experiments (*a*) and (*b*), respectively. The second column contains the observed peak heights corresponding to the masses indicated in the first column. The third column contains normalized values of the molecular ion intensity obtained by setting the sum of the relative molecular ion intensities equal to 100. Masses below 30 are omitted for the sake of conciseness.

The interpretation of the spectra may be simplified by a preliminary consideration of the nitrous oxide molecules containing O^{17}. The natural abundance of O^{17} is approximately 20 percent that of O^{18}. Consequently, an upper limit on the amount of O^{17} present in material containing an excess of O^{18} may be estimated as 20 percent of the O^{18} concentration. Let us assume that all of the 47 peak in the spectra is formed by the ionization of $N^{14}N^{15}O^{18}$ and $N^{15}N^{14}O^{18}$ and that all of the 45 peak results from the ionization of the corresponding O^{16} molecules. Then the concentration of molecules containing O^{18} is $P_{47}/(P_{45}+P_{47})$ or 0.26 percent in (*a*) and 0.98 percent in (*b*). An upper limit of one-fifth these values can be placed on the concentrations of molecules containing O^{17}. In experiment (*a*) we calculate a maximum of 0.05 percent O^{17}. The upper limit of $N^{14}N^{14}O^{17}$ is 0.033 percent, of ($N^{14}N^{15}O^{17}+N^{15}N^{14}O^{17}$) is 0.016 percent, and of $N^{15}N^{15}O^{17}$ is 0.002 percent. Thus the error made in neglecting O^{17} contributions to ion of mass 45 and 47 is trivial in experiment (*a*). The ions of $N^{15}N^{14}O^{17}$ and $N^{14}N^{15}O^{17}$ make up a small though appreciable fraction of the ions at mass 46 and are taken into consideration. Similar results are obtained for the O^{17} molecules in experiment (*b*).

The calculation of the isotopic composition of the N_2O molecules of different masses follows directly from the normalized values presented in Table I. One may calculate the relative contributions of the various molecular ions to the peak at mass 46 as follows. First the contribution of $N^{14}N^{15}O^{17}$ and $N^{15}N^{14}O^{17}$ is subtracted leaving 0.31 percent and 0.55 percent for the sum of $N^{15}N^{15}O^{16}$ and $N^{14}N^{14}O^{18}$ in (*a*) and (*b*), respectively. It was previously shown that 0.26 percent and 0.98 percent O^{18} were present in the isomers containing one N^{15} atom. On this basis we calculate that the $N^{14}N^{14}O^{18}$ species must be present to the extent of 0.175 percent and 0.65 percent in (*a*) and (*b*), respectively. The remaining 0.10 percent in (*a*) must arise from $N^{15}N^{15}O^{16}$. The negative remainder in (*b*) results from an error in estimating the O^{17} concentration. The error in (*a*) is smaller because of the smaller O^{18} enrichment.

[6] L. Friedman and J. Bigeleisen, J. Chem. Phys. **18**, 1325 (1950).

[7] The literature on this subject prior to 1935 is briefly reviewed in *Gmelins Handbuch der Anorganischen Chemie* (Verlag Chemie, Berlin, Germany, 1936), third edition, Vol. IV, p. 855 ff.

[8] A. Bothner-By and L. Friedman, Brookhaven National Laboratory Quarterly Progress Report, January–April 1951, p. 67.

These calculations involve the assumption that there is no isotope effect on the probability of producing a molecular ion, that fractionation of molecules of different masses in the mass spectrometer sample system and leak is negligible, and that voltage discrimination effects in the mass spectrometer are also negligible. In addition, in the analysis of the composition of the ions of mass 46 the assumption of equal concentrations of O^{18} in the $N^{14}N^{14}O$ and ($N^{14}N^{15}O+N^{15}N^{14}O$) molecules is made. It is estimated that all of these factors involve a cumulative error in the concentrations of molecular ions of less than 5 percent.

The value of 0.10 percent for $N^{15}N^{15}O^{16}$ in (*a*) is much too low to be consistent with the mechanism involving nitroxyl as an intermediate. The total N^{15} in the N_2O is about 16 percent, and the random recombination of nitroxyl would produce hyponitrous acid containing 2.56 percent doubly labeled molecules which would decompose into $N^{15}N^{15}O$. Furthermore, only 26.9 percent of the N_2O molecules would be the isomers $N^{15}N^{14}O$ and $N^{14}N^{15}O$. The observed amounts of ($N^{14}N^{15}O+N^{15}N^{14}O$) account, within the experimental error, for all of the excess N^{15}. Mechanisms not involving nitroxyl, which account for the observed isotopic composition of N_2O, will be discussed subsequently.

Consideration of the abundance of the molecular ions provides no information concerning the relative amounts of $N^{15}N^{14}O$ and its isotopic isomer $N^{14}N^{15}O$. The technique for determing the relative abundance of these isomers has been described previously[9] and involves consideration of the abundances of the $N^{15}O^+$ and $N^{14}O^+$ ions produced and of the relative amounts of $N^{14}N^{14}O$ ions and molecular ions containing one N^{15}. Since the $N^{15}N^{15+}$ contribution to mass 30 is negligible, the $N^{14}N^{15}O$ is obtained from the expression $P_{31}/P_{30}+P_{31}$. Values of 17.1 percent $N^{14}N^{15}O$ and 21.4 percent $N^{14}N^{15}O$ are calculated in experiments (*a*) and (*b*), respectively. Concentrations of 15.1 percent $N^{15}N^{14}O$ and 11.0 percent $N^{15}N^{14}O$ in (*a*) and (*b*), respectively, are estimated by difference. These values are subject to errors from the following sources:

(1) A rearrangement by electron impact has been reported[9] in the case of $N^{15}N^{14}O$ in which $N^{15}O^+$ ions are produced. It is assumed in experiment (*a*) that the error caused by this rearrangement is canceled by a similar rearrangement of $N^{14}N^{15}O$ in which $N^{14}O^+$ ions are obtained. A partial cancellation of rearrangements is expected in experiment (*b*). A small isotope effect on this process in which the probabilities of the rearrangements are not identical may exist.

(2) The $N^{14}O^+$ ions from $N^{15}N^{14}O$ are diluted by $N^{14}O^+$ ions from $N^{14}N^{14}O$. Since the probability of $N^{14}N^{14}$ bond rupture is greater than that of $N^{15}N^{14}$ bond rupture, the $N^{14}N^{15}O$ concentration calculated from the 31/30+31 ratio is too small.[10] An additional minor error arises from the fact that the probability of rupture of the $N^{14}N^{15}$ bond by electron impact is not expected to be identical in $N^{14}N^{15}O$ and $N^{15}N^{14}O$.

The combined magnitude of the errors discussed is estimated to be of the order of 5 percent or less in these systems. In view of this, some doubt may exist as to whether the ratio of $N^{14}N^{15}O/N^{15}N^{14}O$ is significantly different from unity in the first experiment. There can be no doubt that in acid medium the 2/1 ratio of $N^{14}N^{15}O/N^{15}N^{14}O$ observed arises from the reaction mechanism rather than the errors cited above.

These results suggest alternate paths for the formation of N_2O in neutral and acid medium, via symmetrical and unsymmetrical intermediates, respectively. Since hyponitrous acid may be isolated[3] from the reaction mixture, it is reasonable to assume that it is the symmetrical intermediate. N-nitroso-hydroxylamine is a plausible unsymmetrical intermediate. On this basis the reaction may be set forth as follows:

$$N^{14}H_2OH+HN^{15}O_2 \rightarrow HO-N^{14}=N^{15}-OH+H_2O \quad (4)$$

$$N^{14}H_2OH+HN^{15}O_2 \rightarrow \begin{matrix} H \\ \diagdown \\ N^{14}-N^{15}=O \\ \diagup \\ HO \end{matrix} + H_2O \quad (5)$$

$$HO-N^{14}=N^{15}-OH \rightleftharpoons N^{14}=N^{15}=O+H_2O \quad (6)$$

$$HO-N^{14}=N^{15}-OH \rightleftharpoons N^{15}=N^{14}=O+H_2O \quad (7)$$

$$\begin{matrix} H \\ \diagdown \\ N^{14}-N^{15}=O \\ \diagup \\ HO \end{matrix} \rightarrow N^{14}=N^{15}=O+H_2O. \quad (8)$$

The experimental results indicate that the over-all reaction represented by Eqs. (5) and (8) would then proceed more rapidly in solutions of lower *p*H. It should be noted that an isotope effect on the relative rates of reactions (6) and (7) may lead to a slight excess, 1.8 percent, of the $N^{14}N^{15}O$.[11]

In summing up, the nitrogen tracer study reveals that the nitroxyl mechanism is untenable, and that while most of the N_2O is formed from hyponitrous acid in neutral solution, excess acid catalyzes a reaction via N-nitroso-hydroxylamine or a similar unsymmetrical intermediate.

The experiments were carried out in O^{18}-enriched water in hopes of obtaining information concerning the source of oxygen in the product nitrous oxide. As previously noted, 0.26 percent and 0.975 percent O^{18}-

[9] L. Friedman and J. Bigeleisen, J. Chem. Phys. **18**, 1325 (1950).
[10] O. A. Schaeffer, J. Chem. Phys. **18**, 1501 (1950).
[11] J. Bigeleisen, J. Chem. Phys. **17**, 675 (1949).

TABLE II.

	a	*b*
(1) % O^{18} in molecules containing one N^{15} = 100 $P_{47}/P_{45}+P_{47}$	0.260%	0.975%
(2) % O^{18} natural abundance =	0.2	...
(3) % O^{18} excess in molecules containing one N^{15} =	0.060	0.775
(4) % O^{18} in $N^{14}N^{15}O^{18}+N^{14}N^{15}O^{16}$ = 100 $P_{33}/P_{33}+P_{31}$ =	0.34	1.42
(5) % O^{18} excess in above =	0.14	1.22
(6) % $N^{14}N^{15}O^{16}$ in $N^{14}N^{15}O^{16}+N^{15}N^{14}O^{16}$ =	53.0	66.0
(7) % excess O^{18} as $N^{14}N^{15}O^{18}$ =	0.07	0.80
(8) Residual excess as $N^{15}N^{14}O^{18}$ =	0	0
(9) Ratio of $N^{14}N^{15}O^{18}/N^{15}N^{14}O^{18}$ =	∞	∞

labeled molecules were obtained in experiments (*a*) and (*b*), respectively. This amounts to an excess of O^{18} above natural abundance of 0.06 percent in (*a*) and 0.775 percent in (*b*), indicating strong acid catalysis of the oxygen exchange reaction. A clue to the source of this exchange may be obtained from an examination of the relative ion intensities of mass 33 and mass 31 peaks corresponding to the ions $N^{15}O^{18+}$ and $N^{15}O^{16+}$. The rather small amount of exchange in (*a*) introduced the possibility of relatively large chart reading errors at $M/e=33$. To minimize this, the spectrum was scanned independently five times and the peak heights were measured with a binocular microscope and a scale calibrated in tenths of a millimeter. The measurements were averaged and a ratio of 0.00305 ± 0.00007 was obtained for P_{33}/P_{31}. This ratio was 0.0142 in experiment (*b*). Table II contains a sequential presentation of the analysis of the data bearing on the use of the oxygen tracer. The ratios of $N^{14}N^{15}O^{18}/N^{15}N^{14}O^{18}$ are important in that they tell whether or not exchange occurs with both reactants or with a symmetrical intermediate. Non-equivalence in the abundances of these molecules indicates exchange with only one reactant or an unsymmetrical intermediate. Furthermore, in the latter case the presence of a particular species in excess provides some information on which reactant or which portion of an unsymmetrical intermediate exchanges its oxygen with water. This analysis in the case of experiment (*a*), suggests the result which is strongly confirmed in experiment (*b*), namely, that the ratio $N^{14}N^{15}O^{18}/N^{15}N^{14}O^{18}$ is very large.

It must be realized that the results are subject to errors similar to those discussed in connection with the determination of the relative amounts of $N^{14}N^{15}O$ and $N^{15}N^{14}O$. In view of this, one may conclude that within the limits of experimental error in (*b*), all of the excess O^{18} is found in $N^{14}N^{15}O^{18}$ and $N^{14}N^{14}O^{18}$ and a negligible amount of excess O^{18} occurs in $N^{15}N^{14}O^{18}$. This strongly suggests oxygen exchange exclusively with nitrous acid or the nitroso oxygen in N-nitroso-hydroxylamine and eliminates the possibility of rapid oxygen exchange between hydroxylamine or hyponitrous acid and water. The result also shows that the oxygen in the product nitrous oxide comes partly from the hydroxylamine and partly from the nitrous acid-water system.

ACKNOWLEDGMENTS

The authors wish to express their appreciation to Dr. R. W. Dodson and Dr. Gerhart Friedlander for helpful discussion and aid in preparation of this manuscript.

Thermal Conductivity of Fluid Argon and Nitrogen*

ARTHUR UHLIR, JR.†
Department of Physics, University of Chicago, Chicago, Illinois
(Received December 7, 1951)

The thermal conductivities of A and N_2 have been measured at pressures up to twice the critical pressures and at temperatures from the normal boiling points to well above the critical temperatures. By combining Enskog's transport theory for a dense gas of hard elastic spheres with free volume calculations for a close-packed lattice (assuming a communal entropy of R per mole), one can calculate the thermal conductivity λ for liquid A between 87.3°K and 141.6°K from liquid and vapor densities and entropy of vaporization. The values so calculated are within 15 percent of the measured values. However, a similarly calculated value of the viscosity is 50 percent lower than the experimental value. A correction for quantum-mechanical effects reduces the disagreement between the theoretical and experimental values of λ to about ± 5 percent, which is within the uncertainty of the thermodynamic data.

INTRODUCTION

IN the program of describing the equilibrium and transport properties of matter in terms of mechanical models, the noble gas elements play a particularly important role, as the models corresponding to these substances are expected to have the simplest dynamical specification. It is plausible that the application of classical mechanics to such models will be fairly satisfactory for liquid radon, xenon, krypton, and argon. Argon is by far the most abundant and least expensive of these elements; measurement of the thermal conductivity of the liquid was undertaken to provide a test of present and future theories of thermal conductivity of liquids. Also, in the absence of complete theories, some idea of the consequences of the greater complexity of polyatomic substances can be obtained by comparison with the results for argon.

APPARATUS

Convection is apt to introduce serious errors in the measurement of the thermal conductivity of liquids. Jakob, in his article on the thermal conductivity of water,[1] criticizes much of the earlier work on such grounds. In his own experiments, Jakob minimized convection by letting the heat flow downward through a horizontal film of water. While such an arrangement is to be recommended, it is not always necessary and is probably not always sufficient to prevent convection. In the apparatus to be described, heat flows through a thin layer of liquid confined in the annular gap between vertical concentric cylinders; this geometry has proved satisfactory in previous work[2,3] and has the advantage that heat losses are small and do not require large corrections or accurate compensating arrangements. Calculations outlined in the part titled "Results" show that, on account of the thin film and small temperature difference used in the present apparatus, convection is possible only in a region near the critical point.

The principle novelty in the present apparatus is the use of helium gas thermometers to measure temperature difference. Gas thermometers are sensitive, vibration-proof, and have an advantage over resistance thermometers, thermocouples, and vapor pressure thermometers in that their sensitivity does not have to be determined by differentiating a calibration curve. Their disadvantages are the large size of the bulbs, the susceptibility to leaks, and the impracticality of automatic recording.

The main parts of the apparatus are the plunger, Fig. 1A, and the barrel, Fig. 1B, both made of copper. The plunger consists of two pieces, a thermometer bulb with a tapered outer surface and a sleeve which fits this taper. The resistor which generates the heat to be conducted through the sample was made of silk-insulated manganin wire and was wound in grooves machined in the tapered surface of the thermometer bulb. The bulb and wires were smeared with petroleum jelly to improve thermal contact and inserted firmly in the sleeve. Just outside of the plunger, copper current and voltage leads are soldered to the heater.

The barrel consists of two pieces shrunk together and hard soldered so that a 49.3 cc cavity is formed to serve as the bulb of the other gas thermometer. The volume of the bulb in the plunger is different, 41.3 cc, because of modifications made in the design during construction. The bore of the barrel is 1.26 in. in diameter and the outside diameter of the plunger is 1.24 in., so that a gap of 0.01 in. is formed when these parts are assembled. The diameter of the bore was measured to 0.0001 in. at 18 locations, that of the plunger at 6 locations, by the Precision Gage Laboratory of the Armour Research Foundation. The length of the gap is 5.58 in. The plunger is centered in the bore by Bakelite rings which are about 0.001 in. undersize (the error due to a small eccentricity is of second order in the eccentricity). Correction was made for thermal expansion. The probable error in the geometrical factor of the apparatus is $1\frac{1}{2}$ percent.

A Bakelite spacer separates the plunger from the

* This experiment was performed at the Institute for the Study of Metals of the University of Chicago.
† AEC Predoctoral Fellow, 1949–1951. Now at Bell Telephone Laboratories, Murray Hill, New Jersey.
[1] M. Jakob, Ann. Physik [4] **63**, 537 (1920).
[2] P. W. Bridgman, *The Physics of High Pressure* (G. Bell and Sons, London, 1931), Chapter 11.
[3] J. M. Lenoir and E. W. Comings, Chem. Eng. Progress **47**, 223 (1951).

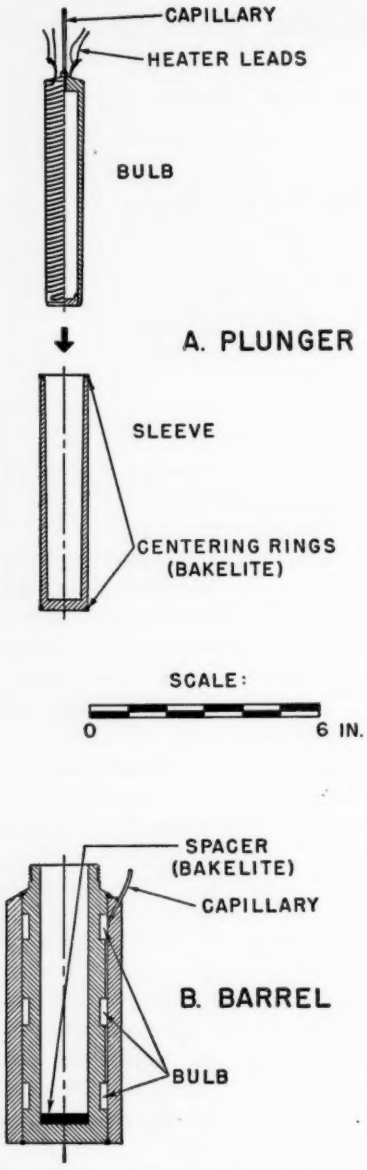

FIG. 1. Gas thermometers and geometry-defining parts of apparatus.

bottom of the bore and two loose-fitting Bakelite pieces (not illustrated) rest on top of the plunger, to insure that the loss of heat through the ends of the plunger will not depend appreciably upon the thermal conductivity of the argon nor be large and variable on account of convection.

Copper-nickel capillary tubing with an inside diameter of 1 mm is soldered to the gas thermometer bulbs and connects to a stopcock manifold which was made of a small block of brass, with steel taper pins for plugs, to minimize dead space. A U-tube made of 2.07 mm precision-bore glass tubing is attached to the stopcock manifold with de Khotinsky cement. Silicone diffusion pump oil, DC 703, was found to be a better manometer fluid in this U-tube than butyl phthalate, Octoil-S, mechanical pump oil, mineral oil, or concentrated sulfuric acid; only the silicone gave freedom from the appearance over a period of days or weeks of a persistent difference in liquid level when the two sides of the U-tube were at the same pressure.

The most obvious procedure for determining thermal conductivity with the apparatus so far described would be to hold the temperature of the barrel constant with some kind of thermostat, so provision was made for surrounding the barrel with liquefied gas under controlled pressure. However, it was expected that it would be satisfactory to let the temperature change slowly. It turned out, in fact, that the latter procedure led to slightly better precision.

In either case, the problem of controlling the temperature of the barrel is simplified by making the assembly, barrel and plunger, appear to its surroundings as a constant source of heat instead of an intermittent source. Therefore, a dummy heater of practically the same resistance as the heater in the plunger was wound on the barrel as indicated in Fig. 2. Current from a storage battery was made to flow through the dummy heater when not flowing through the heater.

The barrel and plunger assembly is suspended inside the heavy-walled aluminum bottle shown in Fig. 2. A brass neck, threaded and soldered to the barrel, has a flange which is closed with a matching flange supported by a $\frac{3}{8}$-in. o.d. stainless steel argon supply tube. This tube passes through and is soldered to the brass lid which is bolted on the aluminum bottle. The flanges and the lid are provided with polyethylene gaskets which were crushed to paper-thinness when the bolts were tightened. The four heater leads are brought through the flange by means of Kovar-glass seals. These leads, together with the leads from the dummy heater and a copper-constantan thermocouple junction taped to the bottom of the barrel, leave the aluminum bottle through another stainless steel tube, which also serves for the introduction of liquifiable gas to the bottle. These wires are brought through Kovar-glass seals at the room temperature end of the tube.

The whole apparatus weighs 37 lb and is suspended in a $5\frac{1}{4}$-in. i.d. Dewar flask by a 1-in. o.d. stainless steel tube attached to the lid of the aluminum bottle.

When measurements were to be made with the temperature slowly rising, the space between the barrel and the aluminum bottle was filled with copper sheets and glycerine, so that the entire mass could warm up at a constant rate.

Argon was obtained from a commercial cylinder to which was attached a pressure regulator of appropriate range. Pressures were measured with Bourdon-tube gauges that were calibrated with a dead-weight tester. Connections in the argon supply system were made with copper tubing and S.A.E. flare joints; needle valves were provided for a controlled leak to the atmosphere, for connecting the various parts of the system to a vacuum pump, and for changing pressure gauges without contaminating the argon. A coil of copper tubing immersed in a Dewar of melting trichlorethylene served as a trap. This trap was probably unnecessary, as a mass

spectrometer analysis of the argon indicated that the principle impurity was 0.2 to 0.4 percent nitrogen.

Helium from a commercial cylinder and regulator was used in the gas thermometers. Connections to the stopcock manifold, vacuum pump, and a mercury manometer were made with rubber tubing. A trap cooled with liquid nitrogen was used.

PROCEDURE

The procedure for the usual kind of run will be described first. At room temperature, the gap for the sample and the connecting lines thereto were rinsed and filled with argon by five or more applications of pressure, the first two of which were preceded by evacuation with a mechanical pump, while the last left the gap connected to the argon cylinder through a pressure regulator set for about the pressure to be used during the run.

The gas thermometers were similarly rinsed and left connected to the helium supply, the only differences being the need for care in changing pressure, so as not to expel the silicone from the U-tube, and the use of about 2 atmos instead of 10 to 100 atmos pressure.

The apparatus was cooled by pouring about 16 liters of liquid nitrogen over it. It was allowed to "soak" in liquid nitrogen for a few hours. The dummy heater was started during this period. Eventually the last of the liquid nitrogen boiled away and the temperature began to rise. After this temperature rise was well established, the helium supply was disconnected from the gas thermometer system and the latter was cautiously bled to atmospheric pressure. An exhaust valve for the argon system was "cracked" to provide a slight leak and the pressure regulator was adjusted to the desired pressure.

The relative temperature distribution became stabilized in the warming apparatus after about two hours. The pressure in the gas thermometer system was above atmospheric again by this time, so the system was momentarily bled to the atmosphere. A minute or two later, the system was again momentarily bled to the atmosphere and the thermocouple voltage was measured. Barometric pressure was measured by connecting one side of a mercury manometer to the vacuum pump. One atmosphere pressure happened to provide a convenient thermometer sensitivity, and obtaining this pressure by bleeding the thermometers to the atmosphere for each run avoided large pressure changes with their considerable thermal effects and the hazard of driving the silicone into the capillary tubing leading to the gas thermometers.

Next, the stopcock between the two gas thermometers was closed. The level difference Δh in the U-tube was measured with a cathetometer as a function of time and, when it appeared to be changing linearly,[4] the current was switched from the dummy heater to the heater in the plunger. After the U-tube reading again varied linearly with time, the heater current and the new thermocouple voltage were noted. Then the current was switched back to the dummy heater. The heater resistance was measured with a small current that was turned off as soon as possible. The U-tube readings were then noted for as long as necessary for a satisfactory interpolation to fix the zero reading to be subtracted from the last reading taken with the heater on, in order to determine the change $\delta\Delta h$ arising from the heater power.

Except at a boiling point or near the critical point, the rate at which the conductivity was changing was slow compared to the 10 to 150 sec thermal time constant of the apparatus.

The heat flowing from the plunger to the barrel is $\lambda_u \Delta T A/L$, where A/L is the geometrical constant of the apparatus and λ_u is the thermal conductivity, uncorrected for series and parallel thermal resistances. The heat balance for the plunger is

$$\lambda_u A \Delta T/L - P + C dT_p/dt = 0,$$

where C is the heat capacity of the plunger, T_p is its temperature, t is time, and P is the power supplied to the heater. If the operator δ signifies the change in steady-state value brought about by a change δP in heater power,

$$\lambda_u A \delta\Delta T/L - \delta P + C\delta(dT_p/dt) = 0.$$

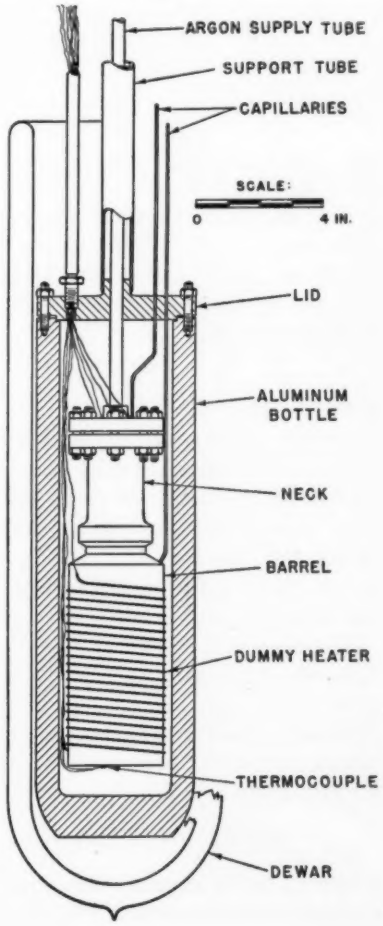

FIG. 2. Cryostat.

[4] The linear variation of the U-tube reading was in the direction and of the order of magnitude expected on account of the difference in thermometer volumes.

TABLE I. Thermal conductivity of argon.

Reduced pressure (nominal)	Pressure atmos	Temperature °K	Thermal conductivity cal/°C-cm-sec
2	96.1	90.3	29.0 $\times 10^{-5}$
	96.0	96.3	27.8
	95.9	109.7	24.5
	95.9	124.4	20.9
	95.8	140.6	16.8
	95.8	149.1	14.63
	95.8	158.9	12.15
	95.8	167.7	9.52
	95.8	174.1	8.36
	95.8	182.8	6.81
	95.8	189.7	6.10
$1\frac{1}{2}$	72.0	159.0	10.82
	72.0	167.1	8.32
4/3	64.2	137.5	16.63
	64.2	142.0	15.47
	64.2	153.0	12.12
	64.2	159.2	9.41
	64.7	167.8	5.57
	64.7	173.3	4.87
	64.7	179.0	4.30
	64.7	188.0	4.10
	64.7	193.8	4.09
1	47.9	91.3	28.7
	48.1	105.8	25.1
	48.1	112.3	23.2
	48.1	124.4	19.8
	48.1	128.3	18.9
	48.1	136.7	16.3
	48.2	137.7	16.2
	48.1	145.7	13.88
	48.1	150.7	9.10
	48.0	155.4	4.89
	48.0	165.5	4.07
	47.8	169.2	3.87
	48.0	173.6	3.80
	47.6	178.5	3.76
	48.0	187.5	3.54
	47.9	188.3	3.60
$\frac{7}{8}$	42.2	126.6	18.7
	41.4	134.7	16.7
	42.0	145.3	13.6
	42.0	146.5	13.1
$\frac{3}{4}$	36.2	122.2	20.2
	36.0	129.9	17.8
	36.1	140.4	14.44
$\frac{1}{2}$	23.6	89.0	28.9
	23.3	89.1	28.8
	23.6	97.9	26.7
	23.6	99.0	26.1
	23.6	109.3	23.6
	23.5	109.5	23.4
	23.4	119.1	20.7
	23.9	126.3	18.5
	23.9	133.1	16.4
	23.3	134.9	2.94
	23.0	147.2	2.66
	23.4	154.0	2.70
	23.2	164.3	2.71
	23.1	189.8	2.86
$\frac{1}{16}$	2.97	86.6	29.8
	2.97	87.7	29.1
	2.97	94.3	27.5
	2.97	98.7	26.4
0.02	0.98	176.4	2.39
	0.98	184.2	2.42
	0.98	191.7	2.65

In the procedure described above, P is initially zero, so δP is just the power supplied to the heater when it is turned on. In the time it takes to make the determination, the change in the steady-state value of $C(dT_p/dt)$ is negligible, so that

$$\lambda_u = L\delta P/A\delta\Delta T.$$

If the dummy heater had not been used, a correction of 1 percent to 10 percent would have been required because the warming-up rate would have been increased by turning the heater on; also, because of the relatively poor thermal conductivity of the glycerine around the barrel, the time for $C(dT_p/dt)$ to reach its steady-state value after the heater was turned on or off would have been unduly long.

The change in temperature difference was calculated from the dimensions and temperatures of the various parts of the apparatus and the observed change in level difference. The following formula represents these calculations within 0.2 percent up to 150°K and within 0.4 percent up to 200°K:

$$\delta\Delta T/\delta\Delta h = 0.0790T_0/H + 2.50\times 10^{-7}T^2,$$

where T_0 is the absolute temperature at which the gas thermometer system was bled to the atmosphere, H is the pressure at that time in mm Hg at 27°C, and T is the absolute temperature at the time $\delta\Delta h$ was measured. The temperatures are in °K.

The procedure for nitrogen was similar except that the thermal conductivity was also determined during the latter part of the period of soaking in liquid nitrogen. Some argon runs were tried with the space between the barrel and the aluminum bottle used for a thermostat bath; a second cylinder of argon was connected to this space during the cooling process, which required several extra liters of liquid nitrogen. After the warming-up began, the thermostat bath was connected to the atmosphere. The temperature arrest at the boiling point lasted about an hour and a half. However, the zero reading of the gas thermometers would meander to the extent of one or two thousandths of a degree in the time it took to make a determination.

The extraneous heat conduction in parallel with the argon gap was determined by measuring the thermal conductivity of nitrogen gas at 1 atmos and subtracting the values obtained by Eucken.[5] The thermal resistance in series with the argon gap was determined by filling the gap with Wood's metal.

[5] A. Eucken, Physik. Z. **12**, 1101 (1911).

The thermocouple voltage measurements were made with a Type K-2 potentiometer; the calibration of the thermocouple wire was checked against the freezing point of argon. The potentiometer and standard resistors were used to measure heater power.

Expressed as probable errors, the precision and expected accuracy of the reported results are, respectively: thermal conductivity, 0.5 percent and $2\frac{1}{2}$ percent; temperature, 0.2° and 0.5°; pressure, 0.5 percent and 0.7 percent.

RESULTS

The thermal conductivity λ of argon is given in Table I, from which Fig. 3 was prepared. Constant pressure curves are labeled with the corresponding reduced pressures.

The shaded region shows where convection is possible according to accepted ideas of heat transfer. The basis for this prediction of a convection region is a dimensional analysis of experiments on free convection between vertical plates. It is customary to use as dimensionless parameters the Grashof number

$$\mathrm{Gr}=\beta g\rho^2 L^3\Delta T/\mu^2,$$

where β is the cubical thermal expansion coefficient, g is the acceleration of gravity, ρ is the density, L is the thickness of the liquid film, ΔT is the temperature difference, and μ is the viscosity, and the Prandtl number

$$\mathrm{Pr}=c_p\mu/\lambda,$$

where c_p is the specific heat at constant pressure (per unit mass).

The assumption that inertial forces are negligible in comparison to viscous forces implies that the criterion for the importance of convection is the value of the product GrPr.[6] A considerable accumulation of engineering data[7,8] shows that very little, if any, convection occurs when this product is less than about 700. In a more complete dimensional analysis, the ratio of the height of the plates to the width of the gap between them would have to be considered. The experiments on convection do not extend to as large a value of this ratio as exists in the present apparatus, but their trend shows that the tendency toward convection decreases slowly as the ratio is increased.

The hard sphere theory, below, indicates that a conservative estimate of the viscosity can be obtained from the relation $\mu=4m\lambda/15k$, where m is the mass of a molecule and k is Boltzmann's constant. The density, expansion coefficient, and specific heat were estimated from the thermodynamic properties of hydrocarbons at corresponding states.[9] Although the value of GrPr calculated in this way for a given point cannot be expected to be very accurate, the boundary of the shaded region in Fig. 3 is fairly well defined, because of the rapid variation in expansion coefficient and specific heat.

Three constant volume lines are drawn in Fig. 3. The one in the vicinity of 90°K is based on a thermal pressure, i.e., $(\partial p/\partial T)_v$, of 25 atmos/°K.[10] The other two

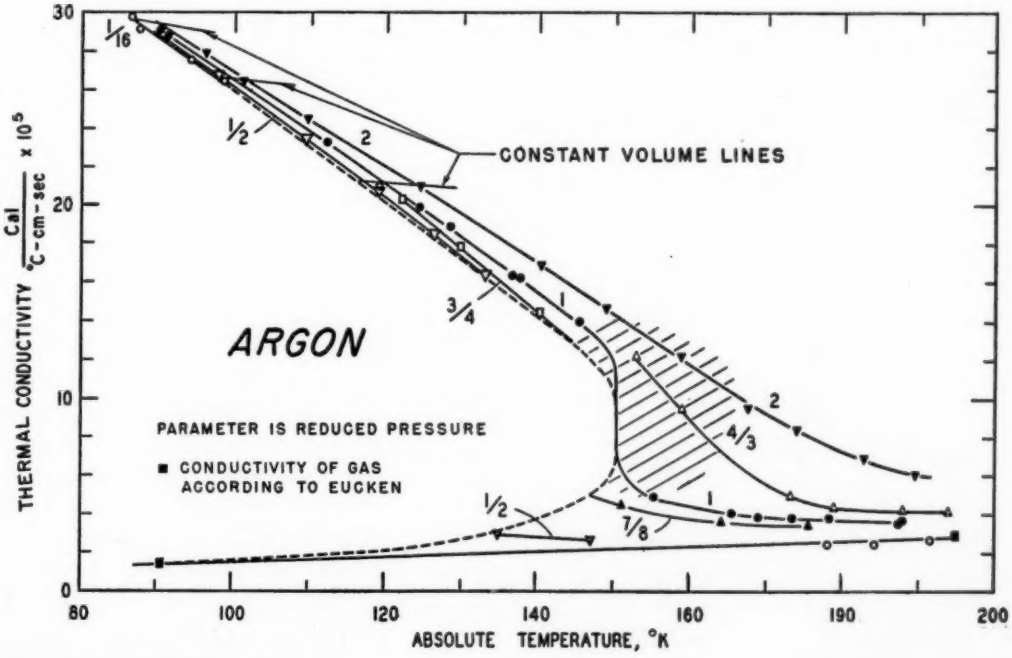

FIG. 3. Thermal conductivity of argon. Pressures are expressed in multiples of the critical pressure, 48 atmos. The dashed line represents extrapolations of constant pressure lines to the saturation temperatures.

[6] W. Nusselt, Z. Ver. deut. Ing. **73**, 1475 (1929).
[7] H. Kraushold, Forsch. Gebiete Ingenieurw. **5**, 186 (1934).
[8] M. Jakob, *Heat Transfer* (John Wiley & Sons, Inc., New York, 1949), pp. 534–542.
[9] W. C. Edminster, Ind. Eng. Chem. **30**, 352 (1938).
[10] F. Simon and F. Kippert, Z. physik. Chem. **135**, 113 (1929).

lines were obtained from the p-v-T diagram given by Rice[11] and based on the densities of the liquid at the vapor pressure and Bridgman's data[12] for much higher pressures than those used in the present experiments.

The thermal conductivity of nitrogen is given in Table II and plotted in Fig. 4. Corresponding values obtained by interpolation (and some extrapolation) from Borovik's graphs[13] are also shown. The errors of interpolation are less than the largest differences, which occur at twice the critical pressure and at the critical and somewhat higher temperatures. For the present apparatus, convection is likely in this region, as in the corresponding region for argon (the shaded area in Fig. 3). However, the discrepancies are probably due in part to an overcorrection applied by Borovik. He had noticed that the apparent thermal conductivity was an increasing function of the temperature difference used in the measurement, especially in this region, and made a linear extrapolation to zero temperature difference to obtain his reported values. His values in this region are therefore apt to be too low, as a unique thermal conductivity is usually found for temperature differences below a certain finite value.[14]

The apparent convection acknowledged by Borovik is particularly noteworthy since he used the desirable arrangement of causing the heat to flow downward through a layer of sample. The thickness of this layer and the temperature differences used were such that the values of the GrPr product were about 10^3 times those for the present apparatus, but the two arrangements cannot be directly compared.

TABLE II. Thermal conductivity of nitrogen.

Reduced pressure	Pressure atmos	Temperature °K	Thermal conductivity cal/°C-cm-sec
2	67.6	76.9	34.0 $\times 10^{-5}$
	67.0	83.3	31.8
	67.0	89.8	29.6
	66.9	100.7	25.7
	66.9	114.5	20.3
	67.0	127.2	16.3
	67.2	142.1	11.0
	67.2	169.0	6.41
	67.3	184.3	5.97
1	33.5	76.6	33.2
	33.5	88.7	29.2
	33.5	97.3	25.6
	33.3	111.0	20.1
	33.3	121.6	15.6
	33.3	132.6	5.06
	33.3	143.4	4.54
	33.3	154.2	4.38
0.25	8.2	76.4	33.1
0.17	5.8	77.2	32.3
0.33	10.9	91.8	27.0
1.15	38.4	107.2	22.3
1.16	38.7	121.3	16.5

[11] O. K. Rice, J. Chem. Phys. **14**, 324 (1946).
[12] P. W. Bridgman, Proc. Am. Acad. Arts Sci. **70**, 1 (1935).
[13] E. Borovik, J. Phys. (U.S.S.R.) **11**, 149 (1947).
[14] See reference 3, Fig. 8.

Hammann[15] measured the thermal conductivity of liquid nitrogen up to the normal boiling point, but there his value is 50 percent higher than that obtained in the present experiment. The practically negligible temperature dependence that he reported is also at variance with the present results. Since the latter are in substantial agreement with those of Borovik, it seems probable that Hammann's values are inaccurate.

HARD SPHERE MODEL

A. Argon

As a model of a liquid, one can take a dense gas o hard spheres in a uniform potential well. The diameter σ of the spheres and the depth of the well can be defined in terms of thermodynamic properties of the real liquid and will then be functions of temperature and the volume v per molecule. The model constructed in this way can be used to calculate the thermal conductivity.

Enskog has solved the thermal conduction problem for hard spheres in terms of a factor χ representing the increased probability of a collision in a dense gas.[16] This factor can be obtained from the equation of state for a hard sphere gas through the relation

$$p^*v/kT=1+b\rho\chi, \tag{1}$$

where p^* is the pressure for the hard sphere gas (not the pressure on the real liquid) and $b\rho=2\pi\sigma^3/3v$. The equation for the thermal conductivity is

$$\lambda=1.02513\frac{25}{32}\left(\frac{\pi k^3T}{m}\right)^{\frac{1}{2}}\frac{\sigma}{v}\left[\frac{1}{b\rho\chi}+\frac{6}{5}+0.7574b\rho\chi\right]. \tag{2}$$

In order to obtain σ and $b\rho\chi$ from the measured thermodynamic properties, one needs the statistical mechanics of a dense gas of hard spheres. Even for this idealized model, arbitrarily exact solutions are not available. The free volume concept[17,18] provides a starting point for making approximations.

For both liquid and gas, the free volume v_f per molecule will be defined in terms of the classical partition function Q by

$$Q=\{Nv_f(2\pi mkT/h^2)^{\frac{3}{2}}\exp[(\bar{\epsilon}-E)/kT]\}^N/N!, \tag{3}$$

where m is the mass and $\bar{\epsilon}=3kT/2$ the average kinetic energy per molecule, N is the number of molecules, and NE is the average energy of the system. The depth of the uniform potential well is thus $\bar{\epsilon}-E$. The definition (3) is equivalent to the assumption of a communal entropy of Nk. This assumption can be examined only in terms of the method chosen for relating v_f to the specifications of the hard sphere gas. For a given

[15] G. Hammann, Ann. Physik [5] **32**, 593 (1938).
[16] S. Chapman and T. G. Cowling, *The Mathematical Theory of Non-Uniform Gases* (Cambridge University Press, London, 1939), Chapter 16.
[17] H. Eyring and J. Hirshfelder, J. Phys. Chem. **41**, 249 (1937).
[18] J. E. Lennard-Jones and A. F. Devonshire, Proc. Roy. Soc. (London) **163A**, 53 (1937); **169A**, 317 (1938); **170A**, 464 (1939).

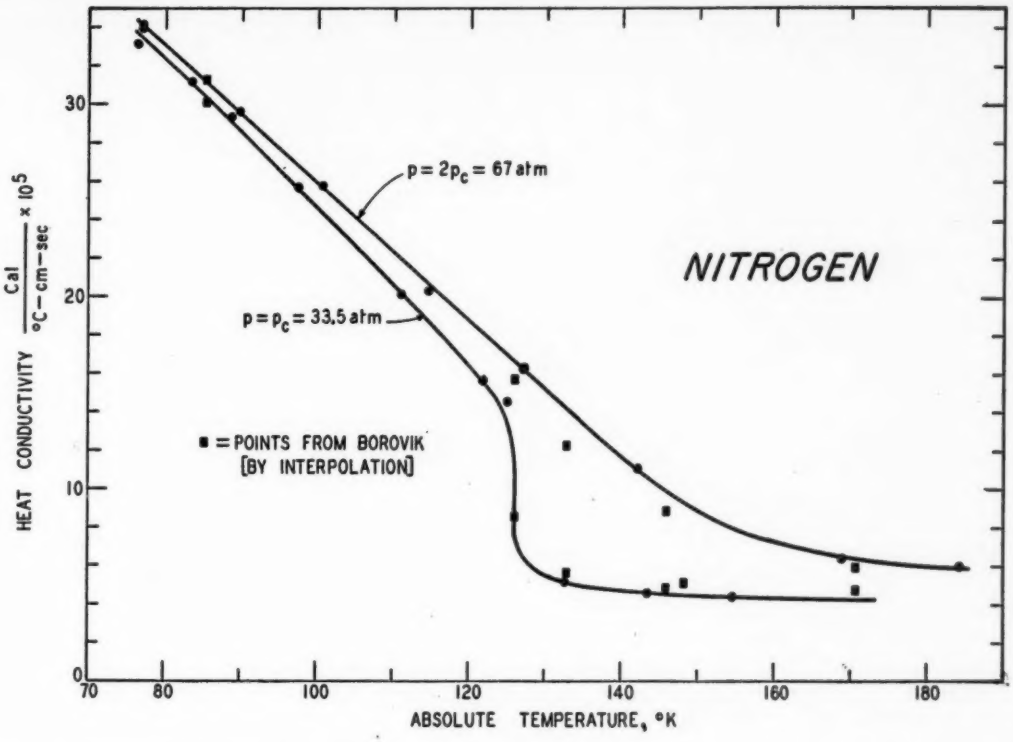

FIG. 4. Thermal conductivity of nitrogen for reduced pressures of 1.00 and 2.00; comparison with Borovik's results. (See reference 13.)

method, however, there are differences of opinion on the amount of communal entropy.[19,20]

The liquid free volume that will be used here is obtained by considering the molecules arranged in a close-packed lattice and calculating the volume that can be traced out by the center of one molecule when the other molecules are fixed in place. A further condition that affects only the calculation for 141.6°K is that the center is not allowed to leave the dodecahedron of volume v centered on the lattice point and whose faces are perpendicular bisectors of the lines between lattice points. Tables of this "exact free volume" have been published recently.[21] Similar compilations for other lattices, e.g., body-centered cubic, would be desirable, since x-ray studies[22] indicate that the number of nearest neighbors in liquid argon is less than the value 12 corresponding to close packing. However, the calculation of the thermal conductivity from measured thermodynamic properties is expected to be rather insensitive to the choice of lattice.

Experimental values of the heat of vaporization ΔH and the volume v_g of the saturated vapor and v_l of the coexisting liquid (per molecule) enable one to carry through the above program and calculate the thermal conductivity of the coexisting liquid. The free volume v_{fl} of the liquid is given by

$$v_{fl}=v_{fg}\exp(-\Delta H/kT), \tag{4}$$

where v_{fg} is the free volume of the saturated vapor and will be taken as

$$v_{fg}\cong v_g-kT_c/8p_c, \tag{5}$$

as suggested by the reduced Van der Waals equation, where T_c is the critical temperature and p_c is the critical pressure. Except within a few degrees of the critical temperature, $v_g \gg kT_c/8p_c$, so that Eq. (5) will not limit the accuracy of any of the calculations made here.

If directly measured values of ΔH are not available, and they are not for argon except at the normal boiling point, ΔH can be obtained from measurements of the vapor pressure p_s according to the Clausius-Clayperon equation

$$\Delta H/T=(v_g-v_l)(dp_s/dT). \tag{6}$$

However, much more accurate vapor densities are required when this equation is used than when the vapor density enters only in Eq. (5).

Table III shows that the experimental results for the thermal conductivity are in reasonably good agreement with the hard sphere model, even when quantum-mechanical effects are neglected. The calculated molecular diameters are fairly constant and their slow decrease with increasing temperature is what one would expect from the closer approach possible for more energetic molecules. The vapor pressure equation given by

[19] O. K. Rice, J. Chem. Phys. **6**, 476 (1938); **12**, 1 (1944); **14**, 348 (1946). Rice obtains a communal entropy of $3Nk$ for a free volume about $\frac{1}{3}$ of the "cage" free volume. Since $e^3 \cong 8$, his conclusions support the use of Nk with the cage free volume.

[20] J. A. Pople, Phil. Mag. **42**, 459 (1951).

[21] Buehler, Wentorf, Jr., Hirshfelder, and Curtis, J. Chem. Phys. **19**, 61 (1951). Their "soft-center" free volumes were used.

[22] A. Eisenstein and N. S. Gingrich, Phys. Rev. **62**, 261 (1942).

TABLE III. Theoretical and experimental thermal conductivities of liquid argon.

Temperature, °K	87.3	90.0	97.8	112.0	122.4	137.7	141.6
$10^5\lambda_{exp}$, cal/°C-cm-sec	29.1	28.7	26.5	22.5	18.3_5	14.9	13.8
N_0v_l, cc/mole[a]	28.5	29.1	30.2	32.7	35.1	41.1	43.6
N_0v_{fl}, cc/mole	0.86[b,c]	1.08[c]	1.5[c]	2.7[c]	4.1	9.3	11.0
Kincaid and Eyring formula							
Eq. (8), $10^5\lambda_{calc}$	21.8	18.6	17.5	15.5	14.4	10.9	10.3
$\lambda_{calc}/\lambda_{exp}$	0.75	0.65	0.66	0.69	0.78	0.73	0.75
Hard sphere model and classical mechanics							
Diameter σ, angstroms	3.44	3.43	3.40	3.34	3.34	3.28	3.30
$b\rho\chi$	5.74	5.32	4.77	3.97	3.50	2.80	2.75
Eq. (2), $10^5\lambda_{calc}$	26.4	24.5	22.5	19.5	17.6	13.9	13.2
$\lambda_{calc}/\lambda_{exp}$	0.91	0.85	0.85	0.87	0.96	0.93	0.95
Eq. (7), $10^3\mu_{calc}$, poise	1.30	1.22	1.12	1.05	0.85	0.67	0.62
$10^3\mu_{exp}$	2.52						
Hard sphere model and quantum mechanics							
$10^5\lambda_{calc}$	29.9	27.4	24.8	21.1	18.7	14.5	13.8
$\lambda_{calc}/\lambda_{exp}$	1.03	0.96	0.94	0.94	1.02	0.98	1.00
$10^3\mu_{calc}$	1.38	1.29	1.18	1.09	0.88	0.69	0.63
Diameter σ, angstroms	3.40	3.39	3.36	3.31	3.31	3.25	3.27

[a] N_0 = Avogadro's number.
[b] Based on measured $N_0\Delta H = 1557.5$ cal/mole. (See reference 26.) All other values of v_{fl} were calculated from vapor density and pressure.
[c] Vapor densities obtained by extrapolation (see text).

Crommelin[23] and the liquid and vapor densities[23,24] measured by Mathias and Crommelin were used, with the following exceptions: Below 122.4°K, there are no measurements of the density of the saturated vapor, so these densities were calculated from a Van der Waals type of equation with an attractive constant a of 1.6 atmos (liters/mole)^2, which agrees fairly well with measured densities[25] of slightly superheated vapor. For 87.3°K, the measured heat of vaporization[26] and Baly and Donnan's liquid density were used.

Enskog's theory enables one to predict the viscosity μ in the same way as the thermal conductivity. His equation is

$$\mu = 1.016\frac{5}{24}(\pi mkT)^{\frac{1}{2}}\frac{\sigma}{v}\left[\frac{1}{b\rho\chi}+\frac{4}{5}+0.7614b\rho\chi\right] \quad (7)$$

and the results of the calculation are given in Table III; the agreement with experiment[27] is much less satisfactory than for thermal conductivity. The existence of more recent viscosity measurements on liquid argon and nitrogen is indicated by abstracts,[28] but we have not succeeded in obtaining the article in question. The abstracts indicate that most of the measurements were for nitrogen and that the results for argon are not extensive enough to check the predictions in Table III. It is interesting to note that the predicted viscosity values agree with the value 1.27×10^{-3} poise calculated by Kirkwood, Buff, and Green[29] for argon at 89°K, using a Lennard-Jones potential and a radial distribution function adjusted to give the measured heat of vaporization.

A simple relation between thermal conductivity and free volume was proposed by Kincaid and Eyring.[30] Their general equation for both monatomic and polyatomic substances is

$$\lambda = (1/12)(9\gamma'-5)v_l^{-\frac{1}{3}}(8kT/\pi m)^{\frac{1}{2}}(v_l/v_{fl})^{\frac{1}{3}}\alpha c_v, \quad (8)$$

where c_v is the specific heat per molecule in the gas, α is an accommodation coefficient to correct for the degrees of freedom that do not fully contribute to the thermal conduction, and γ' is the specific heat ratio for thermal conduction in the gas. The factor $(8kT/\pi m)^{\frac{1}{2}}$ is the average velocity $\bar{u}$. For a monatomic substance, the *a priori* values of γ' and αc_v are 5/3 and $3k/2$ and lead to the first set of λ_{calc} values in Table III. It is evident that a numerical factor of 1.2 would make the Kincaid and Eyring equation a good approximation to the more lengthy calculations based on Enskog's theory and the free volume for a close-packed lattice.

It is conceivable that an approximation to the translational motion of a molecule in a liquid can be obtained from the quantum mechanics of a particle in a box of volume v_f. In estimating a correction for the foregoing classical calculation of the thermal conductivity, it will be convenient to assume that

$$\lambda \propto \langle u\rangle_{Av}v_{fl}^{-\frac{1}{3}}c_v \quad (9)$$

as suggested by Eq. (8). The c_v in Eq. (9) is the specific heat for the model, not for the real liquid.

For the sake of simplicity, the free volume will be taken as cubical in shape; the partition function then shows that it is sufficient to consider the one-dimensional problem of a uniform potential well of width $v_{fl}^{\frac{1}{3}}$. The

[23] *International Critical Tables* (McGraw-Hill Book Company, Inc., New York, 1928), Vol. III.
[24] Landolt-Bornstein, Tabellen (Julius Springer, Berlin, 1923), Vol. I.
[25] J. Y. Oldshue, thesis, Illinois Inst. of Technology (1949).
[26] A. Frank, Z. physik. Chem. **42**, 395 (1939).
[27] N. S. Rudenko and L. W. Schubikow, Physik. Z. Sowjetunion **6**, 470 (1934).
[28] B. I. Verkin and N. S. Rudenko, J. Exptl. Theor. Phys. (U.S.S.R.) **20**, 521 (1950); Chem. Abs. **44**, 8721 (1950); Brookhaven National Laboratory, Guide to Russian Scientific Literature **4**, 82 (1951); Science Abs. **53A**, 980, No. 8518 (1950).
[29] Kirkwood, Buff, and Green, J. Chem. Phys. **17**, 988 (1949).
[30] J. F. Kincaid and H. Eyring, J. Chem. Phys. **6**, 620 (1938).

one-dimensional partition function for kinetic energy is[31]

$$z=\sum_{\nu=1}^{\infty}\exp[-\pi(\nu/2q)^2],$$

where

$$q=(2\pi mkTv_{fl}^{\frac{2}{3}}/h^2)^{\frac{1}{2}}. \tag{10}$$

The Euler-Maclaurin summation formula[31] gives the following approximations:

$$\begin{aligned}
&\sum_{\nu=1}^{\infty}\exp[-\pi(\nu/2q)^2]\cong q-\tfrac{1}{2},\\
&\sum_{\nu=1}^{\infty}\nu\exp[-\pi(\nu/2q)^2]\cong(2q^2/\pi)-(1/12)\cong(2q^2/\pi),\\
&\sum_{\nu=1}^{\infty}\nu^2\exp[-\pi(\nu/2q)^2]\cong 2q^3/\pi,\\
&\sum_{\nu=1}^{\infty}\nu^4\exp[-\pi(\nu/2q)^2]\cong 12q^5/\pi.
\end{aligned} \tag{11}$$

For argon at 87.3°K, $q=3.8$ and direct summations agree very well with Eqs. (11), which are therefore valid for all higher temperatures and larger free volumes. Thus, all the sums can be replaced by their classical values except the partition function itself, which is decreased by a factor $\beta^{-1}=1-\frac{1}{2}q^{-1}$. Therefore the average velocity, the average kinetic energy, and the average square of the energy are increased by a factor β. The specific heat

$$\begin{aligned}
mc_v&=k(\partial/\partial T)T^2(\partial\ \ln z/\partial T)\\
&=k\pi^2[\langle\nu^4\rangle_{Av}-(\langle\nu^2\rangle_{Av})^2]/16q^4\\
&\cong\tfrac{1}{2}k[1+1/4q]\cong\tfrac{1}{2}k\beta^{\frac{1}{3}}
\end{aligned} \tag{12}$$

is increased by a factor $\beta^{\frac{1}{3}}$.

For a given model, then, quantum mechanics gives a thermal conductivity that is larger by a factor $\beta^{\frac{2}{3}}$, because of the increased average velocity and specific heat. However, quantum mechanics affects the construction of the model from the entropy of vaporization. The appropriate modifications of Eq. (3) decrease $v_{fl}^{-\frac{1}{3}}$ by a factor

$$1/\beta\exp[\tfrac{1}{2}(\beta-1)]\cong\beta^{-\frac{1}{3}}. \tag{13}$$

The net correction to be applied to the classical calculation is

$$\beta^{\frac{2}{3}}\beta^{-\frac{1}{3}}=\beta\cong 1+1/2q. \tag{14}$$

Table III shows that this correction brings the calculated thermal conductivities as close to the measured values as the inconsistencies in the thermodynamic data will permit, since the unsystematic deviations that remain can hardly be the fault of the theory.

The correction, Eq. (13), results in slightly decreased molecular diameters. From Eq. (13) and the approximation[32]

$$v_f^{\frac{1}{3}}\cong 2(v^{\frac{1}{3}}-v_0^{\frac{1}{3}}), \tag{15}$$

where $v_0^{\frac{1}{3}}=2^{-1/6}\sigma$ for close packing, one obtains the corrected σ values given in Table III.

In an attempt to repeat the above procedure for the case of viscosity, it was assumed that

$$\mu\propto\langle u\rangle_{Av}v_{fl}^{-\frac{1}{3}}, \tag{16}$$

which gives a net correction of $\beta^{\frac{1}{3}}$, or 7 percent at 87.3°K. But an increase of almost 100 percent would be required to obtain agreement with experiment, so that quantum mechanics cannot account for much of the difference if Eq. (16) is an adequate description of the model.

The unequal success of the hard sphere model for thermal conductivity and viscosity is not too surprising, since the viscosity becomes enormous on freezing, while the heat conductivity does not change in order of magnitude.[33] The faster-moving molecules, for which the hard sphere model should be more suitable, are relatively more effective in thermal conduction than in momentum transport. One would expect the agreement for viscosity to improve rapidly as the free volume and temperature are increased. Viscosity measurements on nitrogen gas at high pressures agree well with Enskog's theory.[16]

B. Nitrogen

A reasonable model for liquid nitrogen would have to take into account its diatomic nature. Unfortunately, there is no rigorous theory of transport processes in dense gases except for hard spheres. A crude approach to the thermal conduction problem is suggested by Eucken's success, for gases, with the assumption that the translational and rotational conductivities are additive.[34]

The translational conductivity is exceptional in that the quantity transported, translational kinetic energy, is correlated with the velocity of transport; this "persistence of velocity" is automatically included in Enskog's theory for hard spheres. The transport of momentum and rotational kinetic energy are not affected by persistence of velocity, so that an estimate of the rotational conductivity can be obtained from $(k/m)\mu$, since k is the rotational specific heat of a diatomic molecule.

A possible prescription for calculating the thermal conductivity of nitrogen is: proceed as if nitrogen were monatomic, i.e., exactly as for argon, and calculate the translational thermal conductivity λ_1 and the viscosity

[31] J. E. Mayer and M. G. Mayer, *Statistical Mechanics* (John Wiley & Sons, Inc., New York, 1940).

[32] Hirshfelder, Stevenson, and Eyring, J. Chem. Phys. **5**, 896 (1937), Eq. (15).

[33] Five measurements, with the present apparatus, of the thermal conductivity of solid argon at 77°K gave $(42\pm2)\times10^{-6}$ cal/°C-cm-sec. However, this value represents a lower limit because of the shrinkage of argon on freezing.

[34] A. Eucken, Physik. Z. **14**, 324 (1913).

TABLE IV. Theoretical and experimental thermal conductivities of liquid nitrogen.

Temperature, °K	78.1	100.0	119.5
$10^5\lambda_{exp}$, cal/°C-cm-sec	32.0	23.5	16.0
N_0v_l, cc/mole	34.8	40.8	52.5
N_0v_{fl}, cc/mole	1.04	3.39	12.9
Kincaid and Eyring formula			
Eq. (8), $10^5\lambda_{calc}$	27.8	20.1	12.9
$\lambda_{calc}/\lambda_{exp}$	0.87	0.85	0.81
Hard sphere model and classical mechanics			
Diameter σ, angstroms	3.69	3.62	3.52
$b\rho\chi$	5.77	3.95	2.76
Eq. (2), $10^5\lambda_1$	25.6	19.1	12.7
Eq. (7), $10^3\mu_1$, poise	0.90	0.65	0.43
Eq. (18), $10^5\lambda_{calc}$	32.0	23.7	15.1
$\lambda_{calc}/\lambda_{exp}$	1.00	1.01	0.94
$10^3\mu_{exp}$	1.54		
Hard sphere model and quantum mechanics			
$10^5\lambda_1$	29.6	20.9	13.4
$10^3\mu_1$	0.97	0.68	0.44
$10^5\lambda_{calc}$	36.5	25.7	16.5
$\lambda_{calc}/\lambda_{exp}$	1.14	1.10	1.03
Apparent free angle ratio, δ_2	0.70	0.77	0.91

μ_1 on the hard sphere model; then let

$$\lambda=\lambda_1+(k/m)\mu_1. \tag{17}$$

The results of such calculations are given in Table IV. Densities from reference 24 and the heats of vaporization selected by Wiebe and Brevoort[35] from the results of several investigators were used.

The experimental values of the thermal conductivity were obtained by extrapolation to the saturation pressure; their remarkable agreement with the values calculated on a classical basis must be regarded as coincidental if the quantum-mechanical corrections, which interfere with the agreement, are to be taken seriously. According to Raman spectra, the rotation of nitrogen may be restricted in the liquid,[36] in which case the free volumes calculated from Eq. (4) are too low by a factor δ_2, the free angle ratio.[30] The correction for this effect would be opposite to the quantum-mechanical corrections and might restore the agreement with experiment; the values of δ_2 that would be required are given in Table IV (solely for the sake of the present argument, as this procedure can hardly be regarded as a means of determining δ_2). They are sufficiently large that quantum-mechanical effects on the rotational energy levels can probably be neglected. The restricted rotation discussed here is to be distinguished from the more extreme variety in which the rotational degrees of freedom perform harmonic oscillations.

[35] R. Wiebe and M. J. Brevoort, J. Am. Chem. Soc. **52**, 622 (1930).

[36] G. Herzberg, *Spectra of Diatomic Molecules* (D. Van Nostrand Company, Inc., New York, 1950), second edition, p. 464.

It will be noted that Eq. (8), which is also based on the assumption of the additivity of translational and rotational thermal conductivities, gives a good approximation to the classical calculations if the right-hand side is multiplied by a factor 1.2. The *a priori* values 7/5 and $5k/2$ were used for γ' and αc_v in Eq. (8).

As in the case of argon, the calculated viscosity is only about half as large as the experimental value, obtained by a slight extrapolation of Rudenko's measurements.[7]

SUMMARY

The thermal conductivity of liquid argon has been measured and correlated with some of its thermodynamic properties under the following assumptions: (a) The atoms are equivalent to hard elastic spheres in a potential well; (b) the statistical mechanics of a dense gas of hard spheres can be approximated by using the free volume for a sphere in the cage formed by its neighbors in a close-packed lattice, along with a communal entropy of Nk; and (c) the energy levels of a sphere are those of a particle confined in the free volume.

Assumption (a) is unsatisfactory at high densities for calculating the viscosity, but thermal conduction appears to be a peculiarly favorable case. Viscosity measurements for somewhat lower densities of the liquid should be interesting.

If, instead of a close-packed lattice, a lattice with a lower coordination number were assumed in (b), the results of the calculations would probably not be altered by more than a few percent. The calculated thermal conductivity would be 25 percent too low if the communal entropy were neglected, so that, apart from the unevaluated error of assumption (a), a communal entropy of at least 80 or 90 percent of Nk is indicated by the experimental results.

The apparent experimental confirmation of assumption (c) is intriguing, but must be regarded as rather tenuous in view of assumptions (a) and (b).

ACKNOWLEDGMENTS

I wish to thank A. W. Lawson for his sponsorship in the Department of Physics and the Institute for the Study of Metals. Encouragement, advice, and assistance has also been received from L. Meyer, E. A. Long, R. W. Keyes, J. Hulm, L. Guttman, and R. Gomer of this Institute, L. Schwarcz and M. G. Mayer of the Institute for Nuclear Studies, and O. Teichman of the Armour Research Foundation.

The ONR assisted the construction of the apparatus, most of which was built by K. Lindholm and N. Nachtrieb.

Infrared and Raman Spectra of Fluorinated Ethanes. III. The Series CH_3-CF_3, CH_3-CF_2Cl, CH_3-CFCl_2, and CH_3-CCl_3*

D. C. SMITH AND GEORGE M. BROWN
Naval Research Laboratory, Washington, D. C.

AND

J. RUD NIELSEN, RAYMOND M. SMITH,† AND C. Y. LIANG
Department of Physics, University of Oklahoma, Norman, Oklahoma

(Received September 5, 1951)

New infrared spectra have been obtained for gaseous CH_3-CF_3 in the region 20–38μ, and in the region 2–38μ for gaseous CH_3-CF_2Cl and CH_3-CFCl_2, and CH_3-CCl_3 vapor and liquid, by use of LiF, NaCl, KBr, and KRS-5 optics. Raman spectra of gaseous and liquid CH_3-CF_2Cl and of CH_3-CFCl_2 and CH_3-CCl_3 in the liquid state have been obtained with a three-prism glass spectrograph of linear dispersion 15A/mm at 4358A. Depolarization ratios were obtained for all of the stronger Raman bands of the liquids.

The spectra are interpreted, a complete assignment of fundamental frequencies is proposed for each molecule, and thermodynamic functions are calculated for the temperature range 298–600°K and at the boiling point.

INTRODUCTION

COMPLETE knowledge of the fundamental vibration frequencies for all of the ethane derivatives listed in Table I is of considerable importance to a variety of problems and is the general aim of an experimental program currently under way. Because of certain advantages resulting from the study of *series* of closely related molecules, the compounds in Table I have been investigated as groups, one of which (No. 2) is treated in the present paper.

The assignment of fundamentals is based primarily upon selection rules, band contours, intensities, polarizations, etc., but also upon satisfactory correlation of the fundamentals with molecular structure through one or more groups of molecules. Such correlations are particularly important and useful in connection with molecules of low symmetry, whose spectra tend to become more complex and have less useful selection rules than those of highly symmetric molecules.

EXPERIMENTAL

Infrared measurements in the range from 2 to 22 μ were made with a large prism spectrometer of high resolution.[1] In the range from 20 to 38 μ a 26° KRS-5 prism was used in a Perkin-Elmer Model 12B spectrometer. Atmospheric water vapor bands were used for calibration of the latter,[2] and checks were provided by a number of sharp bands of certain fluorinated aromatic hydrocarbons in the liquid state common to both infrared and Raman spectra. The resolution obtained with KRS-5 was rather poor, however, so that the positions of sharp bands are probably accurate to no more than ± 2 cm^{-1}. Also, considerable uncertainty is involved in the observation of very weak bands in this region. Liquids were examined between KRS-5 plates separated by Teflon spacers of from 0.01- to 1.8-mm thickness, and gases were studied in 10-cm Pyrex cells with 0.001-in. polythene windows.[3]

All Raman spectra were photographed by means of a three-prism glass spectrograph of linear dispersion 15A/mm at 4358A. The instrument and irradiation apparatus have been briefly described elsewhere.[4]

The sample of CH_3-CF_3 studied previously[5] was used for the additional measurements on this compound. Two samples of CH_3-CF_2Cl, both commercial materials, were studied. That for which vapor state

TABLE I. Groups of related ethane derivatives.

Group No. 1	No. 4	No. 7
CH_3-CH_3	CF_3-CH_3	CCl_3-CH_3
CH_3-CH_2F	CF_3-CH_2F*	CCl_3-CH_2F*
CH_3-CHF_2	CF_3-CHF_2	CCl_3-CHF_2*
CH_3-CF_3	CF_3-CF_3	CCl_3-CF_3
Group No. 2	**No. 5**	**No. 8**
CH_3-CF_3	CF_3-CF_3	CCl_3-CF_3
CH_3-CF_2Cl	CF_3-CF_2Cl	CCl_3-CF_2Cl
CH_3-CFCl_2	CF_3-CFCl_2	CCl_3-CFCl_2
CH_3-CCl_3	CF_3-CCl_3	CCl_3-CCl_3
Group No. 3	**No. 6**	**No. 9**
CH_3-CH_3	CF_3-CH_3	CCl_3-CH_3
CH_3-CH_2Cl	CF_3-CH_2Cl	CCl_3-CH_2Cl
CH_3-CHCl_2	CF_3-CHCl_2	CCl_3-CHCl_2
CH_3-CCl_3	CF_3-CCl_3	CCl_3-CCl_3

* Not available.

* This work has been supported by Contract N7-onr-398, T. O. I., with the ONR and by Contract AT-(40-1)-1074 with the AEC. It was presented in part at the Symposium on Molecular Structure and Spectroscopy held at Ohio State University, June 11–15, 1951. The results for CH_3-$CFCl_2$ are taken from a thesis presented by Raymond M. Smith to the faculty of the Graduate College of the University of Oklahoma in partial fulfillment of the requirements for the degree of Doctor of Philosophy.

† Present address: Battelle Memorial Institute, Columbus, Ohio.

[1] Nielsen, Crawford, and Smith, J. Opt. Soc. Am. **37**, 296 (1947).
[2] Randall, Dennison, Ginsburg, and Weber, Phys. Rev. **52**, 160 (1937).
[3] E. K. Plyler, J. Research Natl. Bur. Standards **41**, 125 (1948).
[4] Smith, Nielsen, and Claassen, J. Chem. Phys. **18**, 326 (1950).
[5] Nielsen, Claassen, and Smith, J. Chem. Phys. **18**, 1471 (1950).

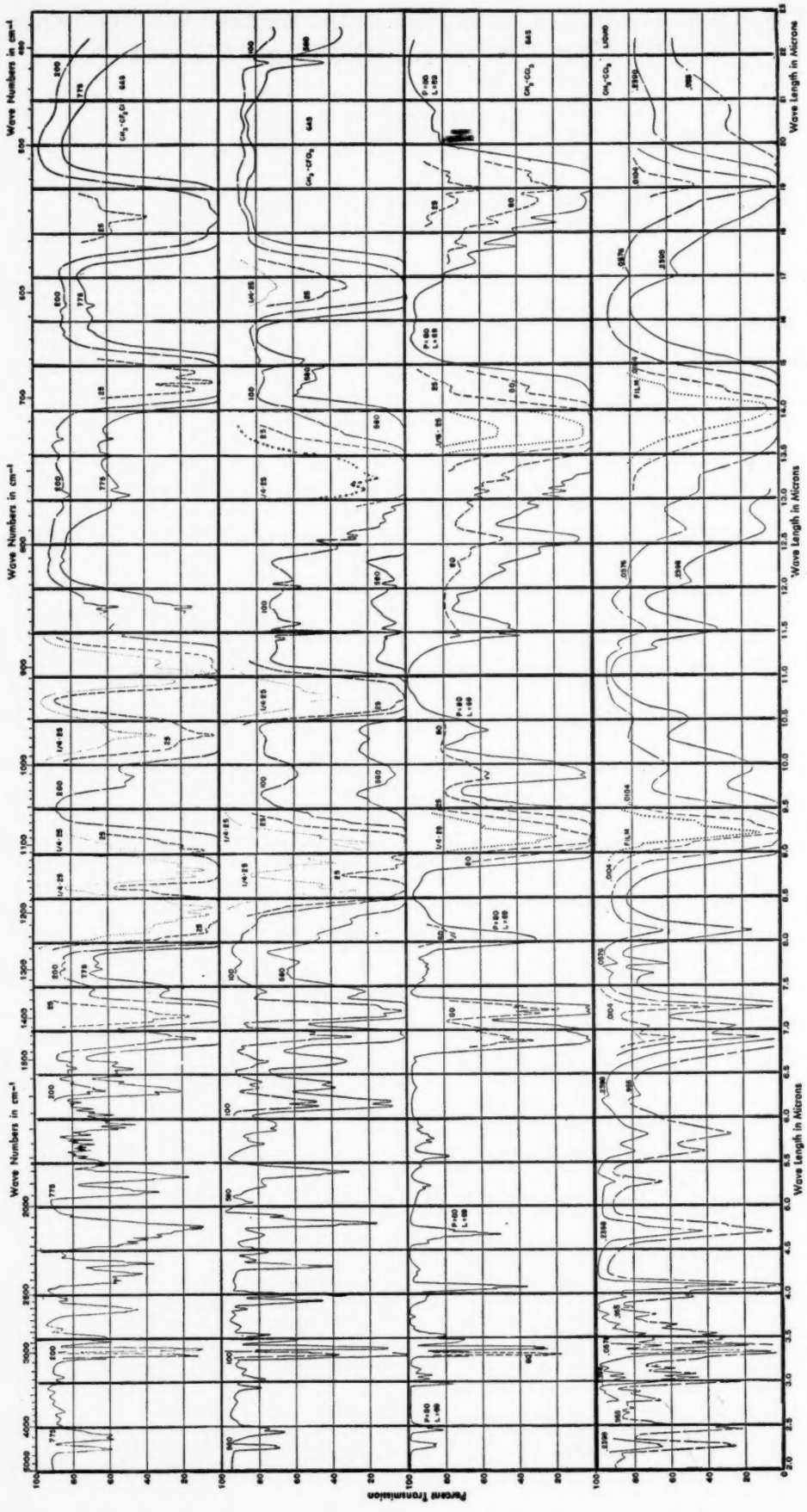

FIG. 1. Infrared spectra of CH_3-CF_2Cl (gas), CH_3-CFCl_2 (gas), CH_3-CCl_3 (gas), and CH_3-CCl_3 (liquid). Vapor pressures are indicated in mm Hg. The cell thickness is 10 cm except for the curve marked $L=69$ for CH_3-CCl_3. The thickness of the liquid cell is given in mm.

TABLE II. Infrared and Raman spectra of CH_3-CF_2Cl.

Infrared (gas) cm^{-1}	Raman (liquid)[a] cm^{-1}	Relative intensity	Depolarization	Interpretation
	144?	vvw		Spurious?
	166?	vvw		Spurious?
~ 295				
305 vs, sh	309	5	(0.6±0.15)	A' fundamental
314				
334 s, sh	335	7	(0.7±0.15)	A'' fundamental
~ 348				
	429 sh	10		A' fundamental, Cl37
~ 435 s	435 sh	33	(0.3)	A' fundamental, Cl35
~ 475 vw(?)				2×238=476?
	526	vvw		A'' fundamental?
~ 533				
543 s, sh	544 sh	8	(0.2)	A' fundamental
554				
~ 600				
611 vw, sh				2×305=610 A'
~ 622				
634 vvw				305+334=639 A''
673				
683 s, sh	679 sh	54	(0.13)	A' fundamental
692				
728				
730 vw, sh				305+430=735 A'?
740 vw				305+437=742 A'
760				
766 w				334+437=771 A'', 334+430=764 A''
~ 773				
811 vvw				Probably CH_3-CH_2F impurity
	827 sh	vw		CH_3-CF_3 impurity
~ 840				
~ 846				
847 w, sh	848	vvw		305+543=848 A'
851				
~ 862				2×430=860 A', or impurity
867 vw, sh	865	vvw		CH_3-CHF_2 impurity
870 vw, sh				334+543=877 A'' or 2×437=874 A'
895				
904 vs, sh	898	9	(0.45)	A' fundamental
912				
~ 955				
967 vs, sh	963 d	2	(0.9±0.1)	A'' fundamental
968				
~ 978				
1013 vw				334+683=1017 A''
1022				
~1060 vvw				CH_3-CH_2F impurity, or 1395−334=1061 A''
~1096				
1101				
1107 s, sh	1103	4	(0.3±0.1)	437+693=1120 A'
				A' fundamental
~1125				
1134 vs, sh	1127	7	(0.2±0.1)	
1143				
~1165				Probably CH_3-CHF_2 impurity
~1180				
1190 vs, sh	1202	0.5		A'' fundamental
1202 vs, sh				
1212	1210	0.5		305+904=1209 A'
1220				
1230 s, sh	1231	1		A' fundamental or 334+904=1238 A''
~1240				
1287				305+967=1272 A''?
1299 w				334+967=1301 A'
1340 w				435+904=1339 A'

[a] The following Raman bands were observed for the gas: 430 w, 437 m, 683 s, sh, 2962 vs, sh, and 3033 cm^{-1} w, d. A different, water-free sample was used for the liquid-state measurements.

TABLE II.—(*Continued*).

Infrared (gas) cm^{-1}	Raman (liquid)[a] cm^{-1}	Relative intensity	Depolarization	Interpretation
~1385				
1395 s, sh	1394	1		A' fundamental
1404				
~1438				
1447 m, sh	1446 d	10	(0.7±0.05)	A' and A'' fundamentals
~1451				
1506				543+967=1510 A''; 305+1196=1501 A''
1522 w, sh				334+1196=1530 A'
1534				305+1230=1535 A'
1541 w, sh				437+1107=1544 } or impurity
1560 w, sh				430+1134=1564 }
1577				
1585 m, sh				683+904=1587 A'
1592				
1600–1850				H_2O impurity bands
1672 w, sh				543+1134=1677 A'
~1695				305+1395=1700 A'
~1750				305+1447=1752
1783 w, sh				334+1447=1781
1808				2×904=1808 A'
1818				683+1134=1817 A'
1821 w, sh				430+1395=1825 A'
1825				437+1395=1832 A'
1873 m, sh				904+967=1871 A''; 430+1447=1877
1883				683+1196=1879 A''; 437+1447=1884
1934				2×967=1934 A'
2041 vvw, sh				904+1134=2038 A'
2096 m, sh }				904+1196=2100 A''
2105 m, sh }				967+1134=2101 A''
2116				683+1447=2130
2135				904+1230=2134 A'
2146				
2160				967+1196=2163 A'
2179				
2198				967+1134=2201 A''
2252 vvw				2×1134=2268 A'?
2299 w, sh				904+1395=2299 A'
2358 w, sh				904+1447=2351; 967+1395=2362 A''
2404				
2415 vw, sh				967+1447=2414
2421				
~2525 vw				1134+1395=2529 A'
2538				1107+1447=2544
~2611 w				1196+1395=2591 A''; 1230+1395=2625 A'
2770 w	2766 sh	6		2×1395=2790 A'?
2778				
~2850 w				1395+1447=2842
2890 w, sh				2×1447=2894 A'
~2955				
2965 m, sh	2956 sh	100	(0.13)	A' fundamental
2975				
~3017				
3026				
3035 s, sh	3025	32	(0.86)	A' and A'' fundamentals
3268 vw				305+2962=3267 A'
3333 vw				305+3034=3339
3460 vw				435+3034=3469
3585 vw				543+3034=3577
3745 vw				683+3034=3717?
3845 vw				904+3034=3866
4150 w				1196+2962=4158 A''; 1134+3034=4168
4240 w				1196+3034=4230
4445 w				1395+3034=4429

TABLE III. Infrared and Raman spectra of CH_3-CFCl_2.

Infrared (gas) cm^{-1}	Raman (liquid) cm^{-1}	Relative intensity	Depolarization	Interpretation
	256	18	(0.6)	A' fundamental
	295 d	6	(0.8)	A'' fundamental
376 s	376 sh	18	(0.05)	A' fundamental
	398 d	13	(0.8)	A'' fundamental
434 s	432 sh	18	(0.10)	A' fundamental
458 m, sh				$2\times229=458$ A', or impurity
~ 465				
~ 490 vvw?				$755-256=499$ A''?
~ 505 vvw, b?				$2\times256=512$ A'?
~ 545 vvw, b				$256+295=551$ A''
~ 586				
596 vs	590 sh	88	(0.05)	A' fundamental
~ 604				
662				
669 m, sh				$295+376=671$ A''
~ 678				
~ 683				
690				$256+434=690$ A'
696				$295+398=693$ A'
~ 722 vvw				
~ 727 vvw				$295+434=729$ A''?
~ 745				
755 vs, sh	745 vd	13	(0.86)	A'' fundamental
~ 762				
776				$376+398=774$ A''
784				
~ 788				
794 m, sh				$2\times398=796$ A'
796 m, sh				
~ 801				
~ 820				
826				$229+596=825$ A''?
831 m, sh				$398+434=832$ A''
~ 835				
~ 851				$256+596=852$ A'?
~ 854				
861 sh				
869 m, sh				$2\times434=868$ A'
874 sh				
~ 884				
~ 920				
929 vs, sh	921 d	6	(0.7)	A' fundamental
~ 936				
~ 971				CH_3-CF_2Cl impurity, or $376+596=972$ A'
~1000				
1011 m				$256+755=1011$ A''
~1020				
~1045				
~1060 vvw				CH_3-CH_2F impurity
~1070				
1088				
1096 vs, sh	1089 d	4	(0.7)	A' fundamental
1106				
1124 vs, sh	1113	6	(0.24)	A' fundamental
1130				
1156				
1164 vs, sh	1157 d	2	(0.9)	A'' fundamental
~1172				
~1185				$256+929=1185$ A''
~1190				CH_3-CF_2Cl impurity, or $434+755=1189$ A''
~1205				CH_3-CF_2Cl impurity, or $2\times596=1192$ A'
1217 w				$295+929=1224$ A''
1242 w				

TABLE III.—(*Continued*).

Infrared (gas) cm^{-1}	Raman (liquid) cm^{-1}	Raman (liquid) Relative intensity	Depolarization	Interpretation
1285 w				
~1302				376+929=1305 A'?
~1312				
1344 m				
~1350				596+755=1351 A'', or 256+1096=1352 A'?
~1373				
1385 s, sh	1386 d	2		A' fundamental
1395				
1416 vw				CH_3-CHF_2 impurity, or 256+1164=1420 A''
1433				
1443 s, sh	1441 d	11	(0.8)	A' and A'' fundamentals
~1451				
1471 vw				376+1096=1472 A'
1504 w				376+1124=1500 A'
1531 vw				434+1096=1530 A'
1560 w				434+1124=1558 A'
1575 w				398+1164=1562 A'
1616 m	1617 sh	4		229+1385=1614 A''? or impurity
1629 m				
~1695 w, b				596+1096=1692 A'
1704 w, sh				256+1443=1699
1730 vw				596+1124=1720 A'
1748 vw, sh				295+1443=1738
1852 m, sh				755+1096=1851 A'', or 2×929=1858 A'
~1908 w				755+1164=1919 A'
1980 w, sh				596+1385=1981 A'
2045 w, sh				596+1443=2039
~2052				929+1124=2053 A'
2079 m, sh				
~2087				929+1164=2093 A''
2141 w				755+1385=2140 A''
2208 vw, sh				755+1443=2198
2217 w, sh				1096+1124=2220 A'
2232 w, sh				2×1124=2248 A'?
2278 vw				1096+1164=2260 A'', or 1124+1164=2288 A''
2315 w, sh				929+1385=2314 A'
2500 w, sh				1124+1385=2509 A'
2545 w, sh				1164+1385=2549 A''
2611 vw, sh				1164+1443=2607
~2653 vw				
2755 vw	2750 sh	8	(0.1)	2×1385=2770 A'
2825 w, sh				1385+1443=2828
2874 w, sh				2×1443=2886 A'
2959 m, sh	2949 sh	100	(0.07)	A' fundamental
3010				
3016	3013	34	(0.8)	
3021 s, sh	3023	25		A' and A'' fundamentals
3086 vw				Impurity?
3185 vw				229+2959=3188 A''?
3300 w				256+3021=3277 or 295+3021=3316
3400 w				376+3021=3397
3600 vw				596+3021=3617
4030 w				1096+2959=4055 A'
4100 w				1096+3021=4117
4385 w				1385 or 1443+2959=4344 or 4402
4425 w				1385 or 1443+3021=4406 or 4464

TABLE IV. Infrared and Raman spectra of CH_3-CCl_3.

Infrared		Raman (liquid)			
Gas cm^{-1}	Liquid cm^{-1}	cm^{-1}	Relative intensity	Depolarization	Interpretation[a]
		241	42	(0.82)	E fundamental
		301	0.3		E fundamental?
	344 vs[b]	344	47	(0.49)	A_1 fundamental
	~ 411 w[b]				(2×205=410 A_1?)
482 vw	~ 483 vw, b	480	0.6		(2×241=482; A_1+E)
~ 495					(205+301=506 E?)
516					
519					
~ 524					
526 s, sh	524 s	523	60	(<0.1)	A_1 fundamental
~ 527					
~ 533					
548 m, sh	~ 541 vw	540 d	vw		(241+301=542; A_1+A_2+E)
~ 556					
565 m, sh					1089−526=563 E?
~ 576					
~ 588 w	587 vw				(241+344=585; E)
~ 621 vw					(2×301=602 A_1)
~ 632 vw					(301+344=645 E)
	~ 662				
~ 686					
690	~ 690				(2×344=688 A_1)
~ 725 vs, b	~ 713 vs, b	712 d	21	(0.87)	E fundamental
~ 749					
755					Impurity?
~ 760					
763 m, sh	~ 763 m, b	757	vvw		(241+523=764 E)
767 m, sh					
~ 773					1075−(301)=774 E?
779					1089−(301)=788; A_1+A_2+E
796 m	~ 790 m				CCl_4 impurity
~ 806 w, b					
~ 819 w, b					
~ 835 vw	~ 829 w				(301)+526=827 E or 1075−(241)=834 E
~ 843 vw					1089−(241)=848; A_1+A_2+E(?)
864					
868 w, sh	867 w				344+526=870 A_1
872 w, sh					
~ 876	883 vw				1089−(205)=884 E?
~ 926 vvw					(205)+725=930 E
~ 952					
962 w	~ 951 w, b				(241)+725=966; A_1+A_2+E
~ 971					
~ 997					
~1003					
1010 m	~1005 m, b				(301)+725=1026; A_1+A_2+E; (301+713=1014)
1016 m					
~1040					1383−(344)=1039E?
~1046					2×526=1052 A_1?
1075 vs	~1071	1069	7	(0.6)	A_1 fundamental?
1089 vs, sh	1086 vs, sh	1083	5	(0.86)	E fundamental
1096 vs	~1100				1427−(344)=1083 E
~1149 vvw					1383−(241)=1142 E
~1190 vvw					1427−(241)=1186; A_1+A_2+E
~1227					
1236 m, sh	1232 m, sh				526+725=1251 E (523+712=1235)
1242 m, sh					
~1282					
1290	1290 w, sh				(205)+1089=1294 E?
1299					
~1309					
1319	1309 w, sh				(241)+1075=1316 E (241+1071=1312)
~1337					
1376					
1383 m, sh	1379 s, sh	1381 sh	2	(0.4)	A_1 fundamental
1391					

[a] Values enclosed in parentheses are for the liquid state.
[b] Observed with KRS-5 prism.

TABLE IV.—(*Continued*).

Infrared Gas cm^{-1}	Infrared Liquid cm^{-1}	Raman (liquid) cm^{-1}	Raman (liquid) Relative intensity	Raman (liquid) Depolarization	Interpretation[a]
~1418					
1427 m, sh	1420 m	1423	5	(0.8)	E fundamental and $2\times725=1450$; A_1+E ($2\times712=1424$ and E fundamental)
~1439					
~1445					
1456 m, sh	1447 m, sh	1447	7	(0.9)	
~1462					
1504 vvw					
1575 vvw	~1600 vvw				$526+1075=1601$ A_1
~1667	~1653 vvw				$(241)+1427=1668$; A_1+A_2+E
1695 vvw					$(241)+1456=1697$; A_1+A_2+E
~1709					
~1718					
1733 vvw, sh	1721 w	~1730	vvw		$(344)+1383=1727$ A_1
1745 vvw, sh					$(301)+1427=1728$; A_1+E
~1751					$(301)+1456=1757$; A_1+A_2+E
	1779 w				$(344+1427=1771$ $E)$
~1795 vw		1790 vd	0.5		$(344+1447=1791$ $E)$ or $725+1075=1800$ E
1832 vvw					$725+1089=1814$; A_1+E
1910 vw	1898 vw				$526+1383=1909$ A_1
1919					
~2110					
2114	2092				$725+1383=2108$ E
~2128					
~2132					
2137 w, sh	2128 w, sh	2133 d	vvw		$725+1427=2152$ $(712+1423=2135)$; A_1+A_2+E
~2141					
~2155					
2179					$725+1456=2181$ A_1+E?
~2336 vvw					CO_2 impurity (air)
~2364 vvw					
~2445					
2451 w, sh	2445 m, sh				$1075+1383=2458$ E
2460	2460 m				$1089+1383=2472$ E
2509	2500 vw, sh				$1089+1427=2516$; A_1+A_2+E
~2538	2525 vw, sh				$1089+1456=2545$ $(1083+1447=2530)$; A_1+A_2+E
	2597 vw, sh				$(2941-344=2597$ $A_1)$
~2660					
2670 vvw	2660 vw, sh				$3017-(344)=2673$ E $(3003-344=2659)$
	~2695				$(2941-241=2700$ $E)$
2755 vvw	2740 vw, sh	2741 sh	6	(0.2)	$2\times1383=2766$ A_1
	2762 vw, sh				$(3003-241=2762)$; A_1+A_2+E
~2809	~2801				$1383+1427=2810$ E $(1379+1420=2799)$
~2825					$3017-(205)=2812$ E?
2829					
2837	2825 w, sh				$1383+1456=2839$ E $(1379+1447=2826)$
~2857	2857	2858	1		$2\times1427=2854$; A_1+E $(2\times1423=2846)$
2874	2882	2886	4		$(2\times1447=2894$; $A_1+E)$
~2899					
2946					
2954 w, sh	2941 w, sh	2938.5	100	(0.1)	A_1 fundamental
2963					
~3008					
3017 m, sh	3003 m, sh	3006 d	48	(0.9)	E fundamental
~3021					
	~3077				
3175 vw	3175 w, sh				$(241)+2954=3195$ E $(241+2941=3182)$
3247 w, sh	3247 w, sh				$(301+2941=3242$ $E)$
3289 w, sh	3289 w, sh				$(344)+2954=3298$ A_1 $(344+2941=3285)$
3356 w, sh	3344 w, sh				$(344)+3017=3361$ E $(344+3003=3347)$
	3460 vw				$526+2954=3480$ A_1 $(524+2941=3465)$
	3584 vw				
	3636 vvw				$(713+2941=3654)$ E
	3704 vw				$(713+3003=3713)$; A_1+A_2+E
	3774 vw				
	~3922				
4000 w, sh	4016 w, sh				$1075+2954=4029$ A $(1071+2941=4012)$
4065 w, sh	4065 w, sh				$1075+3017=4092$ E $(1071+3003=4074)$
4348 w	4367				$1427+2954=4381$ E $(1420+2941=4361)$
4405 w	4425 w, sh				$1427+3017=4444$; A_1+A_2+E $(1420+3003=4423)$
	4651 vvw				

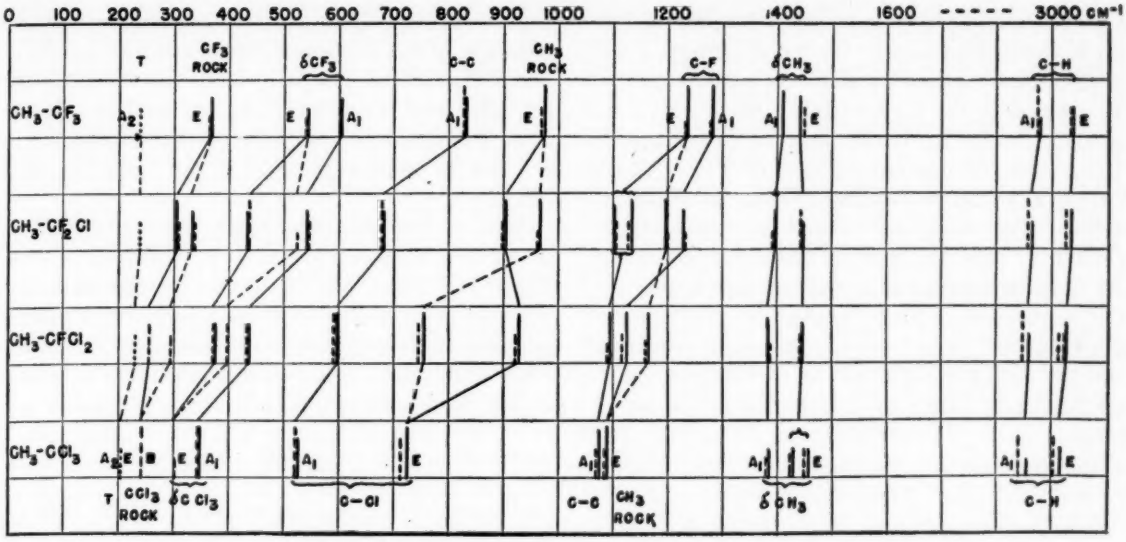

FIG. 2. The fundamental vibration frequencies of CH_3-CF_3, CH_3-CF_2Cl, CH_3-CFCl_2, and CH_3-CCl_3.

data are presented‡ contained water vapor, a trace of CH_3-CH_2F, and about 0.3 percent CH_3-CHF_2, each of which accounts for some impurity absorption. The other sample contained these same impurities (except for water) plus small concentrations of CH_3-CFCl_2 and CH_3-CF_3. It was studied in the Raman effect as a liquid. Nothing is known about the purity of the sample of CH_3-CFCl_2,§ but some evidence of CH_3-CF_2Cl, CH_3-CHF_2, CH_3-CH_2F, and other contaminants were found in the spectra.

The CH_3-CCl_3 was obtained from Eastman Kodak Company and was purified by careful fractional distillation‖ prior to use. It is thought that at least some of the absorption at 796 cm^{-1} is due to CCl_4 impurity that was not removed because of azeotrope formation.

RESULTS

The infrared spectra from 2 to 22 μ of CH_3-CF_2Cl and CH_3-CFCl_2 gases, and of both liquid and vapor CH_3-CCl_3, are shown in Fig. 1. The positions and descriptions of all bands, including those observed with KRS-5 prism and in the Raman effect, are listed in Tables II–IV. The abbreviations v *very*, s *strong*, m *medium*, w *weak*, sh *sharp*, b *broad*, and d *diffuse* are used throughout the tables. The intensities of the Raman bands were measured by photographic microphotometry relative to the strongest band in each spectrum. Depolarization ratios for the stronger Raman bands observed for the liquids are enclosed in parentheses.

‡ This sample was kindly supplied by the General Chemical Division, Allied Chemical Company (Laurel Hill Laboratory).

§ This sample was kindly supplied by the Jackson Laboratory, E. I. duPont de Nemours & Company.

‖ This distillation was kindly performed by Robert Roe, Chemistry Division, Naval Research Laboratory, using a 1-meter jacketed column of 16-mm bore, packed with $\frac{3}{32}$-in. glass helices and having an efficiency equivalent to approximately 50 theoretical plates. The take-off rate was about four drops per minute. The fraction used was one of several taken off at 74.2°C.

INTERPRETATIONS

1. CH_3-CF_3

The fundamental frequencies are known from our previous results for this molecule;[5] their positions are indicated in Fig. 2, where solid lines denote infrared bands, broken lines denote Raman bands (coincident infrared and Raman bands are indicated by slightly separated lines), and dotted lines denote frequencies derived from overtones or combinations, but not observed directly. The relative intensities of the bands are indicated by the heights of the vertical lines. The lowest E fundamental, previously observed only as a weak, diffuse Raman band at 365 cm^{-1}, has now been observed with KRS-5 prism as a strong, partially resolved infrared band with Q branch at 367 cm^{-1}. The fundamentals assigned recently by Cowan, Herzberg and Sinha[6] are identical with those given here, except for interchange of species for 541 and 602 cm^{-1}.

2. CH_3-CF_2Cl

Upon passing from CH_3-CF_3 to CH_3-CF_2Cl each of the degenerate vibrations splits into two components to give a total of eighteen fundamentals, all active in both infrared and Raman effect and differing appreciably only with respect to polarization, the latter depending upon their symmetry with respect to the symmetry plane of the molecule. The relationships of the position, intensity and polarization of the observed bands to those of the related spectra shown in Fig. 2 are therefore the most useful guides in the selection of fundamentals.

The methyl stretching and deformation fundamentals are readily identified with the bands at 2965 and 3035 cm^{-1} and at 1395 and 1447 cm^{-1}. The higher band in each case represents a superposition of A' and A''

[6] Cowan, Herzberg, and Sinha, J. Chem. Phys. 18, 1538 (1950).

fundamentals which fail to split apart because of confinement of these vibrations to the methyl group, which has higher internal symmetry than the molecule.

There appears in the region from 1100 to 1250 cm^{-1} a group of at least five bands that can represent no more than three fundamentals, two of which should be polarized in the Raman effect. These fundamentals involve C—F stretching and methyl rocking, and may be expected to produce intense absorption. The appearance of more than three strong infrared bands suggests the occurrence of Fermi resonance. The bands at 1101 and 1134 cm^{-1}, which are nearly equally intense in both spectra and are polarized in the Raman effect, are therefore attributed to a coincidence of an A' fundamental with the combination $437+683=1120$ cm^{-1} of the same species. The intense infrared maxima at 1190 and 1202 cm^{-1} must also represent a fundamental, which is assumed to have species A'' and to account for the faint Raman band at 1202 cm^{-1}. Whether or not a Raman band occurs at 1190 cm^{-1} is uncertain because of overlapping with the intense band at 2956 cm^{-1} excited by the 4047A Hg line. The other A' fundamental is assigned the value 1230 cm^{-1}, which is observed in both spectra, and the remaining band at 1210 cm^{-1} is interpreted as a combination of species A' whose intensity is enhanced by its proximity to the 1230 cm^{-1} fundamental. An alternative interpretation, equally satisfactory with respect to the correlations of Fig. 2, would be the assignment of 1101 and 1134 cm^{-1} to the two A' fundamentals, 1196 cm^{-1} to the A'' fundamental and both 1210 and 1230 cm^{-1} to binary combinations, the higher of which having the correct species for resonance with the A'' fundamental.

All but two of the remaining fundamentals are readily identified by their relationship to the corresponding fundamentals in CH_3-CF_3. That at 967 cm^{-1} is predominantly a methyl rocking mode, while that at 904 cm^{-1} is primarily C—C stretching. The C—Cl stretching vibration occurs at 683 cm^{-1}, CF_2 deformation at 543 cm^{-1}, and the fundamentals involving rocking of the CF_2Cl group against the methyl carbon appear at 305 and 334 cm^{-1}.

The A' fundamental corresponding to the degenerate CF_3 deformation in CH_3-CF_3 occurs in CH_3-CF_2Cl vapor as an intense, polarized Raman band at 437 cm^{-1}, but the A'' component is not assigned with certainty. It is identified here with the faint Raman band at 526 cm^{-1}, for which no alternative interpretation could be found. However, it might conceivably be the weak infrared band near 475 cm^{-1}, or the Raman band at 430 cm^{-1}. The latter is attributed to the same origin as the A' fundamental at 437 cm^{-1}, the displacement being due to the presence of Cl_{37} isotope. The appearance of this band indicates that it is polarized as is the band at 437 cm^{-1}. The relative intensities and separation of these bands are approximately correct for this interpretation. They were not resolved in the infrared.

The last fundamental, a torsional vibration, may be expected to fall between 238 and 205 cm^{-1}, the wave numbers of the corresponding vibrations in CH_3-CF_3 and CH_3-CCl_3. The only basis for its assignment is the faint and uncertain infrared band near 475 cm^{-1}. This is tentatively interpreted as the overtone, yielding a value of approximately 238 cm^{-1} for the torsional mode.

Most of the remaining bands are readily interpreted as binary combinations, or as impurity bands (see Table II). Some difficulty was experienced in deciding whether certain of the infrared frequencies represented resolved rotational structure, particularly in the region near 1200 cm^{-1}. The infrared spectrum of the liquid would be of help in this connection.

3. CH_3-CFCl_2

The number and positions of the strong infrared and Raman bands observed for CH_3-CFCl_2 fall so nicely into the pattern of Fig. 2 as to leave little doubt about the assignment of fundamentals. The asymmetric stretching fundamental of the methyl group in this case apparently splits into two components that are only partially resolved in either spectrum.

The fundamentals at 1096 and 1123 cm^{-1} are polarized in the Raman effect, and therefore represent C—F stretching and symmetrical rocking of the methyl group. The other methyl rocking mode occurs at 1164 cm^{-1}. The two fundamentals at 929 and 745 cm^{-1} involve C—C and C—Cl stretching, and the low symmetric C—Cl stretching occurs at 596 cm^{-1}.

The five Raman bands at 432, 398, 376, 295, and 256 cm^{-1} are readily identified with the fundamentals involving skeletal deformations, but the low torsional fundamental is not observed in the Raman effect, and is below the range of the infrared measurements. It is assumed to be at 229 cm^{-1}, its overtone accounting for the infrared band at 459 cm^{-1}. As in the previous compound, nearly all of the remaining bands are satisfactorily explained as binary combinations of these fundamentals (see Table III).

4. CH_3-CCl_3

Methyl chloroform has been investigated several times, most recently by Venkateswarlu[7] and by El-Sabban, Meister, and Cleveland.[8] The latter authors summarize previous work and give detailed interpretations for all observed infrared and Raman bands, including those obtained in this investigation.

The assignment of fundamental frequencies proposed here is shown in Fig. 2, and interpretations of the observed infrared and Raman bands are given in the last column of Table IV. It is assumed that $CH_3 \cdot CCl_3$ has the symmetry C_{3v}.

Four of the five A_1 fundamentals can be assigned

[7] P. Venkateswarlu, J. Chem. Phys. **19**, 298 (1951).
[8] El-Sabban, Meister, and Cleveland, J. Chem. Phys. **19**, 855 (1951).

with certainty. They occur at 2954, 1383, 526, and 344 cm^{-1} in the infrared spectrum of the vapor and as highly polarized bands in the Raman effect. Similarly, all but one of the six degenerate fundamentals are readily identified with bands at 3017, 1089, 725, and 241 cm^{-1}, and with the pair at 1427 and 1456 cm^{-1}. The splitting of the latter is undoubtedly caused by resonance with a combination, here assumed to be the overtone $2\times725=1450$ cm^{-1} (A_1+E).

The remaining three fundamentals cannot be assigned with certainty, and it is in respect to these that previous assignments differ among themselves and with that proposed here. The C—C stretching vibration of Species A_1 has been identified by Venkateswarlu with the infrared band at 867 cm^{-1}, and by El-Sabban *et al.* with the infrared band near 1005 cm^{-1}. The former appears to be unusually low, and neither has been observed in the Raman effect. Since alternative explanations can be given for each of these bands, we prefer to identify this fundamental with the Ramen band at 1069 cm^{-1}, which is not easily explained otherwise because of its polarization. The corresponding infrared band occurs at 1075 cm^{-1} in the vapor.

The uncertain E fundamental involves an asymmetric deformation of the CCl_3 group and may be expected near the corresponding A_1 vibration at 344 cm^{-1}. The value 526 cm^{-1} assigned by Venkateswarlu is unacceptable because of the polarization of that band, and the frequency 363 cm^{-1} given by El-Sabban *et al.* has been observed neither in the infrared nor in the Raman effect. The value 363 cm^{-1} could be acceptable as far as the correlations of Fig. 2 go, but since it has not been observed it appears preferable to identify this fundamental with the very weak Raman band at 301 cm^{-1}. This band has been observed previously[9,10] and is not easily explained otherwise, unless as caused by an impurity present in all of the samples studied. El-Sabban *et al.* have interpreted it as the combination $1005-713=292$ cm^{-1} (E), but the numerical agreement is poor for a difference band, and the Boltzmann factor for the initial state would be extremely low.

The third uncertain fundamental is the inactive torsional vibration of species A_2. The weak infrared band at 411 cm^{-1} is assumed to be the overtone of this fundamental giving for the latter a value of approximately 205 cm^{-1}. Since the band at 301 cm^{-1} was not observed in the infrared, the intensity of 411 cm^{-1} is too great for this band to be interpreted as the difference $713-301=412$ cm^{-1} (A_1+A_2+E). Allowed combinations of the torsional vibration at 205 cm^{-1} account for two other infrared bands (at 926 and 1290 cm^{-1}) not otherwise explained. That at 1290 cm^{-1} is one of three bands assumed by Karplus and Halford[11] to be active only in condensed states, but has been observed here also in the vapor.

Binary combinations of the assigned fundamentals account satisfactorily for most of the remaining maxima (see Table IV) which are observed for the liquid, and which therefore represent separate vibrational transitions. Many additional or alternative interpretations involving ternary combinations can be found, but they are not very useful for fixing the fundamentals. The infrared maximum at 796 cm^{-1} in the vapor is considerably stronger in the present sample than in one studied previously[12] and is caused at least in part by an impurity, believed to be carbon tetrachloride, which could not be removed by fractional distillation because of azeotrope formation. The vapor maximum at 755 cm^{-1} also appears to be stronger than in the previous spectrum and may be due to an impurity.

DISCUSSION

The correlation lines in Fig. 2 are drawn according to the vibrational species of the fundamentals. Solid and broken lines denote totally symmetric and asymmetric vibrations, respectively, and crossings of lines connecting the same pair of species may not occur. Because of this restriction, these correlations are more useful than those based on molecular groups. In addition, the latter are usually not as smooth and become ambiguous in cases where two or more groups participate nearly equally in the vibration.

As shown in Fig. 2, only vibrations involving C—H stretching, methyl deformation, and torsion maintain their identity throughout this group of spectra. They are remarkably constant and may be properly regarded as "group frequencies." As chlorine is substituted into the CF_3 group, the rocking and deformation vibrations associated with this group change progressively into those of the CCl_3 group, and to a rough approximation these vibrations may also be considered as "group frequencies." For the remaining fundamental vibrations, however, the motion changes completely with respect to the group involved. Thus, upon passing from CH_3-CF_3 to CH_3-CCl_3, the two C—F stretching vibrations become C—C stretching and methyl rocking, the fundamental associated with CH_3 rocking in CH_3-CF_3 assume progressively the character of C—C stretching and finally C—Cl stretching, and the C—C stretching becomes C—Cl stretching. Particularly in the intermediate, less symmetrical compounds these "group frequencies" lose their meaning, and assignment of fundamentals based upon them tends to become ambiguous.

The over-all consistency of the correlations in Fig. 2 strongly supports the spectral assignments both for the two symmetrical compounds (which served as starting points for the correlations) and for the two intermediates. As mentioned previously, there are a few uncertainties which could not be resolved by consideration of either individual spectra or of correlations. These

[9] Kohlrausch and Koppl, Monatshefte **65**, 185 (1935).
[10] J. Wagner, Z. physik. Chem. **B45**, 341 (1940).
[11] R. Karplus and R. S. Halford, J. Chem. Phys. **18**, 910 (1950).
[12] A. P. I. Project 44 Catalogue of Infrared Spectral Data, Ser. No. 1032 and 1033.

TABLE V. Calculated thermodynamic functions for CH_3-CF_3 at one atmosphere (in cal/deg mole).

	$\frac{H^0-H_0^0}{T}$	C_p^0	S^0	$\frac{-(F^0-H_0^0)}{T}$
$T=250°K$				
Trans+Rot	7.95	7.95	60.69	52.74
Vib	2.17	6.65	2.97	0.80
Tors	1.00	1.94	1.61	0.61
Total	11.12	16.54	65.27	54.15
$T=298°K$				
Trans+Rot	7.95	7.95	62.08	54.13
Vib	3.06	8.66	4.31	1.26
Tors	1.17	2.08	1.97	0.81
Total	12.18	18.69	68.36	56.20
$T=400°K$				
Trans+Rot	7.95	7.95	64.42	56.47
Vib	5.00	12.62	7.43	2.43
Tors	1.42	2.20	2.60	1.18
Total	14.37	22.77	74.45	60.08
$T=600°K$				
Trans+Rot	7.95	7.95	67.64	59.69
Vib	8.59	18.51	13.74	5.15
Tors	1.66	2.05	3.47	1.81
Total	18.20	28.51	84.85	66.65

involve the species of the fundamentals at 541 and 605 cm^{-1} in CH_3-CF_3, the assignment of 526 and 1230 cm^{-1} as fundamentals for CH_3-CF_2Cl, the assignments of 301 cm^{-1} (E) and 1075 (A_1) in CH_3-CCl_3, and the position of the low torsional fundamental in each compound, except possibly CH_3-CF_3 for which the same value has been derived from both infrared and microwave measurements.[5]

It is of interest that the methyl deformation vibrations in this group of compounds suffer the smallest shifts and exhibit the following empirical facts:

(1) For neither of the two compounds of symmetry C_s are the A' and A'' components of asymmetrical methyl deformation separated. However, for both compounds the measured depolarization ratio is somewhat smaller than 6/7 (0.7 for CH_3CF_2Cl and 0.8 for CH_3-CFCl_2).

(2) In the infrared, the intensity of the asymmetrical deformation is for all four compounds considerably lower than that of the symmetrical deformation. In the Raman effect, on the other hand, the relative intensities are reversed.

(3) For all four compounds, the overtone of the symmetrical deformation is much more intense in the Raman effect than the fundamental. Thus, for gaseous CH_3-CF_3 only the overtone was observed; for CH_3-CF_2Cl, CH_3-CFCl_2, and CH_3-CCl_3 the ratio of the intensities is approximately 6:1, 4:1, and 3:1, respectively. In the infrared, on the other hand, the overtone is far less intense than the fundamental for all of the compounds.

(4) For all four compounds the wave number of the overtone of the symmetrical deformation is about 20 cm^{-1} less than twice the wave number of the fundamental. This must be caused by anharmonicity and coupling with totally symmetric levels in the 3000-cm^{-1} region.

If these regularities exist in other compounds containing methyl groups, as a preliminary survey indicates, they are of some practical importance and present an interesting theoretical problem.

Another problem is posed by the suggestion of Cowan, *et al.*[6] that the splitting of the Q branch of the degenerate methyl rocking fundamental at 970 cm^{-1} in CH_3-CF_3 arises from interaction with the torsional vibration. The branch consists of three components of nearly equal intensity at 965, 967, and 973 cm^{-1}.[5] The fundamental near 605 cm^{-1} has a similar Q branch, with maxima at 600, 602, and 605 cm^{-1}, and there are also splittings of from 3 to 5 cm^{-1} in what appear to be the Q branches of other bands near 541, 1086, 1030, and 1005 cm^{-1} in CH_3-CF_3.[5] In the spectra presented here (see Fig. 1) there is also evidence of small splittings in some of the Q branches, particularly of the bands at 967, 904, 847, and 683 cm^{-1} in CH_3-CF_2Cl, at 929, 795, and 755 cm^{-1} in CH_3-CFCl_2, and at 725 and 525 cm^{-1} in CH_3-CCl_3. The splitting can in some cases be attributed to combinations, to "upper stage" bands, or perhaps to effects arising from symmetry considerations alone, but the occurrence seems too frequent for dismissal of other possible causes. Measurements with higher resolution and more detailed consideration of the effect suggested by Cowan *et al.* seem desirable.

THERMODYNAMIC FUNCTIONS

The heat capacity, entropy, free energy function, and heat content function have been calculated previously[5] for CH_3-CF_3. Revised data for this molecule are presented in Table V. Corrections have been made

TABLE VI. Calculated thermodynamic functions for CH_3-CF_2Cl at one atmosphere (in cal/deg mole).

	$\frac{H^0-H_0^0}{T}$	C_p^0	S^0	$\frac{-(F^0-H_0^0)}{T}$
$T=264.15°K$(b.p.)				
Trans+Rot	7.95	7.95	65.01	57.06
Vib	3.01	8.32	4.28	1.27
Tors	1.05	2.05	1.72	0.67
Total	12.01	18.32	71.01	59.00
$T=298°K$				
Trans+Rot	7.95	7.95	65.97	58.03
Vib	3.70	9.72	5.37	1.67
Tors	1.16	2.08	1.97	0.81
Total	12.81	19.75	73.31	60.51
$T=400°K$				
Trans+Rot	7.95	7.95	68.31	60.36
Vib	5.74	13.57	8.78	3.05
Tors	1.42	2.20	2.59	1.18
Total	15.11	23.72	79.68	64.59
$T=600°K$				
Trans+Rot	7.95	7.95	71.53	63.58
Vib	9.35	19.15	15.43	6.08
Tors	1.66	2.06	3.47	1.81
Total	18.96	29.16	90.43	71.47

for computational errors in the original calculation recently discovered, and a more reliable method has been used to estimate the height of the barrier hindering internal rotation. New data for the molecules CH_3-CF_2Cl, CH_3-CFCl_2, and CH_3-CCl_3 are presented in Tables VI, VII, and VIII. In each table the translational-rotational, vibrational, and torsional (hindered rotational) contributions are listed separately and then summed.

The equations and tables of Hougen and Watson[13] were used to obtain all contributions except that involving hindered rotation, which was computed from the tables of Pitzer and Gwinn.[14] The molecular constants used in these calculations are listed in Table IX.

Reduced moments of inertia for the internal rotation were calculated from the formula $I_r=I_1I_2/(I_1+I_2)$, where I_1 and I_2 are the moments of the two groups about the C—C bond axis. The result is only an approximation for CH_3-CF_2Cl and for CH_3-CFCl_2, neither of which has an axis of symmetry. An exact calculation showed that the approximation is good to within one part in 500 for CH_3-CF_2Cl. Obviously an exact calculation for CH_3-CFCl_2 is not required.

The values of V_0, the height of the cosine barrier restricting internal rotation, were calculated by a graphical procedure from the appropriate rotational energy levels, i.e., from the eigenvalues a_r of the Mathieu equation tabulated by Wilson.[15] The differences in a_r between the first and second levels and between the first and third levels were found from Wilson's table, for values of θ from 0 to 40. Plots of a_2-a_1 and a_3-a_1 were made against θ. From the torsional frequency ωc deduced from the analysis of the spectra a value of Δa_r was calculated using the relation

$$\Delta a_r=32\pi^2I_rc\omega/n^2h,$$

where I_r is the reduced moment of inertia of the top, h is Planck's constant, c is the velocity of light, and $n=3$ is the number of maxima in the assumed cosine potential function for one revolution. If ω is the fundamental, Δa_r is a_2-a_1; if ω is the first overtone, Δa_r is a_3-a_1. From the graph of Δa_r against θ, the value of θ corresponding to the Δa_r calculated for each molecule was determined. Then V_0 was calculated from the equation $\theta=8\pi^2I_rV_0/n^2h^2$.

The reliability of the V_0 values (see Table IX) depends mainly on the validity of the torsional frequencies derived from the experimental data. Some error may of course be introduced through assumption of the cosine type potential, but this is generally considered to be small. There is an additional uncertainty of approximately 10 cal/mole in the graphical procedure.

The method used here to obtain V_0 is essentially the inverse of that used by El-Sabban, Meister, and Cleveland[8] in calculating a torsional frequency of 205 cm^{-1} from a barrier height of 2840 cal/mole for CH_3-CCl_3. Their frequency accidentally coincides with the approximate value (see Table IV) deduced from the observed overtone at 411 cm^{-1} when anharmonicity is neglected. Our higher value (3045 cal/mole) for the barrier was obtained from the observed frequency at 411 cm^{-1} (using the curve for $\Delta a_r=a_3-a_1$), and corresponds to a value of 213 cm^{-1}, rather than 205 cm^{-1}, for the fundamental. The barriers for the other molecules, derived from the fundamental frequencies tentatively assigned, are higher than was anticipated. As will be shown in a later paper, however, application of the same procedure to ethane yields a barrier height compatible with calorimetric data.

TABLE VII. Calculated thermodynamic functions for CH_3-CFCl_2 at one atmosphere (in cal/deg mole).

	$\frac{H^0-H_0^0}{T}$	C_p^0	S^0	$\frac{-(F^0-H_0^0)}{T}$
$T=305.15$°K(b.p.)				
Trans+Rot	7.95	7.95	67.54	59.60
Vib	4.82	11.40	7.31	2.49
Tors	1.23	2.12	2.15	0.88
Total	14.00	21.47	77.00	62.97
$T=400$°K				
Trans+Rot	7.95	7.95	69.69	61.75
Vib	6.79	14.73	10.84	4.06
Tors	1.45	2.20	2.69	1.24
Total	16.19	24.88	83.22	67.05
$T=600$°K				
Trans+Rot	7.95	7.95	72.91	64.97
Vib	10.36	19.92	17.87	7.51
Tors	1.67	1.98	3.54	1.87
Total	19.98	29.85	94.32	74.35

TABLE VIII. Calculated thermodynamic functions for CH_3-CCl_3 at one atmosphere (in cal/deg mole).

	$\frac{H^0-H_0^0}{T}$	C_p^0	S^0	$\frac{-(F^0-H_0^0)}{T}$
$T=298$°K				
Trans+Rot	7.95	7.95	66.26	58.32
Vib	5.71	12.42	9.00	3.29
Tors	1.28	2.15	2.22	0.95
Total	14.94	22.52	77.48	62.56
$T=347.3$°K(b.p.)				
Trans+Rot	7.95	7.95	67.49	59.54
Vib	6.79	14.12	11.03	4.24
Tors	1.40	2.17	2.56	1.14
Total	16.14	22.24	81.07	64.92
$T=400$°K				
Trans+Rot	7.95	7.95	68.60	60.66
Vib	7.87	15.78	13.14	5.28
Tors	1.50	2.15	2.85	1.35
Total	17.32	25.88	84.59	67.29
$T=600$°K				
Trans+Rot	7.95	7.95	71.82	63.88
Vib	11.35	20.58	20.52	9.16
Tors	1.68	1.89	3.68	2.01
Total	20.98	30.42	96.02	75.05

[13] Hougen and Watson, *Chemical Process Principles* (John Wiley and Sons, Inc., New York, 1947), Part II, Chapter XVII.
[14] Pitzer and Gwinn, J. Chem. Phys. **10**, 429 (1942).
[15] E. B. Wilson, Jr., Chem. Revs. **27**, 17 (1940).

TABLE IX. Molecular constants.

Molecule	CH_3-CF_3	CH_3-CF_2Cl	CH_3-CFCl_2	CH_3-CCl_3
Dimensions				
C−H (*A*)	1.09	1.09	1.09	1.09
C−C (*A*)	1.45[a]	1.54	1.54	1.54
C−F (*A*)	1.33[a]	1.37[b]	1.40[c]	···
C−Cl (*A*)	···	1.77[b]	1.78[c]	1.76[c]
∠HCH	109°28′	109°28′	109°28′	109°28′
∠CCF	···	111°[b]	109½°[c]	···
∠CCCl	···	111°[b]	111°[c]	110°[c]
∠FCF	108½°[a]	108°[b]	···	···
∠ClCCl	···	···	109½°[c]	109°[c]
$I_AI_BI_C\times10^{113}$ (g³ cm⁶)	0.365	1.18	3.02	6.14
σ (=symmetry number)	3	1	1	3
$I_r\times10^{40}$ (g-cm²)	5.11	5.19	5.23	5.25
Torsional frequency (cm^{-1})	238	238	229	411 (overtone)
V_0 (cal/mole)	3660	3705	3470	3045

[a] From L. O. Brockway and R. L. Livingston, Abstracts, Am. Chem. Soc. Meeting, Buffalo, New York, 1942.
[b] See P. W. Allen and L. E. Sutton, Acta Cryst. **3**, 46 (1950).
[c] From J. Y. Beach and D. P. Stevenson, J. Am. Chem. Soc. **61**, 2643 (1939).

For comparison with the calculated thermodynamic functions there are available the calorimetric measurements of Russell, Golding, and Yost[16] on CH_3-CF_3, and of Rubin, Levedahl, and Yost[17] on CH_3-CCl_3. The former authors obtain for CH_3-CF_3 the value 63.95±0.10 cal/deg mole for the entropy of the ideal gas at 224.40°K and 0.9330 atmosphere, whereas the present calculations yield a slightly lower value of 63.65 cal/deg mole. For CH_3-CCl_3, the calorimetric value $S^0=76.22\pm0.16$ cal/deg mole at 286.53°K was obtained, as compared to a higher value of 76.57 cal/deg mole calculated from the present spectroscopic data. If the uncertainty attached to the calorimetric value is correct, assignment of a higher frequency to one of the three uncertain fundamentals is indicated. No calorimetric data for CH_3-CF_2Cl or CH_3-CFCl_2 in the vapor state were found for comparison with the present results.

[16] Russell, Golding, and Yost, J. Am. Chem. Soc. **66**, 16 (1944).
[17] Rubin, Levedahl, and Yost, J. Am. Chem. Soc. **66**, 279 (1944).

The Hot Atom Chemistry of the Propyl Bromides; Effect of Phase and Recoil Energy on Retentions*

MAURICE S. FOX† AND W. F. LIBBY
Department of Chemistry and Institute for Nuclear Studies, University of Chicago, Chicago, Illinois

(Received October 8, 1951)

The yields of the various organic radiobromides formed by neutron irradiation of liquid and solid iso and normal propyl bromides at various temperatures have been determined. Very careful purification of the propyl bromides has given good reproducibility and evidence that the main features of the hot atom chemistry of the propyl bromides have been discovered.

The solidification at the melting point results in a threefold or larger increase in yield of certain products, presumably those formed by epithermal bromine atoms, and a smaller increase for the remainder of the products, such as the mother molecule, presumably formed by hot reactions. Isomerization of isopropyl to *n*-propyl appears to occur with high probability in epithermal reactions. The epithermal production of bromides of considerably higher boiling point than the mother molecule has been confirmed and the phenomenon discussed theoretically.

Apparently the retentions in the solid phase depend on energy of the recoil bromine, 36-hr Br^{82} showing 93 percent retention in solid *n*-propyl *vs* 80 percent for the 18-min and 4.4-hr Br^{80}'s. This is in contrast to the liquid retentions in which no difference has been observed. On this basis it is concluded that the average recoil energy of the 36-hr Br^{82} is less than those of the two Br^{80} isomers and that the latter two differ relatively little.

The theoretical implications of the observed product distributions and the phase effect on these distributions and the sensitivity to recoil energy are discussed.

I. INTRODUCTION

TWO principal sources of doubt have plagued the field of the hot atom chemistry of the organic halides since the discovery of the Szilard-Chalmers effect[1] in 1934. One of these is the possibility that nonradioactive radicals generated by the radiation decomposition of the target substances seriously affect the chemical fate of the radioactive halogen atoms ejected by the (n, γ) recoil process. This apparently has been rather satisfactorily excluded in many cases by establishing independence of the thickness of gamma-ray shielding placed around the organic halide during the exposure to neutrons. The other principal difficulty has consisted of the possibility that the radioactive halogen atoms might react thermally after losing their initial high energies by collisional deceleration. The thermal reactions with the organic halides which could result in the transfer of radiohalogen from inorganic to organic form and so raise the "retention" are of the exchange type. In most cases proper tests preliminary to the hot atom studies have been made which fairly satisfactorily excluded this type of effect. The second type of thermal reaction—the whole group of possible reactions with minor impurities present in the system—has been much more difficult to control.

Recently evidence of a commanding character[2,3] has accumulated which strongly suggests that many of the data on retentions in the organic halides may be seriously in error because of thermal reactions with the omnipresent impurities. The solution to the difficulty appears to be simple enough but has not been used in general. The importance of reactions with minor impurities can be reduced to insignificance by exchanging the radioactive halogens into species present in larger concentrations such as the allyl or vinyl halides[3,4] or elementary diatomic halogen[2,5] so that the chances of impurity reactions affecting the fate of the radiohalogen become insignificant. With Br_2 added in small amounts to an organic bromide containing minor quantities of olefinic and other impurities, freshly formed thermal Br atoms will most likely exchange with the Br_2 and be diluted so far that the eventual reaction with the olefinic impurity will not incorporate significant quantities of radiobromine.

The basic notion is that additives can be used in the organic halides during exposure in quantities of a fraction of one mole percent so that the presence of the additive can hardly affect the course of the hot and epithermal reactions and yet be quite sufficient to insure a short lifetime for radioactive atomic halogen as such in the solution by exchanging the radioactive atoms into more abundant and less reactive species. We might use the term "thermal scavengers" for these agents, as suggested by Goldhaber and Willard.[2b] In addition, the use of molecular halogen will tend to reduce the concentration of free radicals produced by radiation decomposition by reacting with them so that the danger of radiation chemical effects should be considerably reduced. Of course, if larger quantities are used, the course of the hot and epithermal reactions themselves may be affected[5] in an understandable way by reaction

* Irradiations performed on the 36-in. cyclotron, supported by AEC Contract No. AT(11-1)-86.

† Presented in partial fulfillment of the requirements for the degree of Doctor of Philosophy, Division of Physical Sciences, University of Chicago.

[1] L. Szilard and T. A. Chalmers, Nature **134**, 462 (1934).

[2a] Goldhaber, Chiang, and Willard, J. Am. Chem. Soc. **73**, 2271 (1951).

[2b] S. Goldhaber and J. E. Willard, Paper Phys. and Inorg. Div. American Chemical Society, April, 1951.

[3] Hamill, Williams, Schwarz, and Voiland, Report, March 1, 1951; AEC Contract AT(11-1)-38.

[4a] Hamill, Williams, and Schwarz, J. Am. Chem. Soc. **72**, 2813 (1950).

[4b] R. R. Williams and W. H. Hamill, J. Chem. Phys. **18**, 783 (1950).

[5] L. Friedman and W. F. Libby, J. Chem. Phys. **17**, 647 (1949).

of the excited product molecules containing radiohalogen with the additive.

In an attempt to extend earlier data[5] obtained on the propyl bromides, certain discrepancies have been discovered which probably can best be attributed to inadequate attention to the reaction of thermal radiobromine with impurities and to the use of a distillation column of too low fractionating efficiency. Careful repetition and extension of the earlier work has yielded the data which follow in the main body of this paper. A strenuous attempt has been made to purify the propyl bromides to the point that the total retention and the distribution of the radiobromine among the various organic bromides as revealed by distillation was unaffected by the presence of a small amount of Br_2 during the irradiation. It is believed that these data are reliable. However, an independent check by somewhat different techniques would be desirable.

II. EXPERIMENTAL

A. Procedure

Chemicals

Pure *n*-propyl and isopropyl bromides were obtained from Eastman Kodak and Paragon Testing Laboratories. Olefin impurities were removed by passing a stream of ozone through the propyl bromides for ten times the length of time required for the first appearance of unreacted ozone from the liquids. The resulting mixture was vacuum distilled from an ice bath to separate the higher boiling explosive ozonides. The propyl bromide was then stirred vigorously with concentrated sulfuric acid to remove alcohols, washed with aqueous sodium bicarbonate, then water, and dried over anhydrous sodium sulfate. The final step in the purification was a distillation through a fractionating column of 22 theoretical plates. The first and last 10 percent of the material distilled was discarded. Normal propyl bromide was removed from the column within 0.1 degree of 70.6°C and isopropyl bromide within 0.1 degree of 58.9°C, both at 745-mm pressure.

Irradiation

Fifty milliliter samples of the propyl bromides in amber colored soft glass bottles for room temperature, and Pyrex bottles for the low temperature work, were irradiated at the University of Chicago 37-inch cyclotron. $Be^9(d,n)B^{10}$ and $Li^7(d,n)Be^8$ as target reactions gave a flux of fast neutrons which were moderated by ten centimeters of paraffin as walls of the irradiation box. Samples to be irradiated were placed in the box, in the neutron beam, about twelve inches from the target with an intervening two inches of lead to minimize chemical effects that could be caused by the gamma-radiation from the cyclotron target. Exposures lasted from one to two hours at an average beam current of twelve microamperes. The neutron flux calculated on the basis of the activities produced was about 10^7 neutrons per square centimeter per second. The integrated radiation intensity for an average irradiation of about one hour, measured with a Victoreen meter, was about 700 roentgens. This radiation consisted principally of gamma-rays, of course.

Temperature control for the low temperature irradiations was accomplished by using various liquid-solid mashes. Dry ice acetone was used for −78°C, isopropyl bromide mash for −89°C, *n*-propyl bromide mash for −110°C. Irradiation of the liquid propyl bromides at their melting point was accomplished by cooling them to a few degrees above the melting point and placing in the appropriate liquid-solid mash of propyl bromide. For the solid at the melting point, the propyl bromide was frozen and then placed in the appropriate mash. It was observed by checks during and after the irradiation that, provided the mash was of pure propyl bromide, there was little freezing or melting of the respective liquid or solid.

Extraction

Within five minutes of the completion of the irradiation the samples were extracted with fifty milliliters of aqueous solution, about 0.005 molar in sodium bisulfite and 0.005 molar in sodium bromide. The mixture was shaken vigorously, until all the propyl bromide and ice had melted and then for one minute afterwards, in the irradiation vessel. The two layers were then separated with a separatory funnel and the organic fraction analyzed. Periodic checks were made on the extraction procedure by re-extracting the separated organic layer. No activity was found beyond that which could be attributed to the solubility of the organic bromides, less than 0.5 percent of the organic activity.

Distillation

To a forty-milliliter sample of the extracted irradiated *n*-propyl bromide, about 20 ml of methyl bromide, 40 ml ethyl bromide, 50 ml isopropyl bromide, 30 ml *n*-propyl bromide, and 50 ml each of dibromomethane, 1,2 dibromoethane, 1,2 dibromopropane, and 1,3 dibromopropane were added. With isopropyl bromide, the volume of each carrier was about the same except that 1,1 dibromoethane was added in place of dibromomethane. This mixture was analyzed by distillation. Methyl bromide was taken off by condensing it in a dry ice acetone bath from a stream of nitrogen bubbled through the mixture of carriers at room temperature. The other monobromides were than separated by a pot to receiver distillation at reduced pressure and room temperature. The receiver was held at −78°C. The monobromides were then fractionated at atmospheric pressure and the dibromides at reduced pressure to avoid excessive decomposition. The pot temperatures during distillations never exceeded 110°C. Fractions of 9 to 10 ml were taken off at a time, and since the still

operated at total reflux, the boiling points of each fraction were accurately known. This, coupled with refractive index measurements, determined the purest fraction of each substance. The crudeness of the methyl bromide separation presented quantitative measure of its abundance.

The column used for the distillations was designed by John Hinkley and constructed by the Alpha Apparatus Company, Chicago, Illinois. It was packed with single turn, $\frac{3}{32}$-inch Fenske Pyrex glass helices, and the packed tube was about four feet high. The efficiency was measured with a benzene-carbon-tetrachloride mixture and found to be 22 theoretical plates. The hold-up was about 36 ml.

Radioactivity

The measurements of radioactivity were made with standard Geiger-Müller counters. Samples were counted in a 7-ml standard type thin wall liquid cell counter. The methyl bromide was counted as solution in methyl alcohol, usually about 10 percent, and the other samples were counted as they came off the still. For the analytical work, only the 35.9-hour Br^{82} was counted. Precautions were usually taken to allow the 4.4-hour and 18.5-minute Br^{80} to decay, but a 2-mm lead shield around the counter tube was always present and absorbed this activity when the decay period allowed for the Br^{80} was insufficient.

For the counting of Br^{80} activity, the same liquid cell was used, but without the lead shield. Precautions were taken always to have bromine or bromide ion carrier present to avoid absorption difficulties associated with the carrier free isomeric transition product of the 4.4-hour Br^{80*}. The Br^{82} activity was subtracted to get the activity of pure Br^{80}. The density correction for counting the 2.0-Mev beta-particle was determined empirically. The aqueous solution of density 1.0 counted 10 percent more efficiently than the propyl bromides of density 1.4.

The relative yields of each radioactive compound were determined by correction of the activity of the purest sample of given compound to the total volume of that compound present as carrier in comparison with the total activity produced in the irradiation.

B. Verification of Procedure and Incidental Results

Purification

After observing some difficulty in getting reproducible values of the retention in liquid phase irradiations, it was found that the addition and immediate extraction of radioactive bromine could induce activity in commercial pure propyl bromides. It had also been observed that about 20 percent of the organic radioactivity in the non-reproducible runs appeared as allyl bromide. No such effects were observed in the solid phase irradiations, probably because the impurities were "frozen out" of the propyl bromide lattice and thus unable to interfere with the reactions of the recoil atoms.

TABLE I. Retention of normal propyl bromide.

Temperature Phase	−78°C Liquid	−196°C Solid
Non-ozonized (%)	50.1	86.8
Ozonized (%)	38.7	87.9

Since the presence of bromolefin would be expected to give effects[4, 6] identical with those observed, the ozonization process was introduced to remove them. After ozonization, there was no observed induction of radioactivity by shaking the propyl bromides with radioactive bromine, other than that attributable to photochemical hydrogen substitution. The appearance of allyl bromide activity in the distillation pattern also stopped. The ozonization process had no effect on the solid phase retention as may be noted in Table I.

Irradiation

It was of major importance to establish the absence of any chemical effects of radiation on the hot atom chemistry. From the Victoreen meter measurement of the total gamma-radiation of 700 roentgen for a one-hour irradiation, some estimate can be made of the extent of radiation damage. For 100 ml of propyl bromide, assuming a value for gas phase processes of 30 electron volts per ion pair, a total of about 6×10^{16} ion pairs are produced. Assuming an average lifetime of about 10^{-5} second for recombination or reaction of the ion pairs, a steady state of about 3×10^{8} ion pairs in the system is achieved, or about 10^{-14} mole fraction. The only manifestation of the interference of such fragments with the problem under investigation would be their reaction with radioactive bromine, whose concentration is about 10^{-13} mole fraction. Since the probability of reaction is a function of the product of the two concentrations, little interference is to be expected. If these fragments initiated chains that would interfere with the radioactive bromine, the presence of macroscopic amounts of bromine in the irradiated liquid would be expected to interfere with or eliminate this effect.

To determine the extent of such effects of radiation damage and/or impurities, *n*-propyl bromide was irradiated with 10^{-4} mole fraction of bromine and the distribution of activity compared with irradiations in the absence of bromine. It may be observed from the data in Table II that the presence of bromine in low concentration does not significantly affect either the retention or the distribution of organic radioactivity. This is strong evidence for the absence of effects of radiation or impurities.

To investigate the possibility of radiation effects on the solid, it was considered that in the case of irradiation

[6] W. H. Hamill and R. R. Williams, J. Am. Chem. Soc. 72, 2813 (1950).

TABLE II. Effect of 10^{-4} mole fraction of bromine on hot atom chemistry of normal propyl bromide at room temperature.

	n-Propyl bromide $+Br_2$	*n*-Propyl bromide $+Br_2$	Pure *n*-propyl bromide
Retention (%)	33.3	34.5	34.7
C_2H_5Br (%)	0.6	0.8	0.7
$CH_3CHBrCH_3$ (%)	1.4	1.7	1.7
$CH_3CH_2CH_2Br$ (%)	16.0	16.9	17.1
CH_2Br_2 (%)	1.8	1.8	1.8
CH_2BrCH_2Br (%)	3.2	2.4	3.1
$CH_3CHBrCH_2Br$ (%)	3.3	2.4	2.8
$CH_2BrCH_2CH_2Br$ (%)	2.7	2.9	2.7
Polymer (%)	1.6	1.6	1.5

of solid *n*-propyl bromide, the fragments might be trapped in the crystal lattice and might be able to react upon melting. Melting, of course, is required for extraction. To check this possibility, 20 ml of solid *n*-propyl bromide at −126°C was irradiated in the normal manner and then dissolved without melting in about 80 ml of ethylene, the temperature being held constant at −126°C. It was expected that any fragments frozen in the lattice might react with the solvent ethylene, rather than interfere with the radioactive halogen. Any uncombined halogen atoms would also probably react with the ethylene. If these fragments were of any influence on the final products containing radioactive halogen, a considerable distortion in both the retention and the distribution of organic activity would be expected. Table III demonstrates that there is no significant distortion and thus probably no such effect as that suggested. Some difference may be observed in the dibromopropane and polymer products, but this is within the limits of experimental error.

Again, to demonstrate the absence of radiation effects, it was assumed that the fragments resulting from radiation damage would be caught in the crystal lattice of irradiated solid hydrocarbons. It was also assumed that if radiation damage interfered with this study, these fragments would react with extractable bromine. Samples of solid hydrocarbons and liquid propyl bromide were irradiated simultaneously in separate arms of a single irradiation tube. These hydrocarbons were shaken up immediately after the irradiation so that they would dissolve and melt in the propyl bromide containing extractable bromine. They were extracted, after five minutes, in the normal manner. The data in Table IV demonstrated that this procedure had no significant effect on the retention.

TABLE III. Effect of dissolving solid *n*-propyl bromide irradiated at −126°C in ethylene.

	Ethylene	Normal irradiation
Retention (%)	85.6	88.4
CH_3CH_2Br (%)	2.7	2.8
$CH_3CHBrCH_3$ (%)	3.1	3.4
$CH_3CH_2CH_2Br$ (%)	26.8	26.0
CH_2Br_2 (%)	3.1	2.6
CH_2BrCH_2Br (%)	6.5	6.1
$CH_3CHBrCH_2Br$ (%)	11.2	14.4
$CH_2BrCH_2CH_2Br$ (%)	11.3	8.7
Polymer (%)	13.4	17.6

A critical test on the effect of gamma-radiation was performed by varying the thickness of the protective lead shield during a room temperature neutron irradiation. Table V shows that no observable effects were in evidence.

As important as the problem of the extent of radiation damage is the problem of halogen exchange with alkyl halides.[7] Investigations have demonstrated that in the gas phase bromine does not exchange with ethyl bromide at an appreciable rate, even under drastic conditions.[8,9] Exchange is observed to occur at temperatures above 350°C, but at these temperatures ethyl bromide decomposes to give ethylene and hydrogen bromide, permitting rapid exchange with bromine.[10] To check liquid phase exchange, high specific activity bromine from the irradiation and acidification of aqueous potassium bromate was extracted into 80 ml of isopropyl bromide. The amount of bromine was about 50 milligrams. This mixture was exposed to a 100-watt bulb for twenty-four hours in a sealed flask, then the excess bromine extracted with aqueous sodium bisulfite. Carriers were added to the isopropyl bromide, and the mixture distilled. It was observed that less than 1 percent of the total induced organic activity appeared in iso and normal propyl bromide, all the activity appearing in high boiling dibromides. No analysis was made of the dibromides. Thus it may be assumed that under the conditions of the experiment no exchange occurs between bromine and isopropyl bromide. Although no work was done with *n*-propyl bromide, it would be expected to exchange even less readily than isopropyl bromide since the carbon-bromine bond is stronger.[11]

TABLE IV. Data on solid hydrocarbons at −78°C.

	n-Propyl bromide				Bromide
	Pure	With octane (m.p. −56°C)	With dodecane (m.p. +9°C)	Isopropyl pure	With octane (m.p. −56°C)
Retention (%)	38.7	40.0	38.9	31.7	34.7

Distillation

The fractionating column had a measured efficiency of 22 theoretical plates and a hold-up of about 36 ml. Calculations for the normal and isopropyl bromide separation on the basis of the volumes used demon-

[7] H. Seelig and D. E. Hull, J. Am. Chem. Soc. **64**, 940 (1942).
[8] L. C. Liberatore and E. O. Wiig, J. Chem. Phys. **8**, 349 (1940).
[9] J. B. Peri and F. Daniels, J. Am. Chem. Soc. **72**, 424 (1950).
[10] See reference 9.
[11] H. A. Skinner and J. S. Roberts, Trans. Faraday Soc. **45**, 339 (1949).

strated that the purest fractions of each were more than 95 percent pure for distillation at atmospheric pressure. Since the vapor pressure ratio of normal propyl bromide to isopropyl bromide is the most unfavorable in the monobromide distillation, the purity of ethyl bromide was probably even higher. For the distillation at reduced pressure, the column efficiency is somewhat lower, but except for 1,2 dibromoethane and 1,2 dibromopropane, the vapor pressure ratios are very favorable. This difficulty was somewhat compensated for by the 50 ml of each carrier used, giving a probable purity of about 85 percent for the 1,2 dibromoethane and the 1,2 dibromopropane. The other constituents were separable to better than 95 percent purity. The boiling point of each fraction was accurately known and this coupled with refractive index measurements demonstrated the validity of these calculations.

Carriers were added for all reasonable products from each of the propyl bromides, with the exception of 1,1 and 2,2 dibrompropanes. These were not added because they were not available due to difficulty in their preparation. It is apparent that they did not constitute any significant portion of the total organic activity since their boiling points are sufficiently different from those of the other carriers that they would have shown up as high specific activity fractions in the distillation curves. No such high specific activity fractions were observed in the neighborhood of their boiling points. It was assumed that, as a result of their known instability with respect to rearrangement to 1,2 dibromopropane, if such compounds were formed as a result of the recoil process, rearrangement would occur before the molecule had cooled down to thermal energy.

Some decomposition was observed to occur in the vacuum separation of the dibromides from the monobromides. This was demonstrated by a slight brown discoloration of the dibromide fraction. More decomposition was noted in the dibromide fractionation by the dark brown color of the pot residue at the completion of the distillation. Several experiments were performed to demonstrate that such decomposition had no effect on the distribution of activity in the still, since decomposition of a given fraction of any carrier does not change the specific activity of that carrier. Since the principal bromine product of alkyl bromide decomposition is highly volatile hydrogen bromide, it would not be expected to interfere with other activities in the still.

A sample of pure radioactive isopropyl bromide of known specific activity from another analysis was added to *n*-propyl bromide, ethyl bromide, and dibromopropane carriers. This mixture was refluxed at atmospheric pressure, exposed to the atmosphere, for ten hours. Macroscopic decomposition was manifested at the end of the refluxing by the evolution of hydrogen bromide from the still head. On distillation of the mixture there was no change in the specific activity of the isopropyl bromide other than that due to radioactive decay. Less than 1.5 percent of the total activity appeared in fractions other than those containing isopropyl bromide. This activity appeared in the dibromide fraction and not as ethyl or normal propyl bromide.

TABLE V. Effect of lead shielding on retention of *n*-propyl bromide at room temperature.

	No lead	2 inches of lead	4 inches of lead
Retention (%)	35.5	34.7	34.0

A second experiment involved fractional crystallization of irradiated and extracted *n*-propyl bromide. The solid and liquid fractions were analyzed separately by the normal procedure. This procedure changed the distribution of activities in each fraction, but it may be noted in Table VI that the total distribution of organic activity was not changed.

To establish that the still would not show activity in an inert carrier, 70 ml of benzene were added with the normal volumes of other carriers for a run with *n*-propyl bromide, and although benzene boils only 9.5°C higher than the most active constituent, less than 0.4 percent of the total activity appeared as benzene. The vapor pressure ratio for benzene to *n*-propyl bromide is more unfavorable than for any other two constituents present in a normal distillation.

Special Procedures

To establish the presence of some of the minor products whose boiling points were close enough to interfere with already established major products, a procedure of flooding out was utilized. Carrier for the minor constituent was added with the other carriers, and the mixture distilled. Activities of the purest fraction of the minor constituent were measured, and to about 30 ml of these fractions, about 50 ml more of the carrier were added. This mixture was distilled through a column of about 8 theoretical plates and activities of the various fractions determined. The purest fraction was identified by the boiling point and refractive index, and

TABLE VI. Distribution of products from liquid *n*-propyl bromide irradiated at −78° and fractionally crystallized to disturb the distribution of activity, as compared to the normally treated *n*-propyl bromide.

Retention (%)	Fractionally crystallized I 43.1			Fractionally crystallized II 39.4			Normal treatment
	A[a]	*B*[b]	*C*[c]	*A*	*B*	*C*	*C*
CH_3CH_2Br	0.9	2.1	0.8	1.4	1.9	0.6	0.7
$CH_3CHBrCH_3$	2.2	6.2	2.4	4.9	4.9	2.0	2.2
$CH_3CH_2CH_2Br$	59.0	35.0	16.6	48.6	35.6	16.0	16.3
CH_2Br_2	2.3	6.4	2.5	4.3	6.1	2.3	2.4
CH_2BrCH_2Br	8.4	14.5	5.2	6.9	7.9	3.1	4.2
$CH_3CH_2BrCH_2Br$	7.8	13.5	4.8	13.2	15.3	6.0	4.4
$CH_2BrCH_2CH_2Br$	3.4	8.3	3.3	6.7	7.8	3.2	3.2
Polymer	3.4	5.5	2.1	5.6	7.4	2.8	2.3

[a] Percent yield of solid activity.
[b] Percent yield of liquid activity.
[c] Percent yield of total activity.

TABLE VII. Distribution of activities from *n*-propyl bromide.

Irradiation Temp.	25°C	−78°C	−110°C	−110°C	−125°C	−196°C
Retention (%)	34.7	39.6	39.2	88.1	88.4	88.4
Phase	Liquid	Liquid	Liquid	Solid	Solid	Solid
C_2H_5Br (%)	0.7	0.7	0.8	2.6	2.8	2.7
$CH_3CHBrCH_3$ (%)	1.7	2.2	2.0	3.4	3.4	3.4
$CH_3CH_2CH_2Br$ (%)	17.1	16.3	14.6	26.8	26.0	26.9
CH_2Br_2 (%)	1.8	2.4	1.7	3.0	2.6	2.4
CH_2BrCH_2Br (%)	3.1	4.2	5.6	6.2	6.1	6.0
$CH_3CHBrCH_2Br$ (%)	2.8	4.4	4.2	17.4	14.4	17.8
$CH_2BrCH_2CH_2Br$ (%)	2.7	3.2	2.9	9.0	8.7	10.4
Polymer (%)	1.5	2.3	4.2	16.3	17.6	12.1

TABLE VIII. Distribution of activities from isopropyl bromide.

Irradiation Temp.	25°C	−78°C	−89°C	−89°C	−126°C	−196°C
Retention (%)	31.7	31.5	35.6	88.7	93.9	94.3
Phase	Liquid	Liquid	Liquid	Solid	Solid	Solid
C_2H_5Br (%)	0.7	0.6	0.7	1.2	1.5	1.7
$CH_3CHBrCH_3$ (%)	9.3	9.0	10.1	12.8	11.3	11.7
$CH_3CH_2CH_2Br$ (%)	2.5	3.2	4.1	29.9	30.9	31.8
CH_3CHBr_2 (%)	1.6	1.6	1.4	1.9	1.8	1.3
CH_2BrCH_2Br (%)	5.4	3.6	4.4	4.8	4.1	4.5
$CH_3CHBrCH_2Br$ (%)	2.3	5.2	5.8	18.2	18.2	18.5
$CH_2BrCH_2CH_2Br$ (%)	0.8	1.3	1.5	5.7	6.3	7.5
Polymer (%)	2.9	3.5	2.8	12.4	17.1	12.4

thus the activity of the minor constituent determined. Since the activities involved in this determination are quite low, the counting error is about 10–15 percent, but the procedure is sufficient to determine the presence of a minor radioactive constituent.

An attempt was made to determine the nature of the "polymer" activity. This is the activity that appeared in the pot residue following each distillation. The specific activity of this residue was much higher than that of any of the carriers in the still and therefore could not be the decomposition product of any of the still constituents. To get some idea of the boiling point of the polymer, inert organic compounds (compounds containing no bromine, and that would not react with alkyl bromides or with each other) with boiling points at intervals of about 25° up to 290°C were added to the pot residue, and the mixture was vacuum distilled through an 8-plate column. Reproducible distillation patterns were obtained with wide variation in organic compounds added. About 60 percent of the pot activity came off at atmospheric boiling temperatures, below 220°C and about 30 percent between 220°C and 275°C. There were apparent maxima in activity at about 215°C and 265°C. Typical distillation diagrams are given in Figs. 1 and 2. It may be noted that more than 90 percent of the total polymer activity was distilled below 280°C. The remainder of the activity appeared as decomposition products in the still pot.

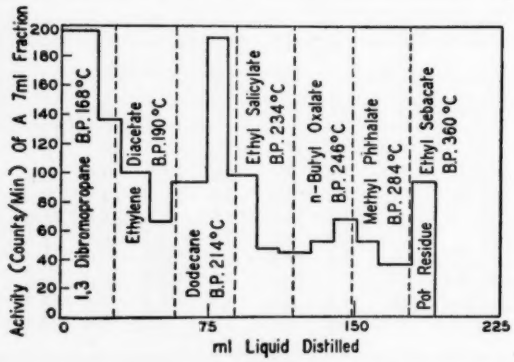

FIG. 1. Distillation curve for polymer from isopropyl bromide irradiated at −196°C.

II. RESULTS

Tables VII and VIII and Fig. 3 give the major experimental results, showing the distribution of non-extractable or organic activity as percentage yields of the total activity at various temperatures. Table VII refers to the experiments in which *n*-propyl bromide was irradiated; Table VIII, isopropyl bromide. The first column gives the compounds that were analyzed, and the adjacent columns give the retention (percent of total activity) and the respective yields of each compound at irradiation temperatures given in the first row. Figure 3 gives the average retention values for various irradiation temperatures for normal and isopropyl bromides. In general the data in Tables VII and VIII are accurate to about one unit. Methyl bromide was added as a carrier

TABLE IX. Retention of radiobromine isotopes in isopropyl bromide produced by (n, γ) reaction.

	25°C	−196°C
Br^{80} (18 min)	33.7±2.0%	81.6±2.0%
Br^{80m} (4.4 hr)	33.9±2.0%	79.9±1.0%
Br^{82} (36 hr)	30.3±2.0%	93.8±0.5%

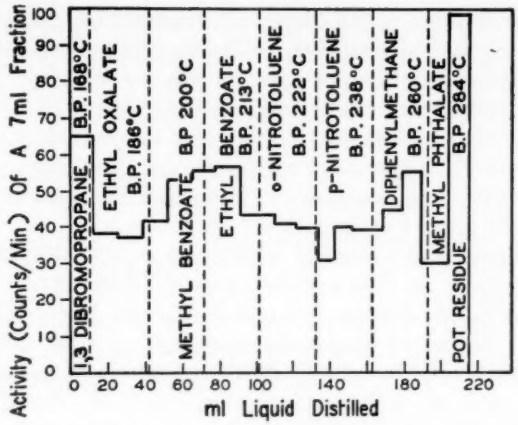

FIG. 2. Distillation curve for polymer from isopropyl bromide irradiated at −196°C.

in all distillations, but because of the crudeness of its separation the absolute value of its contribution to the total activity was uncertain as compared to the other data, so these values were not included in any of the tables. The yield of methyl bromide was about 1–2 percent of the total activity. The products considered accounted for about 95 percent of the total organic activity.

A number of experiments were performed to establish the absence of any observable effects of radiation and minor impurities that might not have been removed by the purification procedure used, as described in Sec. II.

Theoretical consideration, described later, of the theory of the remarkable phase effect shown by the propyl bromides and other substances[2a, b] led to the prediction, detailed in the next section, that retentions in the solid phase could well be dependent on recoil energies, whereas liquid retentions would be less sensitive. Experiments on this point are given in Table IX from which it appears that Br^{82} probably has a lower average recoil energy at birth than does Br^{80} (4.4 hr) or Br^{80*} (18 min) and that the latter two have similar average energies of recoil. The errors given are based principally on the statistics for the counting of the radioactivities.

IV. DISCUSSION

A. Phase Effect

The data reveal a very marked dependence of the yields of certain products on phase—a discontinuous rise of about fourfold occurring on solidification of the

TABLE X. Ratio of yield in solid to yield in liquid phase.

	n-Propyl bromide irradiated	*i*-Propyl bromide irradiated
$CH_3CH_2CH_2Br$	1.65±0.1	9.4 ±2.0
$CH_3CHBrCH_3$	1.7 ±0.5	1.30±0.2
CH_2BrCH_2Br	1.4 ±0.4	1.0 ±0.2
$CH_3CHBrCH_2Br$	4.0 ±1.0	4.2 ±1.0
$CH_2BrCH_2CH_2Br$	3.1 ±0.5	5.5 ±2.0
Polymer	5.7 ±2	4.2 ±1.5

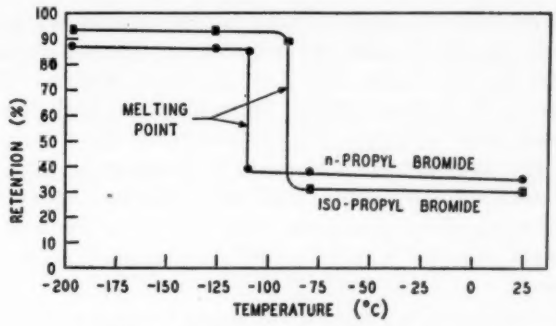

FIG. 3. Temperature *versus* retention.

propyl bromide and very little effect of temperature above and below the melting point being revealed. Table X gives the elevations in retention observed.

The yields of *n*-propyl out of *n*-propyl and isopropyl out of isopropyl target molecules have phase effect ratios of 1.65±0.1 and 1.30±0.2, respectively, while the yield of normal propyl out of isopropyl shows a ratio of 9.4±2.0. It appears that the products divide into two classes corresponding to phase effect ratios greater or less than about three. These groups are given in Table XI.

In this listing the less certain minor constituents generally have been omitted. It appears that C_2H_5Br is hot out of iso and possibly out of normal, CH_2Br_2 is hot out of normal and CH_3CHBr_2 is hot out of iso, but one cannot be certain because the experimental errors in any given retention determination amount to about one percent unit.

The theory previously advanced[5, 12–15] for hot and epithermal reactions in organic systems consisted essentially in the division of the reactions into two classes corresponding to the energy of the recoiling radioactive atom. Reactions occurring in the high energy range where the chemical bonds are small were called "hot" and those occurring in the range where the energy is still somewhat larger than the chemical bond but not over two- or threefold larger were called "epithermal."

In the hot range the only collisions leading to retention of radioactivity in the organic phase are supposed to involve transfer of the momentum of the hot Br* atom so the free radicals generated in the collision and the stopped Br* atom are left in the same solvent cage,

TABLE XI.

Hot (below 3)	Epi (above 3)
n-propyl out of *n*-propyl	*n*-propyl out of *i*-propyl
i-propyl out of *i*-propyl	$CH_3CHBrCH_2Br$ out of either
CH_2BrCH_2Br out of either	$CH_3BrCH_2CH_2Br$ out of either
probably *i* out of *n*[a]	Polymer out of either

[a] The experimental data are so uncertain in this case that the classification of this product is difficult.

[12] W. F. Libby, J. Am. Chem. Soc. **62**, 1930 (1940).
[13] W. F. Libby, Science **93**, 283 (1941).
[14] W. F. Libby, J. Am. Chem. Soc. **69**, 2523 (1947).
[15] Miller, Gryder, and Dodson, J. Chem. Phys. **18**, 579 (1950).

so reactions to form organic radiobromides are very probable. In the case of the propyl bromides it is clear that the only atom heavy enough to decelerate a Br^{82} atom in a single collision is Br, so we expect the original molecule to be a principal product of the hot reactions.

The epithermal reactions are supposed to devolve around solvent cage action also with the important difference that the stopping of the recoiling Br atom no longer requires a collision with a Br atom since the energy and momentum of recoil can be transferred to the molecule struck as a whole by inelastic processes. This means that the free radicals generated by the disruption of the molecule struck can be of any type, and one expects that the formation of new molecules different from the target molecule is extremely likely. In other words, epithermal reactions should lead to H substitution, C—C rupture and replacement, and other types of fundamental chemical change, while hot reactions ought in general to re-form the mother or target molecule.

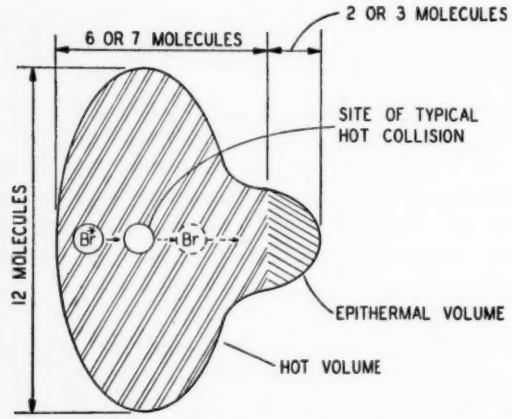

FIG. 4. Postulated nature of instantaneously molten volumes formed by hot atoms in solids.

If the theory outlined is correct, or essentially so, one expects a rather considerable difference in the effect of so fundamental a change in the characteristics of the solvent cage as that brought about by solidification. In a general way the processes involving the most energy, the hot reactions, should be least affected since the solid probably will be melted for a considerable region around the reaction site by the energy passed on to the struck Br atom as well as by that dissipated by the radioactive Br* atom before the head-on Br collision which leads to retention (see Fig. 4). Therefore relatively little difference between the liquid and solid phases might be expected for hot reactions. The epithermal reactions, however, should show a much larger response to solidification because they occur at the very end of the range of the recoiling atom. The epithermal reaction site being at the end of the range is on the surface of the molten drop formed instantaneously in the solid by the recoiling atom. A diagrammatic representation is given in Fig. 4. Since the epithermal site is on the surface it will have a large fraction of its cage wall solidified by the phase change and so rendered much less permeable[16] with a resultant large increase in probability of epithermal reactions. The hot sites residing within the drop are not subject to this effect. In either case the temperature of the phase should have relatively less effect since even the epithermal reaction energies make thermal energies appear small in comparison.

Glancing at Table XI we see that the theoretical expectations are borne out fairly well in that the phase effect ratios fall into two classes above and below 3, with the mother molecules belonging to the low ratio as they should as hot products, while the isomers, H substitution, and polymer products show the larger ratio expected for epithermal reactions. The hot character of the CH_2BrCH_2Br yield together with the data on the minor constituents will be discussed later.

Pursuing our phase effect theory in more detail, the recoil atom is considered to lose energy by two mechanisms. One is by the exchange of momentum, and the other is by breaking chemical bonds. Assuming an average bond energy of four electron volts, the change in the energy of the recoil atom dE in electron volts for a distance dx in units of molecular diameter can be given by

$$dE/dx = -kE - 4. \tag{1}$$

k is calculated by the elastic collision theory for individual atoms from the relation[14]

$$k = 1-(1-\gamma)[1-\ln(1-\gamma)]/\gamma, \tag{2}$$

where

$$\gamma = 4M'M/(M+M')^2,$$

M' and M being the respective masses of the colliding particles.

An approximate k for C_3H_7Br is 0.19. Substituting, and solving the differential equation,

$$E = (E_0+21)e^{-0.19x} - 21, \tag{3}$$

where E_0 is the initial energy of the recoil atom. The heat generated by this process, $H(x)$, neglecting recombination of the fragments produced in the process, would be

$$H(x) = kE = 0.19(E_0+20.7)e^{-0.19x} - 4. \tag{4}$$

If the heat of fusion is about 0.1 ev and there is no heat flow in the direction of the path of the recoil atom, a cone-like volume of liquid results, with a maximum diameter of about 16 molecules for a 100-electron volt bromine atom. Figure 4 presents the model graphically. Allowing heat flow along the path, the ends of the volume become rounded, containing the same volume as

[16] This phenomenon was described somewhat graphically by Rabinowitch (Trans. Faraday Soc. **33**, 1225 (1937)) in his calculation of coordination duration between two particles in a solvent cage as a function of diffusion coefficient. For a liquid whose diffusion coefficient is 10^{-5} cm²/sec this duration is given as 10^{-10} sec or about 10^3 vibrations, whereas for a solid with a diffusion coefficient of 10^{-12} cm²/sec the duration is given as 10^{-3} or about 10^{10} vibrations.

the original cone-like volume, with a maximum diameter of about 12 molecules. This model results in a pear-shaped volume in which the recoil atoms may react.

It is now proposed that the hot reactions occur in the portion of the pear-shaped liquid drop several molecules in diameter, and the epithermal reactions in the little knob, perhaps two molecules in diameter, at the end of the path of the recoil atom. The radioactive atom may appear in either place or anywhere in between. If it makes a hot collision early in its career, it will remain in the center of the drop, while the nonradioactive bromine, having taken on almost all of the energy, continues on the original path to produce the same kind of liquid drop. Here the reactions of the radiobromine would be more independent of phase since the immediate locale is always liquid. If no such head-on collision occurs, the radioactive bromine ends up in the small knob at the end of the path in close proximity to the phase wall in the solid case and the main body of the liquid in the liquid case, causing a phase dependence.

From this model it is predicted that higher recoil energies should be associated with lower retention in the solid phase, since the size of the liquid drop would increase with increasing initial recoil energy and the chance of epithermal reaction be reduced both by increasing the chance of deceleration clear through the epithermal region and by melting more of the wall surrounding the epithermal volume. The liquid phase retention, on the other hand, should show little or no variation in retention since the initial bromine recoil energy is of less consequence in the homogeneous environment. The three isotopes of bromine that may be prepared by (n,γ) reactions were used to test these considerations. The variation in retention between Br^{80} and Br^{82} thus would seem to indicate a higher recoil energy for the Br^{80}, while the absence of variation between Br^{80} and Br^{80m} would indicate a similarity in the high energy portions of their capture gamma-ray spectra. The small variation in the liquid phase retention in contrast to the variation in the solid phase retentions seems to verify the predictions.

Goldhaber, Chiang, and Willard[2a] have studied the effects of phase change on both the neutron capture activated bromine and isomeric transition activated bromine in CCl_3Br and CCl_2Br_2, and of neutron capture activated chlorine in CCl_2Br_2 and CCl_4. Their results, given in Table XII, show increases of retention on solidification less than are shown by the propyl bromides, but nevertheless of considerable magnitude. It appears also that in these cases the increase did not occur abruptly at the phase transition but shows some tendency to continue to rise as the temperature is lowered below the melting point.

The products of the hot and the epithermal reactions in those cases in which the recoiling atom has a mass nearly equal to the masses of the atoms constituting the molecules in the main system are often difficult to distinguish. This applies to CCl_3Br, CCl_2Br_2, and CCl_4. In general one might expect a lower phase effect, on the basis of the theory previously outlined, in a case such as CCl_4 where the probability of reactions occurring in the hot range is much greater and the consequent probability of the hot atoms being degraded completely through the epithermal range into the thermal is much larger. In a general way the data in Table XII do not seem to be in disagreement with these notions.

B. Polymer Production

Willard and co-workers[17,18,2a] and others[19] have repeatedly reported the formation of higher boiling radioactive fractions in neutron bombardment of organic halides. This phenomenon has been more firmly established recently with the observation of the increase of polymer yield on solidification first reported by Goldhaber, Chiang, and Willard,[2a] and confirmed in this research in the case of the propyl bromides. Since the impurities would be frozen out and thermal reactions halted at liquid nitrogen temperatures, and since two samples irradiated at the same temperature but in different phases (Tables VII and VIII) and analyzed in the same way gave higher polymer yields for the solid in all cases, we must conclude that polymerization probably is a phenomenon characteristic of hot atom chemistry. In the present research the polymer fractions were observed to have higher specific activities than any other constituent in the still, so the possibility of "tarring" is excluded further as an explanation.

TABLE XII. Phase effect on retentions (Goldhaber, Chiang, and Willard (see reference 2a)).

Br^{82} in CCl_3Br		Br^{82} in CCl_2Br_2		Cl^{38} in CCl_4	
25°	40	32°	40	30°	43
−3°	44	22°	Freezing point	0°	44
−5°	Freezing point	0°	75	−23°	Freezing point
−6°	58		...	−37°	51
−80°	75		...	−80°	75
−190°	72		...		...

Goldhaber, Chiang, and Willard[2a] have suggested that the polymer formation probably is caused by the recoiling atom rupturing adjacent molecules. This seems eminently reasonable. We would add that the magnitude of the phase effect places the phenomenon in the epithermal range. If we imagine a bromine atom with an energy three or four times the bond energy transferring part of its energy in an inelastic collision which ruptures one molecule, it seems probable that its next collision may lead also to rupture in addition to nearly complete deceleration of the radiobromine atom. Since the mean free path of a bromine atom should be of the order of one molecular diameter, the radiobromine atom and several

[17] E. G. Bohlman and J. E. Willard, J. Am. Chem. Soc. **64**, 1342 (1942).
[18] J. E. Willard, J. Phys. and Colloid Chem. **52**, 1585 (1948).
[19] P. Süe and A. Nouaille, Compt. rend. **230**, 954 (1950).

TABLE XIII. Theoretically predicted and observed hot products.

n-Propyl		Isopropyl	
Expected	Observed	Expected	Observed
$CH_3CH_2CH_2Br$	Yes	$CH_3CHBrCH_3$	Yes
CH_3Br	Possibly	CH_3Br	Possibly
C_2H_5Br	Possibly	C_2H_5Br	Yes
CH_2Br-CH_2Br	Yes	CH_2Br-CH_2Br	Yes
$CH_2Br-CH_2-CH_2Br$	Probably masked by epithermals	$CH_3-CH_2-CH_2Br$	Probably masked by epithermals
$CH_3-CHBr-CH_2Br$		$CH_3CHBrCH_2Br$	
$CH_3-CHBr-CH_3$		CH_3CHBr_2Br	Yes
CH_2Br_2	Yes	No	$CH_3BrCH_2CH_2Br$
$CH_3-CH_2-CHBr_2$	Not tested	$CH_3CBr_2CH_3$	Not tested

radicals produced in these neighboring inelastic collisions may with a fair probability be found to occupy essentially the same cage. Reactions might then proceed with considerable efficiency to form products of increased molecular weight. For example, in our case of the propyl bromides the radicals might be: $C_3H_6Br\cdot$, $C_2H_4Br\cdot$, $CH_2Br\cdot$, and $Br\cdot^*$, one H atom having escaped the cage. Disproportionation then could occur according to

$$C_3H_6Br\cdot+CH_2Br\cdot=CH_3Br+C_3H_5Br. \quad (5)$$

The olefin C_3H_5Br then could react with the remaining radicals to form tribromopentane containing radiobromine:

$$C_3H_5Br+C_2H_4Br\cdot+Br\cdot^*=C_5H_9BrBrBr^*. \quad (6)$$

These types of reactions have been commonly accepted in free radical chemistry.[20,21] Considering all of the possible radicals from *n*-propyl bromide, the olefins that become available for addition are ethylene, propylene, bromoethylene, 1-bromo-1-propylene, and 1-bromo-2-propylene. The addition of two of the other three radicals probably is controlled by steric considerations and energetics. Assuming that atomic radiobromine adds so the product is detectable, the remaining radical will be one of the following: CH_3, C_2H_5, CH_2Br, C_2H_4Br, C_3H_7, $CH_2CH_2CH_2Br$, CH_3CHCH_2Br, and CH_3CH_2CHBr. It may be seen readily that the number of possible compounds is large, including monobrom-, dibrom-, and tribrom- derivatives of propane, the butanes, the pentanes, and the hexanes.

A similar consideration of isopropyl bromide gives a similar though not identical array of possible products. The large number of possible products makes any kind of detailed analysis prohibitively difficult. It was established by an inert carrier technique with vacuum distillation, using two different sets of carriers in the distillation, that about 60 percent of the polymer activity boiled between 168° and 220°C and about 30 percent between 220°C and 275°C, with apparent maxima in activity at about 215°C and 265°C. The maxima accounted for about 25 percent and 10 percent of the total polymer activity, respectively. These boiling ranges are satisfactory from the theoretical point of view set forth above, but certainly by no means completely confirmatory.

The possibility of synthesizing radioactive compounds of higher molecular weight by hot atom chemistry may have some practical applications.

C. Hot Products

The phase effect shows that not only the mother molecules but certain others are formed in hot reactions. According to Tables VII, VIII, X, and XI, CH_2BrCH_2Br and probably C_2H_5Br are formed from either iso or normal propyl bromide in hot reactions. In addition CH_2Br_2 from normal and CH_3CHBr_2 from iso seem to occur.

Considering *n*-propyl bromide struck at the bromine atom essentially head-on by the high velocity radiobromine, the initial results will be the formation of a highly excited propyl radical which is trapped in the same solvent cage with the decelerated projectile radiobromine atom. Obviously the principal reaction should be recombination to form the mother molecule:

$$CH_3\cdot CH_2\cdot CH_2+Br^*=CH_3CH_2CH_2Br. \quad (7)$$

In addition, one can imagine that the propyl radical might decompose before recapturing the Br* atom. The various cases for single bond rupture would be:

A. $CH_3\cdot+CH_2=CH_2$;
B. $C_2H_5\cdot+CH_2$;
C. $CH_3\cdot CH=CH_2+H$;
D. $CH_3\cdot CH_2\cdot CH+H$;
E. $CH_2\cdot CH_2\cdot CH_2+H$.

The products of reaction involving the trapped Br* atom to be expected are:

A. CH_3Br^*, $CH_2Br^*-CH_2Br$, $CH_3CH_2Br^*$, $CH_2Br^*-CH_2CH_3$.

In the last three products it is supposed that the free radical first produced, e.g., $CH_2Br^*-CH_2\cdot$, in the case of ethylene, would eventually capture a Br or H atom from the solvent *n*-propyl bromide or react with the CH_3 radical left in the cage. Similarly,

B. $C_2H_5Br^*$, CH_2Br^*Br, or CH_3Br^*;
C. $CH_3CHBr^*-CH_2Br$, or $CH_3CHBr^*-CH_3$;
D. $CH_3\cdot CH_2\cdot CHBr^*Br$, $CH_3CH_2CH_2Br$;
E. $CH_2Br^*CH_2\cdot CH_2Br$, $CH_2Br^*CH_2CH_3$.

Summarizing, the hot products for *n*-propyl bromide might consist of CH_3Br^*, $C_2H_5Br^*$, $CH_2Br^*-CH_2Br$, $CH_2Br^*-CH_2-CH_2Br$, $CH_3CH_2CHBr^*Br$, CH_2Br^*Br, $CH_3CHBr^*-CH_2Br$, $CH_3CHBr^*-CH_3$, as well as the principal one, $CH_3CH_2CH_2Br^*$.

For isopropyl the same analysis gives

A. $CH_3\cdot+CH_3-CH\cdot$;
B. $CH_3\cdot+CH_2=CH_2$;
C. $CH_3-CH=CH_2+H$;
D. CH_3-C-CH_3+H;

[20] W. H. Waters, *The Chemistry of Free Radicals* (Oxford University Press, London, 1949), p. 129.
[21] E. W. R. Steacie, *Atomic and Free Radical Reactions* (Reinhold Publishing Company, New York, 1946), p. 81.

with the products

A. CH_3Br^*, CH_3CHBr^*Br, $CH_3CH_2Br^*$, $CH_3CHBr^*CH_3$;

B. Same as for *n*-propyl A;

C. Same as for *n*-propyl C;

D. $CH_3CBr^*Br-CH_3$, $CH_3CHBr^*-CH_3$.

Summarizing in Table XIII we see that the predicted and observed products show considerable agreement.

D. Epithermal Products Other than Polymer

The four products showing the large phase effect are the two dibromopropanes, *n*-propyl bromidefrom irradiated isopropyl bromide, and the polymer. The epithermal collisions are imagined to introduce a large internal excitation energy into the target molecule so nearly any type of bond rupture is conceivable. The elimination of a H atom to form the various C_3H_6Br radicals will of course produce the dibromo derivatives as products. The rupture of the C—Br bond to form the propyl radical produces the mother molecule.

In this epithermal production of the propyl bromides it is possible apparently for isomerization of the propyl radical to occur before recombination. The remarkable epithermal production of normal from isopropyl bromide strongly indicates the normal propyl radical to be stabler than the iso. Glazebrook and Pearson[22] have observed that photochemical decomposition of diisopropyl ketone in the gas phase results chiefly in the production of *n*-propyl radical, so it is suggested that, given sufficient time, the isopropyl radicals tend to rearrange into *n*-propyl radicals. Kharasch, Kane, and Brown,[23] on the other hand, failed to find isomerization at 77°C in CCl_4 solution. They thermally decomposed *n*-butyryl peroxide and found only *n*-propyl chloride as product with no trace of isopropyl chloride. Similarly decomposition of isobutyryl peroxide in the same solvent yielded pure isopropyl chloride with no trace of the normal isomer. Perhaps one might conclude that isomerization occurs readily only in excited states of the propyl radical and that our epithermal radicals are sufficiently excited to isomerize.

---

[22] H. H. Glazebrook and T. G. Pearson, J. Chem. Soc. 1777 (1936).

[23] Kharasch, Kane, and Brown, J. Am. Chem. Soc. **63**, 526–528 (1941).

Rotational Structure of the ν_3 Raman Band of Methane*

B. P. Stoicheff,† C. Cumming,‡ G. E. St. John,§ and H. L. Welsh
McLennan Laboratory, University of Toronto, Toronto, Canada

(Received November 12, 1951)

A multiple reflection Raman tube and a high dispersion quartz spectrograph were used to investigate the fine structure of the ν_3 band of gaseous methane. Sixty-eight maxima were measured, and evidence for all but one of the 15 theoretically predicted sub-branches was found. An evaluation of the rotational constants by combination relations for Raman and infrared frequencies gives three different B values for the upper vibrational state and surprisingly, three for the ground state. A more acceptable analysis, based on a single set of rotational constants for the ground state, $B_0=5.253$ cm^{-1} and $D_0=1.9\times10^{-4}$ cm^{-1}, leads to B_1 values for the various branches in the range 5.202 to 5.235 cm^{-1}. The analysis gives $\nu_0=3018.7$ cm^{-1} and $\zeta_1=0.056$. The constants obtained for the ground state are also used in an analysis of the $2\nu_3$ infrared band.

INTRODUCTION

EXPERIMENTAL data on the rotational structure of vibrational Raman bands of polyatomic molecules are extremely meager; only for methane[1] and ethane[2] has a partial resolution of such structures been obtained. Since the intensity of Raman scattering is low, the experimental difficulties associated with high resolution Raman spectroscopy are formidable and are accentuated in fine structure investigations by the necessity of working at low gas densities to prevent excessive line broadening. Nevertheless, it is important to obtain Raman spectra with an instrumental resolution approaching that achieved in infrared absorption, since it is certain that many problems, in particular the interaction of rotation and vibration, cannot be studied adequately by infrared investigations alone. In addition precise frequency data obtained from high dispersion Raman spectra of gases can be used with good effect in increasing the accuracy of molecular structure calculations.

Raman investigations at high resolution have been made feasible to some degree by the development of water-cooled Hg lamps of high intensity and by increasing the efficiency of Raman tubes for gases by multiple reflections in a system of concave mirrors.[3] These methods have been used to obtain considerably greater detail of the ν_3 band of methane than was observed in the early investigation of Dickinson, Dillon, and Rasetti.[1] This Raman band is one of the easiest to investigate with high resolution since its intrinsic intensity is exceptionally high. However, it appears that with an extension of the methods used it will be possible to resolve the fine structure of many Raman bands of the lighter molecules.

EXPERIMENTAL

Since methane is transparent in the ultraviolet, the mercury line 2537A was used for excitation. A two-mirror system for multiple reflections was incorporated in the Raman tube; by this means the intensity of the scattered light entering the spectrograph was increased by a factor of nearly four.[3] The tube was illuminated over 36 cm of its length by four helical lamps of fused quartz with water-cooled mercury pools. The lamps were operated at a current of eight amperes; no gain in intensity of the resonance line 2537A is obtained at higher currents, probably because of self-absorption of the radiation in the lamp. A distressing feature of the high current quartz lamp is the rapid decrease of the ultraviolet transmissivity of the quartz; after 400 hours of operation the intensity of 2537A radiation is reduced by a factor of at least three. The transmissivity can be restored to some extent by treating the inside of the coil with hydrofluoric acid.

The spectrograph used is a two-prism quartz Littrow instrument with an f:22 lens of focal length 155 cm, giving a reciprocal linear dispersion of 27 cm^{-1}/mm at 2537A. The spectrograph and source unit are located in a thermostated room, the temperature of which is held constant to within ±0.2°C; in addition, the spectrograph is lagged with a thick wooden box. The source unit is surrounded by a plywood box from which the air is continuously removed by a fan to the outside, in order to dispose of ozone and excessive heat produced by the Hg lamps. All exposures were taken during periods of relatively constant (±2.5 mm Hg) atmospheric pressure to obtain good definition in the spectrograms. For future work the prisms have been surrounded by a sealed metal box in which a constant density of air is maintained.

In a concurrent investigation on the pressure broadening of Raman lines, it was found that the half-widths of the rotational lines of the ν_3 band of methane increase linearly with pressure. Extrapolation of the results to zero pressure and zero slit width gave a

* A summary of some of the results of this investigation has been published as a Letter to the Editor, Phys. Rev. **84**, 592 (1951).

† Holder of a Garnet W. McKee-Lachlan Gilchrist Post-doctorate Scholarship, School of Graduate Studies, University of Toronto, 1950–51. Now in the Division of Physics, National Research Laboratories, Ottawa, Canada.

‡ Holder of a scholarship under the Research Council of Ontario, 1950–51.

§ Holder of a Garnet W. McKee-Lachlan Gilchrist Scholarship, 1950–51.

[1] Dickinson, Dillon, and Rasetti, Phys. Rev. **34**, 582 (1929).

[2] C. M. Lewis and W. V. Houston, Phys. Rev. **44**, 903 (1933).

[3] Welsh, Cumming, and Stansbury, J. Opt. Soc. Am. **41**, 712 (1951).

TABLE I. Frequencies in the ν_3 Raman band of methane.

Observed frequency, cm^{-1}	Assignment	Calculated frequency, cm^{-1}	Observed frequency, cm^{-1}	Assignment	Calculated frequency, cm^{-1}
3300.5	$S^+(12)$	3301.5	2998.5	$P^+(2)$	2998.7
3288.8	$S^0(12)$	3288.7		$P^0(2)$	2997.6
3280.9[a]	$S^+(11)$	3281.0	2988.0	$P^+(3)$	2988.7
(3269.7)[b]	$S^0(11)$	3269.6		$P^0(3)$	2987.0
3260.4[a]	$S^+(10)$	3260.4	2976.8	$P^+(4)$	2978.6
3250.4[a]	$S^0(10)$	3250.5		$P^0(4)$	2976.2
(3246.4)	$S^-(10)$	...		$P^-(4)$	2974.7
3239.8[a]	$S^+(9)$	3239.9	2966.3	$P^+(5)$	2968.4
3231.1[a]	$S^0(9)$	3231.1		$Q^0(3)$	2966.1
(3227.4)	$S^-(9)$	...		$P^0(5)$	2965.5
3219.5[a]	$S^+(8)$	3219.3		$Q^-(3)$	2965.5
3211.3[a]	$S^0(8)$	3211.6		$P^-(5)$	2963.5
(3207.6)	$S^-(8)$	...	2958.4	$P^+(6)$	2958.2
3198.6[a]	$S^+(7)$	3198.6	(2954.8)[a]	$P^0(6)$	2954.7
3192.1[a]	$S^0(7)$	3191.9	2952.5	$P^-(6)$	2952.2
3177.9[a]	$S^+(6)$	3177.9	(2948.2)	$P^+(7)$	2947.9
3171.8[a]	$S^0(6)$	3172.0	2944.6	$Q^0(4)$	2944.9
3157.2[a]	$S^+(5)$	3157.2		$P^0(7)$	2943.9
3152.2[a]	$S^0(5)$	3152.0		$Q^-(4)$	2943.9
(3147.1)	$R^0(12)$	3147.5	(2940.8)[a]	$P^-(7)$	2940.9
	$R^+(11)$	3145.2	(2937.4)	$P^+(8)$	2937.6
3136.5	$R^0(11)$	3138.2	2933.3[a]	$P^0(8)$	2933.0
	$S^+(4)$	3136.2	(2922.5)	$Q^-(5)$	2922.3
	$R^+(10)$	3135.7		$P^0(9)$	2922.1
3131.9[a]	$S^0(4)$	3131.9	(2912.0)	$P^0(10)$	2911.2
	$R^-(11)$	3131.2	2906.9[a]	$P^-(10)$	2906.5
3126.4[a]	$R^+(9)$	3125.9	2901.2	$Q^0(6)$	2902.3
3115.6[a]	$R^+(8)$	3115.8		$Q^-(6)$	2900.6
	$S^+(3)$	3115.2		$P^0(11)$	2900.3
3105.3[a]	$R^+(7)$	3105.6	2894.7[a]	$P^-(11)$	2894.8
3090.1[a]	$R^0(6)$	3090.0	2889.5[a]	$P^0(12)$	2889.4
3084.8[a]	$R^+(5)$	3084.6	(2882.6)[a]	$P^-(12)$	2883.0
3079.9[a]	$R^0(5)$	3080.0	(2880.9)[a]	$Q^0(7)$	2881.0
3073.9[a]	$R^+(4)$	3073.9	2878.9[a]	$Q^-(7)$	2878.9
(3069.8)[a]	$R^0(4)$	3070.0	(2859.7)[a]	$Q^0(8)$	2859.6
(3066.7)	$R^-(4)$	3067.1	2857.1[a]	$Q^-(8)$	2857.1
(3063.8)	$R^+(3)$	3063.1	(2838.3)[a]	$Q^0(9)$	2838.2
3059.9[a]	$R^0(3)$	3059.9	2835.3[a]	$Q^-(9)$	2835.3
3052.1	$R^+(2)$	3052.2	(2816.5)[a]	$Q^0(10)$	2816.8
(3047.4)	$R^-(2)$	3048.0	2813.3[a]	$Q^-(10)$	2813.1
3041.5	$R^+(1)$	3041.3	(2795.0)[a]	$Q^0(11)$	2795.4
3021.5	$Q^+(\max)$	...	2791.4[a]	$Q^-(11)$	2791.4
			(2773.7)[a]	$Q^0(12)$	2774.0
			2769.2[a]	$Q^-(12)$	2769.2

[a] Frequency used in the analysis.
[b] The bracketted frequencies were measured only from microphotometer traces.

value of 2.5 cm^{-1} for the half-width of the lines. In the fine structure spectrograms a gas pressure of 60 psi and a spectral slit width of 1.5 cm^{-1} were used. Under these conditions the half-width of unblended lines was somewhat less than 3 cm^{-1}.

For frequency calibration an Fe arc spectrum was photographed in juxtaposition with each Raman spectrum. The Raman shifts of most of the lines were determined by measuring the spectrograms with a Hilger comparator and plotting large scale dispersion curves with standard Fe lines. Each plate was measured by two observers and the results averaged. Very weak or diffuse lines were measured from density traces recorded by a Leeds and Northrup microphotometer. Corrections for small displacements of the Fe spectrum with respect to the Raman spectrum were made by using the known frequency of the Hg line, 2759.712A, which falls within the Raman band. Eastman 103a-0 Spectroscopic plates were used.

Methane gas taken directly from commercial cylinders fluoresced under irradiation, producing a dense continuum which obscured the ν_3 band. The fluorescence was eliminated by passing the gas through a glass-wool filter, condensing it at liquid air temperature, and allowing it to evaporate slowly to give the required pressure in the Raman tube.

RESULTS

The final values of the Raman shifts given in the first column of Table I were obtained by averaging the results from four spectrograms with exposure times of 14, 20, 47, and 48 hr. Sixty-eight maxima were measured in the Raman pattern as compared with 14 measured by Dickinson, Dillon, and Rasetti.[1] A microphotometer trace of the 14-hr spectrogram is shown in Fig. 1; beneath the spectrum is plotted the structure of the band as calculated from the results of the analysis given below.

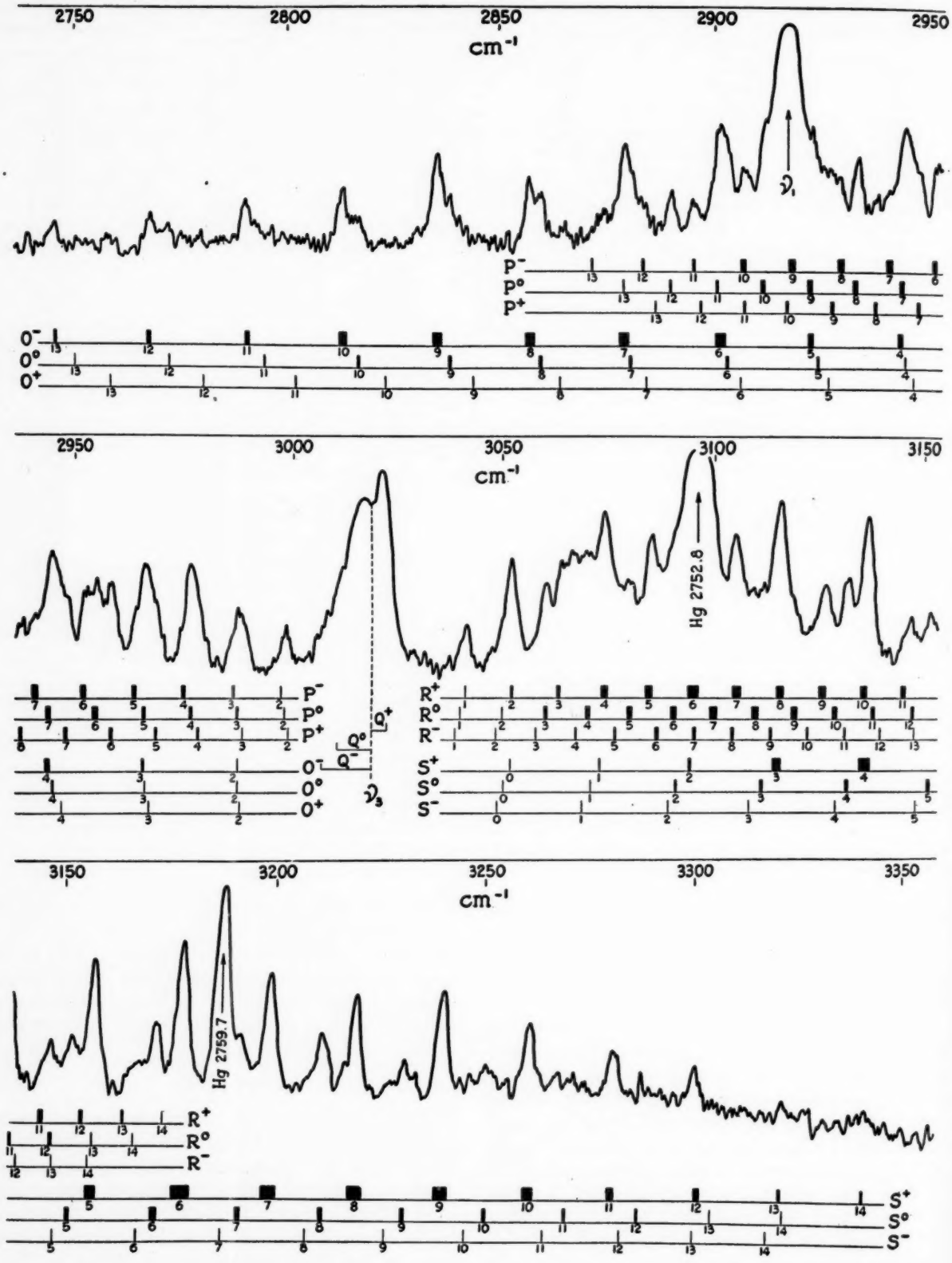

FIG. 1. Microphotometer trace of the ν_3 Raman band of methane. The structure of the band calculated from the results of the analysis is plotted under the trace.

A Raman line at $\Delta\nu=3071.5$ cm^{-1} was measured by Dickinson, Dillon, and Rasetti, and also by MacWood and Urey,[4] who interpreted it as the A_1 part of $2\nu_2$, the upper state of this transition being in Fermi resonance with the upper state of ν_1. In the high dispersion spectrograms there is no indication of any line extraneous to the rotational structure of ν_3 in this region. It is probable that the line measured by the previous investigators at lower dispersion is a group of unresolved lines near the maximum of the R branch. Nevertheless, it is certain that a line observed in liquid methane[5,6] at $\Delta\nu=3053$ cm^{-1} must be interpreted as $2\nu_2$; in this case the rotational lines which are a result of anisotropic scattering are greatly broadened by the intermolecular forces, whereas $2\nu_2$ caused by isotropic scattering remains sharp.

The sharp intense line corresponding to ν_1 falls in the region of the ν_3 band. Since this line was overexposed in the fine structure spectrograms, short exposures of the order of 15 min were made to permit an accurate measurement of the wave-number shift. The value obtained was 2916.5 cm^{-1}; the values found by Dickinson, Dillon, and Rasetti,[1] and MacWood and Urey[4] were 2914.8 cm^{-1} and 2914.2 cm^{-1}, respectively.

ANALYSIS OF THE ν_3 RAMAN AND INFRARED BANDS

The ν_3 band arises from the fundamental transition of one of the 2 triply degenerate (F_2) modes of vibration of the molecule. It was pointed out by Teller[7] that Coriolis interaction between rotation and vibration causes a splitting of the rotational levels of the $v=1$ vibrational state. The energy terms of the three rotational sublevels are given by

$$\begin{aligned} F_1^+(J)&=B_1J(J+1)+2B_1\zeta_1(J+1)-DJ^2(J+1)^2\\ F_1^0(J)&=B_1J(J+1)-DJ^2(J+1)^2\\ F_1^-(J)&=B_1J(J+1)-2B_1\zeta_1J-DJ^2(J+1)^2. \end{aligned} \qquad \text{(I)}$$

In these expressions B_1 is the rotational constant and ζ_1 the vibrational angular momentum for the $v=1$ state; the additional term $DJ^2(J+1)^2$ represents the energy caused by centrifugal distortion. The theory has been further elaborated by Shaffer, Nielsen, and Thomas,[8] who have considered the Coriolis interaction with other vibrational modes, an effect first treated by Jahn,[9] and also second-order interactions including centrifugal distortion and anharmonicity. The calculations of Shaffer, Nielsen, and Thomas show that for a simple valence force field, which is a good approximation for methane, the value of D is given by

$$D=B_0^3[(16/3\nu_1^2)+(5/3\nu_2^2)],$$

where ν_1 and ν_2 are the frequencies of the totally symmetric and doubly degenerate modes of vibration, respectively. Assuming $B_0=5.2$ cm^{-1}, the theoretical value of D is 1.9×10^{-4} cm^{-1}.

In infrared absorption the ground state combines with the $v=1$ state to give 3 branches $R^-(J)$, $Q^0(J)$, and $P^+(J)$ as observed experimentally by Cooley,[10] and Nielsen and Nielsen.[11] According to the analysis of Cooley's results by Childs,[12] the formulas (I) do not satisfy exactly the experimental data.

In the Raman effect all transitions in accordance with the selection rules $\Delta J=0,\ \pm1,\ \pm2,\ J'+J''\geqslant2$ are allowed between the ground state and the Coriolis sublevels of the upper state. Thus, the Raman band consists of 15 sub-branches. The complexity of the band is effectively lessened, however, by the differen relative intensities of the various sub-branches. As stated by Teller,[7] the relative intensities *for high J values* are

$$\begin{aligned} &S^+:S^0:S^-=O^-:O^0:O^+=15:5:1,\\ &R^+:R^0:R^-=P^-:P^0:P^+=10:8:3,\\ &Q^+:Q^0:Q^-=6:9:6. \end{aligned} \qquad \text{(II)}$$

The highest intensities in the outer regions of the band are therefore in the S^+ and O^- branches; this is manifestly the structure observed by Dickinson, Dillon, and Rasetti.

In the present investigation evidence for all but one (O^+) of the 15 sub-branches was found. Because of the complex structure of the band many of the maxima measured are blends of two or more lines. In the analysis, therefore, only those lines were used which had sufficient intensity for accurate frequency measurements, and which were shown by a preliminary analysis to be unblended. These lines are marked in Table I.

Assuming rotational energy terms for the ground state of the form,

$$F_0(J)=B_0J(J+1)-DJ^2(J+1)^2,$$

and the formulas (I) for the $v=1$ state, the molecular constants which can be calculated from the Raman and infrared data are B_0, B_1, D, ζ_1, and the frequency of the band origin ν_0. The infrared frequencies of Nielsen and Nielsen,[11] corrected to cm^{-1} in vacuum, were used.

DETERMINATION OF ν_0, B_0-B_1, AND $B_1\zeta_1$

The values of ν_0, $\nu_0+3B_1\zeta_1$, and B_0-B_1 can be obtained directly from the following sum relations:

$$(\tfrac{1}{2})\{R^-(J)+P^+(J+1)\}=\nu_0-(B_0-B_1)(J+1)^2, \qquad \text{(A)}$$

$$(\tfrac{1}{2})\{S^0(J)+O^0(J+2)\}=\nu_0-(B_0-B_1)(J^2+3J+3), \qquad \text{(B)}$$

$$(\tfrac{1}{2})\{S^+(J)+O^-(J+2)\}=\nu_0+3B_1\zeta_1-(B_0-B_1)(J^2+3J+3). \qquad \text{(C)}$$

It should be noted that only infrared frequencies are used in relation (A) and only Raman frequencies in

[4] G. E. MacWood and H. C. Urey, J. Chem. Phys. **4**, 402 (1936).
[5] Rank, Shull, and Axford, J. Chem. Phys. **18**, 116 (1950).
[6] Crawford, Welsh, and Harrold, Can. J. Phys. March, 1952.
[7] E. Teller, Hand- und Jahrbuch d. Chem. Physik **9, II** (1934).
[8] Shaffer, Nielsen, and Thomas, Phys. Rev. **56**, 895 (1939).
[9] H. A. Jahn, Proc. Roy. Soc. London **168**, 469 and 495 (1938).
[10] J. P. Cooley, Astrophys. J. **62**, 73 (1925).
[11] A. H. Nielsen and H. H. Nielsen, Phys. Rev. **48**, 864 (1935).
[12] W. H. J. Childs, Proc. Roy. Soc. (London) **153**, 555 (1926).

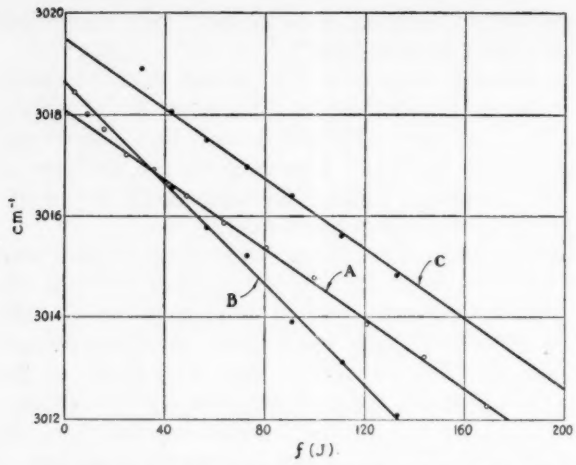

FIG. 2. Determination of ν_0, $\nu_0+3B_1\zeta_1$ and B_0-B_1 from the sum relations (A), (B), and (C).

(B) and (C) and that the centrifugal distortion terms on the right-hand side cancel out, provided D has the same value in both vibrational states. When the left-hand side of (A) or (B) is plotted against the appropriate function, $f(J)$, a straight line is obtained with the intercept on the ordinate axis equal to ν_0 (Fig. 2). A calculation by least squares gives $\nu_0=3018.1$ cm^{-1} from (A) (ignoring the first three points) and $\nu_0=3018.7$ from (B). The small systematic difference which thus appears to exist between the Raman and infrared frequencies is eliminated in the rest of the calculations by raising the infrared frequencies by 0.6 cm^{-1}. The intercept for (C) is $\nu_0+3B_1\zeta_1=3019.6$ cm^{-1}.

A departure from theory is revealed by the fact that the slopes of the three straight lines are not the same. From (A) and (C) in which lines involving F_1^+ and F_1^- states are used, the values of B_0-B_1 are nearly equal, but differ markedly from the value obtained from (B) in which lines involving F_1^0 states are used. It seems advantageous, therefore, at this stage of the analysis to designate by superscripts on the B's the type of states involved in the derivation. Thus, the convergence factors are

$$\left.\begin{aligned} B_0^{+-}-B_1^{+-}&=0.035, \text{ from infrared data,}\\ B_0^{+-}-B_1^{+-}&=0.036,\\ B_0^{0}-B_1^{0}&=0.050,\end{aligned}\right\}\text{from Raman data.}$$

The value of $B_1\zeta_1$ can be found in two ways:

(a) The difference of the intercepts for relations (B) and (C) gives directly $3B_1\zeta_1=0.9$ cm^{-1}.

(b) The combination relation

$$(\tfrac{1}{12})\{S^+(J-1)+O^-(J)-R^-(J)-P^+(J-1)\}=B_1\zeta_1 \quad \text{(D)}$$

gives as the average of six values $B_1\zeta_1=0.29$ or $3B_1\zeta_1=0.87$ cm^{-1}. The two values are in fair agreement; however, the second is considered the more accurate and is used in the subsequent calculations.

DETERMINATION OF THE ROTATIONAL CONSTANTS BY COMBINATION DIFFERENCES

The rotational constants, B and D, for the lower and upper vibrational states are usually evaluated from appropriate difference relations. Since the infrared Q^0 branch has not yet been resolved, Raman data alone must be used in calculating B_0^0 and B_1^0; the S^0 and O^0 lines are most suitable for the purpose. The constants for F^+ and F^- states can be determined from combination differences of Raman and infrared frequencies. This procedure should be most satisfactory when S^+ and O^- lines are used since these are the most accurately measurable Raman frequencies and yield the largest combination differences with the infrared frequencies. The difference relations derived from Eqs. (I) are

$$\{1/(8J+4)\}\{S^0(J-2)-O^0(J+2)\}=B_0^0-D_0^0(2J^2+2J+8), \quad \text{(E)}$$

$$\{1/(8J+4)\}\{S^0(J)-O^0(J)\}=B_1^0-D_1^0(2J^2+2J+8), \quad \text{(F)}$$

$$\{1/(6J+12)\}\{S^+(J)-P^+(J+3)\}=B_0^+-D_0^+(2J^2+8J+12), \quad \text{(G)}$$

$$\{1/(6J+12)\}\{R^-(J)-O^-(J+3)\}=B_0^--D_0^-(2J^2+8J+12), \quad \text{(H)}$$

$$\{1/(6J+6)\}\{S^+(J)-P^+(J)-6B_1\zeta_1\}=B_1^+-D_1^+(2J^2+4J+6), \quad \text{(I)}$$

$$\{1/6J\}\{R^-(J)-O^-(J)+6B_1\zeta_1\}=B_1^--D_1^-(2J^2+4J). \quad \text{(J)}$$

When the left-hand side of each relation is plotted as ordinate with $f(J)$ as abscissa, a straight line is obtained whose intercept and slope are B and D, re-

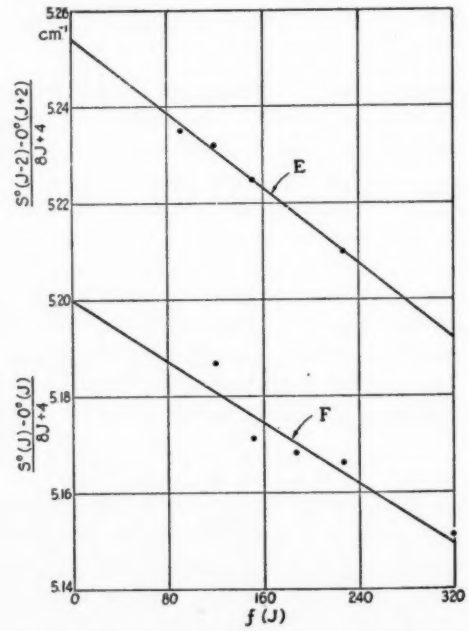

FIG. 3. Determination of B_0^0, D_0^0, B_1^0, and D_1^0 from the difference relations (E) and (F).

spectively. In Fig. 3 the graphs for (E) and (F) are shown. The constants obtained from the six relations by a least-square analysis are

$$\begin{aligned} B_0^0&=5.253, & D_0^0&=1.9\times10^{-4},\\ B_0^+&=5.232, & D_0^+&=1.5\times10^{-4},\\ B_0^-&=5.233, & D_0^-&=1.0\times10^{-4},\\ B_1^0&=5.200, & D_1^0&=1.6\times10^{-4},\\ B_1^+&=5.202, & D_1^+&=1.0\times10^{-4},\\ B_1^-&=5.197, & D_1^-&=0.8\times10^{-4}. \end{aligned}$$

The surprising feature of these results is that B_0^0 is very different from B_0^+ and B_0^- although the three values for B_1 are nearly equal. Also, D_0^0 is 1.9×10^{-4}, equal to the theoretical value, while all the other D values are lower. There is, however, a certain consistency in the analysis since $B_0^0-B_1^0$ is 0.053 in reasonable agreement with the value 0.050 from (B), and $B_0^{+-}-B_1^{+-}$ is 0.033 as compared with the values 0.035 and 0.036 from (A) and (C). The constants also reproduce accurately the frequencies of the lines from which they were derived. It might be expected that these values of the rotational constants would reproduce also the frequencies of the lines not used in the analysis. However, the calculated frequencies of the R^0, P^0, S^-, R^+, and P^- lines differ from the observed frequencies by as much as 2 cm^{-1}, that is by an amount greater than the experimental error.

There is in addition a fundamental difficulty which arises from the results of this analysis; each rotational level of the ground vibrational state, as well as of the upper state, appears to be split and the splitting is proportional to $J(J+1)$. This type of perturbation might well occur in the upper state through a Coriolis interaction with the E part of the nearby $v=2$ state of ν_2. However, according to Jahn's rule,[13] the ground state (A_1) cannot be perturbed by a Coriolis interaction with any of the lower vibrational states of the molecule. A splitting of the rotational levels in consequence of centrifugal distortion[14] also seems unlikely since there is no reason why the sublevels should be designated as F_0^+, F_0^0, and F_0^-, as they are according to this analysis. It must therefore be concluded that the straightforward analysis based on combination relationships has yielded a result which is not understandable from the theoretical viewpoint.

DETERMINATION OF B_1 ASSUMING AN UNPERTURBED GROUND STATE

The basic assumption in the calculation of B_0 by a difference relation is that the upper rotational states are the same for the two branches involved. If the splitting of the rotational levels of the ground state as manifested by the aforementioned different values of B_0 is considered an unacceptable result, it must be assumed that the sublevels of the upper state, $F_1^+(J)$, $F_1^0(J)$, and $F_1^-(J)$, can have different values for the various branches. In the analysis which follows, the ground state is assumed to be unperturbed and the constants, B_0 and D_0, are taken to be equal to B_0^0 and D_0^0 as calculated above from relation (E). It will be shown that these values lead to a consistent analysis of the Raman and infrared ν_3 bands and also of the infrared $2\nu_3$ band.

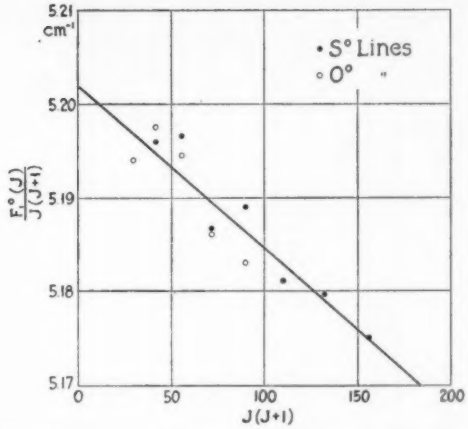

FIG. 4. Determination of B_1^0 and D_1^0 from S^0 and O^0 Raman lines, assuming $B^0=5.253$.

The rotational energy terms of the upper vibrational state can be calculated from the frequencies of the observed transitions and the known values of B_0, D_0, and ν_0. The formula for the S^+ lines is quoted as an example,

$$F_1^+(J)=S^+(J-2)-\nu_0+B_0(J-2)(J-1)-D_0(J-2)^2(J-1)^2. \quad \text{(III)}$$

Rotational constants *for each branch* are then obtained graphically from relations, derived from Eqs. (I), of the type

$$\frac{F_1^+(J)-2B_1\zeta_1(J+1)}{J(J+1)}=B_1^+-D_1^+J(J+1). \quad \text{(IV)}$$

The points for both the S^0 and the O^0 branches (Fig. 4) lie on a reasonably well-defined straight line from which the values, $B_1^0=5.203$ and $D_1^0=1.8\times10^{-4}$ are obtained. The convergence factor, $B_0-B_1^0=0.050$, agrees with that calculated from relation (B). Although comparatively few R^0 and P^0 frequencies are available, the points for the two branches lie on the same straight line, indicating common upper states and giving $B_1^0=5.217$ and $D_1^0=1.8\times10^{-4}$. Thus, the upper states for the R^0 and P^0 lines are not the same as those for the S^0 and O^0 lines.

The points for the S^+ and O^- lines lie on two very different straight lines (Fig. 5) giving $B_1^+=5.206$, $D_1^+=1.0\times10^{-4}$, and $B_1^-=5.235$, $D_1^-=3.8\times10^{-4}$.[15] The average value of the convergence factor, $B_0-B_1^{+-}$, is 0.034, in satisfactory agreement with the value 0.036

[13] H. A. Jahn, Phys. Rev. **56**, 680 (1939).
[14] E. B. Wilson, J. Chem. Phys. **3**, 276 (1935).
[15] Although the D_1 values for the S^+ and O^- branches are not equal to D_0, relation (C) is still valid since a computation shows that the centrifugal stretching terms effectively cancel.

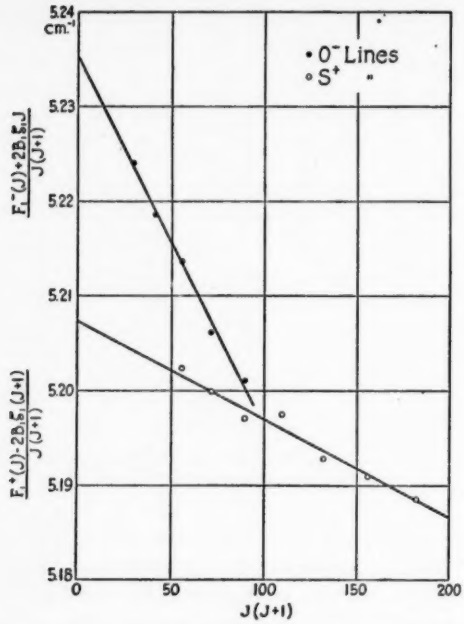

FIG. 5. Determination of B_1 and D_1 from S^+ and O^- Raman lines, assuming $B_0=5.253$.

from relation (C). For the weak S^- and O^+ series the experimental data are insufficient to carry out an analysis. The points for both infrared branches, R^- and P^+, fall on the same straight line (Fig. 6) with $B_1^+=B_1^-=5.217$, $D_1^+=D_1^-=1.8\times10^{-4}$, and $B_0-B_1^+-=0.036$ in good agreement with the value 0.035 from relation (A). Only five lines of the R^- and P^+ series could be measured in the Raman spectrum since these are the weakest of the R and P sub-branches. The average difference between the Raman frequencies and the corresponding infrared frequencies is 0.4 cm^{-1}. Thus, it is probable that the upper states for the R^- and P^+ lines are the same in Raman effect and in infrared absorption. For the R^+ and P^- series the points on the graph (Fig. 7) are more scattered, but there is no doubt that the constants for the two branches are the same,

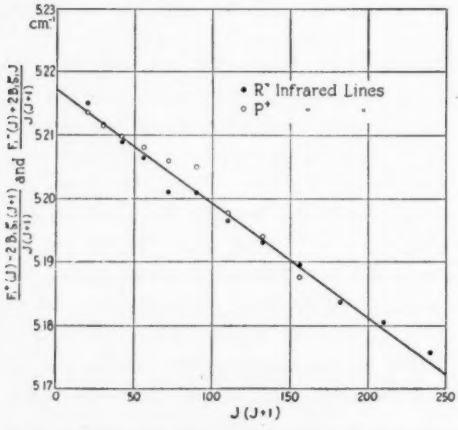

FIG. 6. Determination of B_1 and D_1 from R^- and P^+ infrared lines, assuming $B_0=5.253$.

$B_1^+=B_1^-=5.234$ and $D_1^+=D_1^-=2.9\times10^{-4}$. The results of the analysis are summarized in Table II.

When the constants obtained from the R^- and P^+ branches are used to calculate the infrared frequencies, the experimental values are reproduced to within 0.1 cm^{-1} on the average. Since the analysis shows that the same rotational constants satisfy both R^- and P^+ branches, it should be possible to calculate B_0 and B_1 by combination differences of the infrared frequencies. A least-squares analysis of the data with the relation,

$$\{1/(4J+6)\}\{R^-(J)-P^+(J+2)\} = B_0-B_1\zeta_1-D_0(2J^2+6J+6) \quad \text{(K)}$$

gives $B_0=5.249$, $D_0=1.7\times10^{-4}$, and $B_1=5.216$, $D_1=2.0\times10^{-4}$, which show a satisfactory agreement with the aforementioned values.[16] A further test of the consistency of the analysis is afforded by the evaluation of $B_1\zeta_1$ from infrared data. It can be easily shown from Eqs. (I) that

$$B_1\zeta_1=\{F_1^+(J)-F_1^-(J)\}/2(2J+1). \quad \text{(V)}$$

The average of ten values is $B_1\zeta_1=0.290\pm0.003$ which confirms the value obtained from (*D*).

When the constants of Table II are used to calculate the Raman frequencies, the agreement with the experimental values is very good as shown in Table I. The average discrepancy between observed and calculated frequencies for the 42 lines used in the analysis is only 0.14 cm^{-1}. The diagrammatic presentation of the spectrum under the microphotometer trace in Fig. 1 was prepared from the calculated frequencies. Relative intensities are indicated in the diagram by the *width* of the lines. The total intensity of a given branch line (e.g., $S(6)$) was calculated from the formulas of Placzek and Teller[17] with statistical weights due to nuclear spin as given by Wilson.[18] However, the intensity distribution in the components of a given branch line [e.g., $S^+(6)$, $S^0(6)$, and $S^-(6)$] is only approximate; the matrix elements for the sublevels are not available, and it was necessary to use the relative intensities given in Eqs. (II) which are correct only for high J values. For low J values there are apparent intensity anomalies; thus, for $P(2)$ it is easy to show from the symmetry species of the states involved that $P^-(2)$ has zero intensity, and from the experimental results it appears that $P^+(2)$ has the greatest intensity. For the sake of completeness the weak branches, S^- and O^+, have been included in the diagram although the constants for these lines could not be evaluated; average values, $B_1=5.220$ and $D_1=1.9\times10^{-4}$, were assumed.

It therefore appears that a single value of B_0 and the array of values of B_1, given in Table II, account for the structure of the Raman and infrared spectra. The per-

[16] The lack of agreement with the theoretical formulas, found by Childs (see reference 12) for the infrared ν_3 band, appears to be the result of the use of incorrect combination relations and neglect of the D term.

[17] G. Placzek and E. Teller, Z. Physik **81**, 209 (1933).

[18] E. B. Wilson, J. Chem. Phys. **3**, 276 (1935).

turbation apparent in the spectrum has been ascribed only to the excited vibrational state; in this respect this analysis is more satisfactory from the theoretical viewpoint than the analysis based only on combination relationships. However, the multiplicity of B_1 values is not immediately understandable. The most obvious perturbation of the rotational levels of the $v=1$ state of ν_3 is that resulting from a Coriolis interaction with the nearby and slightly higher $v=2$ state of ν_2. From the calculations of Jahn[9] on a similar but much stronger perturbation of ν_4 by ν_2, it appears that the F_1^+, F_1^0, and F_1^- sublevels are split and also depressed from the unperturbed values. If the perturbation is small, as seems to be the case for ν_3, the splitting of the sublevels would lead only to a broadening of the spectral lines, and the average depression of the sublevels would vary as $J(J+1)$. The depression would not be the same for the three sublevels and would give in effect different values for B_1^+, B_1^0, and B_1^-. These B_1 values could also vary slightly for the different changes in J, $\Delta J=0, \pm1, \pm2$, since the effective center of a given sublevel would not necessarily be the same for different transitions to that sublevel. This explanation, however, does not adequately account for the distribution of B_1 values in Table II. It is probable that second-order perturbations as a result of centrifugal distortion and anharmonicities, such as those considered by Shaffer, Nielsen, and Thomas, are of the same order of magnitude as the perturbation caused by Coriolis interaction with $2\nu_2$. An examination of the problem from this point of view might explain the different values of B_1 and D_1.

TABLE II. Rotational constants of the upper state of the ν_3 band of CH_4, assuming $B_0=5.253$ cm^{-1} and $D_0=1.9\times10^{-4}$ cm^{-1}.

Branch	B_1 (cm^{-1})	D_1 (cm$^{-1}\times10^4$)
O^- (R.E.)	5.235	3.8
R^+, P^- (R.E.)	5.234	2.9
R^0, P^0 (R.E.)	5.217	1.8
R^-, P^+ (I.R. and R.E.)	5.217	1.8
S^+ (R.E.)	5.206	1.0
S^0, O^0 (R.E.)	5.203	1.8

The average internuclear distance for the ground vibrational state r_0, as calculated from the Raman value $B_0=5.253$, is 1.0927×10^{-8} cm. With the value $B_0=5.249$ obtained from infrared data by relation (K), r_0 is 1.0930×10^{-8}. These values of r_0 are probably of the same order of accuracy.

THE STRUCTURE OF THE Q BRANCH

Although the individual lines of the Q branch were not resolved, the contour at high dispersion is striking; there is a sharp maximum of intensity at $\Delta\nu=3021.5$ cm^{-1}, a broad maximum at about $\Delta\nu=3017$ cm^{-1}, and then a gradual decrease in intensity towards smaller frequency shifts (Fig. 1 and on a larger scale Fig. 8). According to Eqs. (I) the structures of the three Q

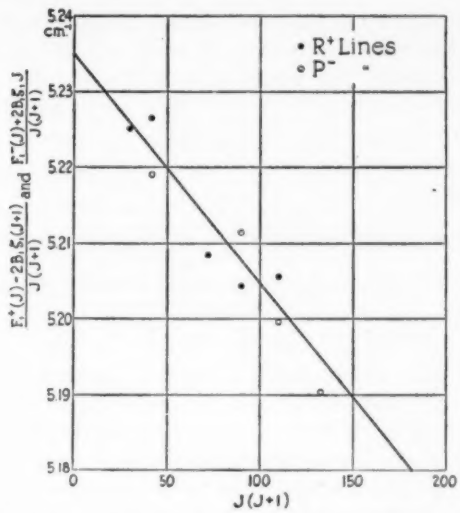

FIG. 7. Determination of B_1 and D_1 from R^+ and P^- Raman lines, assuming $B_0=5.253$.

sub-branches are given by

$$Q^+: \nu=\nu_0-(B_0-B_1)J(J+1)+2B_1\zeta_1(J+1),$$
$$Q^0: \nu=\nu_0-(B_0-B_1)J(J+1),$$
$$Q^-: \nu=\nu_0-(B_0-B_1)J(J+1)-2B_1\zeta_1 J.$$

Since B_0-B_1 and $B_1\zeta_1$ are positive, the Q^0 and Q^- branches are degraded to lower frequency shifts, and the extent of Q^- is greater than that of Q^0. For Q^+, on the other hand, $2B_1\zeta_1(J+1)$ is greater than $(B_0-B_1)\times J(J+1)$ at small J values and less at large J values; hence this branch forms a band head, which corresponds to the observed maximum at $\Delta\nu=3021.5$ cm^{-1}. At low dispersion this head is the most prominent feature of the Q branch and has been measured by the earlier workers as ν_3. Actually, the band origin, as found from

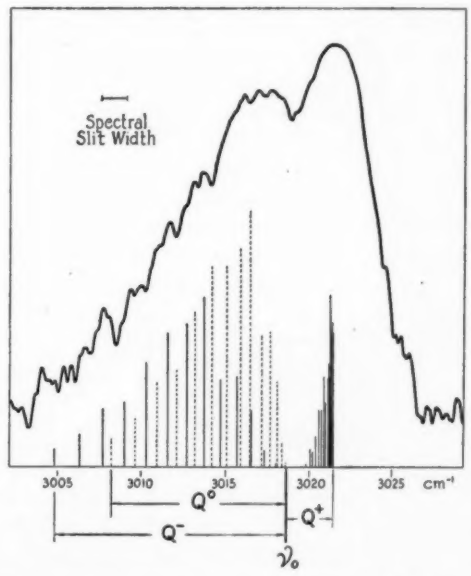

FIG. 8. Microphotometer trace of the Q branch of the ν_3 Raman band. The structure of the branch calculated from the results of the analysis is plotted under the trace.

relation (B), is at $\Delta\nu=3018.7$ cm^{-1}, close to the minimum. Assuming the values $B_0{}^0-B_1{}^0=0.050$ and $B_0{}^{+-}-B_1{}^{+-}=0.035$, the frequencies of the Q branch lines were calculated and are plotted, with approximate intensities, under the microphotometer trace in Fig. 8. It is evident that all features of the contour are reproduced.

ANALYSIS OF THE $2\nu_3$ INFRARED BAND

The values of the rotational constants B_0 and D_0 obtained from the ν_3 Raman band can be used in an analysis of the $2\nu_3$ infrared band, for which experimental data are available in recent papers by Nelson, Plyler, and Benedict,[19] and by McMath, Mohler, and Goldberg.[20] In the following calculations the frequencies quoted by the former authors have been used.

The branches of the $2\nu_3$ infrared band can be designated as $R^+(J)$, $Q^0(J)$, and $P^-(J)$, the upper rotational levels of which are given by equations similar to (I). The band origin ν_0 and the convergence factor B_0-B_2 can be found from the relation

$$(\tfrac{1}{2})\{R^+(J-2)+P^-(J+1)\} = \nu_0-2B_0-(B_0-B_2{}^{+-})J^2, \quad \text{(M)}$$

and also, since the Q branch lines were resolved, from the formula

$$Q^0(J)=\nu_0-(B_0-B_2{}^0)J(J+1). \quad \text{(N)}$$

A graphical solution gives the values $\nu_0-2B_0=5994.22$ cm^{-1}, $B_0-B_2{}^{+-}=0.062$ from (M), and $\nu_0=6004.71$, $B_0-B_2{}^0=0.067$ from (N). Assuming $B_0=5.253$, the value of ν_0 from (M) is 6004.73 in good agreement with the value from (N).

The difference between the values of $B_0-B_2{}^0$ and $B_0-B_2{}^{+-}$ shows that for the $2\nu_3$ band, there is a departure from the simple theory similar to, but not as great as, that found in the ν_3 band. It seems therefore appropriate to carry out an analysis of the same type as that used for ν_3. Assuming $B_0=5.253$ and $D_0=1.9\times10^{-4}$, the upper rotational energy terms $F_2{}^+(J)$, $F_2{}^0(J)$, and $F_2{}^-(J)$ are calculated from the frequencies of the R^+, Q^0, and P^- lines, respectively, by expressions analogous to (III) above. If the B_2 values for the R^+ and P^- branches are equal, as was found for the ν_3 band, the value of $B_2\zeta_2$ can be calculated readily from an equation corresponding to (V). The average of nine values gives $B_2\zeta_2=0.168\pm0.002$ cm^{-1}. The rotational constants for the upper state, calculated by equations corresponding to (IV), are $B_2{}^0=5.187$, $D_2{}^0=2.1\times10^{-4}$, and $B_2{}^{+-}=5.193$, $D_2{}^{+-}=2.3\times10^{-4}$. Consistency in the analysis is shown by the agreement of the values of B_0-B_2 with those obtained from relations (M) and (N). The derived constants reproduce the observed frequencies up to $J=9$ with an average discrepancy of less than 0.1 cm^{-1}. The value of ζ_2 as calculated from $B_2{}^{+-}\zeta_2$ is 0.0324.

These constants for the $2\nu_3$ band differ slightly, but significantly, from those given by Nelson, Plyler, and Benedict. The fact that two values of B_2 are found for $2\nu_3$ from infrared data alone shows that the rotational levels of the $v=2$ vibrational state are probably perturbed in a way similar to that found for ν_3. However, since no Raman data exist for $2\nu_3$, the nature of the perturbation cannot be studied in greater detail.

[19] Nelson, Plyler, and Benedict, J. Research Natl. Bur. Standards **41**, 651 (1948).
[20] McMath, Mohler, and Goldberg, Astrophys. J. **109**, 17 (1949).

Emission and Absorption of Radiation by Spectral Lines with Doppler Contour*

S. S. PENNER
Guggenheim Jet Propulsion Center, California Institute of Technology, Pasadena, California
(Received October 15, 1951)

Equations are developed for observable intensities in emission and absorption for spectral lines with Doppler contour. It is shown that the theoretical relations which are usually employed in estimating effective temperatures of internal energy states (a) require slight modifications when proper allowance is made for the shape of spectral lines, and (b) are not valid unless the product of spectral absorption coefficient and optical density is sufficiently small. Illustrative calculations on several spectral lines belonging to the (0,0) band of the $^2\Sigma \rightarrow {}^2\Pi$ band system of OH suggest that the conditions under which the basic relations hold are probably not satisfied for representative combustion flames.

IT is well known that the emission of radiation in the visible and ultraviolet regions of the spectrum does not make an important contribution to the total equilibrium flux of radiant energy at the temperatures which are normally encountered in combustion chambers. Radiant energy transfer in these spectral regions is, however, of great importance in spectroscopic studies for estimating population temperatures (i.e., rotational, vibrational, and electronic temperatures). Since most of this work is carried out at atmospheric pressure or even at subatmospheric pressures, as in low pressure combustion flames, it is of obvious interest to examine the intensities of radiation emitted for Doppler-broadened lines. The results are immediately applicable to such problems as emission and absorption intensities of OH, C_2, CH, etc., especially in low pressure flames. For emitters with large optical collision diameters such as sodium, and at moderate and elevated pressures for other chemical species, it is necessary to extend the theory discussed in the present report to spectral lines whose contour is described by combined collision- and Doppler-broadening.

Since one of the important applications of the present discussion is to the interpretation of spectroscopic data obtained in emission and absorption on flames, the following treatment will be presented in such a way as to make the results useful to the spectroscopist. In particular, we shall demonstrate† the following:

(1) For Doppler-broadened lines the maximum intensity of spectral lines observed in emission is proportional to the third power of the frequency rather than to the fourth power of the frequency.

(2) For Doppler-broadened lines the maximum intensity of spectral lines observed in absorption is independent of frequency and not proportional to the frequency.

(3) In absorption experiments particular care must be taken to correct for the spectral emission characteristics of the light source.

We shall allow for the possibility of lack of occurrence of equipartition of energy among the various degrees of freedom by designating the translational (kinetic) temperature by T_t, the temperature of the upper energy states by T_u, and the temperature of the lower energy states by T_l. A further generalization to represent the temperatures of internal degrees of freedom as a function of energy level can be introduced without difficulty but will not be considered in the present discussion.

The results of the present analysis indicate that the optical densities of the chemical species OH are too large, in representative combustion flames, to permit the type of interpretation of experimental measurements which is usually made, unless the reported f-values for spectral lines of the $^2\Sigma \rightarrow {}^2\Pi$ band system and (0,0) transitions are much too large.

I. INTENSITIES IN EMISSION

The integrated absorption S_{lu} of a spectral line resulting from an energy change from the upper energy level E_u to the lower energy level E_l is given by the well-known relation[1]

$$S_{lu}=(64\pi^4/3c^3)N_u(\nu_{lu})^4(q_{lu})^2/c\rho^0(\nu_{lu}), \qquad (1)$$

where c = velocity of light; N_u = number of molecules per unit volume per unit pressure in the upper energy state; ν_{lu} = frequency of the emitted or absorbed radiation at the center of the line, which is obtained from the Bohr frequency relation; q_{lu} = matrix element corresponding to transitions between the two given energy states; and $\rho^0(\nu_{lu})$ = volume density of blackbody radiation at the frequency ν_{lu} as given by the Planck distribution law.

The integrated intensity of a single emitted spectral line is obtained from the relation[1]

$$\int_{\Delta\nu_{lu}} R_\nu d\nu=\tfrac{1}{4}\int_{\Delta\nu_{lu}} c\rho^0(\nu)[1-\exp(-P_\nu X)]d\nu, \qquad (2)$$

where $\Delta\nu_{lu}$ is a suitable spectral range including the spectral line under study, R_ν = spectral intensity of the emitted radiation, P_ν = spectral absorption coefficient, X = optical density of the emitters. For the Doppler-broadened spectral line whose center lies at the fre-

* Supported by the ONR under contract Nonr-220 (03), NR 015 210.

† The treatment given in this report does not allow for instrumental distortions of experimental data. If the instrumental distortions do not depend on frequency, then the conclusions of the present analysis will remain unchanged.

[1] For the origin of this relation see, for example, A. C. G. Mitchell and M. W. Zemansky, *Resonance Radiation and Excited Atoms* (Cambridge University Press, London, 1934).

quency ν_{lu} the spectral absorption coefficient P_ν is

$$P_\nu = S_{lu}(mc^2/2\pi kT_t\nu_{lu}^2)^{\frac{1}{2}} \times \exp[-(mc^2/2kT_t\nu_{lu}^2)(\nu-\nu_{lu})^2], \quad (3)$$

where m represents the mass per molecule.

The optical density X of emitters used in combustion spectroscopy for determining rotational, vibrational, or electronic temperatures may be so small that it is permissible to expand the exponential in Eq. (2) retaining only the first two terms.[2] Furthermore, the range of frequencies for which $P_\nu X$ is significantly different from zero is so narrow that $\rho^0(\nu)$ may be replaced by $\rho^0(\nu_{lu})$. Thus

$$\int_{\Delta\nu_{lu}} R_\nu d\nu = \tfrac{1}{4}c\rho^0(\nu_{lu})X\int_{\Delta\nu_l} P_\nu d\nu = \tfrac{1}{4}c\rho^0(\nu_{lu})S_{lu}X. \quad (4)$$

Comparison of Eqs. (1) and (4) leads to the conclusion that

$$\int_{\Delta\nu_{lu}} R_\nu d\nu/(\nu_{lu})^4 g_u(q_{lu})^2 = (16\pi^4 NX/3c^3Q)\exp(-E_u/kT_u), \quad (5)$$

where N_u has been replaced by

$$N_u = Ng_u\exp(-E_u/kT_u)/Q, \quad (6)$$

with N = total number of molecules per unit volume per unit pressure, g_u = statistical weight of the upper energy state, Q = complete partition function. The optical density X appearing in Eq. (5) refers to all of the emitting molecules independently of the energy state in which they happen to be. Hence we obtain from Eq. (5) the following useful result

$$\frac{\partial \ln\left[\int_{\Delta\nu_{lu}} R_\nu d\nu \Big/ (\nu_{lu})^4 g_u(q_{lu})^2\right]}{\partial E_u} = -\frac{1}{kT_u}. \quad (7)$$

Equation (7) is the relation which is usually employed for the determination of temperatures from emission spectra for various internal degrees of freedom.

In practice it is convenient to measure $(R_\nu)_{\max}$, i.e., the maximum intensity of the various spectral lines, rather than the integrated intensity. However, in this case Eq. (7) does not apply exactly since allowance must be made for the frequency dependence of the Doppler-width of spectral lines. From Eq. (3) it is apparent that the maximum value of the spectral absorption coefficient, corresponding to the maximum value of R_ν, is

$$(P_\nu)_{\max} = S_{lu}(mc^2/2\pi kT_t)^{\frac{1}{2}}(1/\nu_{lu}). \quad (8)$$

Hence

$$(R_\nu)_{\max} = \tfrac{1}{4}c\rho^0(\nu_{lu})S_{lu}X(mc^2/2\pi kT_t)^{\frac{1}{2}}(1/\nu_{lu}) \quad (9)$$

and the relation corresponding to Eq. (5) is

$$(R_\nu)_{\max}/(\nu_{lu})^3 g_u(q_{lu})^2 = (16\pi^4 NX/3c^3Q)(mc^2/2\pi kT_t)^{\frac{1}{2}}\exp(-E_u/kT_u). \quad (10)$$

Thus

$$\frac{\partial \ln[(R_\nu)_{\max}/(\nu_{lu})^3 g_u(q_{lu})^2]}{\partial E_u} = -\frac{1}{kT_u}, \quad (11)$$

and the factor $(\nu_{lu})^3$ is seen to replace the factor $(\nu_{lu})^4$ which is normally employed for Doppler-broadened spectral lines. It should be noted that implicit in Eq. (11) is the assumption that the translational temperature, which determines the Doppler-width of spectral lines, is uniform and, in particular, is independent of ν_{lu}.

II. INTENSITIES IN ABSORPTION

In an absorption experiment the integrated intensity of the transmitted radiation is given by the relation[1]

$$\int_{\Delta\nu_{lu}} R_\nu d\nu = \int_{\Delta\nu_{lu}} R_{0\nu}[\exp(-P_\nu X)]d\nu, \quad (12)$$

where $R_{0\nu}$ represents the spectral intensity of the incident radiation. For the sake of simplicity we consider the case in which the light source may be treated as a greybody emitter in the wavelength range for which measurements are made. Thus

$$R_{0\nu} = \tfrac{1}{4}E_s c\rho_\nu^0(T_s),$$

where E_s is a constant independent of frequency and T_s represents the temperature of the source. For absorption measurements on minor component species such as OH, CH, C_2, etc., in flames the assumption is made again that it is sufficient to retain only the first two terms in the expansion of the exponential in Eq. (12).[2] Thus, for a single spectral line,

$$\int_{\Delta\nu_{lu}} R_\nu d\nu \simeq \tfrac{1}{4}E_s Xc \times \int_{\Delta\nu_{lu}} \rho_\nu^0(T_s)d\nu - \tfrac{1}{4}E_s Xc\rho^0{}_{\nu_{lu}}(T_s)S_{lu}; \quad (13)$$

but[1]

$$S_{lu} = (N_l B_{l\to u} - N_u B_{u\to l})h\nu_{lu}/c, \quad (14)$$

where

$$N_l = Ng_l[\exp(-E_l/kT_l)]/Q \quad (6a)$$

represents the number of molecules per unit volume per unit pressure in the lower (initial) energy level E_l whose statistical weight is g_l, $B_{l\to u}$ equals the Einstein coefficient of induced absorption, and $B_{u\to l}$ is the Einstein coefficient of induced emission. Since[3]

$$g_l B_{l\to u} = B_{u\to l}g_u$$

[2] This approximation is examined critically for OH in Sec. III.

[3] See, for example, E. C. Kemble, *Fundamental Principles of Quantum Mechanics* (McGraw-Hill Book Company, Inc., New York, 1935), p. 450.

and

$$B_{u\to l}=(c^3/8\pi h\nu_{lu}{}^3)A_{u\to l},$$

where $A_{u\to l}$ is the Einstein coefficient of spontaneous emission, it follows that[1]

$$B_{u\to l}h\nu_{lu}=(8\pi^3/3h)\nu_{lu}(q_{lu})^2. \quad (15)$$

Introduction of Eqs. (6), (6a), and (15) into Eq. (14) leads to the result

$$S_{lu}=(8\pi^3N/3hcQ)\nu_{lu}(q_{lu})^2gu[\exp(-E_l/kT_l)] \times\{1-\exp[(-E_u/kT_u)+(E_l/kT_l)]\}. \quad (16)$$

For representative spectral lines arising from electronic transitions in the visible and ultraviolet regions of the spectrum and for reasonable values of T_l, T_u

$$\exp[(-E_u/kT_u)+(E/kT_l)]\ll 1,$$

whence Eq. (16) can be replaced by the following close approximation:

$$S_{lu}=(8\pi^3N/3hcQ)\nu_{lu}(q_{lu})^2gu\exp(-E_l/kT_l). \quad (17)$$

From Eqs. (13) and (17) the following useful relation is obtained:

$$\tfrac{1}{4}E_sXc\int_{\Delta\nu lu}\rho_\nu{}^0(T_s)d\nu-\int_{\Delta\nu lu}R_\nu d\nu =(2\pi^3NE_sX/3hQ)\rho^0{}_{\nu lu}(T_s) \times\nu_{lu}(q_{lu})^2gu\exp(-E_l/kT_l). \quad (18)$$

The quantity appearing on the left-hand side of Eq. (18) evidently represents the total integrated absorbed intensity resulting from the energy transition $E_l\to E_u$ and will be designated by the symbol $\int_{\Delta\nu lu}A_\nu d\nu$. From Eq. (18) it is evident that

$$\frac{\partial\ln\left\{\left(\int_{\Delta\nu lu}A_\nu d\nu\right)\Big/\nu_{lu}g(q_u)^2\rho^0{}_{\nu lu}(T_s)\right\}}{\partial E_l}=-\frac{1}{kT_l}. \quad (19)$$

Absorption experiments are generally performed with a greybody light source whose temperature T_s is appreciably greater than the excitation temperature T_l of the lower energy levels. Hence $\rho^0{}_{\nu lu}(T_s)$ will be substantially independent of E_l and Eq. (19) reduces to the usual form for estimates of population temperatures on the lower internal energy states. It is, however, evident from Eq. (19) that the spectral distribution of the light source can affect the experimental results in a very significant way if the light source does not possess the assumed spectral radiation characteristics or if the range of values of E_l considered covers too wide a frequency range.

If peak intensities, rather than integrated intensities, are measured in absorption, then, proceeding as in Sec. II, Eq. (18) should be replaced by the relation

$$(A_\nu)_{\max}=(2\pi^3NE_sX/3hQ)(mc^2/2\pi kT_l)^{\frac{1}{2}}\rho_{\nu lu}{}^0(T_s) \times(q_{lu})^2gu\exp(-E_l/kT_l) \quad (20)$$

and

$$\frac{\partial\ln[(A_\nu)_{\max}/g(q_{lu})^2\rho_{\nu lu}{}^0(T_s)]}{\partial E_l}=-\frac{1}{kT_l}. \quad (21)$$

Reference to Eq. (21) shows that the factor ν_{lu} disappears altogether for Doppler-broadened rotational lines if maximum absorption intensities are measured.

TABLE I. Representative values of integrated absorption for spectral lines of the $^2\Sigma\to{}^2\Pi$, (0,0) band of OH.

Line	ν_{lu}, cm^{-1}	$(T/273.1)S_{lu}\times10^{-4}$, cm^{-2}-atmos^{-1}
Q_1 (1)	32,474.58	1.64
(2)	32,458.65	2.06
(3)	32.441.90	2.28
(4)	32,423.63	2.46
(5)	32,403.47	2.55
(6)	32,380.99	2.64
R_2 (1)	32,415.51	0.97
(2)	32,455.70	1.04
(3)	32,489.49	1.10

III. APPLICATION TO EMISSION AND ABSORPTION STUDIES OF REPRESENTATIVE LINES OF OH

The derivation of Eqs. (7) and (11) was based on the approximations

$$1-\exp(-P_\nu X)\simeq P_\nu X \quad (22)$$

and

$$1-\exp[-(P_\nu)_{\max}X]\simeq(P_\nu)_{\max}X, \quad (23)$$

respectively. Since $(P_\nu)_{\max}\gtrsim P$, we shall examine the range of numerical values $(P_\nu)_{\max}X$ which is encountered in representative combustion flames.

It is readily shown that the experimentally determined oscillator strengths f_{lu} for transitions between the lower energy level E_l and the upper energy level E_u are related to S_{lu} according to the expression

$$S_{lu}=2.3789\times10^7(273.1/T)f_{lu}, \quad (24)$$

where S_{lu} is expressed in cm^{-2}-atmos^{-1} at the temperature T.

Oscillator strengths for representative spectral lines of OH for the $^2\Sigma\to{}^2\Pi$ band system for (0,0) transitions have been reported by Oldenberg and Rieke[4] but should be multiplied by the factor 4.2.[5] Representative numerical values of $(T/273.1)S_{lu}$ for several members of the Q_1- and R_2-branches are summarized in Table I. The numbers in parentheses given after the branch designations refer to the values of K in the notation of Dieke and Crosswhite.[6] Also listed in Table I are the relevant values of ν_{lu}.[6] Representative values of S_{lu} and of

[4] O. Oldenberg and F. F. Rieke, J. Chem. Phys. 6, 439 (1938).
[5] R. J. Dwyer and O. Oldenberg, J. Chem. Phys. 12, 351 (1944).
[6] G. H. Dieke and H. M. Crosswhite, "The ultra violet bands of OH, fundamental data," Bumblebee Series Report No. 87 (November, 1948).

TABLE II. Numerical values of S_{lu} and $(P_\nu)_{max}$ for Q_1 (6) of the $^2\Sigma \rightarrow {}^2\Pi$, (0,0) band of OH, as a function of temperature.

T °K	$S_{lu} \times 10^{-3}$, cm^{-2}-$atmos^{-1}$	$(P_\nu)_{max} \times 10^{-3}$, cm^{-1} $atmos^{-1}$
1000	7.21	38.1
2000	3.61	13.5
3000	2.40	7.32
4000	1.80	4.75
5000	1.44	3.40
6000	1.20	2.59
7000	1.03	2.06
8000	0.901	1.68
9000	0.801	1.41
10,000	0.721	1.20

$(P_\nu)_{max}$ for Q_1 (6) are listed in Table II as a function of temperature. The numerical values of $(P_\nu)_{max}$ were calculated from S_{lu} according to Eq. (8).

Reference to Table II shows that the numerical values of $(P_\nu)_{max}$ for the $Q_1(6)$ spectral line‡ are exceedingly large and that, therefore, the approximation of Eq. (23) can be justified only for very small values of the optical density X. In representative emission experiments from low pressure combustion flames the partial pressure p of OH may be of the order of 10^{-3} atmos, whereas, the radiation path length L is in the neighborhood of 10 cm. For flames burning at higher pressures, p will increase while L decreases in such a way that $X = pL$ remains nearly constant. Hence it appears that the so-called "abnormal rotational temperatures," which have been reported by different investigators,[7–9] may be the result of erroneous interpretation of experimental data unless the experimentally determined oscillator strengths are in error and should really be much smaller than reported by Oldenberg and collaborators.[4,5] On the other hand, it appears likely that for sufficiently large values of K, S_{lu} and $(P_\nu)_{max}$ will decrease sufficiently to validate the approximation of Eq. (23). Thus the rotational temperatures obtained from data on large values of K may be significant although the "more normal rotational distribution" of the lines with small values of K cannot be accepted as valid experimental evidence unless the reported f-values for spectral lines of OH are much too large.

An obvious extension of the preceding discussion to rotational temperatures determined from absorption experiments would appear to raise serious objection to the so called "normal rotational temperatures of OH" reported from absorption measurements. However, in this case the available experimental evidence on the measurement of rotational temperatures[9] seems so convincing that a serious reexamination of f-values appears to be indicated.[10]

‡ It is evident from the data listed in Table I that the numerical values for other lines are of the same order of magnitude as the listed data for Q_1 (see reference 6).

[7] A. G. Gaydon and H. G. Wolfhard, Proc. Roy. Soc. (London) **194A**, 169 (1948), and later publications.

[8] Penner, Gilbert, and Weber, J. Chem. Phys. **20**, 522 (1952).

[9] H. P. Broida, in National Bureau of Standards Report No. 1123 (August 20, 1951).

[10] Theoretical calculations of f-values for OH have been carried out by R. S. Mulliken, J. Chem. Phys. **8**, 382 (1940).

The Use of Isotopic Molecules for the Complete Determination of Force Constants. I. Linear Molecules*

J. C. Decius
Department of Chemistry, Oregon State College, Corvallis, Oregon
(Received October 2, 1951)

Equations are developed which show the maximum amount of information which can be obtained concerning the force constants with isotopic linear molecules. It is demonstrated that a unique solution can be found in terms of the expressions $\Sigma_k\lambda_k$, $\Sigma_k\lambda_k^2$, and $\Sigma_k\lambda_k^3$, where $\lambda_k=4\pi^2\nu_k^2$, provided the ν_k are known for the "unsubstituted" molecule and for certain isotopic molecules involving respectively single, double, and triple substitutions; i.e., if $ABCD\cdots$ is the unsubstituted molecule, isotopic molecules of the types $A^*BCD\cdots$, $AB^*CD\cdots$, etc., $A^*B^*CD\cdots$, etc., and $A^*B^*C^*D\cdots$, etc., are required. More than two isotopic forms (such as A and A^*) of any given atom are not required.

For the triatomic molecule, only the singly substituted forms are required (this is also true for the perpendicular vibrations of the tetratomic molecule). It is also found that the force constants of the symmetrical linear molecule may be found using only symmetrical isotopic molecules; the number of these required is naturally less than the number required for an unsymmetrical molecule having the same number of atoms.

I. INTRODUCTION

It is well known that the number of fundamental vibration frequencies is insufficient for a complete evaluation of all the parameters of the most general vibrational potential energy function except for a few simple and symmetrical polyatomic molecules, such as symmetrical linear XY_2, triangular symmetrical X_3, or tetrahedral X_4. In these exceptional cases, the factoring of the secular determinant by symmetry leads to one-by-one factors of the determinant, so that the number of potential constants is identical with the number of fundamental frequencies. In more general cases, the number of potential constants is given by

$$p=(\tfrac{1}{2})\textstyle\sum_\gamma n^{(\gamma)}(n^{(\gamma)}+1), \tag{1}$$

where $n^{(\gamma)}$ is the size of the secular determinant corresponding to the γth symmetry species. Since the number of fundamental frequencies is

$$f=\textstyle\sum_\gamma n^{(\gamma)}, \tag{2}$$

it is apparent that there are insufficient experimental data unless $n^{(\gamma)}=1$ for all species. Furthermore, the equations connecting the force constants and the frequencies are respectively linear, quadratic, cubic, etc., in the force constants so that even if some force constants were put equal to zero as an approximation, ambiguities would remain on account of the multiple roots of the quadratic, cubic, and higher equations.

However, the potential energy should be independent of the atomic masses, so that isotopically related molecules should yield additional experimental data for the determination of the force constants. In this connection it should be mentioned that not all such data are independent, as is shown by the existence of the product rule,[1] the sum rule,[2] and possibly other relations. It is therefore a problem of some importance to determine the conditions under which a complete solution for the force constants can be obtained. Since the treatment of the linear molecule is considerably simpler than that of the general polyatomic molecule, it will be discussed immediately after the following section, which formulates the general approach to the problem.

II. SYMMETRIC FUNCTIONS OF THE FREQUENCIES

Following the method of Wilson[3] the potential and kinetic energy of the molecule are represented by the (symmetric) matrices **F** and **G**, respectively, where

$$2V=\textstyle\sum F_{ij}q_iq_j \tag{3}$$

and

$$2T=\textstyle\sum G_{ij}p_ip_j, \tag{4}$$

the q's and p's being any suitable set of coordinates and their conjugate momenta, respectively. Since the secular determinant can be written as

$$|\mathbf{FG}-\lambda\mathbf{E}|=0, \tag{5}$$

where

$$\lambda=4\pi^2\nu^2, \tag{6}$$

it follows from the fundamental properties of the characteristic values of matrices that the sum of the diagonal terms of **FG** is equal to the sum of the characteristic values:

$$\sum_{ij}F_{ij}G_{ji}=\sum_k\lambda_k=\sigma_1. \tag{7}$$

It is also possible to find relations between the ele-

* Published with approval of the Monographs Publication Committee, Oregon State College, as Research Paper No. 189, School of Science, Department of Chemistry.

[1] O. Redlich, Z. physik. Chem. **B28**, 371 (1935). E. Teller, quoted in W. R. Angus *et al.*, J. Chem. Soc. 971, 1936.
[2] J. C. Decius and E. Bright Wilson, Jr., J. Chem. Phys. **19**, 1409 (1951).
[3] E. Bright Wilson, Jr., J. Chem. Phys. **9**, 76 (1941).

$$\begin{array}{ccccc} \mu_A+\mu_B & -\mu_B & 0 & 0 & \cdots \\ -\mu_B & \mu_B+\mu_C & -\mu_C & 0 & \cdots \\ 0 & -\mu_C & \mu_C+\mu_D & -\mu_D & \cdots \\ 0 & 0 & -\mu_D & \mu_D+\mu_E & \cdots \\ \cdot & \cdot & \cdot & \cdot & \\ \cdot & \cdot & \cdot & \cdot & \\ \cdot & \cdot & \cdot & \cdot & \end{array}$$

FIG. 1. General form of the G matrix for parallel vibrations of the linear molecule.

ments of F and G and symmetric sums of the λ's such as

$$\sigma_2=\sum_{k<l}\lambda_k\lambda_l, \tag{8}$$

$$\sigma_3=\sum_{k<l<m}\lambda_k\lambda_l\lambda_m, \tag{9}$$

$$\sigma_f=\lambda_1\lambda_2\lambda_3\cdots\lambda_f. \tag{10}$$

In terms of F and G, σ_p is the sum of all p-rowed principal minors (i.e., centered on the principal diagonal) of **FG**.

It is apparent that σ_1 (calculated from the observed frequencies) will yield an equation linear in the unknown F_{ij}, σ_2 will yield an equation quadratic in the F_{ij}, etc., there being f equations in all, of which the last is

$$|\mathbf{F}|=\sigma_f/|\mathbf{G}|. \tag{11}$$

In some respects, however, it is easier to work with a different, but related, set of symmetric polynomials in the frequencies. These are defined by

$$s_1=\sum\lambda_k=\sigma_1 \tag{12}$$

$$s_2=\sum\lambda_k^2=\sigma_1^2-2\sigma_2 \tag{13}$$

$$s_3=\sum\lambda_k^3=-2\sigma_1^3+6\sigma_1\sigma_2-3\sigma_2. \tag{14}$$

The expansions for s_1, s_2, etc., in terms of F and G are simple when the following theorem is recalled: the characteristic values of the p-th power of a matrix are equal to the p-th powers of the characteristic values (of the original matrix). Thus

$$\sum_i(FG)_{ii}=\sum_{ij}F_{ij}G_{ji}=s_1, \tag{15}$$

$$\sum_i(FG)_{ii}^2=\sum_{ijkl}F_{ij}F_{kl}G_{jk}G_{il}=s_2, \tag{16}$$

$$\sum(FG)_{ii}^3=s_3, \tag{17}$$

etc.

It will be shown later that in some cases all the F_{ij} can be determined from the expressions for s_1 and s_2 alone, provided a suitable set of isotopic molecules is available. Such a set is clearly advantageous (1) because the expansions for s_3, s_4, etc., become progressively more cumbersome, and (2) because of the multiplicity of solutions for cubic, quartic, and higher powered equations in the F_{ij}.

The expressions for s_1, s_2, etc., may also be written in the form

$$s_1=\sum_\alpha c_\alpha\mu_\alpha, \tag{18}$$

$$s_2=\sum_{\alpha\beta}c_{\alpha\beta}\mu_\alpha\mu_\beta, \tag{19}$$

where μ_α is the reciprocal mass of the αth atom and c_α and $c_{\alpha\beta}$ are, respectively, linear and quadratic functions of the force constants. This follows from (15) and (16) and the fact that G_{ij} is a linear function of the μ_α. In later sections, methods of computing c_α, $c_{\alpha\beta}$, etc., in terms of the force constants will be given. For the time being, the essential question is how to determine c_α, $c_{\alpha\beta}$, etc., from the experimental data, i.e., from the observed frequencies.

Suppose a molecule is designated by the symbol $ABCD\cdots$ and that s_1 is known for this molecule. In order to find c_A, it is necessary to know the corresponding sum for the molecule $A^*BCD\cdots$ in which the asterisk indicates isotopic substitution. If the sum for $A^*BCD\cdots$ is designated s_1^A, then

$$c_A=(s_1^A-s_1)/(\mu_{A^*}-\mu_A). \tag{20}$$

In the same fashion, c_B, c_C, c_D, etc., can be found. It is only necessary, however, to make isotopic substitutions for $N-1$ atoms of an N-atomic molecule (i.e., to know s_1 for N isotopic molecules in all), since when all but one of the c_α are known, these values can be substituted back in (18) for any molecule of the set in order to solve for the last c_α.

The procedure for finding the $c_{\alpha\beta}$ is only slightly more complex: if s_2^A, s_2^B, and s_2^{AB} refer respectively to the molecules $A^*BCD\cdots$, $AB^*CD\cdots$, and $A^*B^*CD\cdots$,

$$c_{AB}+c_{BA}=2c_{AB}=(s_2^{AB}+s_2-s_2^A-s_2^B)/(\mu_{A^*}\mu_{B^*}+\mu_A\mu_B-\mu_{A^*}\mu_B-\mu_A\mu_{B^*}). \tag{21}$$

Here we consider only the case in which $\alpha\neq\beta$.

III. PARALLEL VIBRATIONS OF LINEAR MOLECULES

The $3N-5$ vibrational motions of a linear molecule of N atoms separate into $N-1$ vibrations parallel to the axis and $N-2$ doubly degenerate vibrations perpendicular to the axis. If there is a center of symmetry, further factoring is possible, but the discussion will be at first confined to the less symmetrical case. Considering first the parallel modes, it is evident that the $N-1$ bond stretches constitute a suitable set of internal coordinates. The **G** matrix can readily be computed[3] in terms of these coordinates: it has the general form indicated in Fig. 1. Upon inserting this **G** matrix in (15) the expression for the sum of the roots of the secular determinant can easily be converted to an equation in which the coefficients of each reciprocal mass are collected. The result is

$$F_{11}\mu_A+(F_{11}+F_{22}-2F_{12})\mu_B+(F_{22}+F_{33}-2F_{23})\mu_C+\cdots+(F_{N-2,N-2}+F_{N-1,N-1}-2F_{N-2,N-1})\mu_{N-1}+F_{N-1,N-1}\mu_N. \tag{22}$$

For the special case of the triatomic linear molecule, this equation is sufficient for the unique determination of all three force constants. Its special form is

$$F_{11}\mu_A+(F_{11}+F_{22}-2F_{12})\mu_B+F_{22}\mu_C, \qquad (23)$$

from which it is evident that F_{11}, $F_{11}+F_{22}-2F_{12}$, and F_{22} can be individually determined if s_1 is known for the three isotopic molecules. ABC, A^*BC, and ABC^*: e.g., HCN^{14}, DCN^{14}, and HCN^{15}. If one designates the sum of roots for these molecules as s_1, $s_1{}^A$, and $s_1{}^C$, respectively,

$$F_{11}=(s_1{}^A-s_1)/(\mu_{A^*}-\mu_A) \qquad (24)$$

$$F_{22}=(s_1{}^C-s_1)/(\mu_{C^*}-\mu_C) \qquad (25)$$

$$F_{12}=(1/2\mu_B)[(\mu_A+\mu_B)F_{11}+(\mu_B+\mu_C)F_{22}-s_1]. \qquad (26)$$

It is also possible to determine the force constants from the sums of roots for a set of isotopic molecules such as ABC, A^*BC, and AB^*C. Note, however, that in the case of the expressions for s_1 no new information could be obtained by studying the isotopic molecule $A^{**}BC$ in which A^{**} designates a third isotopic form of atom A.

For linear molecules having four or more atoms, the expressions for s_1 yield insufficient information to determine the force constants, regardless of how many isotopic molecules are available. It is therefore necessary to resort to the second-power equations (16).

It is desirable at this point to introduce a method for computing the left-hand side of (16) in the desired form, namely with collected coefficients of each reciprocal mass term, such as $\mu_A{}^2$, $\mu_B{}^2$, $\cdots\mu_A\mu_B$, etc. It is possible to write the $\mathbf{G}$ matrix in the form

$$\mathbf{G}=\sum_\alpha \mu_\alpha \mathbf{I}_\alpha, \qquad (27)$$

where $\mathbf{I}_\alpha$ is a matrix which has a particularly simple form when bond stretching coordinates only are employed. An element of $\mathbf{I}_\alpha$, such as $(I_\alpha)_{jk}$, has the value zero unless both bonds j and k meet at atom α; if this is the case, $(I_\alpha)_{jk}=\cos jk$, where jk stands for the angle between the bonds. For the linear molecule $ABCD$ $\mathbf{I}_A$, $\mathbf{I}_B$, $\mathbf{I}_C$, and $\mathbf{I}_D$ have the form shown in Fig. 2.

From Fig. 2 it is apparent that each $\mathbf{I}_\alpha$ has a nonvanishing block centered on the principal diagonal, which is one dimensional for the terminal atoms and two-dimensional for all others. Summarizing these facts in formal symbolism, the expression for a general element of $\mathbf{I}_\alpha$ can be given in the form

$$(I_\alpha)_{jk}=\delta_{j,\alpha-1}\delta_{k,\alpha-1}+\delta_{j,\alpha}\delta_{k,\alpha}-\delta_{j,\alpha-1}\delta_{k,\alpha}-\delta_{j,\alpha}\delta_{k,\alpha-1}. \qquad (28)$$

TABLE I. The coefficients $c_{\alpha\beta}$ for the tetratomic linear molecule.

	μ_A	μ_B	μ_C	μ_D
μ_A	$F_{11}{}^2$	$(F_{12}-F_{11})^2$	$(F_{13}-F_{12})^2$	$(-F_{13})^2$
μ_B		$(F_{11}+F_{22}-2F_{12})^2$	$(F_{12}+F_{23}-F_{13}-F_{22})^2$	$(F_{13}-F_{23})^2$
μ_C			$(F_{22}-F_{33}-2F_{23})^2$	$(F_{23}-F_{33})^2$
μ_D				$F_{33}{}^2$

$$\mathbf{I}_A=\begin{pmatrix}1&0&0\\0&0&0\\0&0&0\end{pmatrix} \qquad \mathbf{I}_B=\begin{pmatrix}1&-1&0\\-1&1&0\\0&0&0\end{pmatrix}$$

$$\mathbf{I}_C=\begin{pmatrix}0&0&0\\0&1&-1\\0&-1&1\end{pmatrix} \qquad \mathbf{I}_D=\begin{pmatrix}0&0&0\\0&0&0\\0&0&1\end{pmatrix}$$

FIG. 2. The matrices $\mathbf{I}_\alpha$ for the tetratomic molecule.

With the aid of this expression, it is shown in the Appendix that if

$$s_1=\sum_\alpha c_\alpha\mu_\alpha$$

and

$$s_2=\sum_{\alpha\beta} c_{\alpha\beta}\mu_\alpha\mu_\beta,$$

the expressions for c_α and $c_{\alpha\beta}$ are simply

$$c_\alpha=F_{\alpha-1,\alpha-1}+F_{\alpha,\alpha}-2F_{\alpha-1,\alpha} \qquad (29)$$

and

$$c_{\alpha\beta}=(F_{\alpha-1,\beta-1}+F_{\alpha,\beta}-F_{\alpha-1,\beta}-F_{\alpha,\beta-1})^2. \qquad (30)$$

In (29) and (30) it is to be understood that F vanishes if either subscript is less than one or greater than $N-1$.

As an illustration of (29) and (30), consider the tetratomic molecule $ABCD$. By (29)

$$s_1=F_{11}\mu_A+(F_{11}+F_{22}-2F_{12})\mu_B+(F_{22}+F_{33}-2F_{23})\mu_C+F_{33}\mu_D.$$

The expression for s_2 is given in tabular form where the entry in the row labeled μ_α and column labeled μ_β is the coefficient $c_{\alpha\beta}$.

Except for the ambiguities inherent because of the second power appearing in (30), one sees that a complete solution for the force constants can be obtained from the expressions for s_1 and s_2 alone, provided a suitable (and rather large!) set of isotopically related molecules is available. Such a set in the tetratomic case could consist of: $ABCD$, A^*BCD, AB^*CD, $ABCD^*$; A^*B^*CD and A^*BCD^*. From the first, second, and fourth of these molecules, F_{11} and F_{33} are obtained directly with the aid of the expressions for s_1. From the first, second, third, and fifth, employing the expressions for s_2, the quantity $(F_{12}-F_{11})^2$ is found and hence F_{12}, since F_{11} is already known. From the first and third $F_{11}+F_{22}-2F_{12}$ is calculated and hence F_{22}. The quantity $F_{22}+F_{33}-2F_{23}$ can now be obtained from the equation

$$(F_{22}+F_{33}-2F_{23})\mu_C=s_1-c_A\mu_A-c_B\mu_B-c_D\mu_D,$$

since c_A, c_B, and c_D have already been determined; this yields F_{23} since F_{22} and F_{33} are already known. Finally, F_{13} can be calculated with the aid of s_2 for the molecules $ABCD$, A^*BCD, $ABCD^*$, and A^*BCD^*. To help clarify this procedure, the coefficients $c_{\alpha\beta}$ actually used in these calculations are underlined in Table I. *All* the coefficients, c_α, are employed.

The generalization of this procedure for a linear polyatomic molecule consisting of any number of atoms

shows that the following set of isotopic molecules is sufficient for the determination of all the force constants. In addition to the "unsubstituted" molecule ($ABCD\cdots$), singly substituted molecules ($A^*BCD\cdots$, $AB^*CD\cdots$, etc.) are required corresponding to substitutions at all but one position. Furthermore, all doubly substituted molecules ($A^*B^*CD\cdots$, $A^*BC^*D\cdots$, etc.) are needed except (1) those involving substitution at a single atom (which may or may not be the same as that omitted from the singly substituted set) and (2) any single molecule in which one of the substitutions is made adjacent to the atom omitted in (1).

Other sets will lead to a solution, but the one just described is most convenient. To illustrate this set more concretely, consider the unsubstituted molecule, $ABCDE$. Instead of A^*BCDE we now write simply A^* and in place of A^*BC^*DE simply A^*C^*, etc. Then, according to the above rule, the singly substituted molecules could be chosen as A^*, B^*, D^*, E^*, and (selecting atom E as the omitted one in the doubly substituted set) A^*B^*, A^*C^*, A^*D^*, B^*C^*, B^*D^*, C^*D^*, with the further privilege of omitting any one of the subset A^*D^*, B^*D^*, and C^*D^*. Naturally, it would be more likely that the atom omitted from the singly

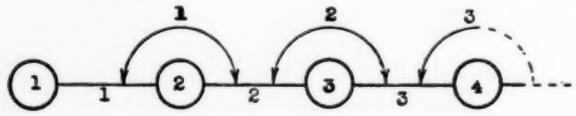

FIG. 3. Atom, bond, and bending coordinate numbering scheme for the linear molecule.

substituted set would be the same as that omitted from the doubly substituted set, on the grounds of availability of isotopes. Thus if no isotope of atom C is available, a solution could also be obtained from the unsubstituted molecule, A^*, B^*, D^*, E^*; A^*B^*, A^*D^*, A^*E^*, B^*D^*, B^*E^*, and D^*E^*, with the further privilege of omitting any one of the doubly substituted molecules except A^*E^*.

Unfortunately, the solution just described is not unique, except in the case of the triatomic molecule. This difficulty arises from the necessity of employing the coefficients $c_{\alpha\beta}$ whose *square roots* are linear combinations of the force constants. Thus with the tetratomic molecule, $F_{12}=c_A\pm c_{AB}^{\frac{1}{2}}$ and $F_{13}=\pm c_{AD}^{\frac{1}{2}}$.

It is possible in principle to make the solution unique by appealing to the coefficients $c_{\alpha\beta\gamma}$ appearing in the sums

$$s_3=\sum_k\lambda_k^3=\sum_{\alpha\beta\gamma}c_{\alpha\beta\gamma}\mu_\alpha\mu_\beta\mu_\gamma.$$

As indicated in the appendix, the relation between these coefficients and the force constants is

$$\begin{aligned}c_{\alpha\beta\gamma}=&(F_{\gamma-1,\alpha-1}+F_{\gamma,\alpha}-F_{\gamma-1,\alpha}-F_{\gamma,\alpha-1})\\&\times(F_{\alpha-1,\beta-1}+F_{\alpha,\beta}-F_{\alpha-1,\beta}-F_{\alpha,\beta-1})\\&\times(F_{\beta-1,\gamma-1}+F_{\beta,\gamma}-F_{\beta-1,\gamma}-F_{\beta,\gamma-1}),\end{aligned}$$

which shows, furthermore, that

$$\begin{aligned}c_{\alpha\alpha\alpha}&=c_\alpha^3\\c_{\alpha\alpha\beta}&=c_\alpha c_{\alpha\beta}\\c_{\alpha\beta\gamma}&=(\pm c_{\gamma\alpha}^{\frac{1}{2}})(\pm c_{\alpha\beta}^{\frac{1}{2}})(\pm c_{\beta\gamma}^{\frac{1}{2}}).\end{aligned}$$

For molecules consisting of four or more atoms, it can easily be demonstrated that there are sufficient terms of the type $c_{\alpha\beta\gamma}$ to determine the correct sign for each $c_{\alpha\beta}^{\frac{1}{2}}$.

This procedure does not recommend itself, however, since the set of additional isotopically substituted molecules required to evaluate the $c_{\alpha\beta\gamma}$ individually would further complicate the already serious problem confronting the chemical synthesist. It is encouraging only to know that a unique solution does exist.

More practical methods of selecting the correct solution, in the event that physical reasonability is insufficient, might involve the evaluation of additional second order coefficients, such as c_{AC} and c_{CD} in the tetratomic case. It should be noted that all the $c_{\alpha\beta}$ can be computed from the specified set of isotopic molecules. Inasmuch as $c_{\alpha\alpha}=c_\alpha^2$, after the c_α are known, there remain only $[N(N-1)]/2$ unknowns of the type $c_{\alpha\beta}$ with $\alpha<\beta$. But from the s_2 expressions for the $N+N(N-3)/2$ isotopic molecules of the specified set there are just the required number of equations to find $[N(N-1)]/2$ unknowns. If these have all been determined, the conditions

$$\sum_\beta c_{\alpha\beta}^{\frac{1}{2}}=0$$

may be used to assist in making the correct choice of signs of the square roots. Also, it is possible to test the alternate solutions by evaluation of the determinant $|\mathbf{F}|$ and comparison with $\lambda_1\lambda_2\lambda_3\cdots\lambda_{N-1}/|\mathbf{G}|$ where $|\mathbf{G}|$ is given by

$$|\mathbf{G}|=(\mu_A\mu_B\cdots\mu_N)M,$$

M being the total mass of the molecule.

IV. PERPENDICULAR VIBRATIONS OF LINEAR MOLECULES

The $N-2$ (doubly degenerate) perpendicular vibrations may be described by a set of $N-2$ bending coordinates whose numbering is illustrated in Fig. 3. The $\mathbf{G}$ matrix elements may be computed with the aid of formulas given by Ferigle and Meister.[4] In terms of the atom, bond, and angle numbering system employed in Fig. 3, the only nonvanishing elements are

$$G_{ii}=\tau_i^2\mu_i+(\tau_i+\tau_{i+1})^2\mu_{i+1}+\tau_{i+1}^2\mu_{i+2}, \tag{31}$$

$$G_{i,i+1}=-\tau_{i+1}(\tau_{i+1}+\tau_i)\mu_{i+1}-\tau_{i+1}(\tau_{i+1}+\tau_{i+2})\mu_{i+2}, \tag{32}$$

$$G_{i,i+2}=\tau_{i+1}\tau_{i+2}\mu_{i+2}, \tag{33}$$

where τ_i is the reciprocal of the length of the ith bond.

[4] S. M. Ferigle and A. G. Meister, J. Chem. Phys. **19**, 982 (1951).

TABLE II. Special coefficients c_γ and $c_{\alpha\gamma}$ for symmetrical linear molecules.

	Neven	Nodd
$\Sigma_g^+(s)$	$c_\gamma=F_{\gamma-1,\gamma-1}+2F_{\gamma,\gamma}-2^{\frac{1}{2}}F_{\gamma-1,\gamma}$	$c_\gamma=0$
	$c_{\alpha\gamma}=c_{\gamma\alpha}=(F_{\alpha-1,\gamma-1}+2^{\frac{1}{2}}F_{\alpha,\gamma}-2^{\frac{1}{2}}F_{\alpha-1,\gamma}-F_{\alpha,\gamma-1})^2$	$c_{\alpha\gamma}=0$
	$c_{\gamma\gamma}=c_\gamma^2$	$c_{\gamma\gamma}=0$
$\Sigma_u^+(a)$	$c_\gamma=0$	$c_\gamma=2F_{\gamma-1,\gamma-1}$
	$c_{\alpha\gamma}=0$	$c_{\alpha\gamma}=c_{\gamma\alpha}=(F_{\alpha-1,\gamma-1}+F_{\alpha,\gamma-1})^2$
	$c_{\gamma\gamma}=0$	$c_{\gamma\gamma}=c_\gamma^2$

Upon introducing matrices $\mathbf{J}_\alpha$ analogous to the $\mathbf{I}_\alpha$ of (27),

$$\mathbf{G}=\sum_\alpha \mu_\alpha \mathbf{J}_\alpha, \tag{34}$$

the following expression for the elements of $\mathbf{J}_\alpha$ is obtained:

$$\begin{aligned}(J_\alpha)_{ij}=&\delta_{i,\alpha-2}\delta_{j,\alpha-2}\tau_{\alpha-1}^2+\delta_{i,\alpha-1}\delta_{j,\alpha-1}(\tau_{\alpha-1}+\tau_\alpha)^2\\&+\delta_{i,\alpha}\delta_{j,\alpha}\tau_\alpha^2-\delta_{i,\alpha-2}\delta_{j,\alpha-1}\tau_{\alpha-1}(\tau_{\alpha-1}+\tau_\alpha)\\&-\delta_{i,\alpha-1}\delta_{j,\alpha}\tau_\alpha(\tau_\alpha+\tau_{\alpha-1})+\delta_{i,\alpha-2}\delta_{j,\alpha}\tau_{\alpha-1}\tau_\alpha.\end{aligned} \tag{35}$$

With the aid of (35), the collected coefficients of the μ_α in the expression for s_1 are found to be

$$\begin{aligned}c_\alpha=&\sum_{ij}F_{ij}(J_\alpha)_{ji}\\=&\tau_{\alpha-1}^2F_{\alpha-2,\alpha-2}+(\tau_{\alpha-1}+\tau_\alpha)^2F_{\alpha-1,\alpha-1}+\tau_\alpha^2F_{\alpha,\alpha}\\&-\tau_{\alpha-1}(\tau_{\alpha-1}+\tau_\alpha)F_{\alpha-2,\alpha-1}-\tau_\alpha(\tau_\alpha+\tau_{\alpha-1})F_{\alpha-1,\alpha}\\&+\tau_{\alpha-1}\tau_\alpha F_{\alpha-2,\alpha},\end{aligned} \tag{36}$$

in which the F's vanish if either index is less than one or greater than $N-2$. For the molecule $ABCD\cdots$, the first few c_α are

$$\begin{aligned}c_A=&\tau_1^2F_{11},\\c_B=&(\tau_1+\tau_2)^2F_{11}+\tau_2^2F_{22}-\tau_2(\tau_2+\tau_1)F_{12},\\c_C=&\tau_2^2F_{11}+(\tau_2+\tau_3)^2F_{22}+\tau_3^2F_{33}\\&-\tau_2(\tau_2+\tau_3)F_{12}-\tau_3(\tau_3+\tau_2)F_{23}+\tau_2\tau_3F_{13},\\c_D=&\tau_3^2F_{22}+(\tau_3+\tau_4)^2F_{33}+\tau_4^2F_{44}\\&-\tau_3(\tau_3+\tau_4)F_{23}-\tau_4(\tau_4+\tau_3)F_{34}+\tau_3\tau_4F_{24},\end{aligned} \tag{37}$$

etc.

It is evident that these coefficients suffice to determine all force constants for both the triatomic and tetratomic molecules, since in the first case F_{11} is the only nonvanishing constant and in the second case, only F_{11}, F_{12}, and F_{22} appear. For longer molecules it would be necessary, as in the case of parallel vibrations, to introduce higher order coefficients, c_{AB}, c_{AC}, etc. With the pentatomic molecule, however, it might be simpler to use the determinant (product of roots) equation to determine the sixth force constant. Multiple roots would occur, of course, and could be eliminated by the procedures described above for the parallel vibrations.

V. THE EFFECT OF SYMMETRY

In case the linear molecule possesses a center of symmetry, the number of independent force constants is reduced in an obvious way. One then has the choice of reformulating the problem in terms of symmetry coordinates, or of employing the equations heretofore developed and appropriately reducing the number of isotopic species employed in accordance with the smaller number of distinct force constants. If the isotopic species employed are all of the maximum symmetry (e.g., C_2H_2 and C_2D_2), the former method is preferable, but if some isotopic molecules employed involved substitution of only one of a pair of equivalent atoms, (e.g., C_2HD) the latter procedure would be more desirable.

If the former approach is adopted, it is found that the previous discussion of the parallel vibrations can readily be carried through in terms of the symmetry coordinates. If the molecule has an even number of atoms, there are $N/2$ coordinates symmetric with respect to the center and $(N/2)-1$ antisymmetric to the center. If the molecule has an odd number of atoms, there are $(N-1)/2$ coordinates of each species.

It turns out that the expressions previously found for c_α and $c_{\alpha\beta}$ still hold, provided neither α nor β refer to the central atom or central pair. The F_{ij}, however, are now the force constants in terms of symmetry coordinates, and the sums s_1, s_2, etc., are taken over the respective species, $\sum_g^+$ (symmetric) or $\sum_u^+$ (antisymmetric). The only necessary modifications are indicated in Table II, where the formulas for c_γ and $c_{\alpha\gamma}$ are given, γ referring to the central atom (or pair).

Applying these results to acetylene, one finds, as is naturally to be expected, that the three force constants of the symmetric ($\sum_g^+$) vibrations may be determined immediately from s_1 and s_2 for C_2H_2 and C_2D_2. The expressions F_{11} and $F_{11}+2F_{22}-2^{\frac{1}{2}}F_{12}$ are found from s_1 for C_2H_2 and C_2D_2. But then

$$s_2=c_{HH}\mu_H^2+2c_{HC}\mu_H\mu_C+c_{CC}\mu_C^2,$$

and, since $c_{HH}=c_H^2$ and $c_{CC}=c_C^2$ are then known, the value of c_{HC} may be determined. Since

$$c_{HC}=(2^{\frac{1}{2}}F_{12}-F_{11})^2,$$

there are sufficient equations with which to determine all three force constants.

It is found on developing the coefficients c_α, etc., for larger molecules that a solution can be found without resorting to isotopic forms of lowered symmetry, such as would result if substitution were made at only one of a set of two equivalent atoms.

APPENDIX

It has been shown that for the parallel vibrations of a linear molecule,

$$\mathbf{G}=\sum_\alpha \mu_\alpha \mathbf{I}_\alpha,$$

where

$$(I_\alpha)_{jk}=\delta_{j,\alpha-1}\delta_{k,\alpha-1}+\delta_{j,\alpha}\delta_{k,\alpha}-\delta_{j,\alpha-1}\delta_{k,\alpha}-\delta_{j,\alpha}\delta_{k,\alpha-1}.$$

Moreover,

$$\begin{aligned} s_2&=\sum_i(\mathbf{FG})_{ii}^2=\sum_{ijkl}F_{ij}F_{kl}G_{jk}G_{li}\\ &=\sum_{ijkl}F_{ij}F_{kl}\sum_{\alpha\beta}(I_\alpha)_{jk}(I_\beta)_{li}\mu_\alpha\mu_\beta\\ &=\sum_{\alpha\beta}c_{\alpha\beta}\mu_\alpha\mu_\beta. \end{aligned}$$

Therefore,

$$c_{\alpha\beta}=\sum_{ijkl}F_{ij}F_{kl}(I_\alpha)_{jk}(I_\beta)_{li}.$$

First, consider the value of the term

$$\begin{aligned}(I_\alpha)_{jk}(I_\beta)_{li}=(&\delta_{j,\alpha-1}\delta_{k,\alpha-1}+\delta_{j,\alpha}\delta_{k,\alpha}-\delta_{j,\alpha-1}\delta_{k,\alpha}\\ &-\delta_{j,\alpha}\delta_{k,\alpha-1})(\delta_{l,\beta-1}\delta_{i,\beta-1}+\delta_{l,\beta}\delta_{i,\beta}\\ &-\delta_{l,\beta-1}\delta_{i,\beta}-\delta_{l,\beta}\delta_{i,\beta-1}).\end{aligned}$$

This vanishes unless $i=\beta-1$ or β, $j=\alpha-1$ or α, $k=\alpha-1$ or α, and $l=\beta-1$ or β. There are therefore 16 possible sets of values for i, j, k, l; if $i=l$ and $j=k$ or if $i\neq l$ and $j\neq k$, the value of $(I_\alpha)_{jk}(I_\beta)_{li}$ (assuming that it does not vanish) is $+1$, otherwise it is -1. The rule for the sign can be stated in the form: positive if there are an even number of inequalities of the index pairs jk and il, negative otherwise.

It is therefore possible to write the expression for $(I_\alpha)_{jk}(I_\beta)_{li}$ in another form, namely

$$\begin{aligned}(I_\alpha)_{jk}(I_\beta)_{li}=(&\delta_{i,\beta-1}\delta_{j,\alpha-1}+\delta_{i,\beta}\delta_{j,\alpha}\\ &-\delta_{i,\beta-1}\delta_{j,\alpha}-\delta_{i,\beta}\delta_{j,\alpha-1})(\delta_{k,\alpha-1}\delta_{l,\beta-1}\\ &+\delta_{k,\alpha}\delta_{l,\beta}-\delta_{k,\alpha-1}\delta_{l,\beta}-\delta_{k,\alpha}\delta_{l,\beta-1}),\end{aligned}$$

which is entirely equivalent to the first expression. When this form is inserted in the expression for $c_{\alpha\beta}$, the summation over $ijkl$ leaves only the following function of the F elements:

$$\begin{aligned}c_{\alpha\beta}=&(F_{\beta-1,\alpha-1}+F_{\beta,\alpha}-F_{\beta-1,\alpha}-F_{\beta,\alpha-1})\\ &\times(F_{\alpha-1,\beta-1}+F_{\alpha,\beta}-F_{\alpha-1,\beta}-F_{\alpha,\beta-1}),\end{aligned}$$

and since $F_{ij}=F_{ji}$, Eq. (30) is obtained:

$$c_{\alpha\beta}=(F_{\alpha-1,\beta-1}+F_{\alpha,\beta}-F_{\alpha-1,\beta}-F_{\alpha,\beta-1})^2.$$

By an extension of these arguments, further coefficients, such as

$$\begin{aligned}c_{\alpha\beta\gamma}=&(F_{\gamma-1,\alpha-1}+F_{\gamma,\alpha}-F_{\gamma-1,\alpha}-F_{\gamma,\alpha-1})\\ &\times(F_{\alpha-1,\beta-1}+F_{\alpha,\beta}-F_{\alpha-1,\beta}-F_{\alpha,\beta-1})\\ &\times(F_{\beta-1,\gamma-1}+F_{\beta,\gamma}-F_{\beta-1,\gamma}-F_{\beta,\gamma-1})\end{aligned}$$

can be obtained.

The Microwave Spectrum of CF_3SF_5

P. KISLIUK AND GENE A. SILVEY
Columbia University, New York, New York

(Received November 28, 1951)

The pure rotational spectrum of CF_3SF_5 has been observed in the microwave region. It is confirmed that the structure is almost certainly trifluoromethyl sulfurpentafluoride, and some evidence relating to the molecular parameters is obtained. Several vibrational states have been observed, including the torsional vibration from which the height of the potential barrier can be estimated as 220 cm^{-1}.

ALTHOUGH the methods of synthesis reported[1] indicate that the structure of CSF_8 is probably trifluoromethyl sulfurpentafluoride, no direct evidence has previously been published. The $J=3\rightarrow4$, $10\rightarrow11$, and $11\rightarrow12$ transitions of the pure rotational spectrum have been observed, yielding $B=1097.6\pm0.4$ Mc. The new evidence favoring this structure is:

(1) The spectrum is that of a symmetric rotor, thus ruling out any proposed structure which does not have an inertial axis of symmetry.

(2) When the values of all bond distances and angles except the C−S distance are estimated and the experimental value of the moment of inertia (460.5 amu A^2 ±0.04 percent) is used to calculate the C−S distance, the reasonable value of 1.86A is obtained. The following bond distances and angles were used for this calculation: $R(CF)=1.35$A and $\angle FCF=107°30'$ from fluorocarbon data, $R(SF)=1.57$A from electron diffraction measurements on SF_6, and $\angle FSF=90°$ for the SF_5 group in CF_3SF_5 because of the octahedral symmetry of SF_6.

A value for the C−S bond distance of 1.87A may be estimated from the sum of a carbon radius of 0.77A and a hexavalent sulfur radius of 1.10A. The latter value is based upon a S−S bond distance of 2.20A found recently in S_2F_{10} from electron diffraction data.[2] The agreement between this estimate and the experimental C−S bond distance indicates that the F−S−F angles in CF_3SF_5 are very close to 90°. One might expect the angle between the fluorine on the molecular axis and each of the other fluorines of the SF_5 group to be slightly less than 90° by analogy with several fluorocarbons such as CF_3CF_3 where the presence of similar groups reduces the F−C−F angle to less than the tetrahedral angle.[3]

Because of the low frequency vibrations of the molecule the population of the ground state falls off very rapidly with increasing temperature. All measurements were therefore made at −78° where these lines are roughly eight times as strong as at room temperature.

Higher vibrational states of two of the lower frequency vibrations were clearly observed. One of these, with 2/11 the intensity of the ground-state line at −78° is lower in frequency by about 26 Mc in the $11\rightarrow12$ transition (whence $\alpha\simeq1$ Mc). If the mode of vibration is nondegenerate, its frequency is roughly 230 cm^{-1}.

The other observed vibration was roughly one-half as intense as the ground-state line at −78°C. The difficulty in measuring the relative intensity arises from the fact that these lines are not completely resolved. These lines probably arise from a torsional vibration of the CF_3 and SF_5 groups about the symmetry axis. There are twelve maxima and twelve minima for such a vibration. The potential is taken to be of the form $V=h/2(1-\cos12\theta)$, where h is the depth of the potential well, and vibration considered to be harmonic by taking only the loading term in the expansion of the potential in powers of θ. From the relative intensity of 0.50±0.10 at −78° we obtain $\nu=93.5$ cm^{-1} ±28 percent, and using the parameters previously considered to calculate the moments of inertia about the symmetry axis of the CF_3 and SF_5 groups we find: $h=4.35\times10^{-14}$ ergs±50 percent = 219 cm^{-1}±50 percent.

If the potential well were parabolic, this depth would contain only 2 or 3 bound states, but the vibrational states should lie closer together near the top of the potential and merge into states with free relative rotation of the two parts of the molecule. Four states were clearly observed at optimum conditions of pressure and stark voltage, but even if a fifth state had been present it is doubtful that it could have been observed.

Because of the different symmetry of the CF_3 and SF_5 groups about the axis, the potential well for torsional vibration would be expected to be shallower than that of CH_3CF_3 or CH_3SiF_3. Both the torsional frequency and the value of α, which is a rough measure of the degree to which the rotating groups move in and out as they rotate back and forth, would then be expected to be smaller in CSF_8. These are given in Table I.

TABLE I.

	Freq of tors vib	Well depth	α
CH_3CF_3[4]	230 ±10 cm^{-1}	1200 cm^{-1}	7.6 Mc
CH_3SiF_3[4]	140 ±30 cm^{-1}	419 cm^{-1}	∼4. Mc
CF_3SF_5	93.5±25 cm^{-1}	219 cm^{-1}	∼0.05 Mc

The authors wish to express their appreciation to Professor C. H. Townes for his help and advice during this work.

[1] G. A. Silvey and G. H. Cady, J. Am. Chem. Soc. **72**, 3624 (1950).
[2] S. H. Bauer, private communication.
[3] G. Glockler in *Fluorine Chemistry* edited by J. H. Simons (Academic Press, Inc., New York, 1950).
[4] H. T. Minden, thesis, Columbia University, 1951.

Letters to the Editor

THIS section will accept reports of new work, provided these are terse and contain few figures, and especially few half-tone cuts. The Editorial Board will not hold itself responsible for opinions expressed by the correspondents. Contributions to this section should not exceed 600 words in length and must reach the office of the Editor not later than the 15th of the second month preceding that of the issue in which the Letter is to appear. No proof will be sent to the authors. A publication charge of $10.00 per Letter is made which, when honored, will entitle the Institution to 100 free reprints.

The Microwave Spectra and Dipole Moment of Stable Pentaborane

HENRY J. HROSTOWSKI, ROLLIE J. MYERS, AND GEORGE C. PIMENTEL
Department of Chemistry and Chemical Engineering, University of California, Berkeley, California
(Received December 4, 1951)

WE have investigated the microwave spectra of stable pentaborane (B_5H_9) in the region near 28,000 Mc and have observed several lines. For two of the strongest of these lines a characteristic Stark effect pattern was obtained. These two lines were found to have two first-order Stark components and two second-order Stark components. This Stark pattern indicates that the lines are a result of $J=1$ to $J=2$ transitions for symmetric top molecules. Most of the remaining lines are satisfactorily interpreted as arising from asymmetric molecules consisting of both B^{10} and B^{11} isotopes.

For a molecule with five boron atoms and a normal isotopic distribution the occurrence of only two prominent symmetric top lines leads to a structure possessing a C_4 symmetry axis with one boron on this axis. Recently, such a structure of symmetry C_{4v} has been determined on the basis of electron and x-ray diffraction measurements.[1,2] From the microwave data alone the two distances, *B–B* (ring-apex) and *B–B* (ring), have been determined as 1.69 ± 0.02A and 1.80 ± 0.01A, respectively, in agreement within experimental error with the electron diffraction results. Evaluation of the remaining five molecular parameters and more precise values for the boron distances must await isotopic hydrogen substitution. Figure 1 compares the observed and calculated microwave spectra for the more abundant isotopic species, and Table I lists the observed frequencies and their assignments. The calculated spectra were determined from the above *B–B* distances with the line at 28,011.4 Mc as a reference point. The 1_{10}–2_{20} frequencies depend very slightly on the moment of inertia about the symmetry axis, and a value consistent with the electron diffraction data has been used in the calculation of these lines. It can be seen from Fig. 1 that the agreement between the calculated and observed spectra is good.

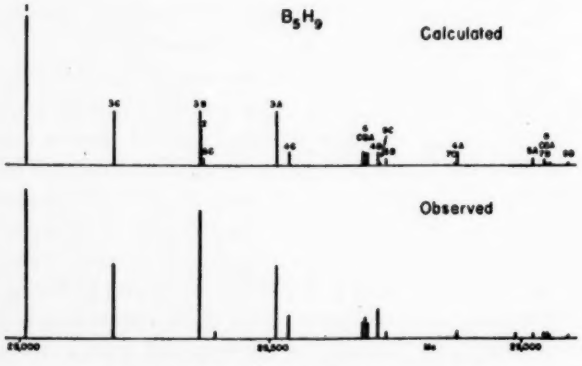

FIG. 1. The calculated and observed spectra of B_5H_9.

TABLE I. The microwave spectra of B_5H_9.

Observed frequency Mc	No.	Assignment Transition	Isotopic species
28,011.4	1	1–2	$B_5{}^{11}H_9$
28,359	2	1–2	$B^{10}B_4{}^{11}H_9$, B^{10} in apex
28,513	3A[a]	1_{11}–2_{21}	$B^{10}B_4{}^{11}H_9$
28,359	3B	1_{10}–2_{20}	B^{10} in ring
28,187	3C[b]	1_{01}–2_{11}	
28,872	4A	1_{11}–2_{21}	$B_2{}^{10}B_3{}^{11}H_9$
28,715	4B	1_{10}–2_{20}	B^{10} in ring and apex
28,538	4C	1_{01}–2_{11}	
29,024	5A	1_{11}–2_{21}	$B_2{}^{10}B_3{}^{11}H_9$
28,732	5B	1_{10}–2_{20}	two B^{10} in ring opposite
28,695	6A	1_{11}–2_{21}	$B_2{}^{10}B_3{}^{11}H_9$
28,690	6B	1_{10}–2_{20}	two B^{10} in ring adjacent
28,685	6C	1_{01}–2_{11}	
29,045	7B	1_{10}–2_{20}	$B_2{}^{10}B_3{}^{11}H_9$
28,870	7C	1_{01}–2_{11}	B^{11} in ring and apex
29,057	8A	1_{11}–2_{21}	$B_2{}^{10}B_3{}^{11}H_9$
29,052	8B	1_{10}–2_{20}	two B^{11} in ring adjacent
29,045	8C	1_{01}–2_{11}	$B_2{}^{10}B_3{}^{11}H_9$
29,095	9B	1_{10}–2_{20}	two B^{11} in ring opposite
28,392	not assigned		
28,989	not assigned		
29,063	not assigned		

[a] Frequency equals $3a+b$, where $a=\hbar^2/2I_a$, etc.
[b] Frequency equals $3b+a$.

Measurements of all four of the Stark components of the line at 28,011.4 Mc give 2.13 ± 0.04 Debye for the dipole moment of pentaborane. This value seems surprisingly large in view of the expected similarity of the electronegativities of boron and hydrogen. It is much greater than the value of 0.6 Debye predicted by Dulmage and Lipscomb[2] on the basis of the Pauling bond order method and a metallic model.

The microwave lines were observed with a Stark modulation spectrograph. The pentaborane was purified by distillation, and the absorption cell was cooled to 200°K to minimize decomposition. Previous observations[3] showed that serious decomposition occurred in the metal wave guide at room temperature. At pressures near 60 microns no quadrupole fine structure was observed and the absorption lines appeared relatively sharp.

We are grateful to Professor W. D. Gwinn for very helpful discussions of this problem, and we wish to thank Dr. A. E. Newkirk of the General Electric Company for providing the sample of pentaborane.

[1] Hedberg, Jones, and Schomaker, J. Am. Chem. Soc. **73**, 3538 (1951).
[2] W. J. Dulmage and W. N. Lipscomb, J. Am. Chem. Soc. **73**, 3539 (1951).
[3] G. L. Cunningham and H. J. Hrostowski (unpublished work).

On the Effect of Iodine in the Radiolysis of the Hydrocarbons*

CLARENCE C. SCHUBERT AND ROBERT H. SCHULER
Department of Chemistry, Canisius College, Buffalo, New York
(Received December 10, 1951)

SCHULER and Hamill[1] have observed a fast electron initiated reaction between the paraffin hydrocarbons and iodine. Weber[2] has shown that, for solutions 10^{-3} to 10^{-4} molar in iodine, this reaction is not dependent upon the iodine concentration. Because of this, it was desired to determine the effect of iodine upon the rate of gas production in these radiolyses anticipating that, as a result of reaction of the radical fragments with the iodine, an appreciable decrease in this rate would be observed.

TABLE I. Hydrocarbon decomposition in the presence of iodine by 120-kev x-radiation.

Sample	(I_2) $M \times 10^3$	Irradiation period	Gas production moles H_2+CH_4/min $\times 10^8$
Cyclohexane			
4	0	50	1.6
13	0	100	1.9
9	0	100	1.9
2	0	200	1.9
14	0.35	100	2.0
3	2.16	250	1.8
8	4.89	100	2.0
10	13.5	100	2.5
11	29.4	100	4.1
15	34.6	100	4.6
5	48	100	5.4
12	50.0	100	4.7
2,2,4 trimethylpentane			
6	0	100	0.92
7	1.92	100	0.99

Ten-ml samples of the hydrocarbons, cyclohexane, and 2,2,4 trimethylpentane, were degassed and sealed on a line capable of evacuation to pressures of less than 10^{-5}. They were then subjected to irradiation with the x-radiation produced by an industrial x-ray unit operating at 120 kev and 5 ma. After irradiation the sample was resealed to the line, frozen in liquid nitrogen, and the gas pumped to a calibrated McLeod gauge. The fraction collected was volatile at −196°C and contained the hydrogen and methane produced in the decomposition but none of the higher hydrocarbons.

In Table I, it is seen that no appreciable quenching of the production of the hydrogen-methane fraction occurs in either the decomposition of cyclohexane or of 2,2,4 trimethylpentane at the low concentration region where there is reaction between the radiation product and iodine. These represent the extreme cases of the formation of almost no methane in the case of cyclohexane and of a relatively large amount in the case of the trimethylpentane.[3]

For samples more concentrated in iodine, the reaction yield is seen, in Fig. 1, to increase approximately in proportion to the amount of added iodine. This increased reaction is interpreted as being a result of the greater absorption of these solutions for x-radiation at the wavelength used ($\lambda_{max} \sim 0.2$A) since iodine has an appreciable photoelectric component here. The incident x-radiation is absorbed in the iodine, producing fast electrons which in turn interact with the hydrocarbon to give a higher yield for the decomposition.

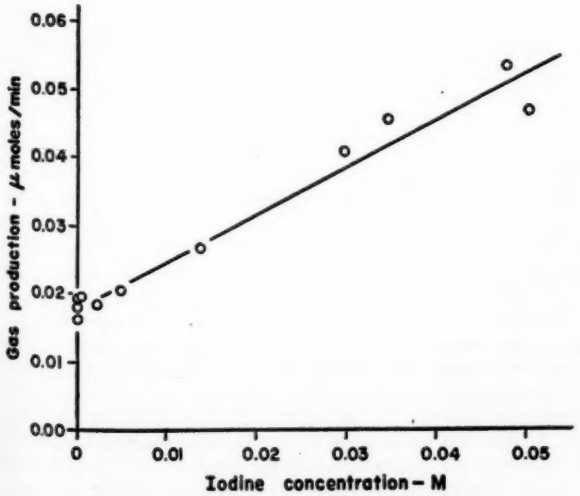

FIG. 1. Effect of iodine in hydrocarbon decomposition at 120 kev.

Further work is in progress on the effect of iodine in the radiation decomposition of the hydrocarbons.

* Supported in part under contract AT-(30-1)-1084 with the AEC.
[1] R. H. Schuler and W. H. Hamill, J. Am. Chem. Soc. (to be published).
[2] E. N. Weber, M.S. dissertation, Canisius College, 1951 (to be published).
[3] C. S. Schoepfle and C. H. Fellows, [Ind. Eng. Chem. **23**, 1396 (1931)] report 1.4 percent CH_4 in the electron irradiation of cyclohexane and 29.3 percent CH_4 in the case of 2,2,4 trimethylpentane.

The Surface Adsorption of Small Ions in Solutions of Surface-Active Agents

CHARLES M. JUDSON, ANN A. LEREW, J. K. DIXON, AND D. J. SALLEY
Stamford Research Laboratories, American Cyanamid Company, Stamford, Connecticut
(Received December 18, 1951)

IN considering the adsorption of a surface-active agent at the air-solution interface, the adsorption of small ions (gegenions or foreign ions) must be examined as well as that of the long chain ion. The need for this is indicated by recent measurements[1] using radiotracer techniques of the sulfate ion adsorption for Aerosol[2] SE cationic agent (stearamidopropyl-2-hydroxyethyl ammonium sulfate). The results indicated that at relatively low concentration, the adsorbed ion was not sulfate but hydroxyl, at least in part. This paralleled an earlier indication[3] for Aerosol[2] OTN anionic agent (di-*n*-octyl sodium sulfosuccinate), where comparison of surface tension and radiotracer measurements of the adsorption of the long chain ion suggested that hydrogen ion and not sodium ion was adsorbed along with the sulfosuccinate ion.

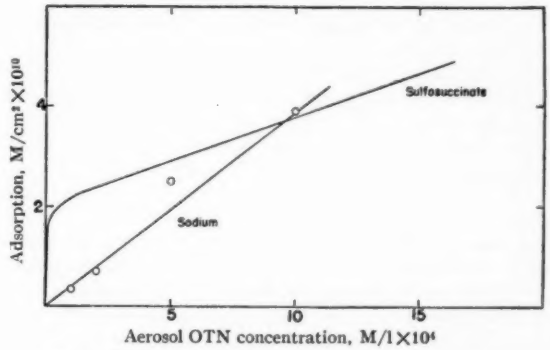

FIG. 1. Adsorption of sodium and of sulfosuccinate ions from Aerosol OTN solutions.

Following up this idea, the adsorption of sodium ions from solutions of Aerosol OTN, labeled with $Na^{22}Cl$, has been measured with Hutchinson's method.[4] In this procedure a film is drawn out of the solution on a platinum loop and the excess concentration of sodium ion in the film determined by counting. Figure 1 shows that at low concentrations the sodium adsorption is quite small compared to the sulfosuccinate adsorption, as determined previously by the direct surface count method.[3] It is realized that the Hutchinson method may lead to values lower than the true ones because the time allowed for withdrawing the loop (which is limited by the stability of the film) may be too short to permit establishment of equilibrium. However, the evidence available from our experience with this method indicates that serious errors from this source will not be encountered at the concentrations in question. The results in Fig. 1 therefore appear to substantiate the suggestion that at low concentrations the adsorbed species from solutions of Aerosol OTN is the undissociated di-*n*-octyl sulfosuccinic acid.

The adsorption of a foreign ion of the same sign as that of the long chain ion has also been investigated for solutions of sodium sulfate and the above Aerosol OTN, with $Na_2S^{35}O_4$ and employing both the direct count method and Hutchinson's method. It might be expected that the adsorption of the sulfate ion would be

essentially zero. Measurements over a wide range of concentrations of sulfate and of surface-active agent showed that sulfate adsorption is indeed small at low sulfate concentrations but becomes appreciable at higher sulfate concentrations. For example, at a constant Aerosol OTN concentration of 10^{-4} molar, sulfate adsorption increases linearly with sulfate concentration, reaching about 500×10^{-10} M/cm² at 0.1 molar sulfate. This represents a sulfate adsorption of 250 times the measured adsorption of a sulfosuccinate monolayer (about 2×10^{-10} M/cm², Fig. 1). The same sort of behavior was observed for solutions of sodium sulfate with Aerosol[2] OT di-(2-ethyl hexyl) sodium sulfosuccinate. It appears that the sulfate adsorption being measured is not an adsorption in the actual interface but is an accumulation of electrolyte in the region of the Gouy-Chapman layer adjacent to the interface.

The Na^{22} and S^{35} used were obtained on allocation from the AEC.

[1] Judson, Argyle, Dixon, and Salley, J. Chem. Phys. **19**, 378 (1951).
[2] Registered trademark, American Cyanamid Company.
[3] Salley, Weith, Argyle, and Dixon, Proc. Roy. Soc. (London) **A203**, 42 (1950).
[4] Hutchinson, J. Colloid Sci. **4**, 599 (1949).

Intensities of Vibration Bands of Carbonyl Sulfide and Carbon Disulfide

D. C. McKean, H. J. Callomon, and H. W. Thompson
The Physical Chemistry Laboratory, Oxford, England
(Received December 14, 1951)

In a recent article Robinson[1] has published data on the intensities of infrared absorption bands of carbon disulfide and carbonyl sulfide, and has calculated values for $\partial\mu/\partial\gamma$ for the linkages concerned. In a paper in course of publication elsewhere,[2] we have described similar work on carbonyl sulfide, and we have also now studied carbon disulfide. Although our results with the latter compounds agree substantially with those of Robinson, there is a discrepancy with carbonyl sulfide which requires comment.

The method used for determining the intensities involved pressure broadening by addition of nitrogen and extrapolation by the procedure of Wilson and Wells.[3] Experimental details are being given elsewhere. The results for carbon disulfide on the band at 1523 cm^{-1} are summarized in Fig. 1, the total pressure including added nitrogen being one atmosphere. The limiting gradient of this plot, which represents the true intensity, was 7700×10^{10} cycles/cm at N.T.P., as compared with 7560×10^{10} found by Robinson. This deviation of about 2 percent is well within possible experimental error, especially since there is an overlapping band of atmospheric water vapor. In the calculation of the normal coordinate, we have computed a value for the normalizing coefficient of 2.90×10^{-12}, whereas Robinson gives 2.8×10^{-12}. The resulting value of $\partial\mu/\partial\gamma$ is 5.9×10^{-10} esu, agreeing with Robinson.

In the case of carbonyl sulfide, the intensities found by us for the bands at 2064 cm^{-1} and 859 cm^{-1} were $12{,}900\times10^{10}$ and 350×10^{10} cycle/cm, respectively, Robinson finding 7900×10^{10} and 110×10^{10} for these two bands. These large deviations might arise as a result of incomplete pressure broadening. We have investigated in detail, with a wide range of pressures of both absorbing and of broadening gas, how the extrapolation is affected in the different circumstances. Comparison of the two sets of data suggests that the conditions of measurement used by Robinson may have led to a somewhat low value for the intensity. It is more likely, however, in our opinion, that the difference may be caused by the fact that the pressure assumed by him was too high owing to the presence of impurity. In our experience the preparation of this gas free from other contaminants and its retention without decomposition are difficult. It was therefore prepared from ammonium thiocarbamate which yields a product free from carbon dioxide, and checks were made for the absence of other gases such as hydrogen sulfide both spectroscopically and by smell.

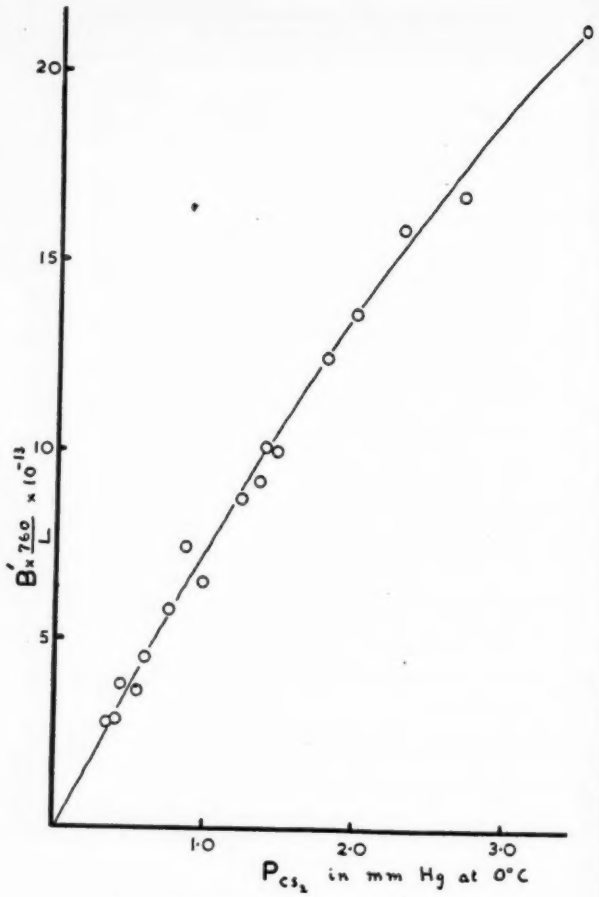

FIG. 1. Plot of intensity *versus* pressure of CS_2.

The correlation of the measured intensities with the values of $\partial\mu/\partial\gamma$ for the linkages involved has been discussed elsewhere.[2]

[1] D. Z. Robinson, J. Chem. Phys. **19**, 881 (1951).
[2] Callomon, McKean, and Thompson, Proc. Roy. Soc. (London) **A208**, 341 (1951).
[3] E. B. Wilson and A. J. Wells, J. Chem. Phys. **14**, 578 (1946).

Infrared Spectrum of SF_6 in the LiF Region

A. de Lattre
Centre d'Analyse spectrale moléculaire de l'Université de Liége, quai Fr. Roosevelt 1B, Liége, Belgique
(Received September 14, 1951)

There recently appeared an article on the infrared spectrum of SF_6 by Lagemann and Jones in this journal, 1951, p. 534. A similar investigation was going on at Liége simultaneously, and it appears worthwhile to publish the results of this separate research in comparison with the previous work, as there appear to be certain points of disagreement between them.

Gaseous SF_6 was studied in the region 1560–2510 cm^{-1} by means of a Beckman spectrometer equipped with LiF optics. Path length was 1 meter and spectra were recorded at 760, 180, 55, and 10 mm Hg pressure, bands being found at 1577 (53, 2; *m*)–1616 (1, 47; *w*) 1634 (1, 47; *w*)–1713 (119; *m*)–1758 (1, 55; *w*)–2027 (0, 06; *vw*)–2225 (0, 85; *w*)–2488 (0, 13; *vw*). The first figure is the frequency in cm^{-1}, the figure between brackets being the reciprocal pressure in atmospheres$\times\log_{10}I_0/I$. Practically perfect agreement in position as well as in the order of intensity is found with

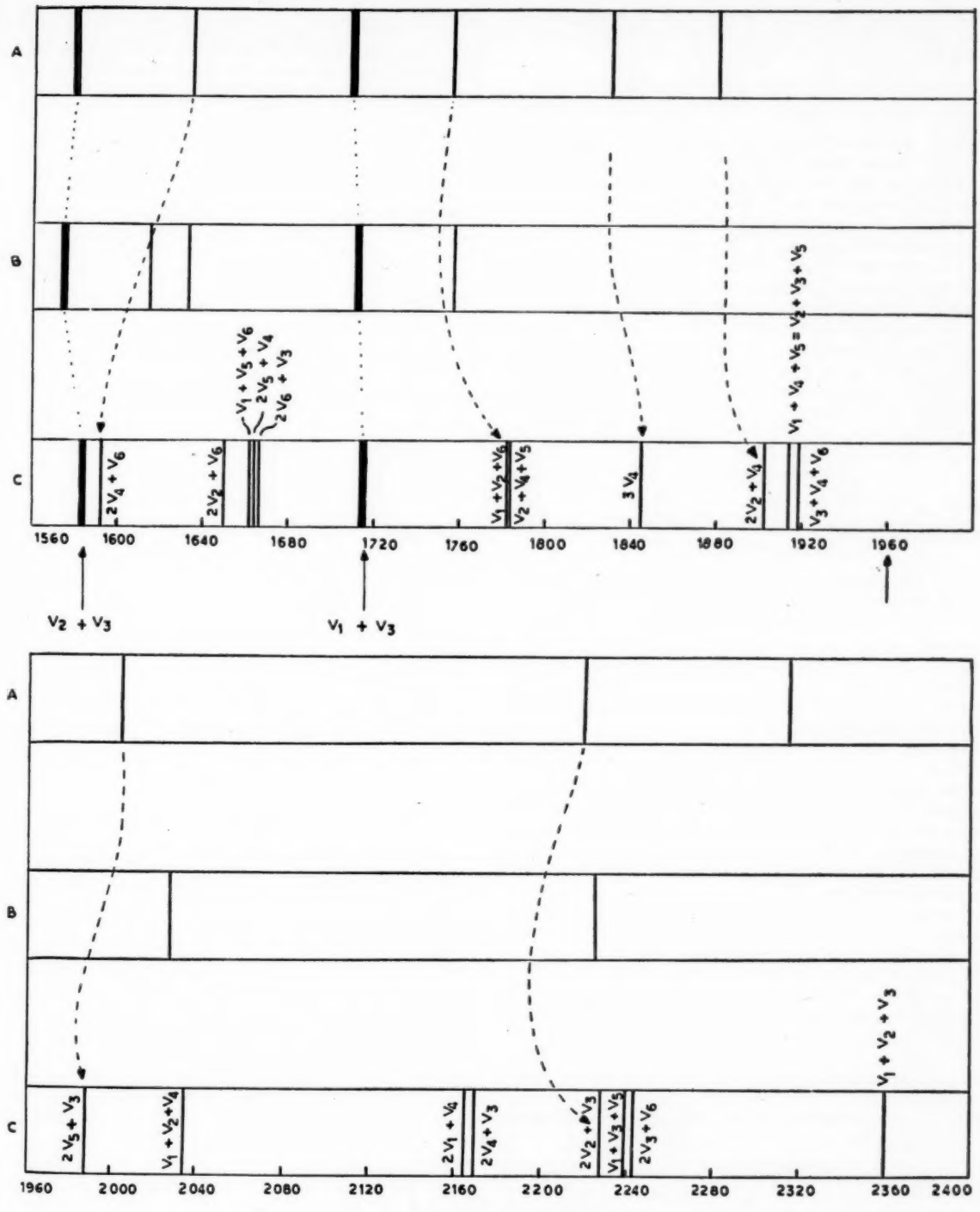

FIG. 1. Near infrared spectrum of SF_6.

Lagemann and Jones for the binary levels and for the bands 1634, 1756, 2004, although the latter is somewhat shifted by us. But we did not observe 1830, 1880, nor 2315, while we observed lines at 1616 and 2488 not mentioned by them (see Fig. 1: upper line gives L. and J.'s frequencies; middle line, our frequencies; and lower line, *all* frequencies having the proper component for infrared activity, these being calculated using L. and J.'s values of the fundamentals).

Our optical path was at least equivalent to that used by L. and J. and our gas was very carefully purified (SF_6 from a cylinder was mixed with N_2; KOH and H_2SO_4 bubblers ensured removal of lower fluorides and most of the moisture; it was then condensed in liquid air, pumped free of noncondensible gas, and sublimed to the desired pressure into the absorption tube. For the low pressure recordings, a further purification was afforded by surrounding the bulb with dry ice while subliming).

As the figure clearly shows, there is an extensive possibility of interaction between the ternary levels allowed by selection rules. It should be borne in mind that the actual order of succession of the zero-order frequencies may be different from that given in

the lower line of the figure to a large extent. It is felt that the following assignment of the ternary levels corresponds better to the actual situation:

$$1634=(2v_4+v_6)+(2v_2+v_6)+(v_1+v_5+v_6)+(2v_5+v_4)+(2v_6+v_3);$$
$$1756=(v_1+v_2+v_6)+(v_2+v_5+v_4); \quad 2004=(2v_5+v_3)+(v_1+v_2+v_4),$$

where the + sign means interaction between the F_{1u} *components* of the levels between brackets. Neither of these levels can be supposed to give the observed band, since interaction between any two close-lying levels gives rise to two new levels, *neither of which* can be described as any of the original ones.

The present writer's opinion is that great caution should be exercised in using any of these interpretations before the discrepancies between L. and J.'s results and ours are settled. Although we disagree only on very weak bands, these play an important part in the assignment of ternary levels, and we conclude that for the present the latter must be considered an open question.

Our best thanks go to Professor D'Or for his guidance and interest, Dr. P. Tarte for valuable help in the experimental part, and Professor A. H. Nielsen for very obligingly discussing the matter with us.

Spectroscopic Studies of Low Pressure Combustion Flames*

S. S. Penner, M. Gilbert, and D. Weber
Jet Propulsion Laboratory, California Institute of Technology, Pasadena, California
(Received December 19, 1951)

A LARGE metal duct with suitable accessory equipment has been constructed for spectroscopic investigations on two-dimensional, low pressure flames.[1] The apparatus represents an improvement over the design used by Gaydon and Wolfhard[2] since larger and more stable flames are obtained. Furthermore, the inlet duct is rectangular thus providing larger and better-defined isothermal regions than can be obtained with cylindrical burners. Spatial explorations of the flame are facilitated by use of the periscopic arrangement shown in Fig. 1. Excellent spatial resolution is obtained at the expense of loss of light intensity. This loss is, however, not serious since long exposures (24 hours or more) can be performed without difficulty.

Spectroscopic studies are being carried out by use of a Perkin-Elmer model 12C-infrared spectrometer provided with complete crystal optics and auxiliary photoelectric receivers for study in the near-infrared region.[3] Preliminary emission studies have been carried out with a 1.5 meter grating spectrograph with a theoretical resolving power of 48,800. Further studies will be performed with improved instrumentation.

Several emission spectra from the luminous zone of a propane-oxygen flame burning at a pressure of 5 mm have been obtained. A complete rotational analysis with the compilation of Dieke and Crosswhite[4] has been carried out for the Q_1, Q_2, P_1, P_2, and R_2 branches of the (0, 0) transitions of the $^2\Sigma \rightarrow {}^2\Pi$ band system of OH. Representative data are shown in Figs. 2 and 3, where the abscissa represents the rotational energy of the initial state (i.e., the excited state in emission studies) and the ordinate equals the logarithm of the peak intensity of lines divided by the product of the transition probability and the cube of the frequency corresponding to the indicated transition.[5] In agreement with the results reported by Gaydon and Wolfhard,[2] the lower rotational states (roughly up to $K=11$) of the upper energy level indicate rotational temperatures somewhat lower than the adiabatic flame temperature (which is 2500°K in the present case). On the other hand, the upper rotational states indicate abnormal rotational

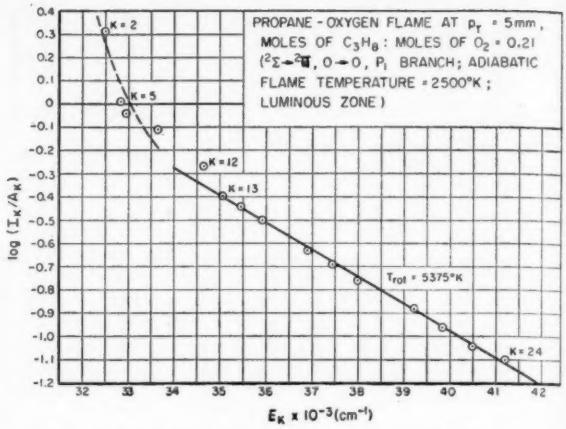
PROPANE - OXYGEN FLAME AT p_T = 5mm,
MOLES OF C_3H_8 : MOLES OF O_2 = 0.21
($^2\Sigma \rightarrow {}^2\Pi$, 0→0, P_1 BRANCH; ADIABATIC
FLAME TEMPERATURE = 2500°K;
LUMINOUS ZONE)
K = 2
K = 5
K = 12
K = 13
K = 24
T_{rot} = 5375°K
log (I_K/A_K)
$E_K \times 10^{-3}$ (cm^{-1})

FIG. 2. Representative plot used for the determination of rotational temperatures of OH (P_1 branch).

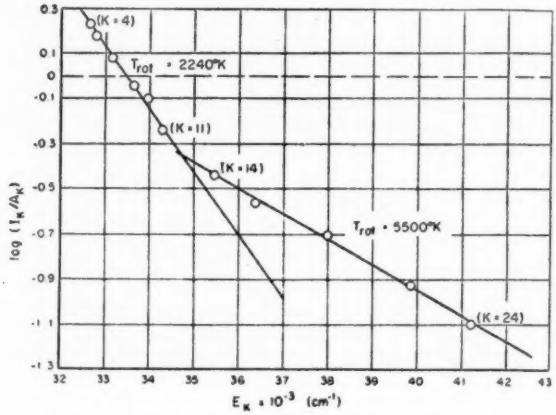

FIG. 3. Curve for determination of rotational temperature of OH (P_2 branch).

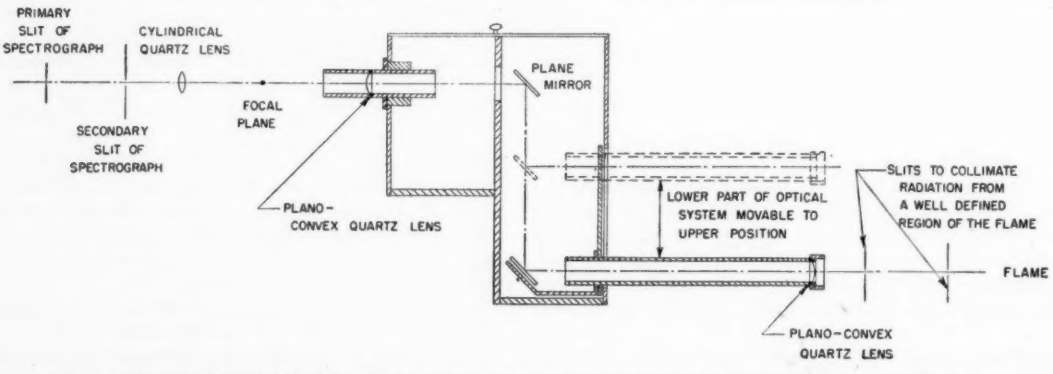
PRIMARY SLIT OF SPECTROGRAPH
CYLINDRICAL QUARTZ LENS
SECONDARY SLIT OF SPECTROGRAPH
FOCAL PLANE
PLANE MIRROR
PLANO-CONVEX QUARTZ LENS
LOWER PART OF OPTICAL SYSTEM MOVABLE TO UPPER POSITION
SLITS TO COLLIMATE RADIATION FROM A WELL DEFINED REGION OF THE FLAME
FLAME
PLANO-CONVEX QUARTZ LENS

FIG. 1. Schematic drawing of optical system used to obtain spatial resolution of low pressure combustion flames.

excitation and temperatures of 5500°K to 8000°K, depending on the position of the luminous zone which is being examined and on the branch for which a rotational analysis is performed. The interpretation of the experimental results described in Figs. 2 and 3 can be shown to imply the validity of the relation,

$$1-\exp[-(P_\nu)_{\max}X]\simeq(P_\nu)_{\max}X,$$

where $(P_\nu)_{\max}$ is the maximum value of the spectral absorption coefficient for a given spectral line and X represents the optical density of the emitter. Calculations of appropriate values of $(P_\nu)_{\max}X$ for representative flames, with the f-values of Oldenberg *et al.*[6] show that the expansion is probably not valid. Hence it follows that the observed "anomalous intensity distributions" may be the result of invalid interpretation of experimental data. This matter will be considered in greater detail in a subsequent publication.

A preliminary rotational analysis of the CH spectrum shows a reasonably normal rotational distribution, in agreement with the work of Gaydon and Wolfhard.[2]

Experimental studies in absorption and emission with improved spectroscopic apparatus are continuing.

* This paper presents the results of one phase of research carried out at the Jet Propulsion Laboratory, California Institute of Technology, under Contract No. W 33-038-ac-4320 sponsored by the Department of the Air Force, Air Materiel Command. Presented before the *Symposium on Energy Transfer in Hot Gases*, National Bureau of Standards, Washington, D. C., September 17–18, 1951.

[1] M. Gilbert, *The Investigation of Low-Pressure Flames*, Report No. 4–54 (Jet Propulsion Laboratory, Pasadena, August 30, 1949).

[2] A. G. Gaydon and H. G. Wolfhard, Proc. Roy. Soc. (London) **A194**, 169 (1948); **A199**, 89 (1949); **A201**, 561 (1950); **A201**, 570 (1950); **A202**, 118 (1951).

[3] S. S. Penner, J. Chem. Phys. **19**, 272, 1434 (1951).

[4] G. H. Dieke and H. M. Crosswhite, *The Ultra Violet Bands of* OH, *Fundamental Data*, Bumblebee Series Report No. 87 (Applied Physics Laboratory, Johns Hopkins University, Silver Spring, Maryland, November, 1948).

[5] It is customary to divide by the fourth power of the frequency rather than by the cube. However, it is easily shown that for Doppler-broadened spectral lines of the type which must occur in the visible and ultraviolet spectra of low pressure flames, the cube of the frequency should be used. The experimental results are actually quite insensitive to the frequency factor.

[6] O. Oldenberg and F. F. Rieke, J. Chem. Phys. **6**, 439 (1938); R. J. Dwyer and O. Oldenberg, J. Chem. Phys. **12**, 351 (1944).

Light Scattering by GR-S Solutions

ROBERT TREMBLAY AND MARCEL RINFRET
Institut de Chimie, Université de Montréal
AND
ROLAND RIVEST
University of California, Berkeley, California

(Received November 13, 1951)

THE light scattered by GR-S (Buna-S type synthetic rubber) solutions of very small refractive index increment presents an anomaly which has been reported.[1] The amount of scattering by a toluene solution of GR-S is approximately ten times as large as would be expected by the light scattering equation,

$$R-Ro=\frac{2\pi^2}{N\lambda^4}\mu_0^2\left(\frac{\mu-\mu_0}{c}\right)^2\frac{c}{(1/M)+2Bc},$$

where R=amount of light scattered by the solution at 90° relative to the light transmitted at 0°, Ro=amount of light scattered by the solvent under the same conditions, N=Avogadro's number, λ=wavelength of the incident light, μ_0=index of refraction of solvent for wavelength λ, μ=index of refraction of solution for wavelength λ, c=concentration of solute in gram per cubic centimeter of solution, M=molecular weight of solute, and B=constant dependent on the solvent.

At the time the validity of the equation for small differences in refractive index between solvent and solution was questioned.

Since then, it has been shown both theoretically[2] and experimentally[2,3] that the equation holds for values of refractive index increment lower than that encountered in toluene solutions of GR-S as shown in Table I.

TABLE I.

Solvent	Solute	$(\mu-\mu_0/c)^2$	Molecular weight: Accepted value	Molecular weight: L.S.	Ref.
Ethylene chloride	GR-S	2.72×10^{-2}	125,000	140,000	1
Toluene	GR-S	0.31×10^{-2}	125,000	1,000,000	1
Chlorobenzene	Polystyrene	0.98×10^{-2}	300,000	310,000	2
Chloroform	Polymethyl metacrylate	0.25×10^{-2}	240,000	232,000	3

The results obtained for GR-S in toluene as recorded in Table I have been explained by Debye and Cashin[2] by assuming the probable presence of microgel.

The work on GR-S was done with a sample prepared for us by the Polymer Corporation at Sarnia, Ontario, Canada. Since according to Baker[4] a conversion higher than 60 percent will produce microgel, this sample was carried to less than 20 percent conversion and we believe that the presence of microgel is improbable in our solutions.[5] Moreover the effect resulting from microgel should be independent of the solvent, as shown by our results with ethylene chloride.

It has been shown[6] that the composition of GR-S copolymer changes during conversion. The refractive index of the bulk polymer formed will be an average value with part of the polymer higher and part lower in index than the average.

In the case of a composition homogeneous co-polymer, a solution prepared with a solvent of refractive index identical to that of the polymer will not give an increase of scattering over that of the solvent. This is predicted by the equation since the value of $(\mu-\mu_0/c)^2$ is obviously zero.

But in the case of GR-S the use of a solvent of refractive index identical to the average refractive index of the polymer will increase the scattering over that of the solvent, even if the refractive index increment is zero.

The reason is that the refractive index increment is a summation of $(\mu-\mu_0)$ terms for values of μ higher and lower than μ_0 and thence can be zero, whereas the scattering is a summation of $(\mu-\mu_0)^2$ terms over the same range for μ and this cannot be zero.

It is then proposed to determine the composition heterogeneity of a sample of GR-S by determining the M.W. by light scattering with a series of solvents of refractive index such that the refractive increment would tend toward zero. If the GR-S is homogeneous in composition, no change in M.W. will appear, but in the other case large differences should occur as shown in Table I for toluene solutions.

[1] R. Rivest and M. Rinfret, J. Chem. Phys. **18**, 1513 (1950).
[2] P. Debye and W. M. Cashin, J. Chem. Phys. **19**, 510 (1951).
[3] R. Tremblay, M.S. thesis, Université de Montréal (1951).
[4] W. O. Baker, Ind. Eng. Chem. **41**, 511 (1949).
[5] A. I. Medalia and I. M. Kolthoff, J. Polymer Sci. **6**, 433 (1951).
[6] E. J. Meehan, J. Polymer Sci. **1**, 318 (1946).

Carrier-Free Radioisotopes from Cyclotron Targets. XXVI. Preparation and Isolation of W^{181} from Tantalum*

JEANNE D. GILE, WARREN M. GARRISON, AND JOSEPH G. HAMILTON
Crocker Laboratory, Radiation Laboratory, Divisions of Experimental Medicine, Radiology and Medical Physics; University of California, Berkeley and San Francisco, California

(Received December 3, 1951)

DEUTERON bombardment of tantalum produces the 140-day W^{181} by the nuclear reaction[1] $Ta^{181}(d, 2n)W^{181}$. This paper reports a radiochemical isolation of carrier-free W^{181} from a tantalum target bombarded with 19-Mev deuterons in the 60-inch cyclotron at Crocker Laboratory. Other possible concurrent reactions include formation of radioisotopes of tantalum by the (d, p) reaction and hafnium by the (n, p) reaction.

The target, a circular plate of tantalum metal[2] approximately 10 mils thick, mounted in a bell-jar type of target assembly, was

bombarded with 19-Mev deuterons for a total of 500 microampere-hours at an average beam intensity of 20 microamperes. The back of the tantalum foil was cooled with a stream of cold water. After bombardment, the tantalum foil was trimmed and the inactive metal discarded. The tantalum was dissolved in a minimum volume of 16 N HNO_3 containing 10 percent HF by volume in a platinum evaporating dish. The HF was removed by boiling with 36 N H_2SO_4 and the cooled acid solution poured slowly into an excess of 20 percent NaOH with constant stirring. The precipitate was digested for 30 minutes and the tantalum hydroxide separated by centrifugation with repeated reductions in volume of the basic solution. The carrier-free tungsten was retained in the supernatant. This process was repeated three times to insure complete removal of the radio-tungsten from the tantalum target. The combined supernatants were evaporated to a small volume, the Na_2SO_4 formed by evaporation was centrifuged out, and the radio-tungsten was recovered in the supernatant. The basic solution was acidified with HCl, 5 mg of Fe^{+3} were added, and the solution carefully brought to pH[4] with NaOH. At this pH the $Fe(OH)_3$ carries the radio-tungsten quantitatively. Three such precipitations were done to insure the complete removal of any tantalum present. The $Fe(OH)_3$ was dissolved in 6 N HCl and the iron extracted with ethyl ether. The aqueous phase containing HCl and W^{181} was evaporated to dryness on 20 mg NaCl. The activity dissolved quantitatively in distilled water.

The decay curve was followed for 130 days and showed the 140-day half-life of W^{181}. Mass absorption measurements in aluminum and lead showed the 0.07-Mev conversion electron and the 0.13 Mev and 1.8 gamma-rays previously reported for W^{181}.[3] A trace amount of carrier-free tungsten was added to a solution containing milligram amounts of tungsten, tantalum, and hafnium—the tungsten fraction was separated chemically and contained 98 percent of the activity.

We wish to thank Professor G. T. Seaborg for helpful suggestions, Mr. B. Rossi and the crew of the 60-inch cyclotron at Crocker Laboratory for bombardments, and Miss Margaret Gee for technical assistance in counting.

* This document is based on work performed under Contract No. W-7405-eng-48-A for the AEC.

[1] G. T. Seaborg and I. Perlman, Revs. Modern Phys. **20**, 585 (1948).
[2] Spectrographic analysis of tantalum foil showed it to be tungsten-free.
[3] G. Wilkinson, Nature **160**, 864 (1947).

Relations between Activation Energy, Rate of Reaction, Bond Dissociation Energy, and Heats of Formation, Atomization, and Reaction for the Substituted Methanes

H. J. Bernstein
Division of Chemistry, National Research Council, Ottawa, Canada
(Received December 4, 1951)

BY considering the contributions from interactions between nonbonded atoms to be additive, the heats of atomization of the molecules in homologous series can be related to one another.[1] For the substituted methanes $CX_{4-n}Y_n$, the heat of atomization Q is a parabolic function of the number of substituents n.[1] This relation becomes linear if the contribution to the heat of atomization from the interaction of two nonbonded X atoms and two nonbonded Y atoms is very nearly equal to twice the contribution from interaction of an X atom with a Y atom.[1]

The heat of the reaction $CX_{4-n}Y_n \rightarrow CX_{3-n}Y_n + X$ is the bond dissociation energy D of the C—X bond. If the bonded and nonbonded contributions to the energy of the radicals are considered to be strictly additive an approximately linear relation between $DCX_{3-n}Y_n - X$ and number of substituents n is obtained. Elimination of n gives an approximately linear relation between $Q_{CX_{4-n}Y_n}$ and $D_{CX_{3-n}Y_n - X}$ for substituted methanes.

For the reaction $M + CX_{4-n}Y_n \rightarrow MX + CX_{3-n}Y_n$ to take place M approaches the substituted methane at an X atom and in a direction collinear with or almost collinear with a C—X axis.[2] We may assume therefore that the activated complex has the structure

$$M \cdots X \cdots CX_{3-n}Y_n,$$

for all the 3-atom reactions of M with this homologous series. Assuming that all bonded and nonbonded contributions to the heat of atomization of these activated complexes are additive, it is readily shown in the manner previously described[1] that the heat of atomization of the complex is also very nearly linear in n. Since the activation energy is

$$Q_{\text{activated complex}} - Q_M - Q_{CX_{4-n}Y_n},$$

it is apparent that the activation energy E_n is also an approximately linear function of n. Hence, the following approximate relations exist between the activation energy (E), the bond dissociation energy (D), the heat of formation (ΔH_f), the heat of atomization (Q), and the heat of reaction[3] (ΔH), for the substituted methanes:

$$\Delta E = c_1 \Delta D = c_2 \Delta(\Delta H_f) = c_3 \Delta Q = c_4 \Delta H. \quad (1)$$

The relations between ΔE and ΔD, and ΔE and ΔH, have been discussed in the literature[4] in the special case where M is a sodium atom. The treatment given here is quite general and M may be polyatomic.

The activation energy and rate of reaction v_n for the nth substituted methane in the 3-atom reactions given above are related by

$$v_n = A_n e^{-E_n/RT} \approx A_n e^{-E_0/RT} \cdot e^{-nE_1/RT}, \quad (2)$$

since $E_n \approx E_0 + nE_1$ with E_0 and E_1 constants. If A_n is nearly constant[5] or if $\ln A_n$ is a linear function of n, it is apparent that

$$\ln v_n = c_0 + c_1 n, \quad (3)$$

where $c_0 = [\ln A_n - (E_0/RT)] \approx \ln v_0$[5] and $c_1 = E_1/RT$. Since[6] $A_n \propto e^{\Delta s/R}$, there must be a linear relation between the energy of activation and the entropy of activation in order that Eq. (3) be valid. Equation (3) has been discussed in the literature[7] for equilibria involving changes of substituents but not in homologous series. It interprets quantitatively the extensive data on sodium "flame" reactions with the halogenated methanes.[8]

A Brønsted-like[9] or Hammett-like[7] relation may be obtained between the equilibrium constants K_1 and K_2 for two types of 3-atom reactions of the substituted methanes since

$$K_1 = v_{1\,(\text{forward})}/v_{1\,(\text{backward})} = v_1/v_{-1}, \quad K_2 = v_2/v_{-2},$$

and $\log K_1 = \log v_1 - \log v_{-1}$ and $\log K_2 = \log v_2 - \log v_{-2}$. When Eq. (3) is valid, $\log K$ is very nearly a linear function of n. Eliminating n gives the relation

$$\log K_1^{(n)} \approx a \log K_2^{(n)} + b, \quad (4)$$

where a and b are constants and $K_1^{(n)}$ and $K_2^{(n)}$ are the equilibrium constants for reactions 1 and 2 involving the nth substituted methanes.

One might expect the relations given in (1) to be approximately valid also for the RX series in which R = methyl, ethyl, isopropyl, and tertiary butyl if the CH_3 group may be treated as a single particle; although here the importance of steric effects can be anticipated.

The detailed derivations of the relations given here will be presented in forthcoming publications.

[1] H. J. Bernstein, J. Chem. Phys. **19**, 140 (1951). In Eq. (3) there has been a printer's error. It should read $P_n = P_0 + (n/4)(P_4 - P_0 + 8\Delta) - n^2 \cdot \Delta/2$.
[2] Glasstone, Laidler, and Eyring, *The Theory of Rate Processes* (McGraw-Hill Book Company, Inc., New York, 1941), p. 88.
[3] Since the heat of reaction is $Q_{MX} + Q_{CX_{3-n}Y_n} - Q_M - Q_{CX_{4-n}Y_n}$ and since both $Q_{CX_{3-n}Y_n}$ and $Q_{CX_{4-n}Y_n}$ are linear functions of n, the heat of reaction is also linear in n.
[4] M. G. Evans and M. Polanyi, Trans. Faraday Soc. **34**, 11 (1938).
[5] "A is not far from being constant for a given type of reaction" (A. F. Trotman-Dickenson and E. W. R. Steacie, J. Chem. Phys. **19**, 329 (1951)).
[6] Reference 2, p. 8.
[7] L. P. Hammett, *Physical Organic Chemistry* (McGraw-Hill Book Company, Inc., New York, 1940), p. 184.
[8] See review article by E. Warhurst, Quart. Rev. V 44, (1951).
[9] R. P. Bell, *Acid-Base Catalysis* (Clarendon Press, Oxford, England, 1941), p. 82.

The Atomic Weight of Silicon

JAMES F. NORTON AND PAUL D. ZEMANY
General Engineering Laboratory and Research Laboratory of the General Electric Company, Schenectady, New York
(Received December 4, 1951)

THE atomic weight of silicon currently[1] accepted is 28.06. This value is based largely on determinations of AgCl from $SiCl_4$ and was adopted[2] after the improved results of Baxter, Weatherill, and Scripture were announced.[3]

An independent determination[4] by the same method gave the value 28.105. The constancy of the value for silicon of different origins was demonstrated[5] also by the same method. There have been, however, some more recent different estimates of the atomic weight of silicon by physical methods. Other chemical evidence[6] suggests the value accepted is too low.

Since the value is of importance to this Laboratory, we have made a mass spectroscopic estimate of the atomic weight of silicon, using the same type instrument to determine both the mass packing fraction and isotope abundance distribution. The instrument used was the General Electric analytical mass spectrometer, essentially a 60° deflection type.[7]

The mass packing fraction was estimated by measuring the linear separation[8] of the chart recording of the doublets $Si^{+28}-CO^+$, $Si^{+28}-N_2^+$, and $Si^{+28}-C_2H_4^+$, which together comprise a quadruplet when a mixture of SiH_4, N_2, CO, and C_2H_4 are admitted simultaneously to the mass spectrometer. The mass scale was determined by continuing the sweep to other adjacent peaks, and interpolating. At the sweep speed used the separation at mass 28 was 32.0 cm/unit mass. The separations of the doublets observed for three separate determinations are given in Table I

TABLE I.

Doublet	Separation cm I	II	III	Atomic weight of Si^{28} [a] I	II	(Physical scale) III
$Si^{28}-CO$	0.66	0.67	0.70	27.9832	27.9829	27.9820
$Si^{28}N_2$	0.95	0.92	0.95	27.9854	27.9863	27.9854
$Si^{28}C_2H_4$	1.90	1.92	1.91	27.9884	27.9897	27.9881
					average	27.9855±0.0030

[a] The molecular weights of CO, N_2, and C_2H_4 are taken as 28.0038, 28.0151, 28.0477 calculated from the values in J. Mattauch, *Nuclear Physics Tables* (Interscience Publishers, Inc., New York, 1946). These are, for our purpose, equivalent to more recent determinations by A. O. Nier and T. R. Roberts, Phys. Rev. **81**, 507, 624 (1951).

together with the calculated values for the atomic weight of silicon.

The final result is taken as 27.986±0.003. This is in agreement with the more precise values of 27.98581 determined by the mass spectrograph[9] and 27.98639 from transmutation data.[10] Fortunately, the excess kinetic energy[11] of the ions measured was small.

The silicon isotope ratios in the SiF_3 ion from SiF_4 were measured and gave the relative amounts listed in Table II, where they are compared with other determinations of this ratio.

We are indebted to Dr. N. C. Cook for the preparation of the SiF_4.

To calculate the atomic weight of silicon the exact masses of the other two isotopes are required, although no sensible error would be made if unit atomic mass were added for the Si^{29} isotope and two for the Si^{30} isotope. To fill this gap in data, the measurements of reference 9 are used. The physical atomic weight ($O^{16}=16.0000$) is then 28.096 and the chemical 28.088±0.004. The conversion factor of 1.000272 was used.[12]

TABLE II.

	This investigation	a	b	c
Si^{28}	92.14	92.28	92.16	92.26
Si^{29}	4.73±0.10	4.67	4.71	4.68
Si^{30}	3.13±0.10	3.05	3.13	3.05

[a] M. G. Inghram, Phys. Rev. **70**, 653 (1946).
[b] J. R. White and A. E. Cameron, Phys. Rev. **74**, 991 (1948).
[c] D. Williams and P. Yuster, Phys. Rev. **69**, 556 (1946).

[1] E. Wichers, Report of Committee on Atomic Weights, J. Am. Chem. Soc. **72**, 1431 (1950).
[2] Bodenstein, Hahn, Hönigschmid, and Meyer, Ber. deut. chem. Ges, **57B**, 1 (1924).
[3] Baxter, Weatherill, and Scripture, Jr., Proc. Am. Acad. Arts and Sci. **58**, 245 (1923).
[4] Hönigschmid and Steinheil, Z. anorg. u. allgem. Chem. **141**, 101 (1924).
[5] P. L. Robinson and H. C. Smith, J. Chem. Soc. 1262 (1926).
[6] Balis, Gilliam, Hadsell, Liebhafsky, and Winslow, J. Am. Chem. Soc. **70**, 1654 (1948).
[7] A. O. Nier, Rev. Sci. Instr. **11**, 212 (1940).
[8] P. D. Zemany, Anal. Chem. **22**, 920 (1950).
[9] H. E. Duckworth and R. S. Preston, Phys. Rev. **79**, 402 (1950); Duckworth, Preston, and Woodcock, Phys. Rev. **19**, 188 (1950).
[10] Ernest Pollard and D. E. Alburger, Phys. Rev. **72**, 1196 (1947).
[11] H. Hagstrum, Phys. Rev. **59**, 354 (1941).
[12] R. T. Birge, Revs. Modern Phys. **13**, 233 (1941).

Brønsted and Lewis Acidity

W. F. LUDER
Northeastern University, Boston, Massachusetts
(Received November 30, 1951)

IN reply to the letter of Ricardo de Carvalho Ferreira,[1] criticizing my position on the electronic theory of acids and bases, I should like to point out that his own position can be maintained only by ignoring an essential part of the Lewis theory.

As has been stressed previously,[2-4] if one follows Lewis, it is unnecessary to make any distinction between "Lewis acidity" and "Brønsted acidity." On the contrary, when applied to hydrogen acids, the two theories are absolutely identical.

Lewis, equally with Brønsted, recognized the importance of the displacement of one base by another. Hydrogen chloride is a secondary acid in which, one may consider, a primary acid (the proton) is combined with a base (the chloride ion). The following equations may emphasize the identity of the two theories for hydrogen acids:

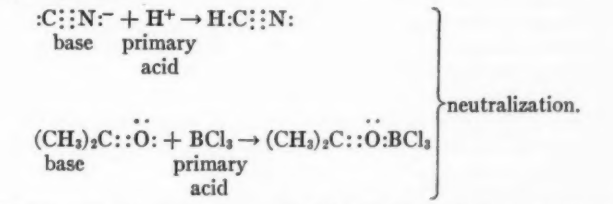

The two products may react with bases by displacement; when so doing, they are called secondary acids.

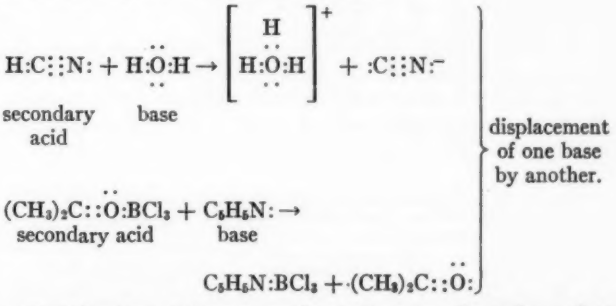

Consideration of these examples and many others shows that "Lewis acidity" is not "solely determined by the partial positive charge of the hydrogen atom," nor is it necessary to "study the two kinds of acidity separately."

In the displacement reactions of hydrogen acids the two theories are identical.

[1] R. Ferreira, J. Chem. Phys. **19**, 794 (1951).
[2] Luder and Zuffanti, *The Electronic Theory of Acids and Bases* (John Wiley and Sons, Inc., New York, 1946).
[3] Luder and Zuffanti, *Teoria Electronica de Acidos y Bases* (Libreria y Editorial Alsina, Buenos Aires, 1950).
[4] Luder, J. Chem. Educ. **25**, 555 (1948).

Potential Constants for Diacetylene*

SALVADOR M. FERIGLE,† FORREST F. CLEVELAND, AND ARNOLD G. MEISTER
Spectroscopy Laboratory, Department of Physics, Illinois Institute of Technology, Chicago 16, Illinois
(Received November 28, 1951)

THE potential (force) constant corresponding to the central carbon-carbon bond stretching of diacetylene (DA) has been given as 3.58[1] and 3.23 md/A.[2] On the other hand, the central carbon-carbon bond distance obtained from electron diffraction measurements[3] is 1.36±0.03A, the low value of the bond distance being interpreted as partly the result of a shortening of the single bond radii, but mainly to some double bond character arising from resonance. The effect of the resonance should be, generally speaking, an increase in the potential constant as compared with that of a single bond, which normally is about 5 md/A. Longuet-Higgins and Wheland[4] tried to justify the low value of the potential constant by using the formulas developed by Coulson and Longuet-Higgins[5] for conjugated hydrocarbons, assuming that the self-polarizability of the bond is very high. Hornig[6] also tried to justify the low potential constant in a rather crude qualitative way.

The low value of the potential constant was obtained as a consequence of the assignment of the 644 cm^{-1} band of DA as an A_{1g} fundamental. It seems that this assignment was based upon the fact that 644 cm^{-1} was the highest observed Raman displacement, with the exception of the 2183 cm^{-1} line which obviously corresponds to the triple bond stretching fundamental. Recently, A. V. Jones[7] has obtained new Raman and infrared spectral data for DA. He assigned the central carbon-carbon stretching fundamental to a polarized Raman line at 874 cm^{-1}, which had not been observed in previous investigations, and ascribed the line at 642 cm^{-1} to a hydrogen bending vibration. Quite independently, the same assignment for the 642 band had previously been made[8] in this laboratory by comparison of the vibrational data of a number of molecules containing the $-C\equiv C-H$ group, for which frequencies close to 644 cm^{-1} have been assigned to bending modes; and also by the measurement of the depolarization factors of the dimethyldiacetylene (DMDA) Raman lines and a correlation study of DA and DMDA.

The fundamental frequencies of DA obtained by Jones[7] are given in Table I. Using these, potential constants have been calculated by the Wilson FG matrix method.[9] The g matrix elements were obtained from the tables of Decius;[10] the justification for using these tables for linear molecules has been given previously.[11] The potential constants thus obtained are given in Table II. With these constants, the calculated wave numbers were within 1 cm^{-1} of the observed values.

The potential constant for the central bond (f_m) is very close to the value recently reported for cyanogen (6.75 md/A).[12] If the formulas of Coulson and Longuet-Higgins[5] are applied, the present results show that the self-polarizability of the bond must be small; Duchesne and Burnelle[12] state that this is practically certain for cyanogen.

TABLE I. Wave numbers corresponding to the fundamental vibrational frequencies of diacetylene ($H-C\equiv C-C\equiv C-H$).[a]

Type	Designation	Wave number (cm^{-1})
A_{1g}	ν_1	(3333)[b]
A_{1g}	ν_2	2184
A_{1g}	ν_3	874
A_{1u}	ν_4	3333
A_{1u}	ν_5	2020
E_{1g}	ν_6	627
E_{1g}	ν_7	482
E_{1u}	ν_8	630
E_{1u}	ν_9	(220)[b]

[a] A. V. Jones, reference 7.
[b] Not observed.

TABLE II. Potential constants for diacetylene.[a]

Constant	Description	Value	
f_a	C−H stretching	5.90149[b]	
f_t	C≡C stretching	15.5039	
f_m	C−C stretching	6.63009	
$f_a{}^t$	C−H, C≡C stretching interaction	−0.132044	
$f_m{}^t$	C−C, C≡C stretching interaction	0.767722	
$f_t{}^t$	C≡C, C≡C stretching interaction	0.0226	
f_{at}	C≡C−H bending	0.20667	0.22080[c]
f_{mt}	C≡C−C bending	0.317476	0.34745
$f_{at}{}^{mt}$	C≡C−H, C≡C−C bending interaction	0.0707	0.1269
$f_{mt}{}^{mt}$	C≡C−C, C≡C−C bending interaction	0.0030711	0.0028745

[a] Bond constants are in md/A, and angle constants are in md A/rad². The number of figures in the potential constants was retained to insure the best reproduction of the frequencies and to secure internal consistency in the calculations; the values are, of course, not reliably known to this many figures. In the constant symbols, m suggests middle bond; t, triple bond; and a, acetylenic hydrogen bond.
[b] Transferred from acetylene.
[c] The 2 values for the bending vibrations result from the solution of a quadratic equation.

The potential constants obtained here are being used to calculate the fundamental frequencies of DMDA. A more complete discussion of the results given in this paper will be presented in the future.

* Supported in part by a research grant from the Research Corporation, and in part by contract DA-11-022-ORD-464 with the Office of Ordnance Research.
† Based upon a part of a Ph.D. thesis.
[1] T. Y. Wu and S. T. Shen, Chin. J. Phys. **2**, 128 (1936).
[2] A. G. Meister and F. F. Cleveland, J. Chem. Phys. **15**, 349 (1947).
[3] Pauling, Springall, and Palmer, J. Am. Chem. Soc. **61**, 927 (1939).
[4] H. C. Longuet-Higgins and G. W. Wheland, Ann. Rev. Phys. Chem. 133 (1948).
[5] C. A. Coulson and H. C. Longuet-Higgins, Proc. Roy. Soc. (London) **A193**, 456 (1948).
[6] D. F. Hornig, ONR Technical Report No. 15 (1950).
[7] A. V. Jones, Paper at the Symposium on Molecular Structure and Spectroscopy, Ohio State University, June, 1951; and private communication.
[8] Ferigle, Cleveland, and Meister, Phys. Rev. **81**, 302 (1951). Also, Paper at the Symposium on Molecular Structure and Spectroscopy, Ohio State University, June, 1951.
[9] E. B. Wilson, Jr., J. Chem. Phys. **7**, 1047 (1939); **9**, 76 (1941).
[10] J. C. Decius, J. Chem. Phys. **16**, 1025 (1948).
[11] S. M. Ferigle and A. G. Meister, J. Chem. Phys. **19**, 982 (1951).
[12] J. Duchesne and L. Burnelle, J. Chem. Phys. **19**, 1191 (1951).

On the Principle of Thermal Interaction

HANS HOLTAN, JR.
Norges Tekniske Hoegskole, Trondheim, Norway
(Received December 17, 1951)

IN a recent Letter to the Editor of this journal,[1] P. Mazur criticizes a paper[2] in which I introduced a new hypothesis, "the principle of thermal interaction." The aim of this hypothesis was to describe the interaction between the flow of entropy connected to the flow of heat and that connected to the transport of matter, leading to relations between thermodynamic variables in the stationary states. This is not the same as an evaluation of the mutual phenomenological coefficients, which of course have to be based on a kinetic treatment. It is quite obvious that it is impossible to express the rate by which these stationary states are reached by thermodynamic methods just as the equilibrium states in isothermal systems are described by classical thermodynamics, whereas the reaction rates have to be treated by the kinetic theory.

The gaseous thermocell treated in my paper is a typical limiting case restricted by (1) the tube is able to maintain the pressure difference ideally (no mass concentration) and (2) the gas is ideal. It follows from (1) that the tube has to be very narrow. It should be obvious that the derivation given is not valid for wider tubes. The calculated pressure difference is the maximum one.

[1] P. Mazur, J. Chem. Phys. **19**, 1431 (1951).
[2] H. Holtan, Jr., J. Chem. Phys. **19**, 520 (1951).

Binding Energies of Gaseous Alkali Hydrides

WILLIAM A. KLEMPERER AND JOHN L. MARGRAVE*
Department of Chemistry and Chemical Engineering, University of California, Berkeley, California
(Received December 17, 1951)

RITTNER[1] has recently proposed a simple procedure for calculating the binding energy of gaseous alkali halide molecules in which the molecule is treated as consisting of ions, each of which is polarized by the electrostatic field of the other. On this basis the following equations give the binding energy $-W$ and the dipole moment μ, respectively, at 0°K:

$$W=\varphi+A\,\exp(-r/\rho)-(C/r^6),$$

$$\mu=er-\left(\frac{r^4e(\alpha_1+\alpha_2)+4re\alpha_1\alpha_2}{r^6-4\alpha_1\alpha_2}\right),$$

where

$$\varphi=-\frac{e^2}{r}-\frac{e^2(\alpha_1+\alpha_2)}{2r^4}-\frac{2e^2\alpha_1\alpha_2}{r^7},$$

α_1 and α_2=polarizabilities of the ions, e=electronic charge, r=equilibrium internuclear distance at the potential minimum, ρ and A=repulsion constants, and C=van der Waals' attractive constant. The value for ρ is obtained by applying the usual requirements for mechanical stability, i.e.,

$$(dW/dr)_{r=r_{eq}}=0$$

and

$$(d^2W/dr^2)_{r=r_{eq}}=P\ \text{(force constant)}.$$

The application of these equations to the entire group of alkali metal halides gave generally good agreement between calculated binding energies and the so-called experimental binding energies given by

$$-W=D+I-E,$$

where D is the dissociation energy of the ionic molecule into neutral atoms, I is the first ionization potential of the alkali atom, and E is the electron affinity of the halogen atom.

There are, however, two objections to the conclusion that the agreement obtained by Rittner indicates complete validity of his proposal: (1) The values for the dissociation energies of the alkali metal halides have not been independently determined from spectroscopic data but are most commonly obtained through the application of thermochemical cycles involving the heats of sublimation of the salts, the dissociation energies of the halogen molecules, the electron affinities of the halogen atoms, and other thermochemical data; and (2) Brewer and Mastick[2] have obtained agreement equally as good as Rittner in calculations considering the alkali metal chlorides, bromides, and iodides as gaseous ionic molecules by making no allowance for either repulsion or polarization effects but merely by using e^2/r, the electrostatic attraction, as the energy of separation of the ions. They conclude that "in the gaseous state distortion of the positive and negative ions may occur to a great extent thereby increasing the bonding energy which, supplemented by increased dispersion forces, apparently cancels the repulsive force."

TABLE I.

Compound	r $\times10^8$ cm	α_M $\times10^{24}$ cm³	α_H $\times10^{24}$ cm³	ω_e cm^{-1}	I_M kcal/mole	E_H kcal/mole	D_e kcal/mole
LiH	1.595	0.029	1.80	1405.65	124.26	17.21	60
NaH	1.887	0.178	1.80	1172.2	118.45	17.21	49
KH	2.244	0.84	1.80	985.0	100.05	17.21	44
RbH	2.367	1.42	1.80	936.77	96.27	17.21	40
CsH	2.494	2.44	1.80	890.7	89.75	17.21	42

TABLE II.

Compound	$-W_{calc}$ kcal/mole	$-W_{exp}$ kcal/mole	μ_{calc} D
LiH	165.4	167	4.05
NaH	141.6	150	6.05
KH	121.4	127	7.60
RbH	117.0	119	7.73
CsH	112.7	114	7.47

It thus seems important to present the results of some calculations concerning the alkali metal hydrides following Rittner's proposed model since (1) the spectra of these molecules have been well analyzed and their dissociation energies are known within a few kcal/mole,[3,4] and the electron affinity of H has been calculated very exactly;[5] and (2) the application of the method of Brewer and Mastick does not lead to the proper results for the binding energies of these hydrides. In Table I are listed the data used[6] and in Table II are the results of these computations.

The agreement between the calculated and experimental values of the binding energies is very satisfactory and within the uncertainties of the values for the dissociation energies. The lack of experimental values for the heats of sublimation of these compounds prevents correlation with thermochemical data on the solid compounds and the calculated crystal energies of the solids. It seems definite, however, that the relative effects of polarization and repulsion as computed are very near to those actually existing in gaseous alkali hydrides. The dipole moments have also been calculated but no experimental data are available for comparison.[7]

In view of the excellent agreement obtained both in this work and that of Rittner, it was thought worthwhile to make similar computations for the gaseous alkaline earth oxide molecules. Very poor agreement between the calculated and experimental values was found, the discrepancies amounting to 80–100 kcal/mole. Similarly, an attempt to apply this method for calculation of the binding energies of HF and HCl failed to yield the correct binding energies and gave negative values for the dipole moments.

* AEC Post-doctoral Fellow, 1951.
[1] E. Rittner, J. Chem. Phys. **19**, 1030 (1951).
[2] L. Brewer and D. Mastick, J. Am. Chem. Soc. **73**, 2045 (1951).
[3] A. Gaydon, *Dissociation Energies* (John Wiley & Sons, Inc., New York, 1947).
[4] G. Herzberg, *Spectra of Diatomic Molecules* (D. Van Nostrand Company, Inc., New York, 1950).
[5] L. Henrich, Astrophys. J. **99**, 59 (1944).
[6] Values for r and ω_e are from reference 4; α_M values are from L. Pauling, Proc. Roy. Soc. (London) **A114**, 181 (1927); α_H was computed from the data of H. Bode, Z. Phys. Chem. **6B**, 251 (1930); I_M values are from L. Brewer, *The Chemistry and Metallurgy of Miscellaneous Materials*, NNES IV-19B (McGraw-Hill Book Company, Inc., New York, 1950), p. 165; E_H is from reference 5; and D_e's were computed from data in references 3 and 4.
[7] A quantum-mechanical calculation of μ_{LiH} indicates a dipole moment of 3.5 D. See M. Adamov, Zhur. Fiz. Khim. **23**, 1172 (1949).

Erratum: Infrared Spectra of *n*-Acetylglycine and Diketopiperazine in Polarized Radiation at 25° and at −185°C

[J. Chem. Phys. **19**, 1147 (1951)]

ROGER NEWMAN AND RICHARD M. BADGER
Gates and Crellin Laboratories, California Institute of Technology, Pasadena, California

THE [10$\bar{1}$] direction in diketopiperazine crystals was erroneously referred to as [101].

Erratum: Thermodynamic Data and Some Notes on the Nature of Adsorbed Helium

[J. Chem. Phys. **19**, 1370 (1951)]

S. V. R. MASTRANGELO AND J. G. ASTON
School of Chemistry and Physics, The Pennsylvania State College, State College, Pennsylvania

THE byline of this article appeared as "The Barrett Division, Allied Chemical and Dye Corporation, Philadelphia, Pennsylvania, and it should have been "School of Chemistry and Physics, The Pennsylvania State College, State College, Pennsylvania."

The Microwave Spectra of POF_3 and PSF_3*

NORVAL J. HAWKINS† AND V. W. COHEN
Brookhaven National Laboratory, Upton, Long Island, New York
AND
W. S. KOSKI
Department of Chemistry, The Johns Hopkins University, Baltimore, Maryland
(Received December 10, 1951)

WE have examined the microwave spectra of $PS^{32}F_3$, $PS^{34}F_3$, $PO^{16}F_3$, and $PO^{18}F_3$ using a 100-kc Stark modulated spectrometer.[1] The PSF_3 and $PO^{16}F_3$ were prepared by reacting PbF_2 with P_2S_5 and P_2O_5, respectively.[2] The $PO^{18}F_3$ was prepared by reacting PF_3 with oxygen.[3] The oxygen in turn was prepared by electrolysis of enriched H_2O (1.5 percent O^{18}) obtained from Oak Ridge. The data are summarized in Table I. Using this data and the FPF angle of 100° in PSF_3 and 106° in POF_3 as obtained from electron diffraction[4,5] we obtain the following bond distances: PS distance of 1.86A and a PF distance of 1.53A in PSF_3; a PO distance of 1.48A and a PF distance of 1.52 in POF_3. It will be noted that the value of the rotational constant for POF_3 4594.26 ±0.01 as measured differs from the value of 4593.50±0.02 as reported by Senatore[6] for $J0 \rightarrow 1$ transition.

TABLE I. Frequencies of PSF_3 and POF_3 lines.

	Line		Frequency
$PS^{32}F_3$	$J3 \rightarrow 4$	$v\,0$	21,260.95 ±0.05 mc/sec
	$J4 \rightarrow 5$	$v\,0$	26,576.36 ±0.03
	$J4 \rightarrow 5$	$v\,1$	26,553.58 ±0.08
	$J4 \rightarrow 5$	$v\,2$	26,595.5 ±0.1
	$J4 \rightarrow 5$	$v\,3$	26,531.5 ±1
$PS^{34}F_3$	$J4 \rightarrow 5$	$v\,0$	25,797.87 ±0.03
	$J4 \rightarrow 5$	$v\,1$	25,775.3 ±0.5
	$J4 \rightarrow 5$	$v\,2$	25,818.0 ±2
$PO^{16}F_3$	$J1 \rightarrow 2$	$v\,0$	18,377.03 ±0.05
	$J2 \rightarrow 3$	$v\,0$	27,565.42 ±0.05
	$J2 \rightarrow 3$	$v\,1$	27,539.39 ±0.05
$PO^{18}F_3$	$J2 \rightarrow 3$	$v\,0$	26,391.61 ±0.10

From the measured linear Stark components in PSF_3 and the quadratic Stark components in POF_3, we calculate the dipole moments to be 0.633±3 percent and 1.69±3 percent, respectively. These values have been determined relative to OCS.[7]

During the course of this investigation, the work of Gordy[8] on these molecules has come to our attention. Good agreement exists in the two investigations in those phases of the work that overlap. It should also be mentioned that a rough measurement of the $PS^{32}F_3$ ($J4 \rightarrow 5$) frequency has been made previously by Roberts.[9]

It will be noted that the PF and PS bond distances reported here are appreciably smaller than the corresponding double bond distances listed by Pauling.[10] This shortening of the bonds and the observed dipole moment can be accounted for if one assumes that *3d* orbitals are involved, that there is an appreciable amount of triple bond contribution to the PF and PS bonds and that the bonds involved in various resonance structures involve considerable amount of ionic character. Similar considerations are applicable to POF_3.

* Research carried out under contract with AEC.
† Present address: G. E. Research Laboratory, Schenectady, New York.
[1] Wentink, Koski, and Cohen, Phys. Rev. **81**, 948 (1951).
[2] Thorpe and Rodger, J. Chem. Soc. **53**, 766 (1888).
[3] Moisson, Compt. rend. **99**, 655 (1884).
[4] Stevenson and Russell, J. Am. Chem. Soc. **61**, 3264 (1939).
[5] Brockway and Beach, J. Am. Chem. Soc. **60**, 1836 (1938).
[6] Samuel J. Senatore, Phys. Rev. **78**, 293 (1950).
[7] Shulman, Dailey, and Townes, Phys. Rev. **78**, 145 (1950).
[8] Quarterly Progress Report of Microwave Research, Duke University, May 1 to August 1, 1950.
[9] Kisliuk and Townes, J. Research Natl. Bur. Standards **44**, 611 (1950).
[10] Linus Pauling, *Nature of Chemical Bond* (Cornell University Press, Ithaca. New York, 1945), second edition, p. 164.

Atmospheric Transmission at High Temperatures*

J. H. TAYLOR, W. S. BENEDICT, AND J. STRONG
The Johns Hopkins University, Silver Spring, Maryland
(Received January 7, 1952)

INFRARED absorption spectra at controlled elevated temperatures provide information on the higher energy levels of molecules and transitions among them. Both are of practical interest. The former are needed to determine thermodynamic properties, and the latter is involved in calculations of radiant heat transfer in the atmosphere and in hot gases.

A Pfund-type absorption cell with two platinized quartz mirrors has been made of porcelain lined steel. This provides a three-meter path which can be uniformly heated to any temperature up to 1000°C. The path length outside the cell is seven meters. The spectra we have taken were obtained with a Perkin-Elmer spectrometer with NaCl prism (4.5–15μ) and a grating spectrometer with four preliminary MgO reflections (14–25μ). A carbon arc source was used.

With our present path lengths and resolving power the spectrum of room temperature air shows a number of pure rotation lines of H_2O from 410 to 650 cm^{-1}, the 619, 667, and 721 cm^{-1} bands of CO_2, and the partially resolved 6μ band of H_2O. The spectrum at 500°C shows nearly 100 new temperature dependent H_2O lines in the pure rotation region from 410 to 950 cm^{-1}, a number of new peaks between 500–828 cm^{-1} which may be identified as (040–050) the Q branches of CO_2 bands from levels as high as (120–130), (200–210) and a considerable broadening of the 6μ water band. Most of the new H_2O lines have been identified as higher level transitions in the pure rotation band. A few rotational transitions within the ν_2 level have also been found. The intensity of the new lines is in agreement with calculations based on the tables of Cross, Hainer, and King,[1] and the energy levels with a few exceptions agree with those inferred from other spectra.[2]

Figure 1 shows the two sample tracings of the spectral region between 513–566 cm^{-1}, one with the cell at 25°C and the other

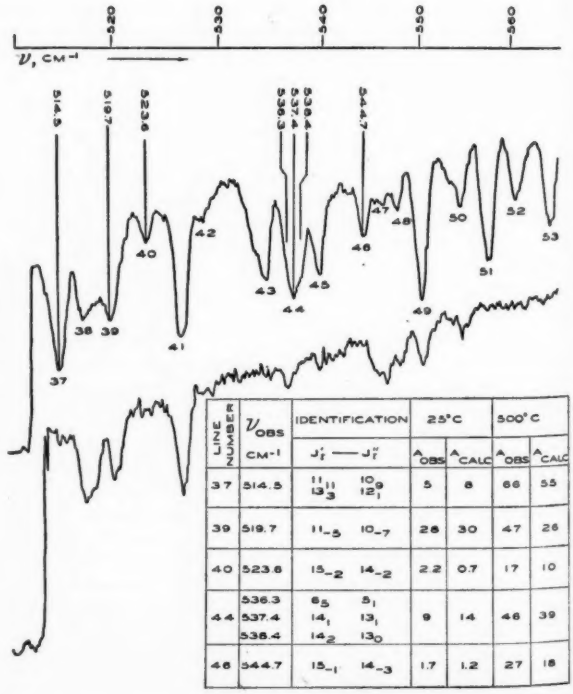

LINE NUMBER	ν_{OBS} CM⁻¹	IDENTIFICATION $J'_i - J''_i$	25°C A_{OBS}	25°C A_{CALC}	500°C A_{OBS}	500°C A_{CALC}
37	514.5	$11_{11}\ 10_9$ / $13_3\ 12_1$	5	8	66	55
39	519.7	$11_{-5}\ 10_{-7}$	28	30	47	26
40	523.6	$15_{-2}\ 14_{-2}$	2.2	0.7	17	10
44	536.3	$6_5\ 5_1$	9	14	46	39
	537.4	$14_1\ 13_1$				
	538.4	$14_2\ 13_0$				
46	544.7	$15_{-1}\ 14_{-3}$	1.7	1.2	27	18

FIG. 1. Lower trace: grating spectrum, 513–566 cm^{-1}, with air-filled cell at 25°C. Upper trace: grating spectrum with cell at 500°C. Tabular insert gives origin, wavelength, and intensity of selected H_2O lines.

with the cell slightly above 500°C. In the table A_{obs} is the absorption at the line center in percent: A_{calc} is proportional to the expression, $A=[(\pi S\alpha x)^{\frac{1}{2}}]/\Delta\nu$, where S is the theoretical line strength, α the line half-width, x the water vapor content in the path, and $\Delta\nu$ the spectrometer slit width.

The investigation is continuing to determine the spectra of various amounts of H_2O, CO_2, and other gases at several elevated temperatures.

* This work was supported by Contract Nonr-248(01).
[1] Cross, Hainer, and King, J. Chem. Phys. **12**, 210 (1944).
[2] Randall, Dennison, Ginsburg, and Weber, Phys. Rev. **52**, 160 (1937); Benedict, Claassen, and Shaw, J. Research, Natl. Bur. Standards (to be published).

Rate of Coagulation of *F*-Centers in KCl*

FLOYD E. THEISEN AND ALLEN B. SCOTT
Department of Chemistry, Oregon State College, Corvallis, Oregon
(Received January 14, 1952)

RECENT studies[1] have shown that *F*-centers in additively colored KCl come to equilibrium with colloid in about 90 minutes at 300°, and 45 seconds at 500°. Intense irradiation results in coagulation to a broad (R') band within 2 minutes, provided the crystal is allowed to warm during the treatment,[2] indicating that the rate of coagulation, as well as some of the products, is strongly influenced by illumination. Because the coagulation of *F*-centers is thought to be analogous to the photographic printout effect, it was desired to investigate the formation of colloid in more detail, in particular the activation energy for thermal coagulation and the effect of optical excitation upon the rate.

A prism monochromator and photomultiplier detection circuit were used to follow the decrease in absorption coefficient at 560 mμ in colored KCl crystals during thermal and optical treatment. The initial concentration of *F*-centers was found spectrophotometrically by the use of the dispersion formula[1] and subsequent concentrations by assuming the concentration proportional to absorption coefficient at 560 mμ. A crystal holder enabled the crystal under study to be plunged rapidly into a small furnace held, within 10°, at each of a series of temperatures, and while in the furnace to be moved in and out of position before an aperture in the path of the monochromatic light for absorption measurements. When desired, the crystal could also be illuminated with approximately 560 mμ light from a carbon arc, filtered by a Wratten No. 74 filter and $CuCl_2$ solution. The intensity upon the crystal was about 0.2 watt cm^{-2}.

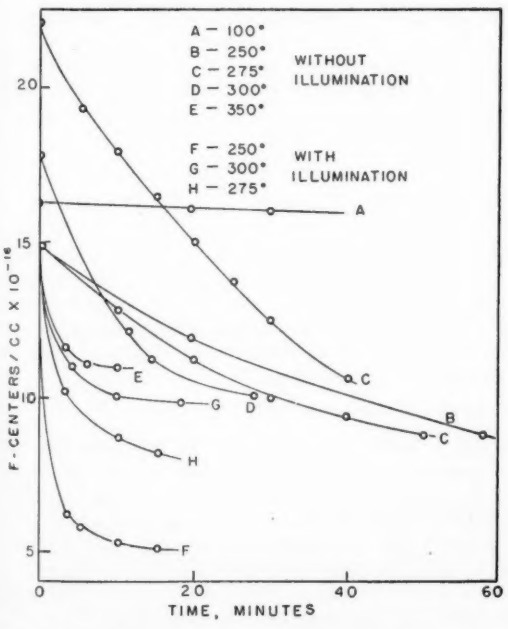

FIG. 1. Conversion of *F*-centers to colloid by heating in darkness and with 560 mμ illumination.

Figure 1 shows the decrease in concentration of *F*-centers with time at several temperatures for typical crystals heated in darkness and under 560 mμ illumination. The acceleration by illumination is very marked.

The rate for thermal conversion, without illumination, corresponded most nearly to that for a second-order reaction; rate constants were obtained from the initial slopes of curves of reciprocal concentration as a function of time. Initial slopes were used because of the reversibility of the reaction; some error is still present because of the lack of knowledge regarding the rate of the reverse process. At least 3 crystals of each concentration were studied at each temperature, to obtain mean rate constants. For the set of measurements on crystals initially having about 17×10^{16} centers/cc, the mean rate constants lay between 0.882×10^{-19} cc$\times F$-center^{-1} min^{-1} at 250° and 3.58×10^{-19} at 350°. The activation energy for the thermal process F-center$=$colloid is 8.7 ± 1.2 kg cal mole^{-1}. The mean rate constants for initial concentrations about 21×10^{16}/cc were somewhat higher, showing that the reaction is not strictly second order; the activation energy for this series was found to be 10.5 ± 1.5 kg cal mole^{-1}.

Second-order curves for illumination-accelerated reactions showed a pronounced change of slope at or before 3 seconds, suggesting that colloid formation was completed very rapidly, followed by slower photochemical formation of *R*-centers. This was substantiated by a negative temperature coefficient of rate constant for the second stage, caused undoubtedly by decreasing stability of *R*-centers with increasing temperature, and by formation of a broader band with illumination than without it.

Two explanations for the acceleration by 560 mμ light seem equally plausible; either the *F*-centers are ionized and the liberated electrons are trapped by colloidal centers already forming, resulting in Coulombic attraction for positive ions or negative ion vacancies and increasing their diffusional velocity toward the colloid, or *R*-centers formed photochemically catalyze the coagulation.

* Presented in part before the Conference on Electrical and Optical Properties of Ionic Crystals, Urbana, Illinois, Oct. 30, 1951. From the MS thesis of Floyd E. Theisen. This work was partially supported by the ONR.
[1] A. B. Scott and W. A. Smith, Phys. Rev. **83**, 982 (1951).
[2] A. B. Scott and L. P. Bupp, Phys. Rev. **79**, 341 (1950).

An Absorption Band of NOCl at 30μ*

W. H. EBERHARDT
School of Chemistry, Georgia Institute of Technology, Atlanta, Georgia
AND
T. G. BURKE
K-25 Laboratories, Carbide and Carbon Chemicals Company, Oak Ridge, Tennessee
(Received December 26, 1951)

BURNS and Bernstein[1] and Pulford and Walsh[2] have recently published studies of the infrared absorption spectrum of NOCl over the region from 1.6 to 25μ. In the vibrational analyses presented in these papers it was necessary to postulate the existence of a band at 332 and 329 cm^{-1} respectively ascribed to the vibration ν_3. The assumption of this band was based on the assignment in both cases of four observed bands to the binary combinations $2\nu_3$, $\nu_1+\nu_3$, $2\nu_1+\nu_3$, and $\nu_2+\nu_3$. In the course of a study of NO_2Cl to be published soon, we have had occasion to examine the spectrum of NOCl as an impurity over the entire region from 1 to 40μ using a Beckman IR-2 spectrophotometer with NaCl optics in the range from 1 through 15μ and a Perkin-Elmer Model 12-C spectrometer with KBr optics in the range 15 to 25μ and with KRS-5 optics in the range from 25 to 40μ. In general, our results are in agreement with those reported in

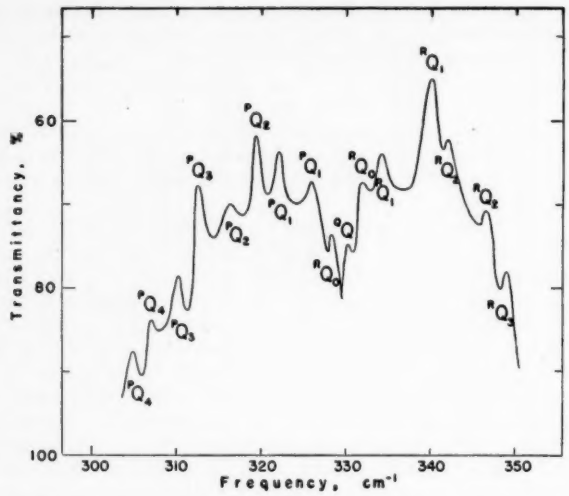

FIG. 1. Fine structure of ν_3 band of NOCl. Bands indicated by assignments above curve are ascribed to $NOCl^{35}$; bands with assignments below curve are ascribed to $NOCl^{37}$.

references 1 and 2 with the addition of a strong band with origin at 329 cm^{-1} for the species $NOCl^{35}$ and at 325 cm^{-1} for $NOCl^{37}$. The rotational fine structure found in this band and its assignment in two sets to the isotopic molecules $NOCl^{35}$ and $NOCl^{37}$ is presented in Fig. 1 and Table I.

The measurements reported for the KRS-5 region were made in a 10-cm cell equipped with KRS-5 windows and at a pressure of NOCl of approximately 25 mm Hg. A slit-width of 0.40 mm was used in the study to obtain maximum resolution. The instrument was calibrated with water bands using the frequencies reported by Randall, Dennison, Ginsburg, and Weber.[3] The accuracy of the measurements is limited principally by the small amplitude and appreciable noise level of the trace resulting from the narrow slits and the small emissivity of the source. These factors introduce considerable uncertainty in the exact location of the features and their magnitude but it is believed that all the features presented in the figure are real.

The rotational structure of the band approaches very closely that of a perpendicular band of a prolate symmetric top with but a very small central branch resulting from the hybrid character of ν_3. The small and indistinct maximum at 330 cm^{-1} is ascribed to this ^QQ branch. The displacement of the ^PQ and ^RQ bands for both $NOCl^{35}$ and $NOCl^{37}$ from their respective origins is approximated by the formula $\Delta\tilde{\nu}=3.3(2m+1)+0.15m^2$ with an uncertainty of about 0.2 cm^{-1} in the first coefficient and 0.05 cm^{-1} in the second. Assuming an average of the electron diffraction values of I_B and I_C for the larger moment of inertia,[1] the least moment of inertia in the ground vibrational state is estimated from this formula as $8.3\pm0.5\times10^{-40}$ g cm^2 and in the excited vibrational state as $8.0\pm0.5\times10^{-40}$ g cm^2. The value for the ground state is in satisfactory agreement with that calculated from the electron diffraction data, 9.05×10^{-40} g cm^2, and corresponds to an average bond angle of 119°. The lower value of I_A for the first vibrational state suggests an average bond angle of about 120° for this state. Both of the values of I_A are considerably lower than those suggested by microwave studies[4] but may be more reliable since the microwave spectrum does not give the rotational constant A directly and I_A must be determined as the difference between I_B and I_C.

TABLE I. Fine structure of the ν_3 band of NOCl.

Rotational transition	$NOCl^{35}$	$NOCl^{37}$
	$-cm^{-1}$	349 cm^{-1}
$^RQ_2$	346.5	342
$^RQ_1$	340	334
$^RQ_0$	332	328.2
^QQ	330	...
$^PQ_1$	325.6	322
$^PQ_2$	319.2	316.2
$^PQ_3$	312.5	310.2
$^PQ_4$	307	305
Band origin	329	325

TABLE II. Force constants and isotopic shift of ν_3 band of NOCl. $\nu_1=1799$, $\nu_2=592$, $\nu_3=329$ cm^{-1}, $\alpha=116°$, $r_{NO}=1.14$A, $r_{NCl}=1.95$A.

Force-field	f_{NO}[a]	f_{NCl}[a]	f_{ClO}[a]	d[a]	$\Delta\nu_{calc}$	$\Delta\tilde{\nu}_{obs}$
Central	1.397	0.192	0.130	...	0.9	4.0
Valence	1.406	0.187	...	0.0334	2.9	
	1.400	0.107	...	0.0588	4.1	

[a] Units are megadynes per centimeter.

A calculation of the isotopic shift by the method of Adel[5] using the central-force field equations of Radakovic and the force constants suggested by Burns and Bernstein leads to a rather low displacement, 0.9 cm^{-1}. A similar calculation using the valence-force field equations of Kohlrausch[6] and the frequencies $\nu_1=1799$, $\nu_2=592$, and $\nu_3=329$ cm^{-1} leads to two possible solutions for the force constants and isotopic shift. These calculations are summarized in Table II. The third set of constants is favored on the basis of the observed isotopic shift of 4 cm^{-1}.

* This document is based on work performed, in part, for the AEC by Carbide and Carbon Chemicals Company, Oak Ridge, Tennessee and for the School of Chemistry, Georgia Institute of Technology, Atlanta, Georgia.

[1] W. G. Burns and H. J. Bernstein, J. Chem. Phys. **18**, 1669 (1950).
[2] A. G. Pulford and A. Walsh, Trans. Faraday Soc. **47**, 347 (1951).
[3] Randall, Dennison, Ginsburg, and Weber, Phys. Rev. **52**, 160 (1937).
[4] Rogers, Pietenpol, and Williams, Phys. Rev. **83**, 431 (1951).
[5] A. Adel, Phys. Rev. **45**, 56 (1934).
[6] K. W. F. Kohlrausch, *Der Smekal-Raman Effekt, Erganzungsband 1931–1937* (Julius Springer, Berlin), p. 66.

Dielectric Relaxation in Sulfuric Acid*

J. C. D. BRAND, J. C. JAMES, AND A. RUTHERFORD
The University, Glasgow W. 2., Scotland
(Received January 18, 1952)

THE high electrolytic conductance of sulfuric acid (0.01 ohm cm^{-1} at 25° for anhydrous H_2SO_4, *cf.* 0.0107 ohm cm^{-1} for 0.1 N sodium chloride solution) is a serious obstacle to the direct measurement at low frequency of the static dielectric constant. An alternative approach is to measure the dielectric constant, ϵ_1, and the total dielectric loss factor, $\epsilon_2{}^T$, in the dispersion region where the disturbances due to the ionic conductance are much diminished. The total loss factor is the sum of the dielectric and conductor losses, so that

$$\epsilon_2{}^T=\epsilon_2+2\sigma/\nu, \quad (1)$$

where ϵ_2 is the loss factor relating to reorientation of the rotating dipoles, σ is the specific ionic conductance in esu, and ν is the frequency of the measuring radiation. ϵ_1 and $\epsilon_2{}^T$ were determined (Eq. (2)) by measuring the refractive index, n, and the absorption coefficient, k, in a section of dielectric-filled coaxial wave guide; n and k being obtained directly from the variation with length of the dielectric column of, respectively, the phase[1] and power[2] of the transmitted wave. Methods

$$\epsilon_1=n^2-k^2; \quad \epsilon_2{}^T=2nk \quad (2)$$

depending on transmission were selected because of the high loss angles involved ($2.5>\epsilon_2{}^T/\epsilon_1>1.5$). The high conductor loss unavoidably lowered the accuracy of both ϵ_1 and ϵ_2, particularly the latter since the term $2\sigma/\nu$ (Eq. (1)) exceeded ϵ_2 throughout the low frequency half of the dispersion region, and the spread of ϵ_1 and ϵ_2 amounted to several units. To evaluate ϵ_2 from $\epsilon_2{}^T$ by Eq. (1), σ was measured at 3000 c sec^{-1} with a conventional ac bridge, and was assumed not to vary with frequency. This assumption was tested with aqueous acids (99.5 and 96.0 percent H_2SO_4) at radiofrequencies outside the dispersion region where

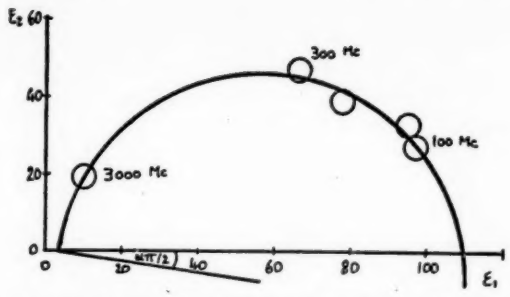

FIG. 1. Dielectric relaxation of anhydrous sulfuric acid at 20°C. $\epsilon_0=110$, $\epsilon_\alpha=3$, $\alpha=0.09$, $\tau_0=4.7\times10^{-10}$ sec and $\lambda_\infty=88$ cm. The chosen value for ϵ_α is greater than n_D^2, which is generally true of polar liquids.

$\epsilon_2{}^T=2\sigma/\nu$ ($\epsilon_2=0$) and was found to be valid within the experimental error. Concentrated aqueous electrolyte solutions also fulfil this condition,[3] the Debye-Falkenhagen dispersion of the conductance being inappreciable at moderate dilution.

The plot of the complex dielectric constant, $\epsilon=\epsilon_1-i\epsilon_2$, at 20° is shown in Fig. 1. Within the rather large experimental error the points fall on a circular arc according to the semi-empirical expression[4]

$$\epsilon=\epsilon_1-i\epsilon_2=\epsilon_\alpha+(\epsilon_0-\epsilon_\alpha)/\{1+(i\omega\tau_0)^{1-\alpha}\};\quad \omega=2\pi\nu,$$

where ϵ_0 and ϵ_α are, respectively, the low and high frequency limiting dielectric constants, τ_0 is the most probable relaxation time, and α is a parameter governing the distribution of relaxation times (hence also the position, below the abscissa, of the center of the arc). In practice the distribution of relaxation times is quite small. It is clear that absorption in the region in question is associated with the molecular rotation, the calculated value of τ_0 by the Debye equation, $\tau=3\eta V/kT$ (which gives rough values only for an abnormal liquid like H_2SO_4) being 13×10^{-10} sec. Unless there is a further relaxation process at lower frequencies, ϵ_0 can be identified with the static dielectric constant of sulfuric acid. The value ~110 is close to formamide (111.5)[5] and anhydrous hydrogen cyanide (114.5),[6] and is characteristic of a polar liquid in which hydrogen bonding leads to a *short-range* cooperative effect of the molecular dipoles.[7]

We wish to thank Professor J. B. Birks for advice and for the gift of apparatus.

* This work was supported by a maintenance allowance (to A.R.) from DSIR.

[1] Redheffer, *M.I.T. Radiation Laboratory Series* (McGraw-Hill Book Company, Inc., New York, 1947), Vol. 11, p. 570.
[2] Turner, J. Inst. Elec. Engr. **93**, 3A, 1474 (1946).
[3] Ritson, Hasted, and Collie, J. Chem. Phys. **16**, 1 (1948); Cooper, J. Inst. Elec. Engr. **93**, 3, 69 (1946).
[4] K. S. Cole and R. H. Cole, J. Chem. Phys. **9**, 341 (1941); W. Kauzmann, Revs. Modern Phys. **14**, 12 (1942).
[5] Leader, J. Am. Chem. Soc. **73**, 856 (1951).
[6] Coates and Coates, J. Chem. Soc. 77 (1944).
[7] Kirkwood, Trans. Faraday Soc. **42A**, 7 (1946) and earlier references.

Hindering Barriers of Ethyl Alcohol

KAZUO ITO
Department of Chemistry, Faculty of Science, Nagoya University, Japan
(Received December 26, 1951)

HINDERING barriers of ethyl and methyl alcohol are not yet determined satisfactorily from thermal and molecular data in spite of the comparative simplicity of molecules. This fact seems to come partly from the fact that in these molecules the gas imperfection correction for entropy may be rather large[1] and, in addition, different results are given by the different approximations used for the analysis of entropy. The present author proposed[2] a method of gas imperfection correction for entropy in which vapor pressure (to calculate an idealized heat of vaporization) and observed heat of vaporization are used, that is,

$$S^\circ-S=2(L^\circ-L)/3T. \qquad (1)$$

By the use of the values obtained by (1) the entropy of ethyl alcohol[1] is

	298.2	351.5	403.2°K
S°	67.30	70.49	73.46 eu

(2)

The product of principal moments of inertia of the ethyl alcohol molecule and moment of inertia of $-OH$ and $-CH_3$ in the molecule are functions of the rotational angle of $-OH$. These can be calculated by Kassel's method[5] and in this case averaged values for *trans*- and *gauche*-positions of $-OH$ can be used because an error in this source is not serious, that is, $A_0B_0C_0=2.287\ 10^{-35}$, $I(OH)=1.20\ 10^{-40}$ and $I(CH_3)=4.39\ 10^{-40}$ g cm^2. The molecular data used are $\angle COH=110°$, C–O=1.42, C–H=1.09, C–C =1.54A, and tetrahedral angles are assumed for all other angles.

Unknown constants to be determined to fit the calculated entropy of ethyl alcohol to that derived from the observed values, that is, to (2) are, then, six rocking frequencies, the hindering barrier of $-CH_3$ for which two values are assigned one of which $V(CH_3)t$ is the value of the barrier of $-CH_3$ when $-OH$ is at a transposition and the other of which $V(CH_3)g$ is that when $-OH$ is at a *gauche*-position, and hindering barriers of $-OH$. The method of calculation of the translational and rotational parts of the entropy is the usual one, and the vibrational frequencies used by Halford[1] are adopted. Six unknown frequencies $(\delta)av$ are treated as 950[3] or 985 cm^{-1} [1] in average. For the part of the entropy caused by the $-CH_3$ rotation a function $V=V(CH_3)(1-\cos3\theta)/2$ is used, assuming $V(CH_3)t-V(CH_3)g=1.0$ kcal/mole and $S(CH_3)$ is calculated by averaging $S(CH_3)t$ and $S(CH_3)g$ with a weight $1:2\exp(-\Delta E/RT)$, where ΔE is the energy difference of the hindering potentials for $-OH$ at *trans*- and *gauche*-position. For the rotation of $-OH$, a function $V=V_1(1-\cos\theta)/2+V_3(1-\cos3\theta)/2$ is used.

There are two methods of calculation of the part caused by $-OH$ rotation, in which one of ethyl alcohol is treated as the mixture of rotational isomers (i) and in the other of which the classical partition function is used for $-OH$ rotation (ii). By use of (i) the entropy of ethyl alcohol can be explained at three temperatures given in (2) by any group as follows (kcal/mole).

	$V(CH_3)t$	$V(CH_3)g$	$V_1(OH)$	$V_3(OH)$	ΔE
	(A) $(\delta)av=950$ cm^{-1}				
(a)	2.6	3.6	1.4	0.76	1.0
(b)	2.2	3.2	1.5	0.83	1.1
(c)	1.5	2.5	2.0	0.89	1.4
	(B) $(\delta)av=985$ cm^{-1}				
(a)	3.0	4.0	1.4	0.58	1.0
(b)	2.3	3.3	1.6	0.64	1.1
(c)	1.6	2.6	2.0	0.73	1.4

By the use of (ii) the calculated and observed entropy are not coincident in the region $(\delta)av=950$ cm^{-1}, $V_1(OH)\leq3.0$, and $\Delta E\leq2.0$ kcal/mole, and the third law entropy S° is explained at the three temperatures by the following parameters satisfactorily.

		$(\delta)av=985$ cm^{-1}		
$V(CH_3)t$	$V(CH_3)g$	$V_1(OH)$	$V_3(OH)$	ΔE
3.0	4.0	2.9	1.17	2.0 kcal/mole

Of these two sets of results the values obtained by (ii) must be adopted because the treatment of (i) corresponds to only a first term in each of the *trans*- and *gauche*-positions when the classical partition function is developed by the saddle point method near the *trans*- and *gauche*-positions.[4] The values obtained seem very reasonable. The reasonable values of the hindering barriers in ethyl alcohol seems to be given as shown above by adopting the proper methods for the gas imperfection correction and the analysis of internal rotation part of entropy.

[1] J. O. Halford, J. Chem. Phys. **17**, 111 (1949).
[2] K. Ito, J. Chem. Phys. **19**, 1313 (1951).
[3] S. C. Schumann and J. G. Aston, J. Chem. Phys. **6**, 480 (1938).
[4] Y. Morino and K. Ito, Lecture in the annual meeting of Chem. Soc. of Japan (1950).
[5] L. Kassel, J. Chem. Phys. **4**, 280 (1936).

Diffusion of Indium into Gallium near the Melting Point

R. E. ECKERT AND H. G. DRICKAMER
Department of Chemistry, University of Illinois, Urbana, Illinois
(Received January 15, 1952)

DIFFUSION of indium into polycrystalline gallium has been measured near the melting point of gallium. The procedure was similar to that described previously[1] by the authors for the systems Tl^{204}—indium and In^{114}—indium, with the exceptions noted below.

(1) The measurements were made in a room maintained at 20°C to permit temperature bath control and slicing at a temperature well below the melting point. Run 114 is the average of three samples run in a room maintained at 8.4°C.

(2) The gallium pellets were $\frac{3}{8}$ in. in diameter as compared with the $\frac{1}{4}$-in. diameter indium pellets.

(3) The gallium pellets were etched in cooled concentrated perchloric acid for one hour. The plating of the indium was carried on as previously described except that the solution was cooled with ice to minimize diffusion during the plating.

The aligning and slicing were identical to that described for indium. The gallium was somewhat more brittle and the accuracy of the slices was about 5 percent except for the 8.4°C pellet where the accuracy was not better than 10 percent per slice. The samples were counted with a fixed geometry on a thin walled Geiger-Müller counter.

The results are shown in Table I and Fig. 1. The accuracy of the points is about ±15 percent except for Runs (110–111) accuracy ±25 percent and Run 114 (accuracy ±25 percent). Gallium at 8.4°C proved to be brittle aud difficult to handle. Several runs were attempted and this is the average of the values obtained. There is no discontinuity in the diffusion coefficient at the melting point, and the rapid rise in D is definitely below the melting point, although much closer than for the polycrystalline indium samples. There are two possible explanations.

TABLE I.

Run No.	Temperature °C	Diffusion coefficient cm²/sec
114	8.4	7×10^{-13}
103	28.99	4.66×10^{-10}
109	29.02	4.53×10^{-10}
105	29.25	2.69×10^{-10}
113	29.34	4.0×10^{-10}
104	29.46	2.70×10^{-10}
106	29.66	1.31×10^{-8}
108	29.73	2.02×10^{-7}
107	29.80	5.82×10^{-7}
110	30.00	1.02×10^{-6}
111	30.00	

(1) The grain diameter in the gallium was one to two millimeters, the same as for the indium samples. Since the gallium pellets were half the diameter of the indium pellets, there were only 3–4 grains at the surface compared with 10–12 indium grains. Thus these data may be more nearly representative of lattice diffusion than of grain boundary diffusion.

(2) The fact that gallium contracts on melting may mean that any premelting or premature lattice disintegration does not have the same tendency to increase diffusion that it would have in an ordinary solid.

From Run 114 and the points at 29°C an equation for diffusion in the solid can be obtained.

$$D=4.4\times10^{26}e^{-(50,000/RT)}\ \text{cm}^2/\text{sec}. \quad (1)$$

Because of the difficulties with the low temperature run, this equation is not very accurate.

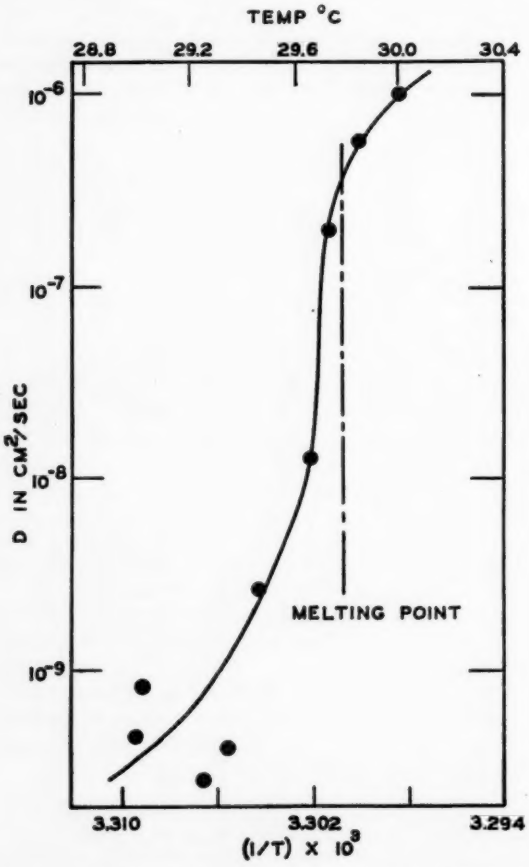

FIG. 1. Plot of lnD *versus* $1/T$ for diffusion of indium and gallium.

[1] R. E. Eckert and H. G. Drickamer, J. Chem. Phys. **20**, 13 (1952).

Analysis of the Near-Ultraviolet Absorption Spectrum of *p*-Cresol Vapor, and the Long Wavelengths Absorption Bands of Benzaldehyde, Acetophenone, and Benzophenone

SUNAO IMANISHI, MITSUO ITO, KIMIO SEMBA, AND TOSHINOBU ANNO
Chemical Laboratory, Faculty of Science, Kyushu University
(Received December 27, 1951)

THE *p*-cresol molecule has the approximate symmetry of C_{2v} or C_s, and its allowed electronic transition of the A_1-B_1 (C_{2v}) or $A'-A'$ (C_s) type lying in the 2480–2945A region has the structure briefly reported below.[1] The spectrum was photographed with a quartz spectrograph having a linear dispersion of 5.0~8.0A per mm in this region, using a vapor path of 40 cm at saturation pressures for 30~140°C.

The most intense 0,0 band of this system is at 2829.0A or 35,338 cm^{-1}. About 170 bands belonging to this system were measured and assigned to combinations of the fundamental vibrational frequencies, directly observed in this spectrum, for this molecule in the ground and the excited states. Nearly all the bands have sharp heads on the short wavelength side, excepting some diffuse blends which generally show no heads. The fundamental vibrational frequencies of the molecule found excited to various quanta in either electronic state involved in this absorption transition, are listed in Table I in comparison with the known Raman and infrared absorption data for the ground state in liquid. The bands with the 310 and 648 cm^{-1} ground-state frequencies which have been assigned to antisymmetric vibrations of the β_1 type are very weak, and their upper state frequencies are not found with certainty, in conformity with the assumption of

TABLE I. *p*-Cresol. Fundamental vibrational frequencies (cm^{-1}).

Raman effect assignment[a]				U. V. absorption			
			(Type in C_{2v})	Ground state	Excited state		
$\Delta\nu$[b]	Int.	ρ[c]		Present work		Sponer[d]	Infrared[e]
				230	217		
338	(4)	1.00	$\omega_{10}(\beta_1)$	310	—		
465	(5)	0.52	$\omega_{11}(\alpha_1)$	458	422	419	
507	(0)			499	469		
649	(3)	0.92	$\omega_2(\beta_1)$	648	585		
703	(0)	0.87					680∼ 690 (w.)
736	(1)			734	694		720∼ 730 (w.)
822	(3)	0.15					818 (st.)
842	(10)	0.07	$\omega_1(\alpha_1)$	839	808	808	860∼ 870 (st.)
							910∼ 920 (m.)
1016	(00)			(1074)	(1016)		1000∼1010 (w.)
1171	(2)	0.34	$\delta_3(\alpha_1)$	1152	1086		1080 (m.)
1214	(5)	0.09	$\omega_4(\alpha_1)$	1231	1153		1170∼1180 (st.)
1256	(3)	0.07	$\omega_3(\alpha_1)$	1259	1196	1187	
1297	(0)	0.55		1296	1226		
1381	(3)	0.49		1396	1272		
1450	(00)	0.92					
1615	(4)	0.74			(1536)		
2864	(1/2)	p					
2922	(2)	p					
3015	(1/2)	p					
3046	(3)	0.47					

[a] K. W. F. Kohlrausch and O. Paulsen, Monatsh. Chem. **72**, 268 (1939).
[b] K. W. F. Kohlrausch and A. Pongratz, Monatsh. Chem. **63**, 427 (1933).
[c] O. Paulsen, Monatsh. Chem. **72**, 244 (1939).
[d] See reference 1.
[e] J. Lecomte, J. phys. et radium **7**, 13 (1938).

the allowed electronic transition. In other respects no intensity anomaly is noticed.

Analyses of *o*- and *m*-cresol vapor spectra are nearly completed, and detailed accounts of the spectra of the three isomeric cresols in the vapor state will be published shortly in the *Science Faculty Memoirs* (*Section Chemistry*) of Kyushu University.

In the benzaldehyde vapor spectrum, Almasy[2] observed a weak and long wavelengths absorption in the 3163–3747A region, apart from the strong and short wavelengths absorption in the 2480–2970A region recently analyzed by Imanishi[3] as arising from the A_1-B_1 allowed electronic transition. We also have photographed this longer wave system with a 3 m focus grating, using 1 m vapor absorption path at saturation pressures for up to 170°C (∼760 mm Hg). This absorption consists of a large number of narrow bands forming four or five prominent groups. The most conspicuous wave-number interval repeated by the strongest band of each group is 1307 cm^{-1}. The total intensity of the system is presumably of the order of 10^{-3} or smaller compared with the A_1-B_1 system.

Now this system may be interpreted as arising from the excitation of a nonbonding electron localized on the oxygen atom of the aldehyde group, as discussed by McMurry,[4] and corresponds to the 30,500 cm^{-1} absorption region observed in alcohol solution of benzaldehyde,[4] while the strong A_1-B_1 system is because of the excitation of the ring π-electron. In that case the electronic transition corresponding to the long wave system would be essentially of a forbidden type ($^1N-{}^1E$, in Mulliken's notation), and the 0,0 frequency may lie at a still longer wavelength than the observed first member 26,923 cm^{-1} of the above progression, by a certain nontotally symmetrical vibration frequency. The 1307 cm^{-1} interval mentioned above may very probably be the upper state frequency of the 1453 cm^{-1} α_1 type[5] vibration observed in the Raman effect for benzaldehyde.[5]

Acetophenone and benzophenone have corresponding weak absorption regions in their vapor spectra at 3060–3500A (31,200 cm^{-1} in alcohol solution) and 3270–3510A (29,500 cm^{-1} in hexane solution), respectively.[4] They are both continuous.

[1] Previously studied by J. Purvis and N. McCleland, J. Chem. Soc. (London) **103**, 1088 (1933); J. Savard, Ann. chim. **11**, 287 (1929); H. Sponer, J. Chem. Phys. **10**, 672 (1942).
[2] F. Almasy, J. chim. phys. **30**, 528, 634, 713 (1933).
[3] S. Imanishi, J. Chem. Phys. **19**, 389 (1951).
[4] H. L. McMurry, J. Chem. Phys. **9**, 231, 241 (1941).
[5] K. W. F. Kohlrausch, *Ramanspektren* (1943).

Polytropic Exponent of Isentropic Expansions in the Coexistence Region*

S. G. REED, JR.
Physics Department, Loyola University, New Orleans, Louisiana
(Received January 4, 1952)

ISENTROPIC expansions in the coexistence region of two phases in equilibrium are often approximated by the polytropic equation

$$pV^\kappa = \text{const},$$

where κ is given as an empirical constant. It has been suggested that κ is purely empirical, having no relation to the heat capacity or other physical properties of the expanding material.[1] The purpose of this note is to show how such a relation may be established.

The polytropic exponent κ is given by

$$\kappa = -v/p(\partial p/\partial v)_s, \tag{1}$$

and in the coexistence region

$$(\partial p/\partial v)_s = -T/C_V(\partial^2 p/\partial T^2)_v, \tag{2}$$

where C_V is the heat capacity of a two phase mixture in equilibrium and at constant volume. Hoge[2] has derived an expression for the specific heat of a saturated mixture, which, appropriately modified for constant volume, gives

$$C_V = C_c + L(1-x)[(\partial \ln(\partial p/\partial T)_v/\partial T)_v] - T(\partial p/\partial T)_v(\partial v_c/\partial T)_v, \tag{3}$$

where C_c is the specific heat of the saturated condensed phase, L the latent heat of vaporization per gram, x the mass fraction of condensate, and v_c the specific volume of the condensed phase. The derivatives are taken at constant total volume. $(\partial p/\partial T)_v$ may be found from vapor pressure data, $p-V-T$ data, or the Clausius Clapeyron equation. The mass fraction in the vapor phase, $1-x$, can be calculated if L and C_c are known as functions of temperature. One has

$$\int_{T_o}^{T} \frac{d}{dT}\left(\frac{L}{T}(1-x)\right)dT = \int_{T_o}^{T} C_c dT/T, \tag{4}$$

the subscript o referring to conditions at the outset of the process.

Equation (1) gives the local value of κ; for the entire expansion, the appropriate exponent κ' satisfying

$$p_o V_o^{\kappa'} = pV^{\kappa'}$$

may be defined according to[3]

$$\kappa' = (\ln p/p_o) \Big/ \int_{p_o}^{p} \kappa^{-1} d \ln p.$$

All the relations given so far are exact.

An approximate expression for C_V and for κ is readily obtained far from the critical point. Then the last term on the right-hand side of Eq. (3) may be neglected, the perfect gas equation of state may be introduced for the vapor phase alone, and the latent heat L may be assumed constant. One finds then

$$C_V \cong C_c + (1-x)(L^2/RT^2 - 2) \tag{5}$$

and

$$\kappa \cong [(1-x)L/RT][(1-x)(L/RT-2) + C_c T/L]^{-1}. \tag{6}$$

Results of an exact and approximate calculation of κ for water vapor at the coexistence line, where $x=0$, for three pressures below 25 atmos, are given in Table I. The empirical κ used in the same range of temperatures and pressures, and near the coexistence line, is $\kappa = 1.135$.[1] The agreement of the exact κ with

TABLE I. κ and C_V for water vapor at the coexistence line.

T, °K	C_V (exact), cal/g—°K	κ (exact)	κ (approx)
266.51	17.79	1.136	1.107
422.07	11.99	1.136	1.125
476.51	8.411	1.136	1.124

this value is within the accuracy of the water vapor tables employed.[4] The approximate κ agrees with the empirical to within the accuracy of the approximations involved.

The polytropic exponent for steam up to the coexistence line is about 1.32 in the same region.[5] The sharp drop in κ is because of a sharp drop in $(\partial p/\partial v)_s$, which has been noted previously.[6]

* Present address: Naval Ordnance Laboratory, White Oak, Silver Spring, Maryland.

[1] F. Bosnjakovic, *Technische Thermodynamik I* (Steinkopf, Dresden, 1935), p. 118.
[2] H. Hoge, J. Research Natl. Bur. Standards **36**, 111 (1946).
[3] A. Iberall, J. Appl. Phys. **19**, 997 (1948).
[4] Keenan and Keyes, *Thermodynamic Properties of Steam* (John Wiley and Sons, Inc., New York, 1936).
[5] See reference 4, p. 82.
[6] Wegener, Reed, Jr., Stollenwerk, and Lundquist, J. Appl. Phys. **22**, 1077 (1951); N. P. Anderson and L. Delsasso, J. Acoust. Soc. Am. **23**, 423 (1951); C. M. Herget, J. Chem. Phys. **8**, 537 (1940); S. Reed, Jr., J. Chem. Phys. (to be published).

Red Hydrogen Chloride*

W. H. Johnston and Robert E. Martin†
Department of Chemistry, Purdue University, Lafayette, Indiana
(Received December 13, 1951)

In connection with exchange studies using hydrogen chloride we have observed a red color in anhydrous solid samples which had been frozen quickly with liquid nitrogen. This color invariably disappeared within a few seconds of the removal of the liquid nitrogen bath. A search of the literature revealed that Giauque reported the same observation in 1927.[1] The purpose of this letter is to describe experiments which appear to rule out impurities as an explanation and suggest that the red color is due to imperfection color centers in the crystals of hydrogen chloride.

Anhydrous tank gas[2] which was white in liquid nitrogen was purified by a series of vacuum distillations whereupon it became pink or red when frozen quickly. Samples were analyzed mass spectrographically[3] before and after purification. These analyses confirmed the purification process and showed less than 0.1 percent of any impurity peak from mass 6 to mass 100.

Furthermore, varying amounts of hydrogen, oxygen, nitrogen, chlorine, mercury, and nitrous oxide, all of which might have persisted in trace amounts, were added to samples of hydrogen chloride. These materials had no effect on the production of the red color. On the other hand, the addition of 10^{-4} or 10^{-5} mole fraction of nitric oxide intensifies the red color.

Various experiments showed the importance of the rate of freezing. When this rate was too slow, white solid was formed. If the gas were frozen quickly, red or pink material was formed. Furthermore, if the hydrogen chloride was introduced in a series of bursts into a cold-finger which was immersed in liquid nitrogen, each burst produced an instantaneous fading and then a return of color in the solid.

One other experiment was done in which a sample of the white solid was bombarded through a thin Pyrex vessel with x-rays from a beryllium window tube with a molybdenum target[4] for two hours. No visible coloration was produced.

It is proposed that the red form of solid hydrogen chloride is due to the production of imperfections in the crystal. Traces of nitric oxide may favor this process. Electrons or perhaps protons may enter these vacancies; the adsorption may be connected with one of these processes or with transitions of the electrons or of the ions formed. Further work to investigate these mechanisms is in progress.

The authors express their appreciation to Dr. H. J. Yearian for the x-ray bombardment, to Mr. John Walton who assisted with the experimental work, and to Dr. Paula Feuer and Dr. H. M. James for valuable discussions.

* This work was supported in part by the AEC under Contract No. AT(11-1)-166.
† Pre-doctoral Fellow of the Purdue Research Foundation.
[1] Giauque, J. Am. Chem. Soc. **50**, 102–103 (1927).
[2] Matheson Company, Joliet, Illinois.
[3] Consolidated-Nier Isotope Ratio Mass Spectrometer Model 21-201, modified to take hydrogen chloride.
[4] A Machlett AEG-50 tube operated at 40 kv and 20 ma was used in this work.

Paramagnetic Resonance Absorption in Organic Free Radicals. Fine Structure*

Clyde A. Hutchison, Jr., Ricardo C. Pastor, and Arthur G. Kowalsky
Institute for Nuclear Studies and Department of Chemistry, University of Chicago, Chicago, Illinois
(Received January 10, 1952)

We have studied paramagnetic resonance absorption at approximately 23,500 mc and room temperature in solutions of diphenyl-picryl hydrazyl,[1–3] $(C_6H_5)_2NNC_6H_2(NO_2)_3$, in benzene. In the cases of dilute solutions a fine structure was observed. The solutions of diphenyl-picryl hydrazyl were prepared by dissolving the weighed solid in a known volume of purified benzene. Known volumes of the solution were transferred in a nitrogen atmosphere to thin walled Pyrex sample tubes; the tubes were sealed off and kept in light-tight containers when not in use.

The magnetic absorption was measured using a right circular cylindrical transmission cavity operated in the TE_{011} mode. The static magnetic field was modulated sinusoidally at 60 cycles with amplitude sufficient to sweep through the entire range of detectable resonance. The output of a crystal detector was amplified and observed on the vertical axis of an oscilloscope on whose horizontal axis was impressed the modulating voltage. The horizontal axis was calibrated in terms of field strength employing the proton resonance. The amplifier gain and phase shift were such as to insure no distortion of the detected signal.

The full width of the resonance at the one-half power point was found to vary with concentration as shown in Table I.

Table I.

Concentration		Width
Pure solid	Crystal	1.9 gauss
	powder	3.7 gauss
0.2	molar	10 gauss
0.02	molar	21 gauss
0.0093	molar	31 gauss
0.00186	molar	48 gauss

The 0.00186 molar solution showed five nearly resolved peaks with maxima approximately equally spaced and with a separation of approximately 10 gauss. The width given in Table I for this concentration was measured between the half power point on one side of the first peak and the half power point on the other side of the fifth peak. The center peak was somewhat more intense and the outside peaks less intense than peaks two and four. The width of the peaks at half maximum height above the intervening minima was approximately 5 gauss. The 0.0093 molar solution showed the fine structure but the components were not sufficiently resolved to give separate maxima. The fine structure was not observable in the more concentrated solutions, and the absorptions were in these cases symmetrical about the maximum.

The absorption in the finely powdered solid was asymmetrical, showing a bulge on the low field side. Single crystals were also studied. These showed no asymmetry, the widths were approximately one-half that for the powder and the measured g-factors varied from 2.0035 to 2.0041 ± 0.0002 depending on the orientation of the crystal. This corresponds to an approximately 2.5 gauss difference in the peak positions.

A possible interpretation of the fine structure in the solutions is that it is a nuclear hyperfine structure. If the two hydrazyl nitrogen nuclear spins and the electronic spin are uncoupled by the static magnetic field to give a complete Paschen-Back effect and if the electron is symmetrically localized on these two nitrogen atoms, then each electronic level would be split into five components by the nuclear perturbation. Five resonance lines would result on the basis of such a model. Sufficient preference for one of the nuclei over the other by the electron should give nine levels. Appreciable interaction with other magnetic nuclei in the mole-

cule might be expected to give a much more complicated pattern than that observed. The observed separations in the most dilute solution would correspond to an IJ coupling of about $M_J(M_{I1}+M_{I2})$ 28 mc. Beringer and Castle[4] have observed a value of 29.8 mc for the magnetic IJ coupling and -1.7 mc for the electric quadrupole IJ coupling in the case of NO.

Townes and Turkevich have reported the examination of two solutions of diphenyl-picryl hydrazyl in benzene at concentrations of 0.07 and 0.03 molar and have found full widths at half maximum absorption of 15 and 10 gauss, respectively. These are somewhat in disagreement with our measured widths particularly as to sign of change of width with concentration. The width which we have observed for the resonance at 0.02 molar is approximately that to be expected on the basis of dipole-dipole broadening. At the higher concentrations the width is much less than that expected on this basis and in the more dilute solutions the nuclear interactions apparently result in the broadening and the appearance of the five peaks. The individual widths of the five components are too large to be accounted for by electronic dipole-dipole broadening and may be the result of other nuclei in the hydrazyl or the solvent.

We have examined other organic free radicals and found g-factors as follows:

di-*p*-anisyl nitrogen oxide, solid	2.0066
benzophenone sodium ketyl, solution in dioxane	2.0031
spiro-cyclohexyl porphyrexide	2.0065
porphyrindine	2.0057

Of these others, only in the case of porphyrindine have we observed a possible fine structure in the form of two bumps symmetrically disposed on either side of the maximum and giving the appearance of three unresolved equally spaced peaks, the center one being somewhat more intense than the others. This preparation contained some impurity which may possibly have accounted for the observed structure.

We have studied magnetic resonance absorption at 3 gauss in the same preparation of hydrazyl as used for the measurements described above and have not been able to observe in the solid the bulge on the low field side. The measured width at half maximum absorption for the powder at this field strength was 1.83 gauss and at the maximum slope points was 1.29 gauss.

We are at present preparing diphenyl-picryl hydrazyl containing N^{15} in the hydrazyl positions which will be used in further investigation of the fine structure.

The porphyrindine and porphyrexide were prepared by Dr. Leslie Hellerman of the Johns Hopkins University.

We wish to thank Clarence Arnow for the development and construction of certain portions of the electronic equipment used.

* This work was supported by the ONR.

[1] Holden, Kittel, Merritt, and Yager, Phys. Rev. **75**, 1614 (1949).
[2] Holden, Kittel, Merritt, and Yager, Phys. Rev. **77**, 147 (1950).
[3] C. H. Townes and J. Turkevich, Phys. Rev. **77**, 148 (1950).
[4] R. Beringer and J. G. Castle, Jr., Phys. Rev. **78**, 581 (1950).

The Stability of Nonpolar Covalent Bonds

R. T. SANDERSON
Department of Chemistry and Chemical Engineering, State University of Iowa, Iowa City, Iowa
(Received January 14, 1952)

RELATIVE electronegativity[1] has recently been shown to be measured by the "stability ratio (SR)",[2,3] defined as the ratio of the average electronic density of an atom or its ion to that of an isoelectronic inert atom (real, or hypothetical as determined by linear interpolation between real values). Accordingly, bonds between atoms of similar stability ratios may be considered to be essentially nonpolar. The purpose of this communication is to state as a general principle the observation that *in a group of nonpolar covalent binary compounds of any particular element, the thermal stability diminishes with increasing difference in radii of the combined atoms.* By means of this principle, a number of hitherto apparently unrelated, and in some instances anomalous, chemical facts are brought into reasonable order.

TABLE I. Some stability ratios and nonpolar covalent radii.

Element	SR	r, A	Element	SR	r, A
Br	4.53	1.14	Pb	3.67	1.47
N	4.49	0.75	Te	3.62	1.35
Se	4.25	1.16	Ge	3.59	1.26
S	4.11	1.02	Tl	3.58	1.48
As	3.91	1.19	H	3.55	0.37
I	3.84	1.33	Hg	3.47	1.49
C	3.79	0.77	Sb	3.37	1.38
Bi	3.78	1.46	P	3.34	1.06

Table I lists the SR values and nonpolar covalent radii of the elements which are relevant to this discussion. These SR values are somewhat modified from those originally reported,[3] being based on inert atomic radii determined from crystal ionic radii instead of from univalent crystal radii as determined by Pauling.[1] These revised radii are: He 0.93, Ne 1.31, A 1.74, Kr 1.89, Xe 2.09, Rn 2.29A.

Perhaps the best application of the above principle is to the covalent hydrides. Somewhat arbitrarily, an SR difference of 0.3 or less is taken to indicate a bond which is essentially nonpolar, being probably less than 7 percent ionic. The "essentially nonpolar" covalent hydrides, then, listed in order of increasing radius difference, are CH_4, PH_3, GeH_4, HI, H_2Te, SbH_3, BiH_3, PbH_4, HgH_2. Data are not available for a complete quantitative comparison, but it is apparent that this sequence is closely similar to that of diminishing thermal stability. Methane of course is the most stable, bismuthine[4] decomposes slowly at ordinary temperatures and plumbane[5] fairly rapidly, and mercury hydride[6] is unstable even below -80°C.

That this is not merely an indication of diminishing ability to form stable bonds with increasing radius is shown by the iodides of sulfur, selenium, and tellurium, which would all be nearly nonpolar. Tellurium iodide[7] is the only compound of this group stable enough to be isolated. Evidence of selenium-iodine compounds in solution has been obtained[8] but none have been isolated, and no evidence whatever of sulfur iodides appears to be known.[9] These facts are consistent with the general principle of diminishing stability with increasing radius difference. A contributing factor may be that in combination with sulfur or selenium but not with tellurium, iodine would be somewhat positive.

Another illustration is that of nitrogen tribromide, NBr_3, which is evidently much less stable than either the chloride or iodide.[10] Both the latter compounds are somewhat ionic, which evidently makes even the iodide more stable than the nonpolar bromide, even though the radius difference in the iodide is greater.

In the nonpolar binary compounds of carbon, the sequence of increasing radius difference is H, Ge, I, Te, Bi, Pb, Tl. With the unexplained possible exception of germanium, which appears to form no carbide,[11] this is also the order of diminishing stability. Carbon tetraiodide is not very stable,[12] carbon ditelluride[13] is evidently too unstable to be prepared, and carbides of bismuth, lead, and thallium seem to be unknown.

Very probably this general principle has previously been observed, but its full significance as an aid to interpreting some of the facts of chemistry seems worthy of greater attention.

[1] L. Pauling, *Nature of the Chemical Bond* (Cornell University Press, Ithaca, New York, 1940), second edition.
[2] R. T. Sanderson, Science **114**, 670 (1951).
[3] R. T. Sanderson, J. Am. Chem. Soc. **74**, 272 (1952).
[4] F. Paneth, Ber. **51**, 1704 (1918).
[5] F. Paneth and O. Nörring, Ber. **53**, 1693 (1920).
[6] Barbaras, Dillard, Finholt, Wartik, Wilzbach, and Schlesinger, J. Am. Chem. Soc. **73**, 4585 (1951).
[7] F. M. Jäger and J. B. Menke, Z. anorg. Chem. **75**, 241 (1912); **77**, 320 (1912).
[8] J. D. McCullough, J. Am. Chem. Soc. **61**, 3401 (1939); E. Montignie, Bull. soc. chim. **4** (5), 132 (1937).
[9] See for example, N. V. Sidgwick, *The Chemical Elements and Their Compounds* (Oxford University Press, London, 1950), p. 947.
[10] See reference 9, p. 707.
[11] Dennis, Tressler, and Hance, J. Am. Chem. Soc. **45**, 2047 (1923).
[12] M. Lantenois, Compt. rend. **156**, 1385 (1913).
[13] A. Stock and P. Praetorius, Ber. **47**, 131 (1914).

The Raman Spectra and Structures of Aluminate and Zincate Ions

ELLIS R. LIPPINCOTT,* JAMES A. PSELLOS, AND MARVIN C. TOBIN
Department of Chemistry, University of Connecticut, Storrs, Connecticut
(Received January 16, 1952)

IT is generally conceded that aluminate, $Al(OH)_4^-$, and zincate, $Zn(OH)_4^=$, ions exist in solution. However, proof of existence of ions in solution is often a matter of some difficulty. The appearance of a well-defined Raman spectrum not only offers proof for the existence of a specific ion, but can give clues to its symmetry and structure.

In order to take Raman spectra of aqueous solutions, it is necessary to obtain optically blank samples. This is ordinarily difficult, but can be done by careful technique.[1]

The samples were prepared by saturating water freshly distilled from a cleaned, all-glass still with the metal salts, and precipitating the hydroxides with Mallinckrodt reagent grade sodium hydroxide. The hydroxides were washed free of anion by decantation, and dissolved in an excess of sodium hydroxide solution. The solutions were loaded into the Raman tube through a Corning 33,900 GVYKU ultrafine bacteriological filter.

The spectra were taken on a Hilger E612 glass Raman spectrograph at the Department of Chemistry at the University of Connecticut. They were taken on Kodak 103J spectroscope plates, with a 0.15 mm slit, and no filter solution. The 4358A mercury line was used for excitation, with 20 minute exposures.†

Neglecting a consideration of the hydrogen atoms, the observed spectra are consistent with a T_d symmetry for these ions although in the absence of an infrared spectrum this cannot be conclusively proved. It must be assumed that the angle binding vibrations are piled up at 300 cm^{-1}, and that the ν_3 line in $Al(OH)_4^-$ is too weak to be seen. The O—H stretching appears as a blackening around 3500 cm^{-1}.

Force constant calculations were carried out for the skeletal frequencies of both ions, using a simple valence force model.[3] The force constants were calculated using the assignment for ν_1 and ν_2 given in Table I. ν_3 and ν_4 were calculated using these force constants. Observed and calculated frequencies are given in Table I, force constants in Table II.

It is seen that the values of the force constants are reasonable, and that the calculated frequencies agree with the observed frequencies, considering the approximate nature of the calculation.

Further support for the tetrahedral configuration of these ions is that the calculated force constants agree well with those obtained using Gordy's relation between force constants and electronegativities for tetrahedral molecules.[4] The electronegativities for the calculations were taken from Gordy's table.[4] Correction for formal charge was made by the method of Pauling.[5] The electronegativity for Zn^{-2} was obtained by assuming the correction for two formal charges to be twice that for one formal charge, and assuming the electronegativity difference between Cu and Zn to be the same as that between Zn and Ga. Gordy's relation gives $3.6 \cdot 10^5$ and $2.5 \cdot 10^5$ dynes/cm for the Al—O and Zn—O bond stretching force constants respectively as compared to $3.79 \cdot 10^5$ and $2.21 \cdot 10^5$ dynes/cm from our spectroscopic data.

TABLE I.

Assignment	Species	Observed	Calculated
		$Zn(OH)_4^=$	
ν_1	A_1	470(5) cm^{-1}	470 cm^{-1}
ν_2	F_2	420(2)	570
ν_3, ν_4	E, F_2	300(1)	300, 290
		$Al(OH)_4^-$	
ν_1	A_1	615(5)	615
ν_2	F_2	...	720
ν_3, ν_4	E, F_2	310(1)	370, 300

TABLE II.

		Force constants
Zn—O	stretching	2.21×10^5 dyne/cm
O—Zn—O	bending	0.30×10^5 dyne/cm
Al—O	stretching	3.79×10^5 dyne/cm
O—Al—O	bending	0.32×10^5 dyne/cm

The authors wish to gratefully acknowledge grants in aid from the Research Corporation and Graduate School Research Fund at the University of Connecticut.

* Present address: Department of Chemistry, Kansas State College, Manhattan, Kansas.

† The ordinary exposure time on this spectrograph is less than five minutes. We attribute this short exposure time to the efficiency of the excitation unit, which is fitted with MgO reflectors (see reference 2).

[1] Marvin C. Tobin, Ph.D. thesis, University of Connecticut (1952).
[2] A. C. Menzies and J. Skinner, J. Sci. Instr. **26**, 299 (1949).
[3] G. Herzberg, *Infrared and Raman Spectra of Polyatomic Molecules* (D. Van Nostrand Company, Inc., New York, 1945), p. 181.
[4] W. Gordy, J. Chem. Phys. **14**, 305 (1946).
[5] L. Pauling, *The Nature of the Chemical Bond* (Cornell University Press, Ithaca, New York, 1948), p. 65.

Effect of Traces of Ammonia on Track Formation in a Continuous Cloud Chamber

RICHARD E. VOLLRATH
Physics Department, University of Southern California, Los Angeles, California
(Received December 20, 1951)

IN 1936 the author[1] described a continuous cloud chamber in which HCl gas from an aqueous HCl solution at the bottom of a jar diffused into H_2O vapor coming from a wet porous porcelain plate closing the top of the jar. The resulting mixture of HCl and H_2O vapor is supersaturated with respect to a dilute solution of HCl and condenses on ions like the water vapor in a Wilson cloud chamber. In spite of numerous attempts to develop this method into a workable continuous cloud chamber, several difficulties persisted and prevented useful photographs of tracks being obtained. One difficulty is caused by a violet turbulence, irregular gusts, that cause the tracks to become distorted. The turbulence is probably caused by sudden release of heat of condensation as the droplets form. The turbulence no doubt also causes a nonuniform condensation at the walls where the liberated heat of condensation would contribute toward the maintenance of the turbulence. Another difficulty was the unaccountable cessation of track formation. It was repeatedly observed that when such a cloud chamber was first put into action the characteristic gusts appear and cosmic-ray tracks were clearly evident. But in a short time the activity diminishes and finally ceases. Analysis of the HCl solution in the chamber proved that the acid had not been measurably diluted with H_2O. Nor had the wet porous plate absorbed significant amounts of HCl. Both effects would of course reduce the degree of supersaturation attained in the vapor mixture. Concentration gradients which might diminish the rate of evaporation at the HCl and H_2O supply surfaces were minimized by flowing the liquids, but without result.

The thought arose that the air initially present in the chamber might contain a substance that facilitates condensation on ions and is used up in the process. Traces of ammonia very likely to be present in this laboratory were suspected. To test this suspicion the ammonia from a one-percent aqueous solution was allowed to diffuse through a paraffined paper diaphragm into a 6 by 6-inch Pyrex jar with a layer of 2.5 N HCl solution at the bottom. A brilliantly iridescent mist immediately formed, and brilliantly colored ion tracks appeared. A remarkable feature of the tracks is that they appear with colors ranging from a coral pink to a deep blue. But each track is of the same color along a large part of its length. This seems to indicate that the droplet size is uniform wherever the color is uniform. The fact that the tracks are of different colors probably indicates that the degree of supersaturation in the chamber varies with time and location in the chamber. Instead of a typical NH_4Cl smoke only liquid droplets form. These presumably consist of aqueous NH_4Cl together with

either NH_3 or HCl in excess. Concentrated HCl and NH_3 always formed a thick NH_4Cl smoke. The most surprising result was that very minute amounts of ammonia suffice for the purpose. The action of the chamber for a week was maintained by 10 cc of a 1-percent NH_3 solution. The turbulence observed with a pure $HCl-H_2O$ system was practically inappreciable here. The reason for this may be that the droplet size is small and it is estimated from the rate of fall to be from 1 to 10 microns. In the pure HCl system the drops were often as large as 10^{-1} mm. Such large drops evolve much more heat during formation. It is also noteworthy that the partial pressure of the HCl above the 2.5 N HCl solution is only about 2×10^{-3} mm. Droplet formation around ions also occurs when ethylene diamine, triethylamine, or pyridine vapor is allowed to diffuse into the $HCl-H_2O$ atmosphere above a 2 to 3 N HCl solution. In all cases air is present at its normal pressure.

There is at present no way of determining the details of the droplet formation process. The author is inclined to believe that highly supersaturated NH_4Cl vapor condenses directly with water vapor around an ion to form an NH_4Cl solution. The observations of Spotz and Hirschfelder[2] are of interest here. They conclude from an NH_4Cl Liesegang ring formation that there is involved a 1000-fold supersaturation of NH_4Cl vapor and suggest the possibility of a cloud chamber in which the tracks are delineated by NH_4Cl crystals. The author has observed that the highly concentrated solutions of HCl and NH_4Cl used by Spotz and Hirschfelder always lead to the condensation of solid NH_4Cl, low partial pressures of HCl and NH_3 in the presence of H_2O at approximately its normal vapor pressure always lead to condensation of NH_4Cl solution droplets.

[1] R. E. Vollrath, Rev. Sci. Instr. **7**, 409 (1936).
[2] E. L. Spotz and J. O. Hirschfelder, J. Chem. Phys. **19**, 1215 (1951).

Photochemical Method of Maintaining a Continuous Cloud Chamber

RICHARD E. VOLLRATH
Physics Department, University of Southern California, Los Angeles, California
(Received December 20, 1951)

ONE of the difficulties met with in a continuous cloud chamber described by the author[1] is to maintain a uniform concentration of HCl throughout the volume of the chamber. When the source of the HCl vapor which is to condense with water vapor on ions is a solution of HCl there will be a concentration gradient of HCl vapor in the chamber. The concentration may be high enough at the upper part of the chamber to produce ion tracks. But the concentration may be so high near the lower part as to result in spontaneous droplet formation with the result that violent turbulence badly distorts the tracks. It occurred to the writer that the HCl might be generated photochemically throughout the volume of the chamber. The photochemical oxidation of chloroform turns out to be suitable for the purpose. The over-all reaction involved is $2CHCl_3+O_2+2H_2O=2CO_2+6HCl$. There is an intermediate step in this reaction in which phosgene is formed $2CHCl_3+O_2=2COCl_2+2HCl$. The phosgene then reacts with the water vapor present in the reaction volume and forms CO_2 and HCl. It was found that this reaction occurs readily and proceeds fast enough in the diffused light of the laboratory to maintain a sufficient HCl concentration. A small amount of NH_3 allowed to diffuse into the chamber facilitates tracks formation (see preceding letter).

The observations were made in a cylindrical Pyrex jar, 6 in. high and 6 in. diameter. A glass plate on a Neoprene gasket closed the top of the jar. At the bottom of the jar was placed a layer of water (100 cc) and about 1 cc of chloroform. A little Cl_2 water added enables the reaction to start immediately. It was found that even without the chlorine the reaction proceeded after a preliminary delay. In sunlight the formation of HCl is so rapid that ion tracks of very large droplets settling out in a few seconds are produced. The track formation diminishes after a while. But traces of ammonia allowed to diffuse into the jar keep the track formation going. In sunlight the turbulence is very violent, as may be expected from the very rapid growth of HCl solution droplets. However with the NH_3 diffusing into the chamber, a much lower rate of production of HCl suffices, and the diffused light of the laboratory is sufficient illumination. Illumination of the chamber with an incandescent lamp makes it possible to control the illumination and hence the rate of the reaction to a value that generates just the right amount of HCl to keep up with its loss by condensation. There are undoubtedly other photochemical reactions that might be utilized in a similar way. For example, the photochemical bromination of toluene would give rise to toluyl bromide and HBr. The toluyl bromide has a low vapor pressure at ordinary temperatures and should form a supersaturated vapor as it accumulates. If toluyl bromide is capable of condensing on ions, then droplets of toluyl bromide should form an ion track. The other product of the photobromination of toluene, HBr, forms ion tracks with H_2O vapor if water is present in the reacting system. The author has found HBr produced in the above reaction to behave exactly like HCl, and droplet formation is facilitated by traces of ammonia or amines. This is somewhat puzzling because it would be expected that the NH_3 would immediately react with bromine to form HBr and N_2.

Another possibility is the photochemical decomposition of certain vapors. Tyndall, the discoverer of the light scattering by small particles, observed that the vapor of amyl nitrite and similar substances decompose in the light of an arc and deposit, in the form of a thick fog of liquid decomposition products. The author has carefully watched strongly illuminated amyl nitrite vapor and found that during the early stages of the decomposition cosmic-ray tracks can be seen. These are very likely the result of the accumulation of low vapor pressure decomposition products. As these accumulate the vapor becomes supersaturated and condenses on ions. It is suspected that nitric acid is one of the decomposition products. Earlier observations made by the author show that HNO_3 vapor condenses with H_2O on ions in the same way as HCl. There are produced, however, in the decomposition of amyl nitrite other products which appear to condense spontaneously and ultimately fill the chamber with a thick fog. Other systems are being investigated in an effort to find a simple photochemical decomposition which can be used to operate a photochemically maintained cloud chamber.

[1] R. E. Vollrath, Rev. Sci. Instr. **7**, 409 (1936).

Erratum: The Ionization Potentials of the Deuterated Methanes

[J. Chem. Phys. **19**, 1254 (1951)]
F. P. LOSSING, A. W. TICKNER, AND W. A. BRYCE

ON page 1258 of the paper referred to above, the sum $\Sigma_i\,\omega_{i_{CH_4}}$ was given as 19,994 cm^{-1}. This value should be

$$\Sigma_i\,\omega_{i_{CH_4}}=18{,}946\ cm^{-1};$$

then

$$G(0)_{CH_4}-G(0)_{CD_4}=0.05\times18{,}946^{-1}=2842\ cm^{-1}.$$

The difference calculated from spectroscopic data is then

$$(18{,}946-13{,}954)/2=2496\ cm^{-1}.$$

While this agreement is not as good as was previously given, it is still sufficiently good for the present purpose. Then

$$G(0)_{CH_4}{}^{+}-G(0)_{CD_4}{}^{+}=0.15\times(7/8)^{\frac{1}{2}}\times18{,}946=2658\ cm^{-1}$$

and

$$I_{CD_4}-I_{CH_4}=2842-2658=184\ cm^{-1}.$$

This is about 0.02 volt instead of 0.03 volt given previously.

The correction of this error, although allowing more latitude in the approximation used, does not in any way affect the conclusion that the experimentally found difference between the ionization potentials of methane and tetradeuteromethane is at least 0.1 volt greater than can be assigned to zero-point energy differences.

The Acid Decomposition of Dilute Sodium Thiosulfate

ETHEL M. ZAISER
Massachusetts Institute of Technology, Cambridge, Massachusetts
(Received December 26, 1951)

IN a recent letter, Kerker[1] reports a marked effect of the concentrations of acid and thiosulfate on the optical density characteristic of the termination of the "induction period" (i.e., t_B, the time required for the appearance of colloidal sulfur). His explanation is that the optical density at t_B is due not only to the critical supersaturation concentration of dissolved sulfur, which must be practically constant, but also to tetra- and pentathionates produced in amounts which depend on the concentrations of acid and thiosulfate.

Kerker fails to point out that the contribution of polythionate to the optical density is important only when the concentrations of these reactants, particularly the acid, are sufficiently high.[2] La Mer and co-workers restricted their studies to that range of *low* concentrations of $Na_2S_2O_3$ (0.001 to 0.003 M) and HCl (0.001 to 0.006 M) in which monodispersed sulfur hydrosols are produced. Over thirty experiments yielded an average of 0.020±5 percent for $\log(I_0/I)$ at t_B.[3] This in turn is responsible for an average deviation of 5 percent in the rate constant calculated for the homogeneous formation of sulfur. These small variations in $\log(I_0/I)$ and the demonstrable absence of a trend with concentration of reactants was taken as indirect evidence that no appreciable concentrations of polythionates are present at t_B in these dilute solutions. This view has been confirmed by Dinegar, Smellie, and La Mer[4] by an independent method. Their chemical analyses of acidified solutions of thiosulfate (in the range of low concentrations described above) show that the rate of formation of polythionates is exceedingly small compared with that of sulfur. Polythionates are present in the early stages of the reaction (e.g., at t_B) in trivial amounts only.

Further evidence comes from Smellie's findings[5] based on electrophoretic studies that the micelles in monodispersed sols in these dilute ranges are positively charged, whereas those in sols prepared from more concentrated solutions are negatively charged. The addition of very small amounts of polythionate ion (2×10^{-5} molar) to dilute sols reverses the sign of charge.

[1] M. Kerker, J. Chem. Phys. **19**, 1324 (1951).
[2] For a summary of relevant work by Bassett and Durant, Janickis, and others, see D. M. Yost and H. Russell, Jr., *Systematic Inorganic Chemistry of the Fifth-and-Sixth-Group Nonmetallic Elements* (Prentice-Hall, Inc., New York, 1944), pp. 387–398.
[3] E. M. Zaiser and V. K. La Mer, J. Colloid Sci. **3**, 571 (1948), Table II.
[4] Dinegar, Smellie, and La Mer, J. Am. Chem. Soc. **73**, 2050 (1951).
[5] R. H. Smellie, dissertation, Columbia University (May, 1951).

The Shape of the Coexistence Curve in the Critical Region

BRUNO H. ZIMM
General Electric Research Laboratory, Schenectady, New York
(Received December 28, 1951)

IN a recent communication Rowden and Rice[1] reported data on the coexistence curve of aniline and cyclohexane and stated that six mixtures of different compositions in the neighborhood of the critical point all separated into two phases within 0.003° of the same temperature. From this they concluded that the coexistence curve had a flat top. However, if one attempts to fit their data by the equation

$$T_c-T=60(x'-x'')^3, \tag{1}$$

where T is the temperature, T_c the highest temperature at which phase separation occurs, and x' and x'' are the mole fractions of the two phases coexisting at T, it is found that the curve passes within 0.003° of all the six mixtures nearest the critical point and in addition fits the mixtures of extreme composition. Hence, we conclude that these data are as consistent with the existence of a cubic coexistence curve as with a flat-topped coexistence curve.

A cubic curve has been found also in the two-liquid system of carbontetrachloride-perfluoromethylcyclohexane[2] and for the liquid-gas coexistence curve of a number of gases.[3] Guggenheim[3] has found that the gas-liquid data may be represented over a wide range by an equation of the form

$$(T_c-T)/T_c=[k(\rho_l-\rho_g)/\rho_c]^3, \tag{2}$$

where ρ_g is the density of the gas, ρ_l the density of the liquid, and ρ_c the critical density. Equation (1) may be expressed in this form if x replaces ρ, and x_c, the critical mole fraction, is replaced by 0.5, its average value for the two components. When this is done, the constant k requires the value 0.3 in order to represent Rowden and Rice's data, 0.32 for the carbontetrachloride-perfluoromethylcyclohexane case, while Guggenheim used a value of 2/7 or 0.286 for the rare gases. It is remarkable that this constant is so nearly the same for such diverse systems.

[1] R. W. Rowden and O. K. Rice, J. Chem. Phys. **19**, 1423 (1951).
[2] B. H. Zimm, J. Phys. and Colloid Chem. **54**, 1306 (1950).
[3] E. A. Guggenheim, J. Chem. Phys. **13**, 253 (1945).

The Kinetics of the Exchange of Tritium between Hypophosphorous Acid and Water

WILMER A. JENKINS AND DON M. YOST
Gates and Crellin Laboratories of Chemistry, California Institute of Technology, Pasadena, California
(Received January 10, 1952)

BECAUSE the reactions of phosphorus and its compounds have long been a source of fundamental interest and even affectionate regard to chemists, to physicists, and to those delving into the chemistry of plant life and because, in particular, the oxidation kinetics of aqueous hypophosphorous acid present some very puzzling features, it was deemed important to approach the kinetics problem from a fresh point of view.

We have, therefore, measured the rates of exchange of radioactive hydrogen (tritium) between tritiated water, HTO, and the two "undissociable" hydrogens of monobasic hypophosphorous acid, H_3PO_2

$$H_2POOH+HTO \rightleftharpoons HTPOOH+H_2O.$$

Exchange runs were carried out as follows: stock solutions of hypophosphorous acid and tritiated water were mixed in a thermostat. Samples were withdrawn from time to time and quenched by neutralizing them with thallous hydroxide. (Preliminary experiments showed that the exchange reaction does not take place in neutral solution.) The resulting solution was then evaporated at room temperature in vacuum to obtain solid thallous hypophosphite. Circular, flat planchets were then filled with the thallous hypophosphite and inserted into a windowless, Q-gas flow, Geiger-Müller counter for tritium assay. The background count of this counter is 36–38 c/m; sample activities ranged from 300 to 1800 c/m. About 45 runs were made at 16 different concentrations to determine the order and the values of the catalytic coefficients (rate constants) given in the following. All runs were carried out in duplicate or triplicate; the average reproducibility of a given run was about 2 percent.

It was found that the kinetics of this exchange in acid solution follow the equation

$$R=k_H(H^+)(H_3PO_2)+k_{H_3PO_2}(H_3PO_2)^2, \tag{1}$$

when H^+ and H_3PO_2 are the only acids present in the system. R is the rate at which the exchange of one "undissociable" hydrogen atom per acid molecule takes place.[1] Experiments in which other acids were added to the system showed that (1) is a special case of the general rate equation

$$R=(H_3PO_2)\Sigma_a\,(HA)_a k_a, \tag{2}$$

that is, the reaction is subject to general acid catalysis in the Brönsted sense.

At 30.0° the values of the catalytic coefficients in (1) are

$$k_H=3.3\pm0.15$$
$$k_{H_3PO_2}=2.9\pm0.14$$

in units of liters per mole hour.

Studies by several investigators[2a–2e] on the rate of oxidation of aqueous hypophosphorous acid to phosphorous acid by various oxidizing agents (Br_2, Cl_2, I_2, $HgCl_2$, $CuCl_2$, IO_3^-) have shown that the rate law, and under certain conditions, the rate *constants* are the same for all of these oxidation reactions irrespective of which oxidizing agent is used. In acid solution the oxidation reaction follows the rate law

$$R^0=\frac{(H_3PO_2)\Sigma_a\, k_a^0(HA)_a}{1+[\Sigma_a\,(HA)_a k_a'^0/k_1^0(Ox)]}, \tag{3}$$

where R^0 is the rate at which hypophosphorous acid is oxidized to phosphorous acid, (Ox) is the concentration of the oxidizing agent, and k_1^0 is a constant which varies with the oxidizing agent. When the concentration of the oxidizing agent is made about $0.1f$ or greater, (3) reduces to

$$R^0=(H_3PO_2)\Sigma_a\,(HA)_a k_a^0, \tag{4}$$

that is, the rate becomes independent of the concentration and nature of the oxidizing agent. This happens because under these conditions, reaction (5) below becomes rate determining.

The mechanism proposed to explain this *oxidation* rate law is as follows:

$$(H_3PO_2)_I \xrightarrow{k_a^0} (H_3PO_2)_{II} \quad \text{slow}, \tag{5}$$

$$(H_3PO_2)_{II} \xrightarrow{k_a'^0} (H_3PO_2)_I \quad \text{rapid}, \tag{6}$$

$$(H_3PO_2)_{II}+Ox \xrightarrow{k_1^0} H_3PO_3+\text{Red} \quad \text{rapid}, \tag{7}$$

where $(H_3PO_2)_I$ denotes the concentration of the "normal" form of hypophosphorous acid in solution, and $(H_3PO_2)_{II}$ denotes the concentration of an "active" form. It is assumed that the oxidizing agent reacts only with the active form to produce phosphorous acid, and that both reactions (5) and (6) are subject to general acid catalysis. The further assumption of a small, steady-state concentration of the active form leads to the aforementioned rate laws, (3) and (4).

The values of the catalytic coefficients for H^+ and H_3PO_2 found at 30.0° for the *oxidation* reactions are[2c]

$$k_{H^0}=21$$
$$k_{H_3PO_2{}^0}=7.6$$

in units of liters per mole hour.

The exact correspondence between the rate laws (1) and (4) and the close correspondence between the values of the catalytic coefficients k_a and k_a^0 for the two acid catalyzed reactions shows that the exchange reaction takes place *via* the equilibrium expressed by reactions (5) and (6). Furthermore, it seems quite likely that the normal and the active forms differ in the position of a hydrogen atom on the H_3PO_2 molecule. The difference between the numerical values of k_a and k_a^0 is a result of isotope effects.

Thus the results of the exchange experiments serve to verify the presence of two tautomeric forms of hypophosphorous acid in aqueous solution and the essential validity of the mechanism of the oxidation reaction originally suggested by Mitchell.[2a] Moreover, a clue emerges regarding the more precise nature of the two tautomeric forms. A detailed account of this research will be published later.

We wish to acknowledge with thanks the helpful discussions with Professor Ernest Swift and Dr. Norman Davidson. The research was supported in part by a grant from the Research Corporation for which we are grateful.

[1] J. N. Wilson and R. G. Dickson, J. Am. Chem. Soc. **59**, 1358 (1937). R. B. Duffield and M. Calvin, J. Am. Chem. Soc. **68**, 557 (1946). Friedlander and Kennedy, *Introduction to Radiochemistry* (John Wiley and Sons, Inc., New York, 1949), p. 288.

[2] a. A. D. Mitchell, J. Chem. Soc. **117**, 1322 (1920); **119**, 1266 (1921); **121**, 1624 (1922). b. R. O. Griffith and A. McKeown, Trans. Faraday Soc. **30**, 530 (1934). c. Griffith, McKeown, and Taylor, Trans. Faraday Soc. **36**, 752 (1940). d. P. Nylen, Z. anorg. u. allgem. Chem. **230**, 385 (1937). e. P. Hayward and D. M. Yost, J. Am. Chem. Soc. **71**, 915 (1949).

Change in Thermodynamic Properties Along Isentropes at the Coexistence Line Far from the Critical Point*

S. G. Reed, Jr.
U. S. Naval Ordnance Laboratory, White Oak, Silver Spring 19, Maryland
(Received December 19, 1951)

THE isentropic curve on a $p-v$ diagram for a single component substance undergoes an abrupt change in slope on passing through the coexistence line.[1] It does not seem to have been noticed that in the region of volumes much larger than critical, the amount of this change can be calculated with a degree of approximation usually employed in analyses of this type.

In the coexistence region the slope of the isentropic is given by

$$(\partial p/\partial v)_S=-T(\partial p/\partial T)_v^2/C_v. \tag{1}$$

Using the Clausius-Clapeyron equation, and assuming that the specific volume of the condensed phase can be neglected compared to that of the vapor and that the specific heat L is constant, is equivalent to taking for the vapor pressure an equation of the type $\ln p=A-B/T$, with A and B constants. At the coexistence line

$$C_v=C_e,\ \text{sat.}+(L^2/RT^2-2L/T), \tag{2}$$

and

$$(\partial p/\partial v)_S=-p^2/RT(1-2RT/L+C_e,\ \text{sat.}RT^2/L^2)^{-1}, \tag{3}$$

where C_e, sat. is the specific heat of the saturated condensed phase. For those substances having C_e, sat.$RT^2/L^2\ll 1$, Eq. (2) reduces to

$$(\partial p/\partial v)_S=(-p^2/RT)(1-2RT/L)^{-1}. \tag{2'}$$

It is interesting to compare this with the slope along the coexistence line

$$(\partial p/\partial v)_{\text{coex.}}=(-p^2/RT)(1-RT/L)^{-1}. \tag{4}$$

Evidently for such substances the saturate disentrope is always steeper, at the coexistence line, than the coexistence line itself.

A calculation for several substances for which virial coefficient data are available indicates that only a very small error will be made if, in computing the slope up to the coexistence line, the perfect gas equation of state is used. Using the perfect gas equation it follows that

$$(\partial p/\partial v)_{S,\text{vap.}}=-\gamma p^2/RT. \tag{5}$$

An example of the abrupt change in slope occurs with nitrogen at 65°K where the slope at the coexistence line decreases sharply by about 10 percent. Equally sharp decreases occur for the related adiabatic compressibility and sound speed defined as $(\partial p/\partial \rho)_S$.[2]

Illuminating discussions on this problem with Dr. K. F. Herzfeld are gratefully acknowledged.

* Some of this material was reported at the New York meeting of the American Physical Society, February 1–3, 1951.

[1] F. Bosnjakovic, Technische Thermodynamik I (Edwards Brothers, Ann Arbor, 1944), p. 188.

[2] Wegener, Reed, Jr., Stollenwerk, and Lundquist, J. Appl. Phys. **22**, 1077 (1951).

Erratum: On the Energetic Treatment of Non-Isothermal Processes

[J. Chem. Phys. **19**, 519–25 (1951)]

Hans Holtan, Jr.
Norges Tekniske Hoegskole, Trondheim, Norway

TEXT to Fig. 1, 350°C should be 327°C; text to Fig. 2, 327°C should be 350°C; the line just after Eq. (21), cation should be anion; and sixth line after Eq. (32), Eq. (8) should be Eq. (32).

Hybridization and Molecular Structure

JULES DUCHESNE
Institute of Astrophysics, University of Liège, Cointe-Sclessin, Belgium
(Received January 15, 1951)

IN recent papers[1] we have shown that the bond properties of many molecules can be properly interpreted by using sp hybridized orbitals with a small amount of s-character, not only in the central atoms, as already well known, but in the end-atoms as well. The analysis of this problem led us to formulate a principle which was expressed in the following way: "The hybridization of an atomic orbital of an atom bonded to a hybridized carbon atom changes with the amount of hybridization of carbon and tends to become equivalent." In this connection it seems worth while to draw attention to the meaning of new experimental results concerned with the structure of particularly appropriate molecules such as CH_3CCH and CF_3CCH.[2] Indeed, the HCH and FCF angles in these molecules have a value of about 107.5° which is definitely less than the tetrahedral one. Furthermore, the CC single bond only amounts to 1.46A in both molecules and is therefore contracted with respect to the sum of the carbon radii, equal to 1.50A, corresponding to the sp^3 and sp hybridization. The possibility of interpreting these facts quantitatively rests on a redistribution of the carbon hybrid atomic orbitals of CH_3 and CF_3. This can easily be performed because the orbital distribution is unequivocally determined by the HCH and FCF angles. The result of the calculation gives more s-character in the CC single bond which becomes almost sp^2+sp instead of sp^3+sp, which would be the case if the angles were 109° 28′. Then the CC bond length becomes 1.478A in satisfactory agreement with the experimental value (1.46A).

Our principle is therefore strikingly confirmed for molecules which can be most adequately handled. It would of course be important to get more experimental data for series of molecules in which the end-atoms are identified as pyramidal radicals. In this case the change of hybridization, which amounts approximately to 8 percent of the s-character, is larger than for the halogen end-atoms considered earlier.[1]

A detailed account will soon appear in the *Mémoires de l'Académie Royale de Belgique.*

[1] J. Duchesne, Trans. Faraday Soc. **46**, 187 (1950); J. Chem. Phys. **19**, 246 (1951).
[2] R. Trambarulo and W. Gordy, J. Chem. Phys. **18**, 1613 (1950); Shoolery, Shulman, Sheehan, Jr., Schomaker, and Yost, J. Chem. Phys. **19**, 1364 (1951).